NASA Conference Publication 2467
Part 2

Structural Dynamics and Control Interaction of Flexible Structures

(NASA-CP-2467-Pt-2) STRUCTURAL DYNAMICS AND N87-22729
CONTROL INTERACTION OF FLEXIBLE STRUCTURES --THRU--
(NASA) 729 p Avail: NTIS HC A99/MF E03 N87-22753
CSCL 22B Unclas
G1/15 0072200

Proceedings of a workshop held at
George C. Marshall Space Flight Center
Huntsville, Alabama
April 22-24, 1986

NASA

NASA Conference Publication 2467
Part 2

Structural Dynamics and Control Interaction of Flexible Structures

Edited by
Robert S. Ryan and Harold N. Scofield
George C. Marshall Space Flight Center
Huntsville, Alabama

Proceedings of a workshop held at
George C. Marshall Space Flight Center
Huntsville, Alabama
April 22–24, 1986

NASA
National Aeronautics
and Space Administration

Scientific and Technical
Information Branch

1987

TABLE OF CONTENTS

Part 1*

Page

SESSION 1 11

Workshop Overview (Dr. J. Blair) 13

Overview of OAST's Large Space Systems Controls Research and Technology Program (John DiBattista) 21

Status of the Mast Experiment (B. R. Hanks, J. L. Allen, Jr., and A. Fontana) 29

Large Space Structures Ground Experiment Checkout (H. B. Waites).... 57

Identification of Large Space Structures, A State-of-the-Practice Report (T. K. Hasselman) 85

SESSION 2 99

Active Damping Experiments (G. C. Horner) 101

A General Method for Dynamic Analysis of Structures (R. C. Engels)... 119

Dynamic Behavior of a Large Flexible Space Station During Space Shuttle Orbiter Docking (N. G. Fitz-Coy and J. E. Cochran, Jr.) 133

Transient Response for Interaction of Two Dynamic Bodies (A. Prabhakar and L. G. Palermo) 175

Mover II - A Computer Program for Model Verification of Dynamic Systems (J. D. Chrostowski and T. K. Hasselman) 199

Consideration in the Design and Development of a Space Station Scale Model (P. E. McGowan) 215

Verification of Large Beam-Type Space Structures (C. G. Shih, J. C. Chen, and J. A. Garba) 247

Verification of Flexible Structures by Ground Test (B. K. Wada and C. P. Kuo) 255

Optimum Mix of Passive and Active Control for Space Structures (L. Rogers) 275

1-CAT: A MIMO Design Methodology (J. R. Mitchell and J. C. Lucas) .. 293

Inter-Stable Control Systems (G. von Pragenau) 335

Status Report and Preliminary Results of the Spacecraft Control Laboratory (J. P. Williams) 359

---

*Pages 1 to 692 are published under separate cover.

PRECEDING PAGE BLANK NOT FILMED

TABLE OF CONTENTS (Continued)

Page

Flexible Spacecraft Control Simulator (J. Bassi)........................ 399

Improving Stability Margins in Discrete-Time LQG Controllers (B. T. Oranc and C. L. Phillips) 417

An Overview of Research Conducted by the Spacecraft Control Branch of the NASA LaRC Grid (R. C. Montgomery) 435

Space Station Structural/Control Interaction (Payload Pointing and Micro-G) (C. R. Larson)...................................... 457

SESSION 3 485

SAFE Dynamic Flight Experiment (R. W. Schock) 487

Application of Robust Projection Operators to the Control of Flexible Structures with Uncertain Parameters (M. H. Bantell, Jr.) 505

Dynamics of Trusses Having Nonlinear Joints (J. M. Chapman) 539

Equivalent Beam Modeling Using Numerical Reduction Techniques (J. M. Chapman).. 567

Dynamic Characteristics of a Vibrating Beam with Periodic Variation in Bending Stiffness (J. S. Townsend) 595

Structural Dynamic System Model Reduction (J. C. Chen, T. L. Rose, and B. K. Wada) 625

Space Telescope Reaction Wheel Assembly Vibration Damping System (R. E. Jewell, P. Davis, and J. Wilson) 669

Part 2

Stiffness Control for Active Damping (J. L. Fanson and J. C. Chen, Jr.) 693

A Quasi-Analytical Method for Non-Iterative Computation of Nonlinear Controls (J. L. Junkins, R. C. Thompson, and J. D. Turner) 759

Decentralized Control of Large Space Structures via the GHR (D. K. Lindner) 775

Control of Flexible Structures and the Research Community (J. S. Pyle and C. R. Keckler) 789

Impact of Space Station Appendage Vibrations on the Pointing Performance of Gimballed Payloads (R. Hughes).................... 841

TABLE OF CONTENTS (Continued)

Page

Maneuvering and Vibration Control of Flexible Spacecraft (L. Meirovitch and R. D. Quinn) 867

Hubble Space Telescope Disturbances Caused by High Gain Antenna Motions (J. P. Sharkey) 881

Preliminary Evaluation of a Reaction Control System for the Space Station (H. H. Woo and J. Finley) 903

SESSION 4 943

Dual Keel Space Station Control/Structures Interaction Study (J. W. Young, F. J. Lallman, and P. A. Cooper) 945

High Speed Simulation of Flexible Multibody Dynamics (A. D. Jacot, R. E. Jones, and C. Juengst) 979

On the Application of Lanczos Modes to the Control of Flexible Structures (R. R. Craig, Jr.) 999

Modal Testing and Slewing Control Experiment for Flexible Structures (J. N. Juang) 1013

MEOP Control Design Synthesis: Optimal Qualification of the Big Four Tradeoffs (David C. Hyland and Dennis Bernstein) 1033

Vibration Isolation for Line of Sight Performance Improvement (J. J. Rodden, H. Dougherty, and W. Haile) 1071

A New Semi-Passive Approach for Vibration Control in Large Space Structures (K. Kumar and J. E. Cochran, Jr.) 1079

Crew Motion Forcing Functions from Skylab Flight Experiment and Applicable to Space Station (B. Rochon) 1095

Modeling of Controlled Structures with Impulsive Loads (M. Zak) 1161

SESSION 5 1177

Critical Issues Forum (S. Seltzer, B. Wada, and L. Pinson) 1179

Notes on Implementation of Coulomb Friction in Coupled Dynamical Simulations (R. J. VanderVoort and R. P. Singh) 1196

On the Control of Structures by Applied Thermal Gradients (D. R. Edberg and J. C. Chen) 1215

TABLE OF CONTENTS (Concluded)

Page

Finite Element Models of Wire Rope for Vibration Analysis (J. E. Cochran, Jr. and N. G. Fitz-Coy) 1251

Experimental Characterization of Deployable Trusses and Joints (R. Ikegami, S. Church, D. Kienholz, and B. Fowler) 1271

System Identification for Large Space Structure Damage Assessment (J. C. Chen and J. A. Garba) 1289

Space Station Structures and Dynamics Test Program (Proposed) (E. W. Ivey, C. J. Moore, and J. S. Townsend) 1319

Analytical Determination of Space Station Response to Crew Motion and Design of Suspension System for Microgravity Experiments (F. C. Liu) 1333

Space Station Structural Dynamics/Reaction Control System Interaction Study (M. Pinnamaneni)................................ 1367

SESSION 6 – PANEL DISCUSSION 1395

N87
22730
UNCLAS

N87-22730

VIBRATION SUPPRESSION BY STIFFNESS CONTROL

James Fanson
Thomas Caughey
Jay Chen

California Institute of Technology

JPL

April 23, 1986

Workshop on Structural Dynamics and
Control Interaction of Flexible Structures

The objectives of large space structure control can be divided into three general categories. They are: 1) Pointing, 2) Vibration Suppression, and 3) Shape Control.

The objective of Pointing is not new to the spacecraft control community. This objective has been part of essentially every space mission of the past 25 years. The Pointing objective includes both spacecraft orientation (in the rigid body sense) and the orbit of the spacecraft.

The other categories are new, however, with the new class of flexible structures. Both vibration and shape are related to the elastic nature of the structure and are therefore fundamentally different phenomena than those encountered in rigid body attitude control. This distinction is true even for nonlinear structures.

In short, the control objectives of Vibration Suppression and Shape Control have more in common with each other than either has in common with the objective of Pointing. We consider this point of view significant.

JPL

CONTROL OF FLEXIBLE STRUCTURES

- Pointing (Rigid Body -- Optimal Control)
- Vibration Suppression (Flexible Body)
- Shape Control (Flexible Body)

The new control objectives have immediate implications for control actuator selection. Traditionally, "external force producing" actuators such as thrusters and momentum wheels have been used. This is in keeping with the traditional Pointing objective for which this type of actuator is required.

This type of actuator is highly undesirable for Vibration Suppression or Shape Control, however, for two reasons. First, external forces will couple the flexible motion to the rigid motion, and second, these devices expend consumables, or otherwise cannot be operated quasi-statically.

There are "internal force producing" devices available for use as actuators which are electrically powered. Among these are piezoelectric and thermoelectric devices. Since electricity is a renewable power source in space these types of actuators are well suited for Vibration Suppression and Shape Control.

JPL

CONTROL ACTUATOR TYPES

- **External Force Producing (Thrusters - Moment Wheel)**
  - -- Required for Rigid Body Pointing
  - -- Undesirable for Vibration Suppression (Rigid Coupling)
  - -- Unusable for Shape Control (Consumables)
- **Internal Force Producing (Piezo /Thermo - Electric)**
  - -- Unusable for Rigid Body Pointing
  - -- Desirable for Vibration Suppression (No Coupling)
  - -- Essential for Shape Control

The ideal actuator or sensor for Vibration Suppression would be electrically powered, would be highly efficient, would weigh nothing, and would have a very high bandwidth. The high bandwidth requirement is important so that the rolloff characteristics of the closed loop system can be designed without regard to actuator dynamics.

IDEAL ACTUATOR/SENSOR FOR VIBRATION SUPPRESSION

- Electrically Powered
- 100% Electro-Mechanical Efficiency
- Zero Mass
- Infinite Bandwidth

Our experiment utilizes piezoelectric ceramics as both sensors and actuators. Two types of piezoelectric materials are available to choose from, piezoelectric ceramics and piezoelectric polymers, and they each have specific advantages and disadvantages.

Both types are electrically powered, are low in mass, and have high bandwidth. The principal advantages of the ceramics are that they have the highest electromechanical efficiency, and operate at low voltage. The major advantage of the polymers is the possibility of casting the material into a dual structure/control element.

PIEZO-ELECTRIC MATERIALS AS ACTUATORS/SENSORS

- **Piezo-Electric Ceramics**
  - -- Electrically Powered
  - -- Highest Electro-Mechanical Efficiency
  - -- Low Mass
  - -- Essentially Infinite Bandwidth
  - -- Low Voltage

- **Piezo-Electric Polymers**
  - -- Electrically Powered
  - -- High Electro-Mechanical Efficiency
  - -- Lowest Mass
  - -- Essentially Infinite Bandwidth
  - -- High Voltage
  - -- Possibility of Being Cast as Structural Member

Most of the significant aspects of structural dynamics for large space structures as they pertain to Vibration Suppression can be understood from a study of the single degree-of-freedom (SDOF) damped linear oscillator. The canonical form of the forced SDOF damped linear oscillator is shown.

Single Degree-of-Freedom Damped Linear Oscillator

$$m\ddot{x}(t) \;+\; c\dot{x}(t) \;+\; kx(t) \;=\; F(t)$$

Substitute: $\frac{k}{m} \equiv \omega_n^2$

$\frac{c}{2\sqrt{km}} \equiv \varsigma$ (Damping Ratio $\frac{c}{c_{\mathrm{critical}}}$)

$$\underbrace{\ddot{x}(t)}_{\text{Inertia Term}} \;+\; \underbrace{2\varsigma\omega_n\dot{x}(t)}_{\text{Damping Term}} \;+\; \underbrace{\omega_n^2 x(t)}_{\text{Stiffness Term}} \;=\; \frac{1}{m}F(t) \;=\; \frac{\omega_n^2}{k}F(t)$$

There are two types of structural dynamic response of interest. The first type is the forced response. When a structure is excited by a persistent disturbance, such as a sinusoidal forcing function, the amplitude of the response increases near structure's natural frequency. For a critical damping ratio ς less than 0.707 the maximum amplitude of response occurs at a frequency of $\omega = \omega_n \sqrt{1 - 2\varsigma^2}$. The quantity of interest in minimizing the amplitude of response is $\varsigma \omega_n^2$. For small damping (less than 0.2) the amplitude of response is inversely proportional to this quantity.

Forced Response:

$$\ddot{x}(t) \; + \; 2\varsigma\omega_n\dot{x}(t) \; + \; \omega_n^2 x(t) \; = \; \frac{\omega_n^2}{k} P \cos\omega t$$

If $\varsigma < 0.707$

$$\left|x(t)\right|_{\max} = \frac{P/k}{2\varsigma\sqrt{1-\varsigma^2}} \qquad \text{At:} \quad \omega = \omega_n\sqrt{1-2\varsigma^2}$$

For ς small

$$\left|x(t)\right|_{\max} \approx \frac{P}{2\varsigma k} = \frac{P}{2m\varsigma\omega_n^2}$$

Quantity of Interest: ςk, *or* $\varsigma\omega_n^2$

The other type of dynamic response of interest is the free response. If a disturbance ceases, how long does it take for the structural response to decay to zero? The quantity of interest in minimizing the settling time is $\varsigma\omega_n$. The free decay of the structural response is enveloped by the term $e^{-\varsigma\omega_n t}$. As $\varsigma\omega_n$ is increased the settling time decreases.

Free Response:

$$\ddot{x}(t) + 2\varsigma\omega_n\dot{x}(t) + \omega_n^2 x(t) = 0$$

$$x(t) \; = \; e^{-\varsigma\omega_n t}(A\cos\omega_d t \; + \; B\sin\omega_d t)$$

Where: $\omega_d \equiv \omega_n\sqrt{1-\varsigma^2}$

Settling Time Requirement $\Longrightarrow \varsigma\omega_n =$ Desired Value

Quantity of Interest: $\varsigma\sqrt{\frac{k}{m}}, \quad or \quad \varsigma\omega_n$

The two aspects of structural response which are significant to the objective of Vibration Suppression are the steady state response amplitude characterized by the quantity $\varsigma\omega_n^2$, and the free decay settling time characterized by the quantity $\varsigma\omega_n$. Ideally, both of these quantities should be maximized to provide the best Vibration Suppression. In practice, however, these two quantites cannot be maximized simultaneously.

Two important observations can be made: First, the stiffness of the structure, or equivalently, its natural frequency, is much more difficult to alter than is the damping ratio ς. This is because ς is usually a small number whereas the stiffness is usually not. Second, the dynamic response is very sensitive to ς.

Dynamic Response Mode	Quantity of Interest
Response Amplitude	$\varsigma\omega_n^2$ *or* ςk
Settling Time	$\varsigma\omega_n$ *or* $\varsigma\sqrt{k/m}$

Observation: k and ω_n are much more difficult to alter than ς.

Observation: Dynamic response is very sensitive to ς.

The derivation of the SDOF damped linear oscillator's open loop poles is presented. The transfer function $T(s)$ is introduced.

Transfer Function:

$$\ddot{x}(t) + 2\varsigma\omega_n\dot{x}(t) + \omega_n^2 x(t) = \frac{\omega_n^2}{k}F(t)$$

$$s^2\hat{x}(s) + 2\varsigma\omega_n s\hat{x}(s) + \omega_n^2\hat{x}(s) = \frac{\omega_n^2}{k}\hat{F}(s)$$

$$\frac{\hat{x}(s)}{\hat{F}(s)} = \frac{\omega_n^2/k}{s^2 + 2\varsigma\omega_n s + \omega_n^2}$$

$$T(s) = \frac{\omega_n^2/k}{(s + \varsigma\omega_n + j\omega_d)(s + \varsigma\omega_n - j\omega_d)}, \quad j \equiv \sqrt{-1}$$

Open Loop Poles:

$$s_1 = -\,\varsigma\omega_n + j\omega_d$$

$$s_2 = -\,\varsigma\omega_n - j\omega_d$$

The general objective of our Vibration Suppression system is to increase ς by active control thereby moving the system poles further into the left half-plane. The direction the pole should be moved from its open loop position in the complex plane depends on the quantity being maximized. To maximize $\varsigma\omega_n$, that is, to minimize the settling time, the pole should be moved directly left into the left half-plane. To maximize the quantity $\varsigma\omega_n^2$, that is, to minimize the response amplitude, the pole should be moved at an angle of $\tan^{-1}\varsigma\sqrt{1-\varsigma^2}$. For small damping values this angle is essentially zero and then the direction becomes straight back into the left half-plane as before.

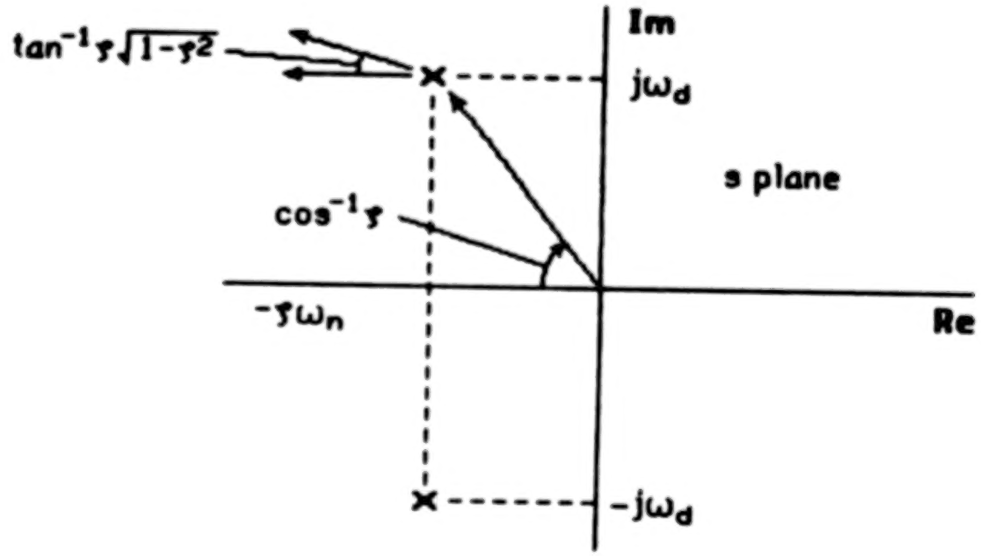
Im
$j\omega_d$
s plane
$\tan^{-1}\zeta\sqrt{1-\zeta^2}$
$\cos^{-1}\zeta$
$-\zeta\omega_n$
Re
$-j\omega_d$

OBJECTIVE: Increase ζ By Active Control Thereby Moving Poles Further Into Left Half-Plane.

Our experiment is intended to simulate some of the inherent difficulties of controlling large space structures. The specimen is a thin cantilever beam. It has low natural frequencies, low mass, and low stiffness.

We are using collocated piezoelectric ceramic sensors and actuators.

JPL

STIFFNESS CONTROL EXPERIMENT

- Vibration Suppression of Cantilever Beam
- Test Specimen Displays LSS Pathologies
  - -- Low Stiffness
  - -- Low Mass
  - -- High Modal Density at Higher Frequency
- Collocated Piezo-Electric Ceramic Sensors and Actuators
- Various Control Strategies

The piezoelectric ceramics are 9.5 mil thick. Two ceramics are adhered to the beam (in sandwich fashion) to operate as sensors to measure bending strain. And two ceramics are adhered next to the sensors to apply a bending moment. The poling directions of the ceramics are arranged such that the actuators operate in a push-pull mode and the sensors operate in parallel.

JPL

Piezo Cantilever Beam

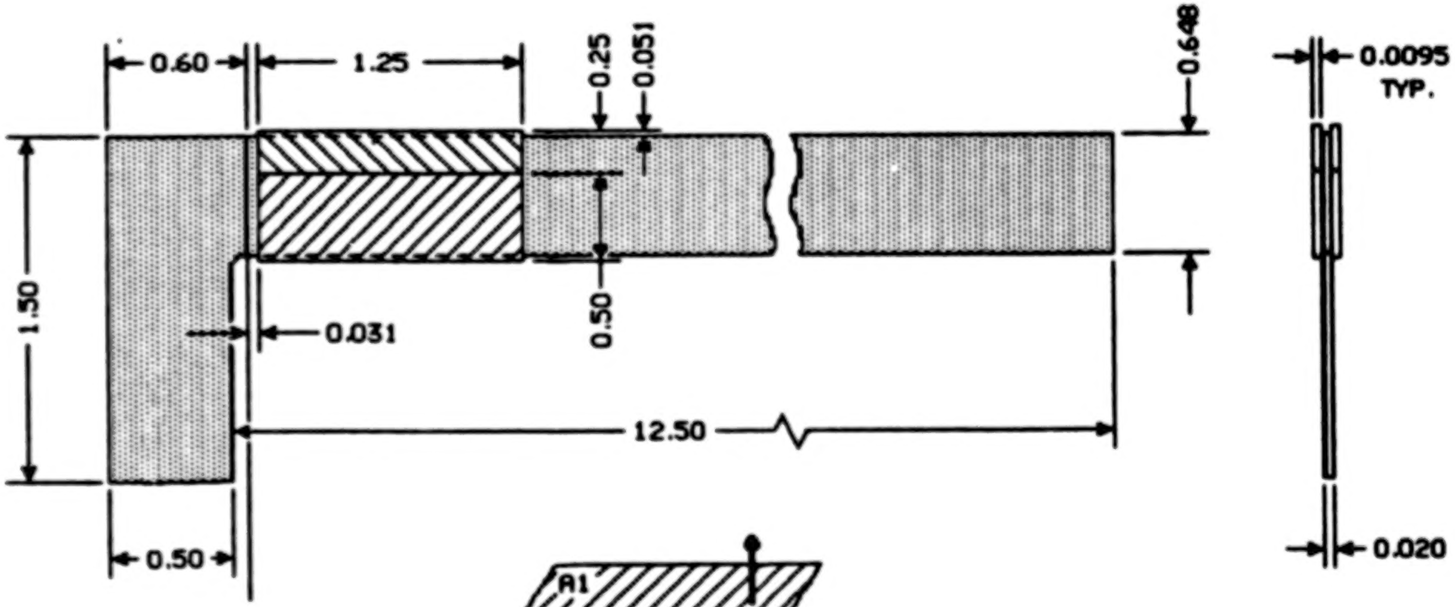
0.60
1.25
0.25
0.051
0.648
0.0095
TYP.
1.50
0.031
0.50
12.50
0.50
0.020

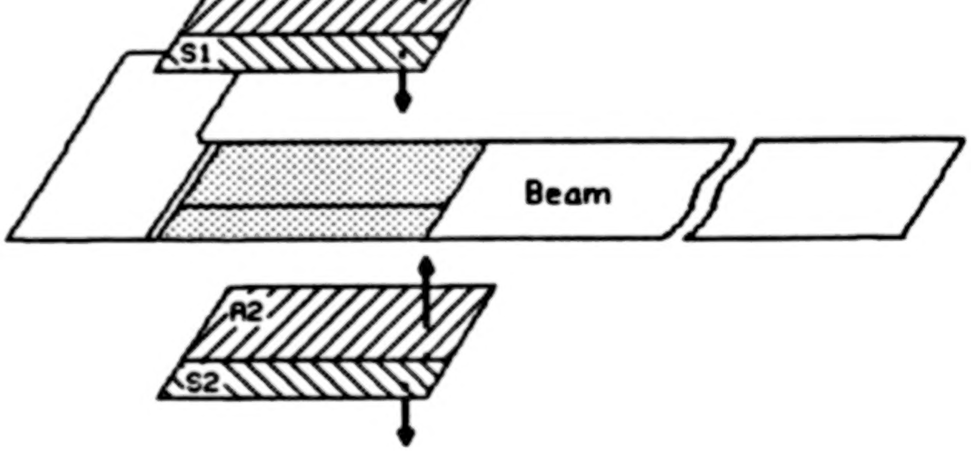
A1
S1
Beam
A2
S2

Actuator/Sensor Poling Orientations

The laboratory setup is shown. The beam is cantilevered out of a clamping fixture which is attached to a linear bearing table. The bearing table is driven by a Brüel and Kjær shaker. The ceramic actuators and sensors can be seen attached to the root of the beam. This setup allows us to excite the structure with a wide range of disturbances to measure control system performance.

ORIGINAL PAGE IS
OF POOR QUALITY

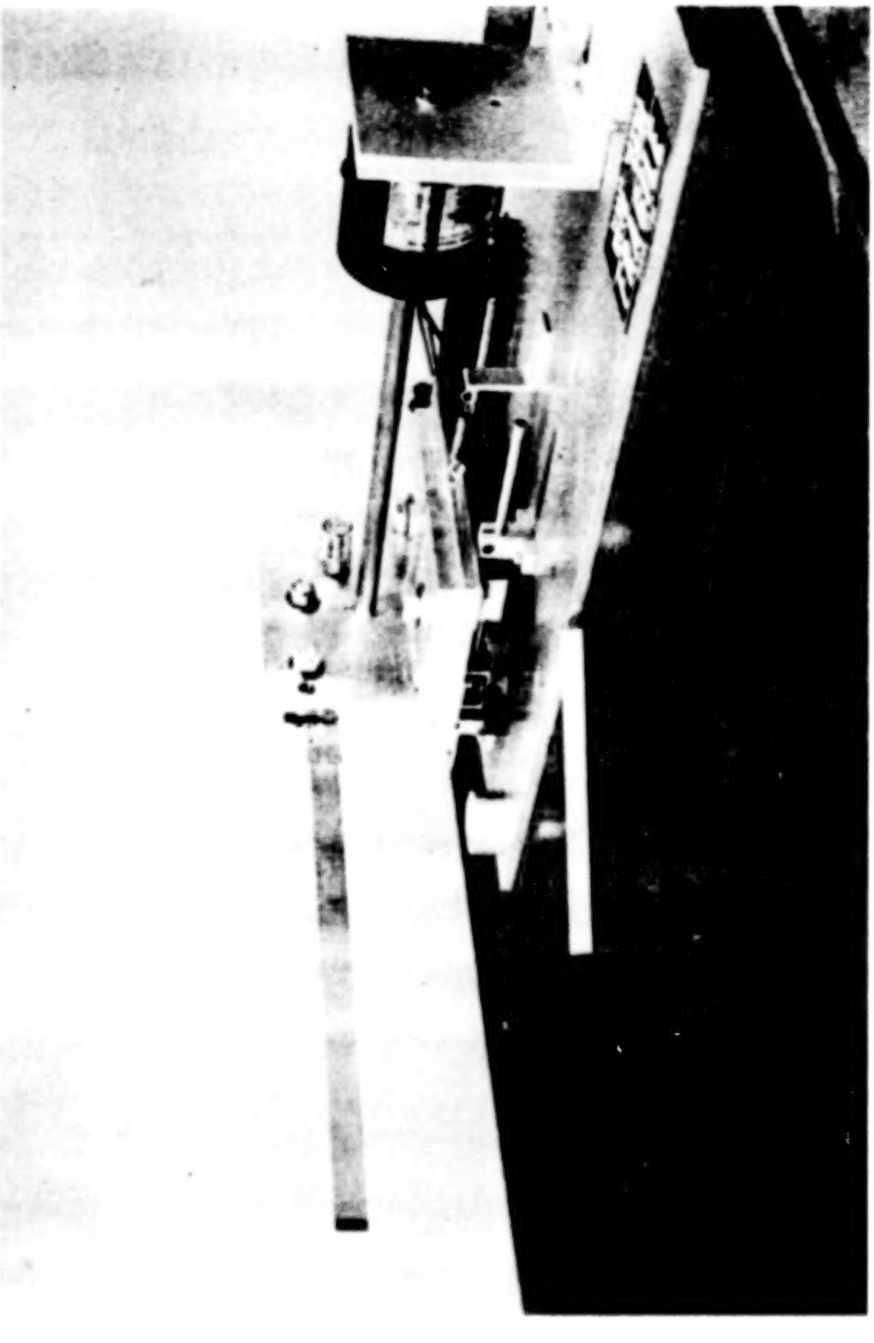

This view shows a close-up of the sensors and actuators. The larger ceramic is the actuator, the smaller is the sensor. The ceramics are attached with a standard cyanoacrylate adhesive in the same manner as strain gauges. Wires are simply soldered to the electrode surfaces.

ORIGINAL PAGE IS
OF POOR QUALITY

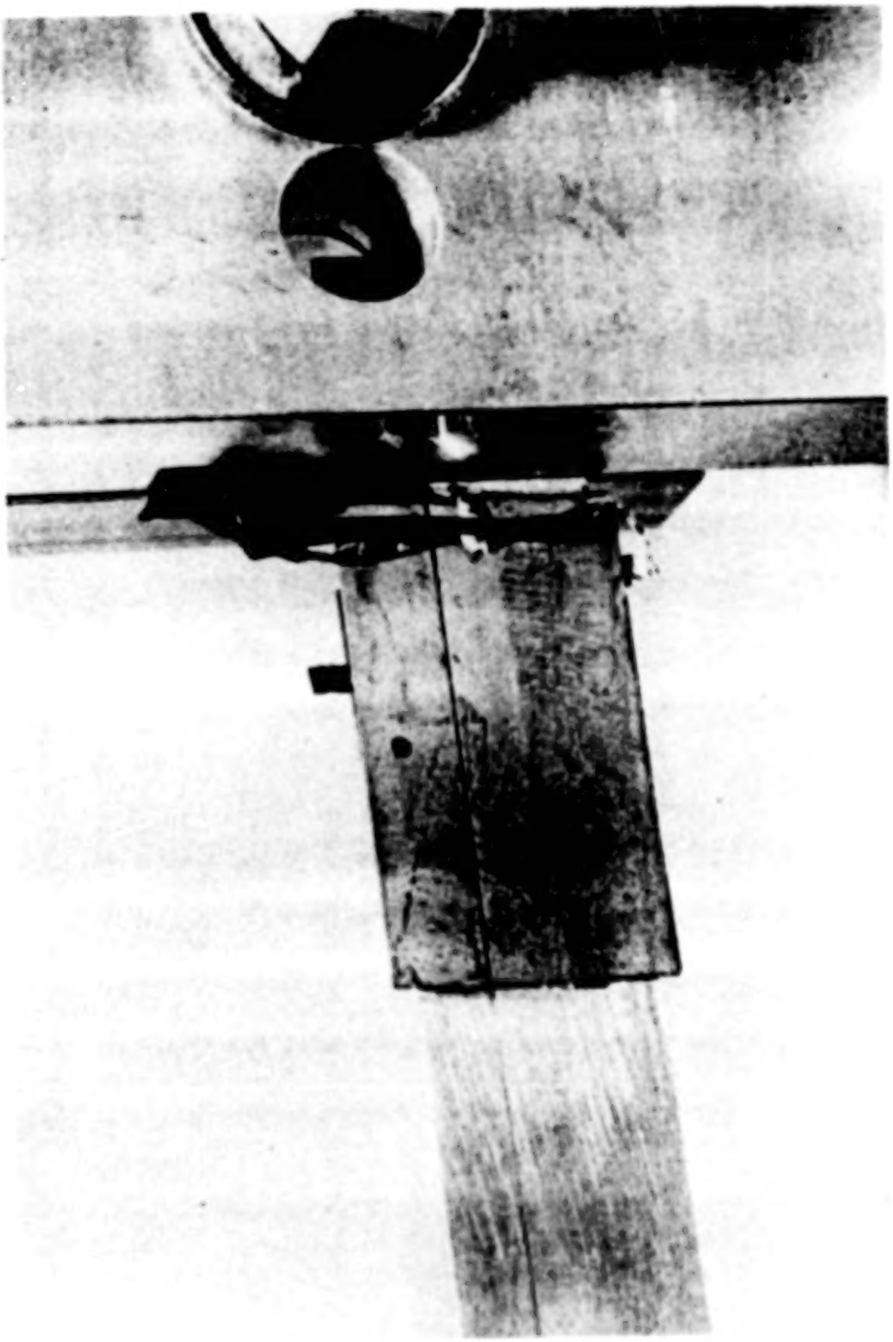

There are limitations in the state-of-the-art of structural modeling for large space structures. In particular, a detailed knowledge of the stiffness matrix of such structures seems very unlikely. Also, good knowledge of mode shapes is uncertain. This has important implications to observer-based control systems since observers are only as good as the structural models available. Furthermore, on-orbit system identification will probably be required for any complicated structure.

REALITIES OF MODELING

- Knowledge of Stiffness Matrix Limited
- Implementation of Observers Uncertain
- On-Orbit Identification Required

In view of the preceding realities of modeling, a set of desired control system features has been developed.

Firstly, a detailed knowledge of the structure should not be required. The compensator should be designed based on the structure's natural frequencies *only* since these are the structural parameters which are most likely to be known with any accuracy. Mode shape information should be used if available.

Secondly, since the objecive is Vibration Suppression, the measurement variables should be only those quantities related to the elastic deformation of the structure. This implies that inertial sensors such as accelerometers should not be used. The only quantity intimately related to elastic deformation is strain, therefore, we measure strain only. Obtaining velocities from displacement measurements requires differentiation which amplifies noise in addition to having other problems, therefore, no velocites are used.

Thirdly, the control system should be idiot proof. That is, it should be simple to implement, should maintain stability and performance in the face of uncertainty (which defines robustness), and should not compromise the structure if an actuator fails.

Finally, the control system should not destabilize unmodelled or uncontrolled modes.

DESIRED CONTROL SYSTEM FEATURES

- **Do Not Require Detailed Knowledge of Structure**
  - -- Use Frequencies Only
  - -- Mode Shapes if Available
- **Feedback Only Quantities Related to Deformation**
  - -- No Accelerometers (Inertial)
  - -- Measure Strain Only, No Velocities
- **Idiot-Proof**
  - -- Simple
  - -- Stability and Performance in the Face of Uncertainty
- **Do Not Destabilize Uncontrolled Modes**

Positive Position Feedback is one control strategy which satisfies the preceding set of desirable features. The strategy is outlined in the following.

The first equation is the equation of motion for the modes of the system. The right hand side is the control force vector which is defined later. For the single-input-single-output (SISO) experiment described in these viewgraphs, the measurement v_s is a scalar voltage proportional to a weighted sum of the modal coordinates of the beam excluding the rigid body modes. The structural frequencies ω are assumed known at least for the modes targeted for control.

A set of electrical filters with second order transfer functions similiar to the structural modes is constructed with designed frequencies ω_f near the structural frequencies ω. The damping values ζ_f are chosed to be large, say 0.2. The tuned electrical filters are driven by the measurement voltage v_s. The filter coordinates η are multiplied by appropriate gains and added to form the control vector. This vector is then imposed on the structure.

Positive Position Feedback:

$$\ddot{\boldsymbol{\xi}} + \left[{}^{\diagdown}2\varsigma\omega_{\diagdown}\right]\dot{\boldsymbol{\xi}} + \left[{}^{\diagdown}\omega^2{}_{\diagdown}\right]\boldsymbol{\xi} = \text{control force vector}$$

$$v_s = \left[\,C\,\right]^T \boldsymbol{\xi}$$

$$\ddot{\boldsymbol{\eta}} + \left[{}^{\diagdown}2\varsigma_f\omega_{f\diagdown}\right]\dot{\boldsymbol{\eta}} + \left[{}^{\diagdown}\omega^2_{f\diagdown}\right]\boldsymbol{\eta} = \left[{}^{\diagdown}\omega^2_{f\diagdown}\right]\left[\,S\,\right]v_s$$

$$v_a = \left[\,G\,\right]^T \boldsymbol{\eta}$$

$$\text{control force vector} = \left[\,D\,\right]v_a$$

The coupled system equation is shown. It is seen that the coupled damping matrix has the standard form but the coupled stiffness matrix has off-diagonal terms. Since the measurement is a generalized displacement, the control couples into the stiffness matrix, hence the term *Stiffness Control*.

JPL

Positive Position Feedback:

$$\begin{bmatrix} \ddot{\boldsymbol{\xi}} \\ \ddot{\boldsymbol{\eta}} \end{bmatrix} + \begin{bmatrix} [{}^{\backprime}2\varsigma\omega_{\smallsetminus}] & 0 \\ 0 & [{}^{\backprime}2\varsigma_f\omega_{f\smallsetminus}] \end{bmatrix} \begin{bmatrix} \dot{\boldsymbol{\xi}} \\ \dot{\boldsymbol{\eta}} \end{bmatrix} + \begin{bmatrix} [{}^{\backprime}\omega^2{}_{\smallsetminus}] & -[D][G]^T \\ -[{}^{\backprime}\omega_{f\smallsetminus}^2][S][C]^T & [{}^{\backprime}\omega_{f\smallsetminus}^2] \end{bmatrix} \begin{bmatrix} \boldsymbol{\xi} \\ \boldsymbol{\eta} \end{bmatrix} = \mathbf{0}$$

$$\ddot{\boldsymbol{\psi}} + [C]\dot{\boldsymbol{\psi}} + \underset{\substack{\uparrow \\ \textbf{New Stiffness Matrix}}}{[K]}\boldsymbol{\psi} = \mathbf{0}$$

A block diagram of the control loop is shown. The sensor and actuator blocks exhibit no dynamics because their bandwidth is far beyond the bandwidth of the loop. Notice that this is a *positive* feedback loop.

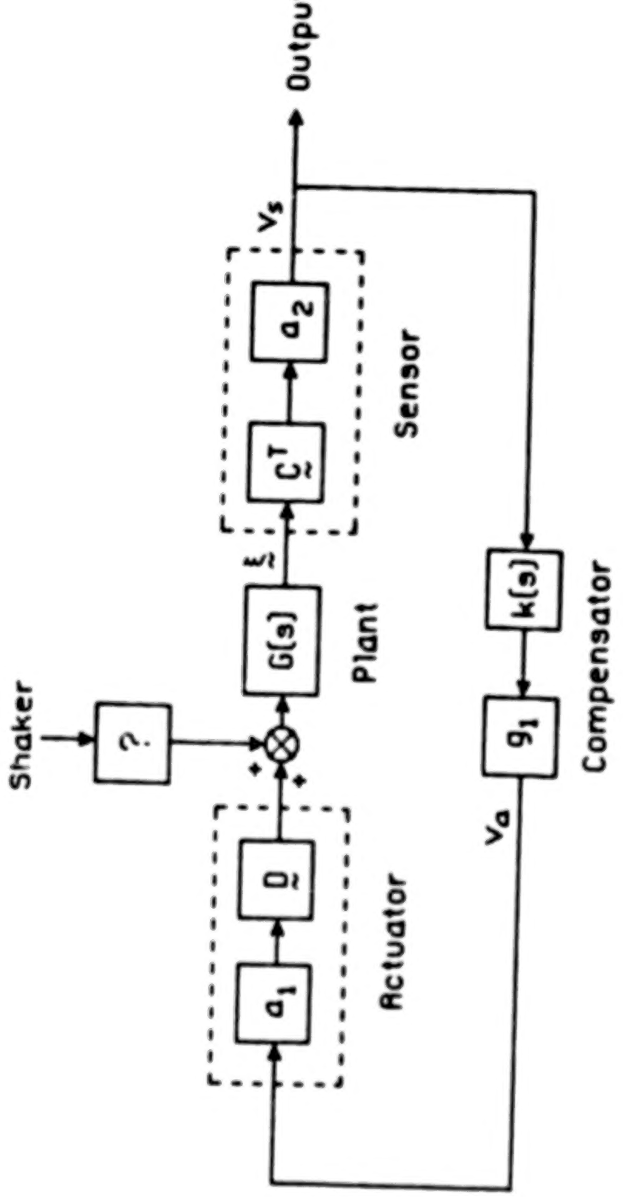
Actuator
a1
D
Shaker
?
+
+
G(s)
Plant
ξ
Sensor
C^T
a2
Vs
Output
Va
g1
k(s)
Compensator

A root locus plot (which traces the location of the closed loop poles in the complex plane as a function of gain) is shown for the case of a single mode and one tuned filter. As the gain is increased the system pole moves into the left half-plane and the filter pole moves toward the imaginary axis. Approximately halfway between the open loop pole locations, the two trajectories bend, the system pole moves upward and the filter pole moves down toward the real axis. Eventually, at sufficiently high gain, the filter pole moves along the real axis into the right half-plane.

JPL

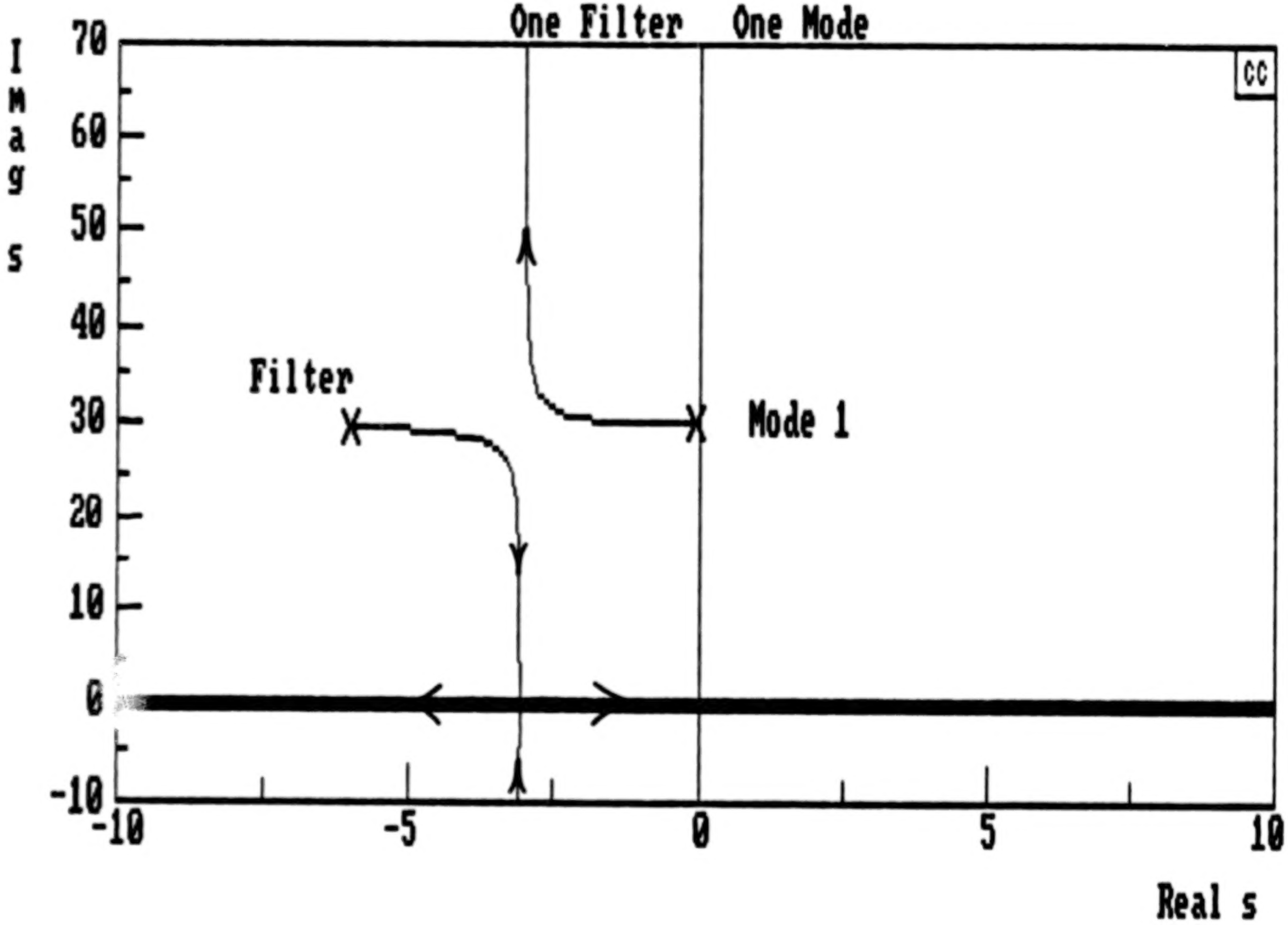
One Filter One Mode
CC
Filter
Mode 1
Imag s
70
60
50
40
30
20
10
0
-10
-10
-5
0
5
10
Real s

If there are densely spaced modes in the vicinity of the filter, we see that all the system poles are moved into the left half-plane with the lowest mode eventually going unstable at sufficiently high gain. The higher poles never go unstable because of the presence of transmission zeros which trap them in the left half-plane. This is characteristic of *Positive Position Feedback*. Instability will only occur either in the lowest frequency mode or the lowest frequency filter.

One Filter Dense Modes

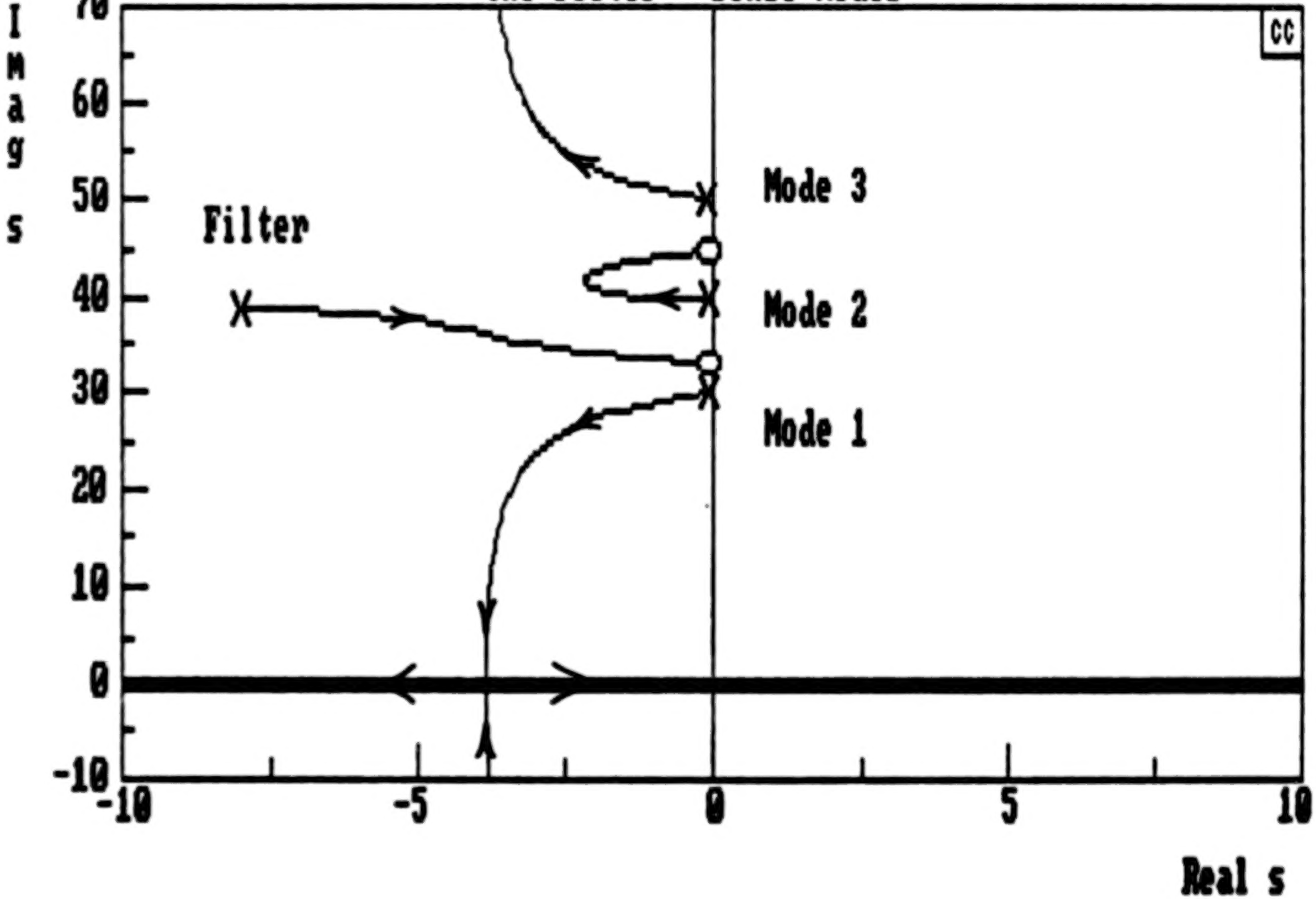

This root locus shows the effect of densely packed control filters in a region of dense structural modes. As can be seen this only improves the movement of the system poles into the left half-plane. Thus, it does no damage to place extra control filters in a region where structural modes are suspected.

Not shown is a technique for trapping the instability by means of an "arresting pole" thus insuring that the instability can only occur in the lowest frequency filter. This means that any instability will occur at low frequency (giving more time to detect it before oscillations become large) and will occur in the electronics which can be built with saturation characteristics.

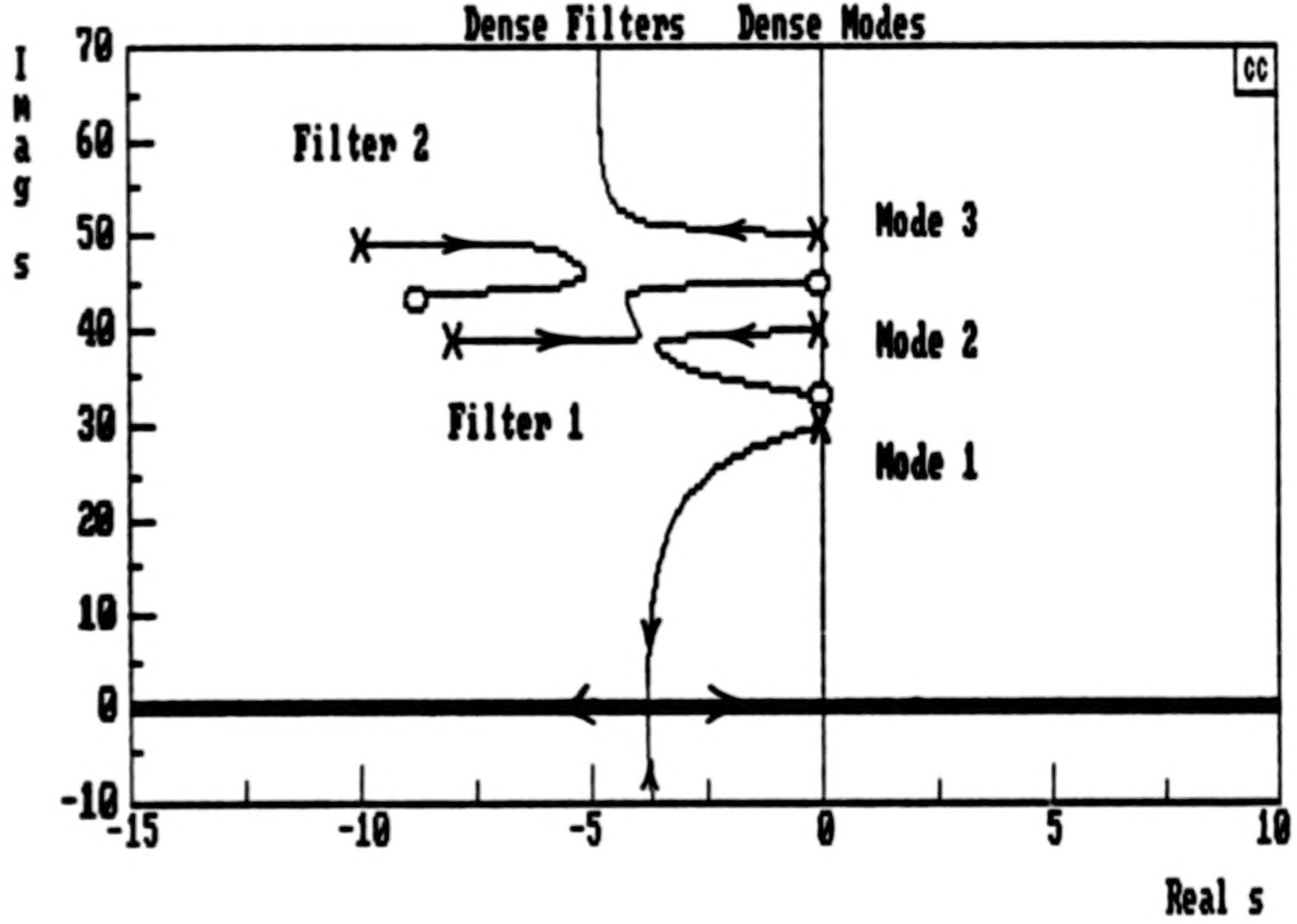
Dense Filters Dense Modes
CC
Filter 2
Filter 1
Mode 3
Mode 2
Mode 1
Imag s
70
60
50
40
30
20
10
0
-10
-15
-10
-5
0
5
10
Real s

This plot shows the response amplitude for the open loop (dashed line) and closed loop (solid line) one mode control case. The first two modes are shown. Because the first two modes of a cantilever beam differ in frequency by a factor of six they are considered far apart. The mode one filter damps mode one but leaves mode two alone. Actually, the damping in mode two is increased slightly. This is another feature of *Positive Position Feedback*: all control spillover is stablizing.

JET PROPULSION LABORATORY
POSITIVE POSITION CHIRP TEST
MODE 1 AND MODE 2

MSC/STI-VAMP

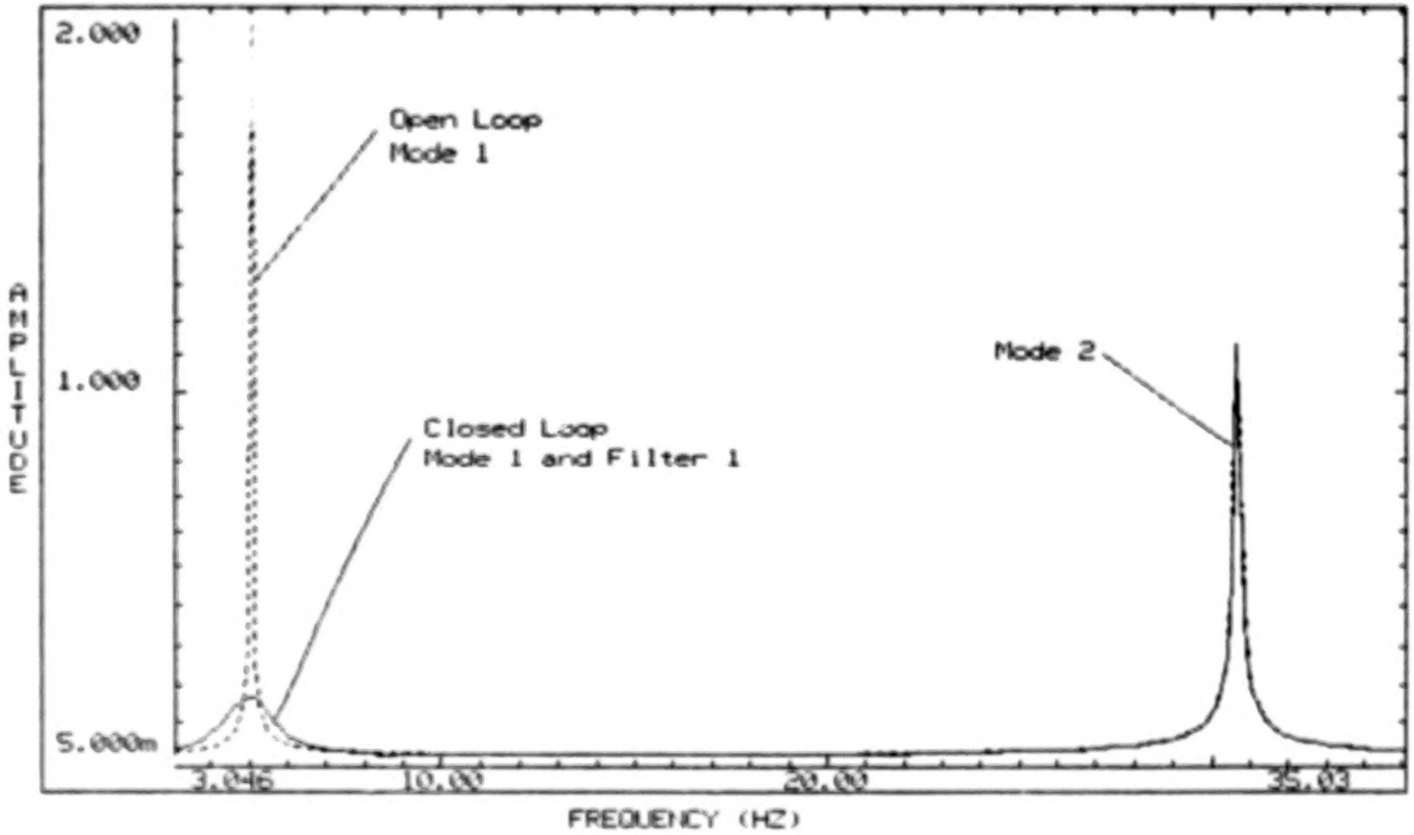

The electrical circuit of the compensator is shown for three mode control. The sensor signal is buffered and then simply split into three parts and fed into three tuned filters, one for each mode since they are not densely spaced. The output of each filter is multiplied by a gain and then added to form a scalar actuator voltage.

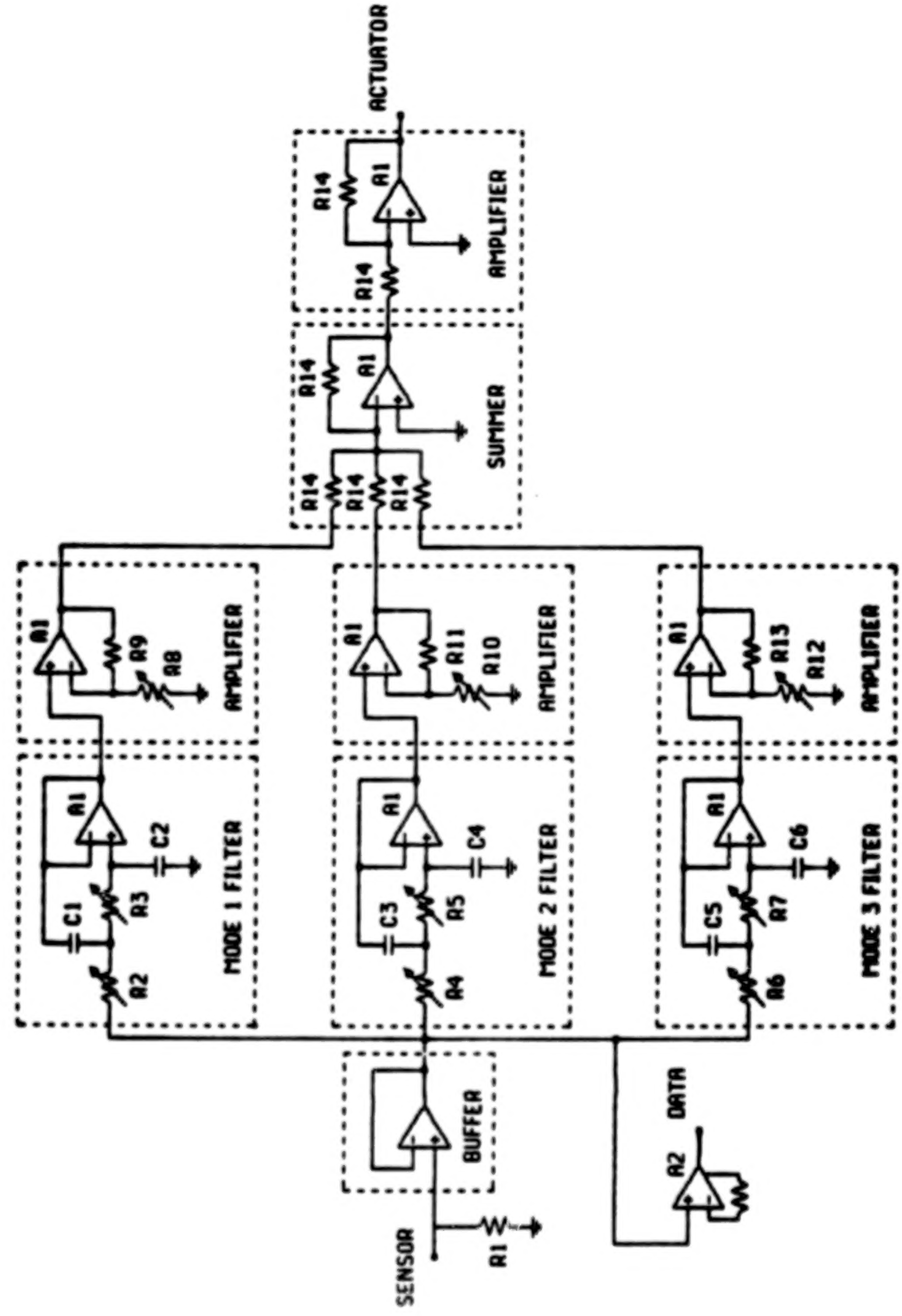
SENSOR
R1
BUFFER
A2
DATA
R2
C1
R3
A1
C2
MODE 1 FILTER
A1
R9
R8
AMPLIFIER
R4
C3
R5
A1
C4
MODE 2 FILTER
A1
R11
R10
AMPLIFIER
R6
C5
R7
A1
C6
MODE 3 FILTER
A1
R13
R12
AMPLIFIER
R14
R14
R14
R14
A1
SUMMER
R14
R14
A1
AMPLIFIER
ACTUATOR

The response amplitude plot is shown for three mode control in the region of modes one and two. The dynamic response is significantly reduced.

JET PROPULSION LABORATORY
POSITIVE POSITION CHIRP TEST
3 MODE CONTROL

MSC/STI-VAMP

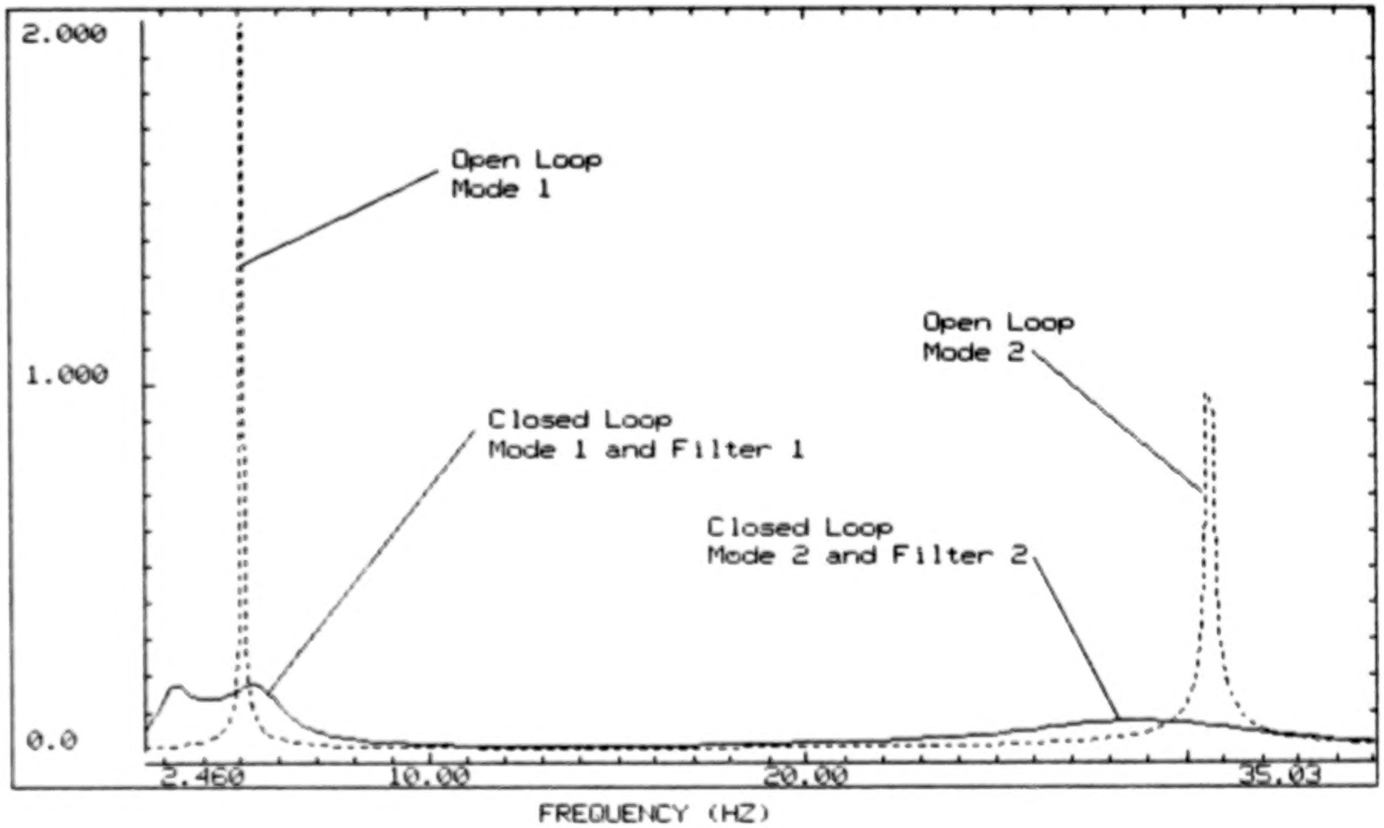

The response amplitude plot for three mode control in the region of modes two and three is shown.

JET PROPULSION LABORATORY
POSITIVE POSITION CHIRP TEST
3 MODE CONTROL

MSC/STI-VAMP

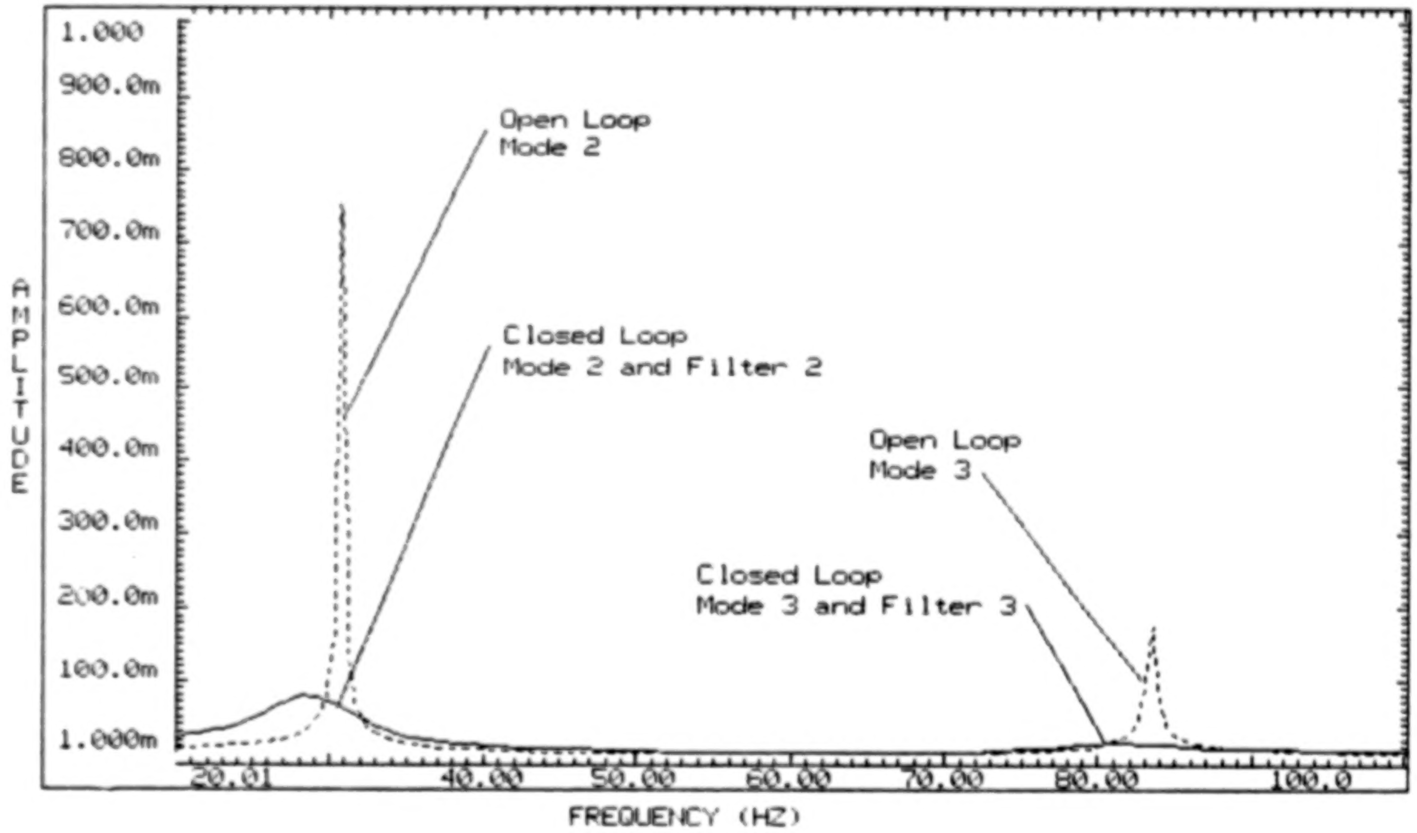

This photograph of an oscilloscope trace shows the free decay of mode one, both open loop and closed loop. The open loop settling time is approximately one minute; the closed loop settling time is approximately one second.

JPL

SISO THREE MODE CONTROL

FREE DECAY -- MODE ONE

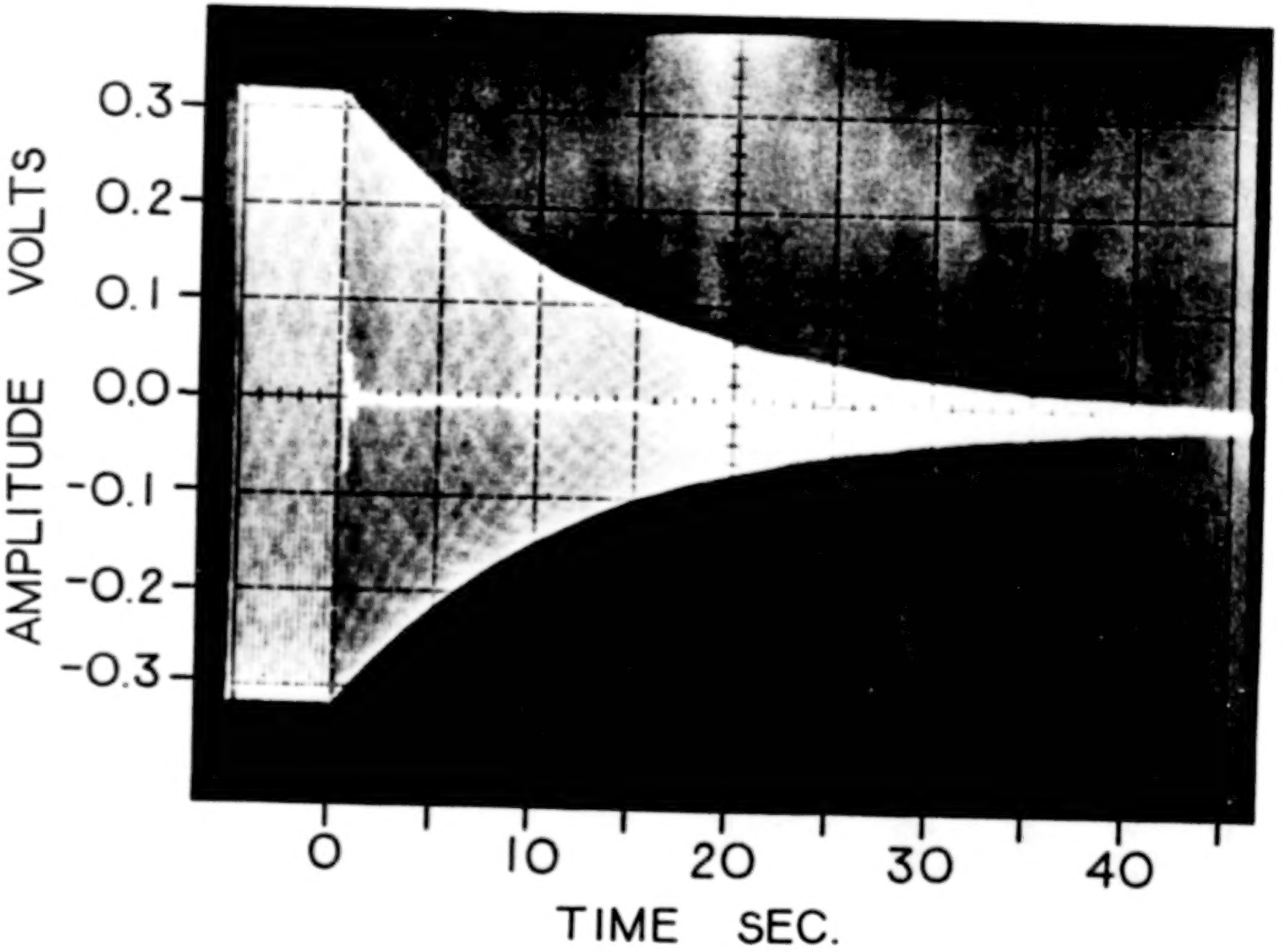

ORIGINAL PAGE IS
OF POOR QUALITY

This oscilloscope photograph shows a blowup of the first part of the preceding free decay comparison. The closed loop settling time is substatially reduced.

JPL

SISO THREE MODE CONTROL

FREE DECAY--MODE ONE

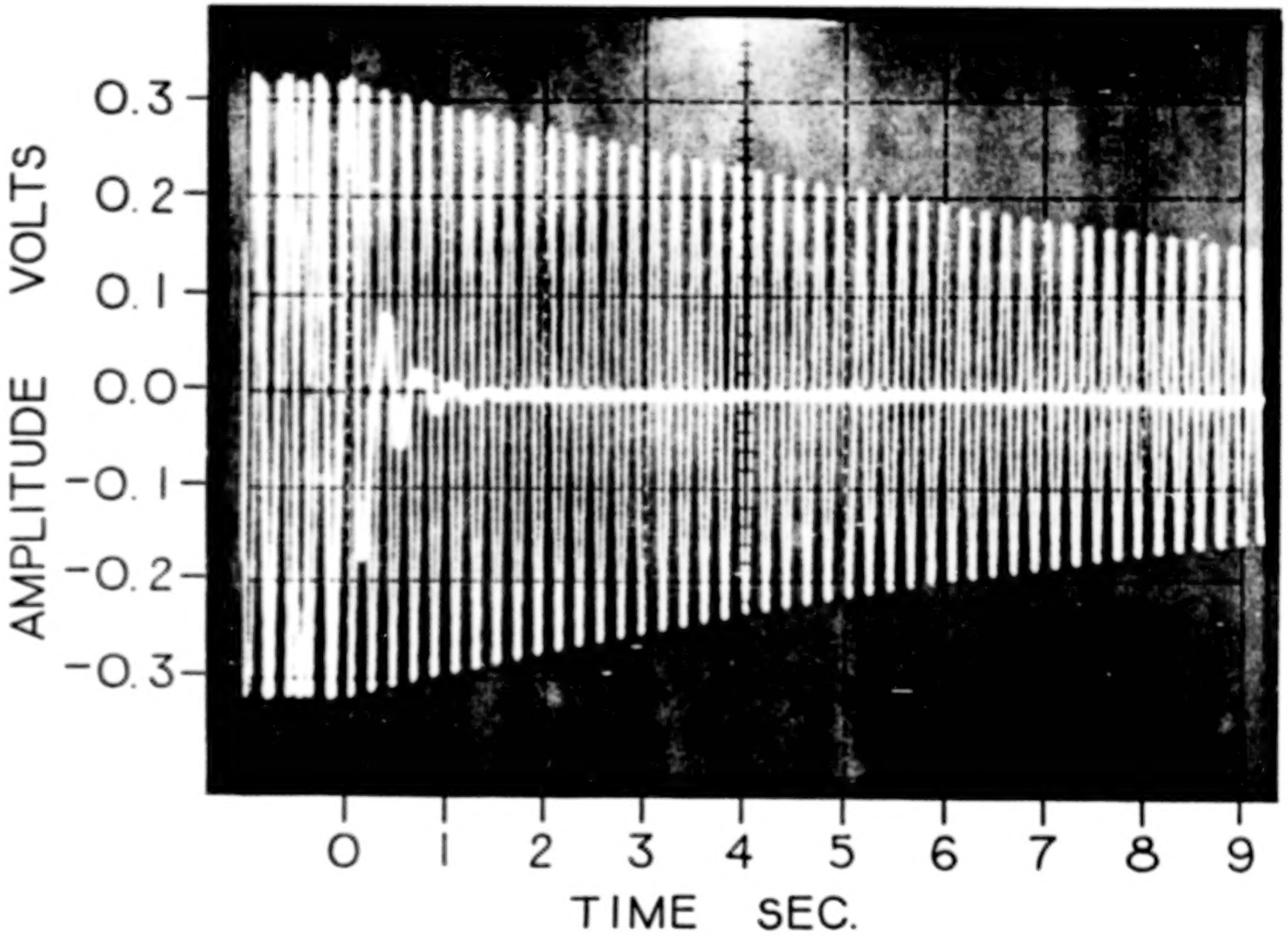

ORIGINAL PAGE IS
OF POOR QUALITY

The three tables show a summary of the open loop vs. closed loop quantities related to dynamic response.

The damping ratio ζ is shown in the first table. The damping ratio is increased by a factor of 67 in mode one, by a factor of 45 in mode two, and by a factor of 15 in mode three.

The quantity of interest for response amplitude is shown in table two. The quantity $\zeta\omega^2$ is increased by a factor of 25 in mode one, by a factor of 44 in mode two, and by a factor of 14 in mode three.

The quantity of interest for settling time $\zeta\omega$ is shown in table three. The quantity $\zeta\omega$ is increased by a factor of 42 in mode one, by a factor of 48 in mode two, and by a factor of 15 in mode three.

Closed Loop Damping Summary

Damping Ratio	ζ_1	ζ_2	ζ_3
Open Loop	0.002	0.002	0.003
Closed Loop	0.134	0.089	0.040

Response Amplitude	$\zeta_1\omega_1^2$	$\zeta_2\omega_2^2$	$\zeta_3\omega_3^2$
Open Loop	1.993	62.87	738.0
Closed Loop	51.68	2,776	10,423

Settling Time	$\zeta_1\omega_1$	$\zeta_2\omega_2$	$\zeta_3\omega_3$
Open Loop	0.063	0.327	1.412
Closed Loop	2.636	15.67	20.39

The Nyquist plot for the three mode control case is shown. Because the control loop is a positive feedback loop, the critical point is (+1,0) instead of the more common location (−1,0). The locus passes under the critical point at low frequency and continues to move farther from the critical point through mode one, mode two, and mode three. The loop begins to roll-off after mode three but the locus stays well away from the critical point.

The peculiar dogleg of the curve at low frequency is due to non-ideal behavior of the piezoelectric ceramic sensors at low frequency.

Because the locus passes below the critical point, the control system is robust with respect to time delays which tend to rotate the Nyquist plot in a clockwise direction. In our case time delays tend to move the locus away from the critical point. The system is also robust to phase lags, which are much more common in structures than phase leads.

JET PROPULSION LABORATORY
POSITIVE POSITION SWIFT TEST
NYQUIST PLOT   LOOP TRANSFER FUNCTION

MSC/STI-VAMP

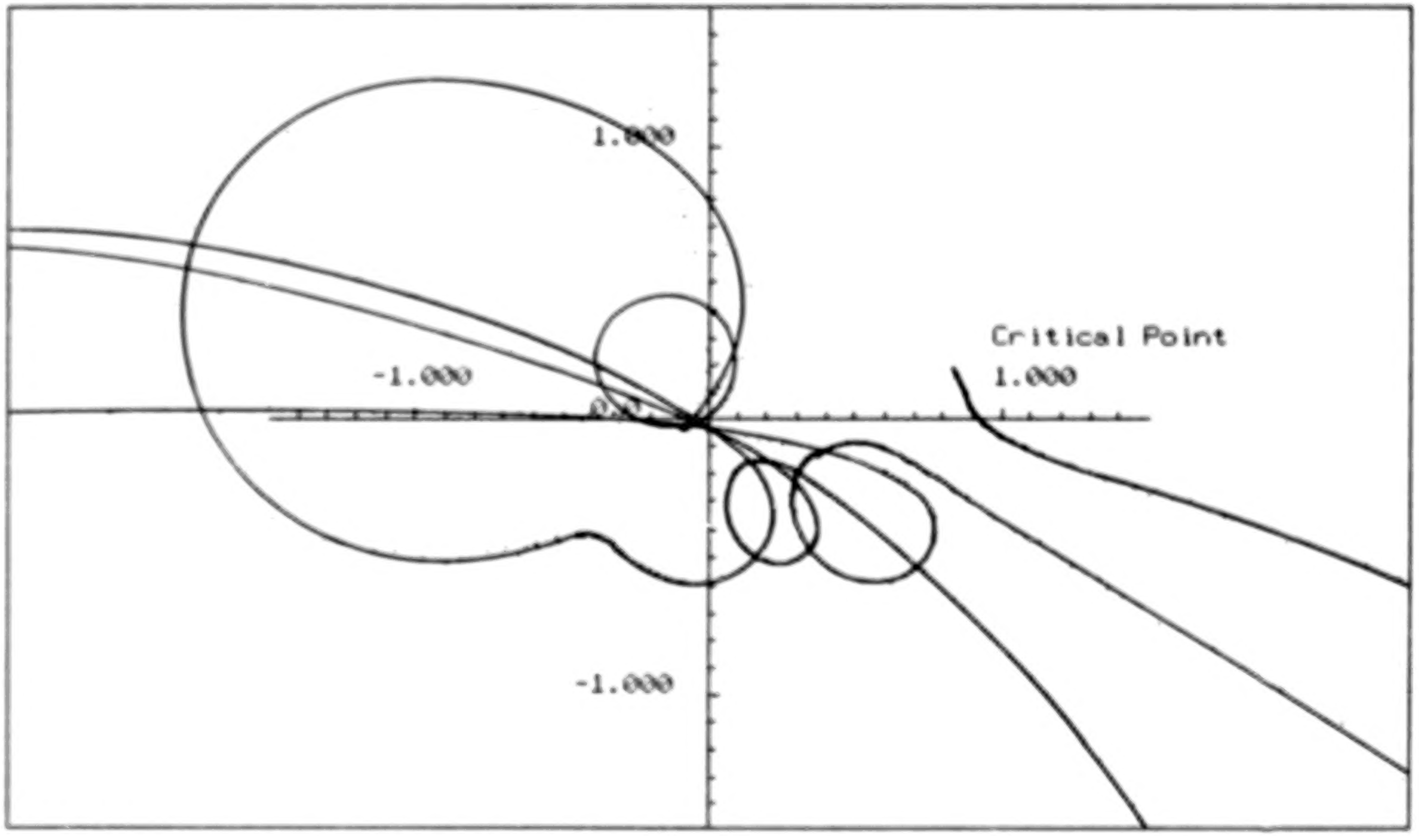

We have demonstrated the feasibility of using piezoelectric ceramics as both sensors and actuators for vibration suppression in a lightweight, flimsy structure. We have acheived multi-mode control using one sensor and actuator pair. The *Positive Position Feedback* control strategy requires only knowledge of the natural frequencies of the structure. Our implementation of *Positive Position Feedback* uses only strain measurements to acheive damping, no velocities or accelerations are needed. All spillover is stabilizing for sufficiently small gains.

CONCLUSIONS

- Demonstrated Feasibility of Using Piezo-Electric Ceramics as Both Sensors and Actuators
- Multi-Mode Control with One Actuator/Sensor Pair
- Control Law Which Requires Only Knowledge of Natural Frequencies of Structure
- Control Law Uses Only Strain Measurements (No Velocities or Accelerations)
- All Spillover is Stabilizing

With *Positive Position Feedback* instability can only occur in the lowest frequency mode or the lowest frequency control filter. Instability can be trapped in the electronics by the use of an "arresting pole." Performance increases with increasing modal density in the sense that one control filter will increase the damping in all nearby modes no matter how densly spaced they are. Since the control loop is a *positive* feedback loop the critical point is $(+1,0)$. The Nyquist locus passes under the critical point so phase lags and time delays tend to move the system away from instability.

CONCLUSIONS (cont.)

- Instability Can Only Occur in the Lowest Frequency Mode or Lowest Frequency Filter
- Instabilities Can be Trapped in the Electronics
- Performance Increases with Increasing Modal Density
- Robust With Respect To Time Delays and Phase Lags

N87
22731
UNCLAS

N87-22731

A Quasi-Analytical Method for Non-iterative Computation of Nonlinear Controls

J. L. Junkins and R. C. Thompson
Texas A&M University

and

J. D. Turner
Cambridge Research Associates

presented to
WORKSHOP ON STRUCTURAL DYNAMICS AND CONTROL
INTERACTION FOR FLEXIBLE STRUCTURES
National Aeronautics and Space Administration
George C. Marshall Space Flight Center
Huntsville, Alabama

April 22-24, 1986

PRECEDING PAGE BLANK NOT FILMED

*Coupling of Spacecraft Structural Modeling with Dynamics/Controls Analysis, Design, and Implementation**

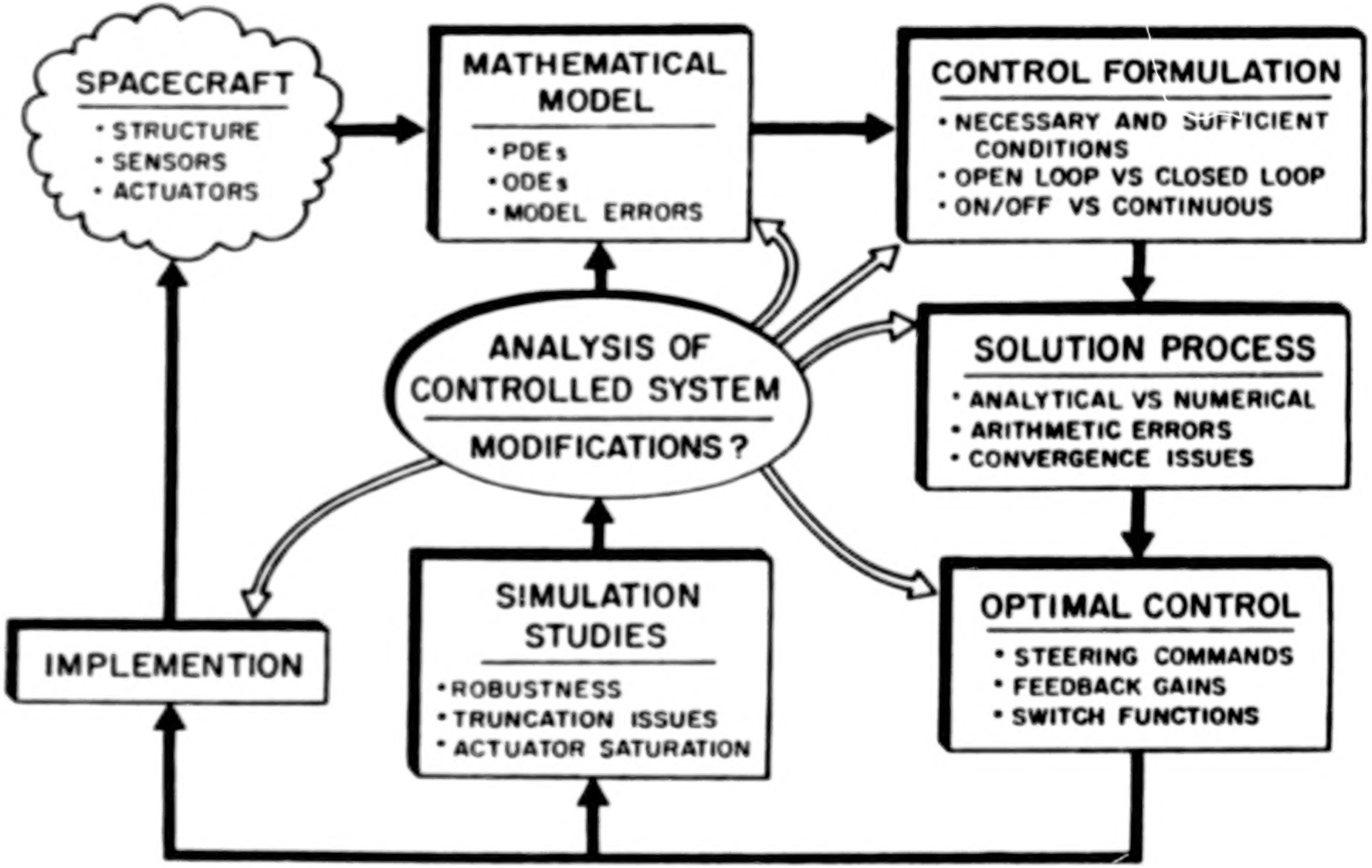
SPACECRAFT
• STRUCTURE
• SENSORS
• ACTUATORS
MATHEMATICAL MODEL
• PDEs
• ODEs
• MODEL ERRORS
CONTROL FORMULATION
• NECESSARY AND SUFFICIENT CONDITIONS
• OPEN LOOP VS CLOSED LOOP
• ON/OFF VS CONTINUOUS
ANALYSIS OF CONTROLLED SYSTEM
MODIFICATIONS?
SOLUTION PROCESS
• ANALYTICAL VS NUMERICAL
• ARITHMETIC ERRORS
• CONVERGENCE ISSUES
SIMULATION STUDIES
• ROBUSTNESS
• TRUNCATION ISSUES
• ACTUATOR SATURATION
OPTIMAL CONTROL
• STEERING COMMANDS
• FEEDBACK GAINS
• SWITCH FUNCTIONS
IMPLEMENTION

---

* the above figure is from our book:
Junkins, J. L. and Turner, J. D. , ***Optimal Spacecraft Rotational Maneuvers***, Elsevier, 1986.

PRELIMINARIES

Consider a dynamical system described by

$$\dot{z} = Fz + Du + \epsilon\, g(z,u,t) \qquad (1)$$

where

z is an $n \times 1$ state vector
u is an $m \times 1$ control vector
F & D are constant matrices
z, u, and the nonlinear terms $g(z,u,t)$ are continuous & differentiable

We seek an optimal control $u^*(t)$ and corresponding optimal trajectory $z^*(t)$ which minimize the quadratic performance measure

$$J = 1/2\,[z^T S z]_{t_f} + 1/2 \int_0^{t_f} (z^T Q z + u^T R u)\,dt \qquad (2)$$

The necessary conditions involve the Hamiltonian $H(z\,,u\,,p\,,t)$

$$H = 1/2\,(z^T Q z + u^T R u) + p^T(Fz + Du + \epsilon g); \qquad (3)$$

These are: $\frac{\partial H}{\partial u} = 0\,, \qquad \frac{\partial H}{\partial p} = \dot{z}\,, \qquad -\frac{\partial H}{\partial z} = \dot{p}$

plus boundary conditions: $z(0) = z_0,\ p(t_f) = Sz(t_f)$ *or* $z(t_f) = z_f.$

Two Point Boundary Value Problem

Pontryagin Necessary Conditions:

$$\dot{z} = Fz + Du + \cdot g \ , \qquad z(0) = z_0$$

$$\dot{p} = -Qz - F^T p - \cdot[\tfrac{\partial g}{\partial z}]^T . \quad p(t_f) = Sz(t_f) \text{, for } z(t_f) \text{ "free"}$$

$0 = Ru + D^T p$, ... *from which the optimal control is* $u^* = -R^{-1} D^T p$.

The state/co-state coupled system can be written as a 2n order system:

$$\dot{x} = A\,x + \cdot h(x,t) \qquad (4)$$

where

$$x^T = [z^T \quad p^T], \quad A = \begin{bmatrix} F & -DR^{-1}D^T \\ -Q & -F^T \end{bmatrix}, \quad h(x,t) = \begin{Bmatrix} g \\ -\frac{\partial g^T}{\partial z} \end{Bmatrix}$$

Due to the nonlinear terms in $h(x,t)$, exact analytical solutions of Eq. (4) are most often impossible. A variety of iterative techniques are available; they are often expensive due to initial ignorance of a "good starting estimate"(of $p(t_o)$ or $p(t_f)$) required for reliable convergence. We seek to avoid iteration through use of a perturbation method & "quasi-analytical" integration. >>>

The Asymptotic Expansion of the Necessary Conditions

We seek a power series solution of the usual form

$$x(t) = x_0(t) + \epsilon x_1(t) + \epsilon^2 x_2(t) + \quad \ldots \quad + \epsilon^k x_k(t) + \ \ldots \qquad (5)$$

Substitution of the power series into the state/co-state system of Eq. (4), and equating like powers of ϵ, leads to the ***sequence*** *of linear systems:*

$$\begin{aligned} \dot{x}_0 &= A\, x_0 && \longrightarrow x_0(t)\,. \\ \dot{x}_1 &= A\, x_1 + g_1(t, x_0(t)) && \longrightarrow x_1(t) \qquad (6) \\ & && \\ \dot{x}_k &= A\, x_k + g_k(t, x_0(t), x_1(t), \ldots, x_{k-1}(t)) && \longrightarrow x_k(t) \end{aligned}$$

with the boundary conditions

$$x_0(0) = \begin{Bmatrix} z(0) \\ \\ p_0(0) \end{Bmatrix}, \ x_0(t_f) = \begin{Bmatrix} z(t_f) \\ \\ p_0(t_f) \end{Bmatrix}; \ \ldots \ ; \ x_k(0) = \begin{Bmatrix} 0 \\ \\ p_k(0) \end{Bmatrix}, \ x_k(t_f) = \begin{Bmatrix} 0 \\ \\ p_k(t_f) \end{Bmatrix}$$

where, at least formally, the sequence of solutions is given by

$$x_k(t) = e^{At}\left[x_k(0) + \int_0^t e^{-A\tau} g_k(\tau, x_0(\tau), x_1(\tau), \ldots, x_{k-1}(\tau))\, d\tau\right], \ k = 1, 2, 3, \ldots \qquad (7)$$

But... how do we make efficient algorithms? Does convergence occur in the "real world"? Can the above be implemented in a way which automates the algebra usually associated with perturbation methods? What about secular terms? Does this approach apply to systems of non-trivial dimensions & "messy" nonlinear terms? We have made some progress in answering these questions.

Van Loan's Identity for Integrating Forced Linear Systems

Consider

$$\dot{x}_k = A\,x_k + g_k, \quad x_k(t) = e^{At}x_k(0) + e^{At}\int_0^t e^{-A\tau}\, g_k(\tau)\,d\tau \qquad ,k = 1, 2, \ldots \quad (8)$$

For the special case that $u(t)$ can be represented as Fourier series, the Fourier series can be rewritten as a matrix exponential

$$g_k(t) = b_{ok} + \sum_{r=1}^{N} b_{rk}\cos(\omega_r t) + a_{rk}\sin(\omega_r t) = G_k\, e^{\Omega t} c \qquad (9)$$

where

b_{ok} , b_{rk} , a_{rk} are 2n x 1 vectors of Fourier coefficients

$G_k = [\, b_o\, b_1\, a_1\, b_2\, a_2 \ldots b_r a_r \ldots b_N a_N\,]_k$, a 2n x (2N + 1) constant matrix

$c = \{\, 1\ 1\ 0\ 1\ 0\ 1\ 0 \ldots\ldots 1\ 0\,\}^T$, a 2N x 1 selection vector

$$\Omega_r = \begin{bmatrix} 0 & -\omega_r \\ \omega_r & 0 \end{bmatrix} \quad , \qquad \omega_r = r(2\pi/(t_f - t_o))$$

$$\Omega = diag\,[\,0\ ,\ \Omega_1\ ,\ \Omega_2\ , \ldots ,\ \Omega_r\ , \ldots ,\ \Omega_N\,]$$

Substituting Eq. (9) into Eq. (8),

$$x_k(t) = e^{At}x_k(0) + [\int_o^t e^{-A\tau}G_k\, e\;\, d\tau\,]c = e^{At}x_k(0) + [\,\psi_k\,]c$$

Van Loan has established the interesting & useful identity which permits computation of the forced response using a matrix exponential (via, for example, Ward's Pade' algorithm):

$$e^{\begin{bmatrix} A & G_k \\ 0 & \Omega \end{bmatrix}t} = \left[\begin{array}{c|c} e^{At} & \psi_k \\ \hline 0 & e^{\Omega t} \end{array}\right] \qquad (10)$$

For large N, we can use superposition & keep the order of the matrix exponentials small .... thus the response to a relatively arbitrary $g_k(t)$ can be calculated via matrix exponentials.

Control Rate Smoothing & State Vector Augmentation

We choose to minimize

$$J = 1/2\{\, z(t_f)^T S z(t_f) + u(t_f)^T S_0 u(t_f) + \dot{u}(t_f)^T S_1 \dot{u}(t_f) \,\}$$

$$+ 1/2 \int_0^{t_f} \{ z^T Q z + u^T R_0 u + \dot{u}^T R_1 \dot{u} + \ddot{u}^T R_2 \ddot{u} \}\, dt$$

Subject to: $\dot{z} = Az + Du$. *This can be converted to standard form via the definitions:*

$$\tilde{z} = \begin{Bmatrix} z \\ u \\ \dot{u} \end{Bmatrix}, \quad \tilde{A} = \begin{bmatrix} A & D & 0 \\ 0 & 0 & I \\ 0 & 0 & 0 \end{bmatrix}, \quad \tilde{D} = \begin{bmatrix} 0 \\ 0 \\ I \end{bmatrix}, \quad \begin{matrix} \tilde{S} = \text{block diag}[S, S_0, S_1] \\ \tilde{Q} = \text{block diag}[Q, R_0, R_1] \\ \tilde{R} = R_2\ ,\ \tilde{u} = \ddot{u} \end{matrix}$$

So we can equivalently minimize

$$J = 1/2\ \tilde{z}(t_f)^T \tilde{S} \tilde{z}(t_f) + 1/2 \int_0^{t_f} \{ \tilde{z}^T \tilde{Q} \tilde{z} + \tilde{u}^T \tilde{R} \tilde{u} \}\, dt$$

Subject to: $\dot{\tilde{z}} = \tilde{A}\tilde{z} + \tilde{D}\tilde{u}$. ***The necessary conditions have the identical form as those developed in the foregoing. Penalizing the control derivatives has been found most constructive in frequency-shaping the torque profiles to decrease excitation of the poorly modeled higher frequency modes.***

Case 1 Optimal Detumble/Attitude Aquisition

STATE DYNAMICS

Euler (quaternion) parameters

$$\begin{Bmatrix} \dot{\beta}_0 \\ \dot{\beta}_1 \\ \dot{\beta}_2 \\ \dot{\beta}_3 \end{Bmatrix} = \frac{1}{2} \begin{bmatrix} 0 & -\omega_1 & -\omega_2 & -\omega_3 \\ \omega_1 & 0 & \omega_3 & -\omega_2 \\ \omega_2 & -\omega_3 & 0 & \omega_1 \\ \omega_3 & \omega_2 & -\omega_1 & 0 \end{bmatrix} \begin{Bmatrix} \beta_0 \\ \beta_1 \\ \beta_2 \\ \beta_3 \end{Bmatrix} \qquad \Bigg\| \quad \text{or} \quad \dot{\beta} = \frac{1}{2}\,(\omega)\,\beta$$

Euler's Equations

$$\begin{Bmatrix} \dot{\omega}_1 \\ \dot{\omega}_2 \\ \dot{\omega}_3 \end{Bmatrix} = \begin{Bmatrix} -I_1\, \omega_2\omega_3 + u_1/I_1 \\ -I_2\, \omega_3\omega_1 + u_2/I_2 \\ -I_3\, \omega_1\omega_2 + u_3/I_3 \end{Bmatrix} \quad \begin{matrix} , & I_1 = (I_3-I_2)/I_1 \\ , & I_2 = (I_1-I_3)/I_2 \\ , & I_3 = (I_2-I_1)/I_3 \end{matrix} \qquad \Bigg\| \quad \text{or} \quad \dot{\omega} = f(\omega,u)$$

BOUNDARY CONDITIONS

$(t_f = 2 \text{ sec})$

$$\beta(0) = \begin{Bmatrix} .9699665 \\ .1318887 \\ .0238626 \\ .2029798 \end{Bmatrix} , \quad \omega(0) = \begin{Bmatrix} .4 \text{ r/s} \\ .2 \\ 1.0 \end{Bmatrix} \quad \beta(t_f) = \begin{Bmatrix} 1 \\ 0 \\ 0 \\ 0 \end{Bmatrix} , \quad \omega(t_f) = \begin{Bmatrix} 0 \\ 0 \\ 0 \end{Bmatrix}$$

Case 1 Numerical Results for the TPBVP Solution

FINAL STATE ERRORS

	LINEAR SOLUTION		FIRST ORDER		SECOND ORDER	
$\Delta\beta_0$	.01999	$\approx 10^\circ$	.00091	$\approx .5^\circ$	7×10^{-7}	$\approx .05^\circ$
$\Delta\beta_1$	−.08232		−.00866		.00058	
$\Delta\beta_2$	.18033		−.00944		.00094	
$\Delta\beta_3$	.01734		−.00412		−.00034	
$\Delta\omega_1$	.01914		−.01525		.00109	
$\Delta\omega_2$	.43150		−.00292		.00295	
$\Delta\omega_3$	.00461		−.00071		.00015	

Case 1 Optimal Detumble/Attitude Acquisition Maneuver

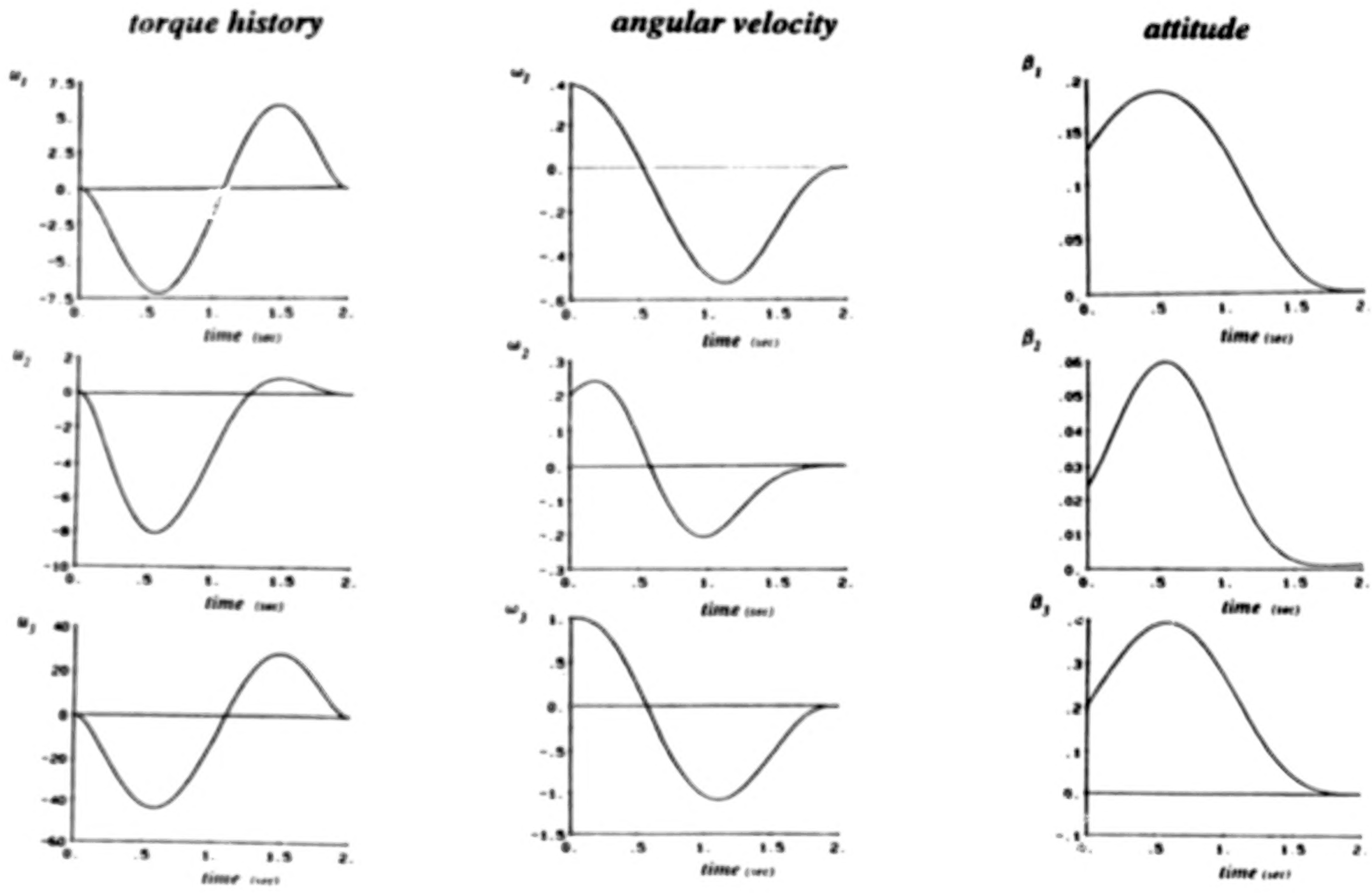

The Draper/RPL Slewing Experimental Configuration

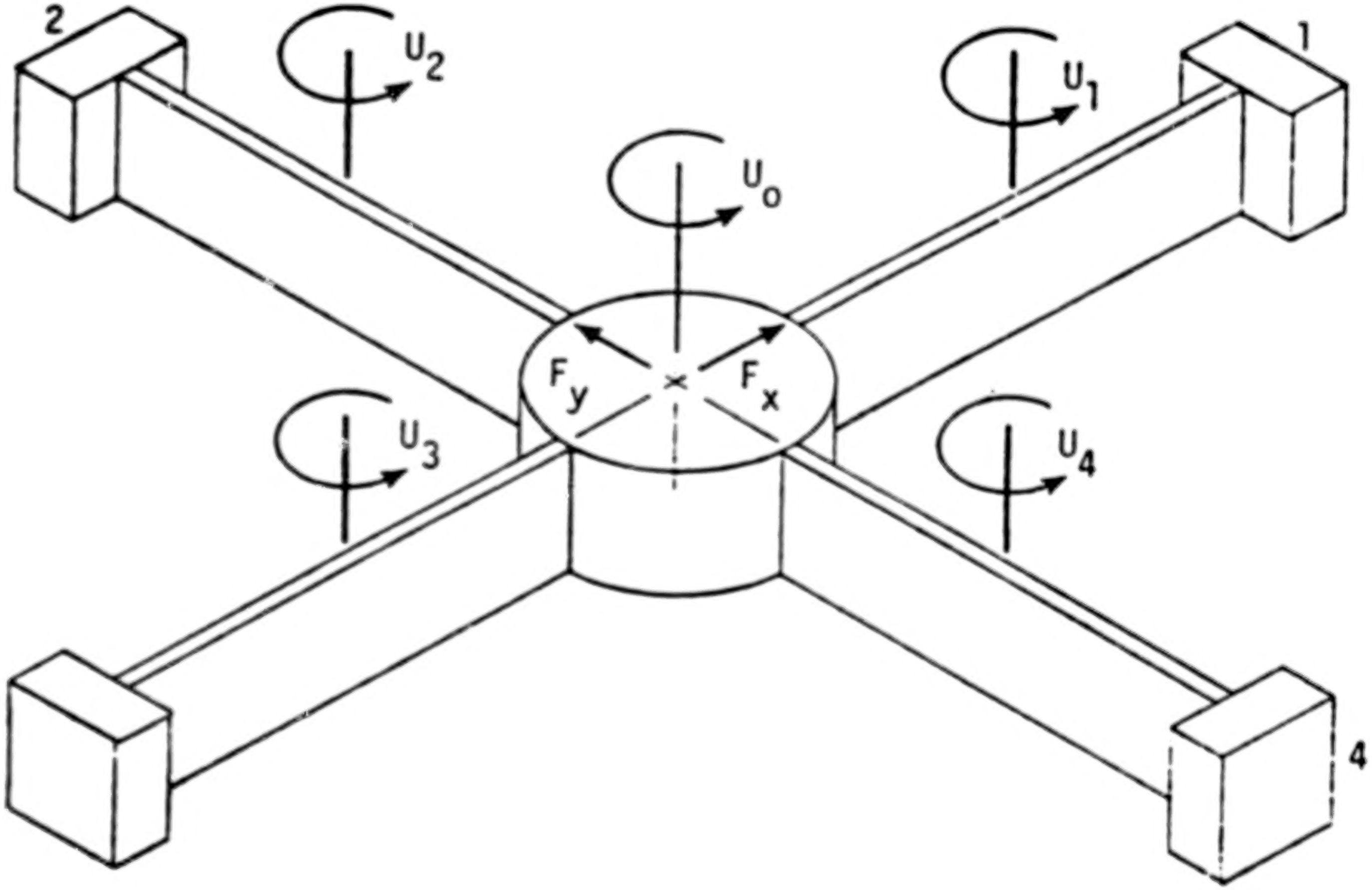
2
U_2
U_1
1
U_0
F_y
F_x
U_3
U_4
3
4

Draper/RPL Configuration: First Eleven in-plane Vibration Modes

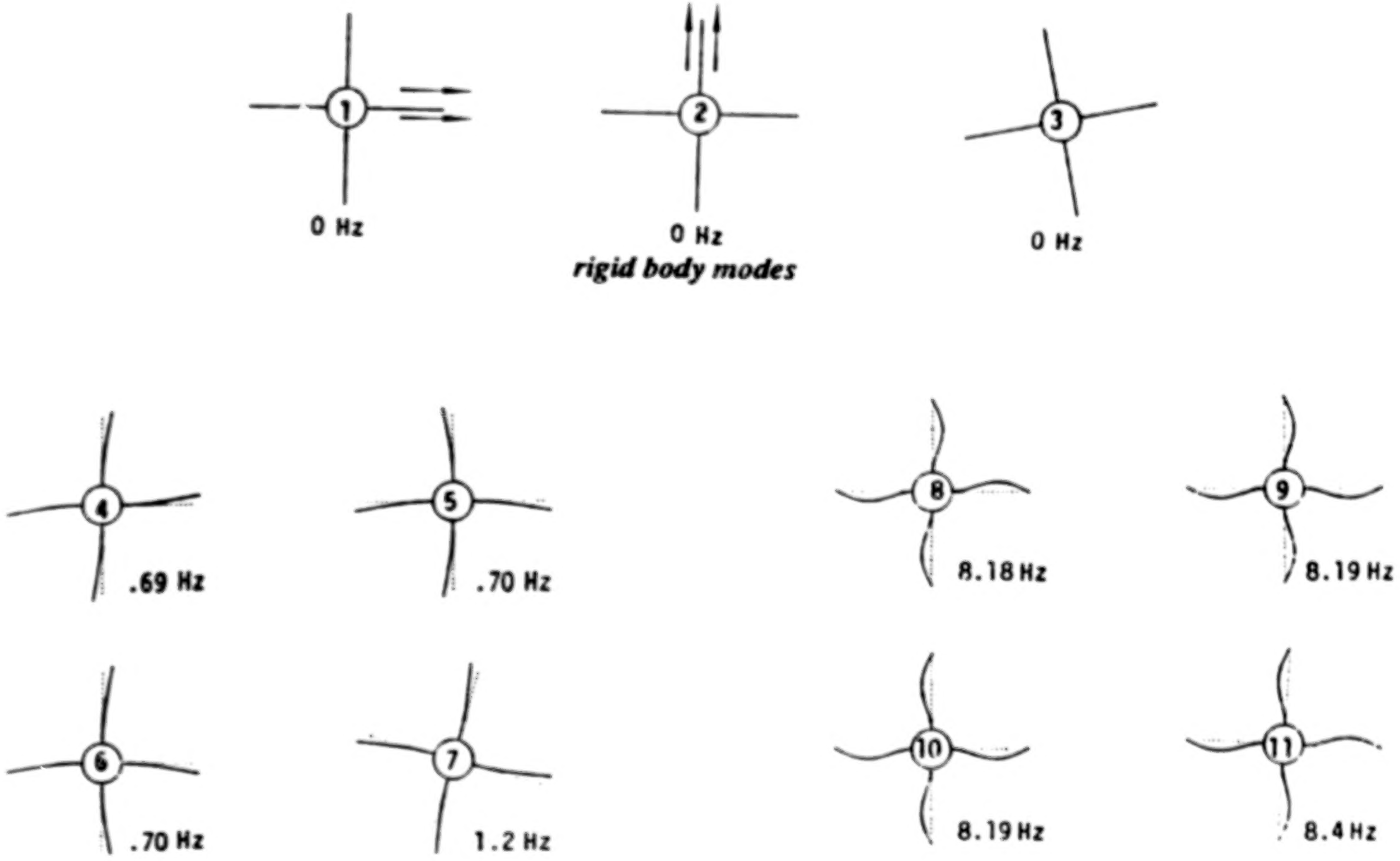
1
0 Hz
2
0 Hz
3
0 Hz
4
.69 Hz
5
.70 Hz
6
.70 Hz
7
1.2 Hz
8
8.18 Hz
9
8.19 Hz
10
8.19 Hz
11
8.4 Hz

rigid body modes

first cantilever modes

second cantilever modes

Case 2 Numerical Results for the TPBVP Solution (small angle flexible body maneuver)

FINAL STATE ERRORS

	LINEAR SOLUTION	FIRST ORDER	SECOND ORDER
ϕ	-0.828E-5	0.276E-4	0.184E-5
θ	0.104E-2	0.667E-5	-0.878E-6
ψ	0.668E-3	-0.270E-4	0.130E-5
ω_1	-0.450E-3	0.150E-3	0.342E-5
ω_2	0.317E-2	0.293E-4	-0.474E-5
ω_3	0.597E-3	-0.396E-5	0.135E-6
η_1 (in plane)	-0.960E-3	-0.120E-5	-0.217E-8
σ_1 (out-of-plane)	0.317E-2	0.293E-4	-0.474E-5

Case 2 Optimal Maneuver with Vibration Suppression/Arrest

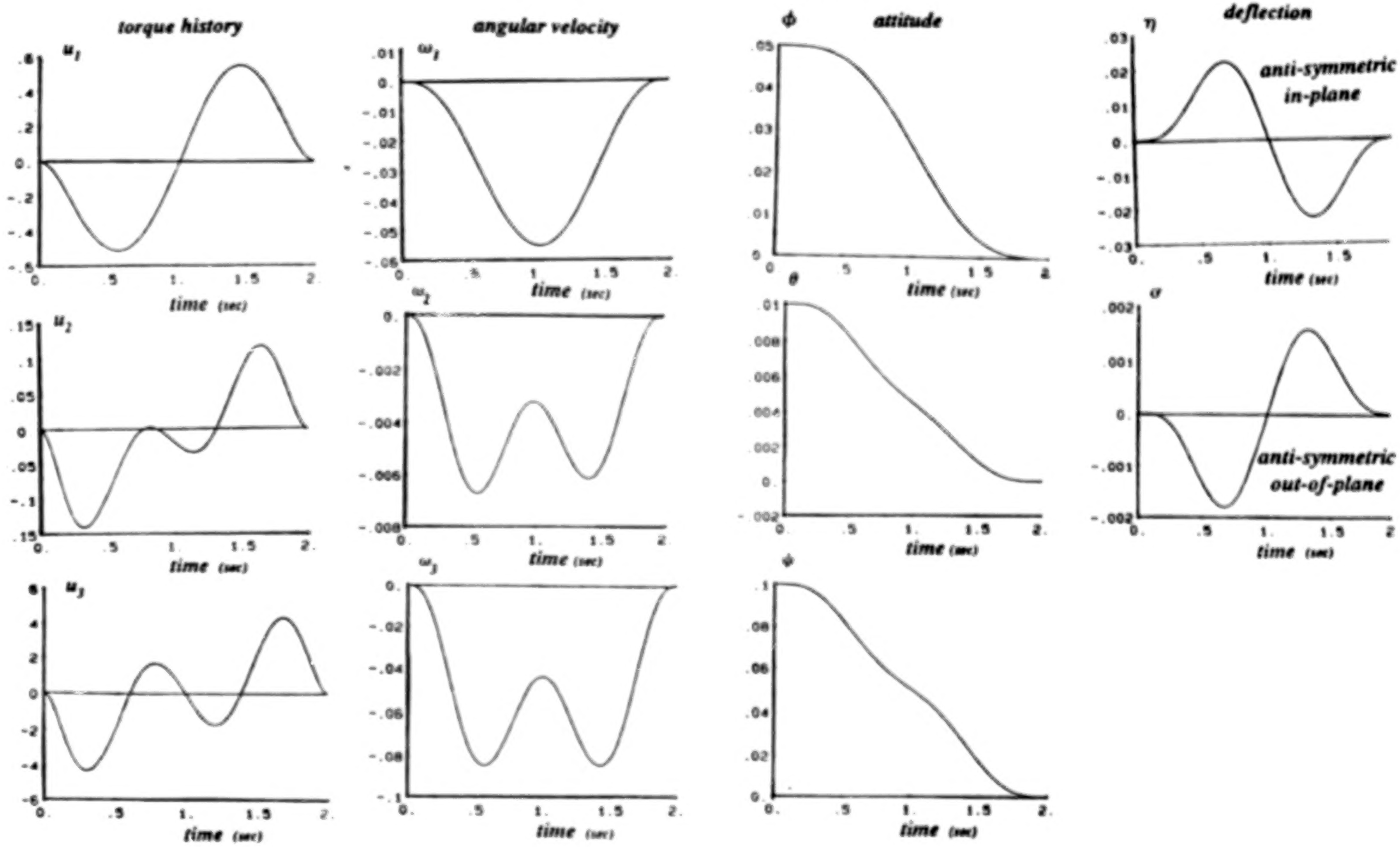

Concluding Remarks

A novel optimal control solution process has been developed for a general class of nonlinear dynamical systems

The method combines control theory, perturbation methods, and Van Loan's recent matrix exponential results

All controlled response integrations are accomplished via matrix exponentials (using Ward's Pade algorithm) and recursions developed herein

A variety of applications support the practical utility of this method; nonlinear rigid body optimal maneuvers are routinely solved; flexible body dynamical systems of order >40 have been solved

The method fails occasionally due to poor convergence of the perturbation expansion or numerical difficulties associated with computing the matrix exponential

The method is attractive because it appears to be a good candidate for semi-automation; no initial guess is required, and it usually converges at 2nd or 3rd order in minutes of machine time

REFERENCES

1. Junkins, J.L., "Comment on Optimal Feedback Slewing of Flexible Spacecraft," AIAA 82-4131, Journal of Guidance and Control, Vol. 5, No. 3, May-June, 1982, p. 318.

2. Turner, J.D., Chun,H.M. and Juang, Jer-Nan, "Optimal Slewing Maneuvers for Flexible Spacecraft Using a Closed Form Solution for the Linear Tracking Problems," Paper No. 83-374, presented at the AAS/AIAA Astrodynamics Conference, Lake Placid, New York, August 22-25, 1983.

3. Nayfeh, Ali Hasan, and Mook, Dean T., Nonlinear Oscillations, John Wiley and Sons, New York, 1979.

4. Van Loan, C.F., "Computing Integrals Involving the Matrix Exponential," IEEE Transactions on Auto Control, Vol. AC-23, No. 3, June, 1978, pp. 395-404.

5. Ward, R.C., "Numerical Computation of the Matrix Exponential with Accuracy Estimate," SIAM Journal of Numerical Analysis, Vol. 14, No. 4, September, 1977, pp. 600-610.

6. Kirk, Donald E., Optimal Control Theory - An Introduction, Prentice Hall, Inc., Englewood Cliffs, NJ, 1970.

7. Thompson, R.C., A Perturbation Approach to Control of Rotational/Translational Maneuvers of Flexible Space Vehicles, M.S. Thesis, Engineering Mechanics, VPI&SU Blacksburg, VA, 1985.

8. Junkins, J.L. and Thompson, R.C., "An Asymptotic Perturbation Method for Nonlinear Optimal Control Problems," Paper No. AAS 85-364, presented at the AAS/AIAA Astrodynamics Specialist Conference, Vail, Colorado, August, 12-15, 1985.

9. Junkins, J.L. and Turner, J.D., Optimal Spacecraft Rotational Maneuvers, Elsevier, Amsterdam, 1986.

DECENTRALIZED CONTROL
OF
LARGE SPACE STRUCTURES
VIA THE GHR

DOUG LINDNER
VA TECH

WHY DECENTRALIZED CONTROL?

- INFORMATION EXCHANGE IS:
  - NOT POSSIBLE
    - * DOCKING MANEUVER
  - NOT DESIRABLE
    - * LIMITED BUS CAPACITY
- ACTUATION IS INHERENTLY DECENTRALIZED
  - * PASSIVE DAMPING
- COMPUTATIONAL POWER IS LIMITED

⇒ MULTIMODELING

= DECENTRALIZED CONTROL

+ REDUCED ORDER MODELING

THE DUAL GHR

$$\begin{tikzcd} \begin{array}{l} \dot{x} = Ax + bu \\ y = cx \end{array} \arrow[d, bend right, "z = Tx"'] \\ \begin{array}{l} \dot{z} = Fz + Gu \\ y = Hz \end{array} \end{tikzcd}$$

$(F\ G, H) =$

$$\left(\begin{bmatrix} F_1 & H_2 & & \\ G_2 & F_2 & \ddots & \\ & \ddots & \ddots & H_r \\ & & G_r & F_r \end{bmatrix}, \begin{bmatrix} G_1 \\ \\ \\ \\ \end{bmatrix}, [H_1 \qquad] \right)$$

where

$$F_k = \begin{bmatrix} a_{k1} & 1 & & \\ \vdots & & \ddots & \\ \vdots & & & 1 \\ a_{k\sigma_k} & & & \end{bmatrix},$$

$$G_k = \begin{bmatrix} \\ \\ \gamma_k \end{bmatrix}, \quad H_k = \begin{bmatrix} \\ \\ \epsilon_k \gamma_k \end{bmatrix}.$$

Ex

$$\begin{bmatrix} a_1 & a_2 & & \\ a_2 & a_3 & -a_4 & \\ & a_4 & a_5 & a_6 \\ & & a_6 & a_7 \end{bmatrix}, \begin{bmatrix} 1 \\ 0 \\ 0 \\ 0 \end{bmatrix}$$

$$\begin{bmatrix} 1 & 0 & 0 & 0 \end{bmatrix}$$

PROPERTIES:

- IDENTIFIES THE INPUT-OUTPUT STRUCTURE OF (A, b, c)

ZERO POLYNOMIAL =

$$\det\left(sI - \begin{bmatrix} F_2 & H_3 & \ddots & \\ G_3 & F_3 & \ddots & H_r \\ & \ddots & G_r & F_r \end{bmatrix}\right)$$

- THERE EXIST RECURRIVE FORMULAS

  FOR THE POLE AND ZERO POLYNOMIALS

THE DUAL GHR DOES

1. DECOMPOSITIONS
   - STRONG COUPLING
   - DECENTRALIZED CONTROL

2. REDUCED ORDER MODELING
   - ESSENTIALLY POLE-ZERO CANCELLATION

Ex

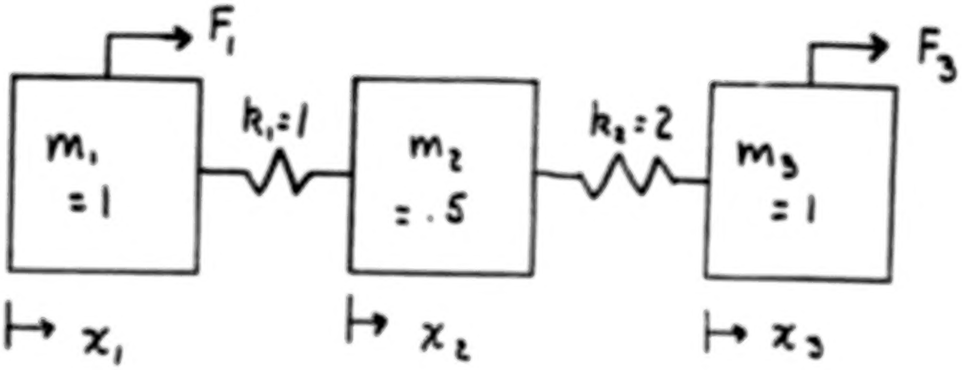

$$\dot{x} = \begin{bmatrix} 0 & 1 & 0 & 0 & 0 & 0 \\ -k_1/m_1 & 0 & k_1/m_1 & 0 & 0 & 0 \\ 0 & 0 & 0 & 1 & 0 & 0 \\ k_1/m_2 & 0 & -\frac{k_1+k_2}{m_2} & 0 & k_2/m_2 & 0 \\ 0 & 0 & 0 & 0 & 0 & 1 \\ 0 & 0 & k_2/m_3 & 0 & -k_2/m_3 & 0 \end{bmatrix} x + \begin{bmatrix} 0 & 0 \\ \frac{1}{m_1} & 0 \\ 0 & 0 \\ 0 & 0 \\ 0 & 0 \\ 0 & \frac{1}{m_3} \end{bmatrix} \begin{bmatrix} F_1 \\ F_3 \end{bmatrix}$$

$$\begin{bmatrix} y_1 \\ y_2 \end{bmatrix} = \begin{bmatrix} 0 & 1 & 0 & 0 & 0 & 0 \\ 0 & 0 & 0 & 0 & 0 & 1 \end{bmatrix} x$$

$$F_1 = m_1 \ell_1 y_1 = m_1 \ell_1 \dot{x}_1$$

$$F_3 = m_3 \ell_3 y_2 = m_3 \ell_3 \dot{x}_3$$

DUAL GHR WITH RESPECT TO (F_1, y_1)

$$\dot{z} = \begin{bmatrix} 0 & -k_1/m_1 & 0 & 0 & 0 & 0 \\ 1 & 0 & -1 & 0 & 0 & 0 \\ 0 & k_1/m_2 & 0 & -k_2/m_2 & 0 & 0 \\ 0 & 0 & 1 & 0 & -1 & 0 \\ 0 & 0 & 0 & k_2/m_3 & 0 & 0 \\ 0 & 0 & 0 & 0 & 1 & 0 \end{bmatrix} z + \begin{bmatrix} \frac{1}{m_1} & 0 \\ 0 & 0 \\ 0 & 0 \\ 0 & 0 \\ 0 & \frac{1}{m_3} \\ 0 & 0 \end{bmatrix} \begin{bmatrix} F_1 \\ F_2 \end{bmatrix}$$

$$y = \begin{bmatrix} 1 & 0 & 0 & 0 & 0 & 0 \\ 0 & 0 & 0 & 0 & 1 & 0 \end{bmatrix} z_1$$

$$z^T = [\, x_2 \;\; x_1 + x_3 \;\; x_4 \;\; x_3 + x_5 \;\; x_6 \;\; x_5 \,]$$

DELETE $x_5 = z_6$

FORM CLOSED LOOP SYSTEM

WITH $F_3 = m_3 \ell_3 z_5$

$$\dot{z}_r = \left[\begin{array}{c:cccc} 0 & -k_1/m_1 & 0 & 0 & 0 \\ \hdashline 1 & 0 & -1 & 0 & 0 \\ 0 & k_1/m_2 & 0 & -k_2/m_2 & 0 \\ 0 & 0 & 1 & 0 & -1 \\ 0 & 0 & 0 & k_2/m_3 & \ell_2 \end{array}\right] z_r + \begin{bmatrix} \frac{1}{m_1} \\ 0 \\ 0 \\ 0 \\ 0 \end{bmatrix} F_1$$

$$y_1 = [\,1 \quad 0 \quad 0 \quad 0 \quad 0\,]\, z_r$$

$$\frac{\dot{X}_1(s)}{F_1(s)} = \frac{Z(s;\ell_2)}{p(s;\ell_2)} = P(s;\ell_2)$$

$$= \frac{z_1(s) + \ell_2 z_2(s)}{p_1(s) + \ell_2 p_2(s)} \quad \text{BY GHR}$$

NOTE:

$$\left.\frac{\dot{X}_1(s)}{F_1(s)}\right|_{\ell_2=0} = \frac{z_1(s)}{p_1(s)} = P(s;0)$$

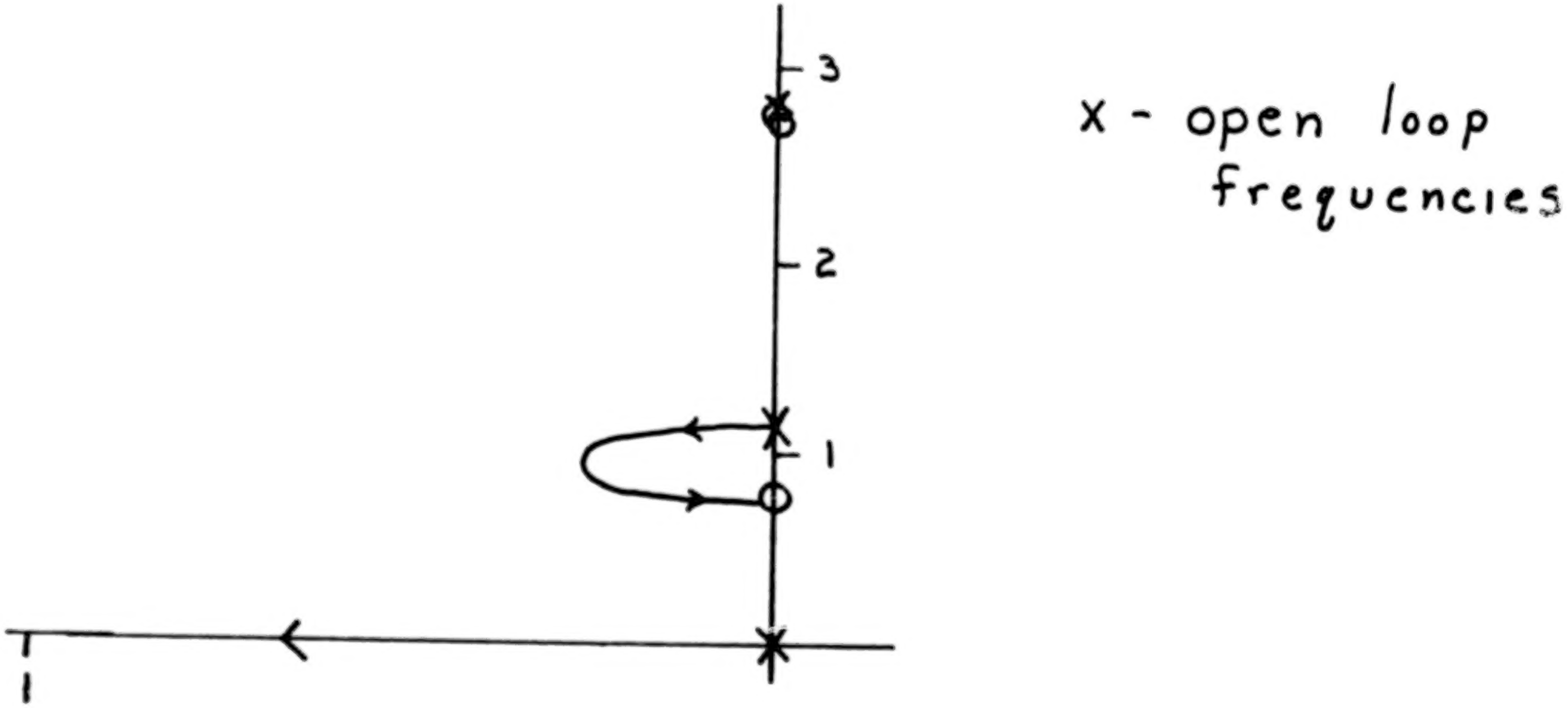
3
2
1
1
x - open loop frequencies

Root Locus wrt ℓ_1 ; $\ell_2 = 0$

$$1 + \ell_1 P(s;0) = 0$$

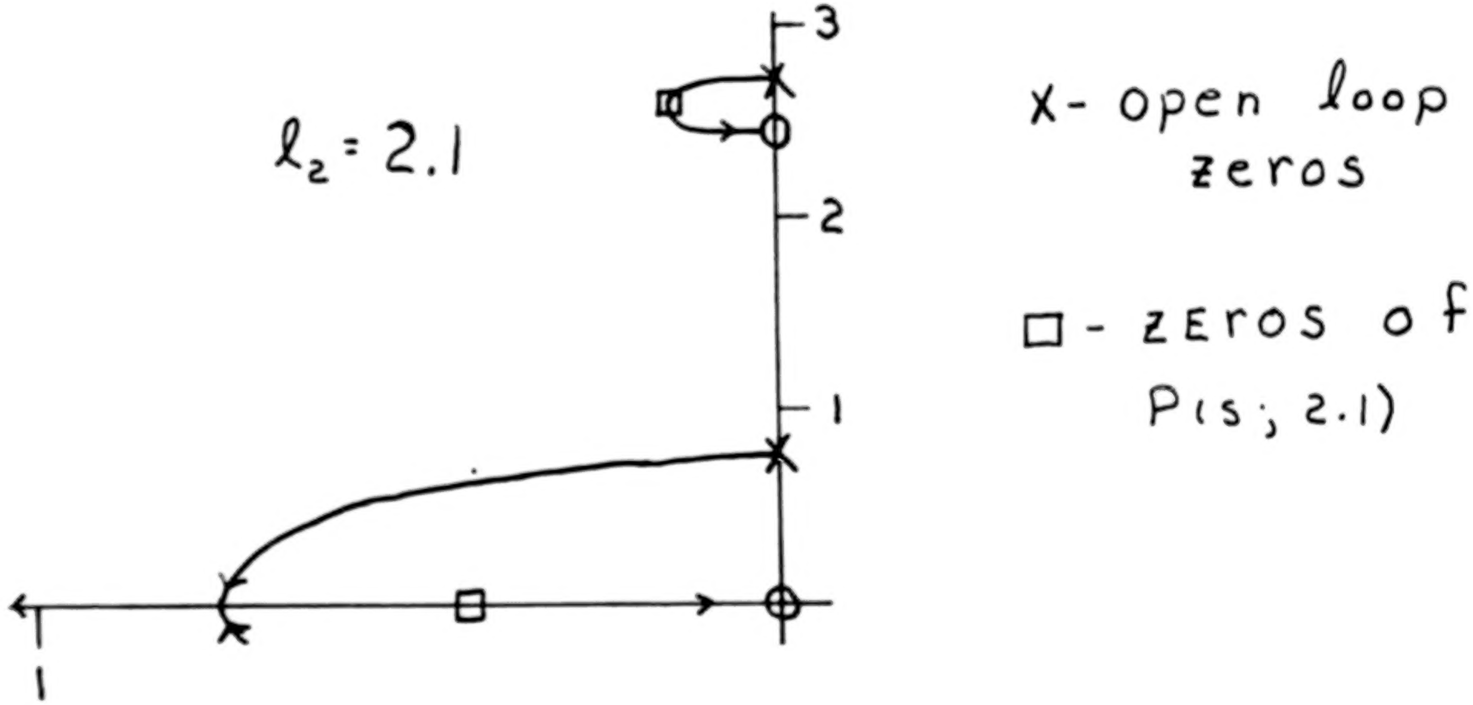

$\ell_2 = 2.1$
3
2
1
1
X - open loop zeros
□ - zeros of $P(s; 2.1)$

ROOT LOCUS OF $z_1(s) + \ell_2 z_2(s) = 0$

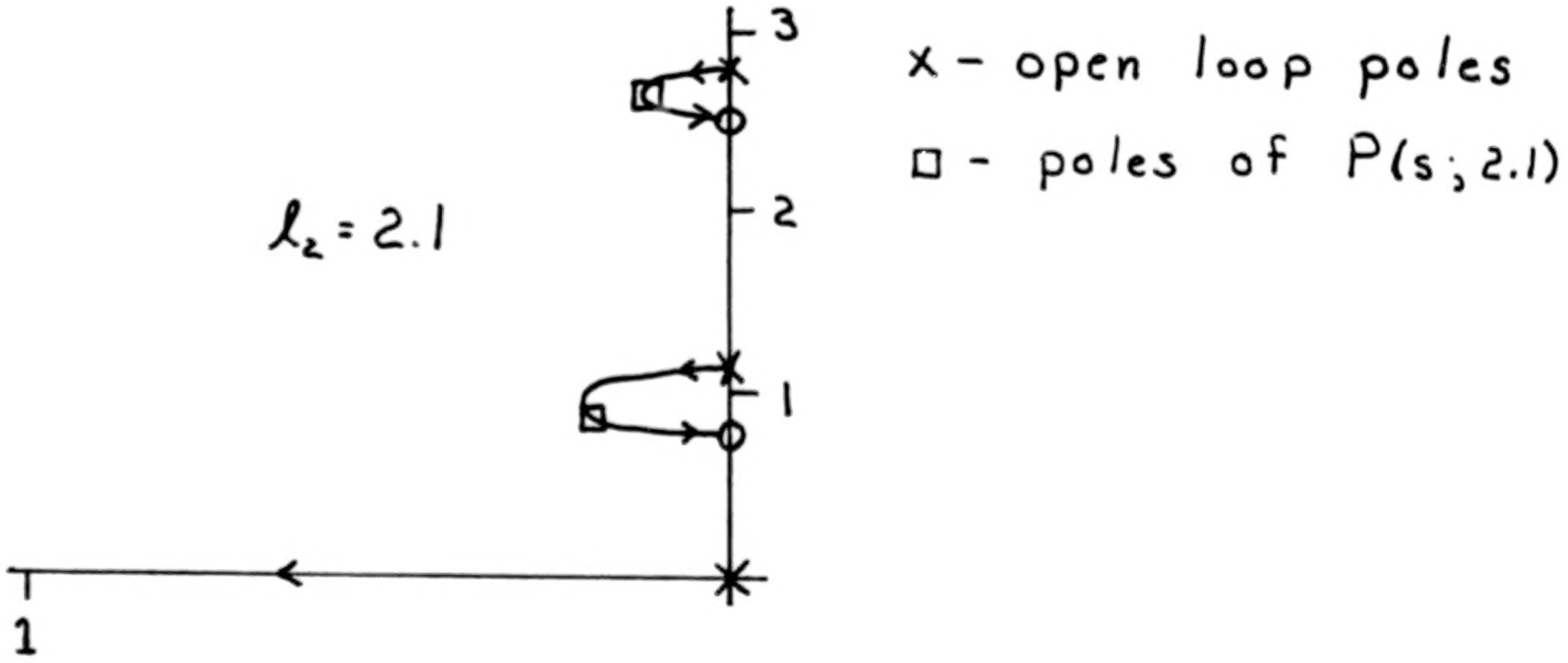
$\ell_2 = 2.1$
3
2
1
1
X - open loop poles
□ - poles of $P(s;2.1)$

ROOT LOCUS OF $p_1(s) + \ell_2 p_2(s) = 0$

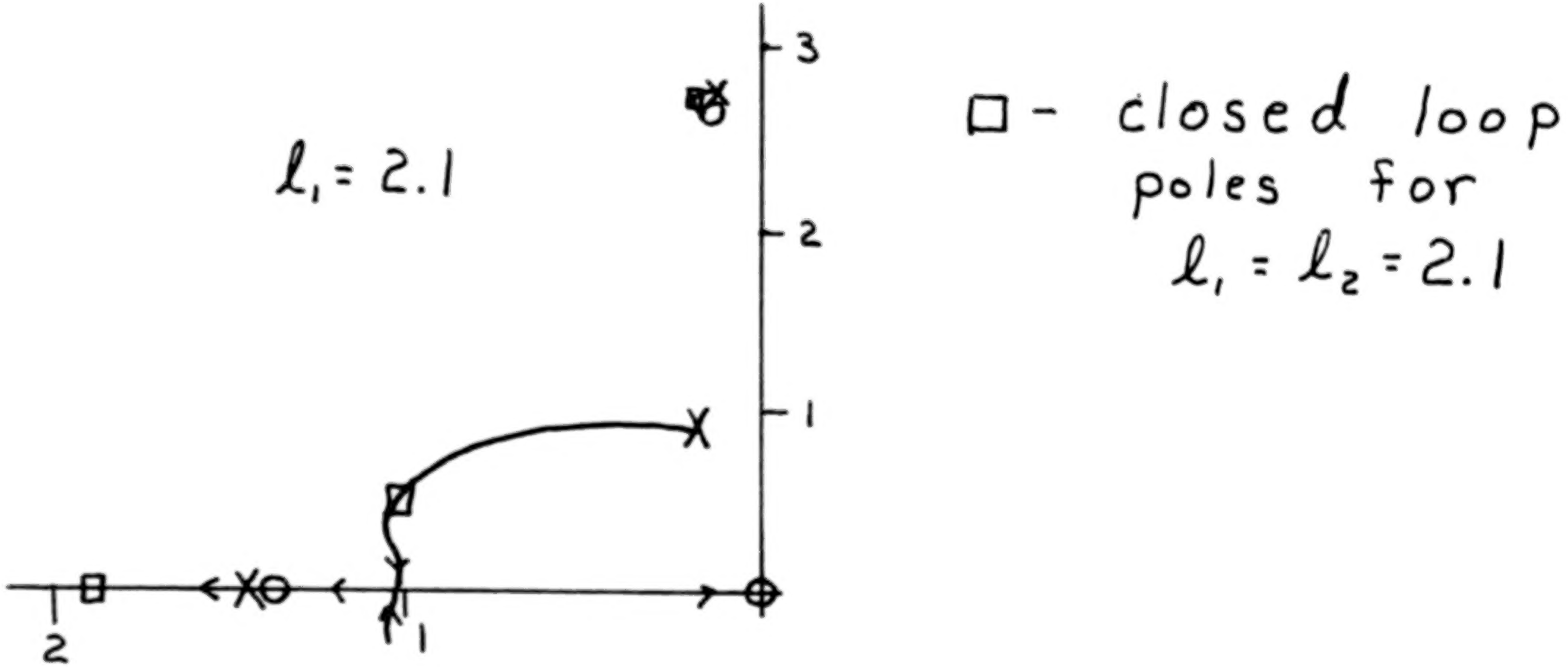

ROOT LOCUS FOR $1 + l_1 P(s; l_2 = 2.1) = 0$

THE DUAL GHR

A TOOL FOR

MULTIMODELING

N87
22732
UNCLAS

N87-22732

CONTROL OF FLEXIBLE STRUCTURES
AND THE
RESEARCH COMMUNITY

BY

CLAUDE R. KECKLER
SPACECRAFT CONTROL BRANCH

AND

JON S. PYLE
COFS II PROJECT MANAGER

NASA LANGLEY RESEARCH CENTER
HAMPTON, VIRGINIA

PRESENTED AT

WORKSHOP ON STRUCTURAL DYNAMICS AND CONTROL
INTERACTION OF FLEXIBLE STRUCTURES

APRIL 22-24, 1986
MARSHALL SPACE FLIGHT CENTER
HUNTSVILLE, ALABAMA

PRECEDING PAGE BLANK NOT FILMED

INTRODUCTION

A major new NASA activity has been initiated to develop the technologies required for understanding the control and structures interaction effects for large, flexible spacecraft structures. This activity, called the Control of Flexible Structures (COFS) program has been separated into three projects: COFS I, the development of ground and flight test hardware for validating the controls and structures interaction effects on a beam structure mounted in the Space Shuttle bay; COFS II, the natural extension of the simple beam testing through the construction of a three-dimensional test bed which will be utilized to validate the methodologies involved in modeling and controlling large, flexible structures in a space environment; and COFS III, the development of the ground test methodologies for multi-body configurations such as the space station concept. The goal of these COFS projects are to generate a technology data base that will provide the designer with alternatives for the improvement of spacecraft performance.

ORIGINAL PAGE IS
OF POOR QUALITY

COFS II HYBRID TEST CONCEPT

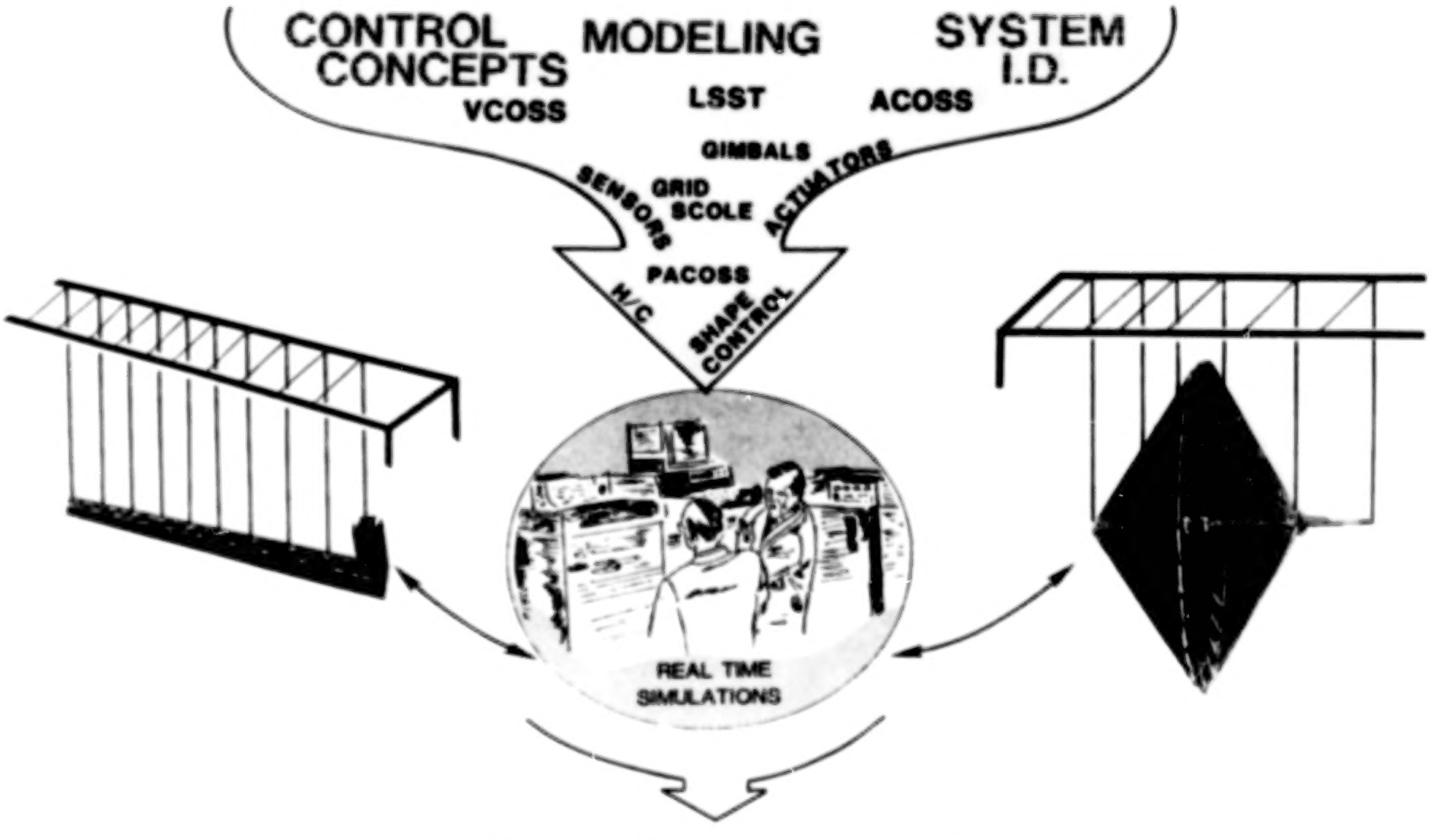

CONTROL CONCEPTS

MODELING

SYSTEM I.D.

VCOSS

LSST

ACOSS

GIMBALS

SENSORS

GRID

SCOLE

ACTUATORS

PACOSS

H/C

SHAPE CONTROL

REAL TIME SIMULATIONS

HI-FI SYSTEM SIMULATION

CONTROL OF FLEXIBLE STRUCTURES

COFS I

Beam Dynamics & Control

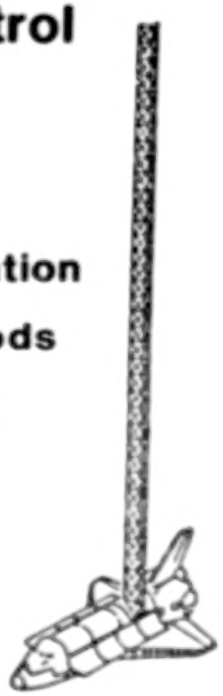

- Systems Identification
- Test Methods
- Distributed Controls

COFS II

Three-Dimensional Dynamics & Control

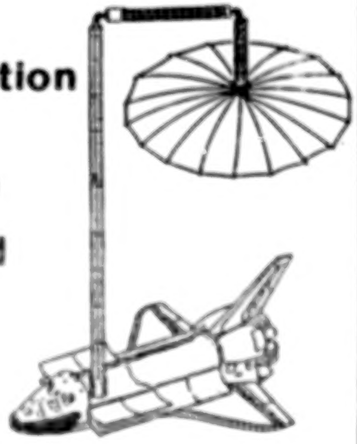

- Systems Identification
- Shape Definition
- Distributed Controls
- Adaptive Controls

COFS III

Multi-Body Dynamics & Control

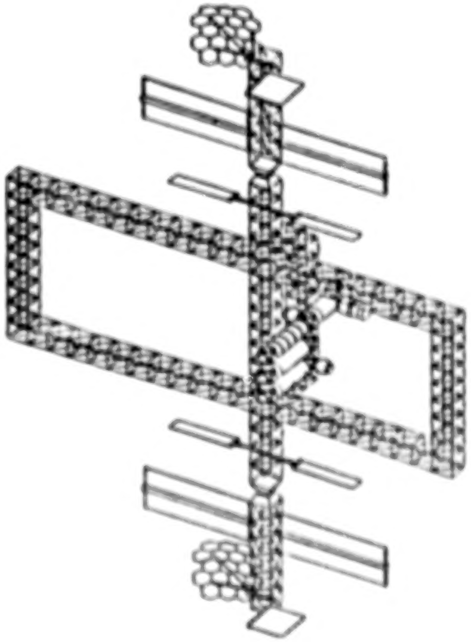

- Test Methods
- Systems Identification
- Model Sensitivities
- Analysis Validation
- Space Station Supporting Technology

PRECEDING PAGE BLANK NOT FILMED

COFS II PROJECT OBJECTIVES

The COFS II project objectives are to develop and evaluate the control/structures interaction technologies needed for effective control of large, flexible, three-dimensional space structures. These functional capabilities are to be developed using sensor and actuator components physically distributed over the flexible flight test structure. The project test hardware will provide a point of focus for the development and evaluation of these functional technologies. Their development requires three types of technical activities; (1) Open-loop Modeling, the prediction of the on-orbit open-loop dynamics and performance using ground-based analytical and experimental methods with validation by orbital testing; (2) Control System Development, the development of control system algorithms and control components to establish the desired functional capabilities; and (3) Closed-loop Modeling, the prediction of the on-orbit closed loop dynamics and performance using ground-based analytical, empirical, and hybrid testing with validation by orbital testing.

CONTROL OF FLEXIBLE STRUCTURES

COFS II Project Objectives

- DEVELOPMENT AND EVALUATE THE METHODOLOGIES INVOLVED IN MODELING AND CONTROLLING LARGE, FLEXIBLE, 3-D STRUCTURES IN SPACE

SPACECRAFT CONTROLS/STRUCTURES INTERACTION (CSI) TECHNOLOGY PROGRAM

The Control of Flexible Structures (COFS) program was developed based on recommendations of the Controls/Structures Interaction (CSI) subcommittee of the Space Systems Technology Advisory Committee (SSTAC) as well as NASA/OAST and the NASA field Centers. The program funds for the conduct of the CSI projects are under the direction of the OAST Director for Space. A steering committee consisting of the NASA/OAST Division Chiefs for Information Sciences and Human Factors, Materials and Structures, and Flight Projects was formed to provide guidance in the development of the CSI technologies and to assure that these results are communicated between the NASA Research Centers and the CSI community. The CSI Technology Program figure indicates representative research efforts being conducted within each of the NASA spacecraft oriented centers and the related NASA Langley Shuttle Technology Experiments Pallet (STEP) and Control of Flexible Structures (COFS) programs.

SPACECRAFT CONTROLS/STRUCTURES INTERACTION (CSI) TECHNOLOGY PROGRAM

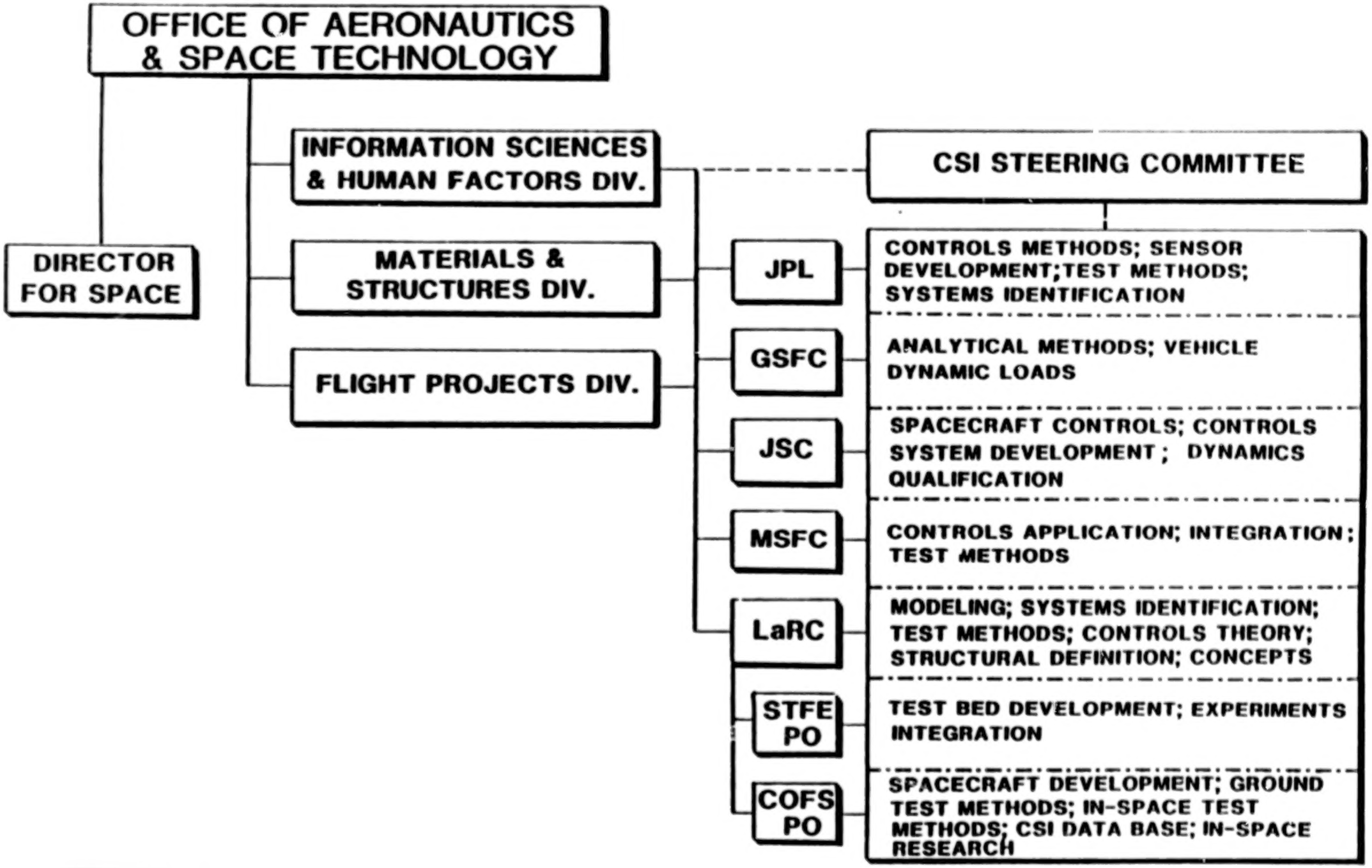

OFFICE OF AERONAUTICS & SPACE TECHNOLOGY

DIRECTOR FOR SPACE

INFORMATION SCIENCES & HUMAN FACTORS DIV.

MATERIALS & STRUCTURES DIV.

FLIGHT PROJECTS DIV.

CSI STEERING COMMITTEE

JPL

CONTROLS METHODS; SENSOR DEVELOPMENT;TEST METHODS; SYSTEMS IDENTIFICATION

GSFC

ANALYTICAL METHODS; VEHICLE DYNAMIC LOADS

JSC

SPACECRAFT CONTROLS; CONTROLS SYSTEM DEVELOPMENT ; DYNAMICS QUALIFICATION

MSFC

CONTROLS APPLICATION; INTEGRATION; TEST METHODS

LaRC

MODELING; SYSTEMS IDENTIFICATION; TEST METHODS; CONTROLS THEORY; STRUCTURAL DEFINITION; CONCEPTS

STFE PO

TEST BED DEVELOPMENT; EXPERIMENTS INTEGRATION

COFS PO

SPACECRAFT DEVELOPMENT; GROUND TEST METHODS; IN-SPACE TEST METHODS; CSI DATA BASE; IN-SPACE RESEARCH

NASA LANGLEY COFS ORGANIZATION

The COFS Project Office is located within the Electronics Directorate at NASA Langley Research Center. This office has the responsibility for implementing the project requirements, goals, and objectives defined by the Langley Structures and Flight Systems Directorates into ground and flight experiments for the development and validation of Controls/Structures Interaction technologies for large, flexible structures. The Project Office is responsible for advocacy of the COFS projects within the CSI community, NASA/OAST and the associated NASA Centers, and for assuring that the COFS projects stay within the costs and schedules accepted by the CSI Steering Committee. In addition, the Project Office is responsible for managing the Guest Investigator contracts and to assure that their experiments are incorporated into each of the COFS projects.

The Project Office is separated into three projects to develop beam dynamics and controls (COFS I), three-dimensional structural dynamics and controls (COFS II), and multi-body structural dynamics and controls (COFS III). Each of these projects have Principal Investigators identified from the Structures and Flight Systems Directorates to guide the project in the development and validation of the technologies. Since a large portion of the experimental effort will be concerned with the ground testing of various scale models of the project hardware, a ground test coordinator has been identified to best utilize the facilities and resources available to the COFS project.

NASA LANGLEY COFS ORGANIZATION

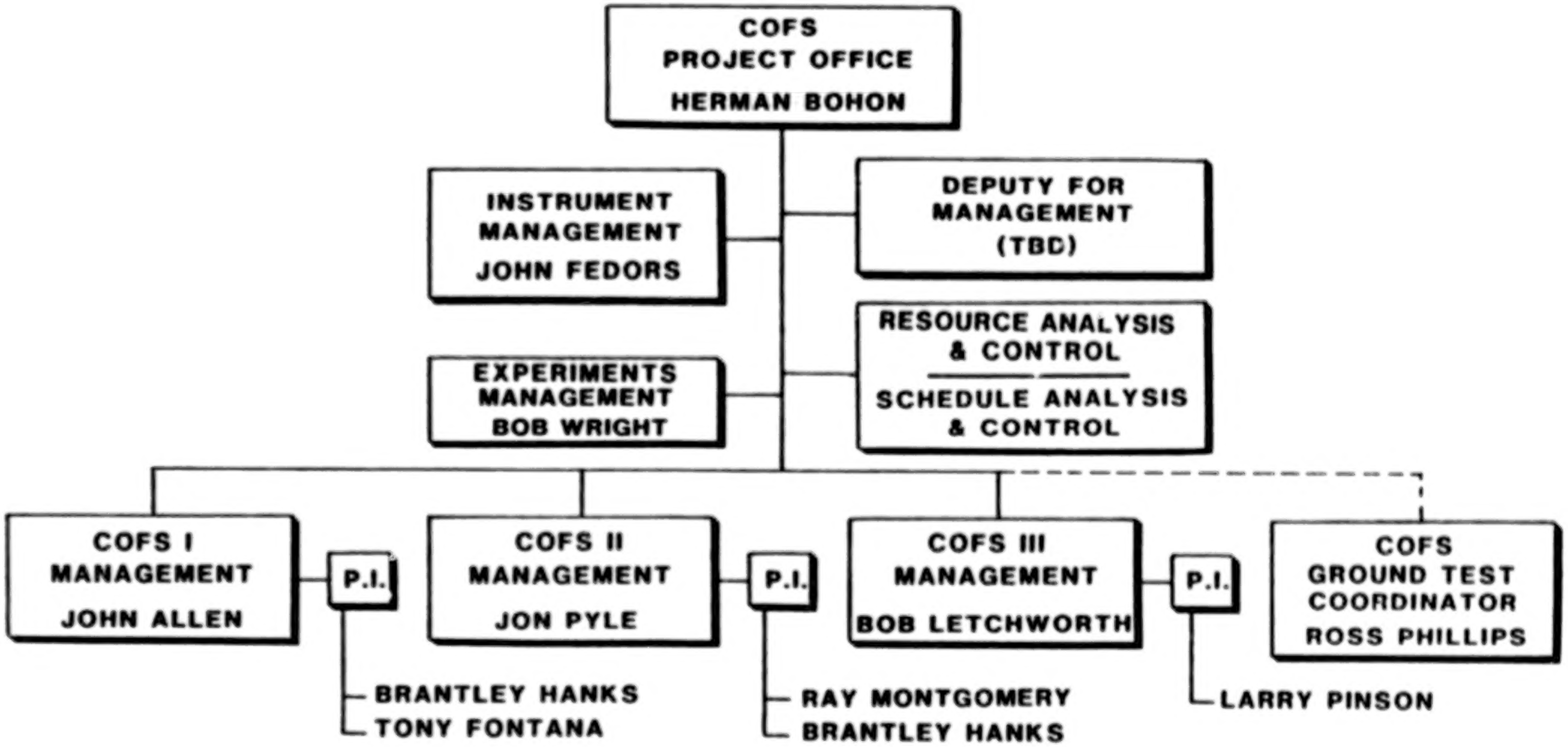

COFS
PROJECT OFFICE
HERMAN BOHON

INSTRUMENT
MANAGEMENT
JOHN FEDORS

DEPUTY FOR
MANAGEMENT
(TBD)

EXPERIMENTS
MANAGEMENT
BOB WRIGHT

RESOURCE ANALYSIS
& CONTROL

SCHEDULE ANALYSIS
& CONTROL

COFS I
MANAGEMENT
JOHN ALLEN

P.I.
- BRANTLEY HANKS
- TONY FONTANA

COFS II
MANAGEMENT
JON PYLE

P.I.
- RAY MONTGOMERY
- BRANTLEY HANKS

COFS III
MANAGEMENT
BOB LETCHWORTH

P.I.
- LARRY PINSON

COFS
GROUND TEST
COORDINATOR
ROSS PHILLIPS

COFS WORKSHOP RESULTS

A Controls/Structures Interaction (CSI) workshop was held at NASA Langley Research Center on August 27-28, 1985. The purpose of the workshop was to review the objectives and hardware proposed for the COFS I project; define the critical technology needs and identify test configurations to develop the critical technologies for large, three-dimensional, flexible structures (COFS II); and to define methods for CSI community participation in the proposed COFS ground and flight tests.

Six discipline panels consisting of approximately ten (10) members each from the CSI community and two members each from NASA LaRC were asked to review the proposed Mast dynamics and controls project and determine the technology needs requiring development in the next generation project. Nine major technology needs were identified requiring the utilization of a three-dimensional configuration as a follow-on to the simple beam experiments of the COFS I project.

After completion of the discipline panel meetings, six configuration panels were organized from members of each of the discipline panels to define viable three-dimensional flight configurations for the COFS II project. Most panels agreed that the configuration should include secondary boom attached by gimbals to a "realistic antenna" and to the Mast beam developed and validated during the COFS I project. Other configurations identified consisted of simpler gimballed booms with masses; however, these configurations did not fully satisfy the development of all the critical technologies.

COFS WORKSHOP RESULTS

August 1985, NASA Langley Research Center

- DEFINED CRITICAL CONTROLS AND STRUCTURES TECHNOLOGY REQUIREMENTS FOR 3-D SPACE EXPERIMENTS
- IDENTIFIED 3-D CONFIGURATION FOR GROUND AND ON-ORBIT TESTING

COFS II WORKSHOP CONFIGURATION TECHNOLOGIES

The COFS II workshop configuration and the critical technologies recommended for development and validation during ground and flight tests are identified in the attached figure. The vertical beam structure shown is the Mast beam which will be extensively ground and flight tested during the COFS I project. Two gimbal assemblies providing a minimum of two (2) degrees of freedom (DOF) each are utilized to connect a secondary deployable boom to the tip of the Mast beam and the boom to the antenna. This secondary boom provides adequate separation between the Mast and an antenna to allow full articulation of the antenna. The secondary boom modal characteristics should be capable of combining with the structural modes of the Mast to provide additional modal characteristics of research interest. The antenna should be realistic in the sense that the technologies developed will have generic application to the industry as a whole rather than to one specific design. The antenna should have a mesh surface with adequate controllability to permit quasi-static changes (long period) in the local surface shape. This controllability will permit validation of control techniques to correct contour errors in the antenna shape caused by over-stretching of the mesh during deployment, thermal distortion or deterioration of the mesh fabric.

The primary technology needs for the three-dimensional configuration are centered around understanding the control of large, flexible structures during repositioning. Therefore, the understanding and development of control techniques for maneuvering, articulation, slewing, pointing or aiming, of the appended bodies, with some degree of precision, and the controllability of the antenna surface shape to assure maximum transmission/reception efficiency are of primary interest. In order to effectively control the secondary boom and antenna, an understanding of the structural characteristics of the three-dimensional configuration is required including the deployment dynamics, system identification/structural evaluation, structural dynamics and vibration characteristics. The successful development and validation of these primary technologies will then permit the further development of adaptive control technologies for this complex configuration.

COFS II
WORKSHOP CONFIGURATION/TECHNOLOGIES

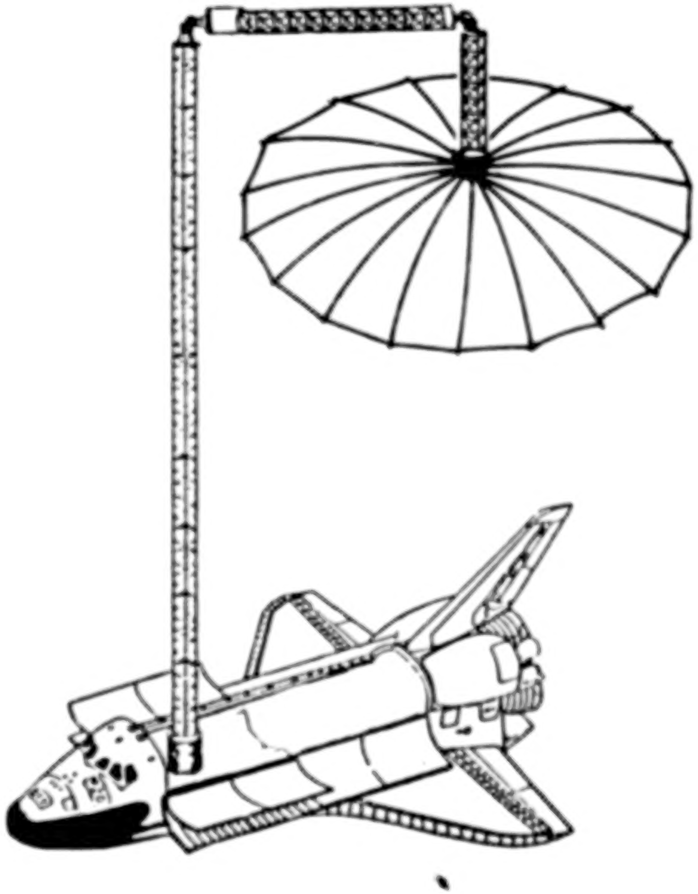

CRITICAL TECHNOLOGY NEEDS

- POINTING/AIMING
- ARTICULATION
- SLEWING
- SHAPE CONTROL
- MANEUVER LOAD
- ALIGNMENT
- SYSTEMS IDENTIFICATION
- STRUCTURAL EVALUATION
- DEPLOYMENT CHARACTERIZATION
- VIBRATION CONTROL
- ADAPTIVE CONTROL

COFS II CONFIGURATION COST OPTIONS

A project cost estimate was completed for various types of large, flexible, three-dimensional configurations which would satisfy the critical technology recommendation of the workshop. The results of this exercise is shown on the figure with increasing project costs as the vertical axis and increasing technology return as the horizontal axis. The COFS I project, Beam Dynamics and Control, was shown as a bench mark of the relative project development costs. Obviously, as the number of technologies and the complexity of the configuration increases, the project costs also increase. Many of the technologies defined at the Langley workshop can be partially developed and validated through the testing of a simplified version of the workshop configuration. However, to achieve full technology development and validation of all the workshop technologies, the configuration recommended by the workshop attendees would probably be required.

CONTROL OF FLEXIBLE STRUCTURES
COFS

COFS II CONFIGURATION COST OPTIONS

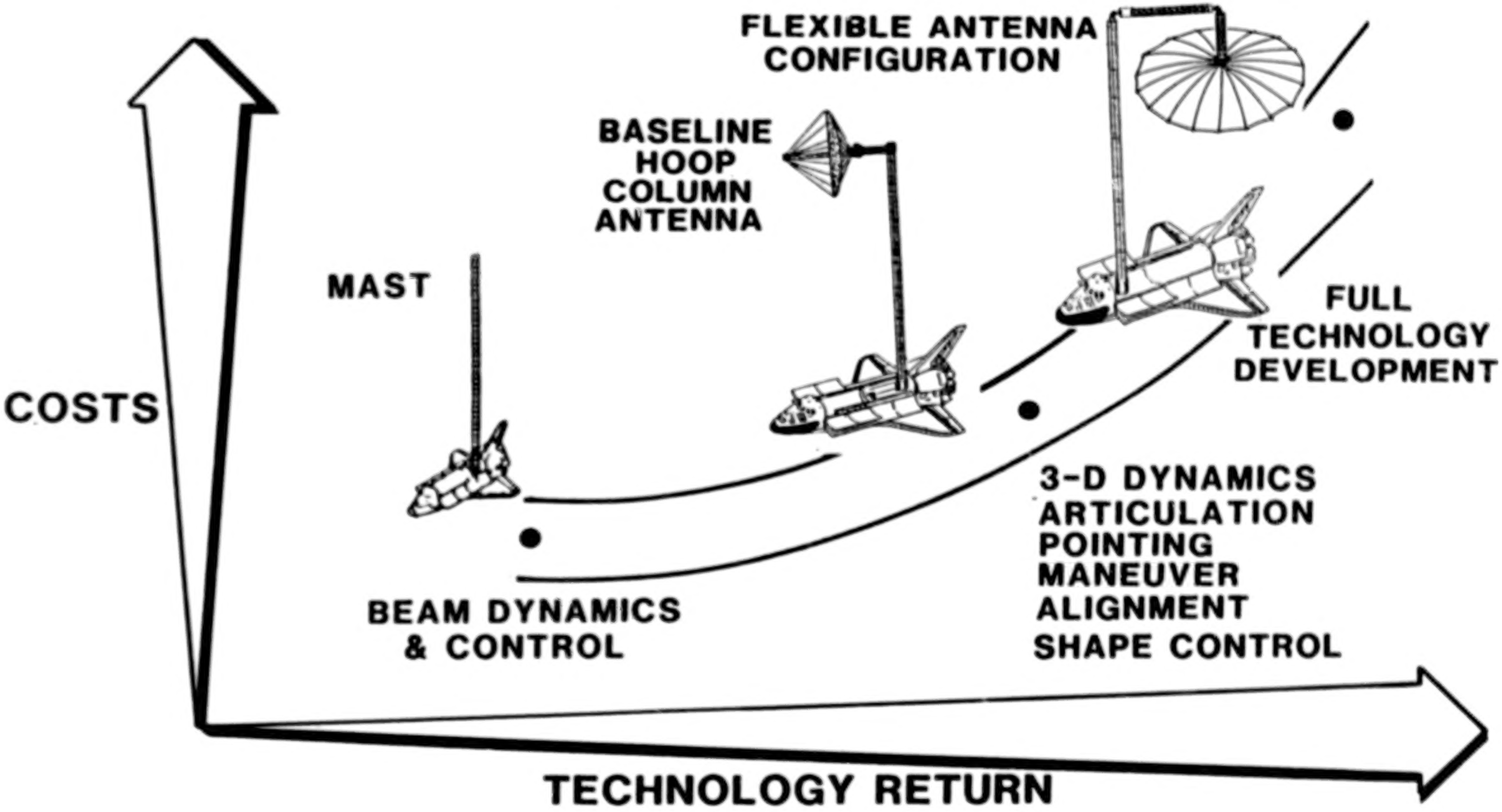
FLEXIBLE ANTENNA CONFIGURATION
BASELINE HOOP COLUMN ANTENNA
MAST
COSTS
FULL TECHNOLOGY DEVELOPMENT
3-D DYNAMICS
ARTICULATION
POINTING
MANEUVER
ALIGNMENT
SHAPE CONTROL
BEAM DYNAMICS & CONTROL
TECHNOLOGY RETURN

ARTIST CONCEPT OF COFS II STUDY CONFIGURATION

The artist rendition of the COFS II configuration shows the Langley designed and developed Hoop/Column antenna attached to the tip of the Mast by means of a two (2) degree of freedom gimbal assembly. This concept, with exception of the feed unit, was utilized as the study configuration for an in-house engineering analysis to determine the feasibility of attaching a realistic antenna to the Mast and developing control and structures technologies. The Hoop/Column antenna has extensive ground testing background plus currently planned development of a quasi-static surface control system for one antenna quadrant (one-fourth of the mesh surface) and is owned by NASA. This configuration will allow partial development of all the critical technologies defined by the COFS Workshop. The canisters will be connected by means of the gimbal assembly and a short (2.5 meters) structural adaptor. During deployment, the Mast will extend to any desired length (up to 60 meters) carrying the undeployed Hoop/Column antenna. The antenna can be fully deployed and then articulated by means of the two degree-of-freedom gimbal assembly. Technology development, evaluation and validation can then be initiated. Upon completion of the flight tests, the antenna and the Mast will be restowed into their respective canisters for the landing phase of the mission.

ORIGINAL PAGE IS
OF POOR QUALITY

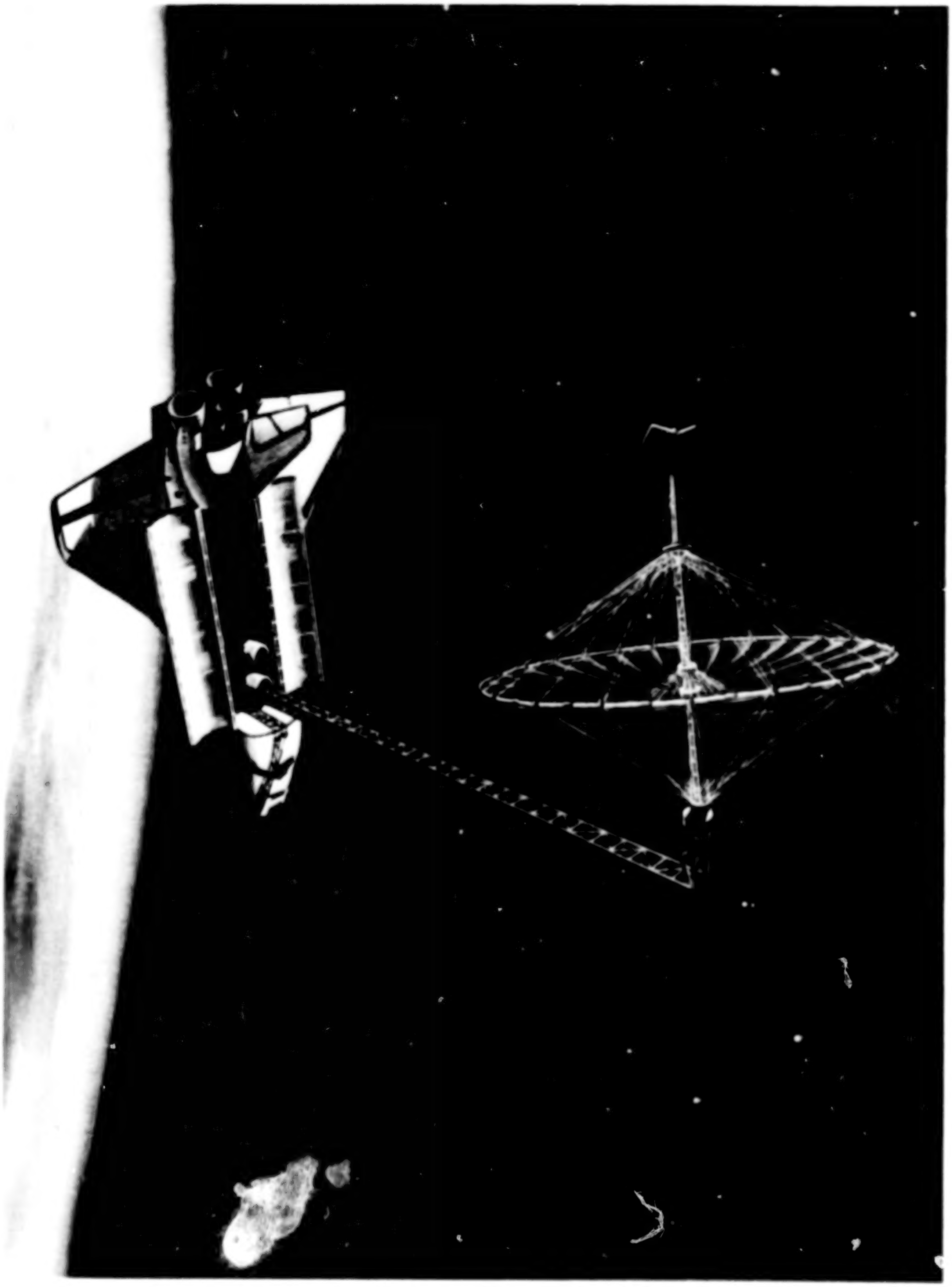

COFS II PROJECT SCHEDULE

The anticipated delay caused by the loss of the Space Shuttle vehicle in January 1986, may slip the expected flight dates for the COFS I project to October 1990 and October 1991. Since the COFS II configuration utilizes the Mast beam developed and validated during the COFS I flight tests, the earliest expected flight date for the COFS II project phase is October 1993. The 18 months identified between the test flight delivery of the Mast and the first COFS II mission will be used for refurbishing the Mast, adding wiring and power, integrating and testing the COFS II hardware, and preparing the COFS II payload for Shuttle integration. The initiation of the hardware development contract in FY 1989 should allow adequate time for the development and verification of the COFS II unique hardware (such as the gimbals and antenna) prior to the required delivery date of the Mast beam for integration. The deployment and pre-design study identified for the FY 1987 through FY 1988 period should provide preliminary solutions to current concerns and issues identified for the COFS II concept.

The ground test schedule is shown as a dashed line representing non-project sponsored basic research development and testing being conducted on related structures which will have a direct input to the COFS II configuration. These tests include work being accomplished through the Air Force with Marshall, development and verification of sensors/actuators at JPL, MSFC and LaRC, and in-house Langley research on the Grid Test Fixture and, SCOLE, as well as the structural surveys and surface controllability efforts on the Hoop/Column antenna. This background information will be utilized in the development of a HYBRID GROUND TEST CONCEPT which will pave the way for understanding and establishing the techniques necessary for ground testing very large flexible structures.

In conjunction with the development of the COFS II hardware and the hybrid ground testing, a guest investigator program will be initiated to encourage participation by industry, universities, and government in the development and validation of the COFS II technologies. Individuals with specific scientific experiments will be invited to support the ground and flight experiments.

COFS II PROJECT SCHEDULE

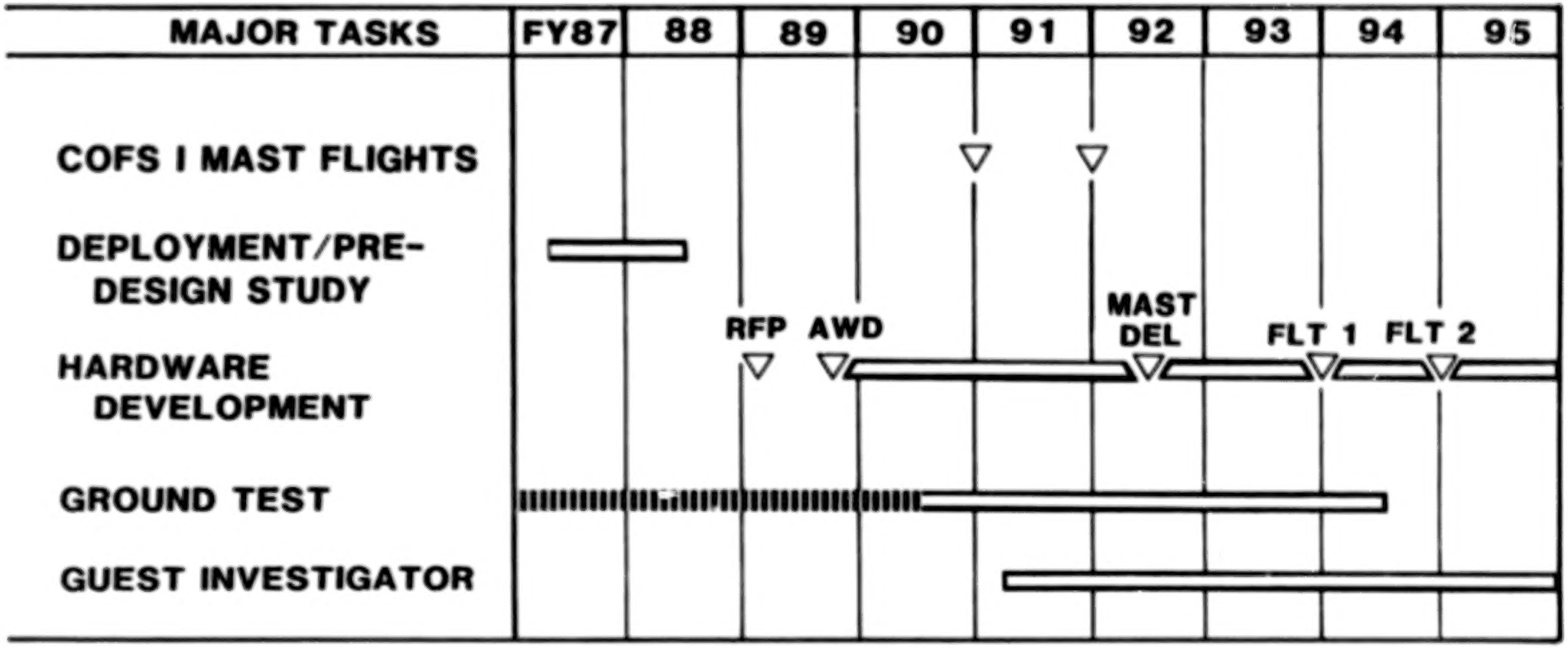

GUEST INVESTIGATOR OPPORTUNITIES

Opportunities for participation by the Controls/Structures Interaction community in the analysis, ground and flight testing of the COFS II configuration can be realized through several research areas. These areas were characterized in the "Guidelines for Participation in the Control Of Flexible Structures (COFS I) Guest Investigator Program" as: (1) STRUCTURES, such as deployment kinematics and beam static precision; (2) STRUCTURAL DYNAMICS, such as dynamic math modeling (partial or complete configuration), systems identification/structural evaluation, damping prediction, ground test methodology, and on-orbit test methods; and (3) CONTROL OF FLEXIBLE STRUCTURES, such as vibration suppression, sensor and actuator dynamic modeling, articulation control, slewing control, pointing and aiming control, maneuver load control, alignment control, antenna surface shape control, adaptive control and failure detection identification, and re-configuration. The COFS II project may provide the opportunity of allowing the integration of unique hardware (sensors, actuators, structures, etc.) into the ground and/or flight test configuration for development and validation. These examples should in no way be construed as preferential and, in fact, innovative and unique experiments are encouraged.

Within the broad technology areas listed above, research may be subdivided into analysis, development of software, and development of hardware. Each of these subdivisions may apply to either ground research or flight research. The "analysis" subdivision involves the development of control algorithms and modeling techniques as well as the use of ground and/or flight test data in a research investigation, e.g., computation of beam damping for joint test data. The "development of software" subdivision involves development of algorithms to be executed by the experiment computer during ground and/or flight tests, e.g., adaptive control law design. The "development of hardware" subdivision involves development of unique hardware that becomes part of the ground and/or flight test article.

GUEST INVESTIGATOR OPPORTUNITIES

(TYPICAL)

- **STRUCTURAL DYNAMICS**
- **FLEX-BODY CONTROL ALGORITHMS**
- **SYSTEM IDENTIFICATION ALGORITHMS**
- **FLIGHT & GROUND TEST METHODS**
- **MATH MODELLING**
- **VIBRATION SUPPRESSION**
- **ANALYSIS OF GROUND & IN-SPACE TEST DATA**
- **FLIGHT TESTING OF UNIQUE HARDWARE**

GUEST INVESTIGATOR TECHNOLOGY TRANSFER

The interaction between NASA and the Guest Investigators (GI's), during conduct of the COFS II project, is shown on the COFS TECHNOLOGY TRANSFER figure. The circles represent those project tasks which will be accomplished within NASA and the squares indicate those tasks to be accomplished by contract (either Hardware Developer or Guest Investigator). The GI's will respond to experiment guidelines generated by the COFS II Principal Investigators and define experiments to be conducted during the ground and flight tests. The experiments will be developed and certified in conjunction with the hardware contractor and the COFS II project office and then validated during the ground and/or flight testing. The data obtained from the testing will be processed through the NASA Data Processing system and distributed to both the GI's and the Principal Investigators. The GI's will have prime responsibility for analyzing the data and reporting the results.

COFS TECHNOLOGY TRANSFER

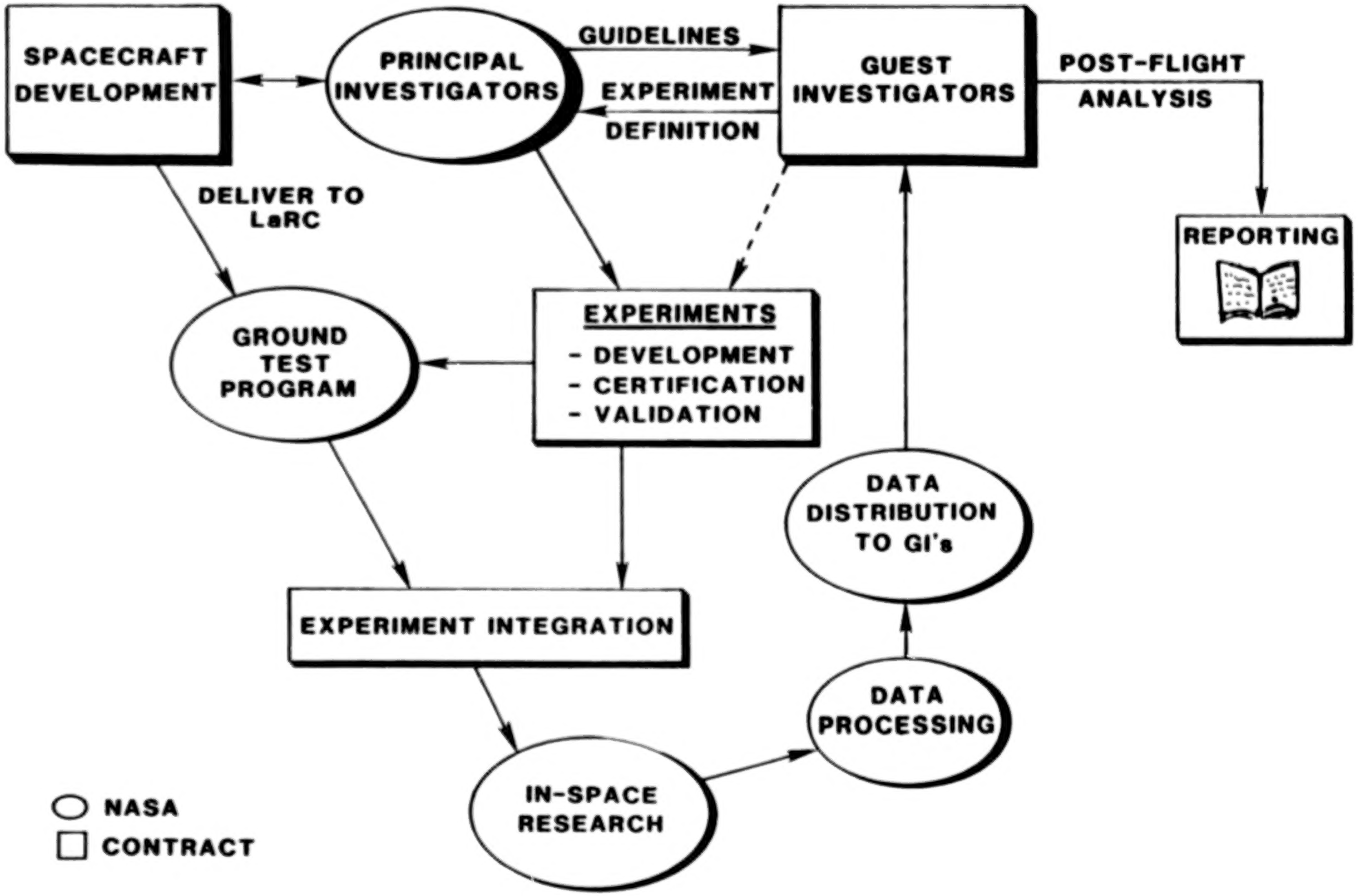

SPACECRAFT DEVELOPMENT

PRINCIPAL INVESTIGATORS

GUIDELINES

EXPERIMENT DEFINITION

GUEST INVESTIGATORS

POST-FLIGHT ANALYSIS

REPORTING

DELIVER TO LaRC

GROUND TEST PROGRAM

EXPERIMENTS

- DEVELOPMENT
- CERTIFICATION
- VALIDATION

DATA DISTRIBUTION TO GI's

EXPERIMENT INTEGRATION

DATA PROCESSING

IN-SPACE RESEARCH

○ NASA
□ CONTRACT

COFS II FLIGHT EXPERIMENT OBJECTIVES

The objectives of the COFS II flight experiment encompass not only the inflight validation of control techniques and methodologies, or the characterization of the large flexible test article, but also the verification of the design approaches applied during the course of the program evolution. These include correlation of flight test results with ground test and analytical predictions to determine the viability of assumptions and modeling decisions made in the development of the system design. In addition, the flight results will be used to establish the viability of the hybrid testing techniques used in predicting on-orbit performance of a large, flexible, and complex structure. Validation of this testing method for large complex systems, as well as verification of the design approaches will be instrumental in the success of future large spacecraft missions.

CONTROL OF FLEXIBLE STRUCTURES

COFS II Flight Experiment Objectives

- DEVELOP AND VALIDATE ADVANCED CONTROL METHODOLOGIES ON A LARGE, 3-D FLEXIBLE STRUCTURE IN A ZERO-G ENVIRONMENT

- IDENTIFY AND CHARACTERIZE THE PLANT DYNAMICS OF A LARGE, 3-D FLEXIBLE STRUCTURE IN A ZERO-G ENVIRONMENT

- CORRELATE FLIGHT TEST RESULTS WITH GROUND TEST AND ANALYTICAL PREDICTION

- ESTABLISH VIABILITY OF HYBRID TESTING TECHNIQUES FOR PREDICTING ON-ORBIT PERFORMANCE OF LARGE, FLEXIBLE, AND COMPLEX SYSTEMS

COFS II TECHNICAL GOALS

The technical goals associated with the COFS II flight experiment program are illustrated in this figure. As can be noted, these goals address issues associated with modeling as well as control of large flexible structures. In the modeling area, it is desired to assess the accuracy of the various models generated for the system configuration, and to evaluate the ability and desirability of utilizing a synergistic combination of analytical, ground and flight test data to develop the high fidelity model of the large flexible structure. Specifically, prediction of the modal frequencies, mode shapes and slopes within five percent, and modal damping within 20 percent for the first ten modes is desired. For the controls discipline, it is deemed essential to establish control synthesis techniques for future missions by comparing the predicted and on-orbit performance of the system incorporated in the COFS flight article. In addition, evaluation of the performance improvements which can be realized from real time, in-situ systems identification must be assessed along with the robustness of the control configuration used on this flight system. Finally, critical technologies in the areas of shape control, articulation, pointing, and failure detection for large, flexible, complex systems must be examined. Specific technical goals for each of these individual tasks are identified on the right hand column of the figure and include goals on stability margins and damping augmentation, bandwidth, impact of modeling uncertainties, and failure detection thresholds.

CONTROL OF FLEXIBLE STRUCTURES

COFS II TECHNICAL GOALS

CONTROL	SPECIFIC GOALS
ASSESS CONTROL SYNTHESIS TECHNIQUES BY COMPARING PREDICTED AND ON-ORBIT SYSTEM PERFORMANCE	● STABILITY MARGINS WITHIN 25% AUGMENT DAMPING TO 5% .... FOR FIRST FIVE MODES
DEMONSTRATE PERFORMANCE IMPROVEMENTS ARISING FROM ON-ORBIT SYSTEMS IDENTIFICATION	● INCREASE BANDWIDTH BY 100% SAME STABILITY MARGINS
EVALUATE SYSTEM ROBUSTNESS	● MODAL FREQUENCIES UP TO 15% MODAL DAMPING UP TO 100% MODE SHAPES AND SLOPES UP TO 20% .... ALL MODES
VALIDATE SHAPE CONTROL, ARTICULATION, POINTING, AND FAILURE DETECTION TECHNIQUES	● SHAPE WITHIN 1 MILLIMETER DETECT ANGULAR VELOCITY FAILURE AT 1 DEG/SEC DETECT ACCELERATION FAILURE AT 0.2 M/SEC^2

MODELING	SPECIFIC GOALS
ASSESS ACCURACY OF MODELS OF 3-D, JOINT DOMINATED STRUCTURE AT ZERO-G	● MODAL FREQUENCIES WITHIN 5% MODAL DAMPING WITHIN 20% MODE SHAPES & SLOPES WITHIN 5% .... FOR FIRST TEN MODES
EVALUATE PROCEDURE OF MODELING VIA COMBINING ANALYTICAL, GROUND & FLIGHT TESTS RESULTS	● MODAL FREQUENCIES WITHIN 2% MODAL DAMPING WITHIN 5% MODE SHAPES & SLOPES WITHIN 2% .... FOR FIRST TEN MODES

LANGLEY GRID TEST FIXTURE

Complementary test programs are being conducted at Langley as part of the base R&T program. A typical example is shown by this view of the Langley grid test fixture. This test article consists of a number of aluminum bars joined at their intersections. The article is suspended from the ceiling by two thin cables, and exhibits a lowest natural structural frequency of approximately 0.5Hz. Typical control actuators and sensors, such as reaction wheels and rate gyros, are attached to the grid. Test programs conducted on this device include control law evaluations on-site and from remote locations, system identification studies, and failure accommodations developments.

ORIGINAL PAGE IS
OF POOR QUALITY

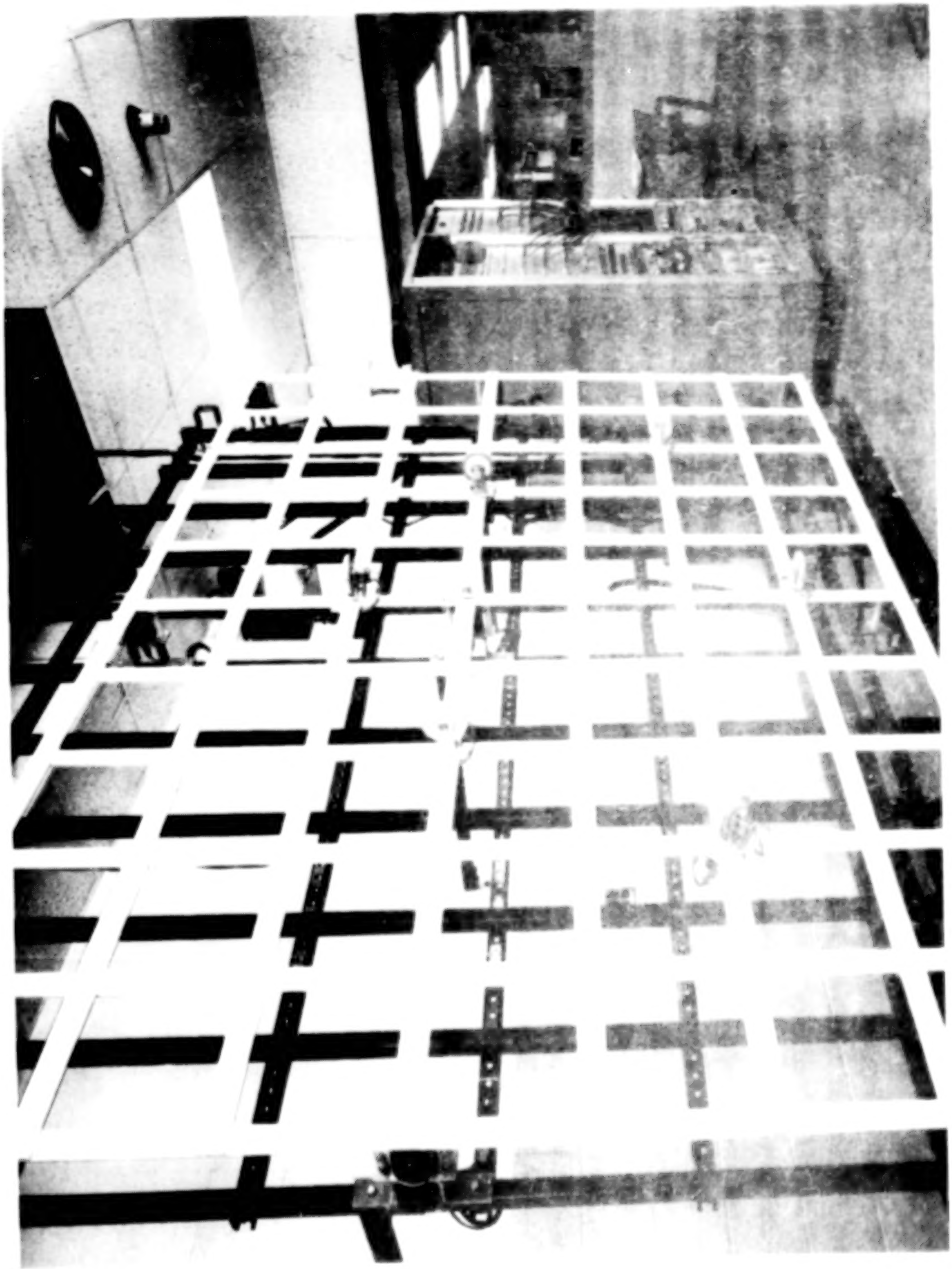

FAILURE ACCOMMODATION

Typical results from failure accommodation studies are examplified in this figure. It can be readily determined that failures can either be anticipated and redundancy provided for that eventuality, or the system design accounts for eventual failures in its original development. For example, if components are known to exhibit a certain Mean Time Between Failures (MTBF) history, and the number of components in the system are known, then it is possible to predict how many of these elements can be expected to fail during the course of the mission. Knowing the predicted failure frequency, it is then possible to develop a cost function which can then be employed in the determination of which control system configuration best accommodates contemplated failures over the postulated mission life. In this figure, two typical system configurations are examined. It is seen that for the long mission cycle, system 2 has the lower associated cost penalty and is thus preferable. Therefore, system design can incorporate contemplated system failure in its definition.

CONTROL OF FLEXIBLE STRUCTURES

Failure Accommodation

SYSTEM RELIABILITY

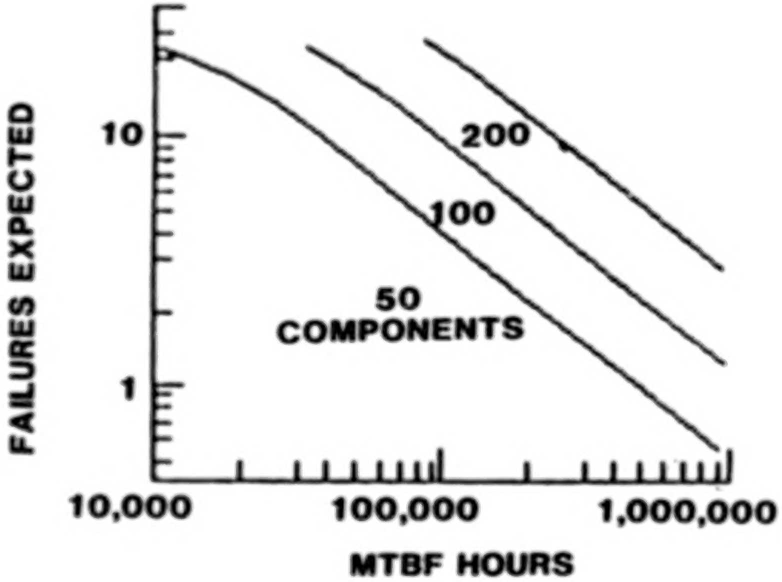

SYSTEM CONFIGURATIONS

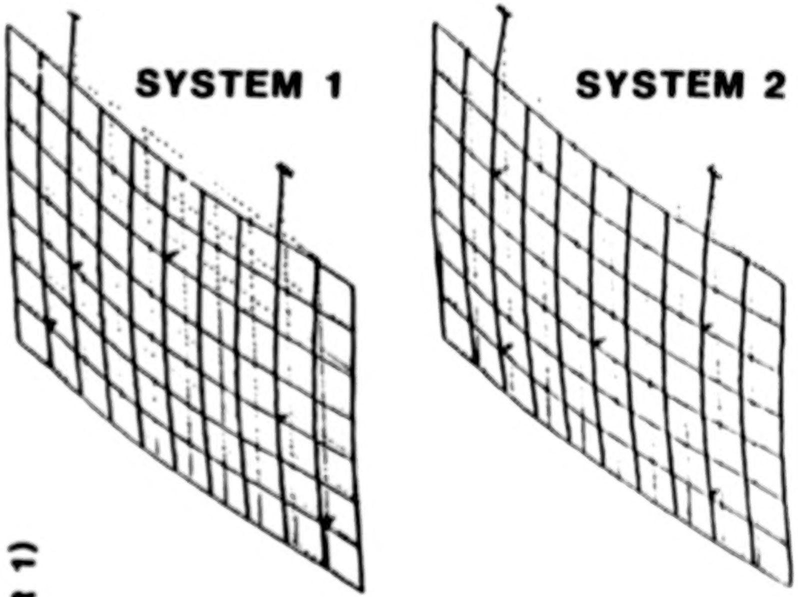
SYSTEM 1
SYSTEM 2

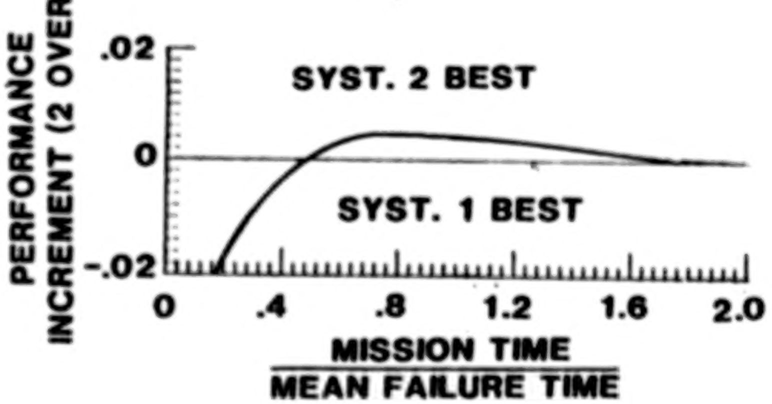

SPACECRAFT CONTROL LABORATORY EXPERIMENT

(SCOLE)

Another test article utilized in the development of control technology is the Spacecraft Control Laboratory Experiment (SCOLE). This system includes a simulated Shuttle vehicle to which is attached a generic reflector and a flexible mast. The shuttle representation is equipped with a set of double gimbal (CMQ's) to provide system control for maneuvering and reorientation. Twin reaction wheel assemblies are attached to the flexible beam for control of the system flexible modes. The reflector is also equipped with a reaction jet package for maneuver load alleviation, vibration suppression and control. Appropriate sensors, such as accelerometers and rate gyros, are also mounted on this test facility and used in system performance evaluation and loop closures. This test apparatus is being studied and used by a contingent of university and government researchers for modeling research, flexible body control and identification, etc.

ORIGINAL PAGE IS
OF POOR QUALITY

SCOLE VIBRATION SUPPRESSION TEST RESULTS

Representative test results from the SCOLE facility are shown in this figure. Suppression of the first vibrational mode of the cantilevered mast of the SCOLE configuration was performed using the reaction jets located at the hub of the reflector. As can be readily noted, the control method utilized in this test was highly effective in damping out the encountered distrubance.

SCOLE VIBRATION SUPPRESSION USING ON-OFF THRUSTERS

Cantilevered Mast – First Mode

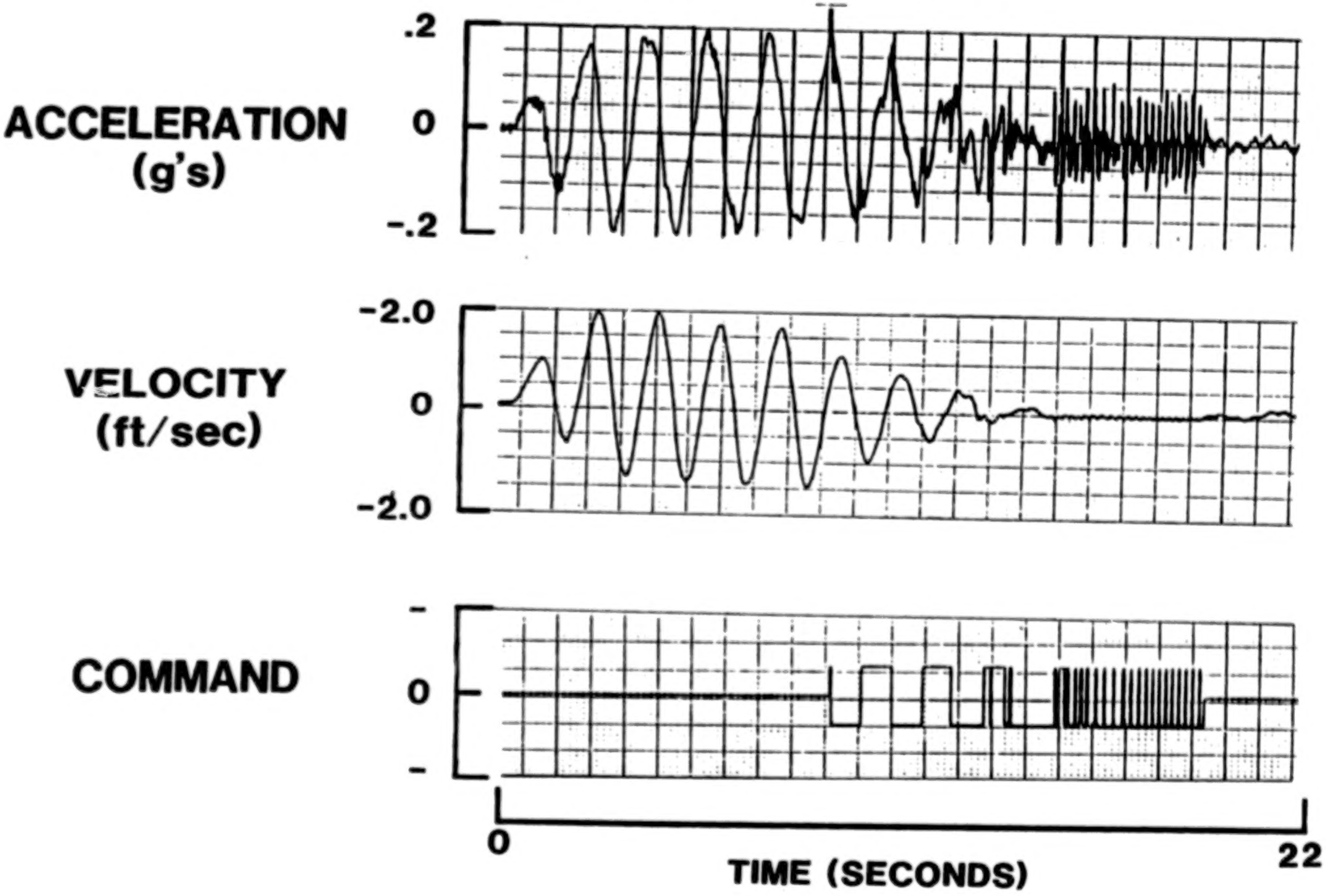

HOOP COLUMN ANTENNA

The Hoop-Column antenna depicted in this figure has been widely used by Langley in a variety of experimental programs dealing with antenna research in the areas of RF performance and structural dynamics evaluations. It is currently being prepared for evaluations of shape control techniques which are essential to providing the antenna efficiencies required by the user community. This article is fifteen (15) meters in diameter and consists of a graphite-epoxy hoop connected to a telescoping graphite-epoxy column via a number of control and alignment cables. The mesh stretched over the surface of the antenna provides four reflector surfaces thus resulting in an antenna with multiple apertures. Testing is expected to begin the summer of 1986.

ORIGINAL PAGE IS
OF POOR QUALITY

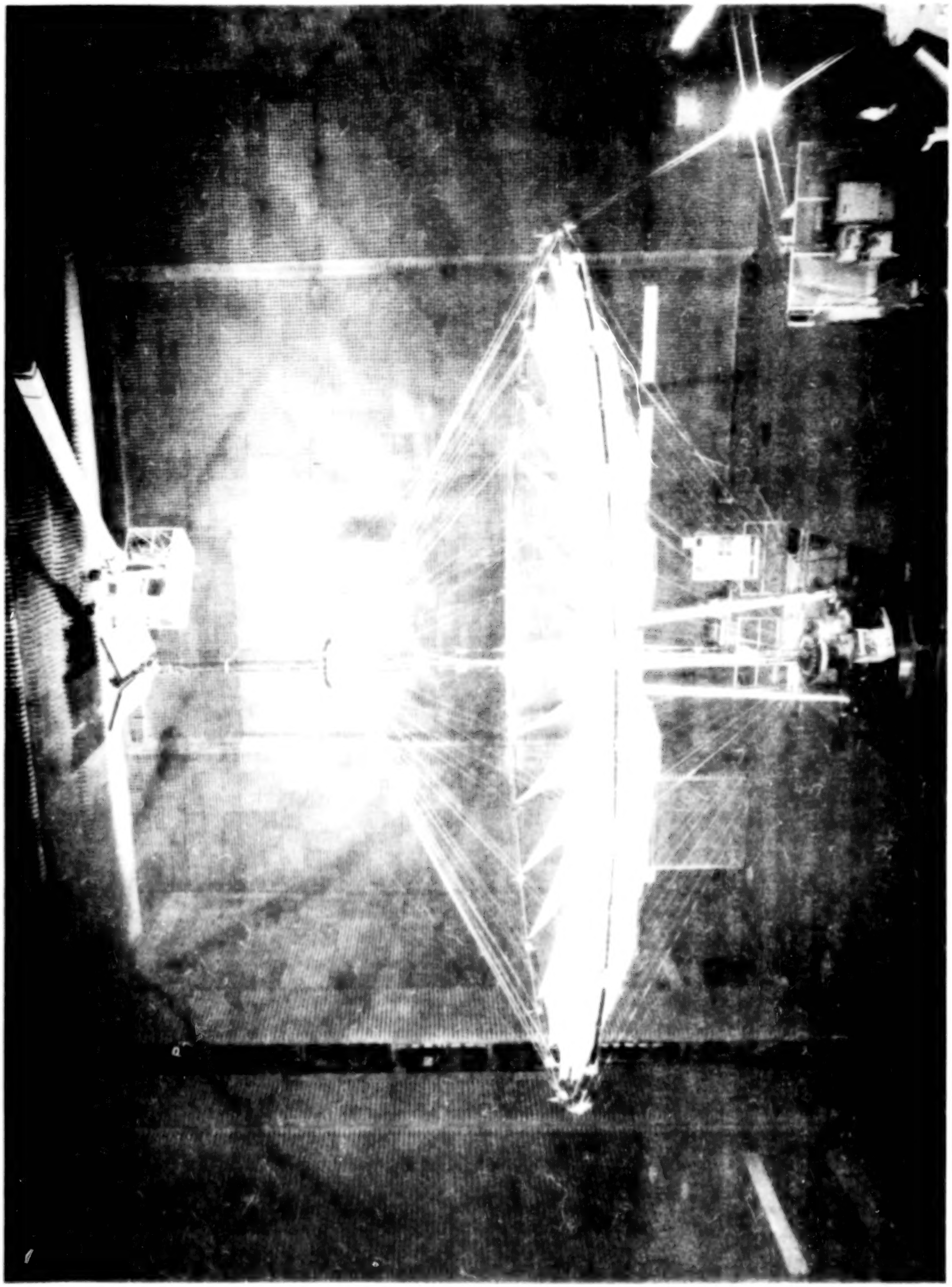

HOOP COLUMN ANTENNA ANALYSIS AND TEST RESULTS

Analytical models of the Hoop-Column antenna were developed during the design phase of the antenna program. These models have been utilized to predict structural dynamics characteristics of this article. Following the fabrication and installation of the antenna at Langley, structural dynamics experiments were conducted to establish the characteristics of this antenna configuration and to evaluate the accuracy of the models and their development techniques. As can be seen from this figure, initial predictions were not unreasonable when compared to the actual physical characteristics. However, as in any program of this nature, some refinement is always needed to overcome the shortcomings of the assumptions made in the generation of the model. In addition, deviations from the hardware design occurring during the fabrication phase will impact the structural characteristics of the system thus requiring mathematical model refinement. It is to be noted that the refined model does subsequently provide very good agreement with the test results when all system anomalies are incorporated into the model. Such research efforts permit the establishment of improved modeling techniques which will be beneficial to the COFS and other programs.

HOOP COLUMN ANTENNA

Analysis and Test Results

MODE	TEST				INITIAL ANALYSIS		REFINED ANALYSIS	
	W/O MESH		W MESH		FREQ	% ERROR	FREQ	% ERROR
	FREQ	DAMP	FREQ	DAMP				
HOOP TORSION	0.068	3.5	0.077	9.5	0.092	19	0.077	0
HOOP ROCKING	0.785	-	0.697	4.4	1.32	88	0.097	0
HOOP IN-PLANE	1.36	4.1	1.76	6.8	2.15	22	1.73	-2
LOWER COL. TORSION	3.13	2.6	3.18	2.6	3.20	5	3.18	4

SURFACE CONTROL CONCEPT

The design of the surface control system for the Hoop-Column antenna will permit active control of each mesh control cord. This is effected by providing a motor for each of four cords per gore to pull on the control cables to achieve the proper surface tension. Release of tension on the mesh, when desired is achieved by actuation of the appropriate motor and a spring mechanism incorporated in the control cord guide to pull the cable out toward the mesh. Since a single quadrant of the antenna will be evaluated, only twenty-eight motors and associated sensors will be required for the initial tests. Control of the hoop alignment and motion relative to the column is also being undertaken by incorporating an additional twenty-four motor and sensor assemblies distributed around the rim and pulling on the appropriate control cord. The actuator/sensor assemblies are to be located at the ends of the antenna mast under the control cord junction plate.

ORIGINAL PAGE IS
OF POOR QUALITY

CONTROL OF FLEXIBLE STRUCTURES

Surface Control Concept

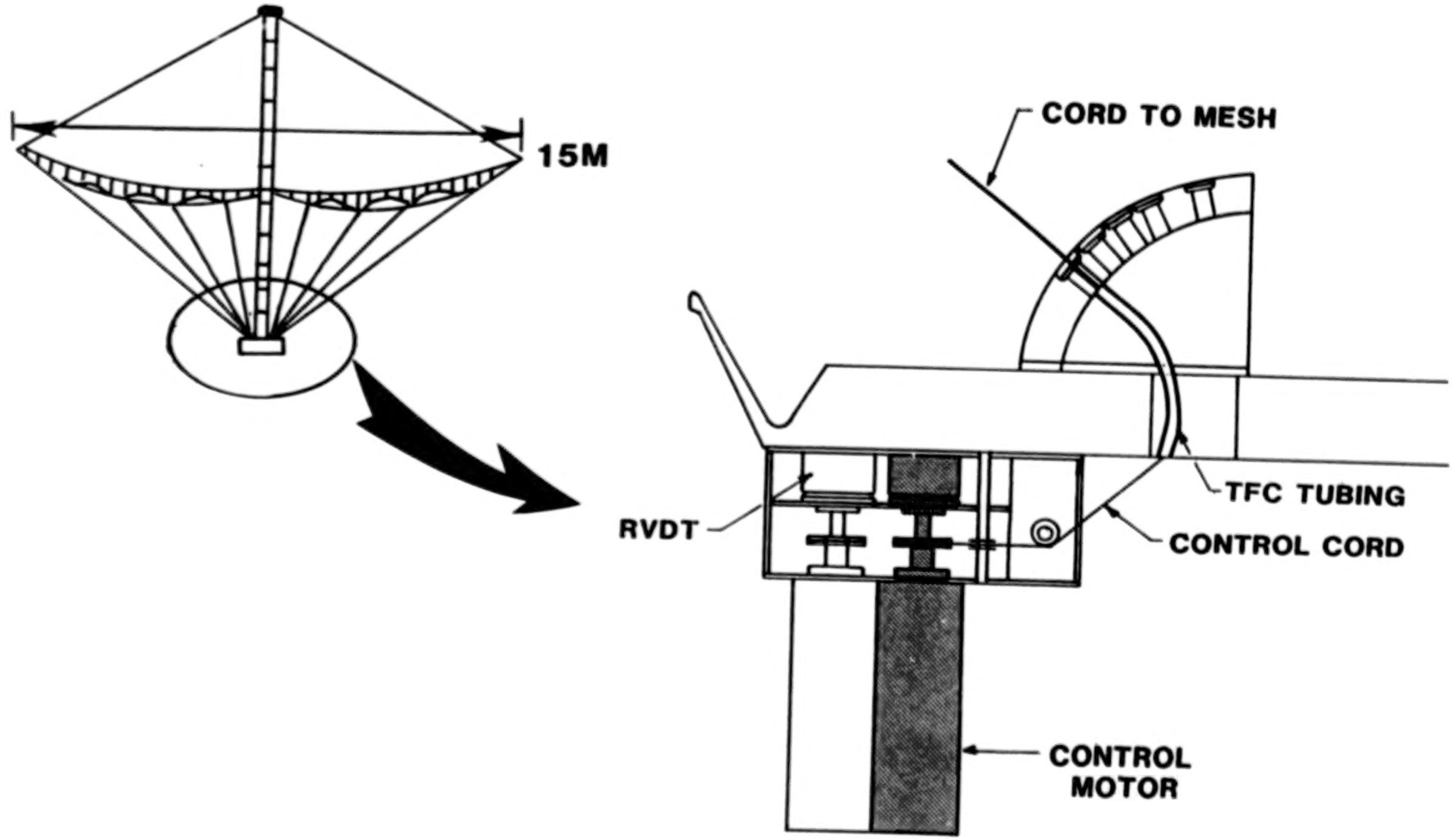
15M
CORD TO MESH
TFC TUBING
CONTROL CORD
RVDT
CONTROL
MOTOR

HYBRID TEST CONCEPT OBJECTIVES

Because of the increasing size of the flight configurations, it becomes necessary to establish some testing techniques which will permit the ground verification of the system design and prediction of its expected on-orbit performance with a high degree of confidence. As such, a hybrid testing concept is contemplated which provides an alternative to full-scale structures and controls ground testing. This concept consists of a combination of real-time simulations and hardware subsystems which are linked through programmed software/hardware interfaces to permit integrated system evaluations. The establishment of this testing technique through the COFS program will be highly instrumental in the ground validation and on-orbit success of future large spacecraft missions.

CONTROL OF FLEXIBLE STRUCTURES

Hybrid Test Concept Objectives

OBJECTIVE:

DEVELOP AND VALIDATE ADVANCED HYBRID TEST CONCEPTS FOR PREDICTING AND CONTROLLING THE DYNAMIC BEHAVIOR OF LARGE FLEXIBLE STRUCTURES

PURPOSE:

PROVIDE ALTERNATIVE TO FULL-SCALE STRUCTURES AND CONTROLS GROUND-BASED EVALUATIONS OF LARGE FLEXIBLE STRUCTURES

APPROACH:

COMBINE REAL-TIME SIMULATIONS AND HARDWARE SUBSYSTEMS THROUGH PROGRAMMED SOFTWARE/HARDWARE INTERFACES TO PERMIT INTEGRATED SYSTEM EVALUATION

COFS II HYBRID TEST CONCEPT

Capitalizing on the legacy of previous programs in the areas of control concepts development, system modeling and identification, as well as in the large, flexible space structures arena such as LSST, VCOSS and ACOSS, synthesis and modeling techniques which proved successful in these programs will be utilized to initiate the COFS analyses and designs. These will be refined by the results obtained from experimental testing and component development efforts as exemplified in the testing of flexible beams, grids, SCOLE, and various sensor/actuator components. Results from ongoing programs, such as the Hoop-Column antenna shape control developments and PACOSS, will be incorporated into the establishment of the high fidelity real-time simulations as they become available. Physical test articles, such as the Mini-Mast, and Hoop-Column antenna, will be combined with these real-time simulations to effect integrated system testing. Physical integration of large test articles is not always possible because of their respective sizes and the requirements they resultantly place on facilities, or because the preferred one-g orientation for one element of the configuration is incompatible with that required for the other elements. Therefore, the simulations will be used to provide the appropriate excitations at the subassembly interfaces, thus producing an integrated system test capability.

ORIGINAL PAGE IS
OF POOR QUALITY

COFS II
CONTROL OF FLEXIBLE STRUCTURES

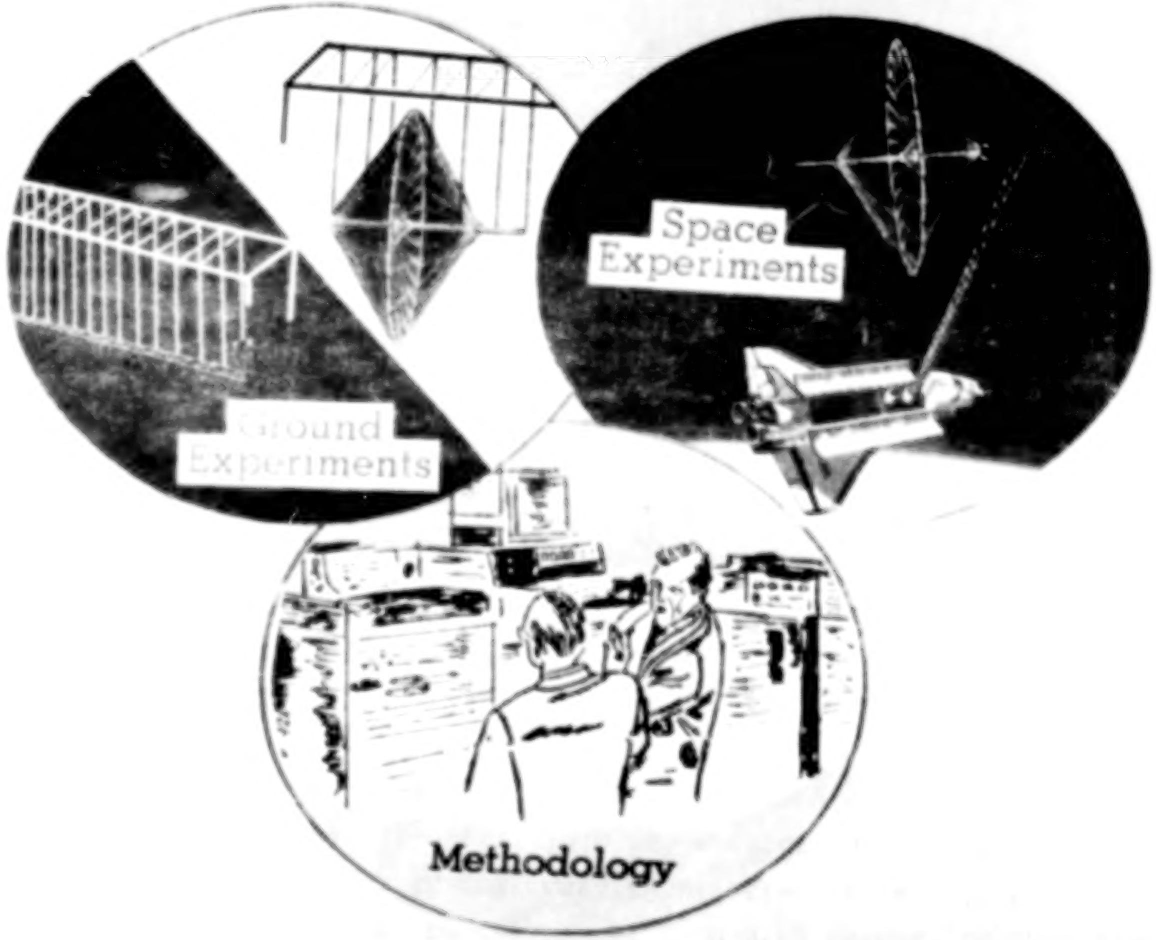
Space Experiments
Ground Experiments
Methodology

ORIGINAL PAGE IS
OF POOR QUALITY

SURFACE SENSOR CHARACTERISTICS

To effect figure control of the antenna surface or the flexible supporting beam, an appropriate sensor is required. This sensor system must be capable of examining several targets simultaneously from a remote location. This tracking of numerous targets must be effected in real time at sampling rates sufficiently high to permit control loop closures. This can provide control of certain dynamic characteristics which could otherwise severely impair the performance of the antenna. A survey of typically available sensors which might be use for such an application, either singly or in multiple pairs, was accomplished and the candidate sensors are shown on this figure. As can be observed, the list is somewhat limited and represents mostly sensors which are still in the development stage. Some, such as the unit employed in the VCOSS program, have progressed to a laboratory operational phase. Further evaluation of these and other to be discovered candidates is continuing.

SPECIFIC SENSOR CHARACTERISTICS

	Number of Targets/Type	FOV	Focal Plane Technology	Sampling Rate	Accuracy
Ball	23/Passive	19°	Array CID	6Hz	2mm/30M • 1/15000
Barnes	12/Active	2°	Array CCD	20Hz	1mm/60M • 1/60000
Grumman	16/Active	35°	Linear Photodiode	200 Hz	.3mm/25M • 1/83000
JPL	1-Dynamic 14-Static / Passive	13°	Streak Tube / Array CCD	8Hz	.1mm/10M • 1/100000
Lockheed	1/Active	19°	Linear Photodiode	100Hz	1A.S/19° • 1/68000
TRW	6/Active	7.5°	Linear Photodiode	4000Hz	.04mm/21M • 1/525000

CONCLUDING REMARKS

As has been shown in this presentation, the COFS II program is a complex and ambitious undertaking which will address several critical technology areas. Among them are modeling, structural dynamics, controls, and ground testing issues which are not only germain to this effort, but to other large space structure programs being contemplated. This effort requires the early integration of controls and structural dynamics considerations in order to achieve mission success. Several technology advances must be achieved in the areas of system modeling, control synthesis and methodology, sensor/actuator development, and ground testing techniques for system evaluation and on-orbit performance prediction and verification. This program offers a unique opportunity for the integration of several disciplines to produce technology advances which will benefit many future programs. In addition, the opportunities available to participate in the various levels in the phases of this program, e.g., analytical development and modeling, ground testing, and flight testing, permit for the involvement of a significant number of interested researchers and organizations from government, universities and industry.

CONCLUDING REMARKS

- COFS II IS AMBITIOUS & COMPLEX EFFORT
- OPPORTUNITIES FOR RESEARCH IN MANY DISCIPLINES
- SYNERGISTIC COMBINATION OF ANALYTICAL, GROUND & FLIGHT EXPERIMENT DEVELOPMENTS
- UNIQUE OPPORTUNITY FOR GUEST INVESTIGATOR PARTICIPATION AT ALL LEVELS

N87
22733
UNCLAS

GENERAL
ELECTRIC

SPACE SYSTEMS DIVISION

IMPACT OF SPACE STATION APPENDAGE VIBRATIONS ON THE POINTING PERFORMANCE OF GIMBALLED PAYLOADS

BY

ROBERT O. HUGHES
GE SPACE DIVISION - VALLEY FORGE
PHILADELPHIA, PA.

PRESENTED AT: WORKSHOP ON STRUCTURAL DYNAMICS
AND CONTROL INTERACTION OF FLEXIBLE STRUCTURES
MARSHALL SPACE FLIGHT CENTER
HUNTSVILLE, ALABAMA
APRIL 22-24, 1986

N87-22733

PRECEDING PA [illegible]

OVERVIEW

A permanently manned Space Station is planned to be launched in the mid 1990's and will orbit at about 460 Km and 28 1/2 degrees inclination. The current baseline configuration is the "dual keel" concept and is about 400 ft. long. The spacecraft will orbit in a nadir pointing, gravity gradient orientation with the X axis in the direction of flight. An initial electrical power capacity of approximately 75 Kw will be generated by a combination of photovoltaic solar arrays and point focusing collectors with heat engines. A central thermal heat rejection system for Attached Payloads is planned and will use fluid loops and large articulating radiators.

OVERVIEW

- SPACE STATION CONFIGURATION
- GIMBALLED PAYLOAD CONCEPTS
- SPACE STATION DISTURBANCE ENVIRONMENT
- VIBRATION RESPONSES AND FAST FOURIER TRANSFORMS
- DYNAMICS/CONTROL SYSTEM MODEL
- PERFORMANCE RESULTS

SPACE STATION CONFIGURATION

The Space Station shown represents a Large Space Structure (LSS). As there are no plans to control the flexible modes (in an active distributed sense) and as there are no plans to estimate (observe) flexible vibrations for feed-forward reasons, non-trivial disturbances will exist at locations where gimballed payloads will be mounted. This base plate disturbance represents the major source of error for the gimbal control system.

The Space Station attitude will be controlled by at least six large Control Moment Gyros (CMGs). Momentum build-up will be managed by off-nadir angles or Torque Equivalent Angles (TEA) that generate desirable, momentum-dumping gravity gradient torques. Current estimates of the maximum nominal TEA angles are ±5° in all axes with rates of .02°/sec per axis.

SPACE STATION CONFIGURATION

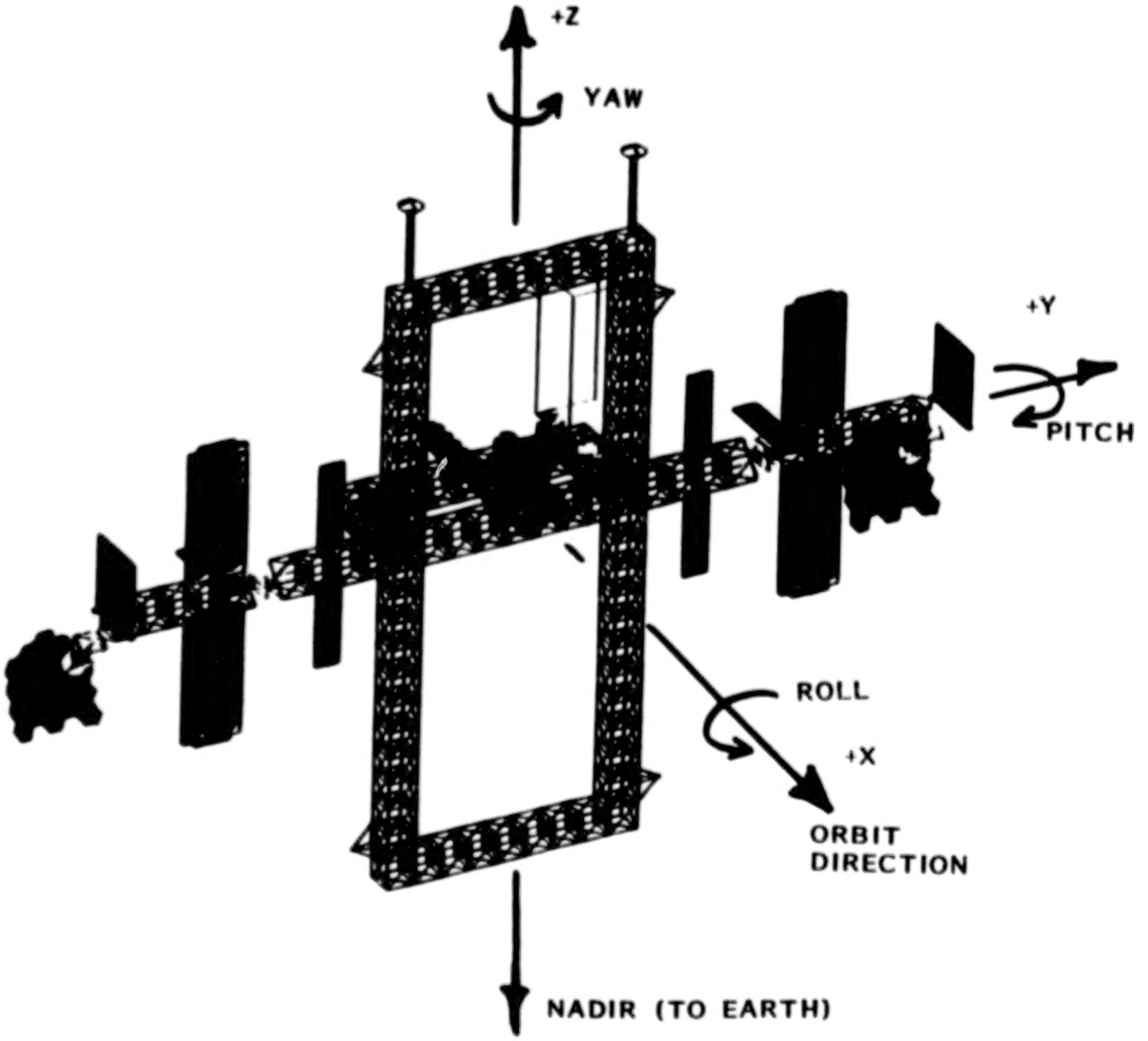
+Z
YAW
+Y
PITCH
ROLL
+X
ORBIT
DIRECTION
NADIR (TO EARTH)

ORIGINAL PAGE IS
OF POOR QUALITY

PAYLOAD GIMBAL CONCEPT

Because the Space Station will not be stationary in its reference frame, generic and reusable pointing mounts are envisioned as the most cost-effective method achieving most payload pointing requirements.

Two types of gimbal concepts exist: one for an end-mount and one for a CG mount. The end-mount design is more versatile in payload accommodation than is the CG mount (shown) but suffers from a CG offset problem. The CG mount arrangement shown has a third axis of rotation which alleviates gimbal lock situations.

PAYLOAD GIMBAL CONCEPT

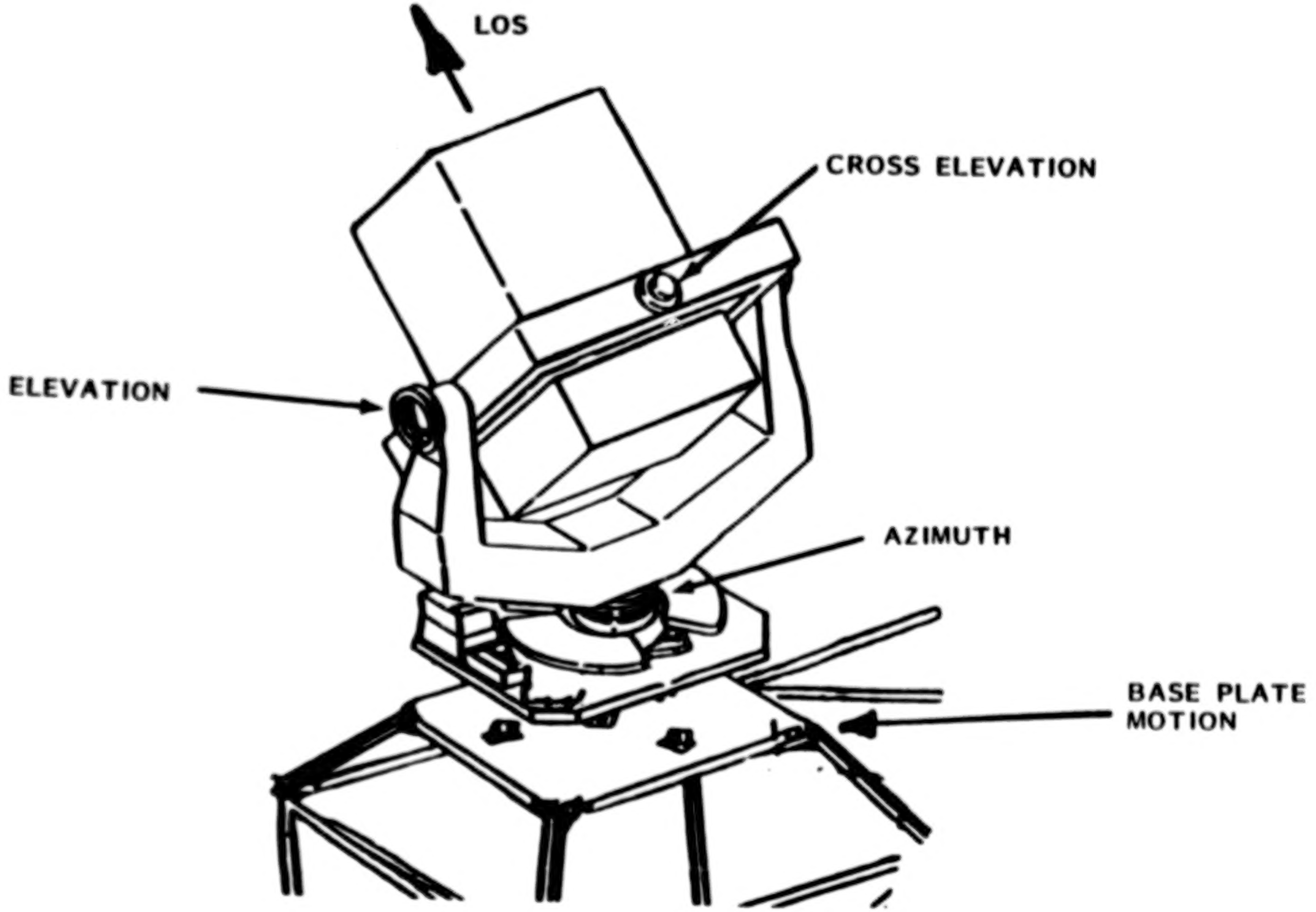
LOS
CROSS ELEVATION
ELEVATION
AZIMUTH
BASE PLATE
MOTION

SPACE STATION DISTURBANCE ENVIRONMENT

Small "ever-present" types of Space Station disturbances include: venting, slosh, machinery and pump vibrations, solar array and radiator motions, CMG torques, payload articulations, and console operations. Larger disturbances which occur in a less random manner include: crew member kickoffs, nominal MRMS (Manipulator) operations, tether operations, laboratory centrifuge operations, and astronaut treadmill activities. Very large disturbances which occur at very predictable and discrete points in time are Shuttle docking, RCS reboost (Station keeping via thrusters), and large excursions of the MRMS with massive payloads. It has been determined that the maintenance of precision pointing during periods of large disturbances would not be cost-effective as the induced vibrations are much larger than the other disturbance types. It is expected that these discrete occurrences will be coordinated with payload objective timelines to minimize data loss. However, payload pointing capabilities must be maintained for the two smaller disturbance levels. These levels represent quiescence or background disturbance levels.

SPACE STATION DISTURBANCE ENVIRONMENT

- SMALL DISTURBANCE SOURCES
  - VENTING, SLOSHING, MACHINERY, CMG's
  - SOLAR ARRAY AND RADIATOR MOTION
  - PAYLOAD MOTIONS, CONSOLE OPS, RODENTS
  - THERMALLY - INDUCED VIBRATIONS
- MODERATE DISTURBANCE SOURCES
  - CREW KICKOFF, TREADMILL OPS, CENTRIFUGE
  - TETHERS, NORMAL MRMS OPS

- DEFINED AS QUIESCENT OR BACKGROUND DISTURBANCES
- REQUIRED TO MEET POINTING SPECIFICATIONS

- LARGE DISTURBANCE SOURCES
  - RCS REBOOST, SHUTTLE DOCKING, LARGE MRMS OPS
  - WILL OCCUR AT PREDICTABLE AND DISCRETE POINTS IN TIME
  - MORE THAN 30X LARGER THAN QUIESCENT LEVELS
  - CURRENT PLAN: RELAX POINTING REQUIREMENTS DURING THESE PERIODS

METHOD OF ANALYSIS

To investigate the effects of background sources of excitation, a NASTRAN model of the Space Station was developed. Forcing functions which modeled a "standard" crew kick-off in the pressurized module, treadmill operations, and a centrifuge with a 20 pound mass imbalance were used as inputs to the NASTRAN Model. Vibration levels were assessed at various locations on the Space Station where pointed payloads were likely to be attached, and the largest rotational/translational case was selected. This location turned out to be at the corner of the upper boom.

METHOD OF ANALYSIS

- SELECT DISTURBANCE SOURCES
    - CREW KICKOFF, CENTRIFUGE, AND TREADMILL OPS
- OBTAIN NASTRAN MODEL OUTPUT RESPONSES
- ASSESS VIBRATION LEVELS AT VARIOUS LOCATIONS OF SPACE STATION WHERE PAYLOADS MAY BE ATTACHED
- SELECT WORST CASE ROTATION AND TRANSLATION
- PERFORM FAST FOURIER TRANSFORM (FFT) ANALYSIS
- USE THE FFTs IN THE CONTROL SYSTEM DYNAMIC MODEL TO ASSESS IMPACT ON POINTING PERFORMANCE

DISTURBANCE RESPONSE

This time history plot is generated from NASTRAN modal data and the selected disturbance inputs. The response is for the rotational motion about the pitch axis. Effects of the crew kick-off can be seen with an initial displacement of approximately 40 microradians (8.3 arc-sec). High frequency vibrations are evident with a maximum peak-to-peak variation of about 7.7 arc-sec.

DISTURBANCE RESPONSE

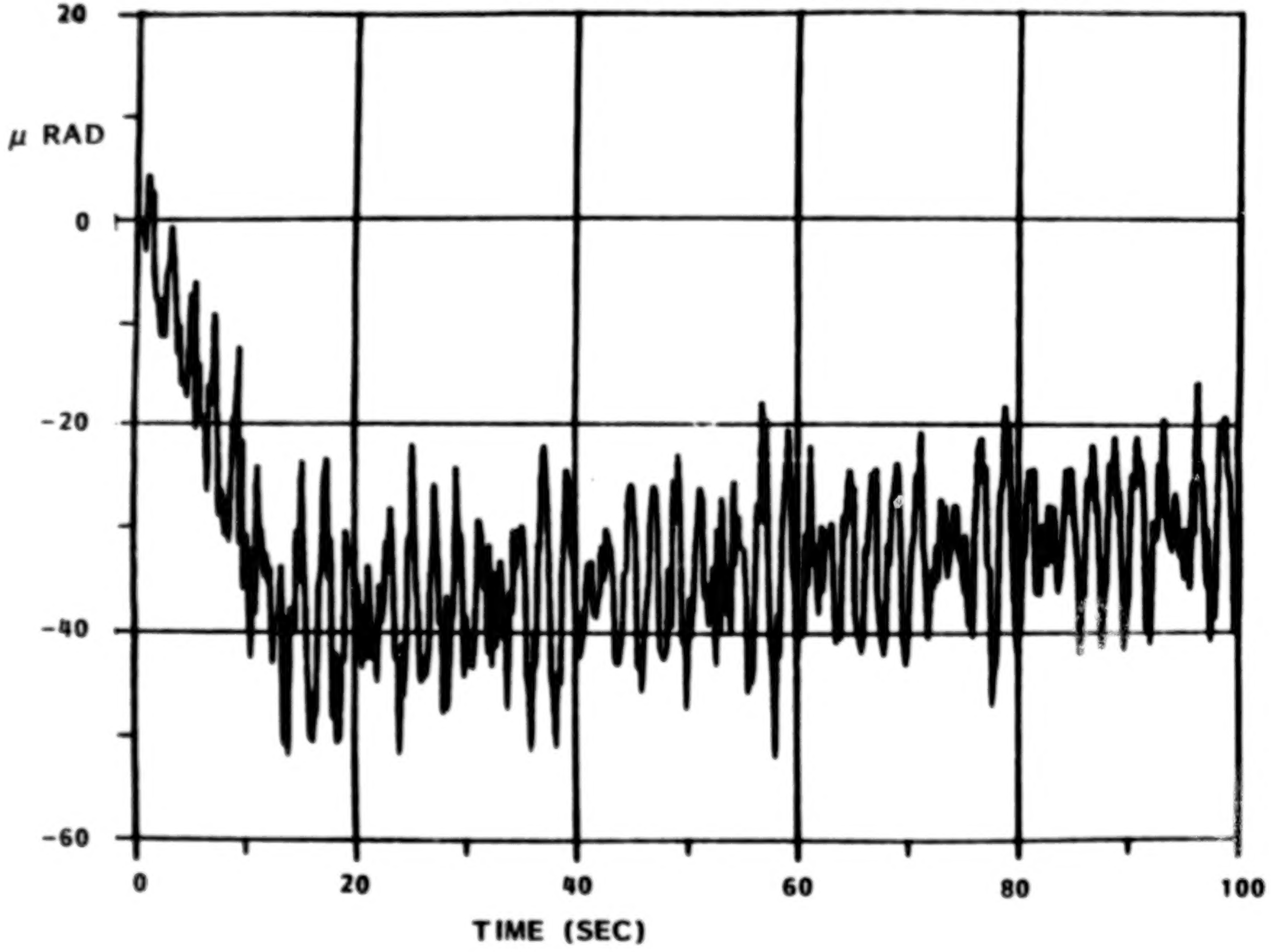

UPPER BOOM ANGULAR DEFLECTION

ROTATION DEFLECTION FFT

The previous time history was analyzed using Fast Fourier Transform (FFT) techniques and the results are shown in this figure. The peaks represent the rotational amplitudes of the major sinusoids present in the signal. In general, base plate motions with frequencies outside the control system bandwidth (nominally 1 HZ) will pass without attentuation. That is, base plate motions cause corresponding pointing errors.

ROTATION DEFLECTION FFT

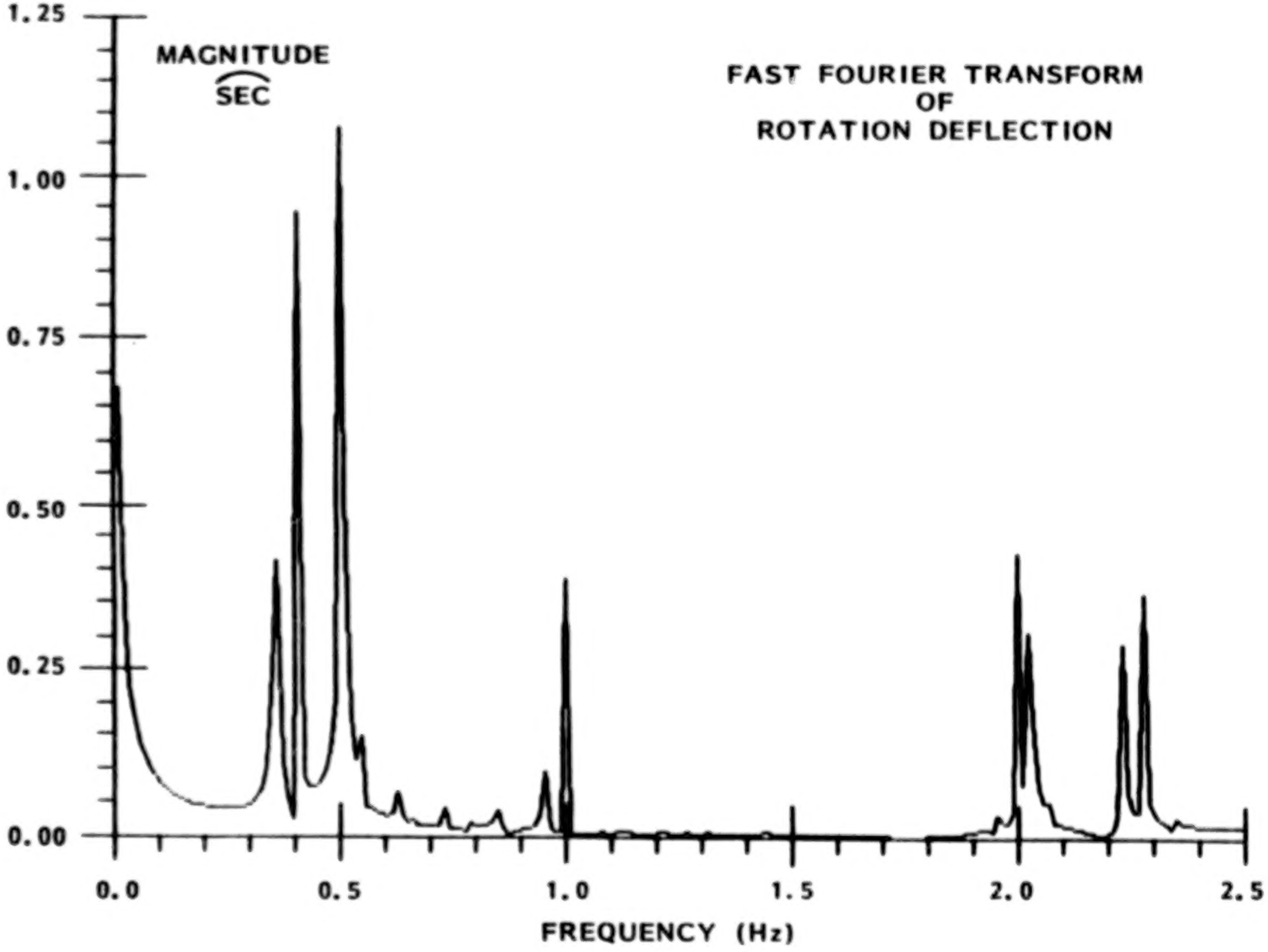

FAST FOURIER TRANSFORM
OF
ROTATION DEFLECTION

LINEAR ACCELERATION FFT

Another time history of worst case linear acceleration (ft/sec^2) was analyzed using the FFT process and the result is shown in this figure. Linear accelerations act through center-of-gravity offsets on the payload mass and cause disturbance torques about the gimbal axes. These torques cause additional pointing errors. The large peaks at 1 HZ and 2 HZ are caused by treadmill operations. Isolation of the treadmill will lower these peaks.

GENERAL
ELECTRIC

LINEAR ACCELERATION FFT

SPACE SYSTEMS DIVISION

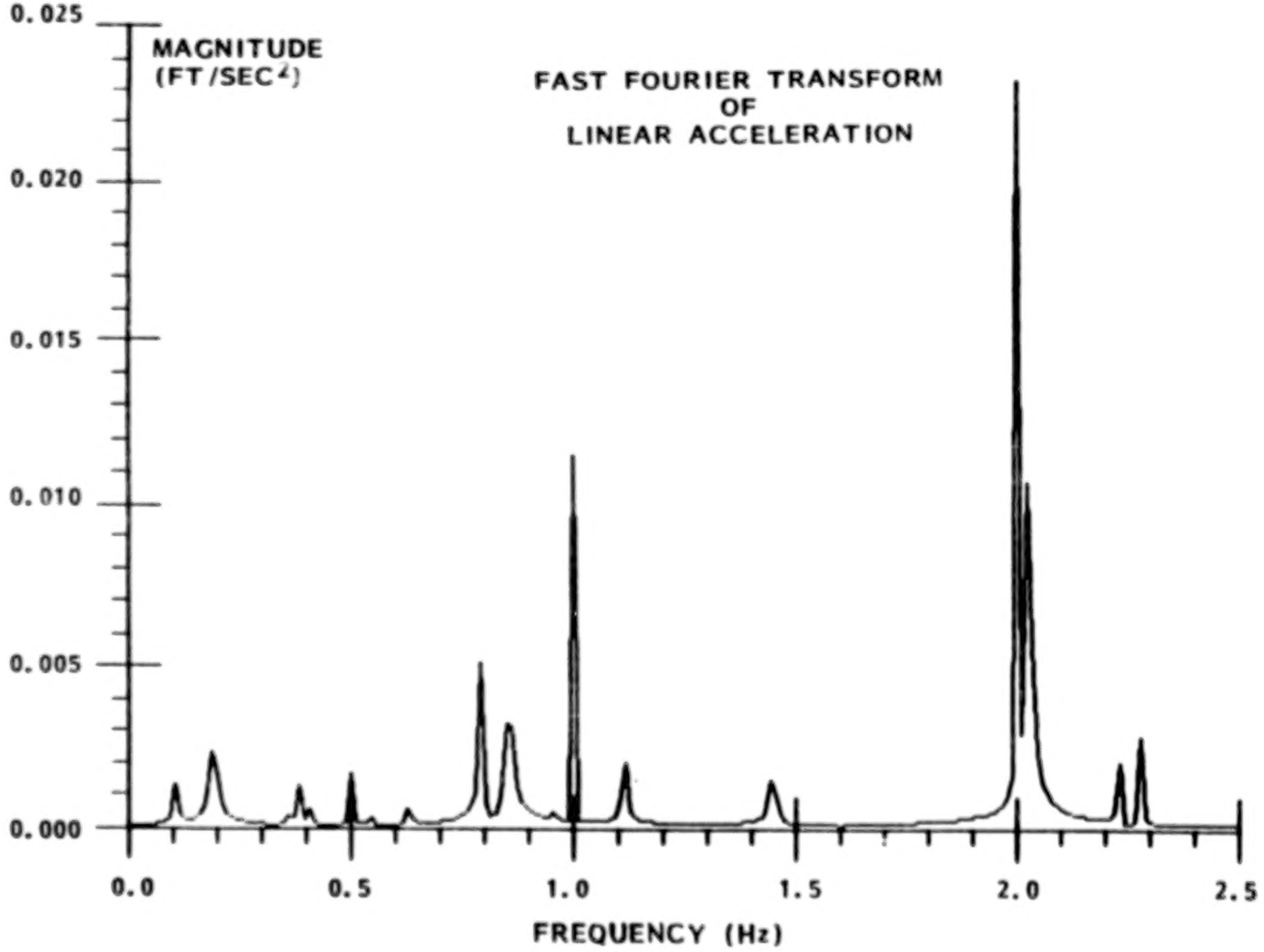

DYNAMIC MODEL

The type of controller chosen for the conceptual design of the PPS is the classic Proportional - Integral - Derivative (PID). This control design is not optimal and other techniques probably could provide higher performance; however, the PID design is well understood and provided needed versatility in the early stages of analysis. Major assumptions for the model included no non-linearities, no noise, no sampling effects, no flexibility problems, perfect torque motor, no cable wrap-up torques, and perfectly known orbital velocity. The accelerometer provided the capability for introducing a feed-forward signal into the loop.

GENERAL ELECTRIC

DYNAMIC MODEL

SPACE SYSTEMS DIVISION

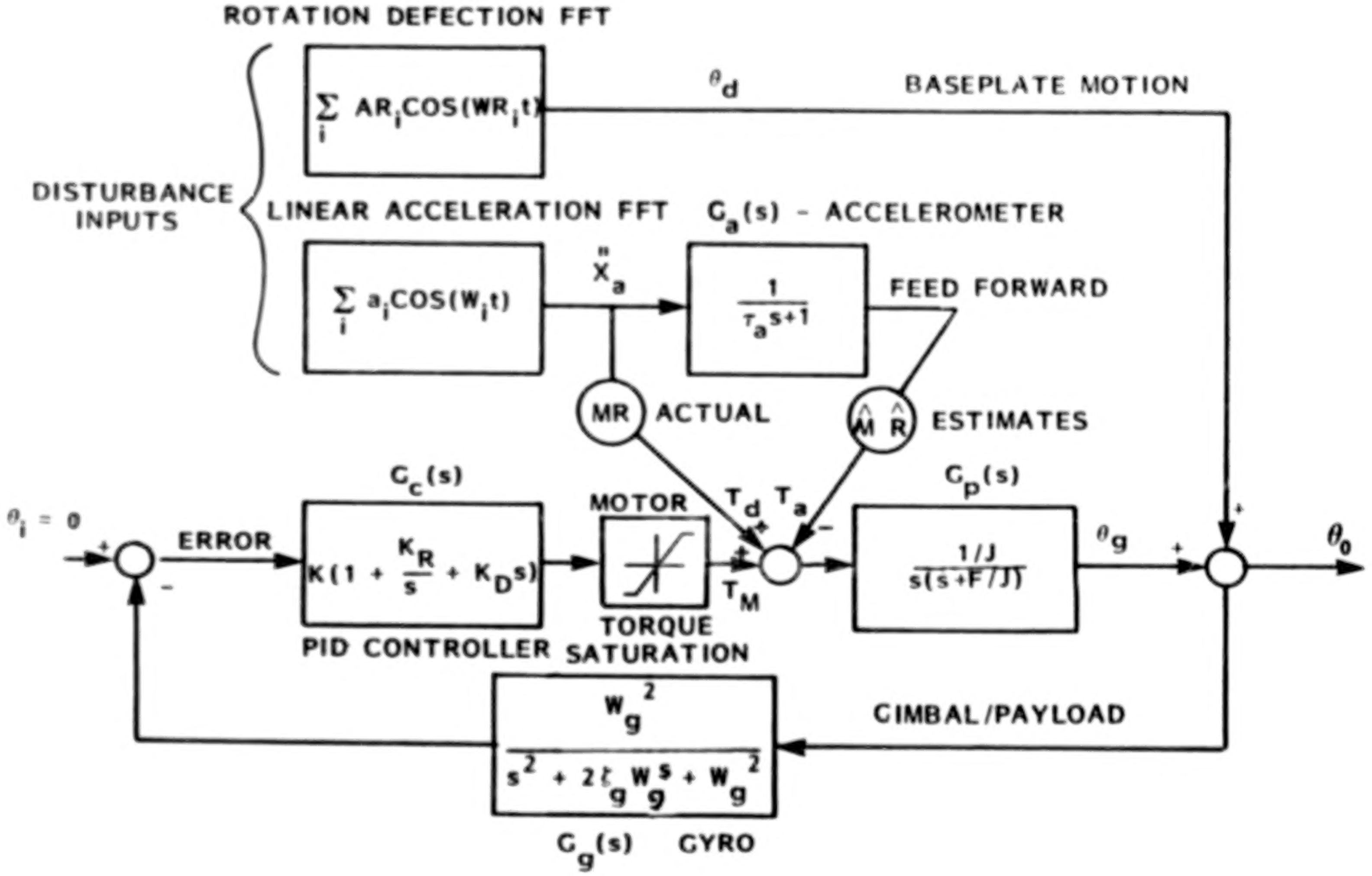
ROTATION DEFECTION FFT
$\sum_i AR_i \cos(WR_i t)$
θ_d
BASEPLATE MOTION
DISTURBANCE INPUTS
LINEAR ACCELERATION FFT
$G_a(s)$ - ACCELEROMETER
$\sum_i a_i \cos(W_i t)$
$\ddot{X}_a$
$\frac{1}{\tau_a s+1}$
FEED FORWARD
MR
ACTUAL
$\hat{M}\hat{R}$
ESTIMATES
$G_c(s)$
MOTOR
T_d
T_a
$G_p(s)$
$\theta_i = 0$
+
-
ERROR
$K(1 + \frac{K_R}{s} + K_D s)$
+
+
-
T_M
$\frac{1/J}{s(s+F/J)}$
θ_g
+
+
θ_0
TORQUE SATURATION
PID CONTROLLER
$\frac{W_g^2}{s^2 + 2\zeta_g W_g s + W_g^2}$
CIMBAL/PAYLOAD
$G_g(s)$ GYRO

TYPICAL SIMULATION RESULTS

A time domain simulation model of the PPS dynamic system was developed and a typical simulation result is shown in the figure. It can be seen that the pointing error is about ±15 $\widehat{\text{sec}}$ while the base plate motion is about ±5 $\widehat{\text{sec}}$. This additional error is due to the CG offset. Nominal parameters are:

M = 2000 Kg
R = .1 m
J = 1100 slug - ft^2
F = 100 ft-lb/rad/sec
Bandwidth = 1 HZ

No Accelerometer Feedforward

GENERAL ELECTRIC

TYPICAL SIMULATION RESULTS

SPACE SYSTEMS DIVISION

CG OFFSET = .1m

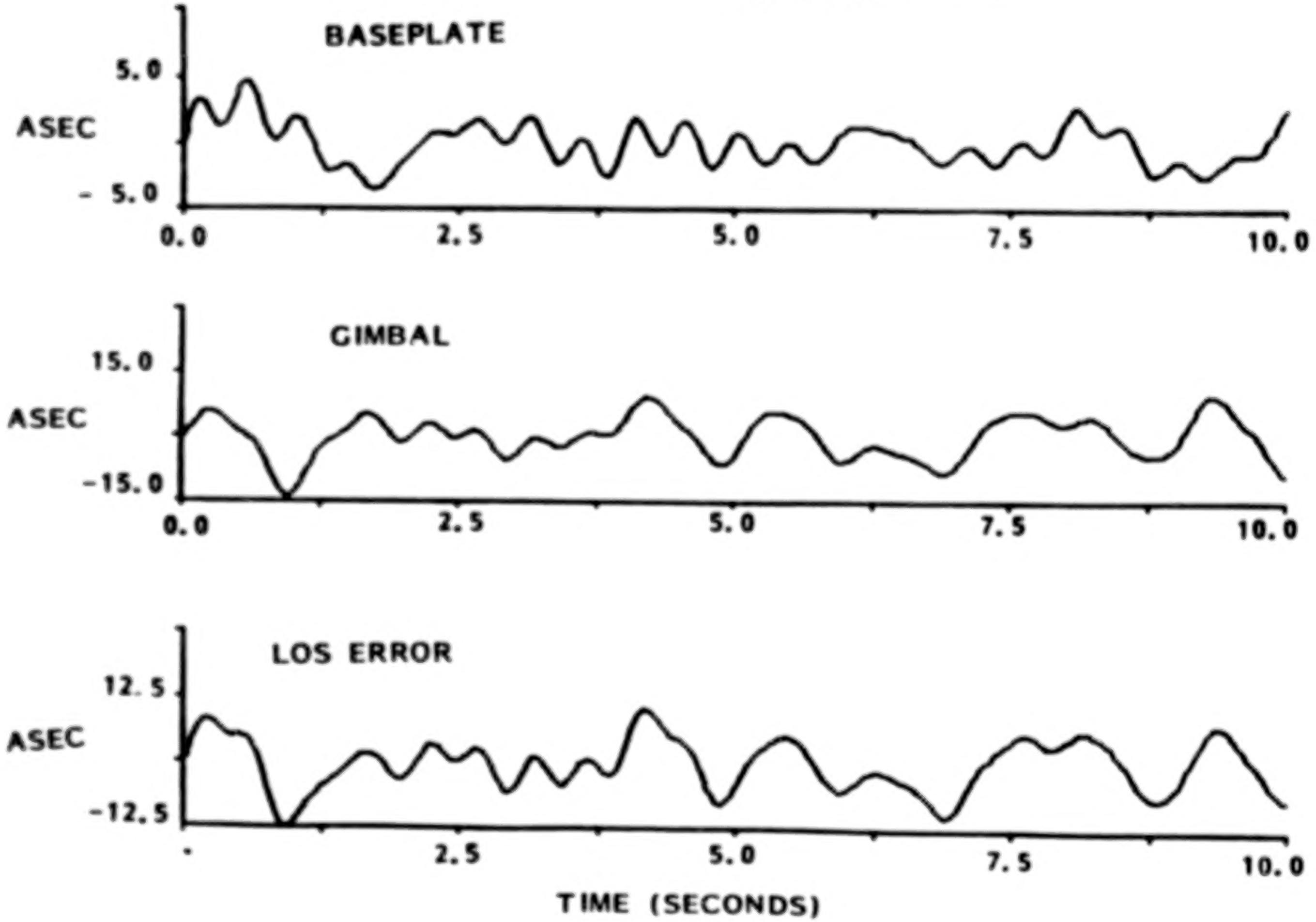

POINTING ERROR SENSITIVITY

One of the most important and descriptive parameters of a control system is its bandwidth. In general, bandwidth, or passband, is the range of frequencies that can pass through a control system. Bandwidth is defined herein as "the -3db point of the closed-loop transfer function". Many factors impact the bandwidth of a system and include: controller design, structural flexibilities, nonlinearities, component bandwidths, component noise characteristics, and gain/phase stability margin specifications.

Variations in pointing error or stability error are shown in the figure for different bandwidths and various CG offsets. It is estimated that there will be a ±.05m CG uncertainty on orbit even with the use of an on-line mass balancing system. Without such a balancing system, an error of about ±.2m is estimated.

POINTING ERROR SENSITIVITY

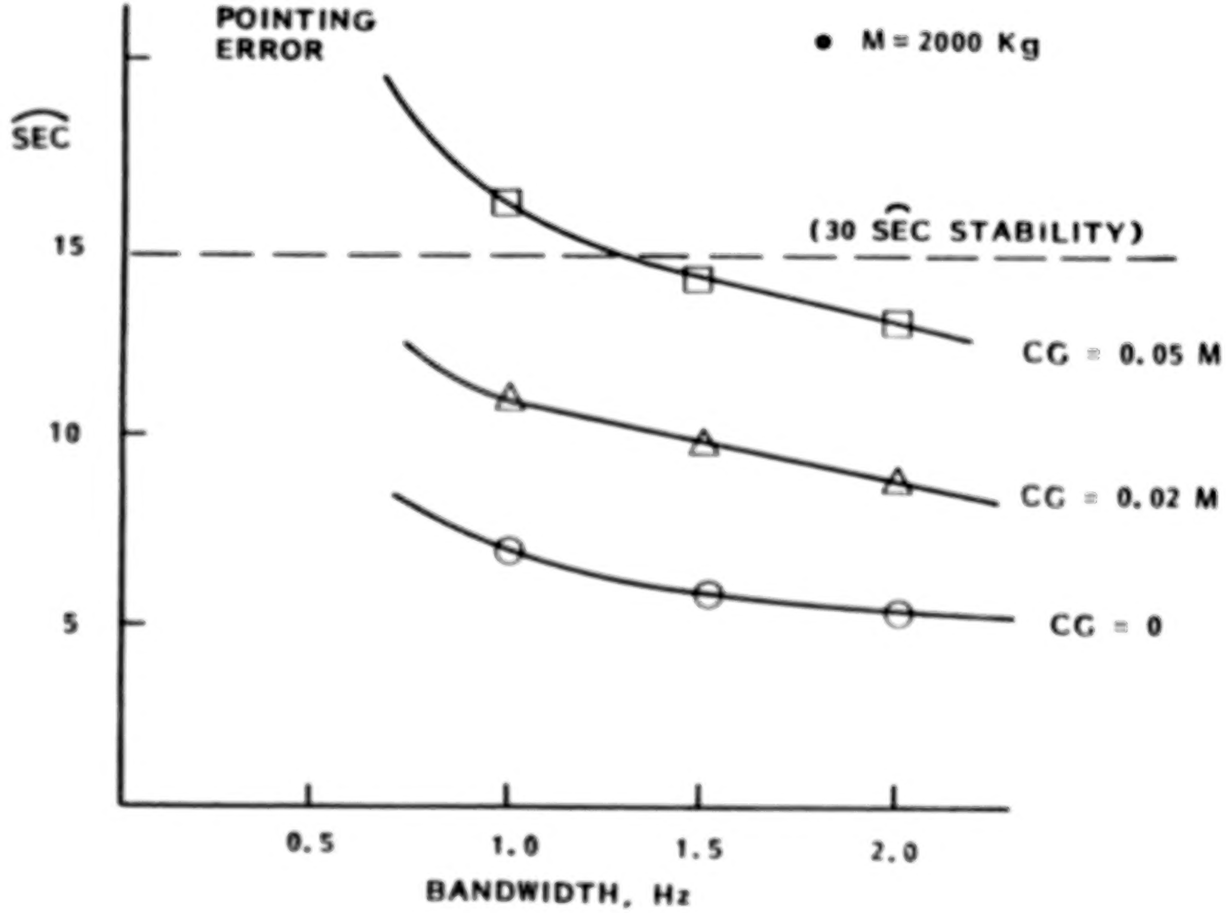

CONCLUSIONS

A study of the interface problems between the Space Station Structure (vibrations) and the Payload Pointing Control System was undertaken. A major goal of the study was to identify any bounding factors that might limit the achievement of required pointing accuracies. A major result is that the Space Station will have a disturbance-rich environment and background levels will be large enough to impact the pointing of some of the payloads. The need for an interface vibration specification between the structure and payloads was identified.

CONCLUSIONS

- PRELIMINARY INTERFACE STUDY BETWEEN SS STRUCTURE AND PAYLOAD POINTING SYSTEMS COMPLETED
  - BASIC RESULT - SS BACKGROUND OR QUIESCENT DISTURBANCE LEVEL IS LARGE ENOUGH TO IMPACT PAYLOAD POINTING.
  - IDENTIFIED NEED FOR SPECIFICATION OF VIBRATION LEVELS AT PAYLOAD INTERFACE.
- STUDY SOUGHT TO IDENTIFY BOUNDING PARAMETERS AND LIMITS
  - INCREASES IN CONTROL SYSTEM BANDWIDTHS CAN DECREASE POINTING ERRORS. HOWEVER, STATE-OF-ART COMPONENTS LIMIT BANDWIDTHS TO ABOUT 1-2 HZ.
  - MASS BALANCING SYSTEM REQUIRED - TO KEEP CG OFFSETS TO WITHIN ±.05 M.
  - DISTURBANCE FREQUENCIES OUTSIDE THE CONTROL BANDWIDTH INDUCE LARGEST ERRORS. ISOLATION OF OFFENDING SOURCES MAY BE REQUIRED.

N87
22734
UNCLAS

N87-22734

MANEUVERING AND VIBRATION CONTROL OF FLEXIBLE SPACECRAFT*

by

L. Meirovitch & R. D. Quinn

Virginia Polytechnic Institute & State University

Department of Engineering Science & Mechanics

Blacksburg, Virginia 24061

---

* Supported by the NASA Research Grant NAG-1-225 sponsored by the Spacecraft Control Branch, Langley Research Center.

PRECEDING PAGE BLANK NOT FILMED

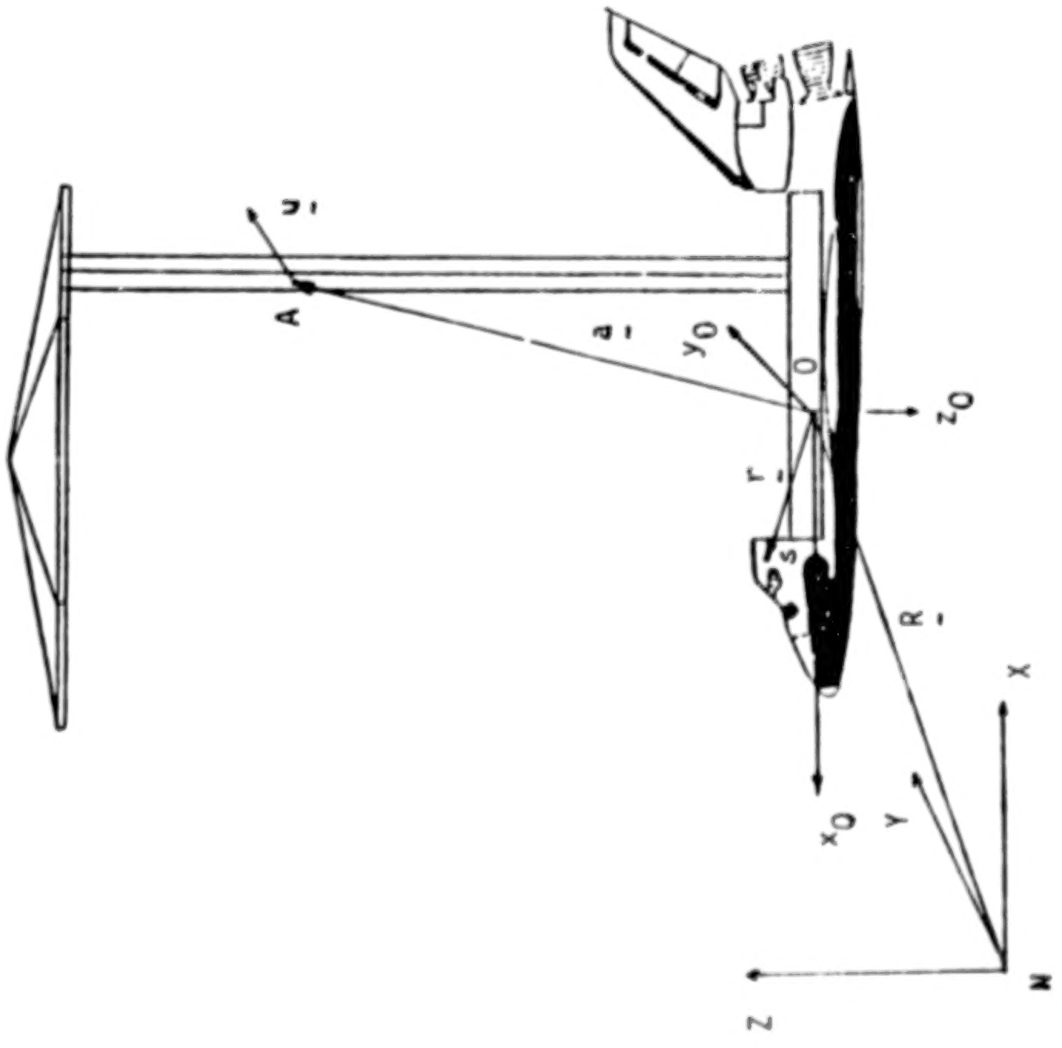
y
A
a
y0
O
z0
r
s
R
X
Y
x0
Z

Figure 1. Spacecraft in Orbit

EQUATIONS OF MOTION

Position and Velocity of Point S: $\underset{\sim}{R}_S = \underset{\sim}{R} + \underset{\sim}{r}$, $\dot{\underset{\sim}{R}}_S = \dot{\underset{\sim}{R}} + \underset{\sim}{\omega} \times \underset{\sim}{r}$

Position and Velocity of Point A: $\underset{\sim}{R}_A = \underset{\sim}{R} + \underset{\sim}{a} + \underset{\sim}{u}$, $\dot{\underset{\sim}{R}}_A = \dot{\underset{\sim}{R}} + \underset{\sim}{\omega} \times (\underset{\sim}{a} + \underset{\sim}{u}) + \dot{\underset{\sim}{u}}$

$\dot{\underset{\sim}{R}}, \underset{\sim}{\omega}$ = translational and angular velocities of frame $x_0y_0z_0$

$\underset{\sim}{u} = \phi \underset{\sim}{q}$ = elastic displacement vector

Lagrange's Equations: $\frac{d}{dt}\left(\frac{\partial T}{\partial \dot{\underset{\sim}{R}}}\right) + \frac{\partial V}{\partial \underset{\sim}{R}} = C^T \underset{\sim}{F}$, $\frac{d}{dt}\left(\frac{\partial T}{\partial \dot{\underset{\sim}{\alpha}}}\right) - \frac{\partial T}{\partial \underset{\sim}{\alpha}} + \frac{\partial V}{\partial \underset{\sim}{\alpha}} = D^T \underset{\sim}{M}$

$$\frac{d}{dt}\left(\frac{\partial T}{\partial \dot{\underset{\sim}{q}}}\right) - \frac{\partial T}{\partial q} + \frac{\partial V}{\partial q} = \underset{\sim}{Q}$$

C = transformation matrix from XYZ to $x_0y_0z_0$

D = matrix of Euler's angles $\alpha_1, \alpha_2, \alpha_3$ $(\underset{\sim}{\omega} = D(\underset{\sim}{\alpha})\dot{\underset{\sim}{\alpha}})$

CONTROL STRATEGY

Rigid-body motions are relatively large.

Elastic deformations are relatively small.

∴ Design a maneuver strategy as if the structure were rigid.

Then, design feedback control to suppress elastic deformations and deviations from the rigid-body maneuver.

Use a perturbation approach to separate the zero-order terms (rigid-body maneuver) from the first-order terms (elastic vibration and deviations from the rigid-body maneuver).

PERTURBATION METHOD

First-Order Perturbation: $\underset{\sim}{R} = \underset{\sim}{R}_0 + \underset{\sim}{R}_1$, $\underset{\sim}{\alpha} = \underset{\sim}{\alpha}_0 + \underset{\sim}{\alpha}_1$

Perturbed Angular Velocity Vector: $\underset{\sim}{\omega} = \underset{\sim}{\omega}_0 + \underset{\sim}{\omega}_1$, $\underset{\sim}{\omega}_1 = \tilde{\underset{\sim}{\omega}}_0^T\underset{\sim}{\beta} + \dot{\underset{\sim}{\beta}}$

$\underset{\sim}{\beta}$ = small angular deflection vector expressed in $x_0y_0z_0$ components

Zero-Order Equations (Rigid Structure):

$$m\ddot{\underset{\sim}{R}}_0 + C_0^T\tilde{S}_0\dot{\underset{\sim}{\omega}}_0 + C_0^T\tilde{\omega}_0^T\tilde{S}_0\underset{\sim}{\omega}_0 + \frac{Gm_e}{|\underset{\sim}{R}_0|^3}\left[m\underset{\sim}{R}_0 + (I - 3\hat{\underset{\sim}{R}}_0\hat{\underset{\sim}{R}}_0^T)C_0^T\underset{\sim}{S}_0\right] = C_0^T\underset{\sim}{F}_0$$

$$\tilde{S}_0^T C_0\ddot{\underset{\sim}{R}}_0 + \frac{Gm_e}{|\underset{\sim}{R}_0|^3}\tilde{S}_0^T C_0\underset{\sim}{R}_0 + I_0\dot{\underset{\sim}{\omega}}_0 + \tilde{\omega}_0^T I_0\underset{\sim}{\omega}_0 = \underset{\sim}{M}_0$$

First-Order Perturbation Equation: $M\ddot{\underset{\sim}{x}} + G\dot{\underset{\sim}{x}} + (K_S + K_{NS})\underset{\sim}{x} = \underset{\sim}{F}^*$

$\underset{\sim}{x} = [\underset{\sim}{R}_1^T \;\; \underset{\sim}{\beta}^T \;\; \underset{\sim}{q}^T]^T$ = perturbation vector

$\underset{\sim}{F}^* = [\underset{\sim}{F}_1^T \;\; \underset{\sim}{M}_1^T \;\; \underset{\sim}{Q}_0^T + \underset{\sim}{Q}_1^T]^T$ = perturbing force vector

RIGID-BODY MANEUVER

Rigid-body maneuver is designed independently of vibration control.

Strategy: single-axis, minimum-time maneuver.

Maneuver Force Distribution Producing Rigid-Body Motion Only:

$$F_1(p,t) = x(p)m(p)\dot{\theta}^2(t)$$

$$F_2(p,t) = -z(p)m(p)\ddot{\theta}(t)$$

$$F_3(p,t) = y(p)m(p)\ddot{\theta}(t)$$

$\theta(t)$ = desired angular motion

$m(p)$ = mass density

$x(p)$, $y(p)$, $z(p)$ = coordinates of p relative to center of rotation

QUASI-MODAL EQUATIONS

Coordinate Transformation: $\underset{\sim}{x}(t) = X\underset{\sim}{u}(t)$

X = rectangular matrix of lower premaneuver eigenvectors

Quasi-Modal Equations: $\ddot{\underset{\sim}{u}}(t) + \bar{G}(t)\dot{\underset{\sim}{u}}(t) + [\Lambda + \bar{K}(t)]\underset{\sim}{u}(t) = \underset{\sim}{f}(t)$

$\underset{\sim}{u}(t)$ = vector of quasi-modal coordinates

$\underset{\sim}{f}(t) = X^T\underset{\sim}{F}^*(t)$ = vector of quasi-modal forces

$\bar{G}(t) = X^T G(t) X$ = reduced-order gyroscopic matrix

$\Lambda = X^T K_0 X$ = matrix of premaneuver eigenvalues

$\bar{K}(t) = X^T K_t(t) X$ = reduced-order stiffness matrix

As maneuver velocity decreases, time-varying terms decrease and equations approach an uncoupled form.

VIBRATION CONTROL

Modal Equations: $\ddot{u}_r(t) + \omega_r^2 u_r(t) = f_r(t) + f_{dr}(t)$

$f_r(t)$ = modal control force

$f_{dr}(t)$ = modal disturbance and maneuver control force (to be neglected)

Actuator Dynamics: $\dot{\underset{\sim}{F}}(t) = a\underset{\sim}{F}(t) + b\underset{\sim}{F}_c(t)$

$\underset{\sim}{F}_c(t)$ = command force vector

Modal Actuator Dynamics: $\dot{f}_r(t) = af_r(t) + bf_{cr}(t)$

Modal State Equations: $\dot{\underset{\sim}{z}}_r(t) = A_r \underset{\sim}{z}_r(t) + \underset{\sim}{b} f_{cr}(t)$

$$\underset{\sim}{z}_r = [u_r \ \dot{u}_r \ \ddot{u}_r]^T \ , \ \underset{\sim}{b} = [0 \ 0 \ b]^T \quad A_r = \begin{bmatrix} 0 & 1 & 0 \\ 0 & 0 & 1 \\ a\omega_r^2 & -\omega_r^2 & a \end{bmatrix}$$

VIBRATION CONTROL (CONT'D)

i. Optimal Control. Performance Index: $J = \sum_{r=1}^{\infty} \int_0^{\infty} (\underset{\sim}{z}_r^T Q_r \underset{\sim}{z}_r + R_r f_{cr}^2)dt$

$Q_r = \mathrm{diag}\,[q_r\ 1\ 1]$

Feedback Control Law: $f_{cr} = -\frac{1}{R_f} \underset{\sim}{b}^T K_r \underset{\sim}{z}_r = -g_{r1}u_r - g_{r2}\dot{u}_r - g_{r3}\ddot{u}_r$

K_r = 3·3 symmetric matrix satisfying steady-state matrix Riccati equation.

Modal Gains: $g_{r1} = bk_{r13}/R_r$, $g_{r2} = bk_{r23}/R_r$, $g_{r3} = bk_{r33}/R_r$

ii. Pole Allocation: Closed-Loop Poles:

$s_{r1} = \alpha_r + i\beta_r,\ s_{r2} = \alpha_r = i\beta_r,\ s_{r3} = \gamma_r$

Modal Gains: $g_{r1} = \frac{1}{b}\,[\text{[illegible]}_r^2 - \gamma_r(\alpha_r^2 + \beta_r^2)]$,

$g_{r2} = \frac{1}{b}\,[2\gamma_r\alpha_r + \alpha_r^2 + \beta_r^2 - \omega_r^2),\ g_{r3} = \frac{1}{b}\,(a - 2\alpha_r - \gamma_r)$

iii. Direct Feedack Control: $\underset{\sim}{F}_C = -M(g_1\underset{\sim}{x} + g_2\dot{\underset{\sim}{x}} + g_3\ddot{\underset{\sim}{x}})$

Gains for Uniform Damping: $g_1 = -a\alpha^2/b,\ g_2 = (2a\alpha + a^2)/b,\ g_3 = -2\alpha/b$

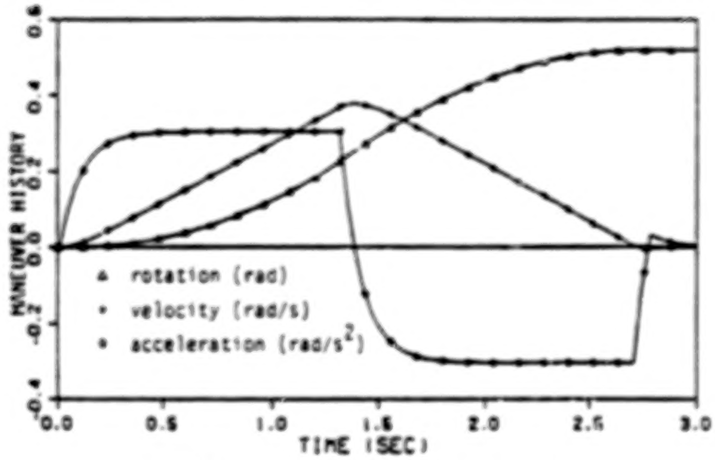

a) 30° roll, M_{max} = 20 ft-lb.

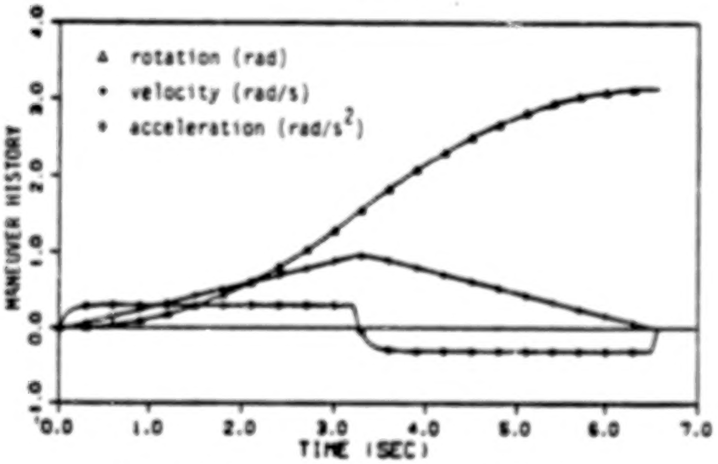

b) 180° roll, M_{max} = 20 ft-lb.

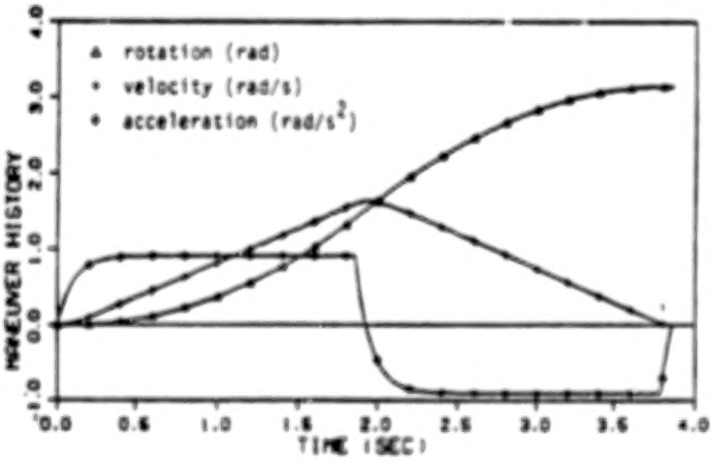

c) 180° roll, M_{max} = 60 ft-lb.

Figure 3. Comparison of Maneuver Strategies

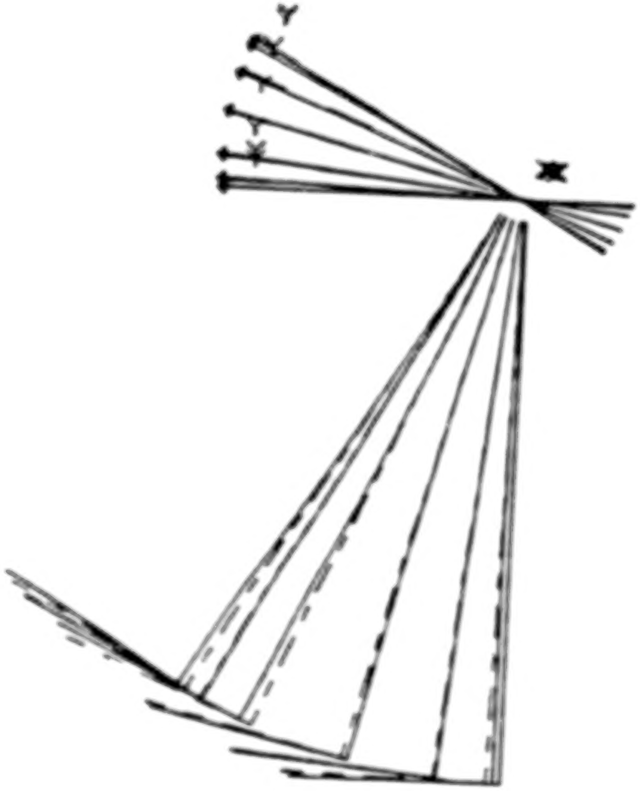

Figure 5. Time-Lapse Plot of 30° Roll Maneuver (No Vibration Control)

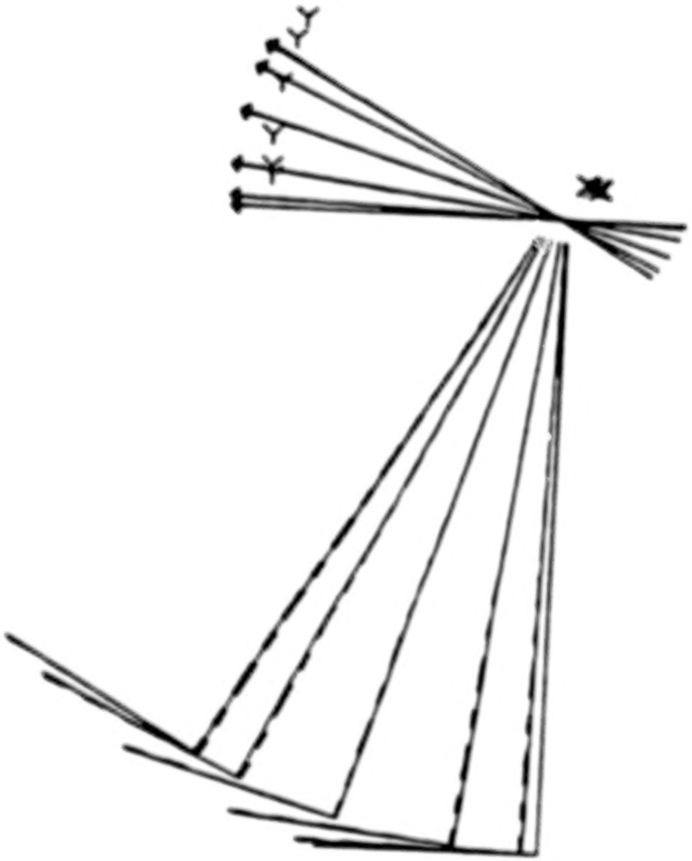

Figure 6. Time-Lapse Plot of 30° Roll Maneuver (Uniform Damping Using 10 Actuators)

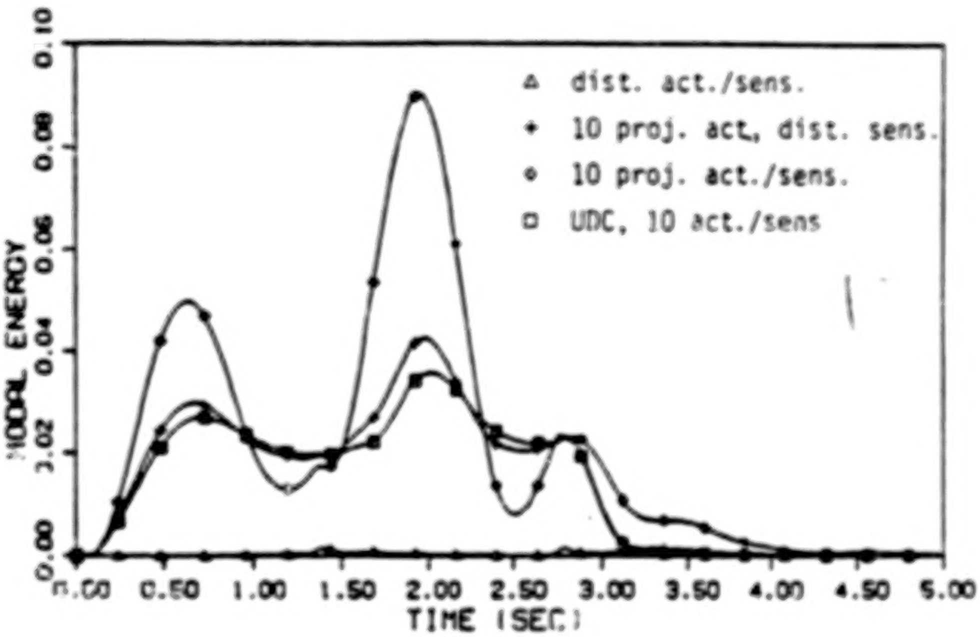

a) Energy

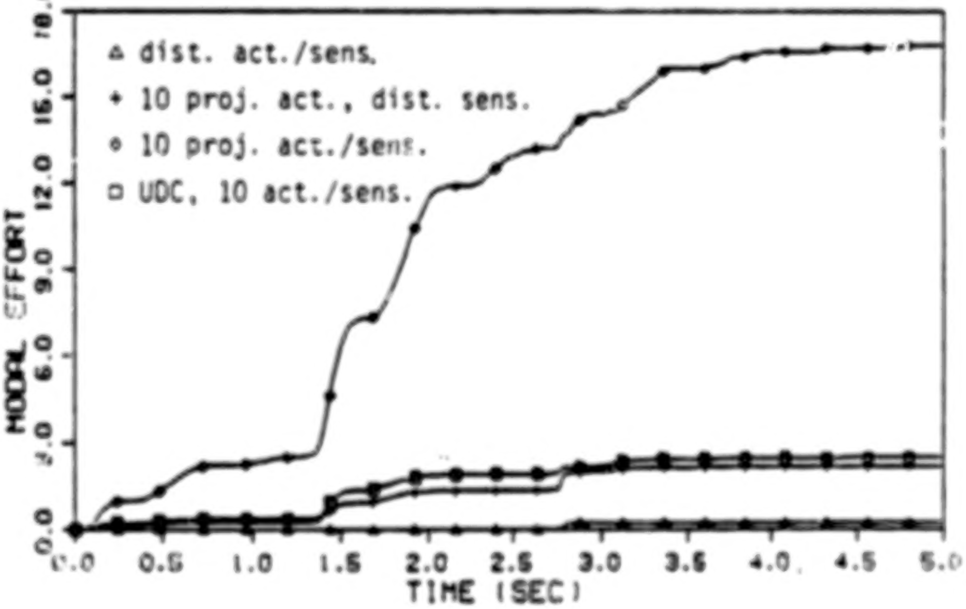

b) Effort

Figure 7. Comparison of Various Vibration Control Implementation Procedures for 30° Roll Maneuver

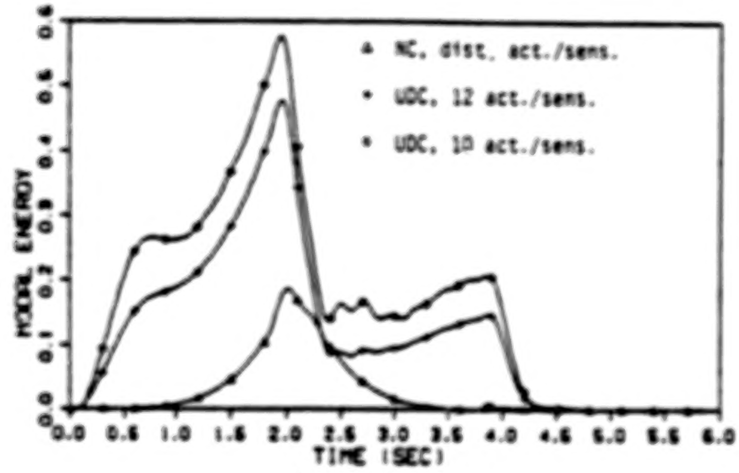

a) Energy

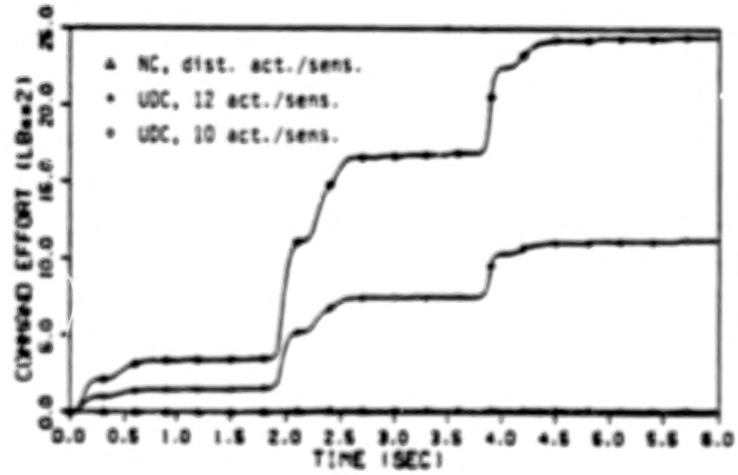

b) Effort

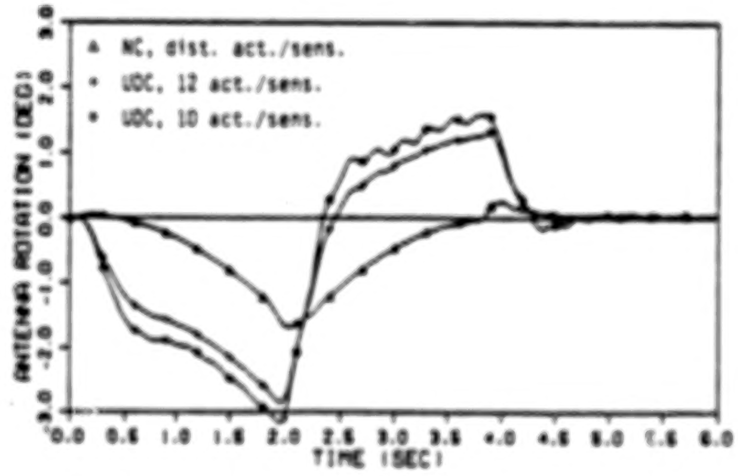

c) Antenna hub rotation in x_0 direction

Figure 12. Implementation of 180° Maneuver with Various Numbers of Actuators

N87
22735
UNCLAS

N87-22735

A TREETOPS SIMULATION OF THE HUBBLE SPACE TELESCOPE-HIGH GAIN ANTENNA INTERACTION

JOHN P. SHARKEY
NASA/MARSHALL SPACE FLIGHT CENTER
HUNTSVILLE, AL

WORKSHOP ON STRUCTURAL
DYNAMICS AND CONTROL INTERACTION
OF FLEXIBLE STRUCTURES
APRIL 22-24, 1986
MARSHALL SPACE FLIGHT CENTER, AL

PRECEDING PAGE BLANK NOT FILMED

C-3

A TREETOPS SIMULATION OF THE HUBBLE SPACE TELESCOPE - HIGH GAIN ANTENNA INTERACTION

Virtually any project dealing with the control of a Large Space Structure (LSS) will involve some level of verification by digital computer simulation. While the Hubble Space Telescope might not normally be included in a discussion of LSS, it is presented at this workshop to highlight a recently developed simulation and analysis program named TREETOPS. This program was developed by Honeywell, Inc. under sponsorship of a Marshall Space Flight Center research and development program called Augmented Flexible Body Dynamics Analysis Program (AFBDAP). TREETOPS, the second program to be developed under AFBDAP, provides digital simulation, linearization and control system interaction of flexible, multibody spacecraft which admit to a point-connected tree topology. The HST application of TREETOPS is intended here to familiarize the LSS community with TREETOPS by presenting a user's perspective of its key features.

Figure 1 outlines some of the outstanding features of TREETOPS. The program is intended as a tool for evaluating the interaction of a LSS and its associative control system. The program

SYSTEMS DYNAMICS LAB	MARSHALL SPACE FLIGHT CENTER OAST RTOP REVIEW CONTROL TECHNOLOGY/GUIDANCE CONCEPTS	J. SHARKEY OCTOBER 1985

NONLINEAR DYNAMICS

SIMULATION OF NONLINEAR DYNAMICS AND CONTROL

OBJECTIVE: PROVIDE AN EFFICIENT MEANS FOR FLEXIBLE BODY CONTROL SYSTEM ANALYSIS OF COMPLEX SPACECRAFT.

APPROACH: HONEYWELL'S AUGMENTED FLEXIBLE BODY DYNAMIC ANALYSIS PROGRAM.

FEATURES:
- NONLINEAR TIME DOMAIN SOLUTION ENCOMPASSING LARGE ANGLES AND LARGE ANGULAR RATES.
- DYNAMICS FORMULATED VIA KANE's METHOD OF GENERALIZED SPEEDS.
- ELIMINATES CONSTRAINED DEGREES OF FREEDOM (D.O.F.).
- ADMITS ARBITRARY, POINT-CONNECTED TOPOLOGIES (CHAIN, TREE, RING).
- STRUCTURE CONNECTED BY ARTICULATED JOINTS WITH ZERO TO SIX D.O.F.
- COMPONENT MODES OF EACH FLEXIBLE BODY ARE UTILIZED.
- LINEARIZED, STATE VARIABLE SYSTEM MATRICES PROVIDED.
- INTERACTIVE PREPROCESSOR PROGRAM GENERATES INPUT DATA BASE.

FIGURE 1

alleviates the control system analyst of the burden of generating the equation of motion (EOM) for flexible, multibody spacecraft. This is accomplished with the Singh-Likins formulation of Kane's method of generalized speeds. This formulation is amenable to the automatic generation of minimal order EOM which eliminate constrained degrees of freedom. The structure is modeled with articulated joints allowing zero to six degrees of freedom. Component modes are used to model flexible substructures, thereby permitting large relative angles and relative rates. Since the system equations are in general nonlinear, a linearization subprogram is provided which generates the linear system matrices suitable for control law development. An interactive preprocessor program is also provided which generates and edits the input data base in an easy to use, menu driven fashion.

The development history of AFBDAP is presented in figure 2. The first simulation program, simply named AFBDAP, was released in 1982. This was a proof of concept program applicable to structures with a chain topology. In 1984, TREETOPS was released featuring the linearization subprogram, an improved interactive preprocessor, an interactive postprocessor for plotting, and the ability to model structures with a tree topology. A limited, closed tree topology modeling capability

ORGANIZATION SYSTEMS DYNAMICS LAB	MARSHALL SPACE FLIGHT CENTER OAST RTOP REVIEW	NAME J. SHARKEY
CHART NO	CONTROL TECHNOLOGY/GUIDANCE CONCEPTS	DATE OCTOBER 1985

NONLINEAR DYNAMICS

DEVELOPMENT HISTORY

1982 AUGMENTED FLEXIBLE BODY DYNAMICS ANALYSIS PROGRAM (AFBDAP)
- PROOF OF CONCEPT
- CHAIN TOPOLOGIES

1984 TREETOPS
- IMPROVED COMPUTATIONAL EFFICIENCY
- TREE TOPOLOGIES
- LOOP CLOSURE SPRINGS

1986 CONTOPS
- CLOSED TOPOLOGIES
- EQUALITY AND/OR INEQUALITY CONSTRAINTS

FIGURE 2

was provided through the use of "loop closure spring," whereby spring force constraints were accommodated, but not kinematic constraints. The CONTOPS program was released in early 1986 as the final product of AFBDAP. CONTOPS admits structures with constrained topologies; both holonomic constraints, such as loop closures or prescribed velocities, and nonholonomic constraints such as Coulomb damping, gimbal stops, etc. Since CONTOPS is still in the verification phase, this presentation will concentrate on TREETOPS.

The basic TREETOPS program structure is shown in figure 3. Working from left to right, HITIP is the interactive preprocessor used to create, edit and error-check the problem specific input data base, which is subsequently read into the basic simulation/linearization program, TREETOPS. HITIP creates and edits two other files, a machine dependent job control file and a parameter dimension file used in compiling the ANSI FORTRAN TREETOP program. The simulation/linearization program, which is usually run in a batch mode, generates three output files: a time-history output file, a linear system matrix file, and a restart file. The restart file can later be used to continue the simulation, perhaps to perform parameter variation studies about a nominal operating point. The output and linear matrice files can be examined with the postprocessor program TREEPLOT.

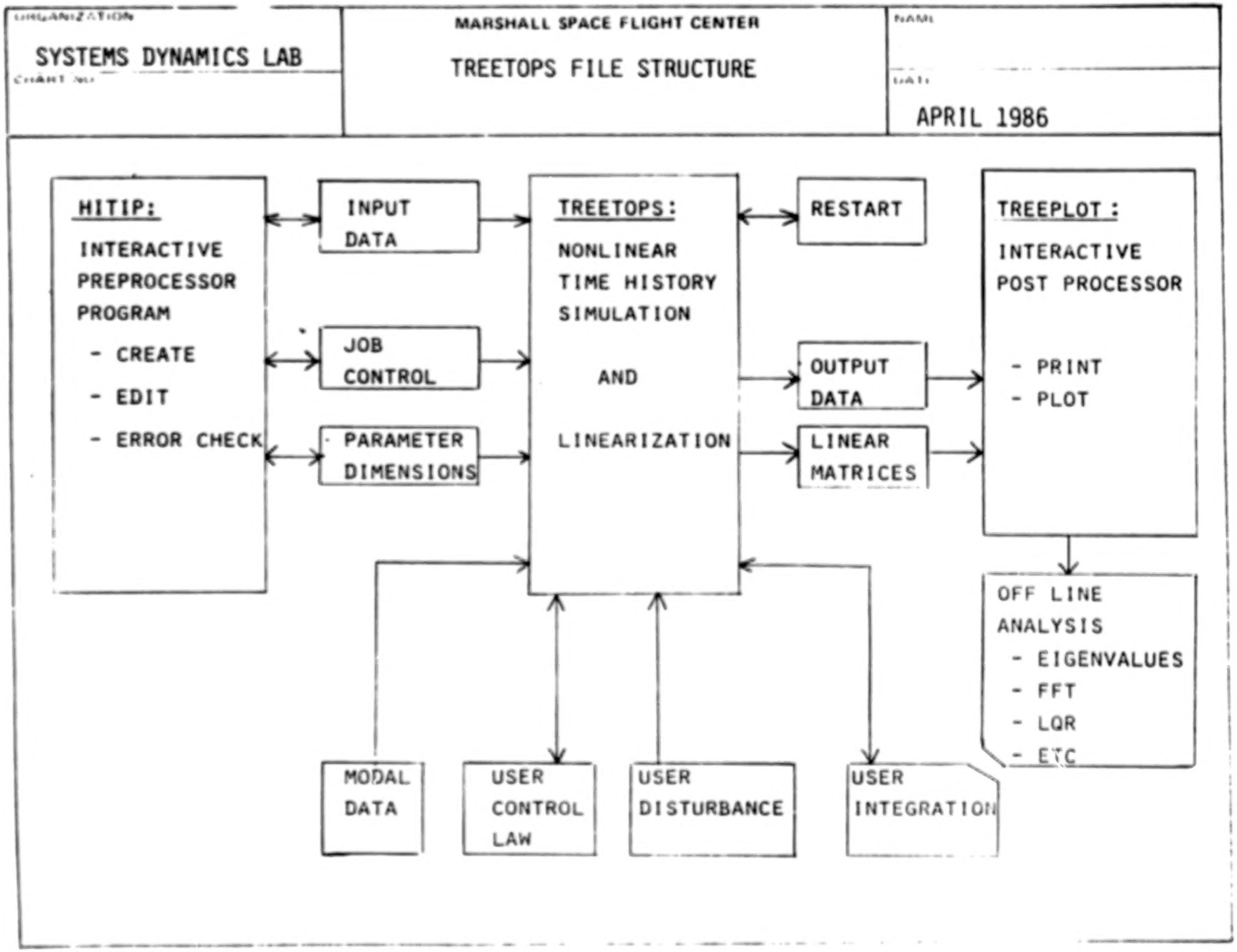
ORGANIZATION
SYSTEMS DYNAMICS LAB
CHART NO.
MARSHALL SPACE FLIGHT CENTER
TREETOPS FILE STRUCTURE
NAME
DATE
APRIL 1986
HITIP:
INTERACTIVE PREPROCESSOR PROGRAM
- CREATE
- EDIT
- ERROR CHECK
INPUT DATA
JOB CONTROL
PARAMETER DIMENSIONS
TREETOPS:
NONLINEAR TIME HISTORY SIMULATION
AND
LINEARIZATION
RESTART
OUTPUT DATA
LINEAR MATRICES
TREEPLOT :
INTERACTIVE POST PROCESSOR
- PRINT
- PLOT
OFF LINE ANALYSIS
- EIGENVALUES
- FFT
- LQR
- ETC
MODAL DATA
USER CONTROL LAW
USER DISTURBANCE
USER INTEGRATION

FIGURE 3

Alternatively, these files can be analyzed off-line to determine eigenvalues, FFT's, LQR's, etc.

The simulation program can also interface with up to four user supplied files: (1) a model data input file, (2) a user supplied control law, (3) a disturbance algorithm, and (4) alternate integration programs as an option to the standard Runga-Kutta four pass.

Figure 4 depicts the conceptual components of a TREETOPS model. The HITIP program allows the user to interactively select the components listed in figure 4 and assemble them into a multibody structure with control laws, sensors and actuators. Function generators can be treated as controller inputs or system disturbances. The control law can be any combination of continuous, discrete or user defined segments. The continuous and discrete controllers are composed of transfer functions (in S or Z), summing junctions and gain blocks. The controllers can be arbitrarily interconnected or tied to any of the ideal actuators listed. The structure is composed of flexible and/or rigid bodies, rotation and translational hinges, and loop closure springs. The bodies are defined on an independent basis, with user defined local coordinate frame locations and orientations. The hinges are used to define Euler angles for

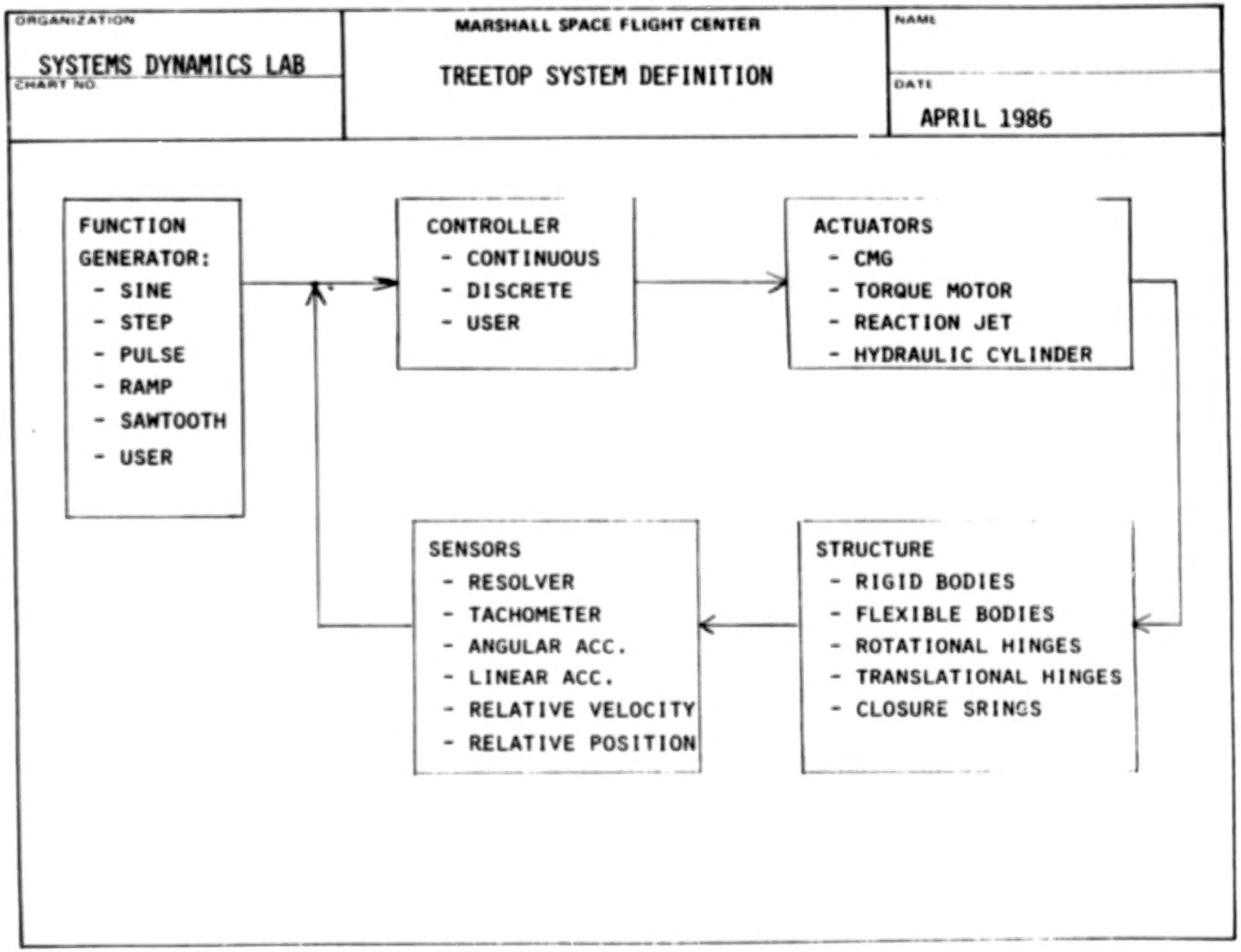
ORGANIZATION
SYSTEMS DYNAMICS LAB
CHART NO.
MARSHALL SPACE FLIGHT CENTER
TREETOP SYSTEM DEFINITION
NAME
DATE
APRIL 1986
FUNCTION GENERATOR:
- SINE
- STEP
- PULSE
- RAMP
- SAWTOOTH
- USER
CONTROLLER
- CONTINUOUS
- DISCRETE
- USER
ACTUATORS
- CMG
- TORQUE MOTOR
- REACTION JET
- HYDRAULIC CYLINDER
SENSORS
- RESOLVER
- TACHOMETER
- ANGULAR ACC.
- LINEAR ACC.
- RELATIVE VELOCITY
- RELATIVE POSITION
STRUCTURE
- RIGID BODIES
- FLEXIBLE BODIES
- ROTATIONAL HINGES
- TRANSLATIONAL HINGES
- CLOSURE SRINGS

FIGURE 4

coordinate transformations. Like the actuators, the sensors also represent ideal devices while the sensor and actuator dynamics can be built into the control law definitions.

Figure 5 presents a segment of the input data base generated by HITIP for the HST TREETOP simulation. Body 1 data is identified as a flexible body which has seven node points and six modes. Hinge 1 is a "fictitious hinge" which connects the base body of a model (always labeled at 1) to the inertial frame, herewith six degree of freedom. Hinge 2 is a single degree of freedom hinge which connects body 2 to body 1. All of the input data appears in a similar format, wherein the user merely fills in the blank of the menu driven preprocessor. Table 1 describes the set of modal data required for each flexible body.

Figure 6 depicts the TREETOPS model of the HST with two High Gain Antennas (HGA's) mounted on flexible masts. Body 1 represents the core of the HST along with the two solar array panels. Bodies 2 and 5 represent 3.27 meter, deployable masts which also serve as waveguides for the antenna RF signals. Each antenna is connected to the mast through a pair of orthogonal, single axis gimbals with dc torque motors. The table on the lower right identifies the vibration frequencies of each

ORIGINAL PAGE IS
OF POOR QUALITY

EXAMPLE OF INPUT DATA FOR HST/HGA TREETOPS MODEL

```
331.000  BODY    0  1 Type of body (R=rigid, F=flexible),ID8           :  F             1.0000
332.000  BODY    0  1 Mass of body (kg)                                :   10881.
333.000  BODY    0  1 Inertia (kg-m2) Ixx,Iyy,Izz                      :   32160.        88772.        83771.
334.000  BODY    0  1 Inertia (kg-m2) Ixy,Ixz,Iyz                      :  -28.000       -1263.0       -5.0000
335.000  BODY    0  1 modal data option (T=tape,D=disc),fname and tape8 :  D            HGATWO:TAPE
336.000  BODY    0  1 Modal inertia opt (N=none,I=inertia M,H,P dyadics):  N
337.000  BODY    0  1 Modal coupling opt (N=none,C=coupling PHIXPHI vec):  N
338.000  BODY    0  1 Number of flexible modes                         :   0.0000
339.000  BODY    0  1 Attach point coordinates (m) x,y,z               :   .00000        .00000        .00000
340.000  BODY    0  1 NODE    1 mass center coordinates (m) x,y,z      :   .00000        .00000        .00000
341.000  BODY    0  1 NODE    2 coordinates (m) x,y,z                  :   1.7617        .00000        1.9736
342.000  BODY    0  1 NODE    3 coordinates (m) x,y,z                  :   1.7617        .00000       -1.9736
343.000  BODY    0  1 NODE    4 coordinates (m) x,y,z                  :   .63430        1.3048        1.3048
344.000  BODY    0  1 >>>>>$$$$$ END OF DATA $$$$$<<<<<                :
345.000  BODY    0  1 >>>>>$$$$$ END OF DATA $$$$$<<<<<                :
106.000  HINGE   0  1 ID8 of hinge, ID8 of inbd body, ID8 of outbd body :   1.0000        .00000        1.0000
107.000  HINGE   0  1 Node index of inboard body attach point          :
108.000  HINGE   0  1 Rotation degrees of freedom                      :   3.0000
109.000  HINGE   0  1 Base body(ID8 1)rotation option(F=free,G=gimbaled):  G
110.000  HINGE   0  1 Rotation axis unit vector L1 inboard body  X,Y,Z :   1.0000        .00000        .00000
111.000  HINGE   0  1 Rotation axis unit vector L1 outboard body X,Y,Z :   1.0000        .00000        .00000
112.000  HINGE   0  1 Rotation axis unit vector L3 inboard body  X,Y,Z :   .00000        .00000        1.0000
113.000  HINGE   0  1 Rotation axis unit vector L3 outboard body X,Y,Z :   .00000        .00000        1.0000
114.000  HINGE   0  1 Rotation spring stiffness (N/M)    k1,k2,k3      :   .00000        .00000        .00000
115.000  HINGE   0  1 Rotation spring damping (N/M/S)    b1,b2,b3      :   .00000        .00000        .00000
116.000  HINGE   0  1 Initial rotation angle (DEG) theta1,theta2,theta3 :   .00000        .00000        .00000
117.000  HINGE   0  1 Null torque angle (DEG)      theta1,theta2,theta3 :   .00000        .00000        .00000
118.000  HINGE   0  1 Translation degrees of freedom                   :   3.0000
119.000  HINGE   0  1 Translation axis unit vector of 1ST DOF  X,Y,Z   :   1.0000        .00000        .00000
120.000  HINGE   0  1 Translation axis unit vector of 2ND DOF  X,Y,Z   :   .00000        1.0000        .00000
121.000  HINGE   0  1 Translation axis unit vector of 3RD DOF  X,Y,Z   :   .00000        .00000        1.0000
122.000  HINGE   0  1 Translation spring stiffness (N/M)  k1,k2,k3     :   .00000        .00000        .00000
123.000  HINGE   0  1 Translation spring damping (N/M/S) b1,b2,b3      :   .00000        .00000        .00000
124.000  HINGE   0  1 Initial translation displacement (M)    y1,y2,y3 :   .00000        .00000        .00000
125.000  HINGE   0  1 Null force position (M)                 y1,y2,y3 :   .00000        .00000        .00000
126.000  HINGE   0  1 >>>>>$$$$$ END OF DATA $$$$$<<<<<                :
127.000  HINGE   0  2 ID8 of hinge, ID8 of inbd body, ID8 of outbd body :   2.0000        1.0000        2.0000
128.000  HINGE   0  2 Node index of inboard body attach point          :   2.0000
129.000  HINGE   0  2 Rotation degrees of freedom                      :   1.0000
130.000  HINGE   0  2 Base body(ID8 1)rotation option(F=free,G=gimbaled):
131.000  HINGE   0  2 Rotation axis unit vector L1 inboard body  X,Y,Z :   .00000        1.0000        .00000
132.000  HINGE   0  2 Rotation axis unit vector L1 outboard body X,Y,Z :   .00000        1.0000        .00000
133.000  HINGE   0  2 Rotation axis unit vector L3 inboard body  X,Y,Z :   .00000        .00000        1.0000
134.000  HINGE   0  2 Rotation axis unit vector L3 outboard body X,Y,Z :   .00000        .00000        1.0000
135.000  HINGE   0  2 Rotation spring stiffness (N/M)    k1,k2,k3      :   4457.3
136.000  HINGE   0  2 Rotation spring damping (N/M/S)    b1,b2,b3      :   13.305
137.000  HINGE   0  2 Initial rotation angle (DEG) theta1,theta2,theta3 :   .00000
138.000  HINGE   0  2 Null torque angle (DEG)      theta1,theta2,theta3 :   .00000
139.000  HINGE   0  2 Translation degrees of freedom                   :   .00000
140.000  HINGE   0  2 Translation axis unit vector of 1ST DOF  X,Y,Z   :
141.000  HINGE   0  2 Translation axis unit vector of 2ND DOF  X,Y,Z   :
142.000  HINGE   0  2 Translation axis unit vector of 3RD DOF  X,Y,Z   :
143.000  HINGE   0  2 Translation spring stiffness (N/M)  k1,k2,k3     :
144.000  HINGE   0  2 Translation spring damping (N/M/S) b1,b2,b3      :
145.000  HINGE   0  2 Initial translation displacement (M)    y1,y2,y3 :
146.000  HINGE   0  2 Null force position (M)                 y1,y2,y3 :
147.000  HINGE   0  2 >>>>>$$$$$ END OF DATA $$$$$<<<<<                :
```

FIGURE 5

Table 1. Modal Data for the j^{th} Body

Symbol	Mnemonic	Dimension	Description
j	IDBODY		Body ID number (j^{th} body)
NM	NMODE		Number of modes for j^{th} body
NN	NNODE		Number of nodes for j^{th} body
$\phi^T M \phi$	MMASS (k, k)	(NM, NM)	Augmented modal mass (kg)
$\phi^T D \phi$	MDAMP (k, k)	(NM, NM)	Augmented modal damping (nt/msec)
$\phi^T K \phi$	MSTIFF (k, k)	(NM, NM)	Augmented modal stiffness (nt/m)
$\underline{\underline{\alpha}}^j_k$	ALPHABJ (i, k)	(3, NM)	Mass center mode shape of k^{th} mode
$\underline{\phi}^j_k(\underline{r}_\ell)$	PHIDNLBJ (i, k, ℓ)	(3, NM, NN)	Mode shape of k^{th} mode at the ℓ^{th} node
$\underline{\phi}'^j_k(\underline{r}_\ell)$	PHIPNLBJ (i, k, ℓ)	(3, NM, NN)	Mode slope of k^{th} mode at the ℓ^{th} node (rad/m)
$\underline{h}^j_k$	RJXPHIBJ (i, k)	(3, NM)	h-Parameter due to the k^{th} mode (kg-m)
$\underline{\underline{M}}^j_k$ *	DINERTM (ICOL, IROW, k)	(3, 3, NM)	Change in inertia of j^{th} body due to the k^{th} mode (kg-m)
$\underline{\underline{P}}^j_{q_k}$ *	PDYADIC (ICOL, IROW, q, k)	(3, 3, NM, NM)	Change in inertia of the k^{th} mode due to the q^{th} mode (kg)
$\underline{Y}^j_{q_k}$ **	PHIXPHIJ (i, q, k)	(3, NM, NM)	Coupling influence of the q^{th} mode into the k^{th} modal equation (kg)

NOTES

1. Index Definition - k = Mode, i = Axis, ℓ = Node, q = Mode, IROW, ICOL = Dyadic matrix elements
2. * indicates optional data is deleted when "time varying inertial option = no."
3. ** indicates optional data is deleted when "PHIXPHI modal term option = no."

HST/HGA TREETOPS MODEL

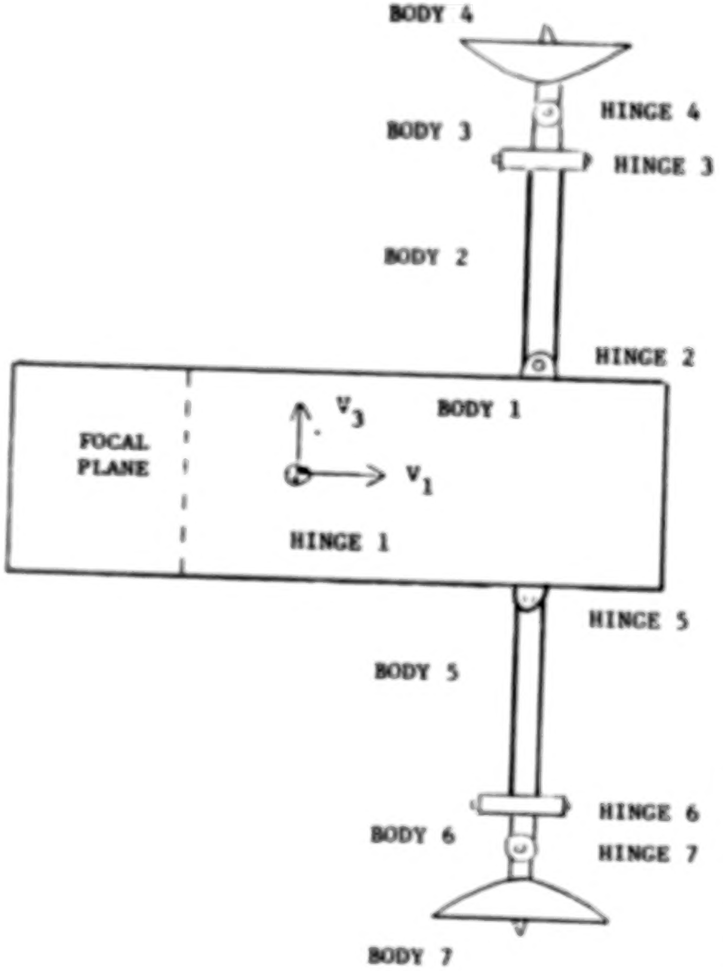
BODY 4
HINGE 4
BODY 3
HINGE 3
BODY 2
HINGE 2
BODY 1
FOCAL PLANE
V_3
V_1
HINGE 1
HINGE 5
BODY 5
HINGE 6
BODY 6
HINGE 7
BODY 7

	HGA		HST & SA	
MODE	FREQ (HZ)	DAMPING	FREQ (HZ)	DAMP
1	0.531	0.005	0.086	0.005
2	1.247	0.005	0.087	0.005
3	8.985	0.005	0.515	0.005
4	21.32	0.005	0.891	0.003
5	24.67	0.005	1.031	0.003
6			2.937	0.003

FIGURE 6

HGA and the core HST. The basic problem to be addressed is the interaction of the fundamental antenna mast modes at 0.531 with the 0.515 HST mode. The stringent 0.007 arc-second pointing stability requirement of the HST budgets only 0.003 arc-second disturbances of the Line of Sight (LOS) to be caused by the HGA's. Analysis showed the possibility of Dahl friction in the HGA gimbal bearings to excite the fundament mast modes during slow HGA tracking maneuvers. TREETOPS was employed to verify the predictions made by the HST prime contractor.

Figure 7 shows the detailed components of the HST TREETOPS model, consisting of seven bodies three of which are flexible, seven hinges with a total of three translational and nine rotational degrees of freedom; eleven sensors, seven actuators, a discrete and a user controller. The discrete controller models the HST fine guidance control system. The user controller models the HGA discrete P-I-D controllers along with bearing friction and roughness, cogging torques and quantization nonlinearities. The model thus contains 22 degrees of freedom plus 14 controller states.

Figures 8, 9, and 10 show results obtained by TREETOPS. In figure 8, a TREETOPS HGA step response compares favorably with simulation results obtained by the HST contractor. This plot

HST/HGA TREETOPS SIMULATION

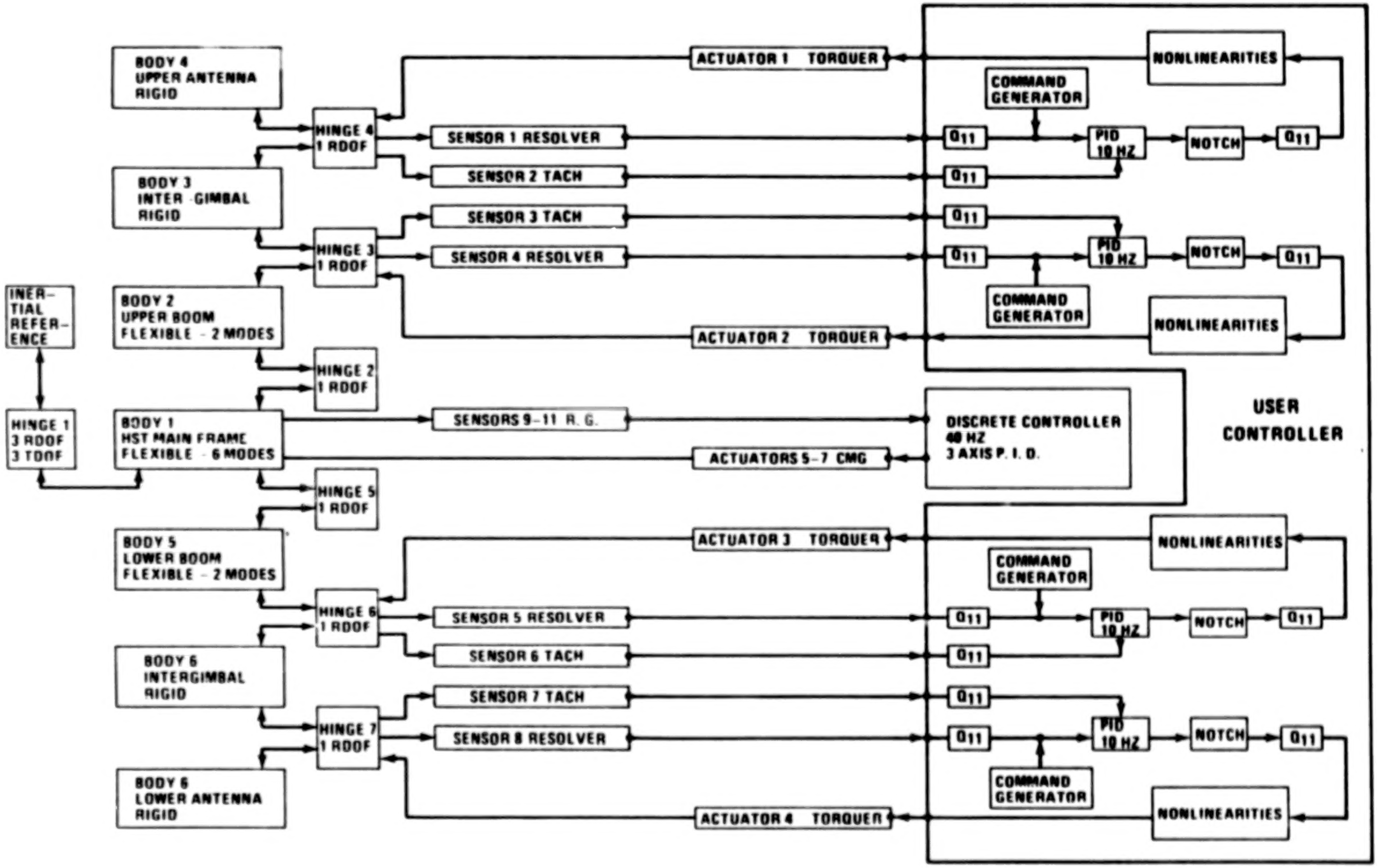
BODY 4
UPPER ANTENNA
RIGID
BODY 3
INTER GIMBAL
RIGID
INER-
TIAL
REFER-
ENCE
BODY 2
UPPER BOOM
FLEXIBLE - 2 MODES
HINGE 1
3 RDOF
3 TDOF
BODY 1
HST MAIN FRAME
FLEXIBLE - 6 MODES
BODY 5
LOWER BOOM
FLEXIBLE - 2 MODES
BODY 6
INTERGIMBAL
RIGID
BODY 6
LOWER ANTENNA
RIGID
HINGE 4
1 RDOF
HINGE 3
1 RDOF
HINGE 2
1 RDOF
HINGE 5
1 RDOF
HINGE 6
1 RDOF
HINGE 7
1 RDOF
ACTUATOR 1 TORQUER
SENSOR 1 RESOLVER
SENSOR 2 TACH
SENSOR 3 TACH
SENSOR 4 RESOLVER
ACTUATOR 2 TORQUER
SENSORS 9-11 R. G.
ACTUATORS 5-7 CMG
ACTUATOR 3 TORQUER
SENSOR 5 RESOLVER
SENSOR 6 TACH
SENSOR 7 TACH
SENSOR 8 RESOLVER
ACTUATOR 4 TORQUER
NONLINEARITIES
COMMAND
GENERATOR
Q11
PID
10 HZ
NOTCH
DISCRETE CONTROLLER
40 HZ
3 AXIS P. I. D.
USER
CONTROLLER

FIGURE 7

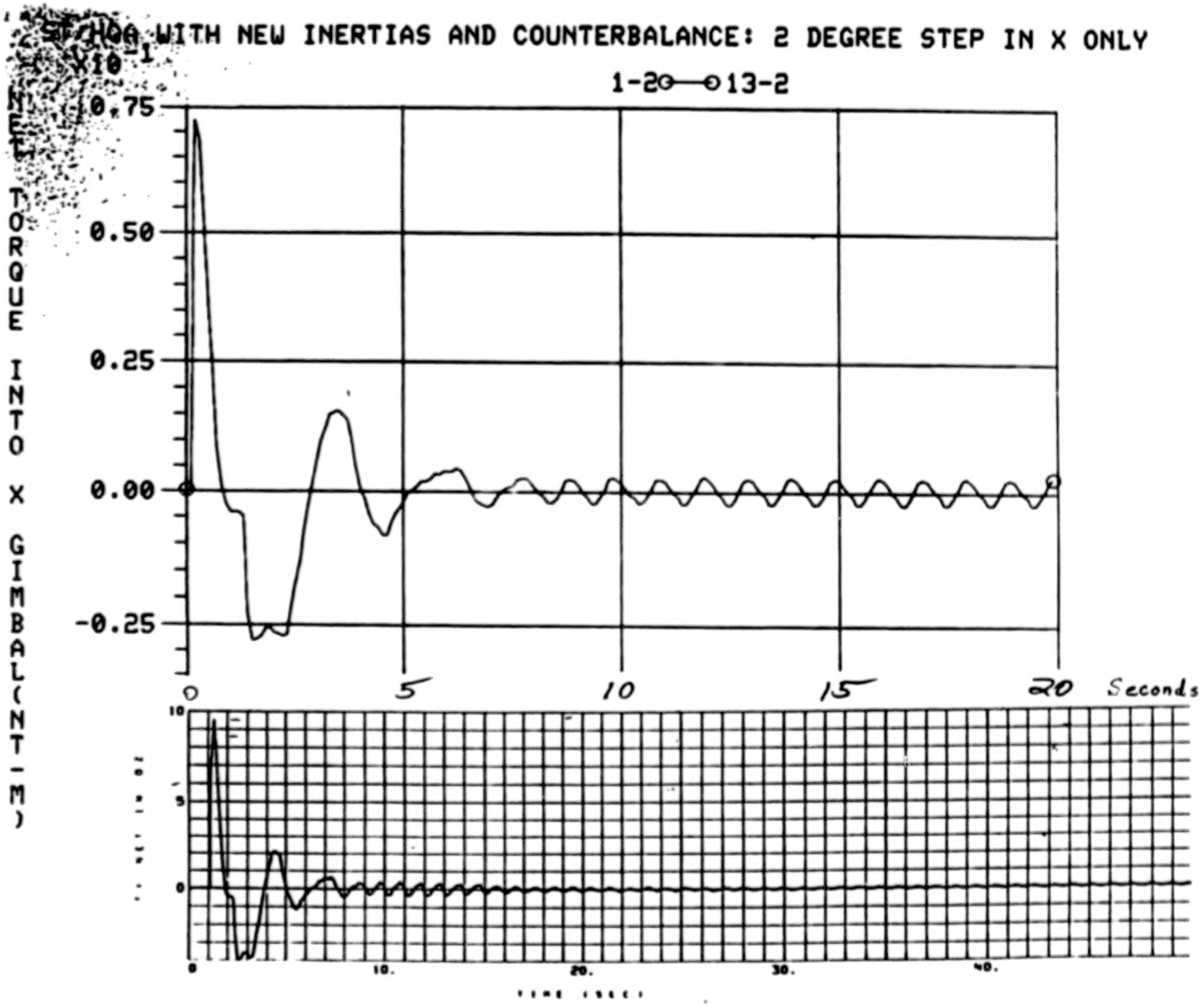
ST/HQA WITH NEW INERTIAS AND COUNTERBALANCE: 2 DEGREE STEP IN X ONLY
1-20—o13-2
X10⁻¹
NET TORQUE INTO X GIMBAL(NT-M)
0.75
0.50
0.25
0.00
-0.25
0
5
10
15
20
Seconds
10
5
0
0
10.
20.
30.
40.
TIME (SEC)

FIGURE 8

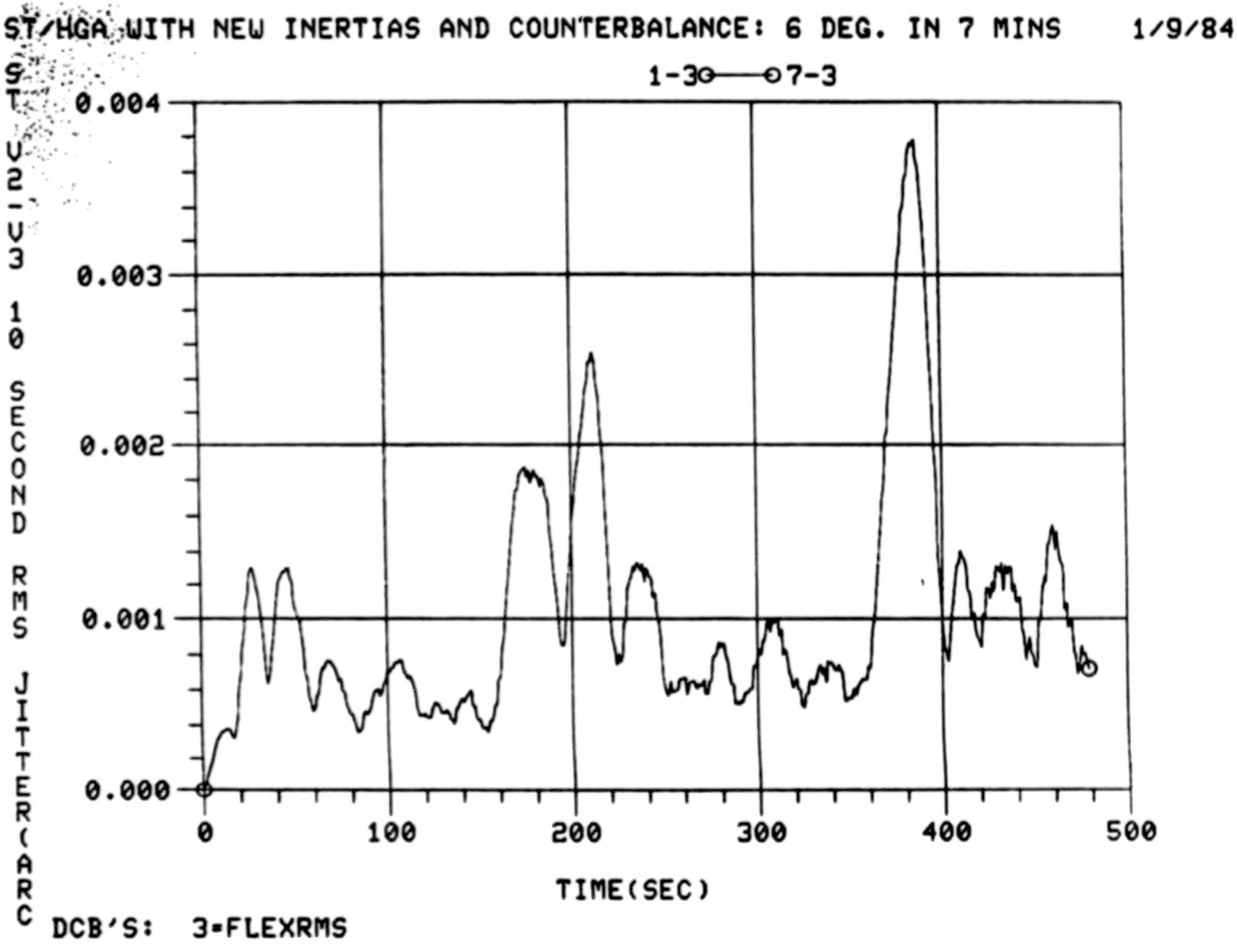
ST/HGA WITH NEW INERTIAS AND COUNTERBALANCE: 6 DEG. IN 7 MINS 1/9/84
1-3 ⊖——⊖ 7-3
ST V2-V3 10 SECOND RMS JITTER(ARC
0.004
0.003
0.002
0.001
0.000
0
100
200
300
400
500
TIME(SEC)
DCB'S: 3=FLEXRMS

FIGURE 9

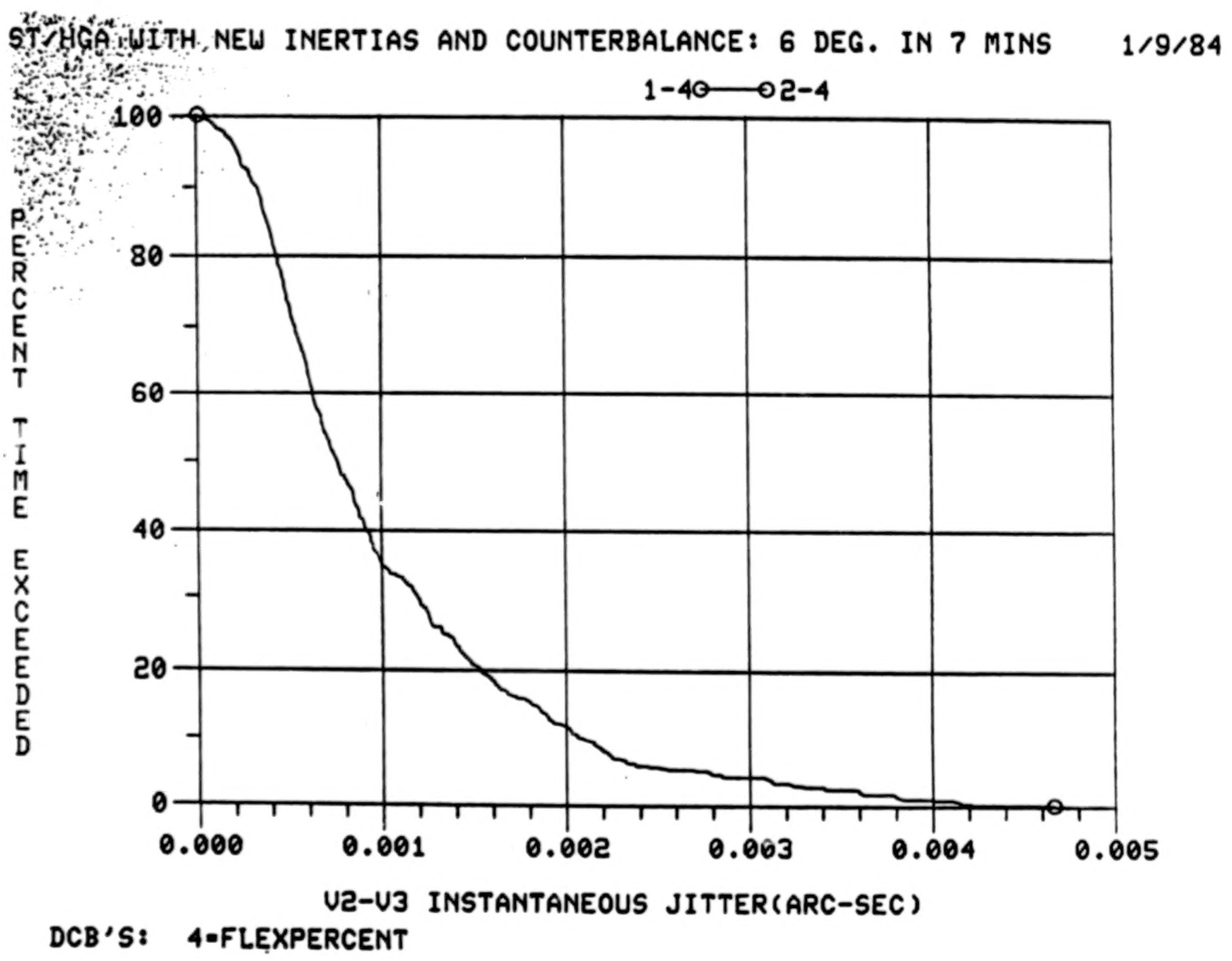
ST/HGA WITH NEW INERTIAS AND COUNTERBALANCE: 6 DEG. IN 7 MINS 1/9/84
1-4 2-4
PERCENT TIME EXCEEDED
100
80
60
40
20
0
0.000
0.001
0.002
0.003
0.004
0.005
V2-V3 INSTANTANEOUS JITTER(ARC-SEC)
DCB'S: 4=FLEXPERCENT

FIGURE 10

shows the net torque applied between bodies 2 and 3 of figure 6 in response to a two degree step command (note the difference in torque units). Figure 9 shows the time history of the HST LOS during a typical HGA tracking maneuver of the Tracking and Data Relay Satellite. Notice that the 0.003 arc-second error budget is exceeded at the end of the maneuver as the HGA pointing control system overcomes the Dahl friction forces at very slow speeds. The 480 seconds of simulation time required approximately 56 minutes of CPU time on a Sigma V computer. Figure 10 summarizes the LOS disturbance caused by the HGA's over the same maneuver. The interaction of the HGA mast modes with the HST is again demonstrated as the error budget is exceeded. Note also that the data plotted in figure 8 is standard TREETOPS output data while the information in figures 9 and 10 were generated during run time in the user controller subroutine, which increased CPU time somewhat.

The proceeding discussion indicates some of the potential applications of the TREETOPS program. Typically, programs of the magnitude receive a rather cool response until a sufficient number of users and check cases have been used to eliminate the unavoidable software bugs and idiosyncrasies. At MSFC, TREETOPS has been employed on the six programs listed in figure 11. In each case alternate simulation results were available

ZATION SYSTEMS DYNAMICS LAB	MARSHALL SPACE FLIGHT CENTER OAST RTOP REVIEW	NAME J. SHARKEY
CHART NO	CONTROL TECHNOLOGY/GUIDANCE CONCEPTS	DATE OCTOBER 1985

NONLINEAR DYNAMICS

FUTURE ENHANCEMENTS

- ORBITAL DYNAMICS (GRAVITY GRADIENT, AERODYNAMIC, AND MAGNETIC FIELD MODELS).
- CMG DYNAMICS.
- NASTRAN INTERFACE PROGRAM.
- MODE SELECTION CRITERIA BASED ON COMPONENT MODE SYNTHESIS.
- SUBMIT TO COSMIC FOR MAINTENANCE SUPPORT.

MSFC PROJECTS UTILIZING TREETOPS

- SPACE TELESCOPE (HIGH GAIN ANTENNA/SOLAR ARRAY INTERACTION STUDIES).
- SPACELAB II INSTRUMENT POINTING SYSTEM.
- SPACELAB II INFRARED TELESCOPE.
- PINHOLE/OCCULTER FACILITY.
- SPACE STATION (REBOOST, POINTING MOUNTS).
- GROUND FACILITY FOR LARGE SPACE STRUCTURES.

FIGURE 11

for verification. Honeywell also has an extensive list of check cases and projects used to verify TREETOPS. Over twenty other companies, universities, or other Government agencies have received a copy of TREETOPS and are currently evaluating its potential applications. Most responses indicate close agreement with other such programs while acknowledging TREETOPS' easy to use format and versatility. Soon CONTOPS will be released to the public domain through NASA's COSMIC network whereby maintenance provision should become available. Figure 11 also list some future enhancement considered for TREETOPS and CONTOPS.

N87
22736
UNCLAS

SPACE STATION

CONTROL SESSION 3B
HENRY WAITES, CHAIRMAN

SSS86-0047

PRELIMINARY EVALUATION OF A REACTION CONTROL SYSTEM FOR THE SPACE STATION

APRIL 22 - 24, 1986,
WORKSHOP ON STRUCTURAL
DYNAMICS AND CONTROL,
INTERACTION OF FLEXIBLE
STRUCTURES, OAST AND MSFC

H. H. WOO
J. A. FINLEY
GN&C

N87-22736

Rockwell International
Space Station Systems Division

PRECEDING PAGE BLANK NOT FILMED

INTRODUCTION

A new configuration called the "Dual-Keel" has been selected by NASA to accommodate the great number of payloads and experiments. The requirements and goals of a Space Station reaction control system (RCS) have been partially defined for this station.

This briefing presents the challenges, the groundrules and criteria, some of the RCS concepts, classical and modern design analysis, and simulation results which are applicable to the Space Station. The objective is to present a preliminary Space Station RCS concept supported by analytical results which meets the given goals and requirements.

BUILDUP PHASES DICTATES GN&C ADAPTABILITY

The buildup phases and the continuously changing configuration dictates adaptability in RCS design. The RCS software must be switched to account for the relocation of the propulsion system during assembly. The gains and filter coefficients need to be updated to improve performance and stability with each new configuration.

Buildup Phases Dictates GN&C Adaptability

FACILITATE OPERATION AND USERS

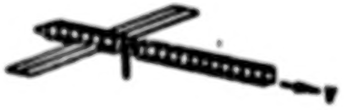

FLIGHT 1

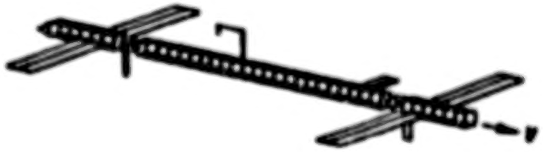

FLIGHT 2

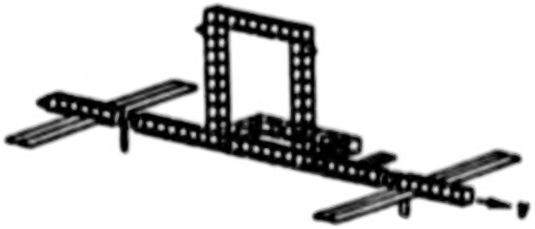

FLIGHT 3

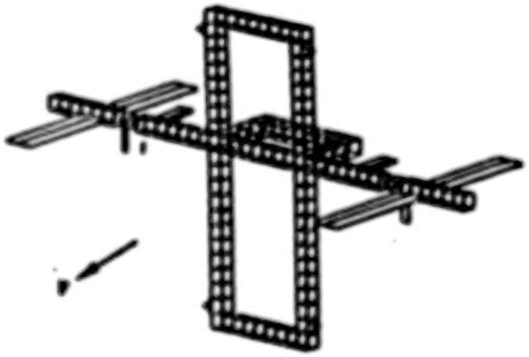

FLIGHT 4

- Relocation of RCS

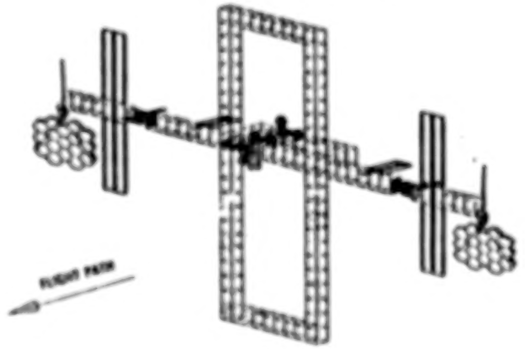

IOC

- Quiet Zone for Users
- USA / International
- Coarse Pointing Subsystem
- Dual Keel for Payload Service and Growth
- Hybrid Power
- Permanently Manned

CONSIDERATIONS:

- Establish Basic GN&C Capability on Flight 1
- Complete 3 Axis CMG and RCS Backup Control
- Place Thrusters for Reboost (Min. Altitude of 180 nmi)
- Allow Larger Angle and Rate for Momentum Dumping for Early Flights
- Add Traffic Control Later
- Add Payload Coarse Pointing as Needed.

Rockwell International
Space Station Systems Division

SCOPE AND METHOD OF APPROACH

The RCS design approach emphasizes groundrules for RCS thruster sizing. Concurrently, the appropriate criteria are determined. The RCS control concept is to develop compensation techniques by employing both modern and classical control methods for stability design and performance analysis with simulations. A non-real time simulation incorporating detailed dynamical models and many subsystem models is used to simulate the overall Space Station response to an RCS design during reboost, maneuvers, and Station disturbances.

RCS design parameters are chosen to meet structural and operational constraints as well as controllability and stability requirements. RCS thrust level, for instance, is chosen to meet the constraints of maximum allowable structural loads, reasonable time for reboost, and minimum structural/RCS interaction.

The thrust level may also have to be chosen so that it lies within a range applicable to a blowdown propulsion system. Overall Station performance requirements drive other RCS parameters such as thrust accuracy, minimum impulse bit, RCS loop gains, and jet select logic.

Scope and Method of Approach

- EMPHASIZE GROUNDRULES FOR RCS THRUSTER SIZING
- DETERMINE APPROPRIATE CRITERIA FOR RCS THRUSTER SIZE
- DEVELOP COMPENSATION TECHNIQUE IN RCS CONTROL CONCEPT
- PERFORM STABILITY AND SIMULATION ANALYSIS

SIZING RCS THRUSTER EMPHASIZES GROUNDRULES

Both the groundrules and criteria for RCS thrust sizing are emphasized by the technical community. The type of propellant feed system (centralized interconnected vs. decentralized) and thruster performance (regulated vs. blowdown) will require the appropriate compensation in RCS design.

Sizing RCS Thrusters Emphasizes Groundrules

BLOWDOWN DESIGN OPTIONS:

- CENTRALIZED INTERCONNECTED FUEL FEED
- DECENTRALIZED FUEL FEED

RCS PROPULSION WILL PROVIDE FOR:

- STATION TRANSLATION AND REBOOST
- BACKUP ATTITUDE CONTROL
- MOMENTUM DUMPING WHEN NECESSARY
- DAMPING TRANSIENTS
- ATTITUDE MANEUVERS

RCS PROPULSION DESIGN DRIVERS IDENTIFY:

- MAXIMUM ALLOWABLE THRUST FOR REBOOST WITHOUT RCS / FLEX COUPLING
- SUFFICIENT THRUST TO SATISFY CONTROL AUTHORITY AND STABILITY REQUIREMENTS

RCS ATTITUDE AND STABILITY RATE GOALS ARE:

- STABILITY RATE OF 0.02 DEG / SEC / AXIS
- ATTITUDE OF +/- 1.0 DEG ABOUT ANY DESIRED ATTITUDE

ATTITUDE AND STABILITY RATE GOALS MAY BE RELAXED DURING:

- REBOOST
- BACKUP TO CMG'S
- MANEUVERS
- ORBITER, OMV, OTV BERTHING / DOCKING
- COLLISION AVOIDANCE
- STATION DISPOSAL
- OTHER CONTINGENCY OPERATIONS

Rockwell International
Space Station Systems Division

CRITERIA HELPS TO DETERMINE RCS THRUSTER SIZE

The functional and performance requirements must be reviewed critically so as to formulate appropriate criteria. The performance of reboost, for example, must be traded off with stability requirements. Due to the flexibility of the structure, the maximum thrust level must be limited as well. Also the jet cycling frequencies must be separated from structural modes. The minimum thrust level is driven by adequate control authority to handle disturbances and by performance during different operations.

Criteria Helps to Determine RCS Thruster Size

SPACE STATION

- MINIMIZE REBOOST TIME -- (ONE CREW SHIFT - 9 HOURS)
- MINIMUM STRUCTURAL / CONTROL INTERACTION -- (STABILITY GAIN MARGIN OF 10 DB AND PHASE MARGIN OF 40 DEG)
- STRUCTURAL LOADS LIMITS AND DEFLECTIONS -- (LIMIT BENDING MOMENT TO 102,000 INCH - POUNDS FOR 16.4 FT / 0.04 INCH TRUSS)
- ADEQUATE CONTROL AUTHORITY WITH REASONABLE DISTURBANCE SETTLING TIME FOR DYNAMIC OPERATIONS -- (LESS THAN 15 MIN)
  - -- ORBITER PLUME IMPINGEMENT (10,000 TO 30,000 FT - POUNDS)
  - -- ORBITER DOCKING / BERTHING (500 POUNDS FOR 1 SEC)
  - -- CREW DISTURBANCE (25 POUNDS FOR 1 SECOND)
- LIMITING OF BENDING AMPLITUDES
  - -- FLEX RATE AT ISA LESS THAN 0.01 DEG / SEC
  - -- FLEX DEFLECTION AT SOLAR ARRAY LESS THAN 1.0 DEG
  - -- FLEX DEFLECTION AT PAYLOAD MOUND LESS THAN 1.0 DEG
  - -- FLEX RATE AT SOLAR DYNAMIC RECEIVER LESS THAN 0.1 DEG / SEC

Rockwell International
Space Station Systems Division

TIME TO REBOOST IS DRIVEN BY THRUST LEVEL

For the operational altitude range of 250 to 270 nmi, the reboost time is about two to four hours for high and low thrust levels (100 and 40 pounds maximum) respectively. During the assembly phase, the reboost time needs to be limited to one crew shift (9 hours) with the application of the appropriate thrust level. The case with the orbiter attached is comparable to a growth station.

TIME TO REBOOST IS DRIVEN BY THRUST LEVEL

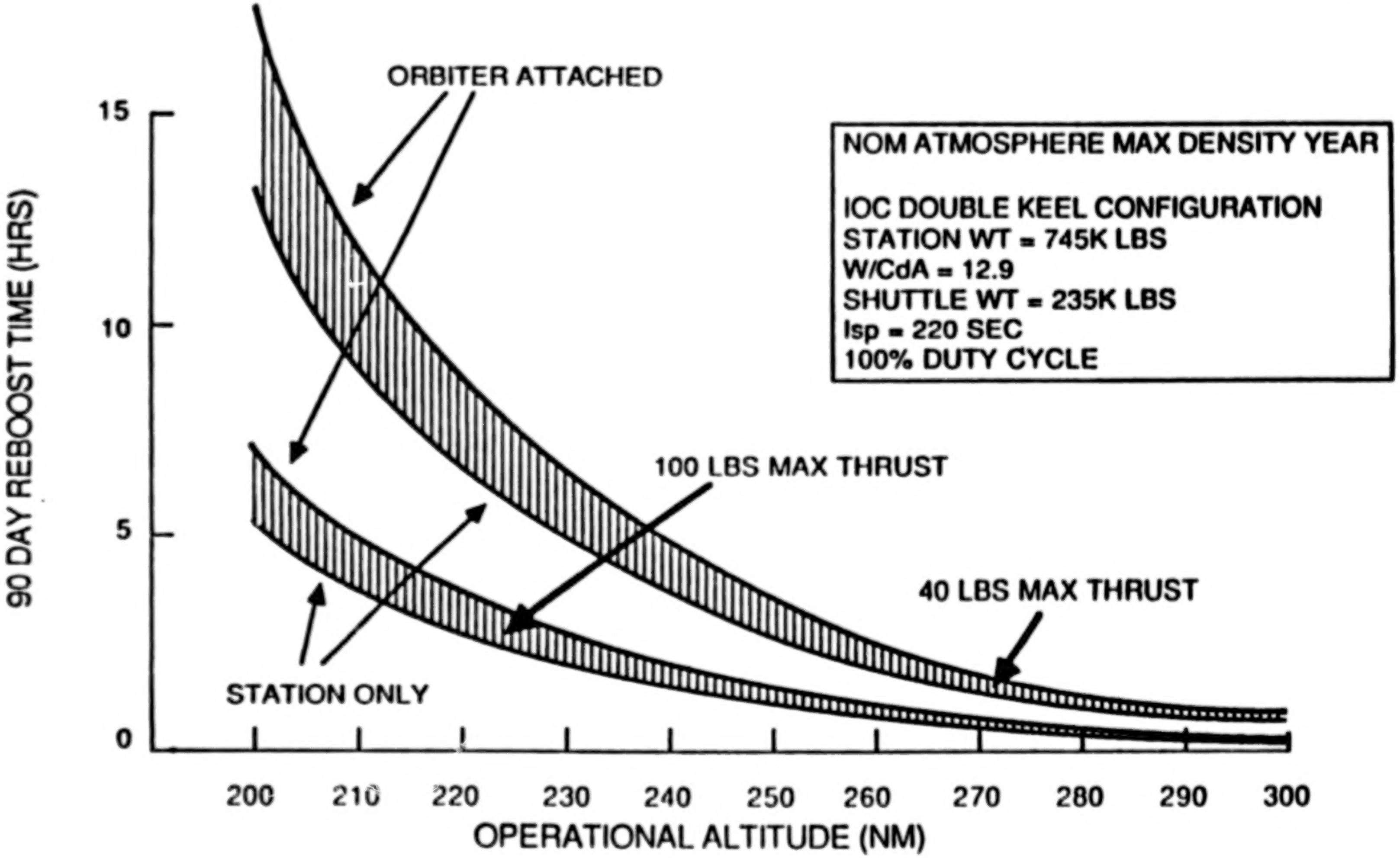

NOM ATMOSPHERE MAX DENSITY YEAR

IOC DOUBLE KEEL CONFIGURATION
STATION WT = 745K LBS
W/CdA = 12.9
SHUTTLE WT = 235K LBS
Isp = 220 SEC
100% DUTY CYCLE

Rockwell International
Space Station Systems Division

DISTURBANCE ACCELERATIONS DEFINE THE DESIRED CONTROL ACCELERATION

The RCS/propulsion system must accommodate disturbances which exceed the CMG momentum management capability. These major disturbances include docking, mission service center (MSC) motion, and orbiter plume impingement effects.

The maximum control acceleration, however, must be selected according to structural loads capability.

Disturbance Moments Define the Desired Control Moments

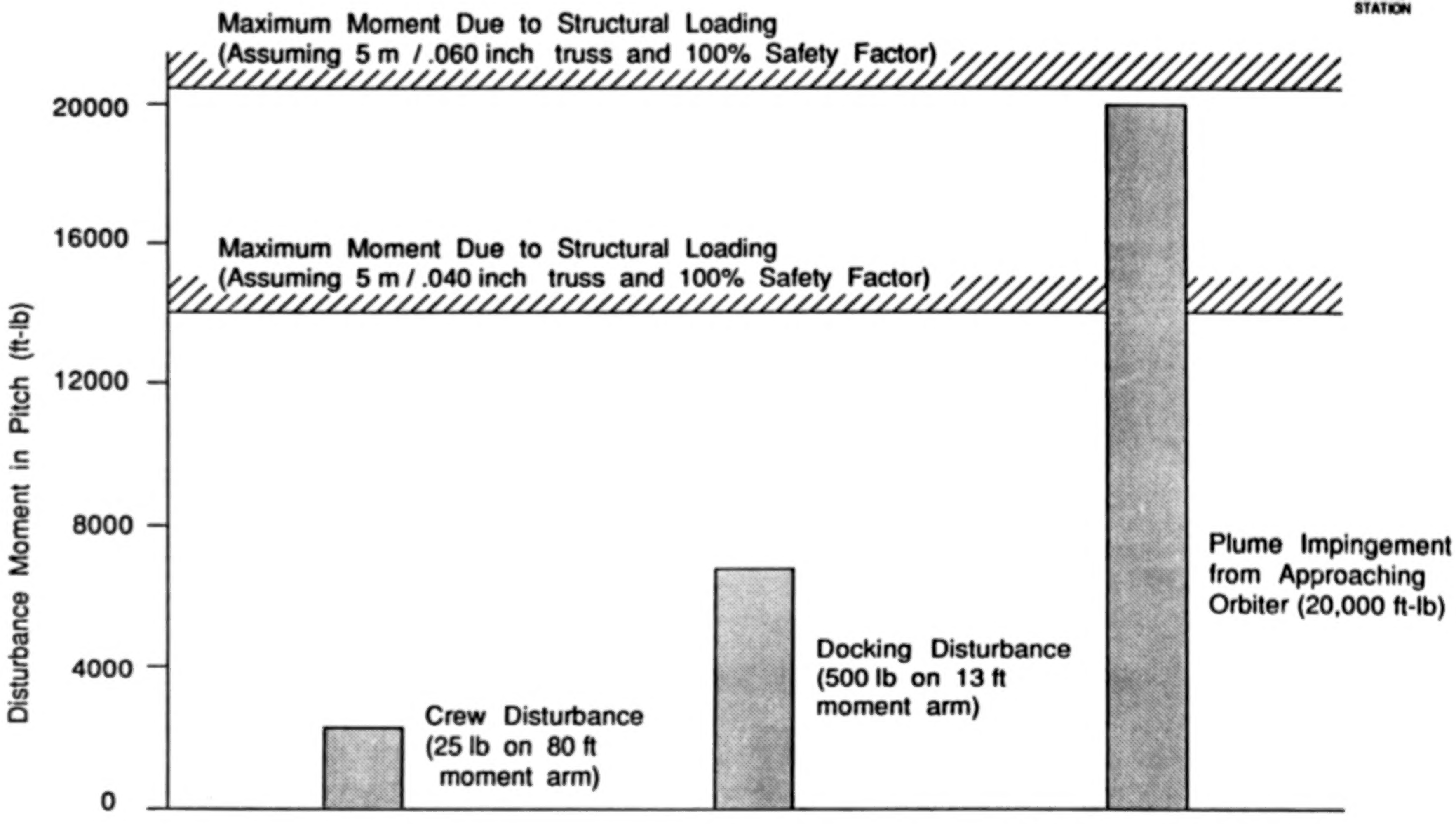

* Assuming IOC Station

Rockwell International
Space Station Systems Division

RCS CONTROL CONCEPTS COMPENSATE FOR PROPULSION SYSTEM VARIATIONS

The proposed RCS control concepts employ modern design techniques for wide notch filter design to attenuate closely spaced dominant structural modes. The rate gain is increased but bounded as the thrust level is reduced. A dual torque control level is practical for control of large and small disturbances. Steady state error due to mistrim moment can be integrated out.

RCS Control Concept Compensates for Propulsion System Variations

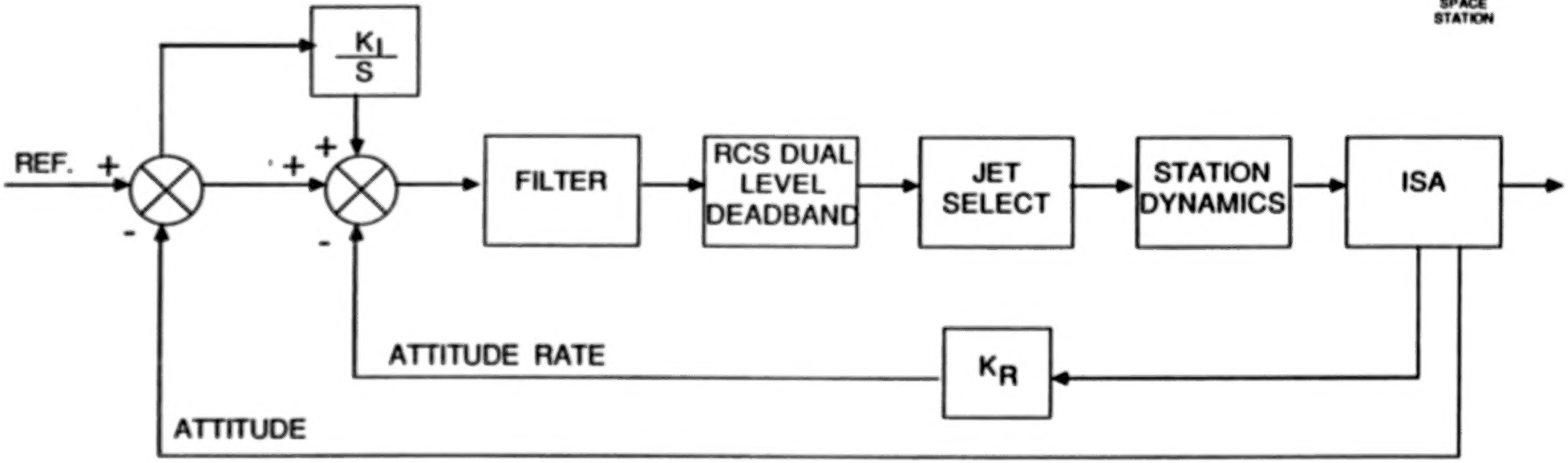

REF.
+
-
$\frac{K_I}{S}$
+
+
-
FILTER
RCS DUAL LEVEL DEADBAND
JET SELECT
STATION DYNAMICS
ISA
K_R
ATTITUDE RATE
ATTITUDE

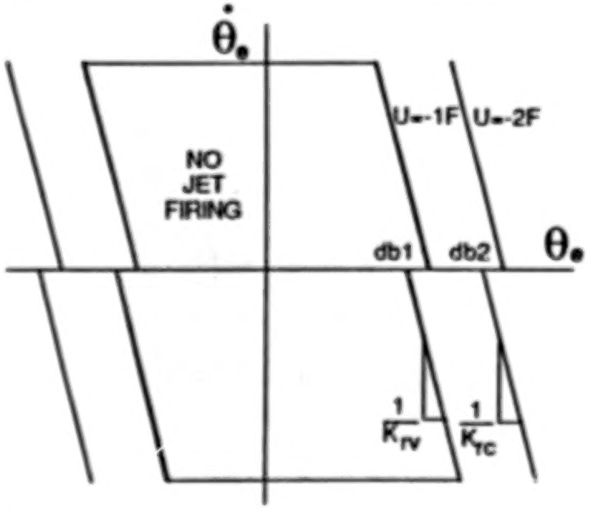

$\dot{\theta}_e$
NO JET FIRING
U=-1F
U=-2F
db1
db2
θ_e
$\frac{1}{K_{rv}}$
$\frac{1}{K_{rc}}$

- USES WIDE BAND NOTCH FILTER FOR COMPENSATION
- SCHEDULES RATE GAIN AS FUNCTION OF THRUST
- PROVIDES VERNIER AND COARSE CONTROL LEVEL
- PROVIDES INTEGRAL LOOP FOR MISTRIM MOMENT

Rockwell International
Space Station Systems Division

THRUST LEVEL OF 20 LB/CLUSTER PROVIDES ADEQUATE GAIN AND PHASE MARGIN FOR COMPENSATED SYSTEM

Adequate gain and phase margin must be achieved for stability while meeting controllability requirements. Describing function analysis is used to model the RCS thrust function as it interacts with a flexible structure. The relationship between attitude deadband, thrust level, and gain and phase margins provides a method necessary to prevent the RCS from interacting with the structure.

Thrust Level of 20 lb / Cluster Provides Adequate Gain and Phase Margin for Compensated System

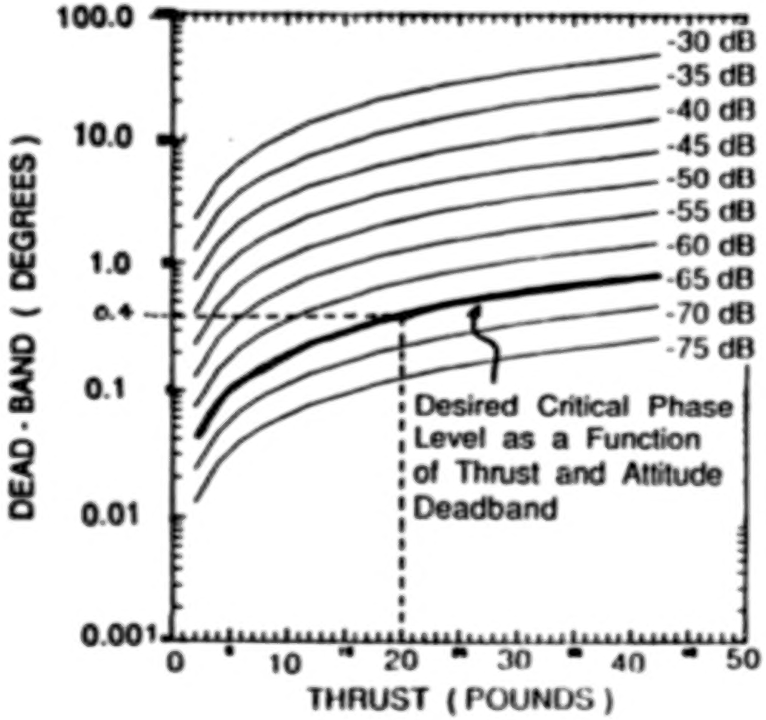

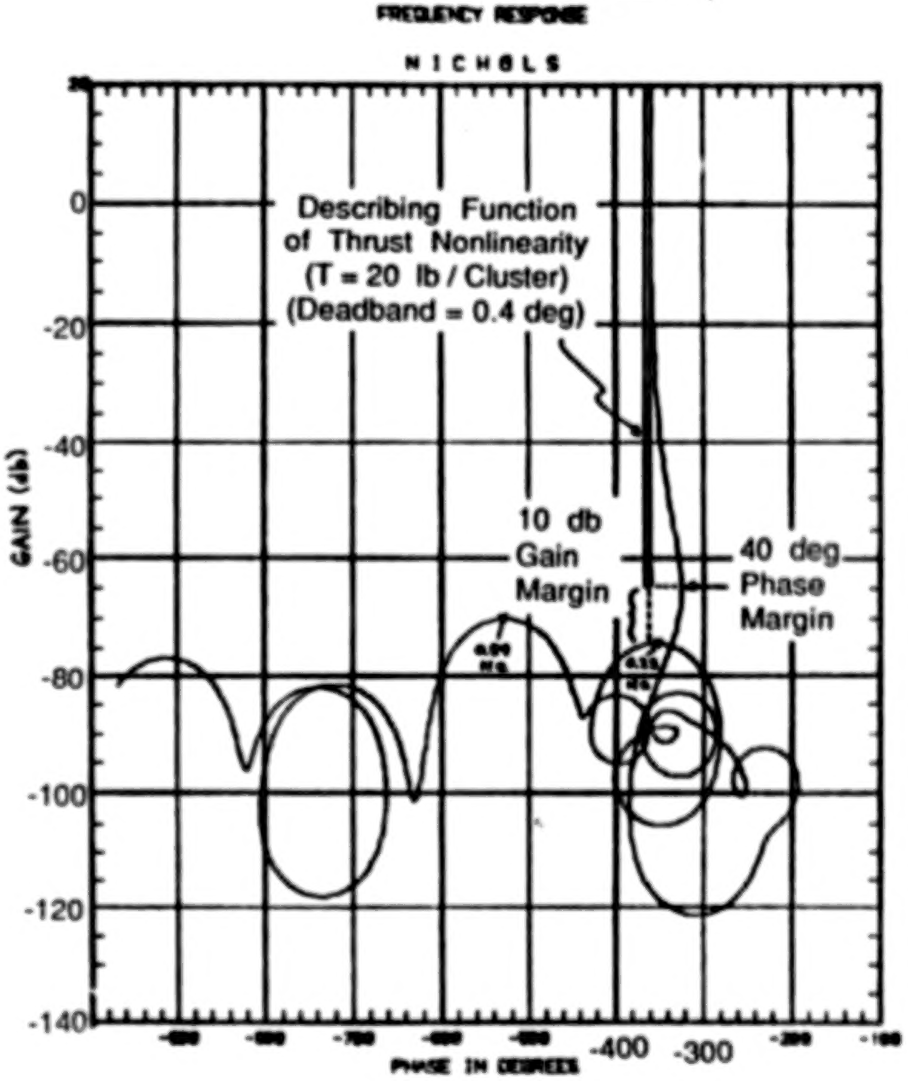

- Phase Margin of 40 deg and Gain Margin of 10 db are Achievable with Thrust Level of 20 lb / Cluster and 4 Clusters Firing in Pitch

Rockwell International

Space Station Systems Division

PEAK DEFLECTION INDICATES ACCEPTABLE DESIGN

Since payload pointing is an important Space Station function, the RCS must be designed so as not to vibrate the structure to a great degree.

Sensitivity data derived from simulation indicates reasonable performance at remote locations on the structure for different configurations.

Peak Deflections Indicate Acceptable Design

SPACE STATION

EARLY FLIGHTS

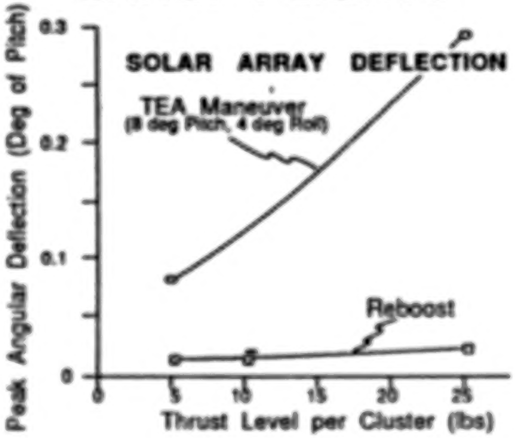

IOC

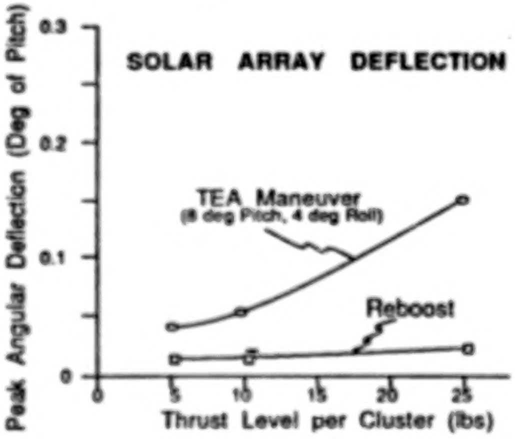

GROWTH

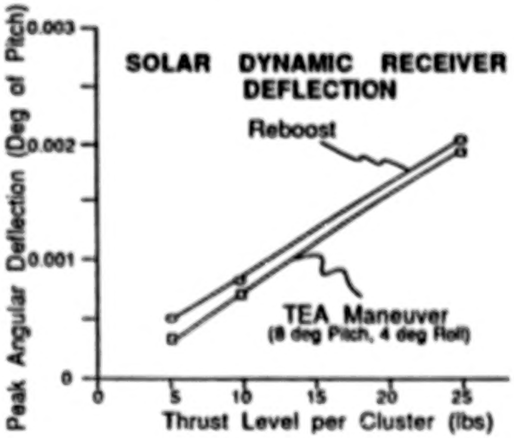

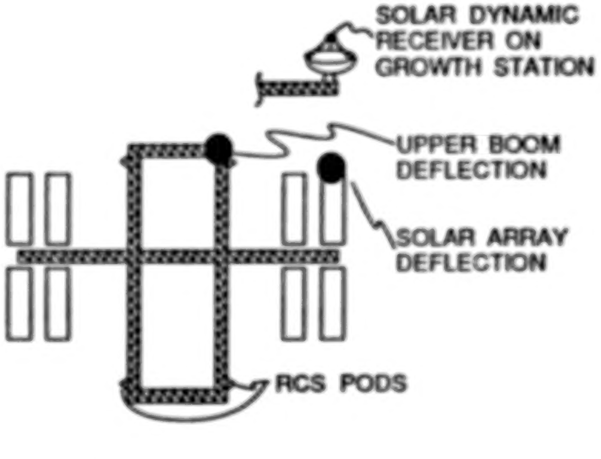
SOLAR DYNAMIC RECEIVER ON GROWTH STATION
UPPER BOOM DEFLECTION
SOLAR ARRAY DEFLECTION
RCS PODS

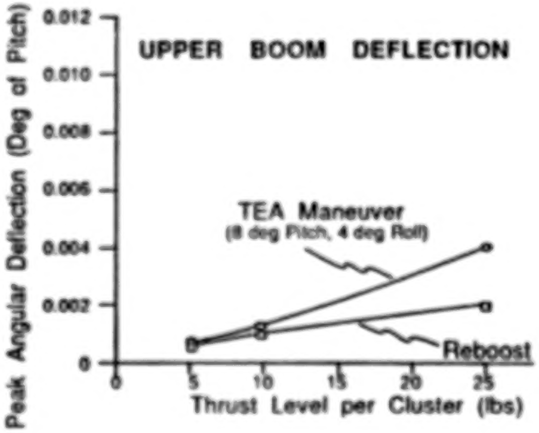

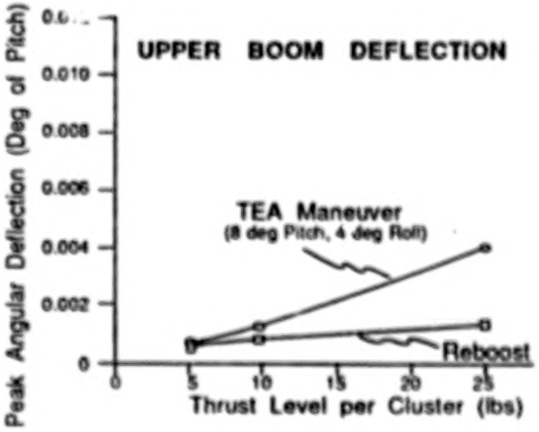

Rockwell International
Space Station Systems Division

RCS PROVIDES ADEQUATE ATTITUDE ERROR CONTROL ASSEMBLY FLIGHT 1

Simulation results indicate that the location of the RCS thrusters provides adequate three-axis control authority and reboost capability.

RCS Provides Adequate Rate Error Control for Assembly Flight 1

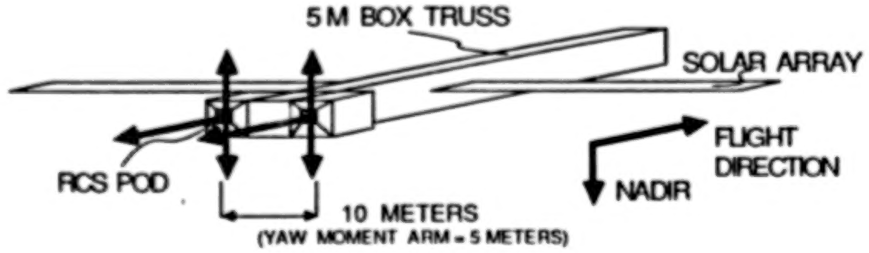
5 M BOX TRUSS
SOLAR ARRAY
RCS POD
10 METERS
(YAW MOMENT ARM = 5 METERS)
FLIGHT DIRECTION
NADIR

$\alpha^{*}_{(roll)} = 6 \cdot 10^{-3} \cdot$ Jet Force

$\alpha_{(pitch)} = 1 \cdot 10^{-3} \cdot$ Jet Force

$\alpha_{(yaw)} = 7 \cdot 10^{-5} \cdot$ Jet Force

* Units in deg/sec/sec

MANEUVER
(8 deg Pitch, 4 deg Roll)

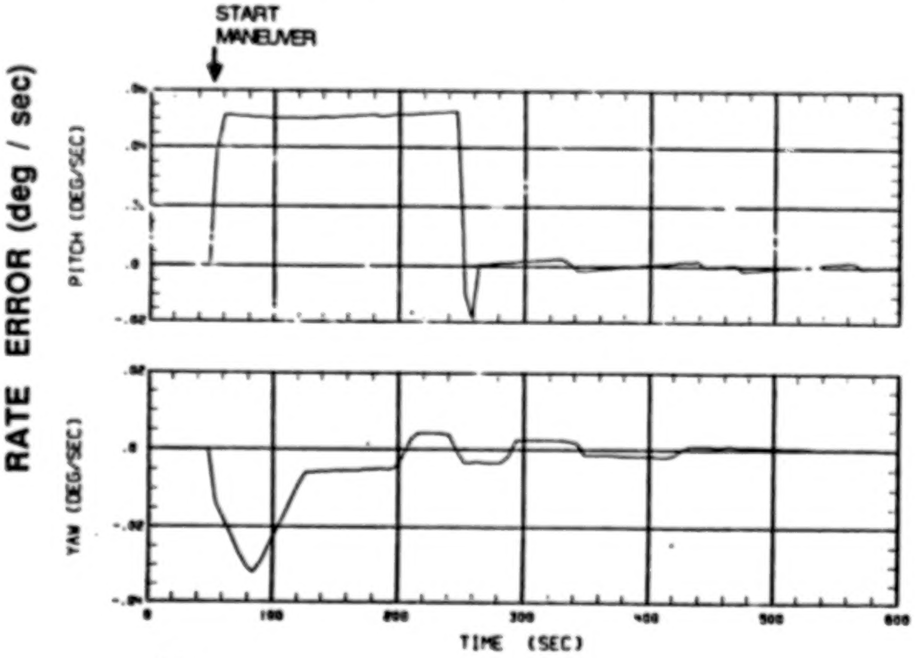

REBOOST
(300 sec x-translation)

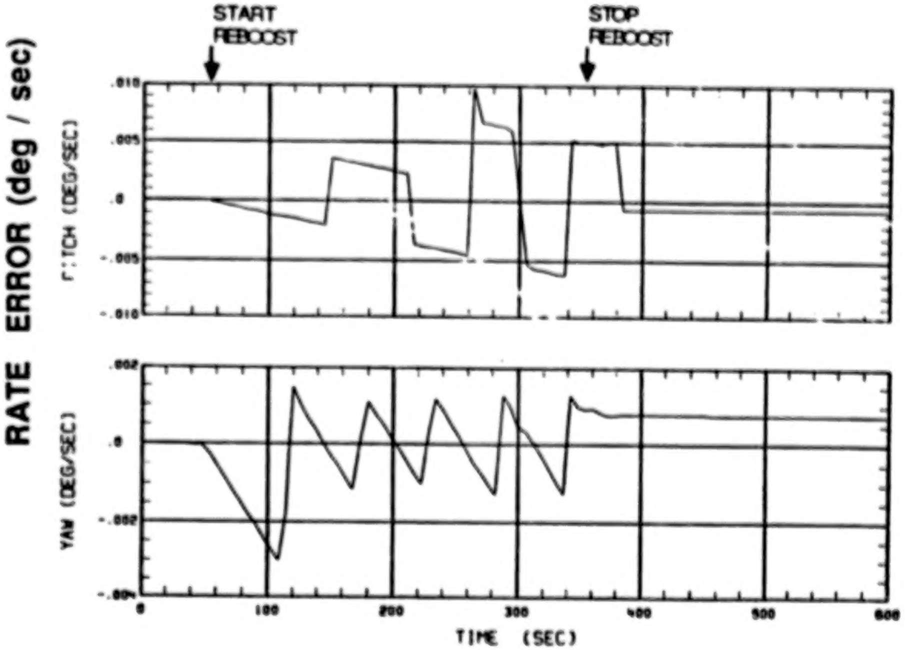

Rockwell International
Space Station Systems Division

RCS PROVIDES ADEQUATE RATE CONTROL FOR ASSEMBLY FLIGHT 1

Simulation results indicates that the location of the RCS thrusters provides adequate three-axis control authority and reboost capability.

RCS Provides Adequate Attitude Error Control for Assembly Flight 1

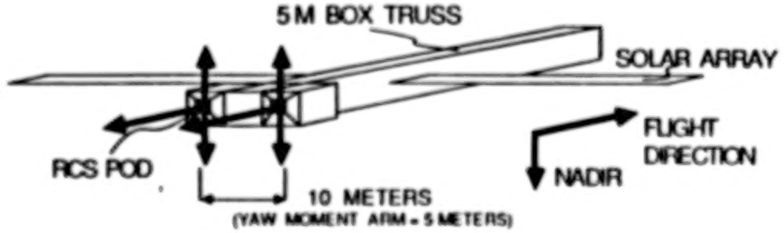
5M BOX TRUSS
SOLAR ARRAY
RCS POD
10 METERS
(YAW MOMENT ARM = 5 METERS)
NADIR
FLIGHT DIRECTION

$\alpha^{*}_{(roll)} = 6 \cdot 10^{-3} \cdot$ Jet Force

$\alpha_{(pitch)} = 1 \cdot 10^{-3} \cdot$ Jet Force

$\alpha_{(yaw)} = 7 \cdot 10^{-5} \cdot$ Jet Force

* Units in deg/sec/sec

MANEUVER
(8 deg Pitch, 4 deg Roll)

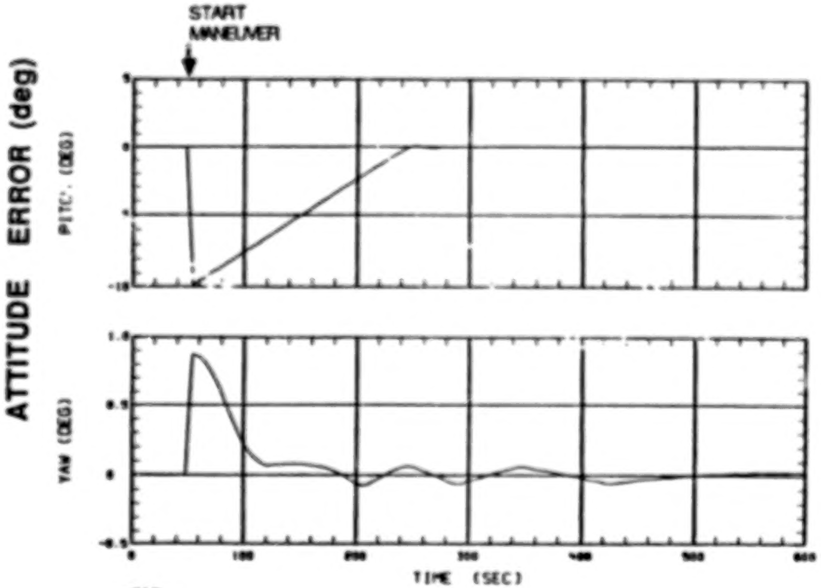

REBOOST
(300 sec x-translation)

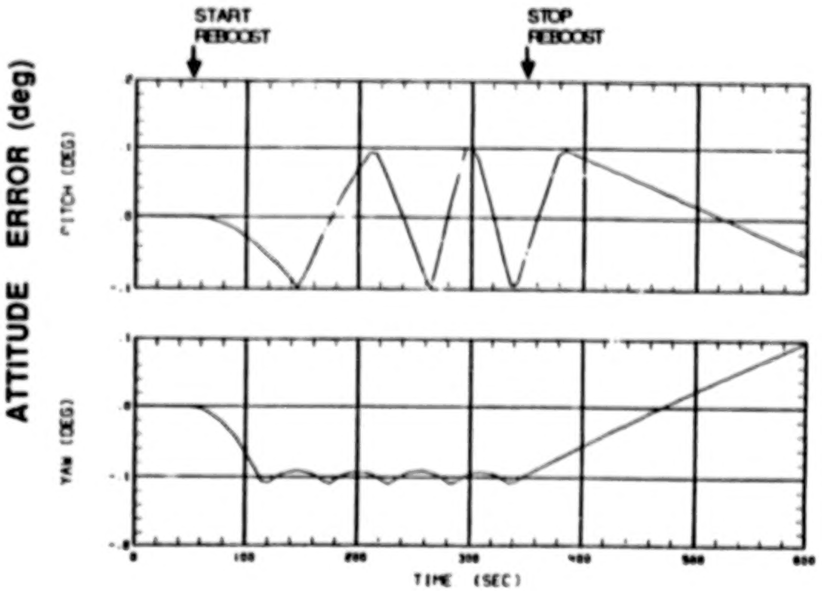

Rockwell International
Space Station Systems Division

REBOOST AND ATTITUDE MANEUVERING PRODUCE ACCEPTABLE SOLAR ARRAY DEFLECTIONS AND RATES

Solar array deflection is acceptable during reboost and maneuver operations.

Reboost and Attitude Maneuvering Produce Acceptable Solar Array Deflections and Rates *

SPACE STATION

ATTITUDE MANEUVER (8 DEG PITCH, 4 DEG ROLL)

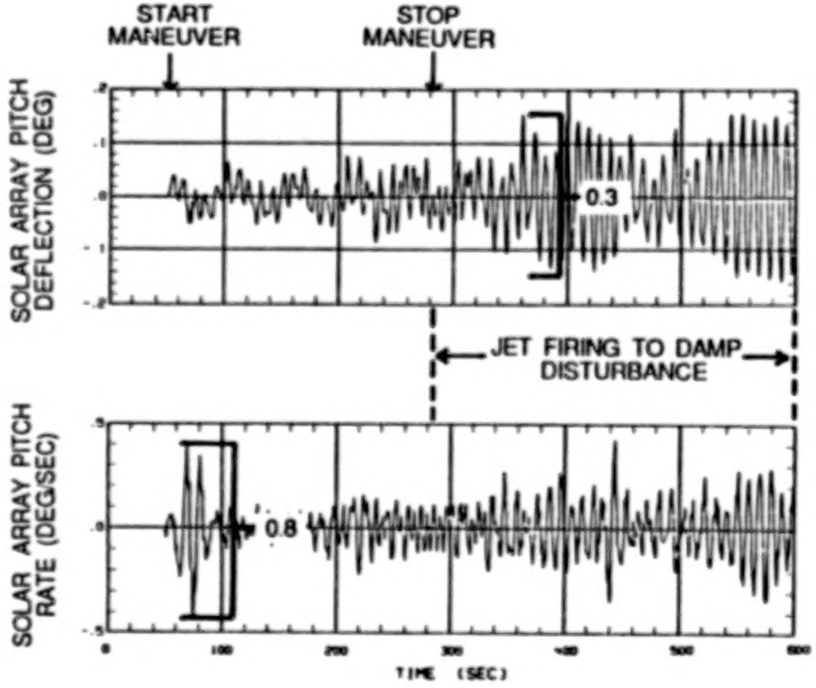

REBOOST -- 300 SECOND TRANSLATION

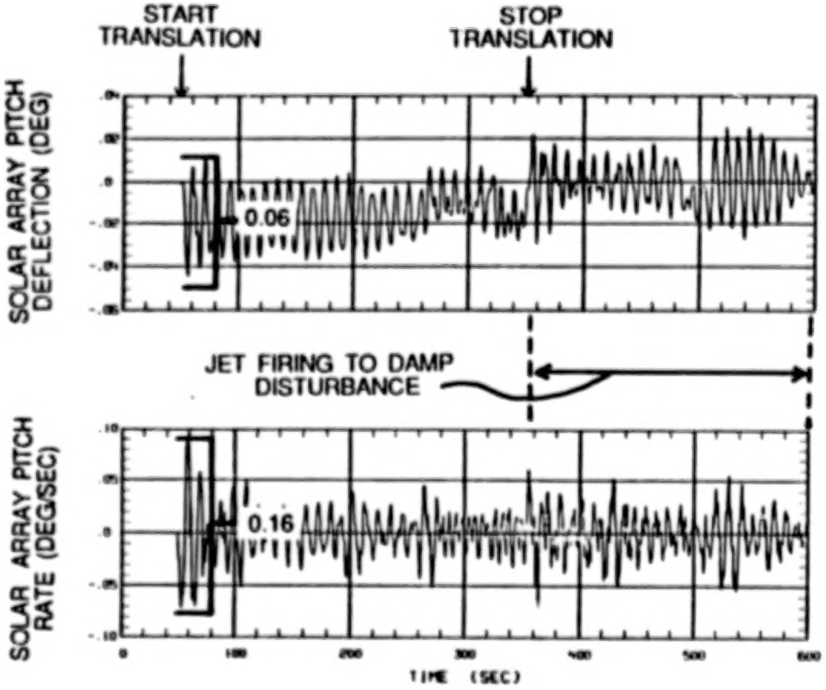

Rockwell International
Space Station Systems Division

* 25 lb / Cluster Thrust Level

REBOOST AND ATTITUDE MANEUVERING PRODUCE ACCEPTABLE UPPER BOOM DEFLECTIONS AND RATES

A remote location on the upper boom exhibits reasonable deflection during reboost and attitude maneuver operations.

Reboost and Attitude Maneuvering Produce Acceptable Upper Boom Deflections and Rates *

ATTITUDE MANEUVER
(8 DEG PITCH, 4 DEG ROLL)

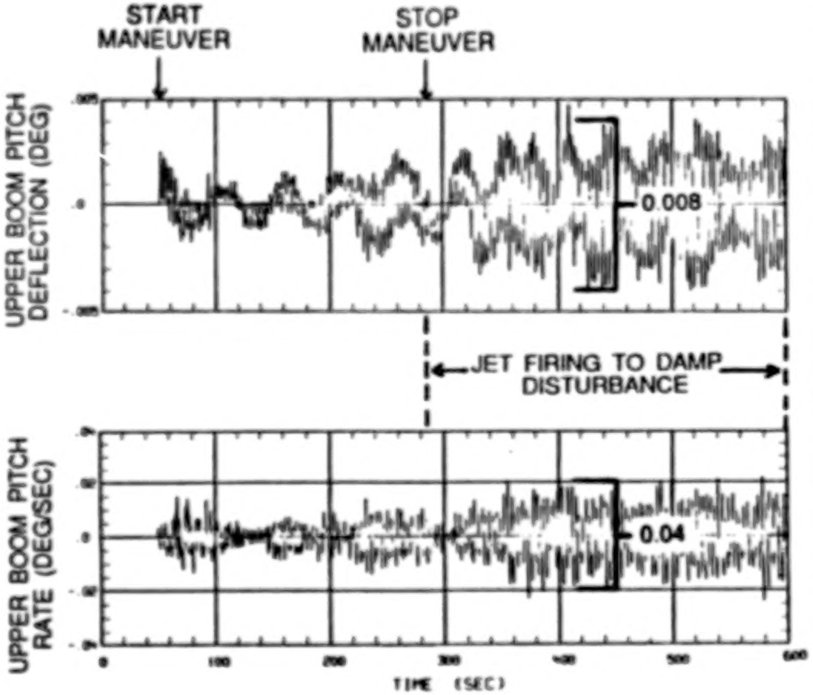

REBOOST -- 300 SECOND TRANSLATION

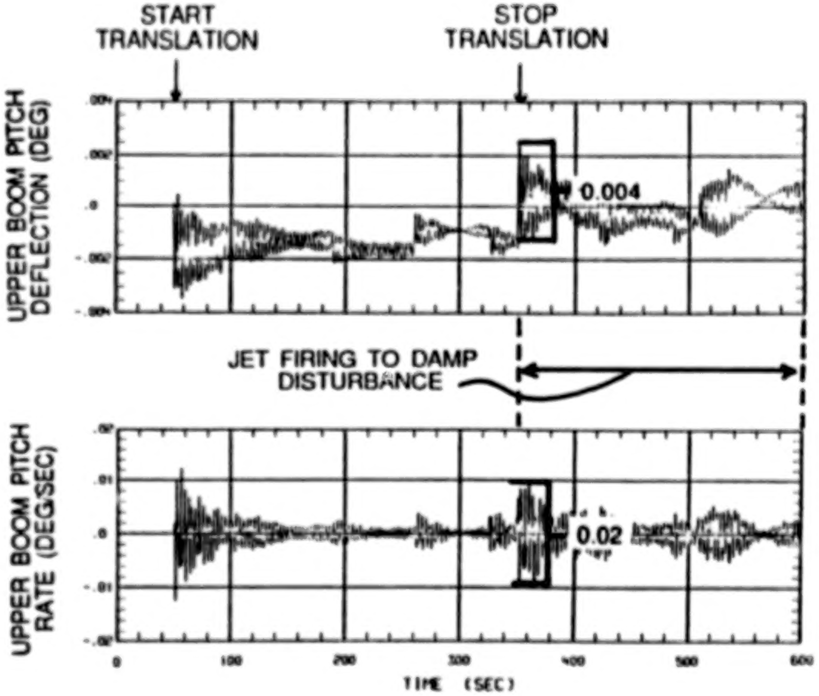

Rockwell International
Space Station Systems Division

* 25 lb / Cluster Thrust Level

THRUST LEVEL OF 10 LB/CLUSTER PROVIDES ACCEPTABLE CONTROL AUTHORITY

The ability of a reaction control system to damp disturbances quickly is of interest as a measure of control authority. The settling-time-versus-thrust-level indicates the sensitivity of performance during the damping of a maneuver-related disturbance.

Thrust Level of 10 lb / Cluster Provides Acceptable Control Authority

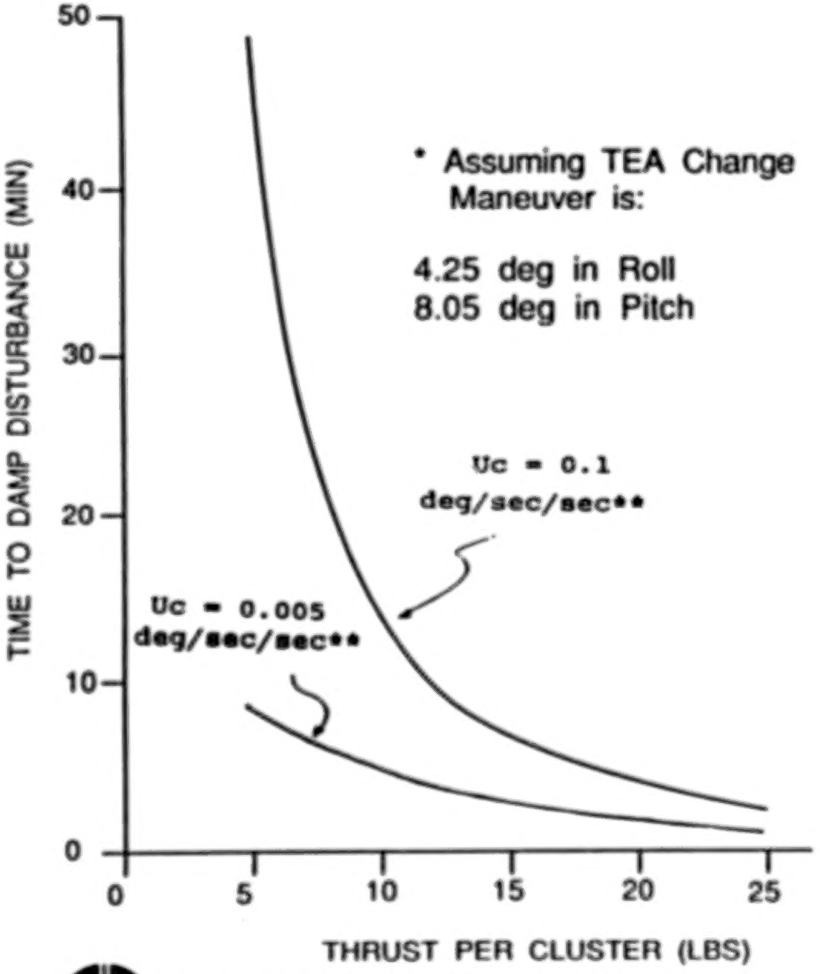

* Assuming TEA Change Maneuver is:

4.25 deg in Roll
8.05 deg in Pitch

BODY RATE ERROR

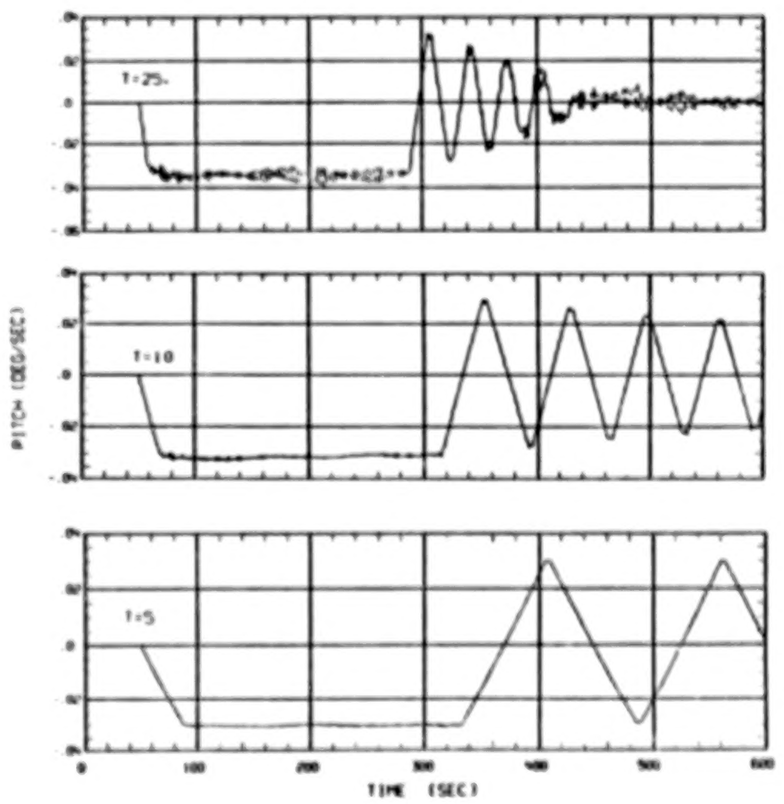

Rockwell International
Space Station Systems Division

RCS PROVIDES ADEQUATE RATE ERROR AND ATTITUDE ERROR CONTROL FOR PLUME IMPINGEMENT DAMPING

The effect of orbiter plume impingement disturbance was evaluated in terms of control authority, attitude excursion, and settling time. Worst case study of HIGH Z orbiter primary RCS firing indicates significant disturbance torque impulse of at least 161,000 ft-lb in pitch axis. Thrust level/cluster greater than 5 lb/jet is preferred to minimize attitude excursion and settling time. A more realistic case of LOW Z orbiter jet firing indicates less severe torque impulse of 26,188 ft-lbs at close range.

RCS Provides Adequate Rate Error and Attitude Error Control for Plume Impingement Damping

CONDITIONS:
- HIGH Z ORBITER BURN
  AT DOCKING PORT FOR 1 SECOND
- (-19,000 ft-lb in roll)
- (161,000 ft-lb in pitch)
- (-61,000 ft-lb in yaw)

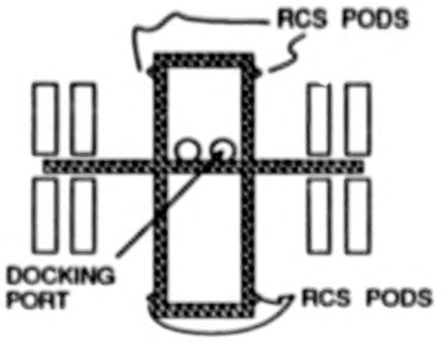
RCS PODS
DOCKING PORT
RCS PODS

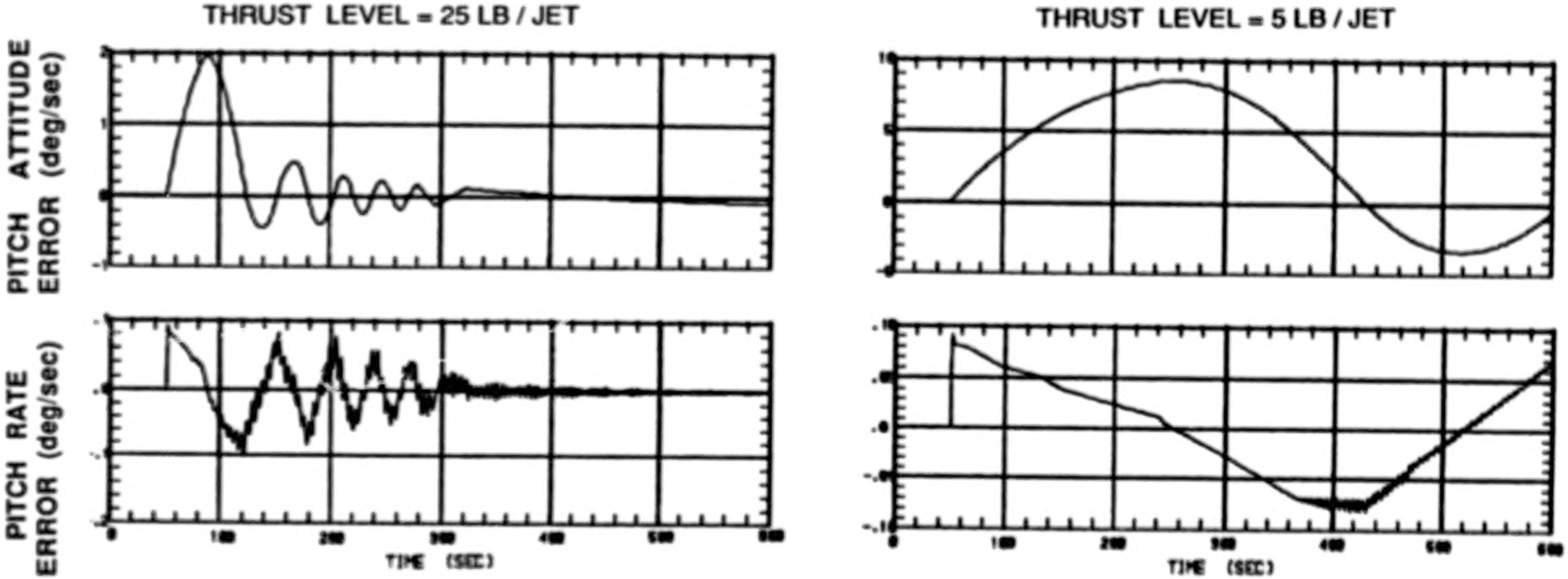

Rockwell International
Space Station Systems Division

CONTINGENCY OPERATION DISTURBANCES HANDLED WITHIN REASONABLE SETTLING TIME

The HIGH Z RCS mode of the orbiter may be applied during a contingency braking condition. It is reasonable to allow settling time to be longer than it would be for a nominal operation, as long as the attitude excursion of the Station does not reduce the clearance between the orbiter and the Station.

Contingency Disturbances Controlled Within Reasonable Settling Time

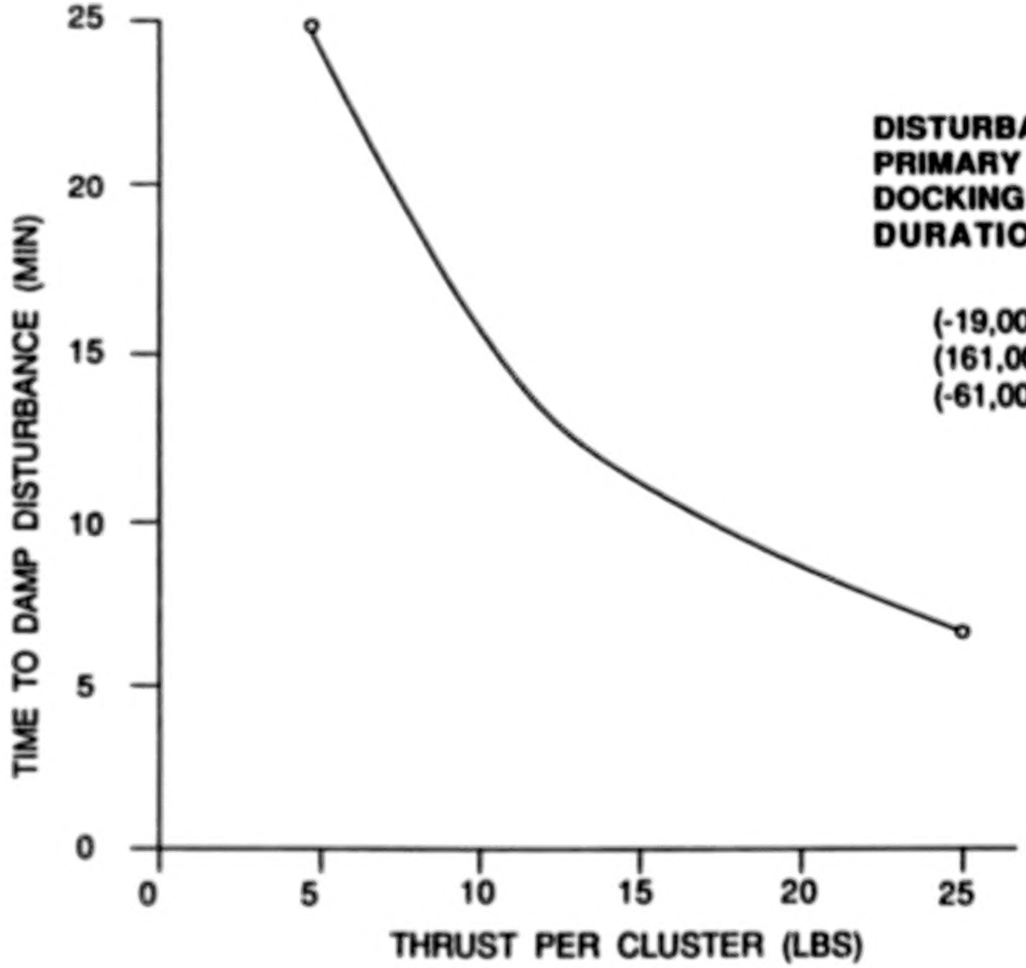

DISTURBANCE IS HIGH Z PRIMARY JET FIRING AT DOCKING PORT FOR 1 SECOND DURATION

(-19,000 FT-LB IN ROLL)
(161,000 FT-LB IN PITCH)
(-61,000 FT-LB IN YAW)

RCS CONTROL/STABILITY ACHIEVED BY COMPENSATION TECHNIQUE

A compensated RCS controller can provide adequate stability and performance. These techniques include wide notch filter, rate gain scheduling, dual control level, and integral loop.

A two-level RCS utilizing three engines per direction is applicable to the Space Station. A pressure regulated thrust level of 10 lb / engine or a blowdown thrust range of 15-7.5 lb / engine provides adequate control authority without unnecessary loading of the structure. Results also indicate that with proper choice of loop gains and phase plane parameters, system constraints and performance requirements can be met during reboost, maneuvers, and disturbance conditions.

RCS Control / Stability Achieved by Compensation Techniques

- A COMPENSATED RCS CONTROLLER CAN PROVIDE A PHASE MARGIN OF 40 DEGREES AND A GAIN MARGIN OF 10 db.

- THOUGH THE YAW MOMENT ARM IS SMALL FOR ASSEMBLY FLIGHT 1, THREE AXIS CONTROL CAN BE MAINTAINED DURING MANEUVERS AND REBOOST

- MAXIMUM RATES AND DEFLECTIONS EXPERIENCED OVER THE RANGE OF ACCEPTABLE THRUST VALUES ARE:

	Upper Boom	Solar Array
Deflection (deg)	< 0.004 peak	< 0.15 peak
Rate (deg / sec)	< 0.02 peak	< 0.40 peak

DESIGN ANALYSIS ESTABLISHES GN&C REQUIREMENTS FOR THRUST MAGNITUDE

By following the design criteria and performing the design analysis, we can achieve the design goals, fall within structural truss load limits, meet stability requirements, satisfy reasonable reboost time, assure adequate control authority, and cover the range of center of gravity variation.

Design Analysis Establishes GN&C Requirements for Thrust Magnitude

SPACE STATION

DESIGN GOALS:
- Can be met with 10 lbf Minimum Thrust / Cluster

STRUCTURAL TRUSS LOAD LIMITS:
- Satisfied with Thrust Less Than 25 lbf / Cluster

ADEQUATE STABILITY GAIN MARGIN:
- Satisfied with Thrust Less Than 20 lbf / Cluster

REBOOST TIME:
- Reboost Time Less Than One Crew Shift with Thrust at 20 lbf / Cluster

ADEQUATE CONTROL AUTHORITY:
- Met with 10 lbf Minimum Thrust / Cluster

CLUSTER LOCATIONS FOR DUAL - KEEL
- Provide Large Control Moment Arm and Cover Range of CG Variations
- Need Further Study on CGx Offset

CONCLUSION/RECOMMENDATIONS FOR GN&C THRUST MAGNITUDE REQUIREMENTS

Complying with loads and deflection constraints, the thrust range is limited to 20 pounds per cluster. If a pressure regulated system is chosen, 10 pounds thrust per thruster is required. If a blowdown system is chosen, a 15 to 7.5 thrust range/thruster is required.

A pressure regulated system is preferred in light of control logic simplicity, less cost for software development and verification, and straightforward performance verification.

Conclusions / Recommendations for GN&C Thrust Magnitude Requirements

CONCLUSIONS:

- Limit Thrust Range to 20 lb / Cluster Maximum
- If a Pressure Regulated System is Chosen, 10 lb Thrust / Thruster is Required
- If A Blowdown System is Chosen, a 15 to 7.5 lb Thrust Range / Thruster is Required
- Require 3 Thrusters / Cluster, 9 Thrusters / Module (3 in +x, 3 in +y, 3 in -x)

RECOMMENDATIONS:

- Baseline Pressure Regulated System
  - 3 Jets / Cluster, 9 Thrusters / Module (3 in +x, 3 in +y, 3 in -x)
  - 10 Pound Thrust / Thruster

Rockwell International
Space Station Systems Division

April 23, 1986

SESSION 4

Integrated Session 4A - Don Skoumal, Chairman

Dual Keel Space Station Control/ Structures Interaction Study	J. W. Young, F. J. Lallman, P. A. Cooper, LaRC
High Speed Simulation of Flexible Multibody Dynamics	A. D. Jacot, R. E. Jones, C. Juengst, Boeing
On the Application of Lanczos Modes to the Control of Flexible Structures	R. R. Craig, Jr. U. of Texas
Modal Testing and Slewing Control Experiment for Flexible Structures	J. N. Juang, LaRC
MEOP Control Design Synthesis: Optimal Qualification of the Big Four Tradeoffs	David C. Hyland and Dennis Bernstein, Harris Corp.

Integrated Session 4B - Harry J. Buchanan, Chairman

Vibration Isolation for Line of Sight Performance Improvement	J. J. Rodden, H. Dougherty, W. Haile, LMSC
A New Semi-Passive Approach for Vibration Control in Large Space Structures	K. Kumar and J. E. Cochran, Jr. Auburn Univ.
Crew Motion Forcing Functions from Skylab Flight Experiment and Applicable to Space Station	B. Rochon, JSC
Modeling of Controlled Structures with Impulsive Loads	M. Zak, JPL

PRECEDING PAGE BLANK NOT FILMED

N87
22737
UNCLAS

N87-22737

DUAL KEEL SPACE STATION CONTROL/STRUCTURES INTERACTION STUDY

by

John W. Young
Spacecraft Control Branch

Frederick J. Lallman
Analytical Methods Branch

and

Paul A. Cooper
Structural Concepts Branch
NASA Langley Research Center
Hampton, VA 23665

ABSTRACT

A study was made to determine the influence of truss bay size on the performance of the space station control system. The objective was to determine if any control problems existed during reboost and to assess the level of potential control/structures interactions during operation of the control moment gyros used for vertical stabilization. The models analyzed were detailed finite-element representations of the 5-meter and 9-foot growth versions of the 300 KW dual keel station.

Results are presented comparing the performance of the reboost control system for both versions of the space station. Standards for comparison include flexible effects at the attitude control sensor locations and flexible contributions to pointing error at the solar collectors. Bode analysis results are presented for the attitude control system and control, structural, and damping sensitivities are examined.

PRECEDING PAGE BLANK NOT FILMED

The purpose and objectives of the study are presented in figure 1. Details of the space station models and the control systems studies are given in references 1 and 2.

PURPOSE

To determine the influence of truss bay size (5–meter vs. 9–foot) on the performance of the space station control systems

OBJECTIVES

- To assess the level of potential control/structures interactions during operation of the control moment gyros used for vertical stabilization
- To investigate possible control problems during operation of the Reaction Control System Jets used for orbit reboost

Figure 1

DUAL KEEL SPACE STATION

The 5-meter and 9-foot versions of the dual keel space station studied in the present paper had approximately the same dimensions and mass properties with the only difference being the truss bay size. The 5-meter station is shown in figure 2 to illustrate several points of interest in the control study. The control sensors and control moment gyros which constitute the Attitude Control Assembly (ACA) are co-located at the origin of the coordinate system shown in figure 2. The ACA package is located about 10 feet above the center of gravity of the station. The four reaction control system (RCS) thrusters shown are used in the reboost control system with each thruster producing a 75-pound force along the orbit plane (x-axis) of the station. The solar dynamic units are explained in a following figure. They are of interest in the reboost analysis since they must be oriented toward the solar vector for efficient operation as power generators.

DUAL KEEL SPACE STATION

5m truss

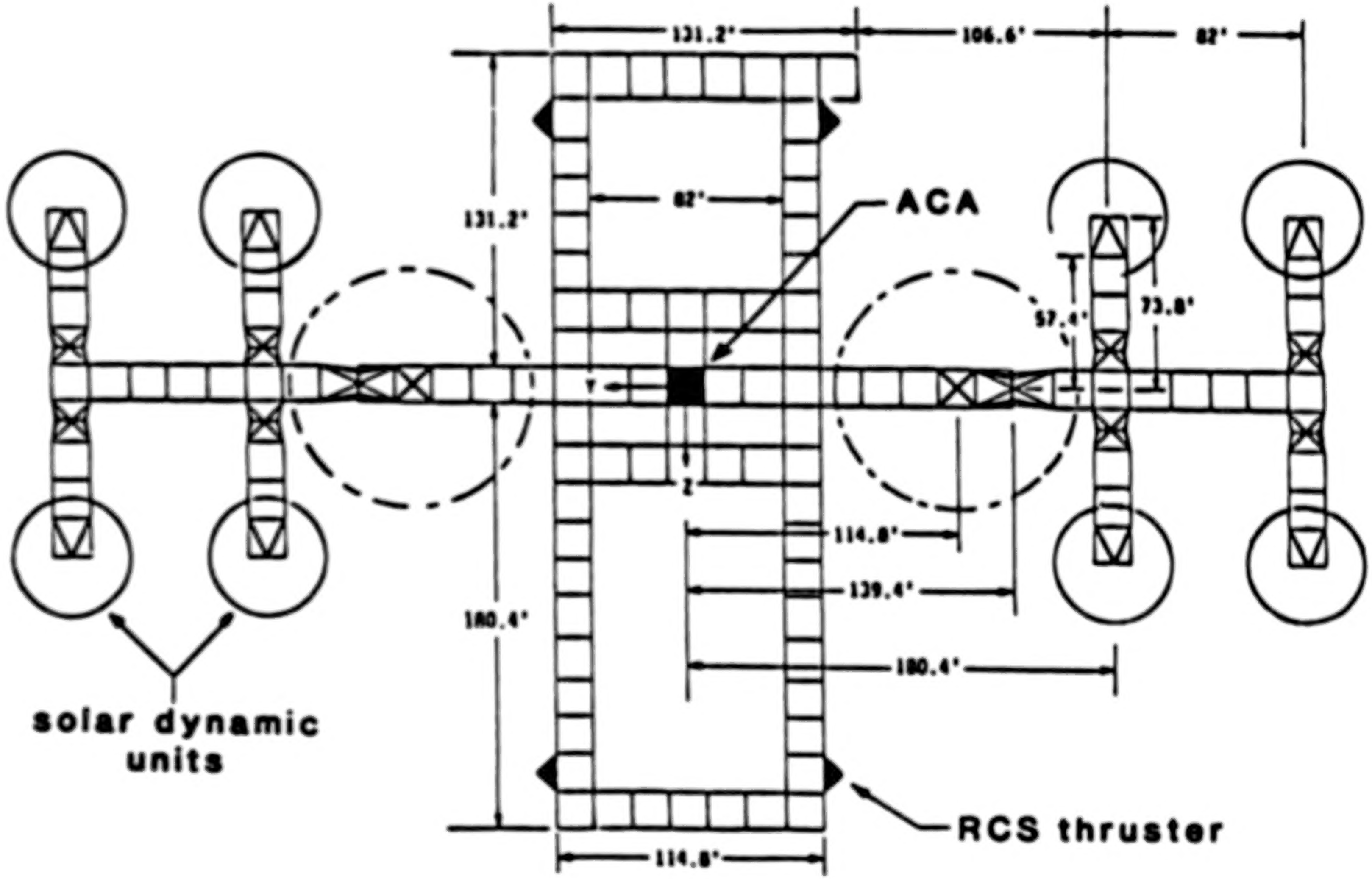
131.2'
106.6'
82'
131.2'
82'
ACA
57.4'
73.8'
Y
Z
114.8'
139.4'
180.4'
180.4'
solar dynamic units
RCS thruster
114.8'

Figure 2

ATTITUDE CONTROL SYSTEM STUDY

The attitude control system is designed to regulate the orientation of the space station to keep the longitudinal axis (z-axis) aligned with the gravity vector. The control system consists of y-axis pitch and pitch rate sensors, control moment gyros (CMG's), and electronics to cause corrective moments to be applied to the station whenever it deviates from the commanded attitude. The attitude control system study is outlined in figure 3. Control system performance indicators are listed in the figure.

ATTITUDE CONTROL SYSTEM STUDY

- Control System stability investigated using frequency response (Bode) Analysis

  Control Laws:
  1– Angular error and rate feedback (PD)
  2– PD + 1st order lag compensation

- Control System Performance Indicators

  1– Gain margin for structural modes
  2– Structural damping required for specified gain margin
  3– Modal frequency change for structural instability
  4– Control bandwidth

Figure 3

BLOCK DIAGRAM OF ATTITUDE CONTROL SYSTEM

A block diagram of the y-axis control system used in the study is shown in figure 4. The attitude angle (and its rate of change) responds to moments applied to the station by the CMG's and external and internal disturbances. The effect of structural vibrations is included in this angle. The electronic controller mechanized a control law to produce a commanded control moment based on the error signal. The closed loop bandwidth and damping ratio of the system was specified to be .01 Hz. and .275 respectively.

BLOCK DIAGRAM OF ATTITUDE CONTROL SYSTEM

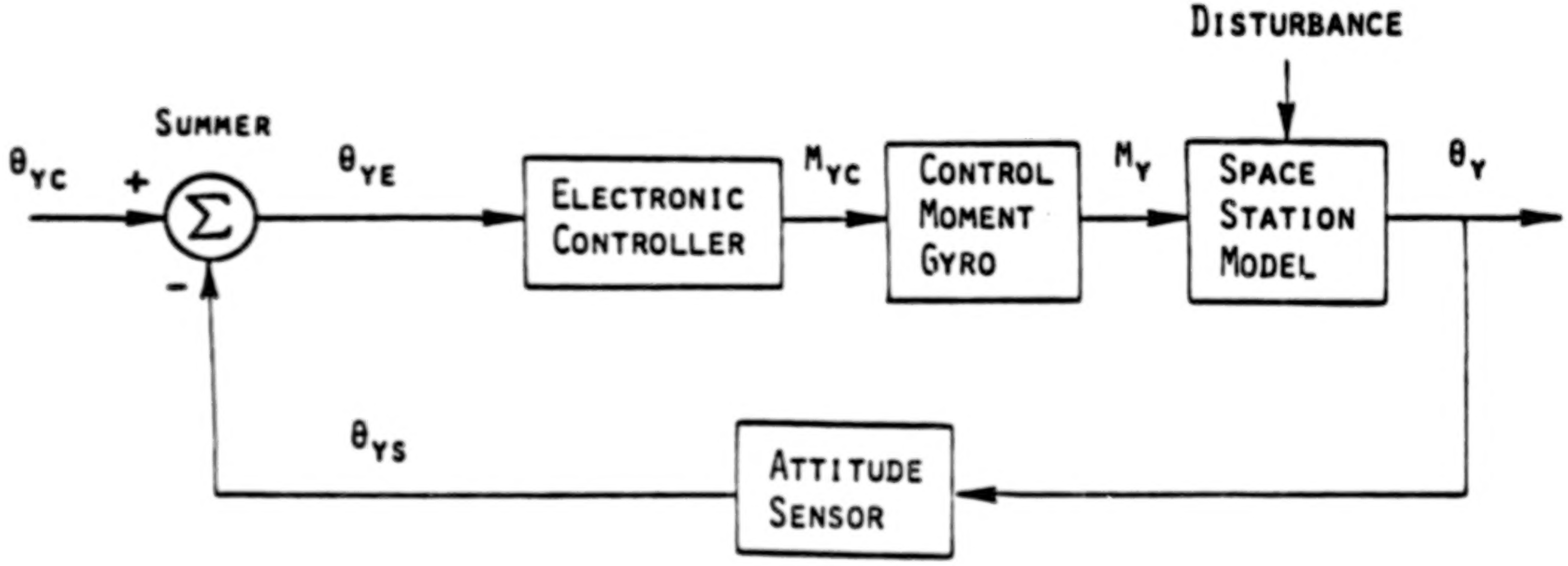
DISTURBANCE
SUMMER
θ_{YC}
+
Σ
-
θ_{YE}
ELECTRONIC CONTROLLER
M_{YC}
CONTROL MOMENT GYRO
M_Y
SPACE STATION MODEL
θ_Y
θ_{YS}
ATTITUDE SENSOR

θ_Y - SPACE STATION ATTITUDE

θ_{YS} - SENSED ATTITUDE

θ_{YC} - COMMANDED ATTITUDE

θ_{YE} - ATTITUDE ERROR

M_Y - CONTROL MOMENT

M_{YC} - COMMANDED CONTROL MOMENT

Figure 4

FREQUENCY RESPONSE, PD CONTROLLER

Frequency response plots for loop gain using a PD controller are given in figure 5. The PD controller is the simplest that can stabilize the rigid-body dynamics while meeting the bandwidth requirement. The low frequency portions of the plots reflect the rigid-body dynamics and are nearly identical since the moments of inertia of the two station models are approximately the same. The higher frequency portions of figure 5 show the effect of including the structural dynamics in the station models (50 structural modes were included). The major difference in the two models was that the structural mode frequencies of the 5-meter station were approximately twice those of the 9-foot configuration because of its greater stiffness. The frequency response plots of figure 5 indicate unstable gain margins for both station models with higher resonant peaks occurring with the 9-foot model.

FREQUENCY RESPONSE, PD CONTROLLER

Control Low: $\frac{M_y}{\theta_{ye}}(s) = K's + K$

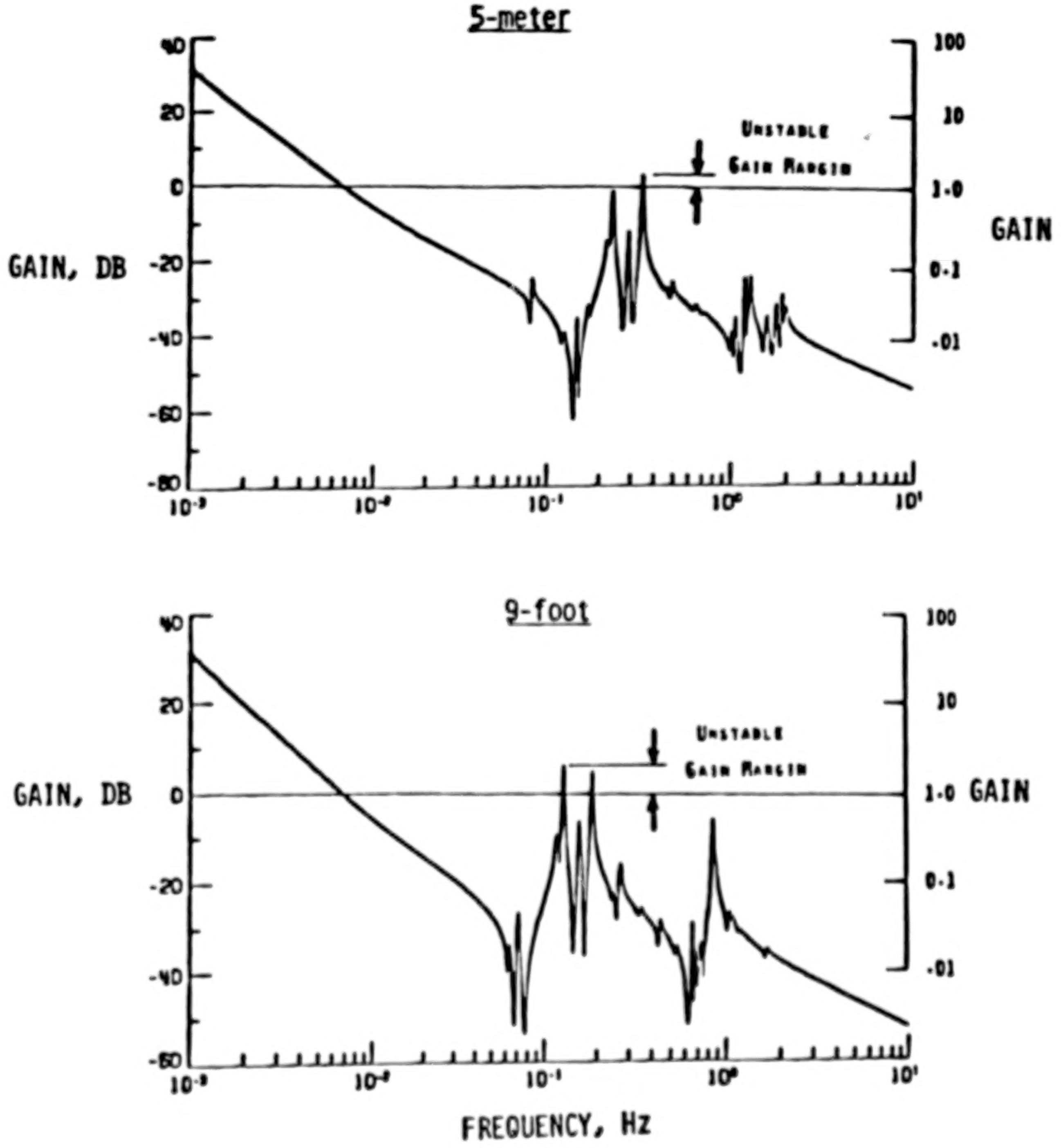

Figure 5

FREQUENCY RESPONSE, COMPENSATED PD CONTROLLER

Since the PD control law resulted in unstable structural modes, a second control law was designed to correct the problem. The object of the redesign was to reduce the magnitude of the frequency response for the higher frequency range while maintaining the rigid-body bandwidth and damping ratio. This was accomplished by adding a first-order lag to the control law and adjusting the proportional and differential gains to form a compensated PD controller. Frequency response plots for loop gain using the compensated PD controller are given in figure 6. The addition of compensation reduces the higher frequency portions of the gain plots and results in stable gain margins for both station models.

FREQUENCY RESPONSE, COMPENSATED PD CONTROLLER

Control Low: $$\frac{M_y}{\theta_{ye}}(s) = \frac{K's + K}{s/p + 1}$$

5-meter

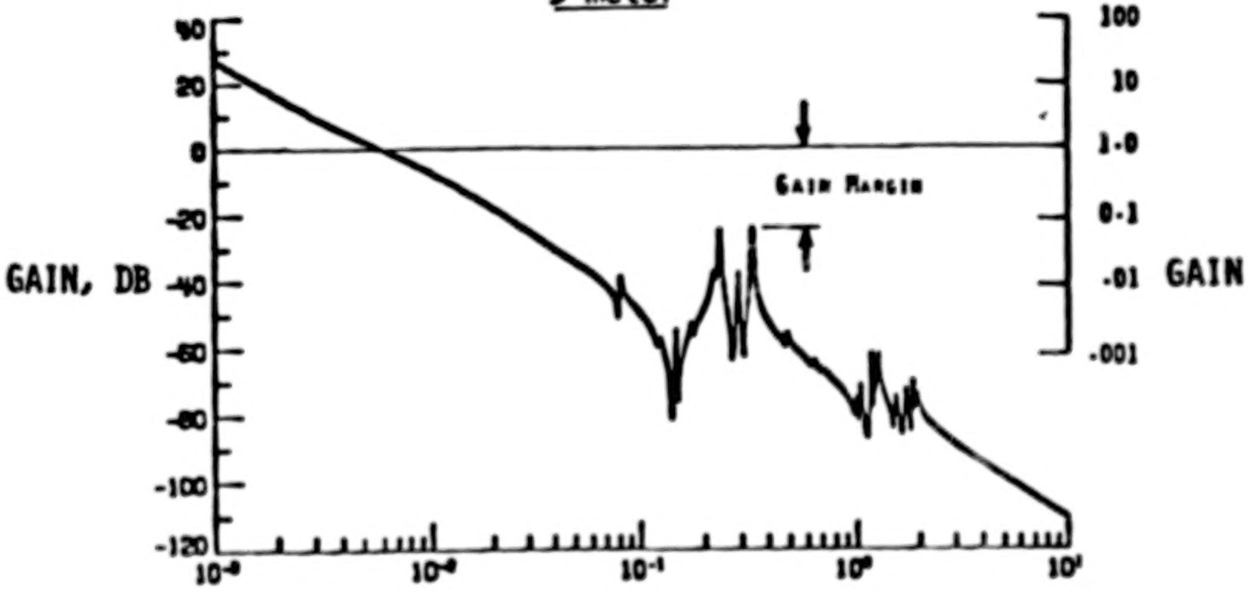

9-foot

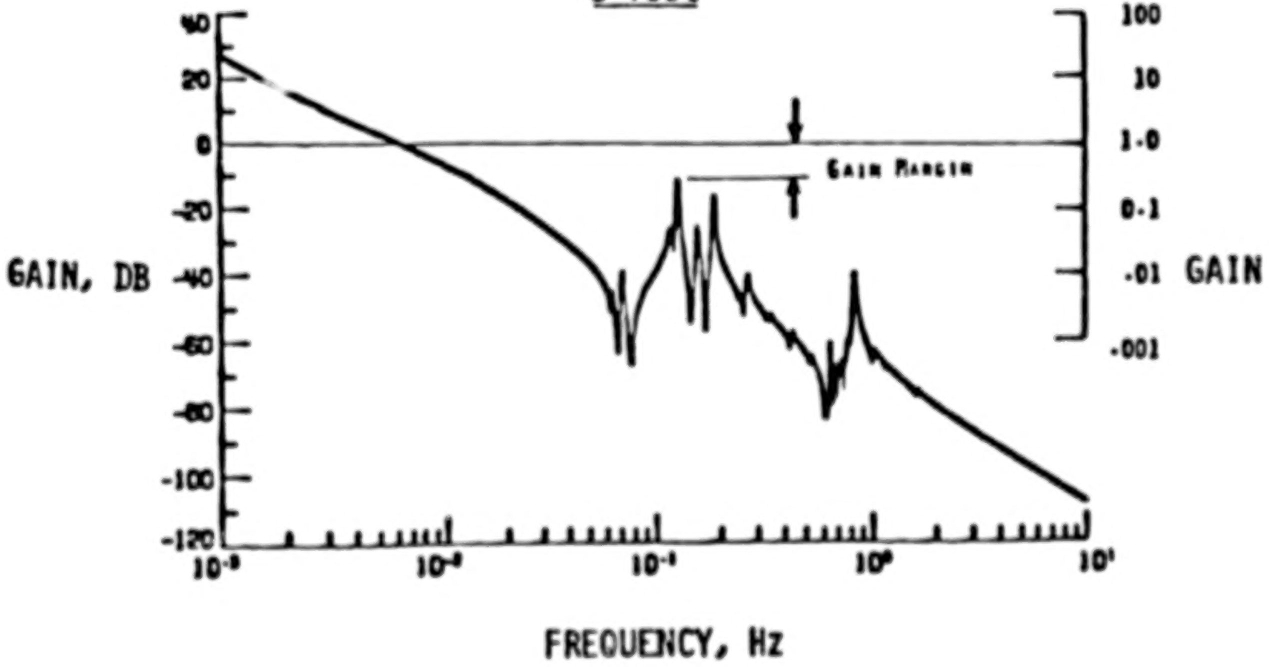

Figure 6

SPACE STATION BODE ANALYSIS RESULTS

The results of the attitude control system study using the compensated PD controller are given in figure 7. Gain margin comparisons (Fig. 6) show a 12 DB advantage for the 5-meter station. Estimates of the structural damping required to meet a hypothetical gain margin specification of 20 DB show that the 5-meter station required about 4.4 times less damping than the 9-foot model. The 5-meter station was found to be more tolerant to possible modal frequency changes and to have twice the bandwidth of the 9-foot station for a gain margin specification of 20 DB.

SPACE STATION
BODE ANALYSIS RESULTS*

	5 METER	9 FOOT	COMMENTS
GAIN MARGIN	23 dB	11 dB	12 dB ADVANTAGE FOR 5-METER
REQUIRED STRUCTURAL DAMPING FOR 20 dB MARGIN	0.34%	1.5%	5-METER REQUIRES 4-5 TIMES LESS STRUCTURAL DAMPING
MODAL FREQUENCY CHANGE FOR STRUCTURAL INSTABILITY	-75%	-47%	5-METER IS MORE TOLERANT OF MODAL FREQUENCY CHANGES
MAXIMUM BANDWIDTH FOR 20 dB MARGIN	.012 Hz	.0060 Hz	5-METER ATTITUDE CONTROL IS TWICE AS RESPONSIVE

*PD CONTROLLER WITH 1st ORDER COMPENSATION

Figure 7

REBOOST CONTROL SYSTEM STUDY

The reboost control system study performed is outlined in figure 8. Control system performance indicators are listed in the figure.

REBOOST CONTROL SYSTEM STUDY

- Control System performance comparisons between the 5–meter and 9–foot configurations were made using time history response calculations

  Control Law:
  Nonlinear switching logic for RCS jets based on sensed pitch and pitch rate

- Control System Performance Indicators

  1– Flexible interference in sensor outputs
  2– Structural vibrations at the solar collectors

Figure 3

REBOOST CONTROL LOGIC

The Space Station must be periodically reboosted to maintain a desired orbit. The maneuver is performed using four 75-pound, constant thrust jets located as shown on figure 2 with two jets above and two below the station center of gravity. The purpose of the reboost control system is to maintain attitude control during the maneuver. The system operates either with all jets on or using only the upper jets. With all jets on, a torque is generated about the y-axis of the station causing it to rotate away from the local vertical. The station attitude is kept within desired limits by off-modulation of the lower-keel jets. The control logic which governs the firing of the lower jets is given in figure 9. The logic results in a near periodic firing of the RCS jets as shown in the control history given on figure 9. The 1-degree deadband results in the space station oscillating about a 1-degree offset from the local vertical.

REBOOST CONTROL SWITCHING CURVE FOR RCS JETS

(Deadband = 1°, Hysteresis = .05°, K = 1 sec)

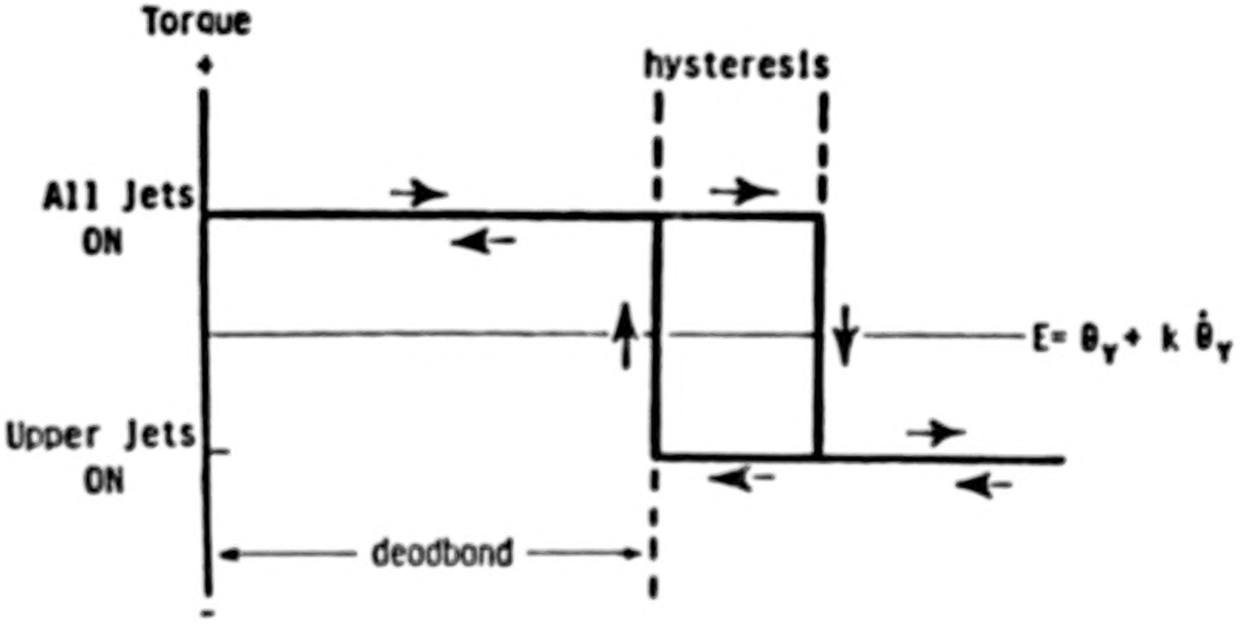
Torque
+
hysteresis
All Jets ON
$E = \theta_Y + k\,\dot{\theta}_Y$
Upper Jets ON
deadband
-

TYPICAL CONTROL HISTORY

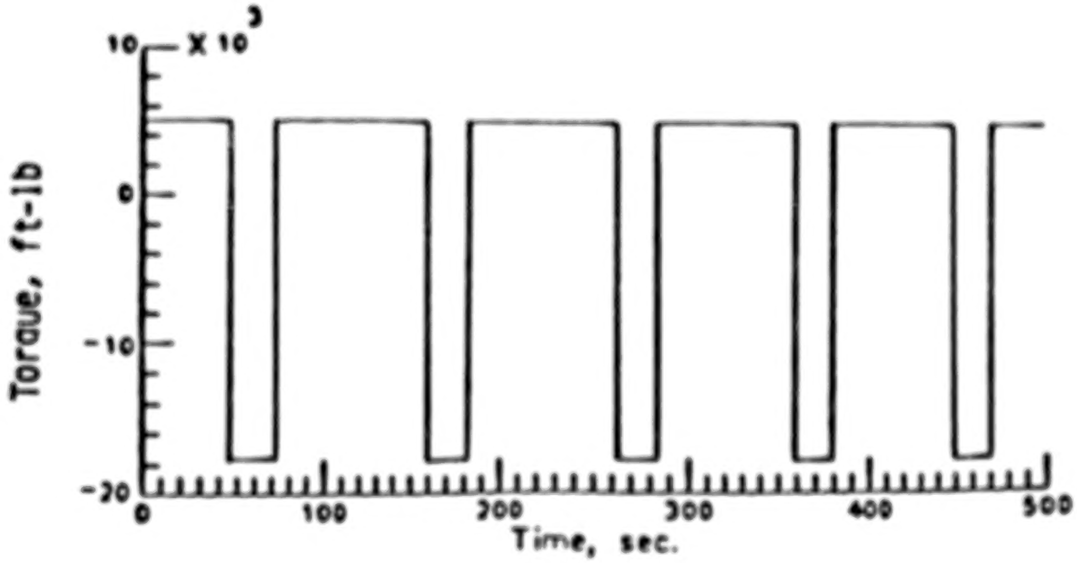

Figure 9

FLEXIBLE CONTRIBUTION TO ERROR SIGNAL DURING REBOOST MANEUVER

The error signal (E) used to control the RCS jet firing was an unfiltered pitch and pitch rate signal as measured at the ACA package location (Fig. 2). Since this signal contains both the rigid body and local flexible response, it is of interest to examine the flexible interference in sensor outputs during a reboost maneuver. Comparisons of the flexible contribution to the error signal are given in figure 10 for the 5-meter and 9-foot stations. The .03° peak in flexible interference for the 9-foot model could be reason for concern since it represents 60 percent of the .05° hysteresis used in the switching logic. However, no adverse effects were noted when an unfiltered error signal was used in the reboost logic. Nevertheless, with flexible deviations such as those shown on figure 10, the potential exists for deterioration of the hysteresis switching loop, and, in actual practice the reboost control error signal should be filtered to reduce flexible interference at the sensors.

FLEXIBLE CONTRIBUTION TO ERROR SIGNAL DURING REBOOST MANEUVER

$(E_{flex} = \Theta_{y\ flex} + K\,\dot{\Theta}_{y\ flex})$

ORIGINAL PAGE IS
OF POOR QUALITY

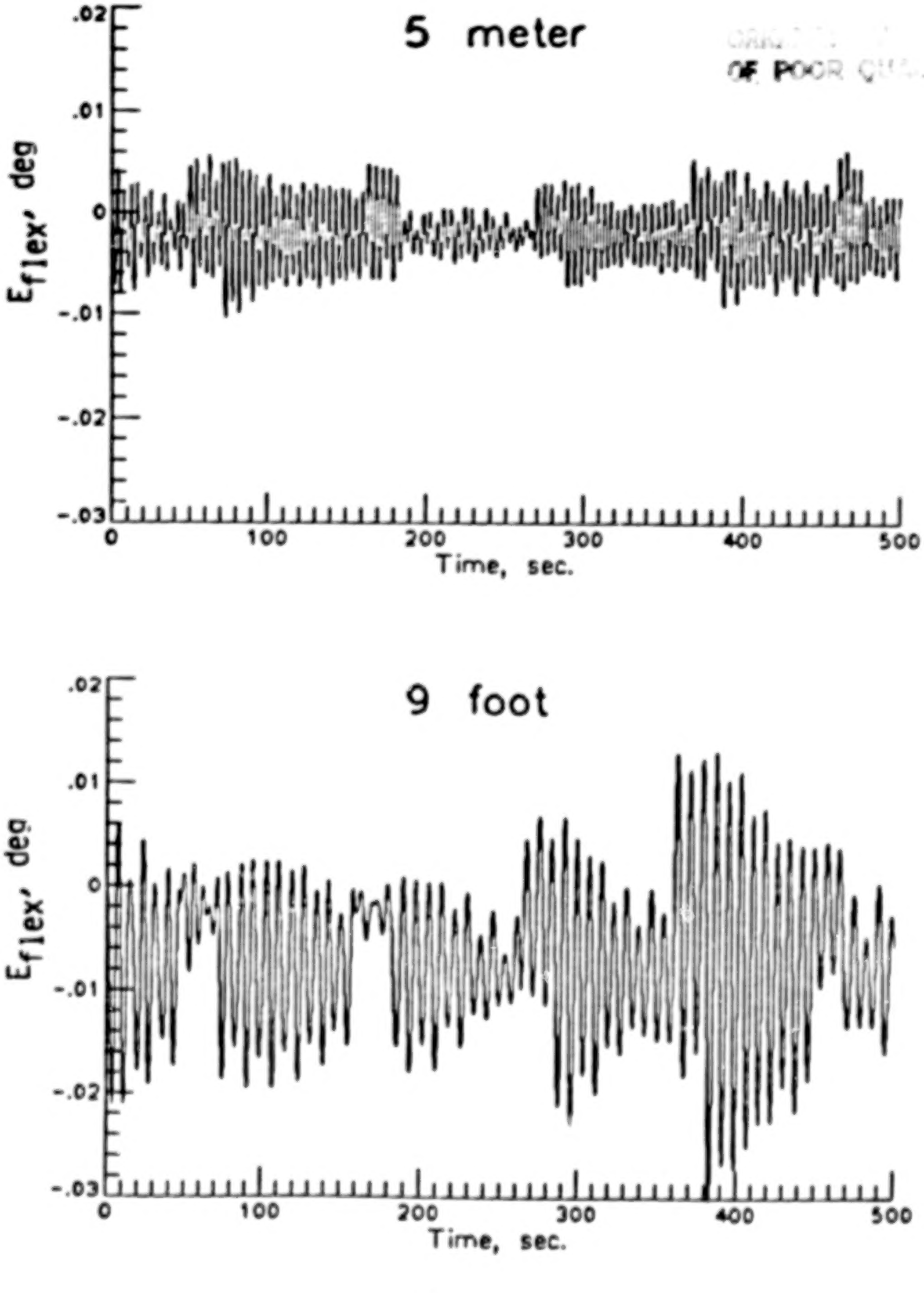

Figure 10

SOLAR DYNAMIC COLLECTORS

The station is powered by eight solar dynamic systems located as shown on figure 2. A typical solar dynamic collector is shown in figure 11. For maximum efficiency, the direction of the symmetric axis of each of the solar dynamic systems must be held to within .1° of the solar vector, even during an orbit reboost maneuver. This is done using controllers which command rotary joints located on the transverse truss and a rotary joint attached to the reflector symmetry axis. For the current study, these controllers are assumed inactive.

TYPICAL SOLAR DYNAMIC COLLECTOR UNIT

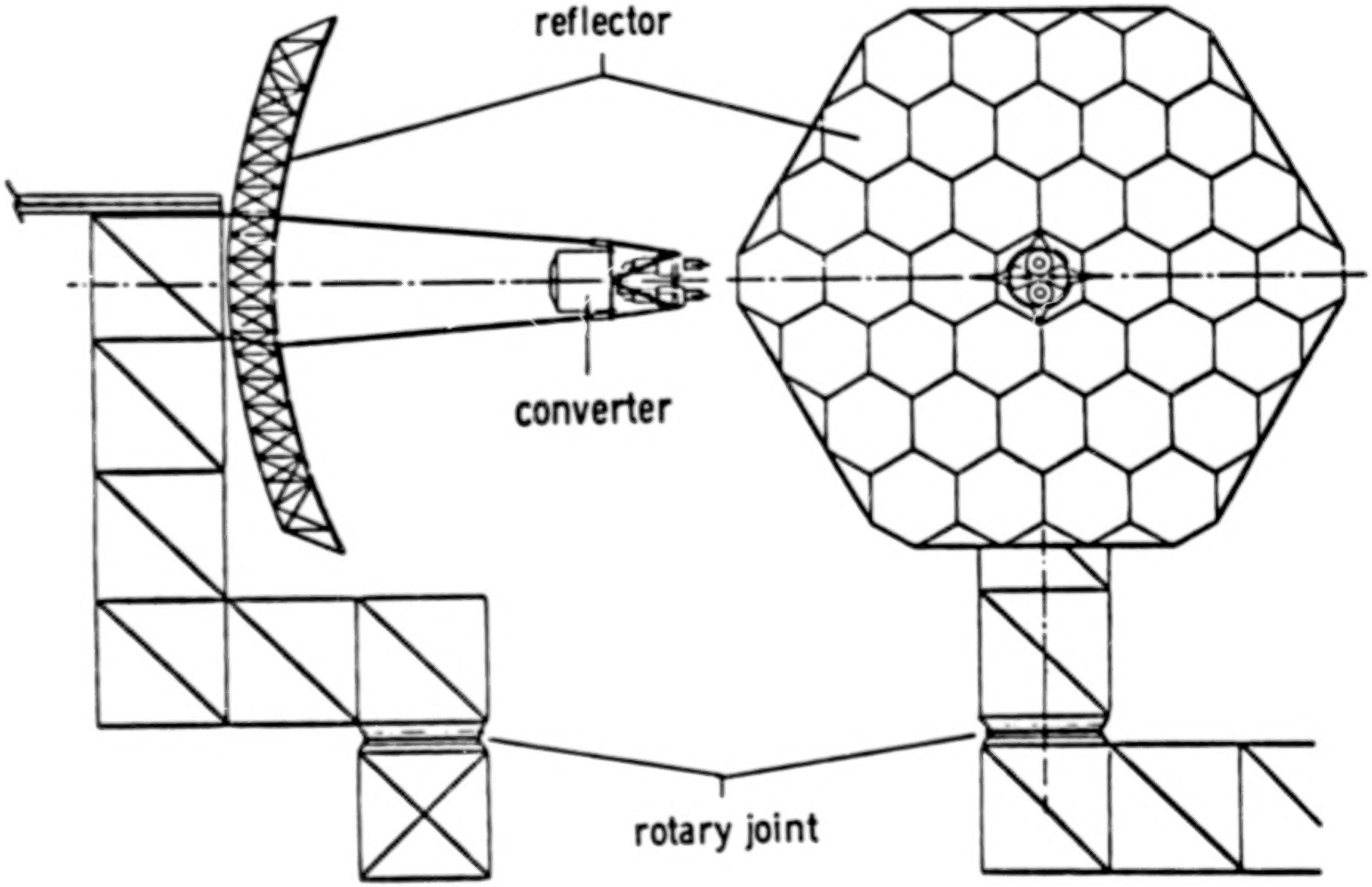
reflector
converter
rotary joint

Figure 11

VARIATION OF SUN-LINE AT OUTER SOLAR COLLECTOR DURING REBOOST

Sun-line variations at the outer collector during reboost are shown on figure 12 for the 5-meter and 9-foot stations. The responses contain a low-frequency rigid-body oscillation with a superimposed, higher frequency oscillation caused by the flexible modes. Due to the 1-degree offset requirement during reboost, sun-line variations always exceed the .1° pointing requirement for the solar collectors. However, if the rigid-body pitch angle were known, it could be nulled using the previously discussed rotary joints. Note that the flexible variations shown in figure 12 are larger for the 9-foot station than for the 5-meter configuration.

VARIATION OF SUN LINE AT OUTER SOLAR COLLECTOR DURING REBOOST

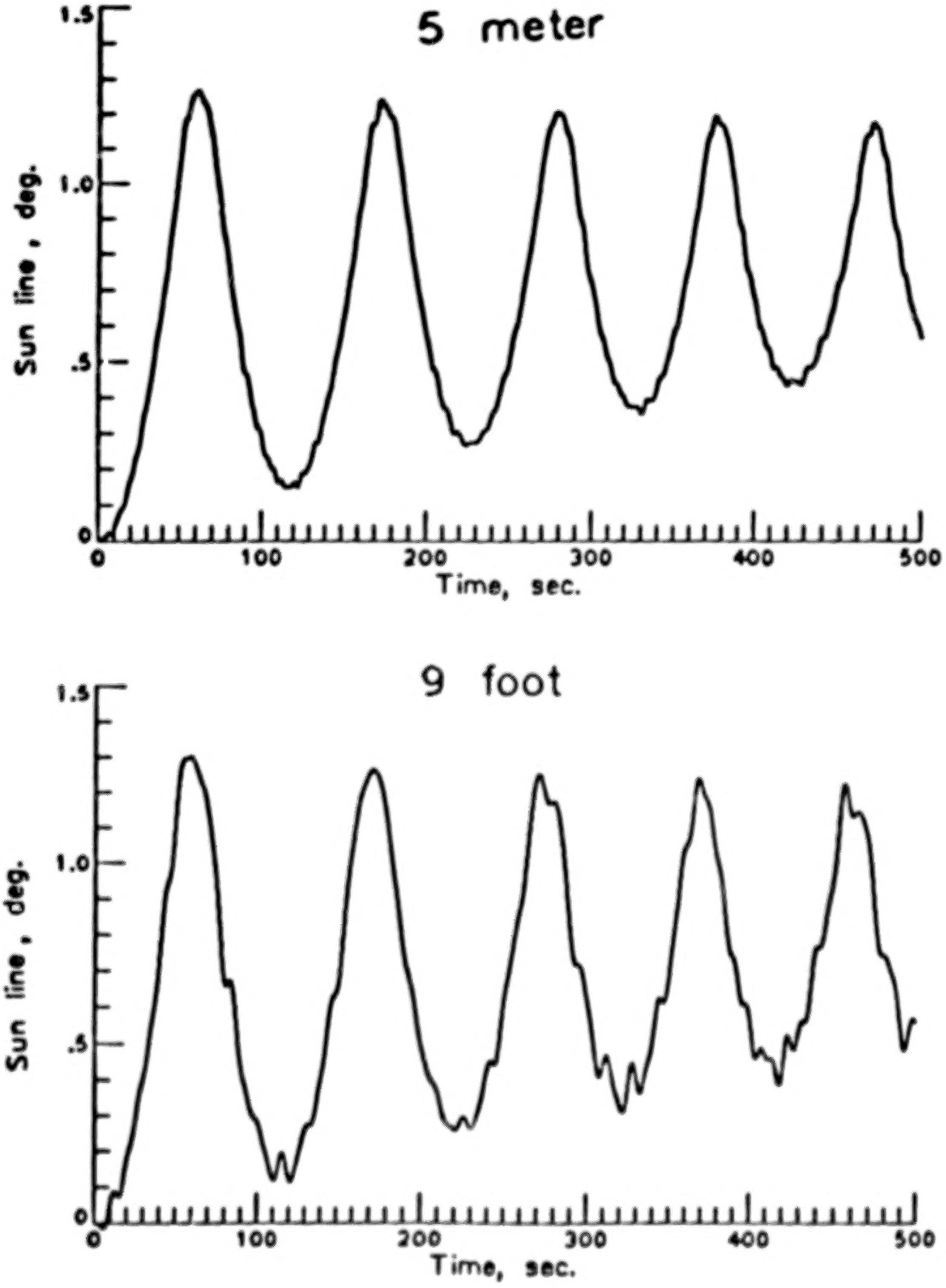

Figure 12

FLEXIBLE SUN-LINE EXCURSIONS DURING REBOOST

Flexible contributions to sun-line variations during reboost are given in figure 13 for the two station models. Shown is a continuous trace of the flexible sun-line at the outer solar collector during a reboost maneuver. While both flexible responses are within the .1° requirement, the 5-meter excursions are about one-fourth those for the 9-foot station.

SUN–LINE EXCURSIONS DURING REBOOST

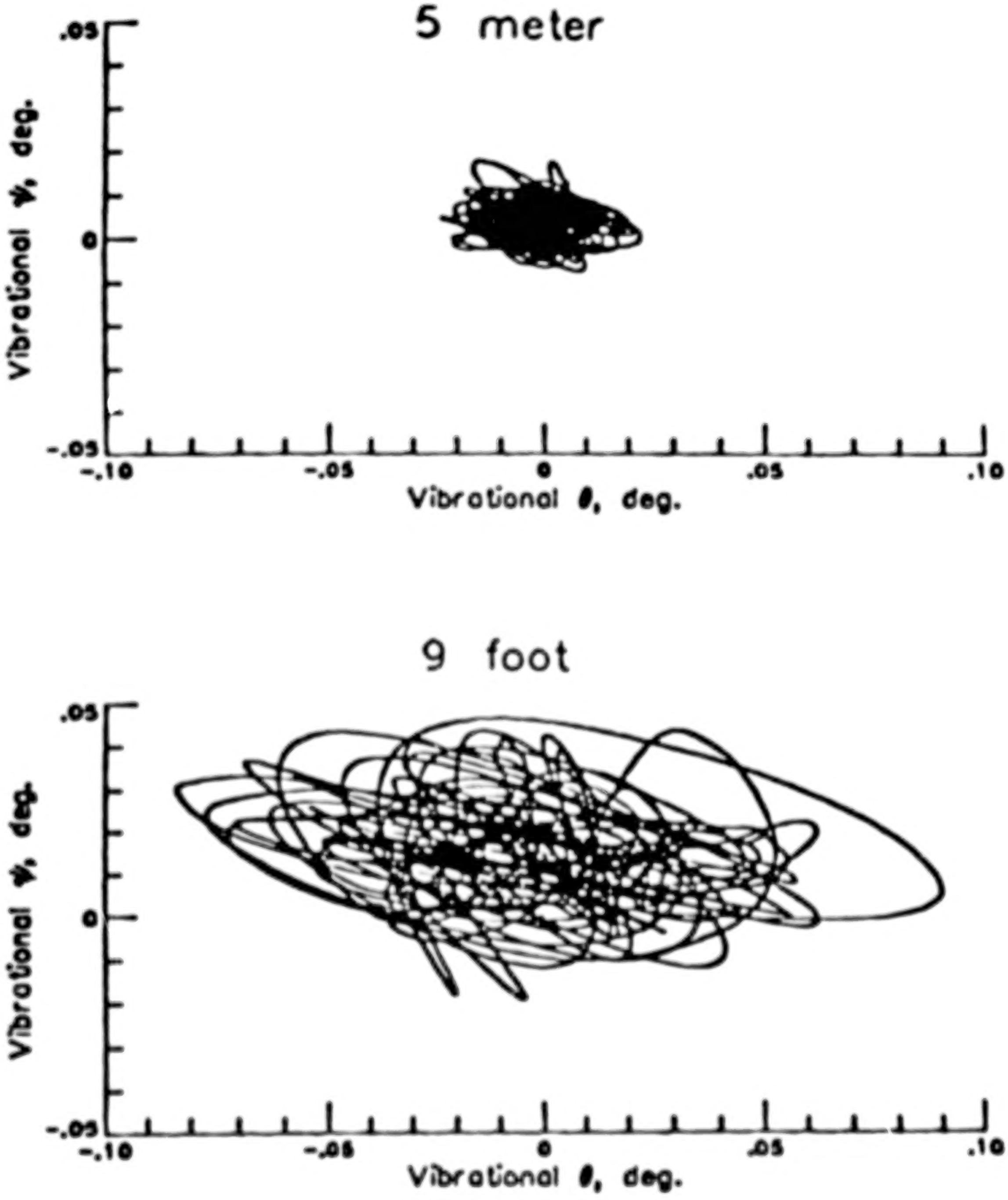

Figure 13

SUMMARY OF FLEXIBLE RESPONSE RESULTS FOR REBOOST MANEUVER

A summary of the results of the reboost control analysis are given in figure 14. The minimum structural frequency for the 5-meter station is double that for the 9-foot station. Since the reboost control frequencies are the same for both models, a greater separation between control and structural frequency exists for the 5-meter station. This is reflected in the lower flexible interference in the sensor outputs and the smaller collector transients shown in figure 14 for the 5-meter configuration.

SUMMARY OF FLEXIBLE RESPONSE RESULTS FOR REBOOST MANEUVER

	5 meter	9 Foot	Comments
Min. Structural Freq, Hz	.124	.062	5–meter freq double that for 9–foot
Reboost Control Freq, Hz	.014	.014	No difference
Peak Sensed E_{flex}, deg	.010	.030	5–meter interference 1/3 that for 9–foot
Peak Collector Transient, deg	.028	.095	5–meter peak sun–line transient about 1/4 that for 9–foot

Figure 14

REDESIGNED REBOOST MANEUVER

The previous reboost analysis assumed 75-pound thrust RCS jets, a 1-degree offset from the local vertical, and control logic hysterisis of .05°. An additional study was made in which the control logic was redesigned such that total sun-line variations at the solar collectors would never exceed the .1° pointing requirement during the reboost maneuver. The redesign consisted of reducing the upper and lower RCS jets from 75 pounds to 12.5 pounds and 20 pounds respectively. This produced opposing torques of equal magnitude with all jets on or with only the upper jets active. The deadband in the control logic was set to zero and a hysteresis of .00875° was used. The resulting sun-line variation at the outer solar collector for the 5-meter station during reboost is shown in figure 15. Note that rigid-body plus flexible deviations remain within the .1° requirement throughout the maneuver.

VARIATION OF SUN LINE AT OUTER SOLAR COLLECTOR FOR REDESIGNED REBOOST MANEUVER

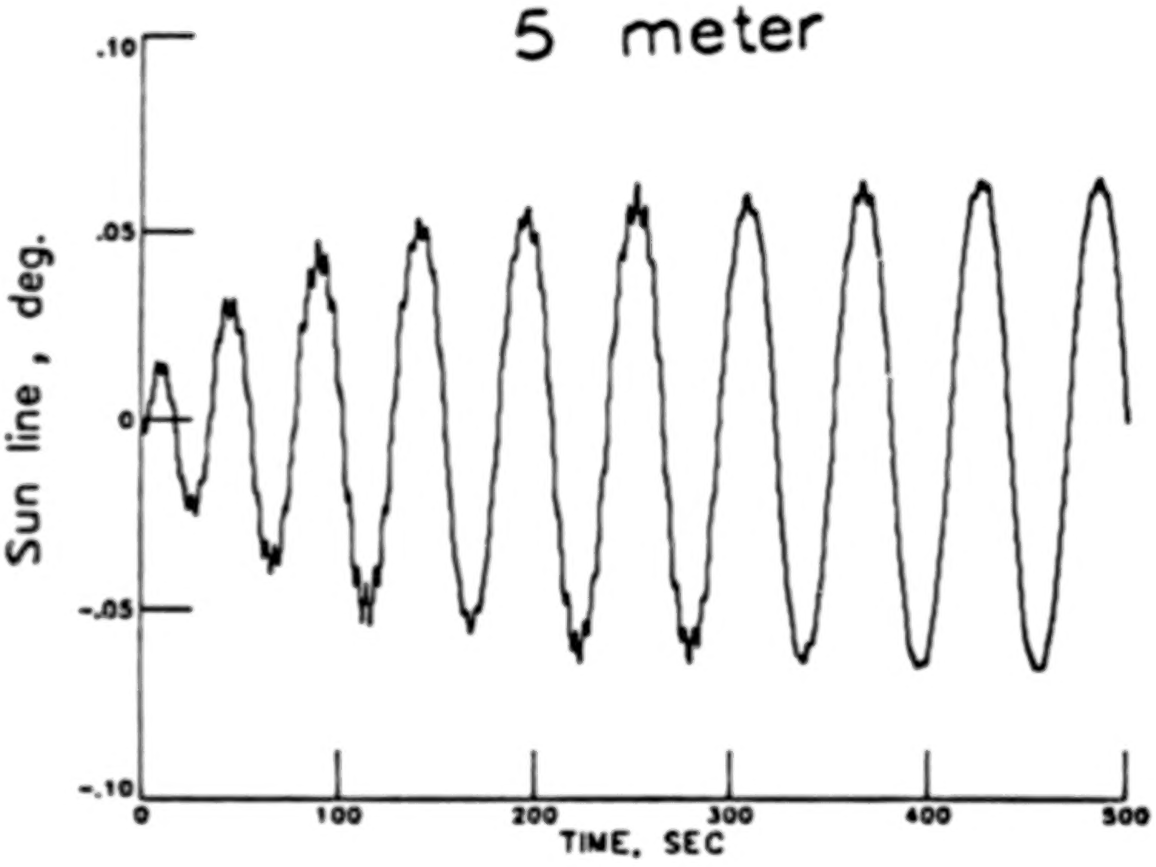
5 meter

Figure 15

SUMMARY OF RESULTS

The reboost and attitude control study results are summarized in figure 16. All aspects of the control study indicated a preference for the 5-meter configuration.

SUMMARY OF RESULTS

REBOOST ANALYSIS

5-METER CONFIGURATION PREFERRED DUE TO:

- LOWER AMPLITUDE, HIGHER FREQUENCY INTERFERENCE IN SENSED PITCH AND PITCH RATE
- SMALLER STRUCTURAL VIBRATIONS AT SOLAR DYNAMIC COLLECTORS

ATTITUDE CONTROL (BODE) ANALYSIS

5-METER CONFIGURATION PREFERRED DUE TO:

- HIGHER GAIN MARGINS
- LOWER STRUCTURAL DAMPING REQUIREMENTS
- LOWER SENSITIVITY TO MODAL FREQUENCY VARIATIONS
- HIGHER BANDWIDTH

CONCLUSION

ALL ASPECTS OF THE CONTROL STUDY INDICATED A PREFERENCE FOR THE 5-METER CONFIGURATION

Figure 16

REFERENCES

1. Dorsey, J. T.; Sutter, T. R.; Lake, M. S.; and Cooper, P. A.: Dynamic Characteristics of Two 300 KW Class Dual-Keel Space Station Concepts. NASA TM-87680, March 1986.

2. Young, J. W.; Lallman, F. J.; Cooper, P. A.; and Giesy, D. P.: Controls/Structures Interaction Study of Two 300 KW Dual-Keel Space Station Concepts. NASA TM-87679, May 1986.

N87
22738
UNCLAS

N87-22738

HIGH SPEED SIMULATION OF FLEXIBLE MULTIBODY DYNAMICS

A.D.Jacot, R.E.Jones, and C.D.Juengst
The Boeing Aerospace Company, Seattle, Wash.

ABSTRACT:

A multiflexible body dynamics code intended for fast turnaround control design trades is described. Nonlinear rigid body dynamics and linearized flexible dynamics combine to provide efficient solution of the equations of motion. Comparison with results from the DISCOS code provides verification of accuracy.

INTRODUCTION

Control design for complex multiflexible body dynamical systems requires many computer runs of simulations with high CPU usage. The high fidelity computer codes which currently address this nonlinear dynamics problem (for example, DISCOS, ref. 1, and TREETOPS, ref. 2) cannot provide sufficiently fast computer turnaround. To adequately address the control structure interaction problem, structural analyzers for this work should be embedded within a control design code having available an entire repertoire of control simulation and analysis tools. The high fidelity dynamics codes are not designed for convenient use in this way. High fidelity analysis methods are needed, however. The nonlinearities of large motion multibody dynamics suggest that control design based on linear analysis will fail to assess performance accurately, and may also fail to identify stability problems during prolonged slewing motions. Thus there appears to be a deficiency in control structure interaction design methodology for nonlinear multiflexible body systems. The SADACS (Spacecraft Appendage Dynamics And Control Simulation) code attempts to address a range of problems in this category.

Most multiflexible body dynamics problems are essentially linear in their flexible behavior even though their rigid body motions may be strongly nonlinear. SADACS was specifically developed for this type of problem. The present work is a follow-on to the approach described by Hassul and Heffernan in reference 3. SADACS is embedded within the Boeing EASY5 control design and simulation system which provides a wide range of simulation tools, linear control design methods, and nonlinear time domain integration options. The approach achieves high computational speed by solving the flexible dynamics equations in diagonalized system mode form. It solves the fully nonlinear rigid motion problem in parallel with the flexible solution, providing an accurate total motion prediction for most nonlinear dynamic response problems.

* C-4

Large angular motions cause gradual changes in the flexible system modes, and these changes are handled by updating the system modes. Very little error in the flexible motion is caused by this updating, no error is induced in the rigid solution, and little increase in computational time occurs.

SADACS is operational in a number of Boeing applications involving complex control structure interaction problems. It has been verified by comparisons with predictions of the DISCOS code. Computational speeds have varied from several times faster than DISCOS for small problems to 100 or more times faster for larger problems. It is routinely used for problems that are computationally infeasible for the high fidelity codes which solve the coupled, nonlinear structural equations of motion in terms of the flexible modes of individual appendages.

Because SADACS is an approximate approach, it must be verified when it is used for problems which have a stronger degree or different type of nonlinearity than that previously studied. To date, however, it has been found highly accurate for complex multiflexible body dynamics problems.

TECHNICAL APPROACH

The handling of structural flexibility in SADACS parallels the approach of conventional structural analysis. The several bodies of the system are represented by their component modes, retaining corresponding freedoms at the attachment points. They are then coupled to form the equations of the total system by performing a conventional structural merge. This greatly simplifies setting up the flexible equations of motion in comparison with the fully nonlinear formulation used by codes such as DISCOS.

Since this approach omits all nonlinearities, a separate nonlinear analysis is performed in parallel with the flexible solution. This solution addresses only the rigid motions, thereby retaining the nonlinearities of greatest importance in most problems. The separation of rigid and flexible solutions can only be done with the flexible formulation in system mode form. Therefore, SADACS performs an eigensolution to obtain a system normal mode representation of structural flexibility. The use of normal modes provides the improvement in computational time which is the aim of the SADACS development.

Though this approach appears both simple and logical, its implementation involves approximations in mathematical derivations which are difficult to justify and to understand as regards physical meaning and probable consequences in problem solutions. The concerns center on the handling of the rotations and their rates. Each of the technical sections which follow attempts to identify the mathematical approximations as they are introduced and to describe the physical nature and possible magnitude of errors which may occur in simulations.

The technical details of SADACS center on three main subjects:

1. Definition of the flexible structural model in terms of

the modes of its component bodies.

2. Use of the structural definition to set up the multiflexible body equations of motion, accounting for the gimbal freedoms and torques.

3. Eigensolution, truncation of system modes, and handling of truncated modes in dynamic analysis.

4. Simultaneous solution and combination of separate rigid and flexible dynamic response problems.

These subjects and the important matters of verification of accuracy and computational speed are discussed in the sections which follow.

Definition of the Structural Model

Figure 1 illustrates the type of multiflexible body system to be studied. A four body chain topology is shown, although SADACS also handles a tree topology. Each body has a coordinate frame which is used for its structural analysis. Bodies 1 and 2 in this figure are each attached to two other bodies. At their attachment points these bodies each have 6 degrees of freedom. Using the Craig-Bampton component body modal formulation (refs. 3, 4), these freedoms are defined by stiffness and mass data. They are treated as coordinates, called constraint modes, and have modeshapes which involve deformations of the interiors of the bodies. The modeshapes are computed by imposing, one at a time, the displacements and rotations of the attachment points and performing static structural analyses of the resulting deformations. Taken as a group, the attachment point freedoms combine to provide rigid body motion. For this reason, the constraint mode set cannot be easily truncated. They also provide the flexibility of the bodies in response to forces and torques applied externally to the attachment points.

To supplement the constraint modes, dynamic flexible modes of the bodies are computed with the attachment points completely fixed. These are called the fixed interface modes. Taken together, the constraint and fixed interface modes provide a complete description of the motions of the bodies in modal coordinate form. The fixed interface modal set is usually truncated.

The structural modelling described above contains implied approximations due the handling of the rotations. The use of the constraint modal coordinates to define rotations is a superposition procedure. It ignores the fact that rotations are only superimposable in a specific sequence defined by the physical construction of a gimbal device and properly accounted for in mathematical procedure. If the rotations are sufficiently small, however, they can be treated by superposition. Therefore, the modal approach taken here is only valid for the flexible portion of the motion, in which the rotations are very small. In addition, the use of the body structural analysis frame as a basis for the definition of the constraint mode coordinates ignores the fact that the actual orientations of the axes of the interbody attachment constraints are influenced by flexibilty. There are situations in which this is important, as in the case of a very flexible body attached to another body which is massive or which has large angular momentum. SADACS does not attempt to address these types of problems. Finally, the structural analysis frame is treated effectively as an inertial frame because the constraint modes referred to this basis provide the only means of rigid motion of a body. If a body has large motions in either rotation or translation, they must be represented by large values of the constraint mode coordinate values. Numerical difficulty could then be encountered in the use of the constraint mode stiffnesses. These are typically very large and are not well suited to analyses in which they must create reactions to large, nearly rigid motions. Therefore, if SADACS were to simulate a transient response using the structural model rather than the separate rigid motion solver to compute the rigid motion, errors typical of inertial grounding would likely occur. However, the code is never used in this mode, and the restriction of the structural model to simulate only the flexible motion eliminates this concern.

Equation 1 gives the relationship of the Craig-Bampton modal coordinates to the discrete physical freedoms of a single body.

$$\begin{Bmatrix} d_B \\ d_I \end{Bmatrix} = \begin{bmatrix} 0 & I \\ P_{IF} & P_{IC} \end{bmatrix} \begin{Bmatrix} q_F \\ q_C \end{Bmatrix} \tag{1}$$

where $\langle d_I \rangle$ and $\langle d_B \rangle$ are the discrete motions of the interior and boundary gridpoints, $[P_{IC}]$ and $[P_{IF}]$ are the modeshapes defining the interior motions due to the constraint and fixed interface modes, and $\langle q_C \rangle$ and $\langle q_F \rangle$ are the constraint and fixed interface modal coordinates, respectively. The vectors $\langle d_B \rangle$ and $\langle q_C \rangle$ are identical. The discrete freedoms include both displacements and rotations.

The Craig-Bampton modal coordinates are not uncoupled as structural normal modes are. The equations of motion of the body in this form have inertial coupling between the constraint and fixed interface modes. Equations 2 and 3 show the forms of the symmetric modal coordinate mass and stiffness matrices for a single body

$$[M] = \begin{bmatrix} M_{FF} & M_{FC} \\ M_{CF} & M_{CC} \end{bmatrix} \tag{2}$$

$$[K] = \begin{bmatrix} K_{FF} & 0 \\ 0 & K_{CC} \end{bmatrix} \tag{3}$$

where the subscripts FF, FC/CF, and CC indicate the fixed interface modes, the coupling between the fixed interface and constraint modes, and the constraint modes, respectively. The matrices $[K_{FF}]$ and $[M_{FF}]$ are diagonal. $[K_{CC}]$ is generally full, but there is no stiffness coupling between the constraint and fixed interface modes. The mass coupling matrices $[M_{FC}]$ and $[M_{CF}]$ and the constraint mode mass matrix $[M_{CC}]$ are generally full.

Bodies 3 and 4 in figure 1 are each attached to only one other body. These bodies also have both constraint and fixed interface modes, but they have a simpler and more familiar form in these cases. The constraint modes are simply the rigid body displacements and rotations of the bodies imposed by their attachment point motions. The fixed interface modes are simply the cantilever modes of conventional structural analysis.

SADACS handles tree topology structural systems in which there are bodies with more than two attachment interfaces. In figure 1, for example, body 1 could have several additional appendages. In such cases, a larger number of constraint modes is defined. As the number of constraint modes is thus increased, the body becomes effectively stiffer in the numerical descriptions of both its constraint and fixed interface modes. The modes become less effective descriptors of the system dynamics, modal convergence deteriorates, and retention of large modal sets becomes necessary. In the SADACS approach, this does not cause any difficulties because the system is subjected to eigensolution and truncation. However, for approaches which solve the equations of motion in component mode form, the Craig-Bampton formulation may lead to large problem size and difficulty in integrating the equations of motion.

The coordinate systems of the structural modal analysis dictate procedures for the use of the modal data in subsequent multibody analysis. Figure 1 shows that each body has a coordinate triad which is used for its structural analysis. No generality is lost if all of these triads are parallel. Thus, each body's displacements and rotations are referred to the same basis vectors, called herein the structural analyzer global basis. The structural analysis is performed with the bodies in specific relative orientations to this global basis, called herein the nominal orientations. The modal data are therefore readily used to study the system in its nominal condition. If the bodies are to be studied in off nominal orientations, the structural data are still valid and the structural analyses need not be repeated. Transformations of the appendage constraint mode vectors can return these vectors to the global basis. Figure 2 illustrates this situation. Body 2 in the figure has been rotated to an off nominal position. The structural analysis has not been repeated for this new orientation. The body 2 modal data are still valid, but are referred to the rotated body 2 basis rather than to the global basis. This requires a compensating transformation of the constraint mode data when the multibody attachment equations are formulated.

Multibody Structural Merge

Figure 1 shows all bodies of the system oriented nominally, so that their body frames are parallel to the global frame. The modal data of each body are referred to the global basis system. The fixed interface modeshapes contain displacements along, and rotations about, the axes of the global system. The constraint mode coordinate vectors contain displacements along and rotations about these axes. If any bodies are rotated to off nominal orientations, their modal data become referred to the correspondingly rotated material frames as indicated by figure 2. The derivations of this section consider both nominal and off nominal orientations in imposing the interbody connectivity conditions.

The first step of the derivation is the transformation of the constraint modal coordinates to the basis systems of the gimbals. This allows the individual body mass, damping, and stiffness matrices to be combined into total system coupled matrices by enforcing compatibility of adjacent body displacements and rotations. This procedure is called a structural merge. No transformation is required for the fixed interface modal data.

It is in the structural merge that the approximations of the flexible body linearization become difficult to visualize and understand. The present approach differs in part from the fully nonlinear formulations in that it omits second and higher order terms in the acceleration equations. This causes approximations in inertia load distributions on the structural components and therefore in the equations of motion. The higher order terms are present in high fidelity codes because at the outset they assemble the equations of motion for bodies residing in a rotating assemblage. This defines accelerations due to products of the angular rates with themselves (centrifugal and gyroscopic effects), and with the modal rates (Coriolis effects). These are omitted at the outset when the modal equations are developed in conventional structural dynamics form. The omitted terms are very small except in cases where large angular rates and large flexibility combine. Hence SADACS is seen to be limited by the combination of angular rate and structural flexibility.

Other approximations are made in the procedure for imposing connectivity between the bodies, due to the manner of handling the orientations of the gimbal axes. In the high fidelity codes, the motions of the gimbal axes are represented exactly, including the effects of large rotations and structural flexibility. The influences of the gimbal motions on the motions of the bodies are therefore computed exactly. In the approximate derivations of the present approach, however, modal data are used to define flexible rotations and modal coordinate rotation quantities are transformed as though they were the components of a vector. The influences of the gimbal orientations are therefore approximated. This treatment is accurate if the flexible rotations are very small, so that superposition of angular motions can be done without regard for the order in which they occur. The justification of this treatment is that the structural merge is used only to model the small flexible contributions to the rotations.

In addition, transformations are applied to all of the matrices of the modal coordinate formulation without including the influences of the rates of change of the transformations with time. Since differentiation of the transformation matrices generates quantities that are proportional to the angular rates, this is equivalent to omitting nonlinearities due rotational rates. The justification of this approximation is that the inertial loadings applied to the flexible modes due to the rotational nonlinearities cause very small deformations for most problems. If extremely flexible structures were to be simulated, or if the angular rates were very large, then this would not be an acceptable approximation. Therefore it is again seen that SADACS is limited in the degree of both flexibility and angular rate which it can accurately address.

Finally, the structural merge is performed at a particular set of body orientations, and the structural model is only valid for this particular condition of the system. To address the changes in the flexible character of the system as the relative orientations of the bodies change with time, SADACS incorporates an updating feature which re-merges the system and computes new flexible modes. The details of this procedure are not covered in this paper.

Figure 3 shows the coordinate systems which are required to set up the multibody structural merge. To simplify the figure only two bodies are shown, but the discussion is easily extended to the case of many bodies. Each body has the same global coordinate system, designated by the letter "N". The hinge between the bodies uses two coordinate triads to describe the gimbal rotations. Following the nomenclature of DISCOS, reference 1, a "p" triad is defined on the "inboard" body of the pair, and a "q" triad is defined on the "outboard" body of the pair. These triads are bound to the material of the bodies, and it is convenient to refer to a "p" body and a "q" body. A sequence of three Euler rotation angles, TH1, TH2, and TH3, rotate the p triad into the q triad. Since the triads are material bound, this rotates the q body, positioning it relative to the p body.

The p triad must contain the axis about which TH1 occurs. This can be any one of its axes. The p triad must also contain the axis which, after the TH1 rotation, will be the physical gimbal axis for the TH2 rotation. This can be any axis of p other than that of the TH1 rotation. The q triad must contain the axis of the final rotation of the Euler sequence, TH3, and, when TH3 is zero, also the axis of the TH2 rotation. In general, these requirements prevent the N system from being identical to either the p or the q system.

There is a degree of arbitrariness in the definition of TH1 and the p system. The p frame may contain the TH2 axis when TH1 has a zero value. In this case, the value of TH1 positions the q body with respect to the p body subsequent to the nominal positioning and the initial value of TH1 in dynamic analysis is zero. The rotation from N to p participates in the body 2 nominal positioning in this case. Figure 3a illustrates this definition. Alternatively, the p frame may not contain the axis of TH2 when TH1 has a zero value. In this case, the value of TH1 orients the q body with respect to the p body for both nominal and subsequent positioning, and the initial value of TH1 in dynamic analysis is nonzero. There need not be a rotation from N to p in the nominal orientation in this case. Figure 3b illustrates this definition.

Consider a general gimbal device which allows three Euler angular motions TH1, TH2, and TH3. The direction cosine transformations of each angular motion are easily computed and are defined here by the matrices [T1], [T2], and [T3]. Defining the basis vectors of the p and q frames by $\langle \underline{U}_p \rangle$ and $\langle \underline{U}_q \rangle$, the total direction cosine transformation from the p basis to the q basis is

$$\langle \underline{U}_q \rangle = [T3][T2][T1]\langle \underline{U}_p \rangle \qquad (4)$$

The product of the direction cosine matrices above will be denoted by [T321]. Defining the p frame cartesian components of the angular rate of the q body with respect to the p body by $\langle w_p \rangle$ and the Euler angle rates as $\langle \dot{TH} \rangle$, these components are related by

$$\langle w_p \rangle = [Pi]\langle \dot{TH} \rangle \qquad (5)$$

The matrix [Pi] is a function of the Euler angles TH1 and TH2 and is not orthogonal. There are 12 possible forms of [Pi] depending on the particular physical axes of the gimbal which correspond to the sequenced angles TH1, TH2, and TH3 (ref. 6). Equation 5 allows definition of the non-orthogonal basis system of the gimbal axes, defined by $\langle \underline{G} \rangle$, as

$$\langle \underline{G} \rangle = [Pi]^T\langle \underline{U}_p \rangle \qquad (6)$$

The angular rate of the q body with respect to the p body can be expressed in either the p basis, as in equation 5, or in the q basis. Denoting the latter by $\langle w_q \rangle$, the [T321] transformation of equation 4 gives

$$\langle w_q \rangle = [T321]\langle w_p \rangle \qquad (7)$$

Combining equations 5 and 7 gives

$$\langle w_q \rangle = [T321][Pi]\langle \dot{TH} \rangle \qquad (8)$$

The matrix product above is defined as [Qi]. Thus,

$$[Qi] = [T321][Pi] \qquad (9)$$

and

$$\langle w_q \rangle = [Qi]\langle \dot{TH} \rangle \qquad (10)$$

The gimbal basis can now be determined in terms of the q basis. Following the forms of equations 5 and 6,

$$\langle \underline{G} \rangle = [Qi]^T\langle \underline{U}_q \rangle \qquad (11)$$

The transformation from the p basis to the N basis is defined as [pTN], and that from the q basis to the N basis is defined as [qTN]. In SADACS these matrices are approximated by their rigid body definitions and are therefore constant in time. The transformations are

$$\langle \underline{U}_N \rangle = [pTN]\langle \underline{U}p \rangle \qquad (12)$$

and

$$\langle \underline{U}_N \rangle = [qTN]\langle \underline{U}_Q \rangle \tag{13}$$

and define the structural analysis basis, $\langle \underline{U}_N \rangle$, in terms of the two hinge cartesian bases, neglecting the effects of flexibility within the individual bodies.

The p body constraint mode transformation to the gimbal basis can now be defined. Denoting the transformed $\langle q_C \rangle$ vector for the p body by $\langle r_{CP} \rangle$,

$$\langle q_C \rangle = [[pTN][Pi]]^{\bullet}\langle r_{CP} \rangle \tag{14}$$

where the notation $[\ ]^{\bullet}$ indicates that this transformation "stacks" the [pTN][Pi] matrix as 3x3 partitions along the diagonal in order to transform both the displacement and rotation freedoms.

For the q body the transformation must consider the possibility that the body may be in an off nominal orientation. This makes it most convenient to transform from the q basis to the gimbal basis. Denoting the transformed $\langle q_C \rangle$ vector for the q body by $\langle r_{CQ} \rangle$,

$$\langle q_C \rangle = [[qTN][Qi]]^{\bullet}\langle r_{CQ} \rangle \tag{15}$$

The matrix [Qi] contains the positioning information which accounts for the off nominal orientation of body q.

The transformation matrix products in equations 14 and 15 will both be denoted by $[rTN]^{\bullet}$ and it will be recognized in their use below that they are numerically different for the p and q bodies.

The mass matrix of a single body, equation 2, is transformed to the gimbal rotation components by

$$\begin{bmatrix} I & 0 \\ 0 & [[rTN]^{\bullet}]^{T} \end{bmatrix} \begin{bmatrix} M_{FF} & M_{FC} \\ M_{CF} & M_{CC} \end{bmatrix} \begin{bmatrix} I & 0 \\ 0 & [rTN]^{\bullet} \end{bmatrix} \tag{16}$$

The stiffness matrix, equation 3, is also transformed by equation 16. In this case there are no off diagonal partitions in the calculation or the result.

The generalized loads applied to interior points of bodies are transformed by the matrix on the left in equation 16. The gimbal torques are defined in the gimbal bases and do not require transformation.

The compatibility condition for the attachment, or structural merge, of the bodies is

$$\begin{Bmatrix} r_{CP} \\ r_{CQ} \end{Bmatrix} = \begin{bmatrix} I1 & I2 & 0 \\ I3 & 0 & I4 \end{bmatrix} \begin{Bmatrix} r_{C1} \\ r_{CP+} \\ r_{CQ+} \end{Bmatrix} \tag{17}$$

where $\langle r_{C1} \rangle$, $\langle r_{CP+} \rangle$, and $\langle r_{CQ+} \rangle$ are the common p body and q body freedoms which are locked and the p and q body freedoms which are free to have relative motion, respectively. I1, I2, I3, and I4 are selector matrices which define the interbody compatibility conditions.

For simplicity of notation the vector r_c will be defined,

$$\langle r_c \rangle = \begin{Bmatrix} r_{cl} \\ r_{cpf} \\ r_{cqf} \end{Bmatrix} \qquad (18)$$

To derive the equations of motion of coupled bodies, the mass, damping, and stiffness matrices and the generalized loads of the individual bodies are first assembled without imposing the constraint conditions. The result is illustrated for two bodies by the mass matrix below.

$$\begin{bmatrix} M_{FF} & Mr_{FCp} & Mr_{FCq} \\ Mr_{CpF} & Mr_{CpCp} & 0 \\ Mr_{FCq} & 0 & Mr_{CqCq} \end{bmatrix} \qquad (19)$$

The matrix partitions denoted by [Mr] have been transformed to the gimbal bases as described by equations 14-16. The subscripts F, Cp, and Cq denote the fixed interface modes, the constraint modes on the p body, and the constraint modes on the q body, respectively. The stiffness matrix corresponding to expression 18 has null off diagonal partitions. This form of the equations expects the freedoms to be ordered $\langle q_F \rangle$, $\langle r_{cp} \rangle$, and $\langle r_{cq} \rangle$. The extension to the entire system is accomplished by stacking additional partitions in expression 19.

The equations of motion are to be assembled by subjecting the freedoms to the constraint of equation 17. The constraint is written

$$\begin{Bmatrix} q_F \\ r_{cp} \\ r_{cq} \end{Bmatrix} = \begin{bmatrix} I & 0 & 0 & 0 \\ 0 & I1 & I2 & 0 \\ 0 & I3 & 0 & I4 \end{bmatrix} \begin{Bmatrix} q_F \\ r_{cpl} \\ r_{cpf} \\ r_{cqf} \end{Bmatrix} \qquad (20)$$

Defining the selector matrix in equation 20 by [II], the transformations are accomplished by pre-multiplying the system mass, damping, and stiffness matrices by $[II]^T$ and post-multiplying the result by [II]. The generalized loads are transformed by pre-multiplying by $[II]^T$. This procedure involves only simple row and column operations and is most easily performed by additions rather than by the matrix multiplication process. The result of this final step is the component mode equations of motion of the SADACS flexible body solver.

System Modal Analysis

The coupled component mode equations of motion are diagonalized by eigensolution of the merged, second order structural equations of motion. No linearization of the rigid motion equations is required for this task. Damping is usually omitted in the component mode equations, leading to a generalized real symmetric eigenvalue problem with pure imaginary frequencies. Damping is then added to the system modes after the eigensolution. SADACS optionally solves the complex eigenvalue problem using assigned component modal damping. This option has not proved advantageous. The system modal damping produced usually varies greatly among the system modes, a situation felt to be unrealistic, and the complex eigenvalue problem is felt to be less reliably solved than the real form.

The flexible modeshapes of the system eigensolution are denoted by $[S_F]$. The system flexible modal coordinates are denoted by $\langle x_F \rangle$. The recovery of the component modal coordinate data for the purely flexible motion is given by

$$\begin{Bmatrix} q_F \\ r_C \end{Bmatrix} = [S_F]\langle x_F \rangle \tag{21}$$

The system flexible mode mass and stiffness matrices are computed by pre-multiplying the corresponding component mode matrices by $[S_F]^T$ and post-multiplying the result by $[S_F]$. The resulting matrices are diagonal. The generalized load vector is computed by pre-multiplying the component mode load vector by $[S_F]^T$.

The flexible system modal set is truncated to reduce computational effort in the time stepping integration procedure. Denoting the retained modes by $\langle x_{FR} \rangle$ and the truncated modes by $\langle x_{FT} \rangle$, the equations which are solved are

$$\langle \ddot{x}_{FR} \rangle = \langle X_{FR} \rangle - [C_{FR}]\langle \dot{x}_{FR} \rangle - [K_{FR}]\langle x_{FR} \rangle \tag{22}$$

and

$$\langle x_{FT} \rangle = [\ K_{FT}]^{-1}\langle X_{FT} \rangle \tag{23}$$

where the symbol $\langle X \rangle$ denotes the generalized load, $[C]$ and $[K]$ denote the modal damping and stiffness matrices, and the $[K]^{-1}$ matrix in equation 23 is the diagonal of inverse modal stiffnesses of the truncated flexible system modes. The subscripts in all terms follow the definitions given above for the vector $\langle x \rangle$. Equation 22 is given for the case of unit flexible mode generalized mass, which is the normalization provided by the eigensolver.

The eigensolution, truncation, and time stepping solution procedure outlined above is extremely fast and has encountered no numerical difficulties. Several of the advantages of the approach are discussed briefly in the paragraphs which follow.

The truncation of the higher flexible modes allows the use of a much larger integration time step than would be required if all modes were retained. This benefit is not available to approaches which integrate component mode equations of motion because truncation of the component modal set can cause serious loss of accuracy. This is especially true when cantilever appendage modes are used to simulate systems with free or controlled gimbal freedoms. The loss of accuracy is due to the fact that the higher cantilever modes are important participants in the low frequency behavior of the dynamical system and therefore need to be retained in the component mode simulation. SADACS is typically used with very large numbers of component modes and severe truncation of the system modal set. This provides a substantial reduction of computational time and does not cause noticeable loss of accuracy.

The use of equation 23 is critical to the accuracy of problem solutions. This equation provides the quasi-static responses of the higher frequency system modes. If the contribution of equation 23 is omitted, the gimbal angle responses to control torques may be either under- or over-predicted by substantial amounts. In addition, the locations of transfer function zeros are made highly inaccurate by the omission of the quasi-static responses. It is the use of equation 23 which permits truncation of the modal set for the integration of equation 22, thereby speeding the computational process.

Equations 22 and 23 are easily solved because of the absence of coupling between the modes. The entire flexible solution has been reduced to a very simple form, leaving the difficult, coupled, nonlinear analysis problem to the rigid motion dynamics, where it is known to be most important in the majority of applications. The computational price which is paid for the modal analysis simplification is the effort of the eigensolution. This has proved to be very small in problems solved to date, in comparison with the computational effort of coupled modal analysis and integration with small time steps.

Separation of Rigid and Flexible Motions

The SADACS formulation uses separate rigid body (RB) and flexible body (FB) computer codes. The rigid body code currently used is the MBDY subroutine due to Likins and Fleischer (ref. 4). This code was chosen because it is a proven standard and because it could easily be integrated into the Boeing EASY5 system. It has proven reasonably fast in applications. Other rigid body codes could equally well be used. The flexible body code is the linear, small motion formulation of conventional structural dynamics, derived in the form outlined herein. It is used in system mode form and omits rigid modes. The flexible body solver is called from EASY5 as a subroutine.

Figure 4 shows a block diagram of this procedure. The figure identifies the rigid body solver, RB, the flexible body solver, FB, and the control simulation. The rigid motion prediction of FB is seen to be unused, and the flexible prediction is combined with the RB solution to create the total motion. The total motion provides the performance of the simulated system and the feedback data for the controller. It also is used to determine if the body orientation angles have changed sufficiently to require the calculation of new system modal data.

The figure indicates the geometric and modal transformations which have been discussed in the above sections. The gimbal torques are generated in the gimbal axis bases and are directly applicable to the model gimbal freedoms. They must, however, be transformed to correspond to the system modal coordinates. Torques applied to the interiors of the bodies are generated in the body bases, and these must be transformed to account for the use of constraint modal coordinates referred to the gimbal bases. They must also be transformed to correspond to the system modal coordinates.

After the time integration, the FB responses are back transformed from the system modal form to the constraint mode form referred to the gimbal bases. After this transformation, they can be combined directly with the gimbal rotation data from RB. Because the flexible contributions to the gimbal rotations are small, they can be added directly to the Euler positioning angles computed by RB. The internal body rotations similarly require a modal back transformation. Since they are needed in the body bases, they require an additional back transformation to account for the use of constraint modal coordinates referred to the gimbal basis systems.

MBDY computes the main body angular rates in the body basis. If main body angular position relative to the inertial frame is needed, an integration of these rates is done, taking proper account of the rotations of the body axes. This is not shown in the figure. The FB module computes the small flexible angular rates and positions of identified sensor points in the body basis. If it is required to obtain these quantities in the Euler angle basis which defines the inertial attitude of the body, they are transformed in the manner of equation 10. The equation is applicable to both rates and positions in this case because the flexible angles are very small.

The figure shows the modal coordinates and their rates returned to the equations of motion block. This is required to form the right hand sides of equation 22.

The decision whether to update the system modes is based on the magnitudes of the gimbal angles. If updating is not required, the solution continues with the commanded data and the feedback signals returning to the controller. If updating is required, the computational process exits to a set of updating routines. After computing new system modes and modal coordinate values and rates, the process returns to the integration routine as indicated by the figure. At the return, the new modal data have replaced the old modal data.

DISCOS-SADACS Comparisons

The approximations which have been used to reduce the computational time of SADACS cannot be quantified as to their accuracy on the basis of judgement alone. The magnitudes of errors which might occur depend on the magnitudes of the rotations and the rotational rates and on the sensitivity of the particular dynamical system to nonlinear influences. An effective way to verify that an approximate approach is accurate is to perform comparisons with high fidelity predictions of proven codes for problems of the type under study. For this purpose, an extensive verification of SADACS in comparison with DISCOS was done. The comparison used identical component mode models in SADACS and DISCOS. A number of problems were solved for the verification, all involving large angular motions at rates which caused the rigid motions to be strongly nonlinear. The results showed that the SADACS approach is extremely accurate and fast for complex multiflexible body systems with large motions at moderate rates.

All of the calculations showed that the simplifications of the SADACS approach result in a large reduction of computer time. The reduction was about 100-times for most of the problems studied. Run time reduction estimates are strongly problem sensitive. Larger problem sizes would significantly increase the speed advantage of the SADACS type approach over fully nonlinear approaches. Very small problems have shown only a two to three times speed advantage. The DISCOS open loop simulations in some cases required 40 or more CPU hours on a VAX 11-780. These problems were not large in comparison with other simulations of complex control structure interaction problems. For many problems it would not be feasible to run DISCOS simulations, or probably any other similar simulations using component modes and retaining fully nonlinear equations. An approach such as SADACS is probably the only way to attack such large control design problems.

The elimination of certain nonlinearities within a high fidelity code can speed its calculations appreciably. The TREETOPS code has such valuable options and Boeing has developed similar options within DISCOS. However, it appears that achieving a major speed increase necessitates transforming the equations to diagonalized form and truncating the system in order to increase the integration time step. Thus, the elimination of nonlinearities may not achieve the level of computational speed increase which is needed for really large control design problems. In the authors' view, the real need for high computational speed in high fidelity codes is to allow verification of approximate codes for simulations of realistic complexity. This is barely possible at the present time.

Figures 5-8 show comparisons of DISCOS-SADACS time history predictions. The figures give the responses of the main body and one appendage of a complex system. The command for this problem was a large rotational excursion of one appendage and the problem was run without control. Torques were applied to all system bodies through an inverse inertia matrix such that the rotations of the main body and the uncommanded appendages were very small for the initial stages of the motion. At the later stages, however, nonlinear effects cause all of the bodies to have large rotations, since no feedback was used to control the motions.

Figure 5 shows the main body x-rotation. Large motions occur in the later stages of the response due to the effects of nonlinearities. These motions are not predicted by linearized simulations. This figure shows that the SADACS use of simultaneous nonlinear rigid body and linearized flexible body solutions provides excellent large motion accuracy.

The triangular excursion at the start of the motion in figure 5 is due to the effects of flexibility in response to the applied torque pulse. Figure 6 shows an enlargement of this portion of the response. In this figure, the SADACS and DISCOS predictions are separated by two plot divisions in order to permit detailed examination of the flexible oscillations. It is seen that the flexible motion predictions are virtually identical. This figure verifies the FB system mode formulation and shows that the angular rates have little effect on the flexible responses.

The responses shown on figure 6 and the early portion of figure 5 are changed greatly if the correction given by equation 23 is omitted. The magnitude can change several-fold and the sign of the early response may also change due to such omission. This was observed in comparisons of DISCOS with a linearized code which omitted the quasi static deformation correction. In this case, the modal truncation was done by the structural analysis procedure before creating the data for the control design simulation.

Figure 7 shows the main body z-rotation, again in an enlarged plot to allow close examination of the flexible response. The SADACS and DISCOS predictions are indistinguishable on the plot.

Figure 8 shows the rotation about one gimbal axis of an uncommanded appendage. The late motions have a strongly nonlinear response which is predicted accurately by the SADACS simulation. The comparison verifies the accuracy of the approach of separate RB and FB solution procedures. This calculation is a more critical test of the prediction method than that of figure 5 because it emphasizes the coupling effects of the main body translational motions and the sensitivity of the rigid body inertia matrix to the angular motions of the main body and the torqued appendage.

Conclusions

A computer code for multiflexible body dynamic analysis has been developed based on linearizing flexible motions while retaining fully nonlinear rigid motions. The code is conceptually simple because its flexible formulation is that of conventional structural dynamics. It is embedded within a control design system, so that it is well adapted to both frequency and time domain control design applications.

The accuracy and computational speed of the code have been evaluated by comparisons with the predictions of DISCOS for problems with strong rigid motion nonlinearities and moderately flexible structural components. The approach has been found to be exceptionally accurate and fast.

The accuracy evaluations have shown that multibody flexible nonlinearities are usually extremely small while rigid nonlinearities are almost always sufficiently large to require simulation in control design work.

The computational speed evaluations have shown that the key factor in the slow speeds of the fully nonlinear, high fidelity multibody simulations is their integration of the coupled equations of motion in terms of component modal coordinates. This type of formulation is required to permit full retention of flexible nonlinearities. It results in excessive computation time because of the processing of the flexible rotations as large quantities, the handling of coupling terms in the equations, and especially because of the small integration time step required by the component mode representation. The actual computation of the nonlinear numerical terms in the equations of motion is not a dominating factor in the slow computational speeds of these types of formulations.

The omission of the flexible nonlinearities allows all of these time consuming computations to be eliminated. The result is a very fast approximate approach which can attack the computationally demanding problem of control design trades while maintaining sufficient accuracy for performance predictions.

References

Bodley, C., Devers, A., Park, A., and Frisch, H., "A Digital Computer Program for Dynamic Interaction and Simulation of Controls and Structures (DISCOS)," NASA Tech. Paper 1219, May 1978

Singh, R. and VanderVoort, R., "Dynamics of Flexible Bodies in Tree Topology-A Computer-Oriented Approach," J. Guidance, Vol. 8, No. 5, pp. 584-590, Sept.-Oct. 1983

Hassul, M. and Heffernan, D. L., "Simulation of Large Spacecraft with Rotating Appendages," AIAA-80-1667, AIAA/AAS Astrodynamics Conference, Danvers, Mass., Aug. 11-13, 1980

Craig, R. R. and Bampton, M. C. C., "Coupling of Substructures for Dynamic Analysis," AIAA Journal, Vol. 6, July 1968, pp. 1313-1319

Fleischer, G. E. and Likins, P. W., "Attitude Dynamics Simulation Subroutines for Systems of Hinge-Connected Rigid Bodies," NASA-JPL Technical Report 32-1592, May 1, 1974

"Spacecraft Attitude Determination and Control," Edited by J. R. Wertz, the D. Reidel Publishing Co., 1978

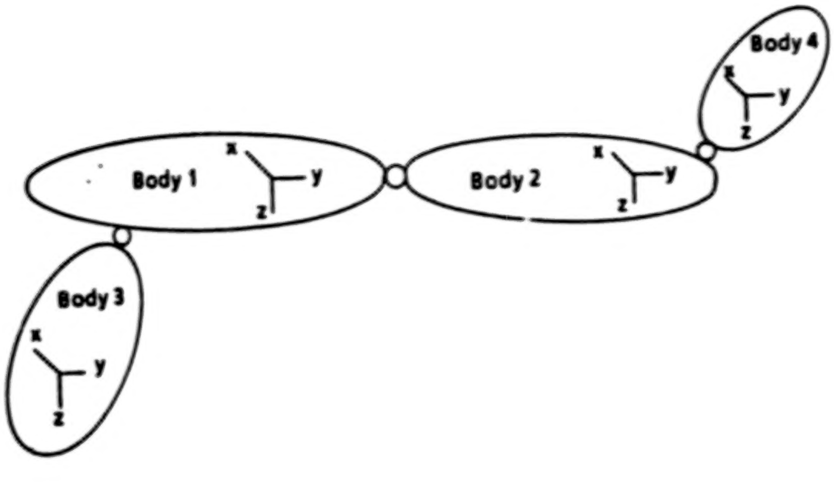
Body 4
x
y
z
x
Body 1
y
z
Body 2
x
y
z
Body 3
x
y
z

Figure 1 **Multibody System Example**

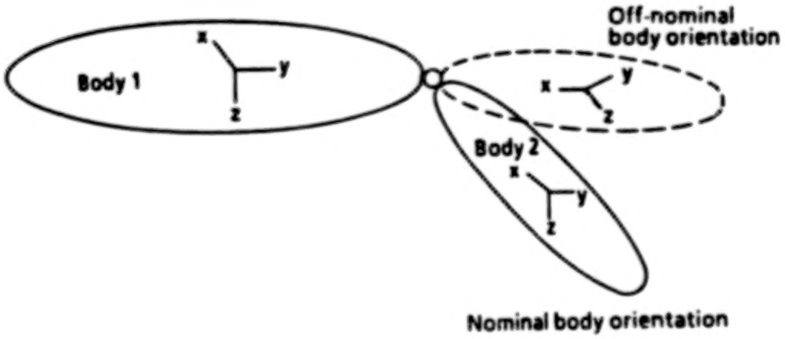
Off-nominal body orientation
x
Body 1
y
z
x
y
z
Body 2
x
y
z
Nominal body orientation

Figure 2 **Nominal and Off-Nominal Body Frames**

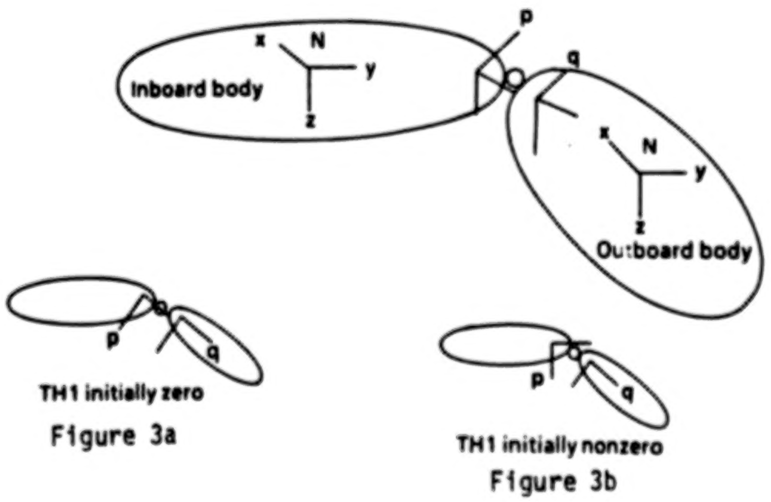
p
x
N
y
Inboard body
z
q
x
N
y
z
Outboard body
p
q
p
q

TH1 initially zero

Figure 3a

TH1 initially nonzero

Figure 3b

Figure 3 **Definitions of Gimbal Coordinate Frames**

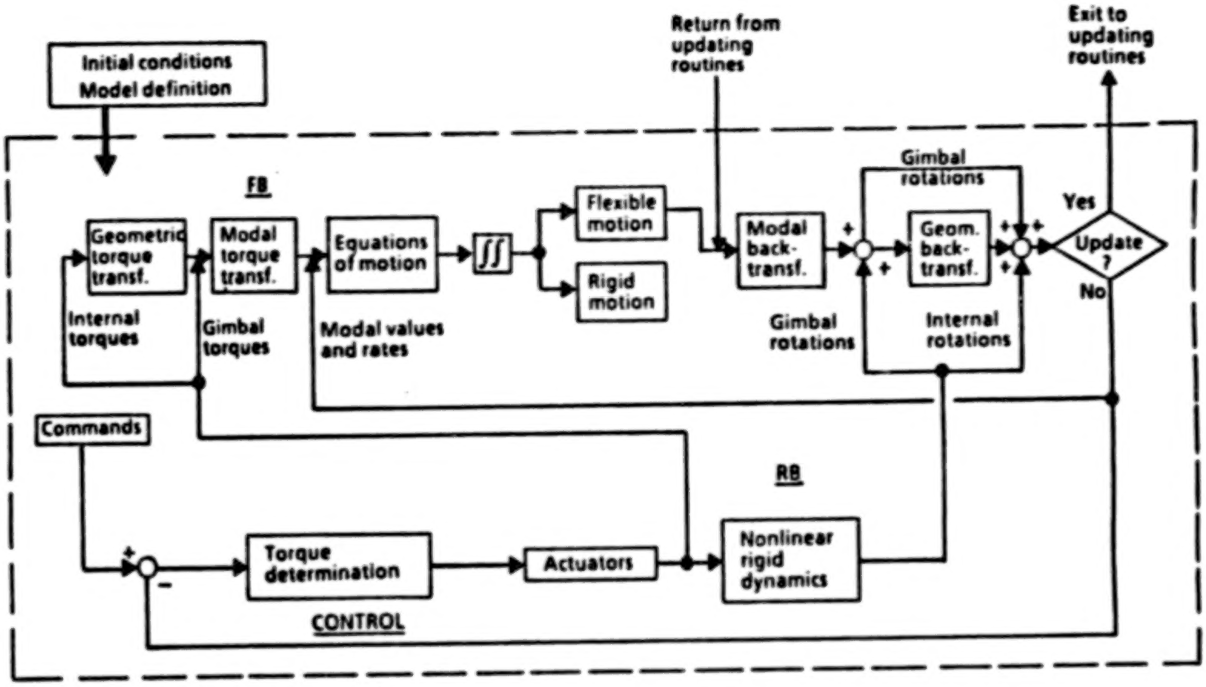
Initial conditions
Model definition
Return from updating routines
Exit to updating routines
FB
Geometric torque transf.
Modal torque transf.
Equations of motion
∫∫
Flexible motion
Rigid motion
Modal back-transf.
Gimbal rotations
Geom. back-transf.
Update ?
Yes
No
Internal torques
Gimbal torques
Modal values and rates
Gimbal rotations
Internal rotations
Commands
RB
Torque determination
Actuators
Nonlinear rigid dynamics
CONTROL

Figure 4 **SADACS Computational Flow**

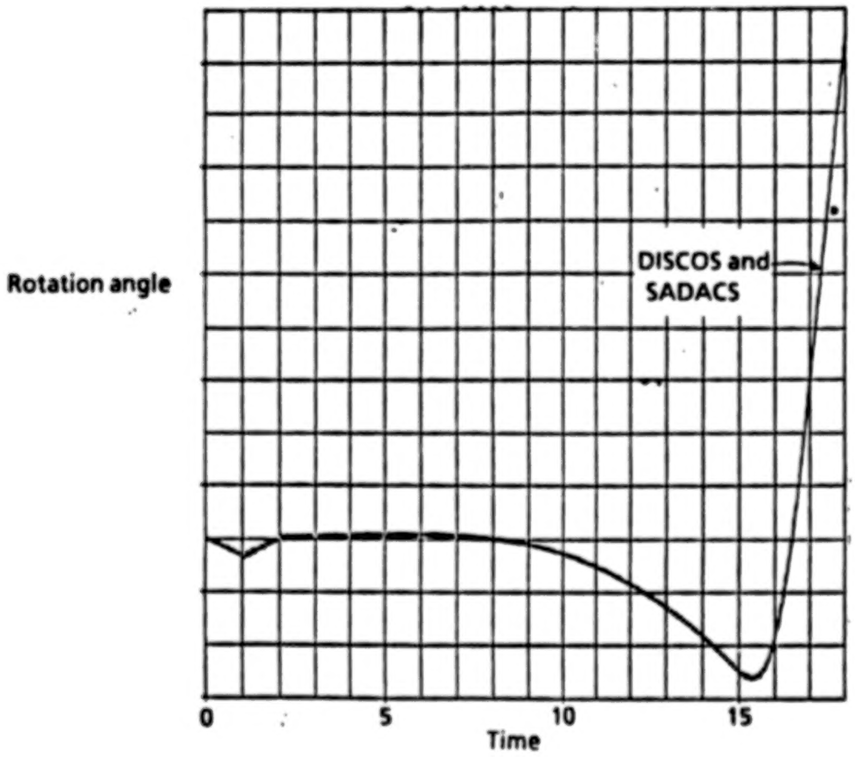

Figure 5 **DISCOS-SADACS Comparison:**
Main Body Sensor X Rotation Due To Appendage Command

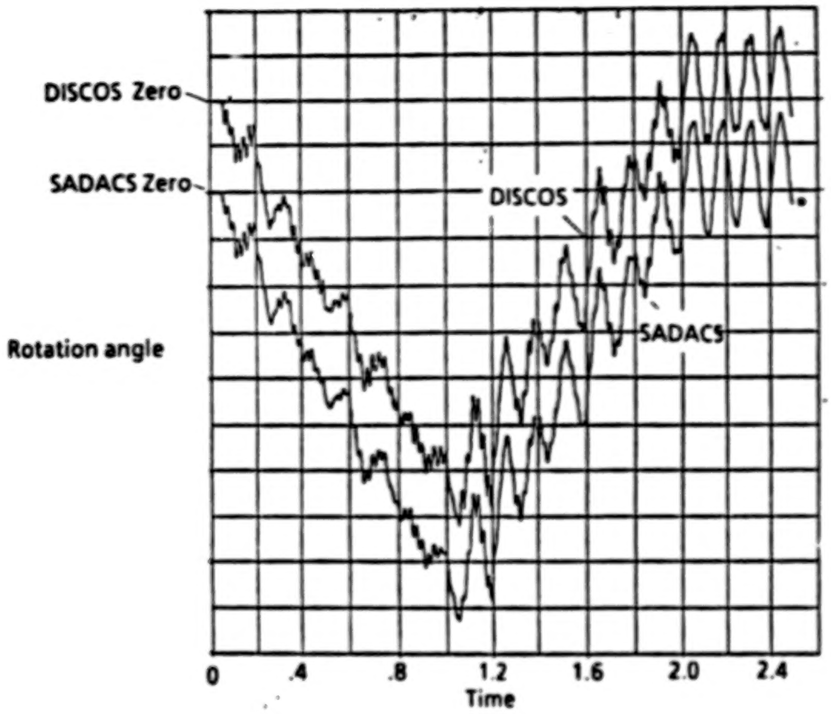

Figure 6 **DISCOS-SADACS Comparison:**
Main Body Sensor X Rotation Due To Appendage Command

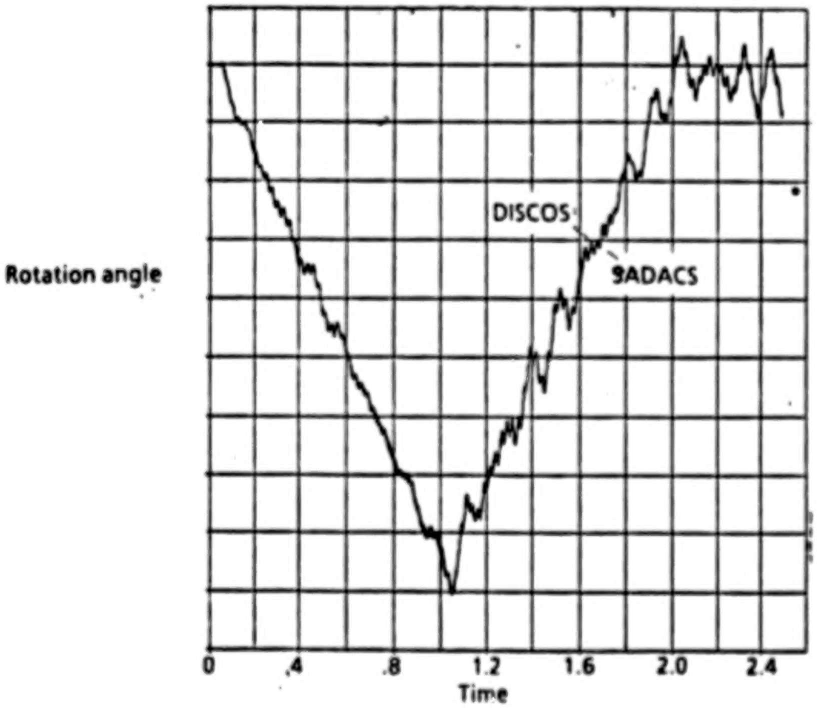

Figure 7 **DISCOS-SADACS Comparison:**
Main Body Sensor Z Rotation Due To Appendage Command

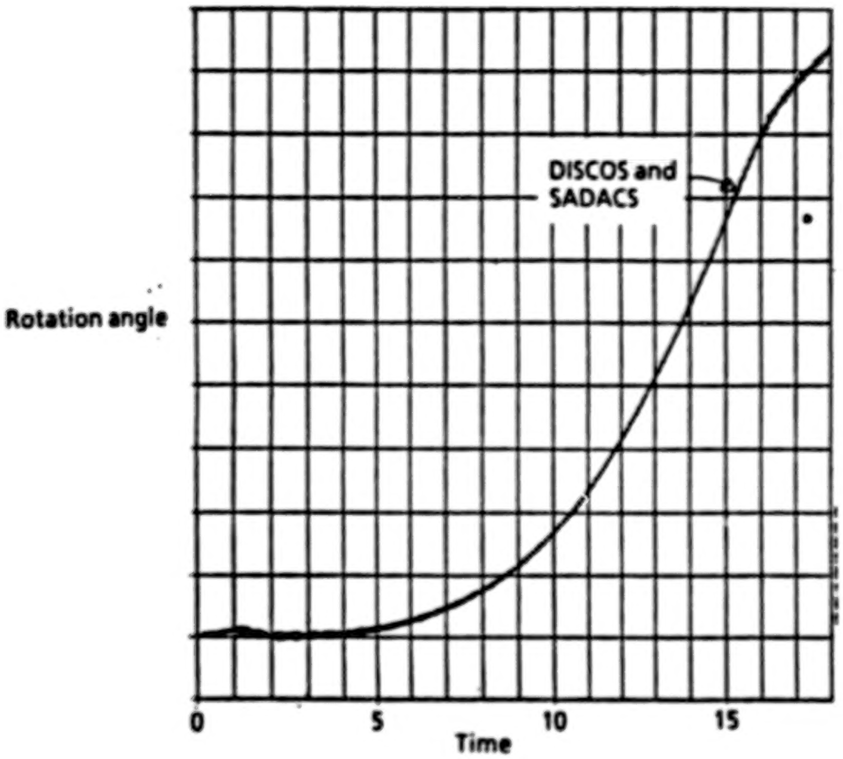

Figure 8 **DISCOS-SADACS Comparison:**
Hinge Rotation of Un-Torqued Appendage Due To Command on Another Appendage

N87
22739
UNCLAS

N87-22739

LANCZOS MODES FOR REDUCED-ORDER CONTROL OF FLEXIBLE STRUCTURES

by

Roy R. Craig, Jr.
Russell M. Turner

ASE-EM Department
The University of Texas at Austin

LANCZOS ALGORITHM - FE VERSION

$$\bar{r}_j = K^{-1}Mq_j$$

$$r_j = \bar{r}_j - \alpha_j q_j - \beta_j q_{j-1}$$

$$\alpha_j = q_j{}^T M\bar{r}_j$$

$$\beta_j = (r_{j-1}{}^T M r_{j-1})^{1/2}$$

$$q_{j+1} = (1/\beta_{j+1})r_j$$

$$\beta_{j+1} = (r_j{}^T M r_j)^{1/2}$$

The algorithm for recursively forming Lanczos vector q_{j+1} from Lanczos vector q_j for the case of nonsingular K is shown. It involves an orthogonalization step and a normalization step.

STARTING VECTOR

$$F = b\varepsilon(t)$$

$$r_o = K^{-1}b$$

$$q_1 = (1/\beta_1)r_o$$

$$\beta_1 = (r_o{}^T M r_o)^{1/2}$$

Lanczos mode [illegible] most useful when the spatial distribution of the excitation is constant. This load distribution then determines the starting vector.

LANCZOS EQUATION FORMAT

$$M\ddot{u} + Ku = F$$

$$MK^{-1}M\ddot{u} + Mu = MK^{-1}F$$

$$u = Q_m z$$

$$Q_m = [q_1 q_2 \ldots q_m]$$

$$Q_m^T MK^{-1}MQ_m\ddot{z} + Q_m^T MQ_m z = Q_m^T MK^{-1}F$$

Lanczos vectors are used in a mode-superposition manner which is not exactly the same as the familiar Rayleigh-Ritz version of mode-superposition. Multiplication by the equation of MK^{-1} "smooths" the loading.

LANCZOS EQUATION FORMAT - CONT.

$$T_m\ddot{z} + z = g_m$$

$$g_m = Q_m^T MK^{-1}F$$

$$T_m = \begin{bmatrix} \alpha_1 & \beta_2 & & & & \\ \beta_2 & \alpha_2 & \beta_3 & & & \\ & \beta_3 & \cdot & \cdot & & \\ & & \cdot & \cdot & \cdot & \\ & & & \cdot & \cdot & \beta_m \\ & & & & \beta_m & \alpha_m \end{bmatrix}$$

The final Lanczos equations have a tridiagonal generalized mass matrix and have a unit matrix for the generalized stiffness matrix. The form of the generalized force vector g_m is very special.

EXAMPLES

- Lanczos Modes and Equations
- Comparison of Normal Mode Models and Lanczos Mode Models
  - + Poles and Zeros
  - + Frequency Response Functions
  - + Transient Response

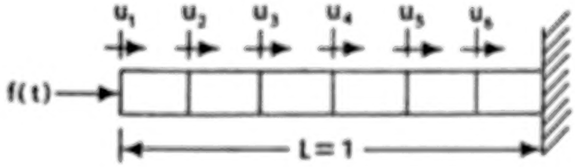
u1
u2
u3
u4
u5
u6
f(t)
L = 1

FINITE ELEMENT MODEL

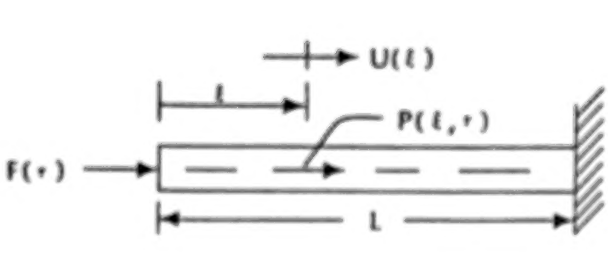

CONTINUOUS MODEL

FE LANCZOS MODE MODEL

$$T_m\ddot{z} + z = g_m$$

$$T_6 = \begin{bmatrix} 0.39770 & 0.04361 & 0.0 & 0.0 & 0.0 & 0.0 \\ 0.04361 & 0.04234 & 0.01238 & 0.0 & 0.0 & 0.0 \\ 0.0 & 0.01238 & 0.01564 & 0.00516 & 0.0 & 0.0 \\ 0.0 & 0.0 & 0.00516 & 0.00830 & 0.00221 & 0.0 \\ 0.0 & 0.0 & 0.0 & 0.00221 & 0.00505 & 0.00083 \\ 0.0 & 0.0 & 0.0 & 0.0 & 0.00083 & 0.00320 \end{bmatrix}$$

$$g_6 = \begin{Bmatrix} 0.57735 \\ 0.0 \\ 0.0 \\ 0.0 \\ 0.0 \\ 0.0 \end{Bmatrix} f(t)$$

Note that there is tridiagonal inertia coupling of the Lanczos generalized coordinates, but note that the only Lanczos coordinate directly excited by the external force is the first coordinate.

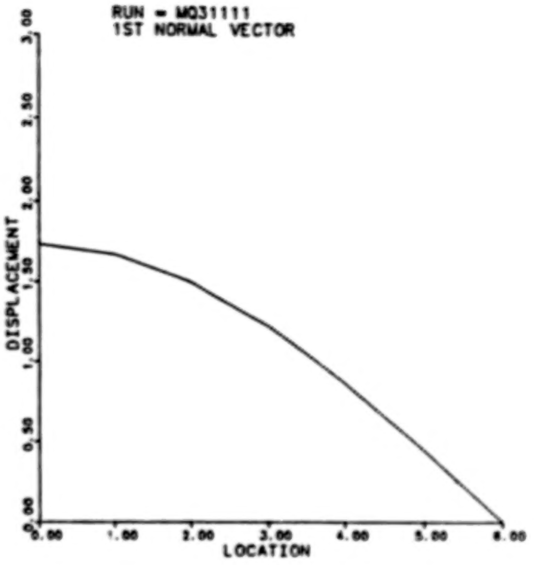

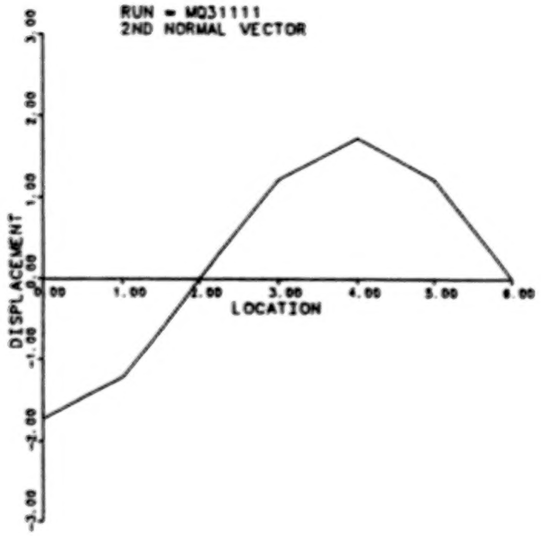

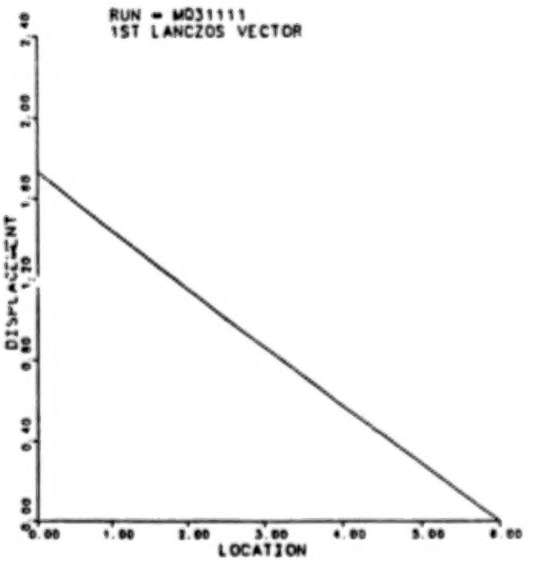

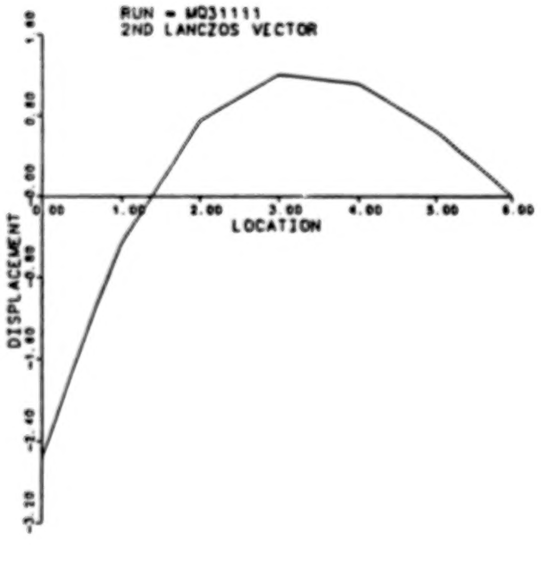

Typical normal modes and Lanczos vectors are shown here for axial deformation of a clamped-free rod. The starting Lanczos vector is based on a single force applied at the "free" end. Although finite element normal modes do have some stain near the free end, "exact" normal modes would all be strain-free at the end where the excitation force is applied.

TRANSFER FUNCTIONS IN MODAL COORDINATES

$$\begin{bmatrix} s^2+2.48152 & 0 & 0 & 0 \\ 0 & s^2+23.36993 & 0 & 0 \\ 0 & 0 & s^2+70.87551 & 0 \\ 0 & 0 & 0 & s^2+156.16108 \end{bmatrix} \hat{\eta}(s)$$

$$= \begin{Bmatrix} 1.42231 \\ -1.48875 \\ 1.62980 \\ -1.85632 \end{Bmatrix} \hat{f}(s)$$

TRANSFER FUNCTIONS - NORMAL MODE MODELS

$$\hat{u}_1(s)/\hat{f}(s) = 10.34151[s^2+3.28270)^2][s^2+(6.82929)^2]$$

$$[s^2+(10.94259)^2]/\Delta_4$$

$$\Delta_4(s) = [s^2+(1.57528)^2][s^2+(4.83424)^2]$$

$$[s^2+(8.41876)^2][s^2+(12.49644)^2]$$

$$\hat{u}_1(s)\ /\hat{f}(s) = 4.23934[s^2+(3.52834)^2]/\Delta_2(s)$$

$$\Delta_2(s) = [s^2+(1.57528)^2][s^2+(4.83424)^2]$$

$$\hat{u}_1(s)\ /\hat{f}(s) = 2.02296\ /\ [s^2+(1.57528)^2]$$

TRANSFER FUNCTIONS - LANCZOS MODE MODELS

$$\hat{u}_1(s)/\hat{f}(s) = 18.29893[s^2+(3.17763)^2][s^2+(6.59014)^2]$$

$$[s^2+(10.97092)^2]/\Delta_4(s)$$

$$\Delta_4(s) = [s^2+(1.575285)^2][s^2+(4.83427)^2]$$

$$[s^2+(8.48668)^2][s^2+(15.21009)^2]$$

$$\hat{u}_1(s)\ /\hat{f}(s) = 7.14344[s^2+(3.06112)^2]/\Delta_2(s)$$

$$\Delta_2(s) = [s^2+(1.57529)^2][s^2+(5.19414)^2]$$

$$\hat{u}_1(s)\ /\hat{f}(s) = 2.51446\ /\ [s^2+(1.5857)^2]$$

POLES AND ZEROS OF REDUCED-ORDER MODELS

EXACT POLES (6DOF)	4DOF NORMAL	4DOF LANCZOS	2DOF NORMAL	2DOF LANCZOS
1.57528	1.57528	1.57529	1.57528	1.57529
4.83424	4.83424	4.83427	4.83424	5.19414
8.41876	8.41876	8.48668	-	-
12.49644	12.49644	15.21009	-	-

TABLE 2. POLES OF REDUCED-ORDER MODELS

EXACT POLES (6DOF)	4DOF NORMAL	4DOF LANCZOS	2DOF NORMAL	2DOF LANCZOS
3.17759	3.28270	3.17763	3.52834	3.06112
6.57266	6.82929	6.59014	-	-
10.39230	10.94259	10.97092	-	-
14.69693				
18.85315				

TABLE 3. ZEROS OF REDUCED-ORDER MODELS

STATIC RESPONSE COMPARISON

	Normal Mode Model	Lanczos Mode Model	No. of Modes
$(\hat{u}_1/\hat{f})_{s=0}$	0.96961	0.99951	4
"	0.91005	0.99980	2
"	0.81521	1.00000	1
"	1.00000	1.00000	6(EXACT)

TABLE 1. TRANSFER FUNCTIONS EVALUATED AT s=0

These two tables compare poles and zeros of normal mode models and Lanczos vector models and the static response of normal mode and Lanczos vector models.

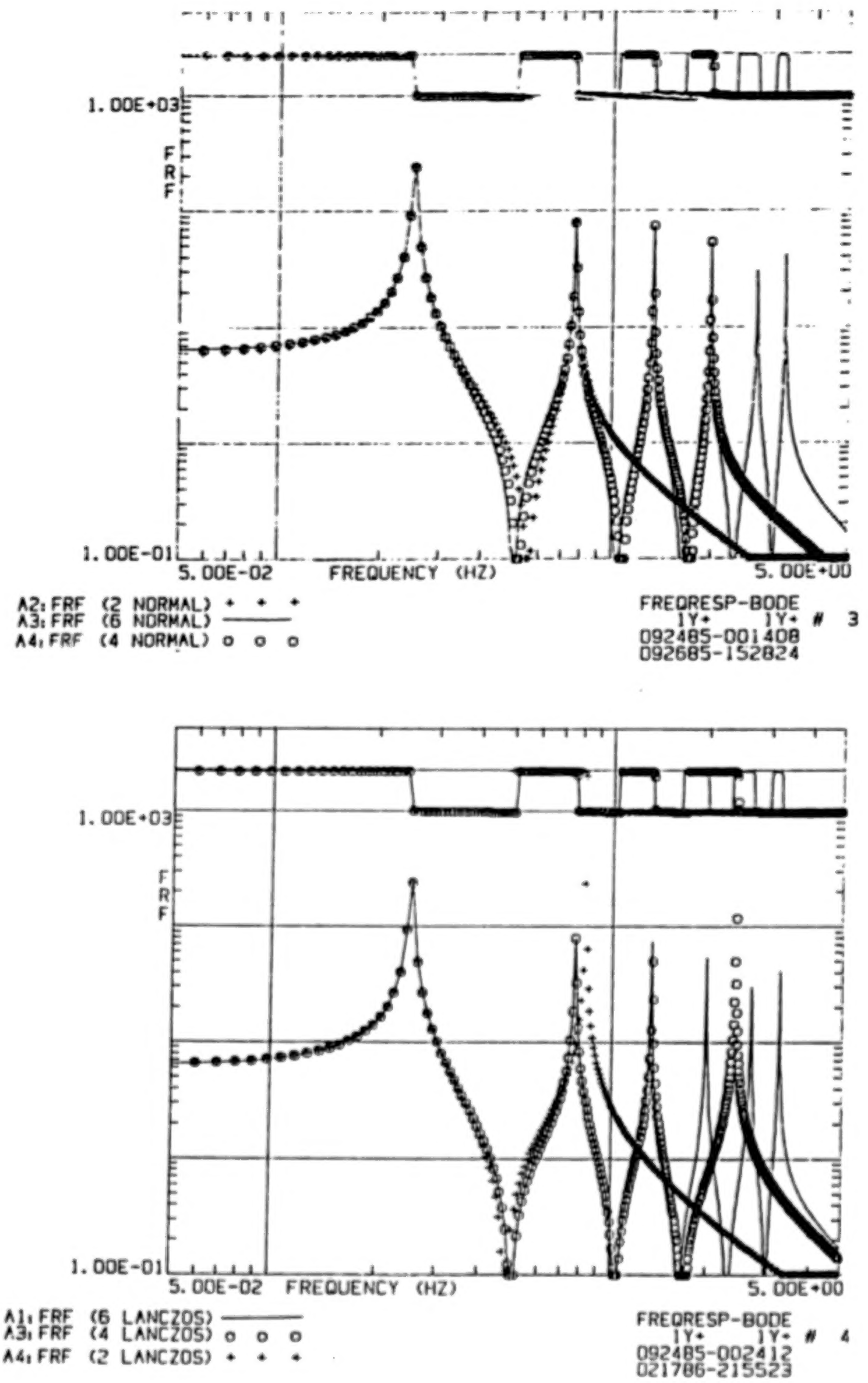

Direct frequency response functions (tip displacement/tip force) are shown for normal mode models and Lanczos vector models. The Lanczos models have improved low-frequency performance.

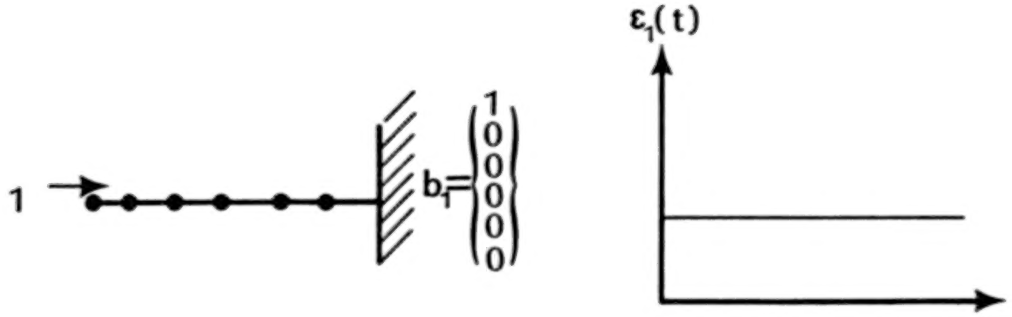
1
b1=
1
0
0
0
0
0
ε1(t)

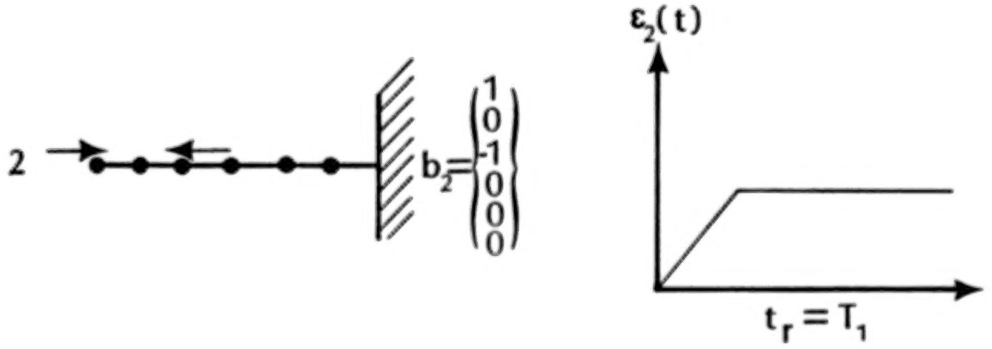
2
b2=
1
0
-1
0
0
0
ε2(t)
tr = T1

Control maneuvers, such as slewing, are transient response problems. The next examples compare transient response solutions of normal mode an Lanczos vector models when the structure is subjected to step and ramp excitation. Two force distributions are illustrated.

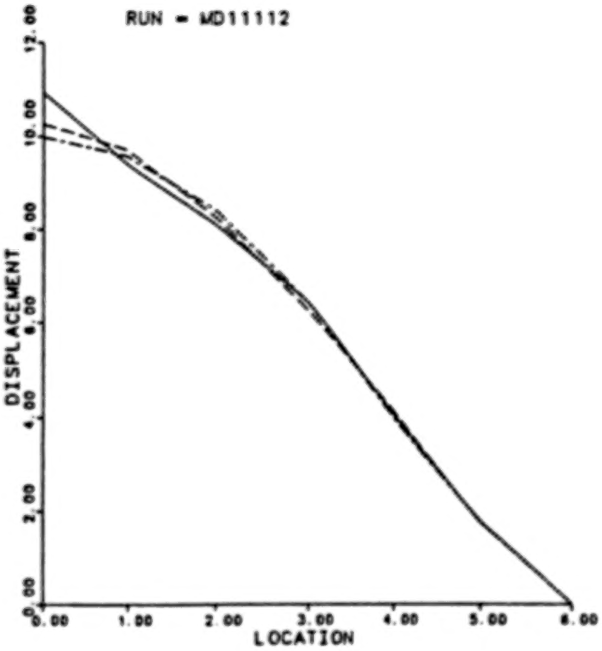

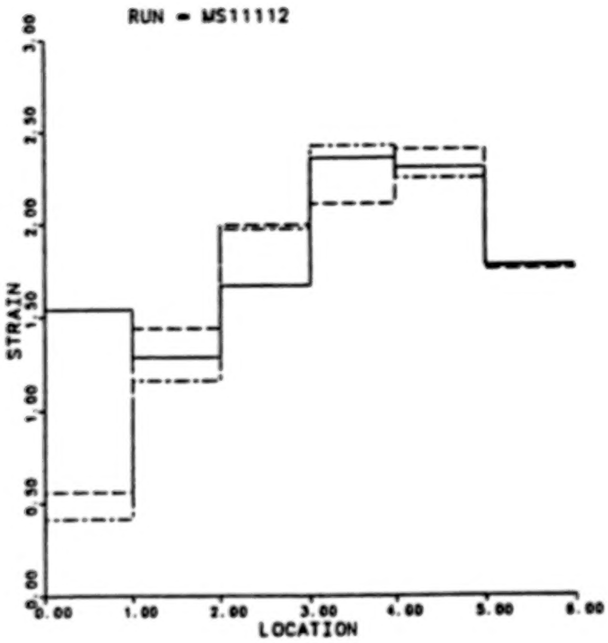

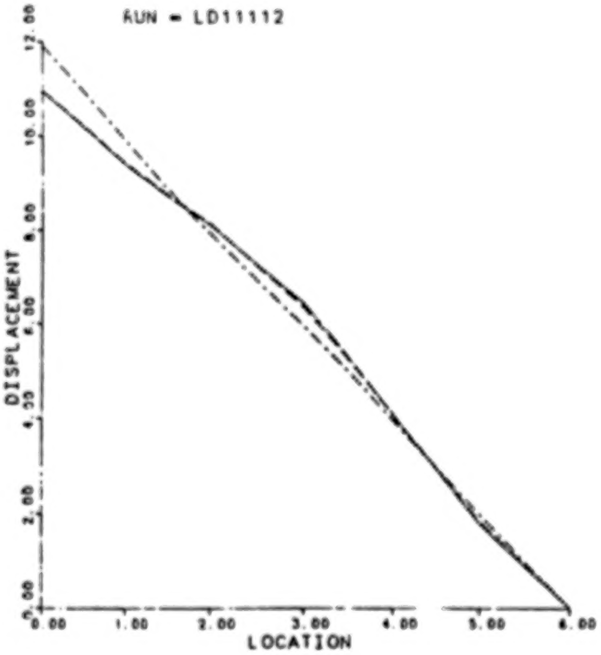

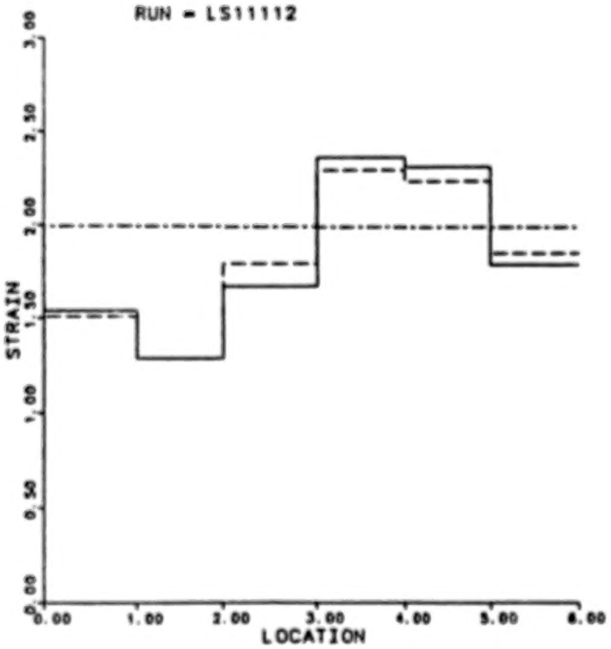

These are modal and Lanczos solutions for a step force applied at the tip. Both displacement and strain solutions are shown. Note that the Lanczos solutions converge a little better than the normal mode solutions do.

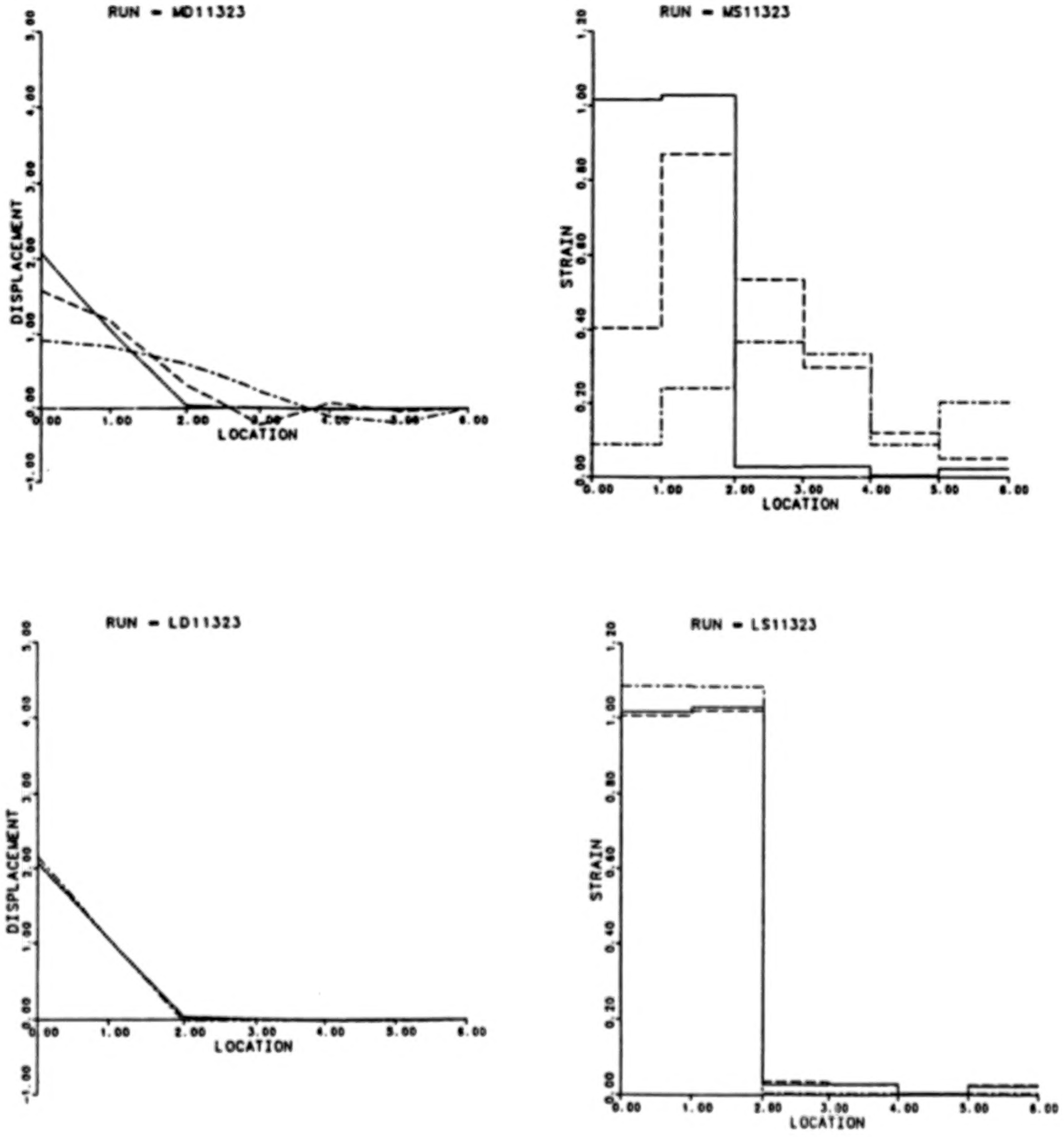

These are modal and Lanczos solutions for opposing forces applied at nodes 1 and 3 with a ramp time history. Note that the modal solutions are very poor, while the Lanczos solutions show excellent displacement and strain convergence.

CONCLUSIONS AND RECOMMENDATIONS

- Lanczos mode models represent low-frequency forced response better than do normal mode models.
- Lanczos mode models can be developed for both continuous and finite element structural representations.
- Lanczos mode models for systems with multiple inputs and/or rigid body modes should be developed.
- Numerical stability of the Lanczos algorithm should be assessed.
- Control system designs employing Lanczos mode models should be attempted.

N87
22740
UNCLAS

N87-22740

SLEWING CONTROL EXPERIMENT FOR A FLEXIBLE PANEL

Jer-Nan Juang

Structural Dynamics Branch
NASA Langley Research Center
Hampton, Virginia 23665

Marshall Workshop on Structural Dynamics and Control
of Large Flexible Structures

April 22-24, 1986

INTRODUCTION

This research is intended to identify technology areas in which better analytical and/or experimental methods are needed to adequately and accurately control the dynamic responses of multibody space platforms such as the Space Station. A generic space station solar panel (ref. 1) is used to experimentally evaluate current control technologies. Active suppression of solar panel vibrations induced by large angle maneuvers is studied with a torque actuator at the root of the solar panel. These active suppression tests will identify the hardware requirements and adequacy of various controller designs (ref. 2).

GENERIC SPACE STATION MODEL DYNAMIC TESTS

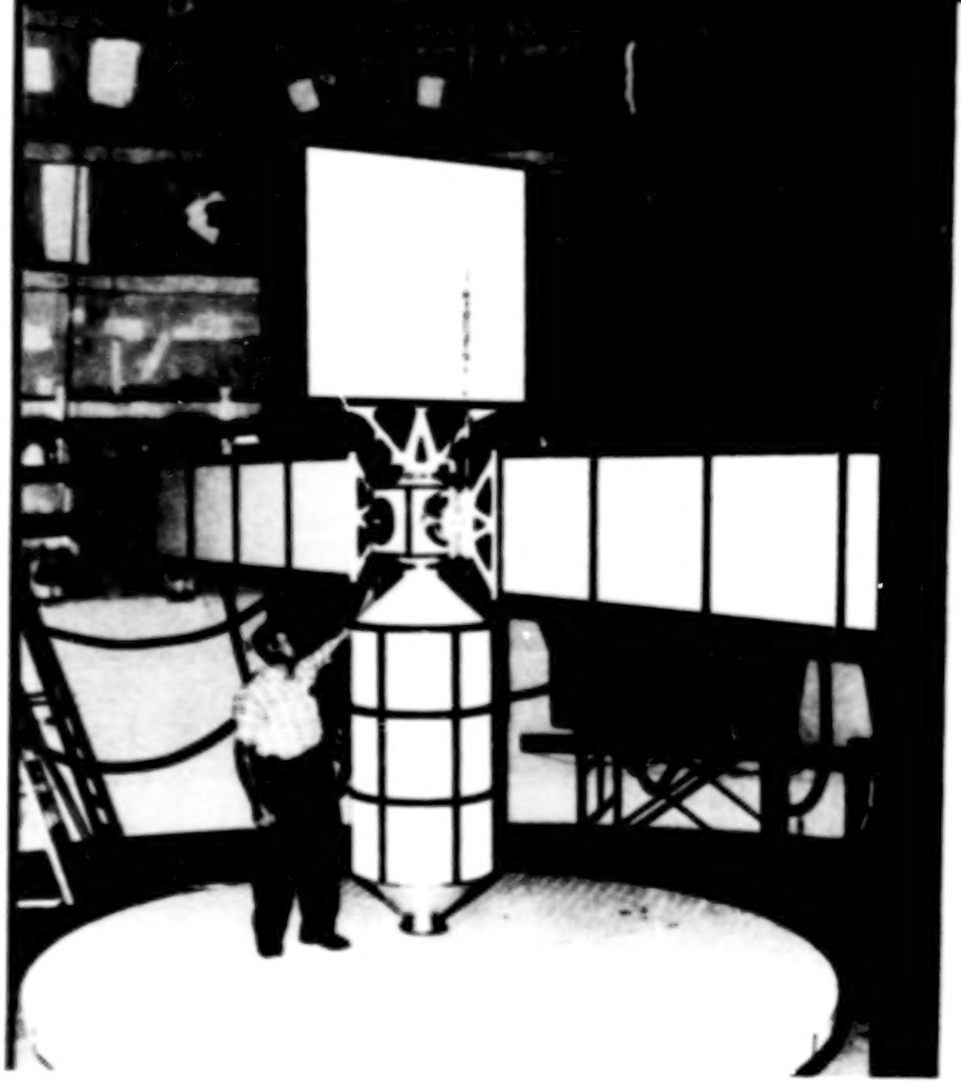

MULTIBODY SYNTHESIS

OPEN LOOP MANEUVERS

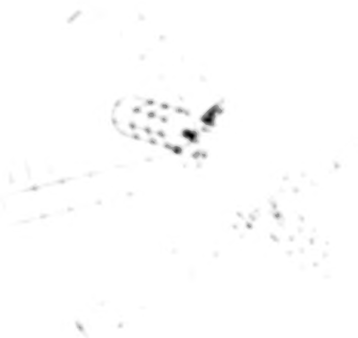

VIBRATION SUPPRESSION

ORIGINAL PAGE IS
OF POOR QUALITY

RAPID MANEUVERING OF FLEXIBLE STRUCTURES

The objective of the present experiment is to demonstrate slewing of a flexible structure in a single axis while simultaneously suppressing vibrational motion by the end of the maneuver. This experiment is designed to verify theoretical analyses concerning the application of modern control methods to the control of flexible structures (refs. 3 & 4).

RAPID MANEUVERING OF FLEXIBLE STRUCTURES

- **OBJECTIVE:** TO UNDERSTAND THE SUPPRESSION OF VIBRATIONS IN FLEXIBLE STRUCTURES.

- **APPROACH:** PERFORM FUNDAMENTAL EXPERIMENTS IN SLEWING OF FLEXIBLE STRUCTURES WHILE SIMULTANEOUSLY SUPPRESSING VIBRATIONAL MOTION AT THE END OF MANEUVER.

EXPERIMENT SET-UP

A 13-foot-long flexible solar panel model having a cross section of 2.1 ft x .13 in. is used for experimental validation. The test model is cantilevered in a vertical plane and rotated in the horizontal plane by an electric gearmotor. Instrumentation consists of three full-bridge strain gages to measure bending moments and two angular potentiometers to measure the angle of rotation at the root. The strain gages are located at the root, at twenty-two percent of the panel length, and at the mid-span. Signals from all four sensors are amplified and then monitored by an analog data acquisition system. An analog computer closes the control loop, generating a voltage signal for the gearmotor based on a linear optimal control algorithm with terminal constraints in finite time. The Figure shows an example of results for a 30-degree slew in 3.5 seconds. When no control is used, residual motion is significant, whereas the controller produces the same maneuver with virtually no residual motion.

SLEWING CONTROL SUCCESSFULLY DEMONSTRATED FOR FLEXIBLE SOLAR PANEL

TEST SET-UP

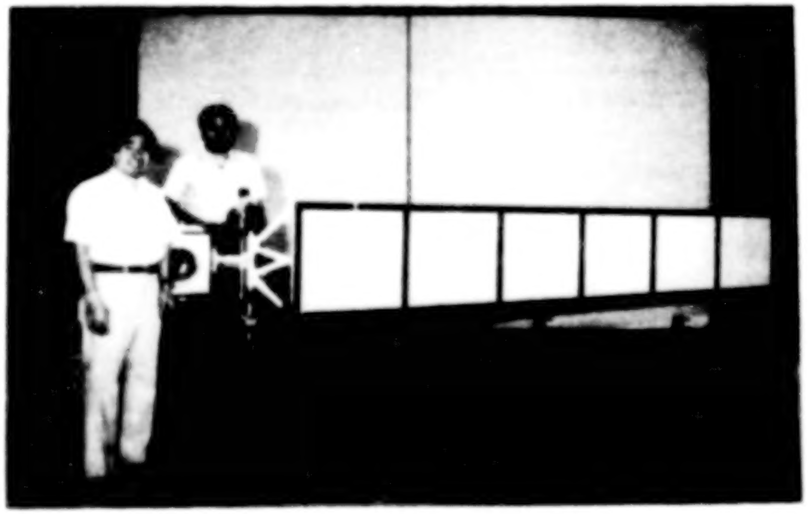

13-foot long aluminum/honeycomb panel

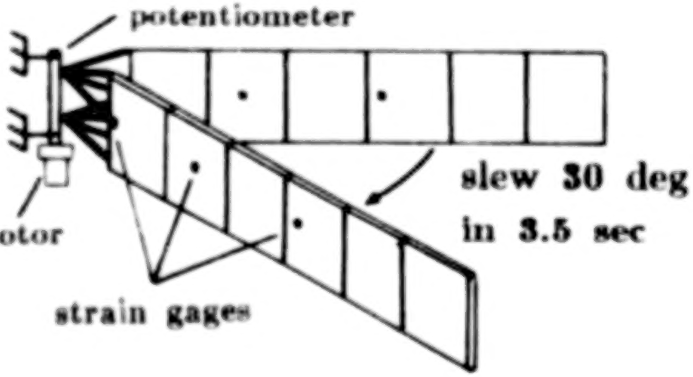
potentiometer
motor
strain gages
slew 30 deg
in 3.5 sec

EXPERIMENT

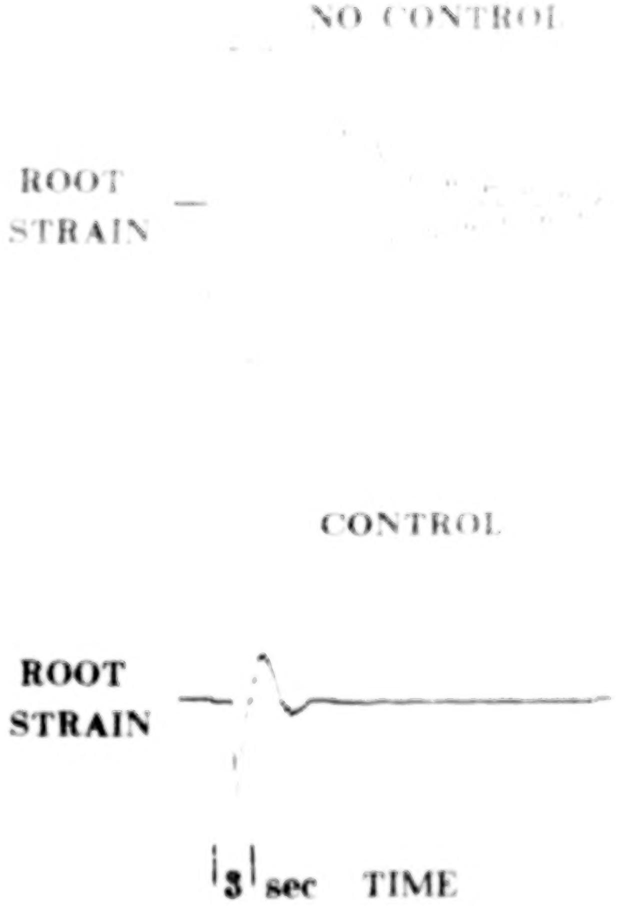

ORIGINAL PAGE IS
OF POOR QUALITY

CONTROL STRATEGY FOR TERMINALLY CONSTRAINED MANEUVER

The control design which is used in this experiment is the optimal terminal control law (refs. 3 & 4). The optimal terminal control law is formulated by findind the control input to minimize a cost function which consists of an integral of quadratic forms in the state, control, and control-rate with appropriate weighting matrices, subject to specified terminal constraints. The feedback gains thus derived consists of constant (steady state) and time varying gains. The weighting matrices determine the relative importance of the constant gain and time varying gain.

CONTROL STRATEGY FOR TERMINALLY CONSTRAINED MANEUVER

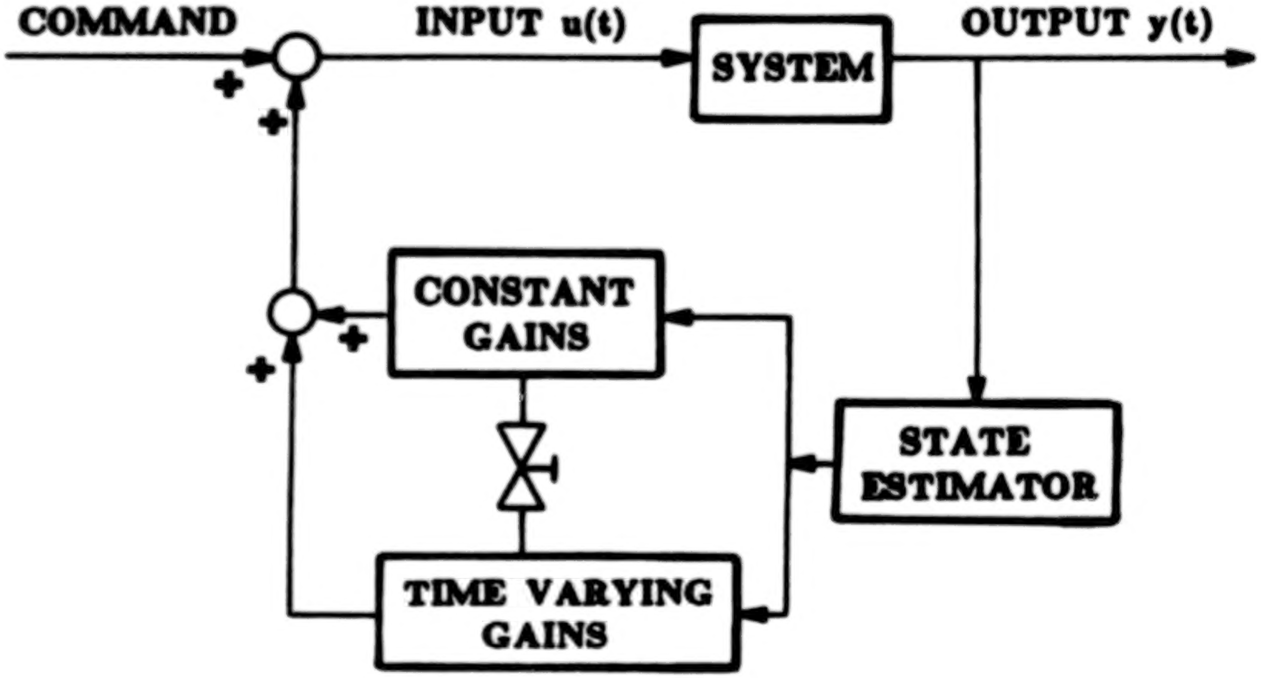
COMMAND
INPUT u(t)
SYSTEM
OUTPUT y(t)
+
+
CONSTANT GAINS
+
+
STATE ESTIMATOR
TIME VARYING GAINS

TYPICAL ANALYSIS/TEST COMPARISON

This figure shows the results for 30-degree maneuvers in air and in vacuum. The root strain is shown to illustrate the comparison of the analytical simulation with the experimental results. The solid line represents simulation data, whereas the dashed line represents the experimental data. Reasonable agreement is observed in the transient responses. The ordinate is in millivolts which can be converted to strain by using the conversion factor (ref. 5).

TRANSIENT RESPONSES FOR SIMULATED AND EXPERIMENTAL DATA
(For a 30 degrees maneuver)

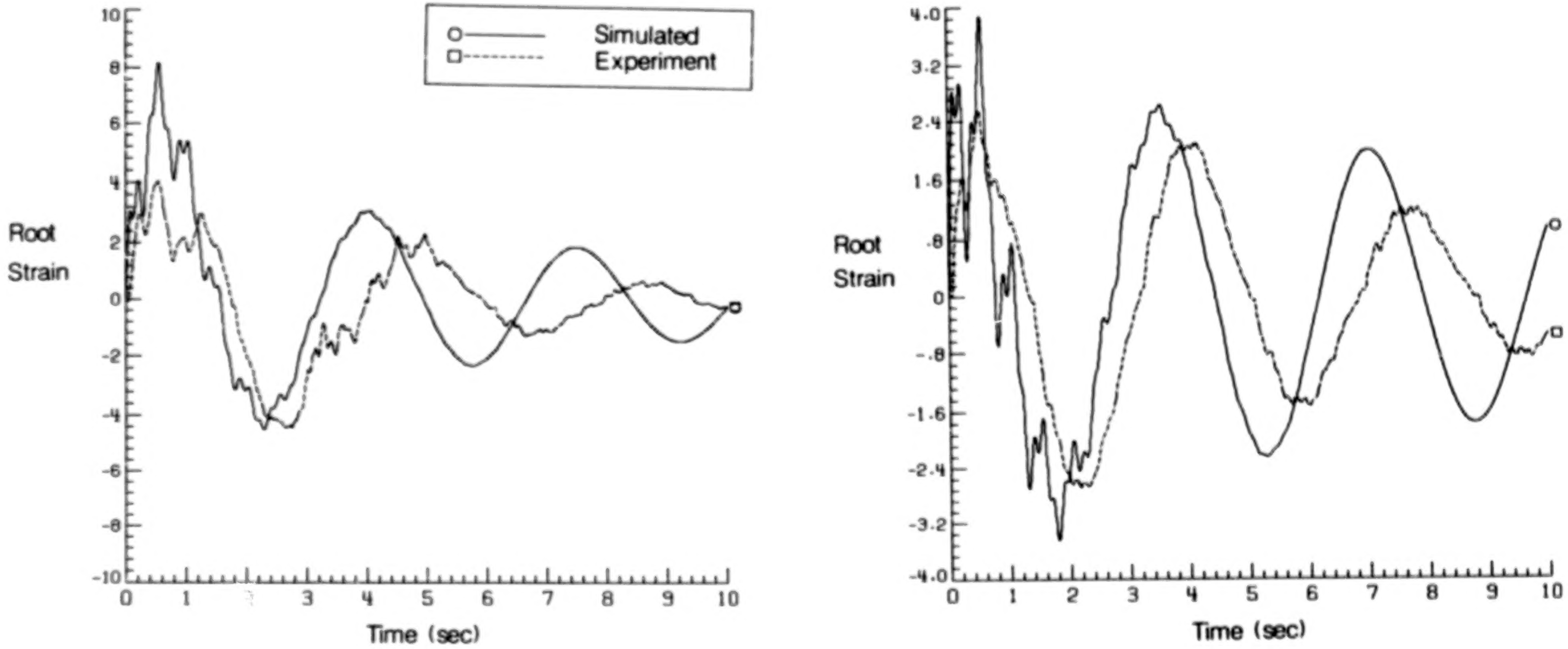

a) Air

b) Vacuum

TYPICAL ANALYSIS/TEST COMPARISON (CONTINUED)

The predicted and experimental frequencies and damping values are shown in the Table. In addition to the transient analysis, the laboratory data was analyzed using the Eigensystem Realization Algorithm (ERA) (Refs. 6 & 7). Since the system dynamics including air damping are nonlinear, the data length must be considered in the interpretation of modal parameters. However, examination of modal parameters identified using several different data lengths indicates that no significant variation of results occurs. Harmonic frequencies which reflect nonlinearities of the system dynamics do appear (see ref. 8). As a result, the dynamic behavior for those cases in air can be approximately described by the modal parameters. The predicted first mode frequency in air is lower than measured in the experiment. This is because of the softening effect of the gear train backlash which is not properly modeled if cantilever modes are used in the beam discretization. The same phenomena in vacuum is also observed. In both cases (in air and in vacuum), the analytically predicted damping values are lower than experiment. The differences are attributed to the dissipative effect of the gear train backlash not modeled. A reduction of the peak strain is also observed in vacuum because no air opposes the maneuver.

TYPICAL ANALYSIS/TEST COMPARISON

	DAMPING	FREQUENCY
● ANALYSIS	5%	0.28 HZ
● EXPERIMENT		
IN AIR	16%	0.25 HZ
IN VACUUM	9%	0.27 HZ

TYPICAL ANALYSIS/TEST COMPARISON (CONTINUED)

This figure shows the results for the same maneuver in air and vacuum when the control torque profile is shaped (ref. 5). Good agreement is observed in the transient analysis in vacuum. The experiment data in air depict a residual motion caused by air circulation in the laboratory while conducting the experiment. With the exception of the peak strain values, the curves in the figure agree reasonably. It is believed that the geartrain backlash and deadband effects contribute significantly to the increase of the peak strain value when air is opposing the slew maneuver particularly for the case with torque shaping. The discrepancy is also attributed to modeling errors of the drag forces. The drag coefficient is generally a function of vibration amplitude.

TRANSIENT RESPONSES FOR SIMULATED AND EXPERIMENTAL DATA
(For a 30 degrees maneuver with torque shaping)

ORIGINAL PAGE IS
OF POOR QUALITY

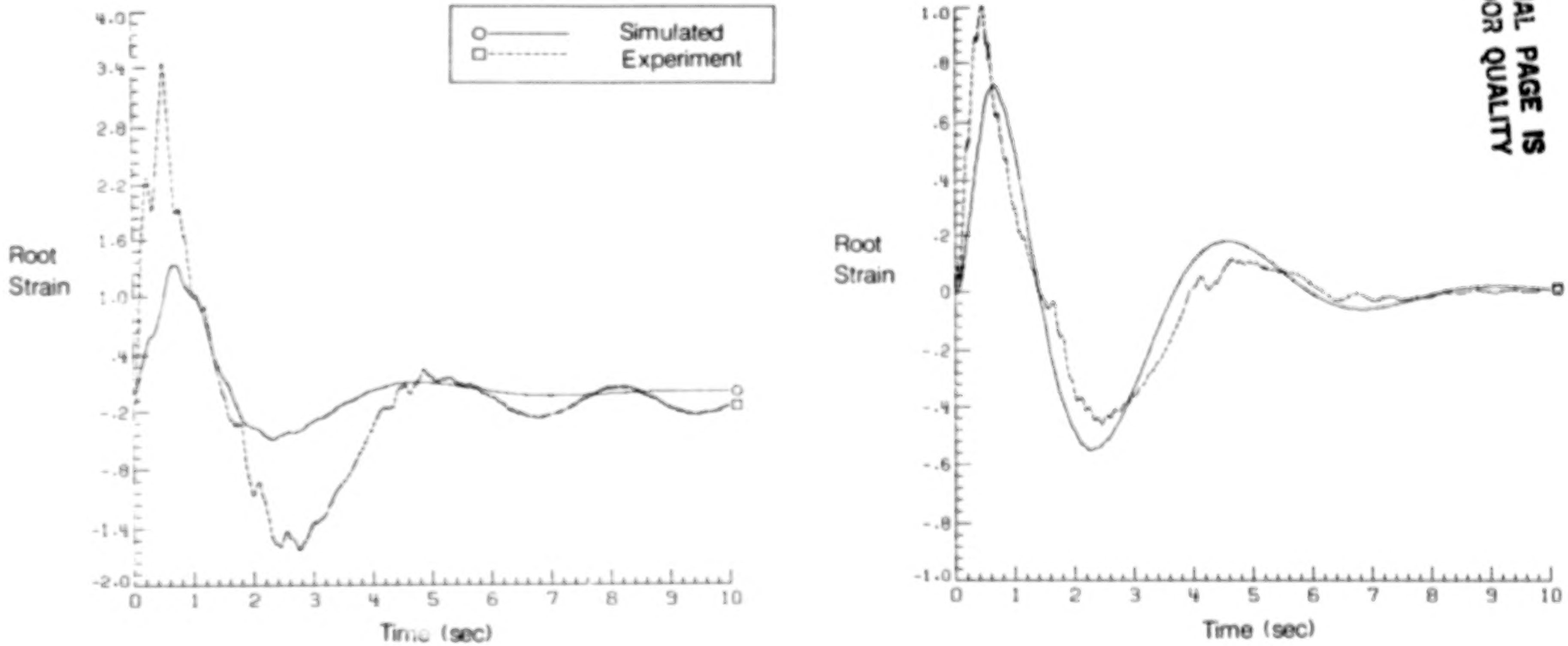

a) Air

b) Vacuum

ACCOMPLISHMENT

Prediction of transient responses, frequencies, and damping ratios is compared with experimental results. Satisfactory agreement was achieved between experimental measurements and theoretical predictions. Nonlinear effects due to large bending deflections during the maneuver did not cause significant changes in performance of the control laws, which were designed using linear control theory. To minimize the excitation of flexible modes, a low-pass filter was used to shape the control torque input. This shaping proved beneficial for fast slewing maneuvers. Damping effects due to atmosphere can be systematically and effectively included in the equations for slewing maneuvers of a flexible panel. By using the analysis technique shown here, one can include air damping in the numerical simulation to extrapolate the characteristics of the system in vacuum. The significance of air damping effects depends on the controller design for flexible structures. The smoother the controller is, the less the effects of air damping will be.

ACCOMPLISHMENT

- FAST SLEWING MANEUVERS WITH VIBRATION SUPPRESSION HAVE BEEN SUCCESSFULLY DEMONSTRATED FOR FLEXIBLE STRUCTURES.

- SATISFACTORY AGREEMENT WAS ACHIEVED BETWEEN EXPERIMENTAL MEASUREMENTS AND THEORETICAL PREDICTION USING A LINEAR CONTROL THEORY

FUTURE PLANS

The hardware will be modified to study the slewing control of multiple solar panels hinged to a rigid body, which produces a kinematically nonlineal dynamic system for large angle maneuver. Three actuators are required to slew the system which has three rigid body axes.

ORIGINAL PAGE IS
OF POOR QUALITY

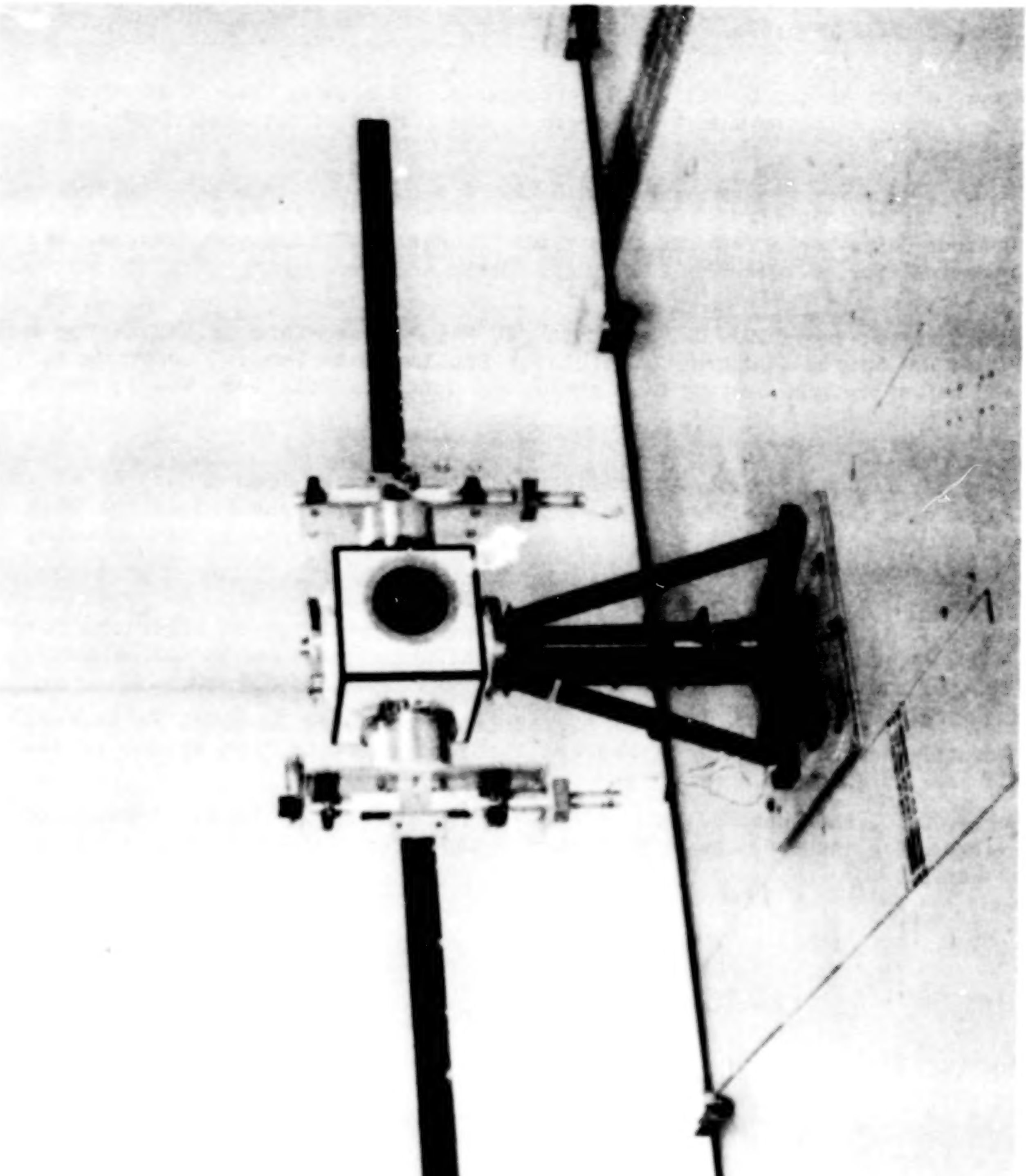

REFERENCES

[1] Belvin, K. W., "Experimental and Analytical Generic Space Station Dynamic Models," NASA TM-87696, March 1986.

[2] Juang, J. N., Horta, L. G., and Robertshaw, H., "A Slewing Control Experiment for Flexible Structures," To appear in the Journal of Guidance, Control and Dynamics.

[3] Juang, J. N., Turner, J. D., and Chun, H. M., "Closed-Form Solutions of Control Gains For a Terminal Controller," Journal of Guidance, Control and Dynamics, Vol. 8, Jan.-Feb. 1985, pp. 38-43.

[4] Juang, J. N., Turner, J. D., and Chun, H. M., "Closed-Form Solutions For a Class of Optimal Quadratic Regulator Problems with Terminal Constraints," Journal of Dynamic System, Measurement and Control, Vol. 108, No. 1, March 1986, pp. 44-48.

[5] Juang, J. N. and Horta, L. G., "Effects of Atmosphere on Slewing Control of a Flexible Structure, "AIAA Paper No. 86-1001-CP, Presented at the 27th Structures, Structural Dynamics, and Materials Conference, San Antonio, Texas, May 19-21, 1986.

[6] Juang, J. N., and Pappa, R. S., "An Eigensystem Realization Algorithm for Modal Parameter Identification and Modal Reduction," Journal of Guidance, Control and Dynamics, Vol. 8, No. 5, Sept.-Oct. 1985, pp 620-627.

[7] Juang, J. N., and Pappa, R. S., "Effects of Noise On Modal Parameters Identified with the Eigensystem Realization Algorithm," To appear in the Journal of Guidance, Control and Dynamics.

[8] Horta, L. G. and Juang, J. N., "Identifying Approximate Linear Models for Simple Nonlinear Systems," To appear in the Journal of Guidance, Control and Dynamics.

N87
22741
UNCLAS

N87-22741

MEOP CONTROL DESIGN SYNTHESIS: OPTIMAL QUANTIFICATION OF THE MAJOR DESIGN TRADEOFFS

D. C. Hyland
and
D. S. Bernstein
Harris Corporation
Government Aerospace Systems Division
Melbourne, Florida

Workshop on Structural Dynamics and Control Interaction
of Flexible Structures
MSFC, Huntsville, Alabama
April 22-24, 1986

INTRODUCTION: OPTIMAL PROJECTION/MAXIMUM ENTROPY DESIGN SYNTHESIS

In this presentation we (1) discuss the underlying philosophy and motivation of the optimal projection/maximum entropy (OP/ME) stochastic modelling and reduced order control design methodology for high order systems with parameter uncertainties, (2) review the OP/ME design equations for reduced-order dynamic compensation including the effect of parameter uncertainties, and (3) illustrate the application of the methodology to several Large Space Structure (LSS) problems of representative complexity. The basis for this paper is references [1-25] along with recently obtained results.

The OP/ME approach, as its name suggests, represents the synthesis of two distinct ideas: (1) reduced-order dynamic compensator design for a given high-order plant (i.e., optimal projection design) and (2) minimum-information stochastic modelling of parameter uncertainties (i.e., maximum entropy modelling). Maximum entropy modelling is discussed in [1-13,15] and optimal projection design is studied in [6,10,12,14,16-25].

Before attempting an overview of the OP/ME approach, it is important to discuss the class of problems that motivated this work, namely, control of large flexible space structures. A finite-element model of a large flexible space structure is, generally, an extremely high-order system. For example, a version of the widely studied CSDL Model #2 includes 150 modes and 6 disturbance states, i.e., a total of 306 states, along with 9 sensors and 9 actuators. The size of the model and the coupling between sensors and actuators render classical control-design methods useless and all but confound attempts to use LQG to obtain a controller of manageable order. Indeed, these difficulties were a prime motivation for the optimal projection approach. Besides the high order of these systems, finite element modelling is known to have poor accuracy, particularly for the high-order modes. Reasonable and not overly conservative uncertainty estimates predict 30-50 percent error in modal frequencies after the first 10 modes, with the situation considerably more complex (and pessimistic) for damping estimates. Otherwise-successful control-design methodologies widely promulgated in the aerospace community were severely strained in the face of such difficulties.

As indicated in Figure 1, maximum entropy modelling addresses the robustness problem by permitting direct inclusion of parameter uncertainties in the plant and disturbance models so that quadratically optimal system design plus maximum entropy modelling automatically yield system designs that trade performance off against modelling uncertainties. Furthermore, complexity and cost generally preclude implementation of very high dimension controllers (as in standard LQG techniques). Optimal projection design deals directly and rigorously with the question of system dimension by trading controller order off against performance.

OPTIMAL PROJECTION/MAXIMUM ENTROPY DESIGN SYNTHESIS

- Parameter uncertainties are directly incorporated into the design process
  - ⇨ Optimal quantification of robustness/performance tradeoff
- Controller order fixed by implementation constraints
  - ⇨ Optimal quantification of order/performance tradeoff

Figure 1

MAXIMUM ENTROPY MODELLING

Maximum entropy modelling is a form of stochastic modelling. Although external disturbances are traditionally modelled stochastically as random processes, the use of stochastic theory to model plant parameter uncertainty has seen relatively limited application. All objections to a stochastic parameter uncertainty model are dispelled by invoking the modern information-theoretic interpretation of probability theory. Rather than regarding the probability of an event as the limiting frequency of numerous repetitions (as, e.g., the number of heads in 1,000 coin tosses) we adopt the view that the probability of an event is a quantity which reflects the observer's certainty as to whether a particular event will or will not occur. This quantity is nothing more than a measure of the information (including, e.g., all theoretical analysis and empirical data) available to the observer. In this sense the validity of a stochastic model of a flexible space structure, for example, does not rely upon the existence of a fleet of such objects (substitute "ensemble" for "fleet" in the classical terminology) but rather resides in the interpretation that it expresses the engineer's certainty or uncertainty regarding the values of physical parameters such as stiffnesss of structural components. This view of probability theory has its roots in Shannon's information theory but was first articulated unambiguously by Jaynes (see [26-29]).

The preeminent problem in modelling the real world is thus the following: given limited (incomplete) a priori data, how can a well-defined (complete) probability model be constructed which is consistent with the available data but which avoids inventing data which does not exist? To this end we invoke Jaynes' Maximum Entropy Principle: First, define a measure of ignorance in terms of the information-theoretic entropy, and then determine the probability distribution which maximizes this measure subject to agreement with the available data. The smallest collection of data for which a well-defined probability model (called the minimum information model) can be constructed is known as the minimum data set.

The reasoning behind this principle is that the probability distribution which maximizes a priori ignorance must be the least presumptive (i.e., least likely to invent data) on the average since the amount of a posteriori learned information (should all uncertainty suddenly disappear) would necessarily be maximized. If, for some probability distribution, the a priori ignorance and hence the a posteriori learning were less than their maximum value then this distribution must be based upon invented and, hence, generally incorrect data. The Maximum Entropy Principle is clearly desirable for control-system design where the introduction of false data is to be assiduously avoided.

It is shown in [1] that the stochastic model induced by the Maximum Entropy Principle of Jaynes is a Stratonovich multiplicative white noise model. The earlier developments considered a relatively restricted class of parameter uncertainties. At present, however, the theory extends to the most general modelling uncertainties encountered in flexible mechanical systems. Moreover, the minimum data set presently used to induce the maximum entropy stochastic model consists of stipulated bounds on the deviations of physical parameters about their nominal values. This description is both convenient and deeply rooted in engineering tradition. As indicated in Figure 2, these parameter bounds are the basic data needed to implement maximum entropy modelling in practice.

MINIMUM-INFORMATION MODELLING

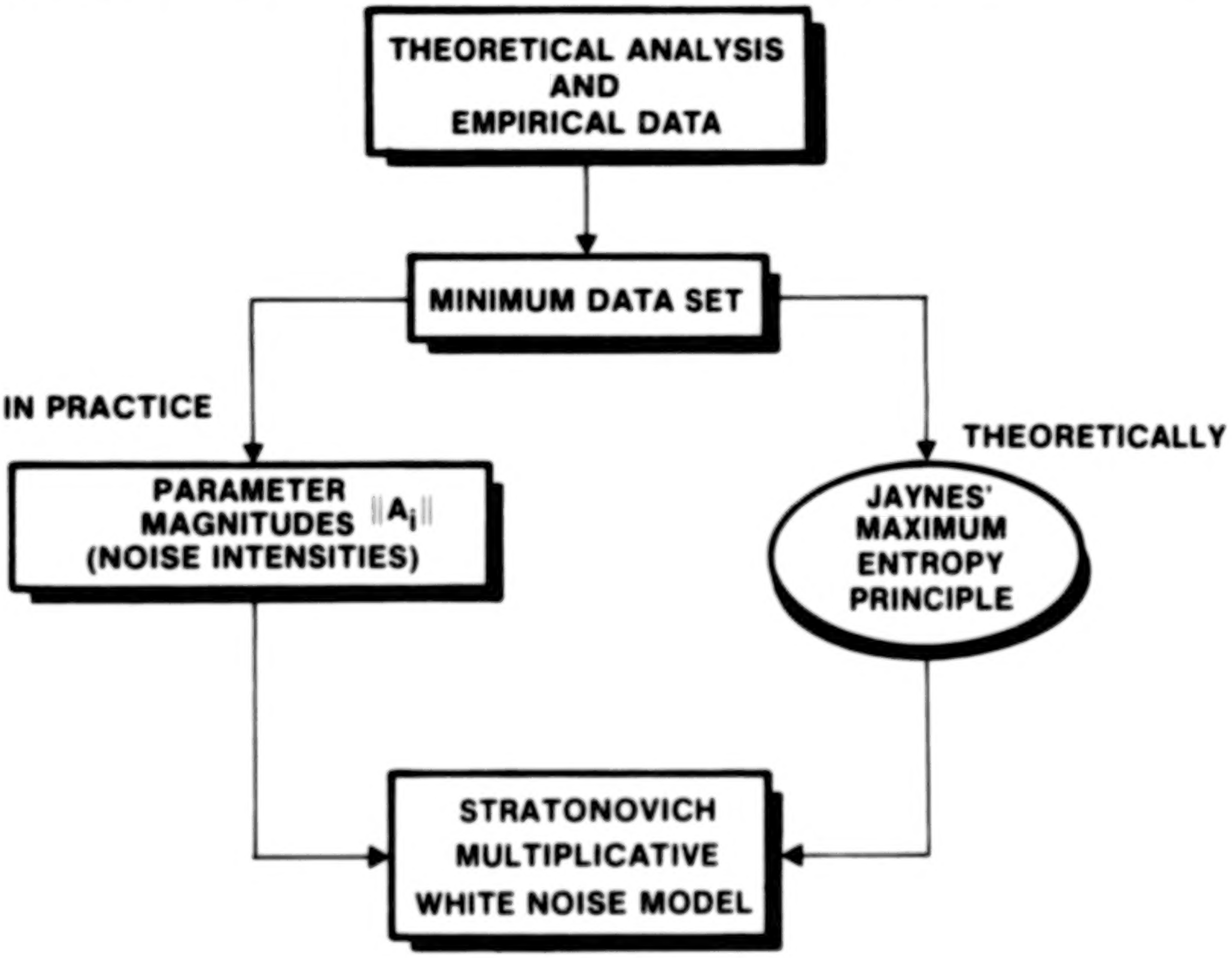
THEORETICAL ANALYSIS AND EMPIRICAL DATA
MINIMUM DATA SET
IN PRACTICE
THEORETICALLY
PARAMETER MAGNITUDES $\|A_i\|$ (NOISE INTENSITIES)
JAYNES' MAXIMUM ENTROPY PRINCIPLE
STRATONOVICH MULTIPLICATIVE WHITE NOISE MODEL

Figure 2

REPRESENTATION OF PARAMETER UNCERTAINTIES

Once significant types of parameter uncertainty have been identified and bounds on parameter variations established, the maximum entropy model can be placed in the general form shown in Figure 3. The set $\{A_i, i=1,\ldots,N\}$ of deterministic matrices defines the geometric pattern of the uncertain perturbation, ΔA, of the dynamics matrix. The norm $\|A_i\|$ defines the magnitude of uncertainty and is uniquely related to the originally stipulated parameter deviation bound. The stochastic model which follows in consequence of Jayne's Maximum Entropy Principle is a form of Stratonovich white noise. This model is extremely mathematically tractable since the second moment equation for the state can be closed. Moreover, the Stratonovich formulation allows crucial effects of uncertainty to be reproduced.

A = Nominal Dynamics Matrix
$A + \Delta A$ = Actual Dynamics Matrix (But ΔA Is Unknown)

WHITE NOISE REPRESENTATION

$$\Delta A = \sum_{i=1}^{p} \alpha_i(t) A_i$$

$\alpha_i(t)$ = Zero-Mean, Unit-Intensity, Uncorrelated White Noise Processes
A_i = Uncertainty Pattern
$\|A_i\|$ = Uncertainty Magnitude

MULTIPLICATIVE WHITE NOISE MODEL

$$\dot{x}(t) = \left(A + \sum_{i=1}^{p} \alpha_i(t) A_i\right) x(t)$$

Figure 3

STOCHASTIC DIFFERENTIAL EQUATIONS AND THE STRATONOVICH CORRECTION

Figure 4 displays the stochastic differential equation (second equation in the figure) arising from the Stratonovich model. To illustrate the crucial features of this model, a brief review of the literature on multiplicative white noise is absolutely essential. The theory of stochastic differential equations was placed on a firm mathematical foundation by Ito [30] and has been widely developed and applied to modelling, estimation and control problems [31-59]. The basic linear multiplicative white noise model is given by the Ito differential equation:

$$dx_t = (Adt + \sum_{i=1}^{p} d\alpha_{it} A_i) X_t$$

where the $d\alpha_{it}$ are Wiener processes. Although such models were studied extensively for estimator and control design [40-56], this approach fell into disrepute with the publication of [58,59] where it was shown for discrete-time systems that sufficiently high uncertainty levels (i.e., magnitudes $\|A_i\|$ above a threshold) led to the nonexistence of a steady state solution. Although it was purported in [58] that this "phenomenon" was an "obvious" consequence of high uncertainty levels, these conclusions failed to take into account (possibly because of the discrete-time setting) the subtle relationship between the ordinary differential equation (the first equation in Figure 4) and the stochastic differential equation. Indeed, it was shown in [31] that if a stochastic differential equation is regarded as the limit of a sequence of ordinary differential equations, then the above Ito equation is not correct. Instead, the ordinary differential equation with multiplicative white noise corresponds to the corrected Ito equation appearing as the second equation in Figure 4. It is seen that this differs from the "naive" equation by a systematic drift term (the Stratonovich correction). Although skepticism regarding this unusual result was admitted to in [31], the form of the second equation in Figure 4 was corroborated completely independently by Stratonovich in [32], whose results actually appeared in the Russian literature prior to 1965. His approach is based upon an alternative definition of stochastic integration which differs from Ito stochastic integration by a mathematical technicality. The Stratonovich approach, it should be noted, has the interesting feature that approximating sums involve future values of a Brownian motion process which, although physically unacceptable in the classical view of probability, is completely consistent with the information-theoretic interpretation.

In spite of the glaring technicality of the Stratonovich correction, almost all research on the estimation and control of such systems failed to perceive its physical significance. To the author's knowledge, the work of Gustafson and Speyer [56] was the only paper prior to the appearance of [1] which demonstrated the crucial feature: The Stratonovich correction neutralizes the threshold uncertainty principle. In particular for systems which are inherently stable under particular parameter variations (e.g., structures with uncertain stiffness matrices), the Stratonovich formulation correctly predicts unconditional second-moment stability - in contrast to the Ito formulation within which a stringent uncertainty threshold is encountered.

STRATONOVICH CORRECTION

Stratonovich, 1966 [31]; **Wong and Zakai, 1965** [32]

Ordinary Differential Equation: $\dot{x}(t) = (A + \sum_{i=1}^{p} \alpha_i(t) A_i) x(t)$

Itô Stochastic Differential Equation: $dx_t = (A_s dt + \sum_{i=1}^{p} d\alpha_{it} A_i) x_t$

$$A_s = A + \underbrace{\frac{1}{2} \sum_{i=1}^{p} A_i^2}_{\text{correction}}$$

Figure 4

MAXIMUM ENTROPY MODIFICATION OF THE STATE CONVARIANCE EQUATION

Note that when undertaking quadratic optimization within the maximum entropy model, one minimizes the mathematical expectation of the usual quadratic performance penalty taken over the maximum entropy statistics. Thus the feature of the stochastic model most utilized in practice is the second moment equation for the system state. The form of this equation that results from the Stratonovich white noise model is given explicitly in Figure 5. The "stochastic modification" term given by the bottom expression in Figure 5 distinguishes this stochastic Lyapunov equation from the ordinary Lyapunov equation that would result from a deterministically parametered model.

The importance of the stochastic modification term cannot be underrated. In particular, for most types of parameter uncertainty encountered in structural systems, the Stratonovich corrections in M[Q] imply progressive decorrelation between pairs of dynamical states. This informational or statistical damping phenomenon is a direct result of parameter uncertainties that is captured by the multiplicative white noise model. The Stratonovich correction, moreover, is crucial: By neutralizing the threshold uncertainty principle, it permits the consideration of long-term effects for arbitrary uncertainty levels.

$$\dot{Q}(t) = A_sQ(t) + Q(t)A_s^T + \sum_{i=1}^{p} A_iQ(t)A_i^T + V$$

$Q(t) = E[x(t)x(t)^T]$ (The quantity of interest in quadratic optimization)

E = Average over parameter uncertainties and disturbances

$$A_s = A + \frac{1}{2}\sum_{i=1}^{p} A_i^2 \qquad V = \text{Disturbance Intensity}$$

STOCHASTIC MODIFICATION

$$M[Q] = \frac{1}{2}\left(\sum_{i=1}^{p} A_i^2 Q + Q\sum_{i=1}^{p} A_i^{2T}\right) + \sum_{i=1}^{p} A_iQA_i^T$$

Figure 5

RAMIFICATIONS FOR THE STRUCTURE OF THE STEADY STATE COVARIANCE

The far-reaching ramifications of the foregoing observations are explored extensively in [1-10]. As an example, assume (as is usually the case in practice) that uncertainties in modal frequency obtained from a finite-element analysis of a large flexible space structure increase with mode number. From the form of M[Q(t)] it is easy to deduce that the steady state covariance becomes increasingly diagonally dominant with increasing frequency and thus assumes the qualitative form given in Figure 6. The benefits of this sparse form are important: The computational effort required to determine the steady state covariance (and thus to design a closed-loop controller, for example) is directly proportional to the amount of information reposed in the model or, equivalently, inversely proportional to the level of modelled parameter uncertainty. This casts new light on the computational design burden vis-a-vis the modelling question: The computational burden depends only upon the information actually available. A simple control-design exercise involving full-state feedback for a simply supported beam presented in [4] illustrates this point. The gains for the higher-order modes of the beam, whose frequency uncertainties increase linearly with frequency, were obtained with modest computational effort in spite of 100 structural modes included in the model. Another important ramification of the qualitative form of Q is the automatic generation of a high/low-authority control law. Note that for the higher order and hence highly uncertain modes the control gains reported in [3,4] indicated an inherently stable, low performance rate-feedback control law, whereas for the lowest order modes the control law is high authority, i.e., "LQ" in character.

EFFECT OF FREQUENCY UNCERTAINTIES ON THE QUALITATIVE STRUCTURE OF THE STEADY-STATE COVARIANCE $Q = \lim_{t \to \infty} E[x(t)x(t)^T]$

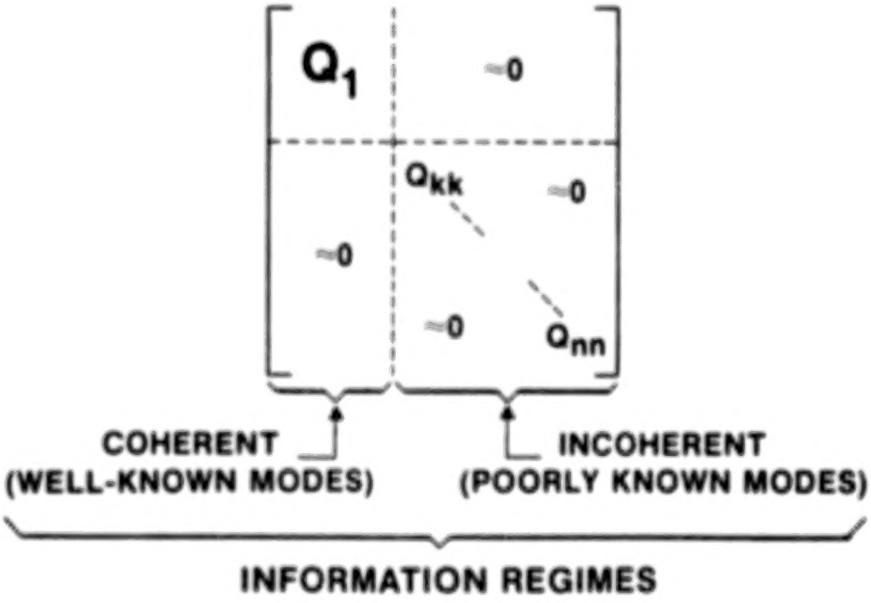

Figure 6

PERFORMANCE ROBUSTNESS

Figure 7 illustrates the basic concept of robustness with respect to performance that is so essential to adequate LSS control design. The curves shown sketch the variation of closed-loop performance (e.g., line-of-sight error) for particular control designs when system parameters deviate from their nominal values. As illustrated in one example below, standard LQG design provides a sharp minimum at the nominal parameter values but can be extremely sensitive to off-nominal variations. On the other hand, since the maximum entropy formulation includes the deleterious effects of uncertainty within the basic design model, it provides the mechanism to assure satisfaction of performance objectives not only for the nominal model but also over the likely range of parameter deviations. Note that the price paid for this is a degradation of performance (relative to a deterministic model, LQG design) whenever the system parameters happen to be near their nominal values. However, this tradeoff between nominal performance and robustness is widely recognized as an inescapable fact of life. The prime motivation for the maximum entropy development is to achieve a design methodology which sacrifices as little near-nominal performance as possible while securing performance insensitivity over the likely range of modelling errors.

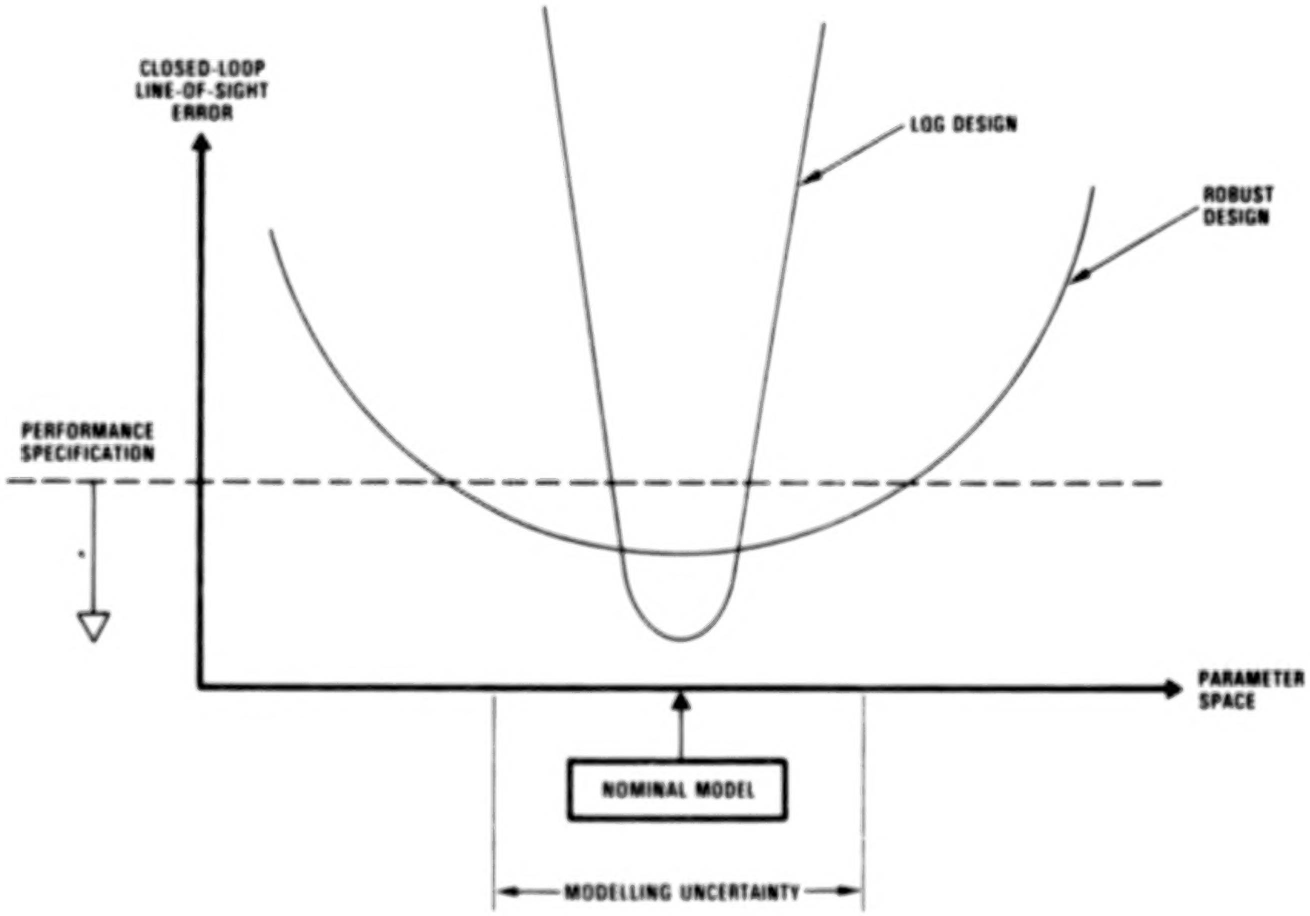

Figure 7

DEVELOPMENT OF THE OP/ME SYNTHESIS

At this point, we consider the optimal projection approach and its amalgamation with maximum entropy modelling. Figure 8 illustrates that the overall development proceeded along two distinct paths, starting from standard LQG theory. One path of development (the right branch) retained the LQG assumption that the dynamic controller to be designed is of the same dimension as the plant but extended the theory by including the effects of parameter uncertainty via stochastic modelling. The optimality conditions for full-order dynamic compensation under a maximum entropy model are the principal design results and consist of two modified Riccati equations coupled to two Lyapunov equations by the stochastic modification terms. These equations were presented in [5,15] and were also independently discovered by a Soviet researcher [57].

The second path of development from LQG retained the assumption of a deterministically parametered model but removed the restriction to full-order compensation - i.e., a quadratically optimal but fixed-order compensator is sought for a higher order plant in order to simplify implementation. This led to the optimal projection approach to fixed-order compensation.

The optimal projection approach is based entirely on a theorem which characterizes the quadratically optimal reduced-order dynamic compensator. Assuming a purely dynamic linear system structure for the desired compensator whose order is determined by implementation constraints (e.g., reliability, complexity or computing capability), a parameter optimization approach is taken. There is, of course, nothing novel about this approach per se and it has been widely studied in the control literature [60-73]. Clearly, the parameter optimization approach fell into disrepute because of the extreme complexity of the grossly unwieldy first-order necessary conditions which afforded little insight and engendered brute force gradient search techniques. The crucial discovery occurred in [6] where it was revealed that the necessary condition for the dynamic-compensation problem gives rise to the definition of an optimal projection as a rigorous, unassailable consequence of quadratic optimality without recourse to ad hoc methods as in [74-83]. Exploitation of this projection leads to immense simplification of the "primitive" form of the necessary conditions for this problem. The novel equations consist of two modified Riccati equations and two modified Lyapunov equations (analogous to the four optimality conditions for full-order compensation under maximum entropy models) coupled, in this instance, by a projection of rank equal to the desired controller dimension. This "optimal projection" essentially characterizes the geometric structure of a reduced-order plant model employed internally by the compensator.

OPTIMAL PROJECTION/MAXIMUM ENTROPY APPROACH TO LOW-ORDER, ROBUST CONTROLLER DESIGN

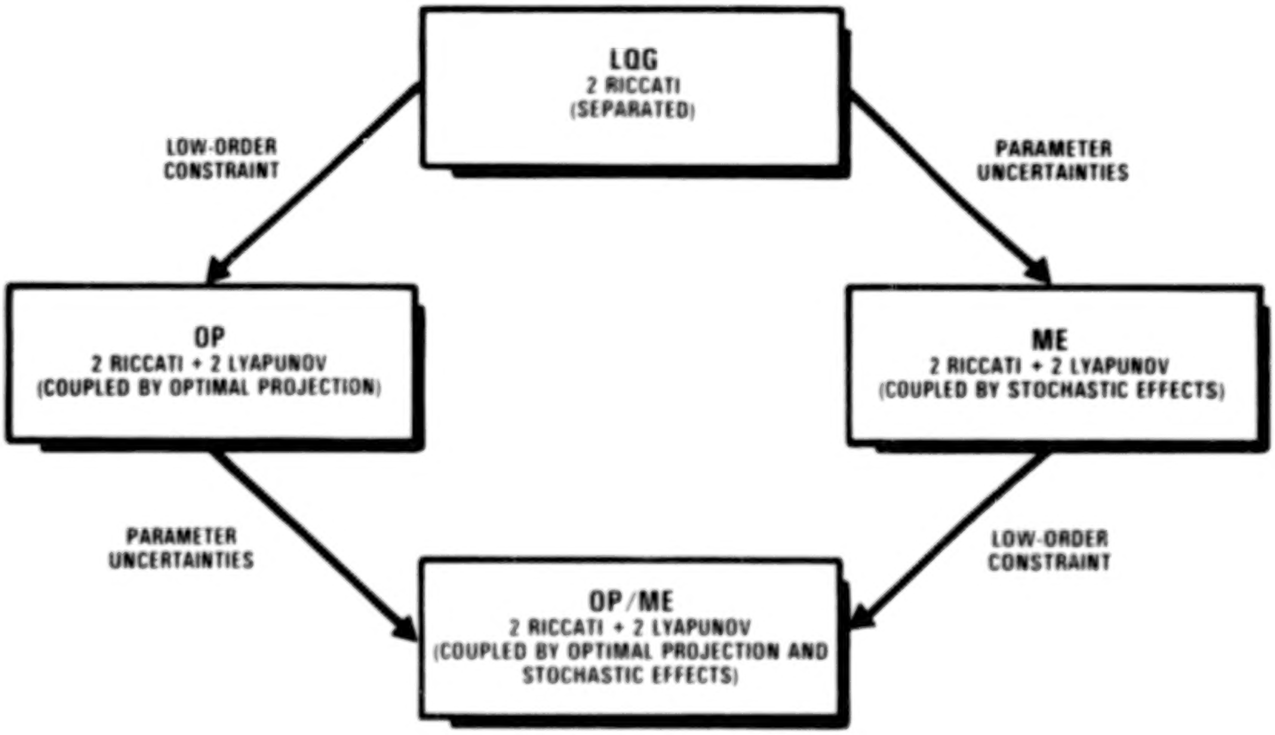

LQG
2 RICCATI
(SEPARATED)

LOW-ORDER CONSTRAINT

PARAMETER UNCERTAINTIES

OP
2 RICCATI + 2 LYAPUNOV
(COUPLED BY OPTIMAL PROJECTION)

ME
2 RICCATI + 2 LYAPUNOV
(COUPLED BY STOCHASTIC EFFECTS)

PARAMETER UNCERTAINTIES

LOW-ORDER CONSTRAINT

OP/ME
2 RICCATI + 2 LYAPUNOV
(COUPLED BY OPTIMAL PROJECTION AND STOCHASTIC EFFECTS)

Figure 8

SURVEY OF APPROACHES TO FIXED-ORDER DYNAMIC COMPENSATOR DESIGN

Before describing the synthesis of the optimal projection (OP) and maximum entropy (ME) approaches, we sketch the relationship between optimal projection and previously proposed techniques for reduced-order compensator design. The general relationships among general categories of approaches are illustrated in Figure 9.

The basic premise is that the plant to be controlled is distributed parameter in character (as are structural systems). The usual engineering approach (the right branch in Figure 9) is to replace the distributed parameter system with a high-order finite-dimensional model. However, fundamental difficulties remain since application of LQG leads to a controller whose order is identical to that of the high-order approximate model. Attempts to remedy this problem usually rely upon some method of open-loop model reduction followed by LQG design or LQG design followed by closed-loop controller reduction (see, e.g., [74-83]). Most of these techniques are ad hoc in nature, however, and hence guarantees of optimality and stability are lacking.

A more direct approach that avoids both model and controller reduction is to fix the controller structure and optimize the performance criterion with respect to the controller parameters. This is the optimal projection formulation. As noted above, the new forms of optimality conditions discovered in [6] harbor the definition of an oblique projection (i.e., idempotent matrix) which is a consequence of optimality and not the result of an ad hoc assumption. By exploiting the presence of this "optimal projection," the originally very complex stationary conditions can be transformed without loss of generality into much simpler and more tractable forms. The resulting equations (see (2.10)-(2.17) of [22]) preserve the simple form of LQG relations for the gains in terms of covariance and cost matrices which, in turn, are determined by a coupled system of two modified Riccati equations and two modified Lyapunov equations. This coupling, by means of the optimal projection, represents a graphic portrayal of the demise of the classical separation principle for the reduced-order controller case. When, as a special case, the order of the compensator is required to be equal to the order of the plant, the modified Riccati equations immediately reduce to the standard LQG Riccati equations and the modified Lyapunov equations express the proviso that the compensator be minimal, i.e., controllable and observable. Since the LQG Riccati equations as such are nothing more than the necessary conditions for full-order compensation, the "optimal projection equations" appear to provide a clear and simple generalization of standard LQG theory.

On the other hand (see the left branch of Figure 9), the approach taken by the mathematical community accepts the distributed parameter model, extends LQG results to obtain a controller of similarly infinite dimensional nature and then resorts to discretization and truncation to achieve a suitably low-order (and finite dimensional) controller for implementation. However, the finite-dimensional approximation schemes that have been applied to optimal infinite-dimensional control laws [84-87] only guarantee optimality in the limit, i.e., as the order of the approximating controller increases without bound. Hence, there is no guarantee that a particular approximate (i.e., discretized) controller is actually optimal over the class of approximate controllers of a given order which may be dictated by implementation constraints. Moreover, even if an optimal approximate finite-dimensional controller could be obtained, it would almost certainly be suboptimal in the class of all controllers of the given order.

It should be mentioned that notable exceptions to the above-mentioned work on distributed parameter controllers are the contributions of Johnson [88] and Pearson [89,90] who suggest fixing the order of the finite-dimensional compensator while retaining the distributed parameter model. Progress in this direction, however, was impeded not only by the intractability of the optimality conditions that were available for the finite-dimensional problem, but also by the lack of a suitable generalization of these conditions to the infinite-dimensional case. Recent results [18,21,23] made significant progress in filling these gaps by deriving explicit optimality conditions which directly characterize the optimal finite-dimensional fixed-order dynamic compensator for an infinite-dimensional system and which are exactly analogous to the highly simplified optimal projection equations obtained in [6,12,14,16,22] for the finite-dimensional case. Specifically, instead of a system of four matrix equations we obtain a system of four operator equations whose solutions characterize the optimal finite-dimensional fixed-order dynamic compensator. Moreover, the optimal projection now becomes a bounded idempotent Hilbert-space operator whose rank is precisely equal to the order of the compensator.

As Figure 9 suggests, this represents the most direct approach yet taken to designing low-order controllers for infinite-dimensional systems. Computational techniques for solution of the operator equations remain the object of research, but success in the finite-dimensional case leads to confidence that existing solution techniques can be appropriately generalized.

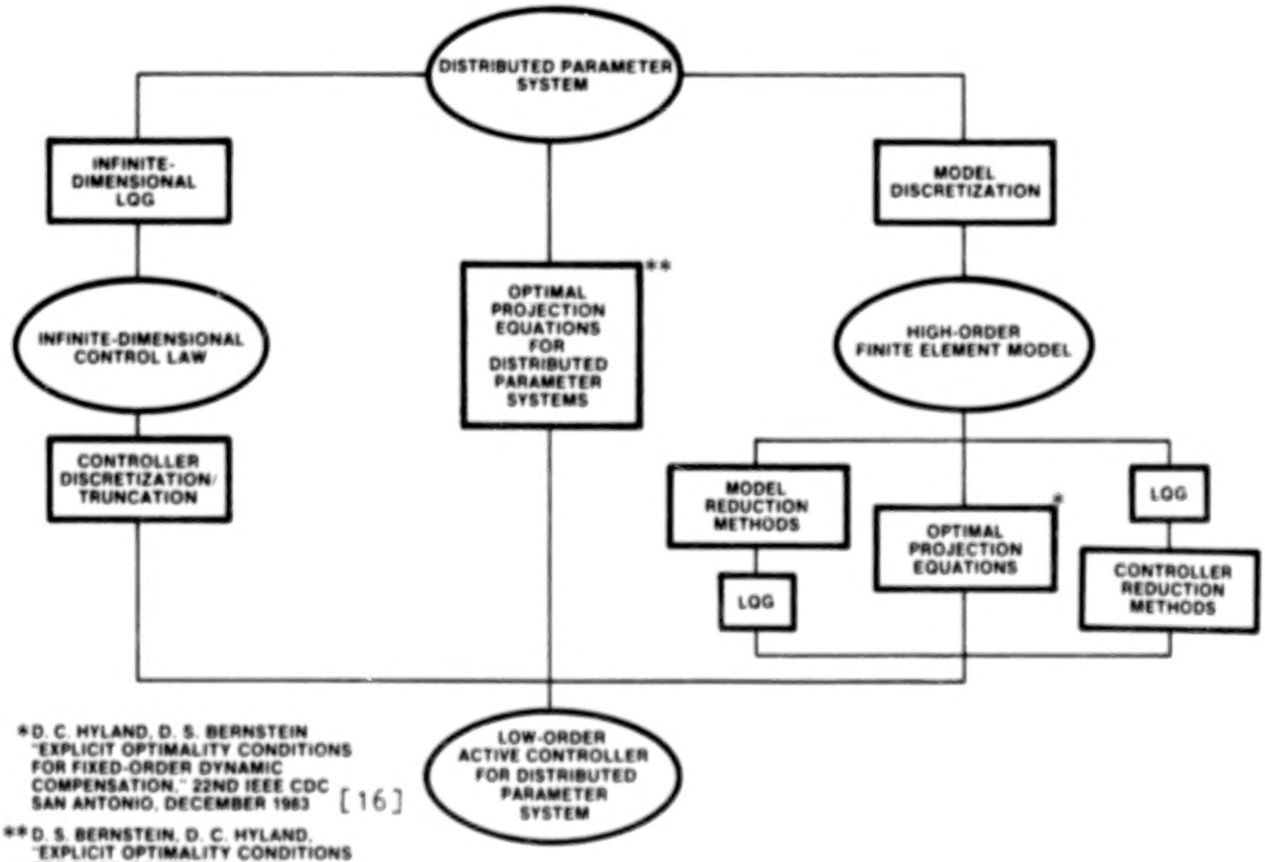
DISTRIBUTED PARAMETER SYSTEM
INFINITE-DIMENSIONAL LQG
MODEL DISCRETIZATION
OPTIMAL PROJECTION EQUATIONS FOR DISTRIBUTED PARAMETER SYSTEMS
**
INFINITE-DIMENSIONAL CONTROL LAW
HIGH-ORDER FINITE ELEMENT MODEL
CONTROLLER DISCRETIZATION/TRUNCATION
MODEL REDUCTION METHODS
OPTIMAL PROJECTION EQUATIONS
*
LQG
LQG
CONTROLLER REDUCTION METHODS
LOW-ORDER ACTIVE CONTROLLER FOR DISTRIBUTED PARAMETER SYSTEM

*D. C. HYLAND, D. S. BERNSTEIN "EXPLICIT OPTIMALITY CONDITIONS FOR FIXED-ORDER DYNAMIC COMPENSATION," 22ND IEEE CDC SAN ANTONIO, DECEMBER 1983 [16]

**D. S. BERNSTEIN, D. C. HYLAND, "EXPLICIT OPTIMALITY CONDITIONS FOR FIXED-ORDER DYNAMIC COMPENSATION OF INFINITE-DIMENSIONAL SYSTEMS" 1983 SIAM FALL MEETING, NORFOLK, VA. NOVEMBER 1983 [23]

Figure 9

STEADY STATE REDUCED-ORDER DYNAMIC COMPENSATION PROBLEM WITH PARAMETER UNCERTAINTIES

Now we explicitly present the combined OP/ME design equations. First, Figure 10 gives the problem statement. The high-order, uncertain plant has state $X \in \mathbb{R}^N$ where N is finite. As indicated using previous notation, uncertainties in the dynamics matrix, A, the control input matrix, B, and the sensor output matrix, C, are all modelled via the maximum entropy approach. Furthermore, the general formulation allows cross-correlation between the disturbance noise, w_1, and the observation noise, w_2.

The object is to design a lower order dynamic controller with state $X_c \in \mathbb{R}^{N_c}$ where $N_c < N$ by choosing the controller matrices A_c, B_c and C_c so as to minimize the indicated quadratic performance criterion. Note that the possibility of cross terms ($R_{12} \neq 0$) in the performance index is accounted for in this formulation.

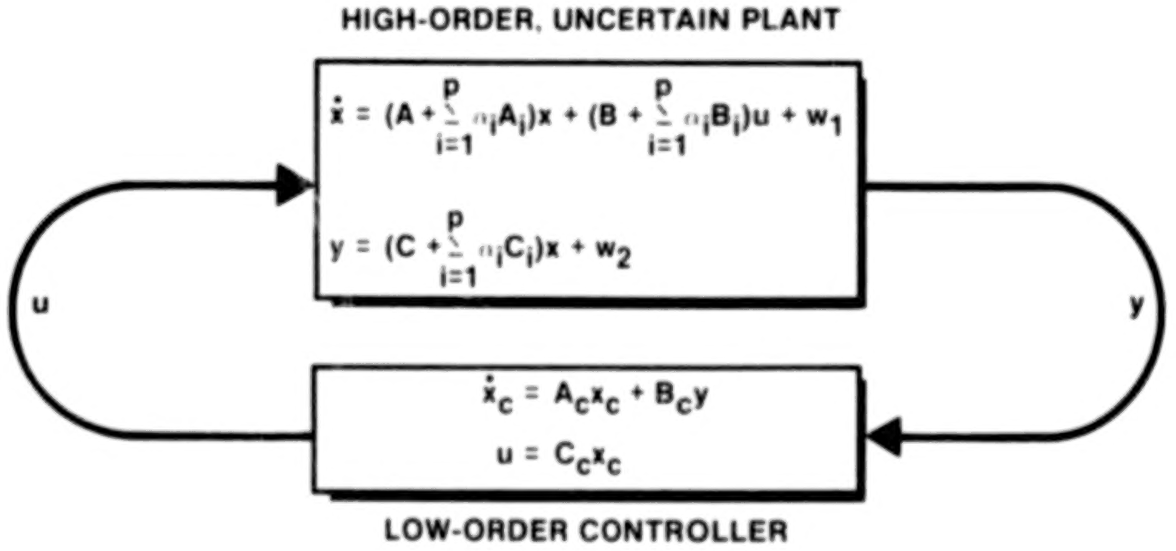
HIGH-ORDER, UNCERTAIN PLANT
$\dot{x} = (A + \sum_{i=1}^{p} \alpha_i A_i)x + (B + \sum_{i=1}^{p} \alpha_i B_i)u + w_1$
$y = (C + \sum_{i=1}^{p} \alpha_i C_i)x + w_2$
u
y
$\dot{x}_c = A_c x_c + B_c y$
$u = C_c x_c$
LOW-ORDER CONTROLLER

PERFORMANCE CRITERION

$$J(A_c, B_c, C_c) = \lim_{t \to \infty} E[x^T R_1 x + 2x^T R_{12} u + u^T R_2 u]$$

Technical Assumption: $B_i \neq 0 \Rightarrow C_i = 0$

Figure 10

MAIN THEOREM OF OP/ME: OPTIMAL COMPENSATOR GAINS

With the foregoing problem statement, the quadratically optimal gains are given by the first three expressions in Figure 11. These relationships are basically LQG in character - the major modification being brought about by the appearance of the matrices $\Gamma \epsilon \mathbb{R}^{N_c \times N}$ and $G \epsilon \mathbb{R}^{N_c \times N}$. A particular factorization of the optimal projection τ, i.e., $\Gamma G^T = I_{N_c}$, is represented by Γ and G so that $\tau = G^T \Gamma$ is idempotent. Note that any rank N_c projection can be factored in this way and, for given τ, any and all such factorizations yield the same closed-loop performance (see [22]).

Determination of A_c, B_c and C_c requires that we first solve the basic design equations (shown in Figure 12) for the quantities Q, P, and $\hat{Q}$, $\hat{P}$ and τ. The notational conventions given on the lower half of Figure 11 serve to define these design equations precisely.

CONTROLLER GAINS (Functions of Q, P, $\hat{Q}$, $\hat{P}$)

$$A_c = \Gamma(A_s - B_s R_{2s}^{-1} \mathcal{P}_s - \mathcal{Q}_s V_{2s}^{-1} C_s) G^T$$

$$B_c = \Gamma \mathcal{Q}_s V_{2s}^{-1}$$

$$C_c = -R_{2s}^{-1} \mathcal{P}_s G^T$$

NOTATION

$$\hat{Q}\hat{P} = G^T M \Gamma, \quad \Gamma G^T = I_{n_c} \; (\Rightarrow \tau = G^T \Gamma = \tau^2)$$

$$\mathcal{A} Q \mathcal{A}^T = \sum_{i=1}^{p} A_i Q A_i^T, \quad \mathcal{A} Q \mathcal{B} = \sum_{i=1}^{p} A_i Q B_i, \text{ etc.}$$

$$A_s = A + \frac{1}{2}\mathcal{A}^2 \qquad B_s = B + \frac{1}{2}\mathcal{A}\mathcal{B} \qquad C_s = C + \frac{1}{2}\mathcal{C}\mathcal{A}$$

$$R_{2s} = R_2 + \mathcal{B}^T(P+\hat{P})\mathcal{B} \qquad V_{2s} = V_2 + \mathcal{C}(Q+\hat{Q})\mathcal{C}^T$$

$$\mathcal{Q}_s = QC_s^T + V_{12} + \mathcal{A}(Q+\hat{Q})\mathcal{C}^T \qquad \mathcal{P}_s = B_s^T P + R_{12}^T + \mathcal{B}^T(P+\hat{P})\mathcal{A}$$

Figure 11

OPTIMAL PROJECTION/MAXIMUM ENTROPY DESIGN EQUATIONS

Finally, Figure 12 shows the fundamental OP/ME design equations for determination of P, Q, $\hat{P}$, $\hat{Q}$ and τ. The nonnegative-definite matrices P and Q are analogous to the regulator and observer cost matrices of LQG and are determined by two modified Riccati equations. The two modified Lyapunov equations satisfied by matrices $\hat{Q}$ and $\hat{P}$ are analogous to the Lyapunov equations determining controllability and observability Grammians that are employed by many of the current, suboptimal, controller-order reduction schemes. Note that the optimal projection, τ, is given explicitly in terms of the group generalized inverse of the product $\hat{Q}\hat{P}$. Thus, the nonnegative-definite matrices $\hat{Q}$ and $\hat{P}$ largely serve to determine τ.

In contrast to LQG, all four equations are coupled both by the optimal projection and by the stochastic modification terms - indicating that the classical separation principle generally breaks down under restrictions on controller dimension and/or under the impact of parameter uncertainties.

The four equations in Figure 12 summarize a generalized LQG-type approach wherein robust controllers of low dimension follow as a direct consequence of the optimality criterion and *a priori* uncertainty levels. Moreover, the computational task is well-defined: solve a system of two Riccati and two Lyapunov equations coupled by the optimal projection and stochastic effects. A variety of computational procedures are presented in [1, 4, 14-15, 17, 19] and these are currently included in an automated design software package. We illustrate this automated design capability in the example problems that follow.

SOLVE FOR NONNEGATIVE-DEFINITE Q, P, $\hat{Q}$, $\hat{P}$

$$0 = A_sQ + QA_s^T + \;Q\;^T + V_1 + (\;R_{2s}^{-1}\;_s)\hat{Q}(\;R_{2s}^{-1}\;_s)^T - \;_sV_{2s}^{-1}\;_s^T + \;_sV_{2s}^{-1}\;_s^T\;^T$$

$$0 = A_s^TP + PA_s + \;^TP\; + R_1 + (\;_sV_{2s}^{-1}\;)^T\hat{P}(\;_sV_{2s}^{-1}\;) - \;_s^TR_{2s}^{-1}\;_s + \;^T\;_s^TR_{2s}^{-1}\;_s\;$$

$$0 = (A_s - B_sR_{2s}^{-1}\;_s)\hat{Q} + \hat{Q}(A_s - B_sR_{2s}^{-1}\;_s)^T + \;_sV_{2s}^{-1}\;_s^T - \;_sV_{2s}^{-1}\;_s^T\;^T$$

$$0 = (A_s - \;_sV_{2s}^{-1}C_s)^T\hat{P} + \hat{P}(A_s - \;_sV_{2s}^{-1}C_s) + \;_s^TR_{2s}^{-1}\;_s - \;^T\;_s^TR_{2s}^{-1}\;_s\;$$

$$\text{RANK } \hat{Q} = \text{RANK } \hat{P} = \text{RANK } \hat{Q}\hat{P} = n_c$$

$$\tau = \hat{Q}\hat{P}(\hat{Q}\hat{P})^{\#} \qquad \tau_\perp = I_n - \tau$$

# GROUP GENERALIZED INVERSE

Figure 12

EXAMPLE 1: CSDL MODEL #2

The first two examples considered here illustrate application of the optimal projection approach without inclusion of parameter uncertainty effects. The third and final example serves to illustrate the combined OP/ME design capability.

The first case was treated in [17] and is depicted in Figure 13. Specifically, it is a version of the CSDL, ACOSS Model 2 previously considered in [91]. The steady state performance index has the form

$$J = E\left[X^TR_1X\right] + RE\left[U^TU\right]$$

where R_1 represents the state penalties on mean square line-of-sight errors and defocus and R is a positive scalar. Clearly, controller authority and bandwidth are both inversely proportional to R.

This example was used to compare both theoretically and numerically the optimal projection approach with a variety of suboptimal controller-order reduction methods. The theoretical comparison shows that all current suboptimal techniques essentially define a (suboptimal) projection characterizing the reduced-order compensator. In contrast, the optimal projection design equations define the needed projection by rigorous application of optimality principles. Moreover, all the approaches considered in [7] can be displayed in a common notation, and this graphically reveals the suboptimal design equations as special cases of or approximations to the optimal projection equations.

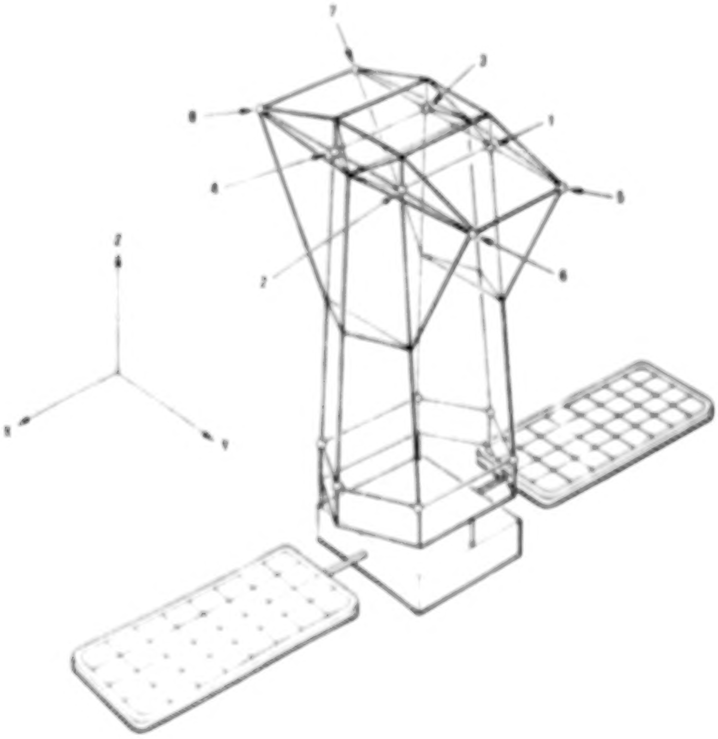

REFERENCE [91]

R. E. Skelton and P. C. Hughes, "Modal Cost Analysis for Linear Matrix Second Order Systems," J. Dyn. Syst. Meas. and Control, Vol. 102, September 1980, pp. 151-180.

Figure 13

NUMERICAL COMPARISON OF SUBOPTIMAL AND OPTIMAL PROJECTION APPROACHES

Now for the numerical comparisons. As is standard in the application of quadratic optimization, one characterizes each design for a fixed compensator order by plotting the "regulation cost" ($E[X^TR_1X]$) as a function of the "control cost" ($E[U^TU]$). Results for these tradeoff curves are shown in Figure 14. The very bottom-most curve represents the full-order, LQG design. Since this is the best obtainable when there is no restriction on compensator order, the problem is obtaining a lower order design whose tradeoff curve is as close to the LQG results as possible.

The thin black lines in Figure 14 show the N_c = 10, 6, and 4 designs obtained via Component Cost Analysis [83], where N_c denotes the compensator dimension. This appears to be the most successful suboptimal method applied to the example problem considered here. Note that the 10th and 6th order compensator designs are quite good, but when compensator order is sufficiently low (N_c = 4) and controller bandwidth sufficiently large (R<5.0), the method fails to yield stable designs. This difficulty is characteristic of all suboptimal techniques surveyed, and, in fairness, it should be noted that most other suboptimal design methods fail to give stable designs for compensator orders below 10.

In contrast, the width of the grey line in Figure 14 encompasses all the optimal projection results for compensators of orders 10, 6, and 4.

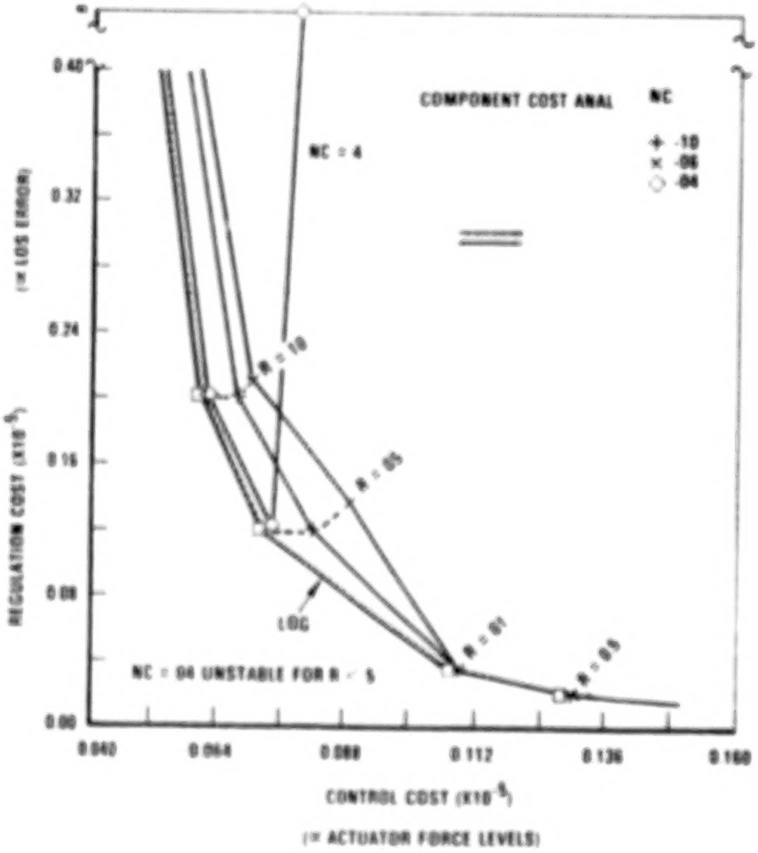

Figure 14

OPTIMAL PROJECTION RESULTS FOR PERFORMANCE/COMPLEXITY TRADEOFF

To provide a more detailed picture of the optimal projection results, Figure 15 shows the percent of total performance increase relative to the full-order, LQG designs as a function of 1/R (proportional to controller bandwidth and to actuator force levels) for the various compensator orders considered.

Even for the 4th order design, the optimal projection performance is only ~5 percent higher than the optimal full-order design. Furthermore, the performance index for the optimal projection designs increases monotonically with decreasing controller order - as it should. Such is not the case for suboptimal design methods.

These results reinforce our belief that the optimal projection approach is a powerful and highly reliable alternative to current reduced-order control design methods.

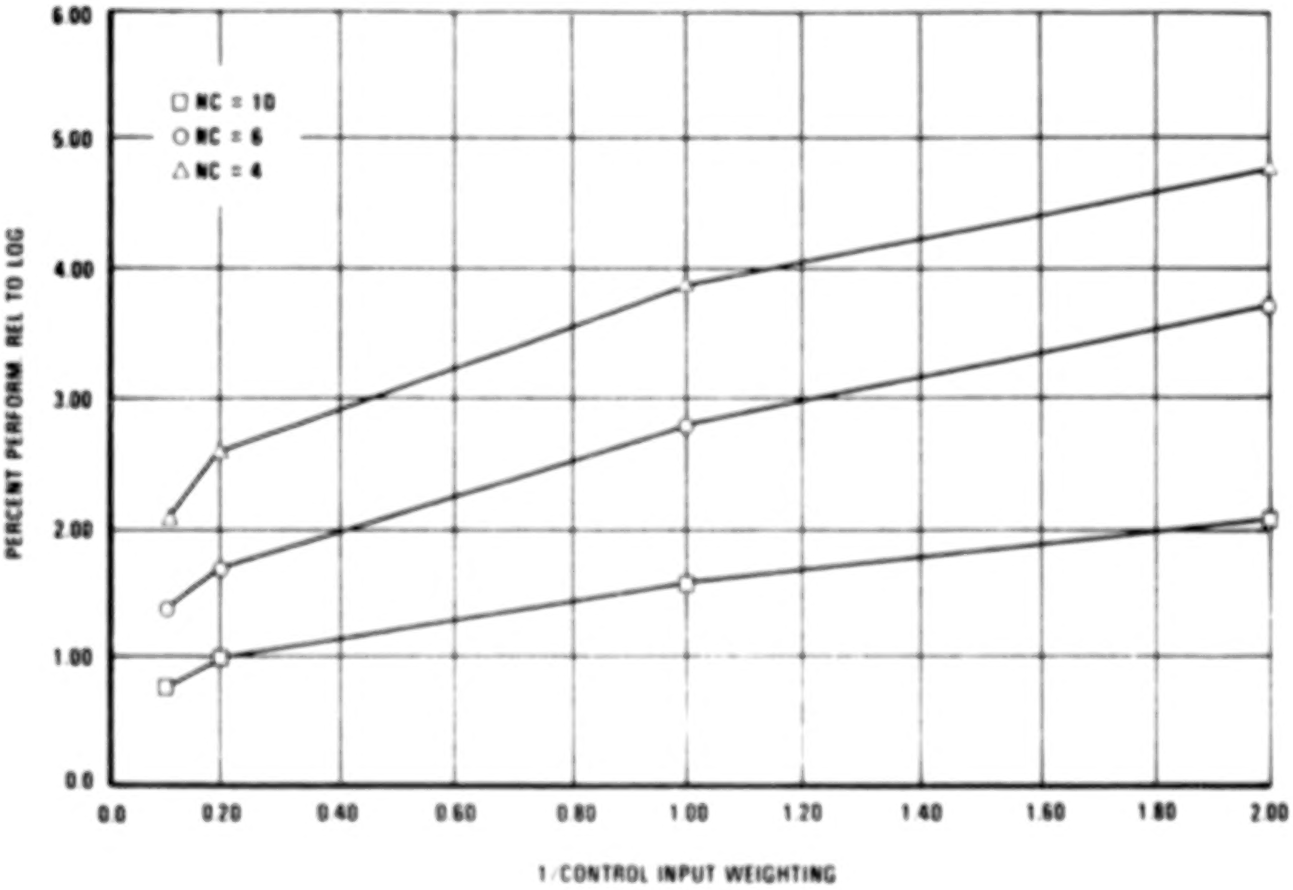

Figure 15

EXAMPLE 2: 15-M HOOP/COLUMN ANTENNA CONTROLS/DYNAMICS EXPERIMENT CONCEPT

The second example of the application of optimal projection involves significant interplay among controller design, experiment design, and control hardware selection.

To further the technology development goals of the planned Large Space Antenna Flight Experiment, Harris GASD has undertaken a preliminary study for design of a ground-based controls and dynamics experiment involving the 15-M Hoop/Column Antenna. This structure is a deployable mesh reflector design for space communications applications.

In designing the experimental apparatus, it was our goal to establish performance requirements, disturbance spectra, etc., to emulate (not simulate a flight test) the generic pathologies of large space systems. Care was also taken in selecting control hardware and software in such a way as to provide a good test-bed for a variety of system identification and control design approaches.

The basic experimental configuration motivated by the above considerations is depicted in Figure 16. As shown, the entire spacecraft is suspended by a cable secured to the ceiling of a radome. The point of attachment to the structure is inside the primary column segment approximately 1.5 inches above the center of mass. The resulting gravity moment arm provides some slight restoring stiffness and prevents the cable from resting against the column. Absence of an RF feed (replaced by equivalent weights) permits the suspending cable to run clear through the aperture of the upper column segment, thereby permitting approximately 5° of rotational motion along both horizontal axes.

Steady-state random disturbances are to be supplied by two-axis torquers located within the spacecraft bus. The selected location provides significant disturbability to the first hundred modes and a high degree of disturbance to ~50 modes.

15-METER H/C MODEL CABLE SUSPENDED CONFIGURATION FOR GROUND TESTING

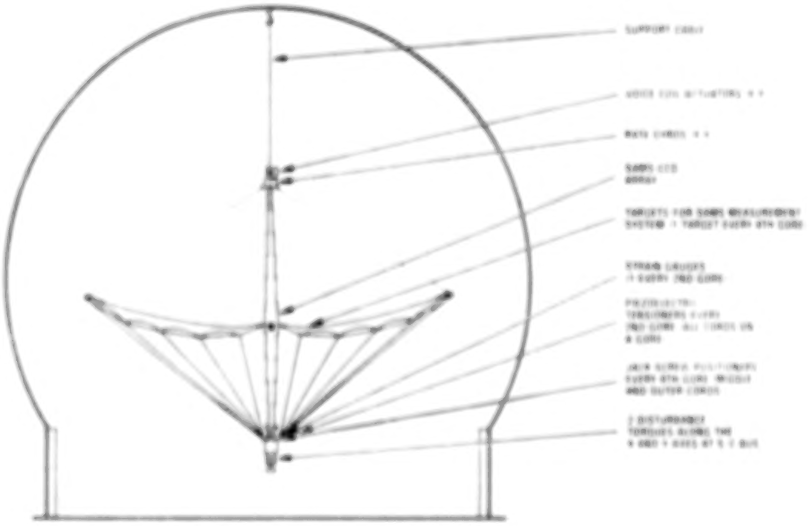
SUPPORT CABLE
VOICE COIL ACTUATORS X Y
RATE GYROS X Y
SAMS CCD ARRAY
TARGETS FOR SAMS MEASUREMENT SYSTEM (1 TARGET EVERY 8TH CORD)
STRAIN GAUGES (1 EVERY 2ND CORD)
PIEZOELECTRIC TENSIONERS EVERY 2ND CORD
JACK SCREW POSITIONERS EVERY 8TH CORD (MIDDLE AND OUTER CORDS)
2 DISTURBANCE TORQUES ALONG THE X AND Y AXES AT S/C BUS

Figure 16

DISTRIBUTION OF MODAL FREQUENCIES FOR 15M CONTROLS/DYNAMICS EXPERIMENT CONCEPT

Detailed finite element analyses of this cable-suspended configuration have been carried out, and the overall distribution of modal frequencies can be summarized as in Figure 17. The figure shows the "mode-count" versus frequency; i.e., $N(\omega)$ denotes the number of modes below a given frequency, ω. As indicated, there is a collection of "quasi-rigid-body" nodes at low frequencies. Each of these modes involves a compound pendulum motion on the cable with the spacecraft undergoing essentially rigid-body rotations and translations. The quasi-rigid-body modes provide a rather accurate simulation of rigid body degrees of freedom. At ~7.5 Hz and above, there emerge the overall beam bending or "spacecraft" modes involving bending of the supporting hoop and central column. Finally, the rapid increase in mode count above ~11 Hz is accounted for by the very closely spaced "antenna surface" modes - involving motion primarily of the mesh surface and its underlying tensioning and control cords.

$N(\omega) \triangleq$ NUMBER OF MODAL FREQUENCIES BELOW ω

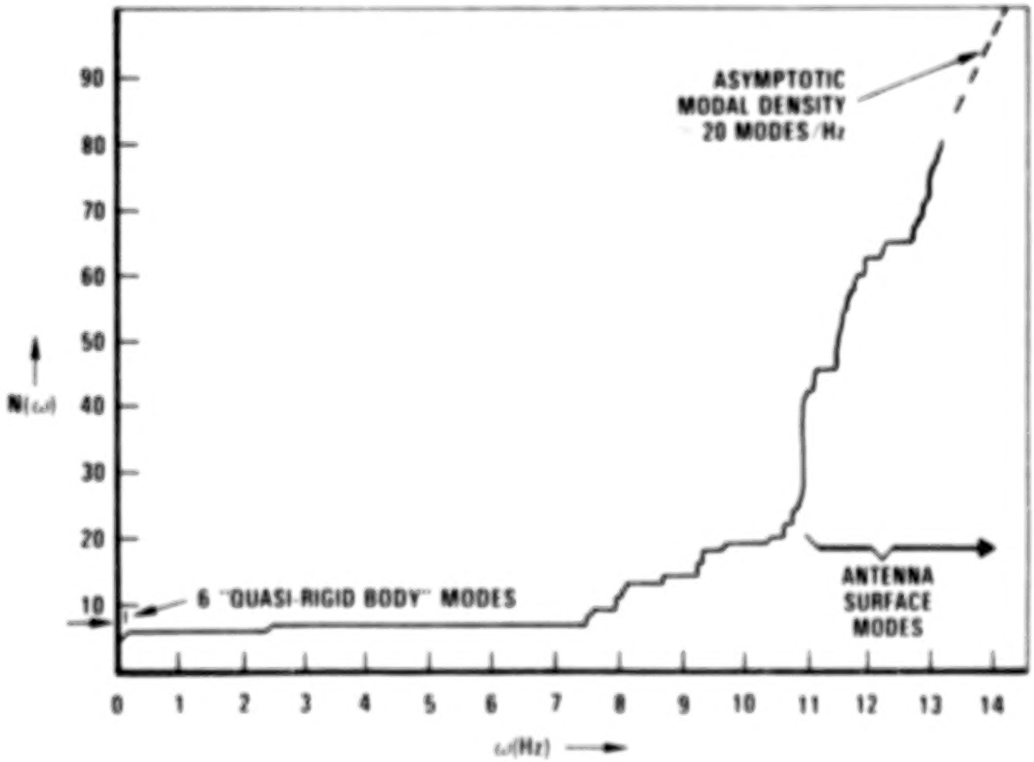

15-M MODEL GROUND TEST CONFIGURATION
MODE-COUNT VERSUS FREQUENCY

Figure 17

15-M EXPERIMENT - INSTRUMENTATION CONCEPT AND DESIGN RESULTS

Because there is a wide dispersion of disturbability for the selected disturbance source, it is possible to deliberately shape the disturbance spectrum to provide significant excitation of a desired number of modes. The selected spectrum is broad band with a half-power band limit of 15 Hz. As is evident from Figure 17, the 15 Hz bandwidth easily covers more than 100 modes.

Of course, significant disturbance on a large number of modes does not alone suffice to create a challenging control problem - selection and scaling of performance criteria are also necessary tasks in the experiment design. Refs. [92, 93] give details on the selected quadratic performance index. Basically, the state penalty consists of three main terms which impose performance penalties on (1) pointing errors, (2) misalignment and defocus errors, and (3) antenna surface shape errors.

With the control objectives thus defined, the control design and actuator/sensor selection methodologies were exercised iteratively to obtain a set of applicable, low-cost devices. The resulting instrumentation plan is depicted in Figure 18 a and detailed in [93].

Design results including dynamics models for the full complement of control hardware devices indicated in Figure 18 a are reported in [93]. For simplicity, we consider results on a subproblem involving only elastic mode vibration control using four jackscrew positioner devices and four strain gauges mounted on the control cords.

Despite a large number of modes included in the design model, optimal projection designs were successfully obtained and the effect of decreasing the control input penalty (progressively increasing the control authority) on closed-loop system poles is indicated in Figure 18 b. It is seen that while high order modes remain stable, significant increases in damping can be achieved for lower order modes within the limitations (force/bandwidth) of the actuators and sensors.

ORIGINAL PAGE IS
OF POOR QUALITY

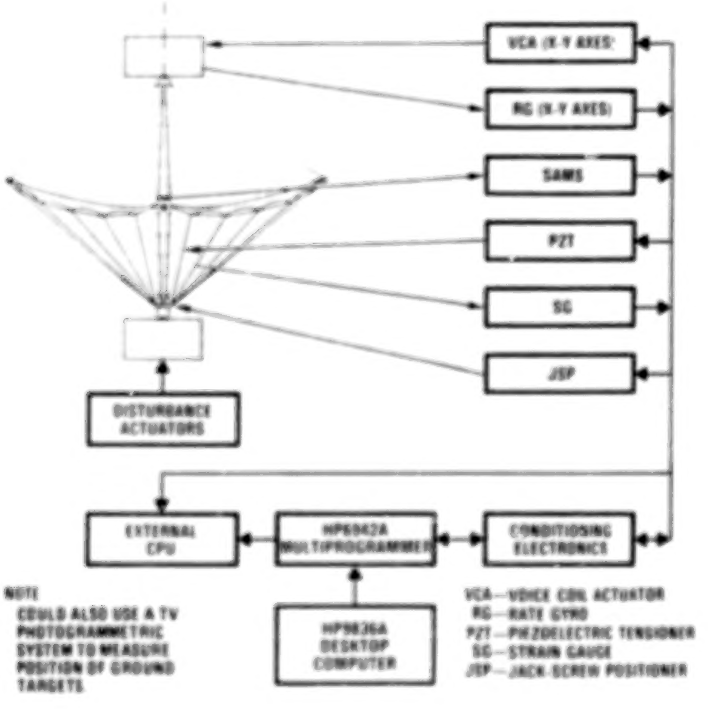

OVERALL EXPERIMENT HARDWARE CONCEPT

VCA (X-Y AXES)
RG (X-Y AXES)
SAMS
PZT
SG
JSP
DISTURBANCE ACTUATORS
EXTERNAL CPU
HP6942A MULTIPROGRAMMER
CONDITIONING ELECTRONICS
HP9836A DESKTOP COMPUTER
NOTE
COULD ALSO USE A TV PHOTOGRAMMETRIC SYSTEM TO MEASURE POSITION OF GROUND TARGETS
VCA—VOICE COIL ACTUATOR
RG—RATE GYRO
PZT—PIEZOELECTRIC TENSIONER
SG—STRAIN GAUGE
JSP—JACK-SCREW POSITIONER

Figure 18 a

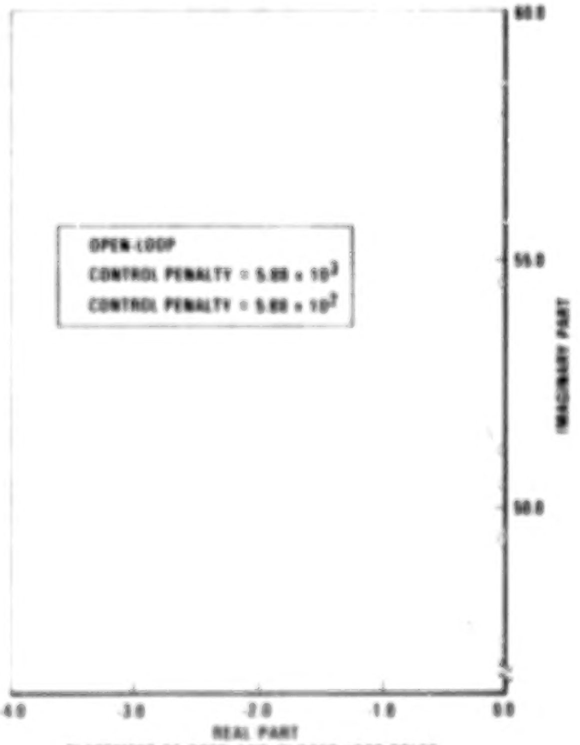

Figure 18 b

15-M EXPERIMENT: PERFORMANCE/COMPLEXITY TRADEOFF RESULTS

For the problem considered above, Figure 19 summarizes the tradeoffs of performance versus controller complexity (compensator dimension) and control authority (control input weighting in the performance index). Generally, it is seen that compensators of dimension > 10 yield negligible improvement in performance. This conclusion holds for the general problem including all hardware devices and rigid body modes. Thus, memory and throughput requirements for the processor needed to implement the control algorithm were sized on the assumption that $N_c \leq 10$. These estimates were then used to arrive at the processor selection indicated in Figure 18.a. Specifically, the control algorithm would be implemented on the HP 9836A Desktop Computer. This is a Motorola MC68000 microprocessor-based (16-bit) machine. Also, the HP-6942A Multiprogrammer can be utilized to perform all a/d and d/a conversions as well as data handling. An external CPU is included to assist in data handling and route data to off-line storage. After completion of a given experimental sequence, stored data can be analyzed, parameter identification tests can be performed and results can be correlated with analytical predictions.

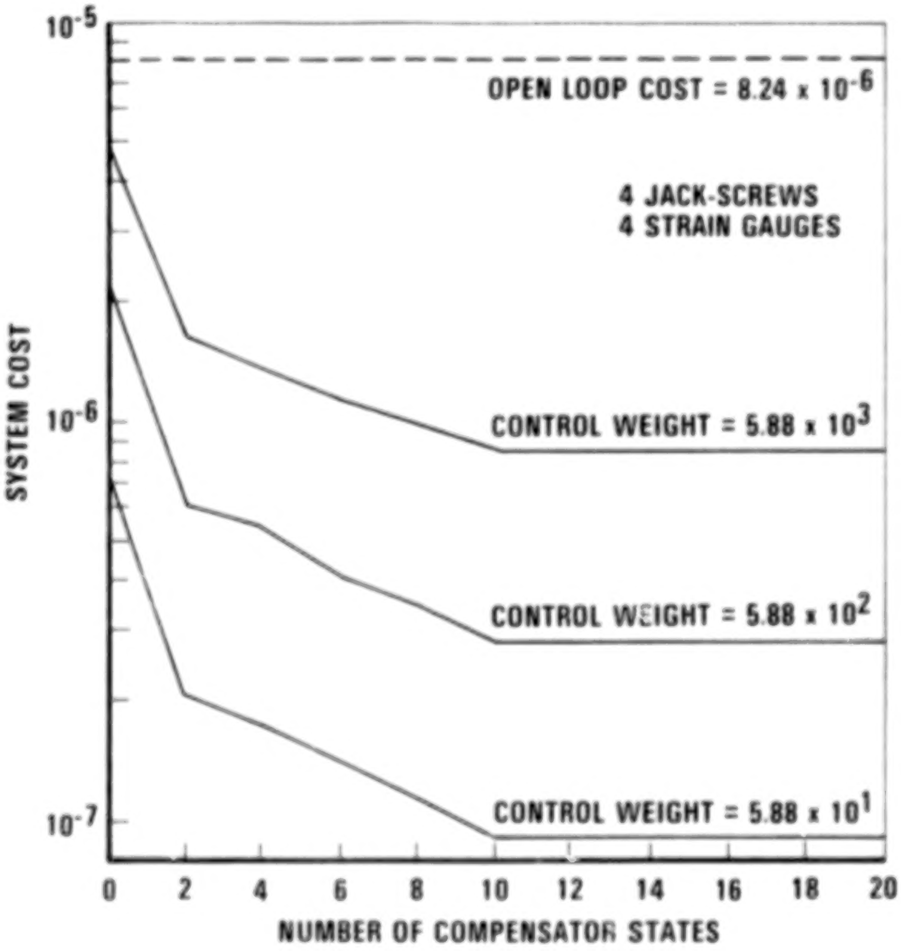

Figure 19

EXAMPLE 3: SPACECRAFT CONTROL LABORATORY EXPERIMENT (SCOLE)

Our third and last example is used primarily to illustrate application of the maximum entropy design-for-uncertainty approach. Harris GASD has just completed a NASA LaRC supported study on the Spacecraft Control Laboratory Experiment (SCOLE) configuration shown in Figure 20. This is the subject of the NASA/IEEE Design Challenge described in [94]. Since the study is specifically aimed at exploring the maximum entropy approach, its scope is restricted in other areas. Specifically, we consider the steady state pointing problem using linear, continuous-time models of all subsystems.

A high order finite element model was constructed for SCOLE, treating the Shuttle and reflectors as rigid bodies and the connecting mast as a classical beam with torsional stiffness. This model includes the Shuttle products-of-inertia and the offset between reflector center-of-mass and its attachment point on the mast. The quadratic performance penalty on the system state is simply the total mean square line of sight error (as defined in [94]). Full details of our model and design results are given in [95].

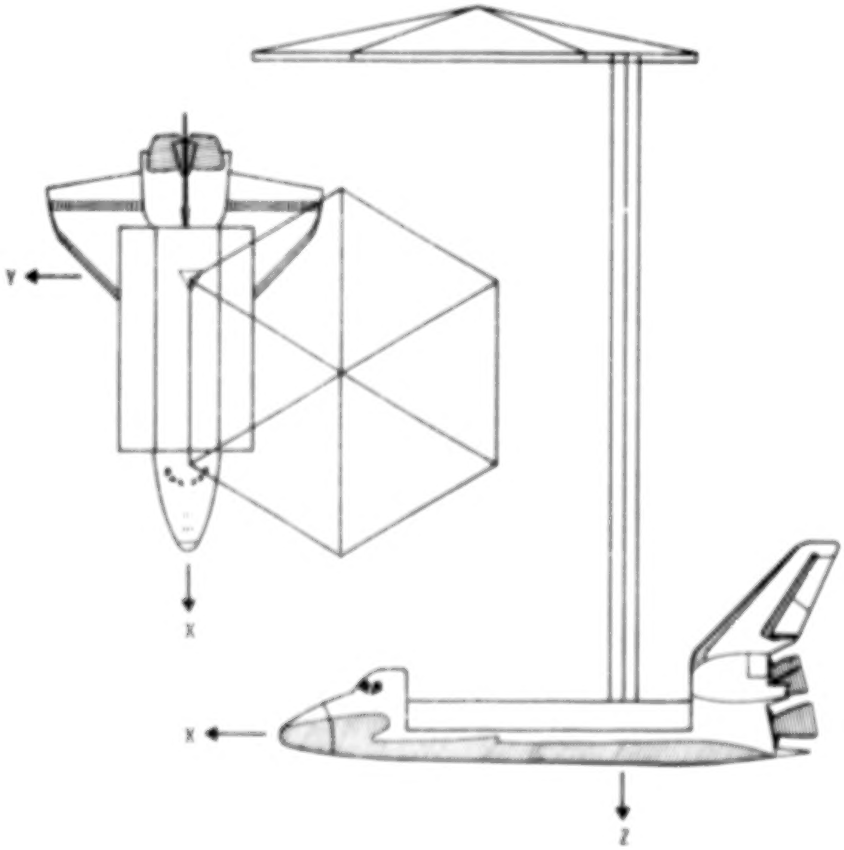

Figure 20

COMPARISON OF CLOSED-LOOP POLE SENSITIVITY FOR LQG AND MAXIMUM ENTROPY DESIGNS

As part of the SCOLE study, we considered a system model including the first eight modes and (1) performed LQG studies to select the control authority and establish a baseline and (2) designed full-order (16 state) compensators with a maximum entropy model of modal frequency uncertainties. The maximum entropy model assumed that all elastic mode frequencies were subjected to independent variations (due to modelling error) of $+\sigma$ to $-\sigma$ relative to their nominal values. Thus the positive number σ denotes the overall fractional uncertainty.

Although robust stability is obtained under these independent and simultaneous variations, the robustness properties of specific designs are simply illustrated here by looking at the variation of performance and closed-loop poles when all modal frequencies are varied by the same fractional change from the nominal values. In other words, we interconnect a given controller design (be it LQG or maximum entropy) with a perturbed plant model wherein all modal frequencies are changed by δ x (nominal values) and evaluate the closed-loop performance and pole locations. This is repeated for a range of values of δ.

Figure 21 a shows how the pole locations for an LQG design wander under a $\pm 5\%$ variation of the modal frequencies. It is seen that two of the pole pairs are particularly sensitive and are nearly driven unstable by only this $\pm 5\%$ variation. This happens because the associated structural modes contribute little to performance and the LQG design attempts a "cheap control" (small regulator and observer gains) by placing compensator poles very close to the open-loop plant poles. For nominal values, this scheme achieves significant shifts of open-loop poles with very small gains, but it is highly sensitive to off-nominal perturbations.

Figure 21 b shows closed-loop poles for the same conditions except that a maximum entropy compensator design with $\sigma = 0.1$ (10% variation modelled) was utilized. In contrast with Figure 21 a, the maximum entropy design makes the compensator poles "stand-off" deeper in the left half plane. (This is a direct consequence of the Stratonovich correction.) Consequently, the strong and sensitive interactions noted above are entirely eliminated. The poles associated with higher-order structural modes are seen to vary only along the imaginary axis and are not destabilized.

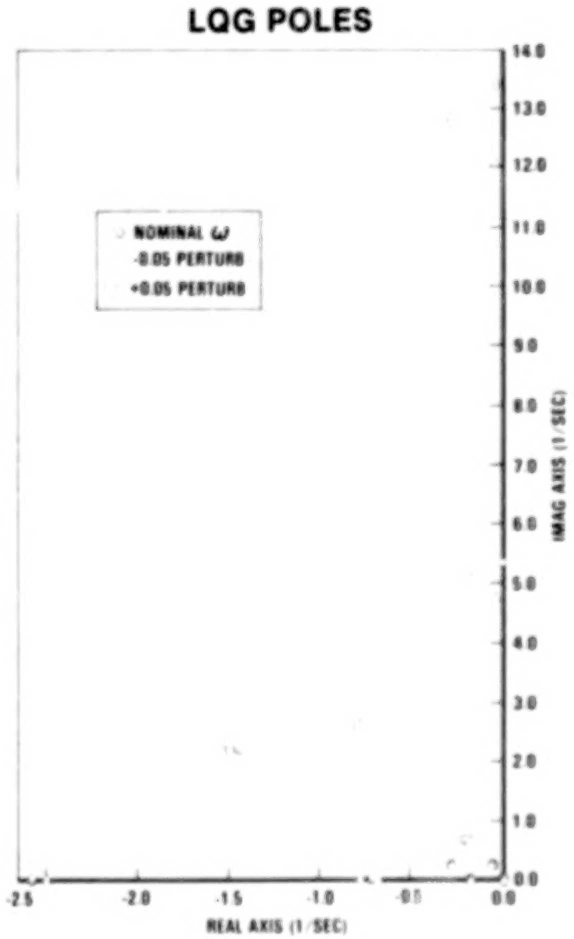

Figure 21 a

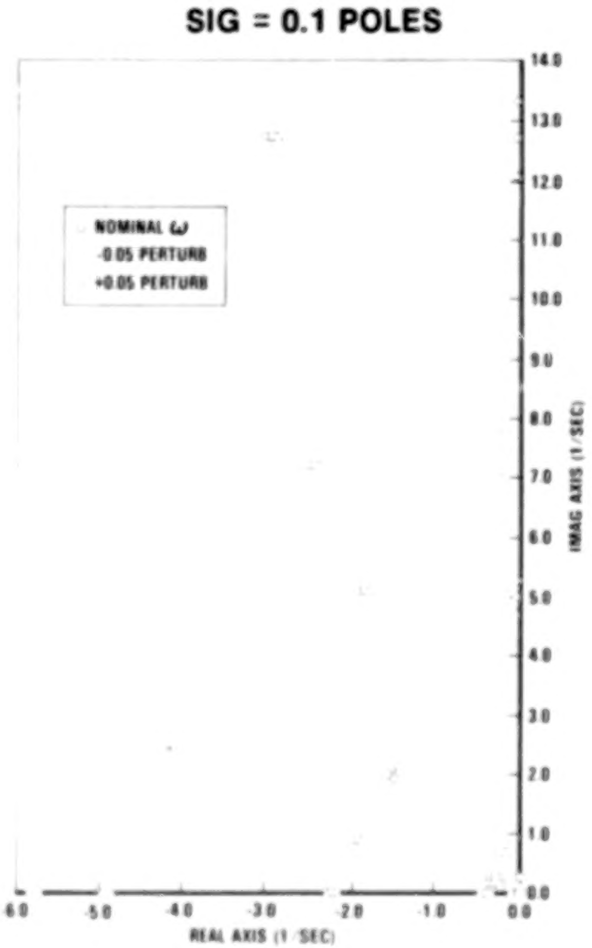

Figure 21 b

VARIATION OF PERFORMANCE WITH SYSTEM PARAMETER DEVIATIONS: DETERMINISTIC MODELLING VERSUS MAXIMUM ENTROPY DESIGN

Figure 22 illustrates how the total performance index for given controller designs varies as the structural mode frequencies are perturbed relative to their nominal values. The LQG design (which is simply a maximum entropy design for $\sigma = 0$) becomes unstable for > 7% and < -14% variations. In contrast and even with a modest 10% level of modelled uncertainty, the maximum entropy designs completely eliminate the sensitivity. Note that within the parameter range for which LQG is stable, the $\sigma = 0.1$ maximum entropy design experiences only a ~12-15% degradation. Of course, over the regions for which LQG is unstable, the maximum entropy designs are qualitatively superior.

These results serve to illustrate a general fact: By incorporating parameter uncertainty as an intrinsic facet of the basic design model, the maximum entropy formulation is able to secure high levels of robustness with little degradation of nominal performance.

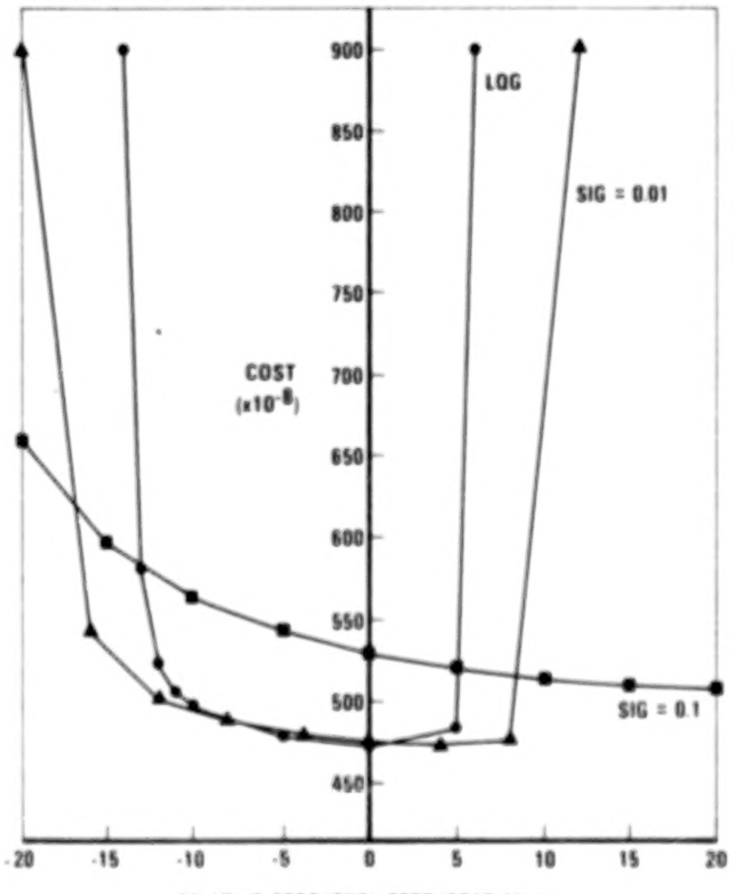

ROBUSTNESS STUDY

Figure 22

COMBINED OP/ME DESIGN: PERFORMANCE/COMPLEXITY TRADEOFF

Finally, the combined OP/ME design capability was exercised, taking the 16-state maximum entropy compensator design with $\sigma = 0.10$ frequency uncertainty level as the starting point. Reduced order compensator designs were constructed for compensators of order 14,12,10,8,6 and 5. Figure 23 shows the tradeoff between performance (total, closed-loop performance index evaluated for nominal values of modal frequencies) and controller dimension. The Figure clearly shows that performance degradation for compensator orders above 6 is negligible. The 6th order controller sacrifices only 3% of the performance of the full-order (16 state) controller. This would seem to be acceptable in view of the better than sixfold decrease in implementation costs (e.g., flops required in matrix multiplication) which results from order reduction.

In conclusion, these results, together with much additional material included in [95], demonstrate automated solution of the full OP/ME design equations (shown in Figure 12) and illustrate the performance and implementation benefits to be expected under this unified approach.

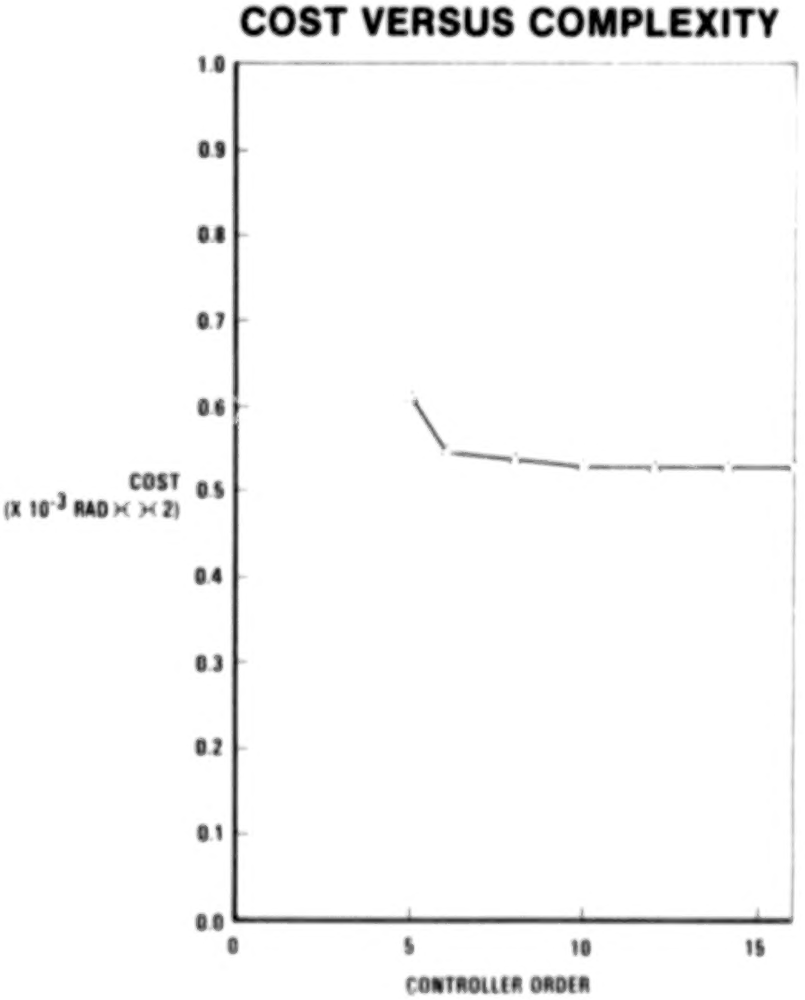

Figure 23

References

1. D. C. Hyland, "Optimal Regulation of Structural Systems With Uncertain Parameters," MIT, Lincoln Laboratory, TR-551, 2 February 1981, DDC# AD-A099111/7.

2. D. C. Hyland, "Active Control of Large Flexible Spacecraft: A New Design Approach Based on Minimum Information Modelling of Parameter Uncertainties," VPI&SU/AIAA Symposium, Blacksburg, VA, June 1981.

3. D. C. Hyland, "Optimal Regulator Design Using Minimum Information Modelling of Parameter Uncertainties: Ramifications of the New Design Approach," VPI&SU/AIAA Symposium, Blacksburg, VA, June 1981.

4. D. C. Hyland and A. N. Madiwale, "Minimum Information Approach to Regulator Design: Numerical Methods and Illustrative Results," VPI&SU/AIAA Symposium, Blacksburg, VA, June 1981.

5. D. C. Hyland and A. N. Madiwale, "A Stochastic Design Approach for Full-Order Compensation of Structural Systems with Uncertain Parameters," AIAA Guidance and Control Conference, Albuquerque, NM, August 1981.

6. D. C. Hyland, "Optimality Conditions for Fixed-Order Dynamic Compensation of Flexible Spacecraft with Uncertain Parameters," AIAA 20th Aerospace Sciences Meeting, Orlando, FL, January 1982.

7. D. C. Hyland, "Structural Modeling and Control Design Under Incomplete Parameter Information: The Maximum Entropy Approach," Modelling, Analysis and Optimization Issues for Large Space Structures, NASA CP-2258, 1983, pp. 73-96.

8. D. C. Hyland, "Maximum Entropy Stochastic Approach to Control Design for Uncertain Structural Systems," American Control Conference, Arlington, VA, June 1982.

9. D. C. Hyland, "Minimum Information Stochastic Modelling of Linear Systems with a Class of Parameter Uncertainties," American Control Conference, Arlington, VA, June 1982.

10. D. C. Hyland and A. N. Madiwale, "Fixed-Order Dynamic Compensation Through Optimal Projection," Proceedings of the Workshop on Applications of Distributed System Theory to the Control of Large Space Structures, JPL, Pasadena, CA, July 1982.

11. D. C. Hyland, "Minimum Information Modelling of Structural Systems with Uncertain Parameters," Proceedings of the Workshop on Applications of Distributed System Theory to the Control of Large Space Structures, JPL, Pasadena, CA, July 1982.

12. D. C. Hyland, "Mean-Square Optimal Fixed-Order Compensation - Beyond Spillover Suppression," AIAA Astrodynamics Conference, San Diego, CA, August 1982.

13. D. C. Hyland, "Robust Spacecraft Control Design in the Presence of Sensor/Actuator Placement Errors," AIAA Astrodynamics Conference, San Diego, CA, August 1982.

14. D. C. Hyland, "The Optimal Projection Approach to Fixed-Order Compensation: Numerical Methods and Illustrative Results," AIAA 21st Aerospace Sciences Meeting, Reno, NV, January 1983.

15. D. C. Hyland, "Mean-Square Optimal, Full-Order Compensation of Structural Systems with Uncertain Parameters," MIT, Lincoln Laboratory TR-626, 1 June 1983.

16. D. C. Hyland and D. S. Bernstein, "The Optimal Projection Equations for Fixed-Order Dynamic Compensation," IEEE Trans. Autom. Contr., Vol. AC-29, pp. 1034-1037, 1984.

17. D. C. Hyland, "Comparison of Various Controller-Reduction Methods: Suboptimal Versus Optimal Projection," Proc. AIAA Dynamics Specialists Conference, Palm Springs, CA, May 1984.

18. D. S. Bernstein and D. C. Hyland, "The Optimal Projection Equations for Fixed-Order Dynamic Compensation of Distributed Parameter Systems," Proc. AIAA Dynamics Specialists Conference, Palm Springs, CA, May 1984.

19. D. S. Bernstein and D. C. Hyland, "Numerical Solution of the Optimal Model Reduction Equations," AIAA Guidance and Control Conference, Seattle, WA, August 1984.

20. D. C. Hyland and D. S. Bernstein, "The Optimal Projection Approach to Model Reduction and the Relationship Between the Methods of Wilson and Moore," 23rd IEEE Conference on Decision and Control, Las Vegas, NV, December 1984.

21. D. S. Bernstein and D. C. Hyland, "The Optimal Projection Approach to Designing Optimal Finite-Dimensional Controllers for Distributed-Parameter Systems" 23rd IEEE Conference on Decision and Control, Las Vegas, NV, December 1984.

22. D. C. Hyland and D. S. Bernstein, "The Optimal Projection Equations for Fixed-Order Dynamic Compensation," IEEE Trans. Autom. Contr., Vol. AC-29, No. 11, pp. 1034-1037, 1984.

23. D. S. Bernstein and D. C. Hyland, "The Optimal Projection Equations for Finite-Dimensional Fixed-Order Dynamic Compensation of Infinite-Dimensional Systems," SIAM J. Contr. Optim., Vol. 24, pp. 122-151, 1986.

24. D. C. Hyland and D. S. Bernstein, "The Optimal Projection Equations for Model Reduction and the Relationships Among the Methods of Wilson, Skelton and Moore," IEEE Trans. Autom. Contr., Vol. AC-30, 1985.

25. D. C. Hyland and D. S. Bernstein, "The Optimal Projection Equations for Reduced-Order State Estimation," IEEE Trans. Autom. Contr., Vol. AC-30, pp. 583-585, 1985.

26. E. T. Jaynes, "New Engineering Applications of Information Theory," Proceedings of the First Symposium on Engineering Applications of Random Function Theory and Probability, J. L. Bogdanoff and F. Kozin, pp. 163-203, Wiley, New York, 1963.

27. E. T. Jaynes, "Prior Probabilities," IEEE Trans. Sys. Sci. Cybern., Vol. SSC-4, pp. 227-241, 1968.

28. E. T. Jaynes, "Where Do We Stand on Maximum Entropy," The Maximum Entropy Formalism, D. Levine and M. Tribus, eds., The MIT Press, pp. 15-118, Cambridge, MA, 1979.

29. R. D. Rosenkrandtz, ed., "E. T. Jaynes: Papers on Probability, Statistics and Statistical Physics," Reidel, Boston, 1983.

30. K. Ito, On Stochastic Differential Equations, Amer. Math. Soc., Providence, RI, 1951.

31. E. Wong and M. Zakai, "On the Relation Between Ordinary and Stochastic Differential Equations," Int. J. Engrg. Sci., Vol. 3, pp. 213-229, 1965.

32. R. L. Stratonovich, "A New Representation for Stochastic Integrals," SIAM J. Contr., Vol. 4, pp. 362-371, 1966.

33. R. L. Stratonovich, Conditional Markov Process and Their Application to the Theory of Optimal Control, Elsevier, NY, 1968.

34. A. H. Jazwinski, Stochastic Processes and Filtering Theory, Academic Press, New York, 1970.

35. E. Wong, Stochastic Processes in Information and Dynamical Systems, McGraw-Hill, New York, 1971.

36. E. J. McShane, Stochastic Calculus and Stochastic Models, Academic Press, Press, New York, 1974.

37. L. Arnold, Stochastic Differential Equations: Theory and Applications, Wiley, New York, 1974.

38. W. H. Fleming and R. W. Rishel, Deterministic and Stochastic Optimal Control, Springer-Verlag, New York, 1975.

39. H. J. Sussmann, "On the Gap Between Deterministic and Stochastic Ordinary Differential Equations," The Annals of Probability, Vol. 6, pp. 19-41, 1978.

40. W. M. Wonham, "Optimal Stationary Control of Linear Systems with State-Dependent Noise," SIAM J Contr., Vol. 5, pp. [illegible]-500, 1967.

41. M. Metivier and J. Pellaumail, Stochastic Integration, Academic Press, New York, 1980.

42. W. M. Wonham, "On a Matrix Riccati Equation of Stochastic Control," SIAM J. Contr., Vol. 6, pp. 681-697, 1968.

43. W. M. Wonham, "Random Differential Equations in Control Theory," in Probabilistic Analysis in Applied Mathematics, A. T. Bharucha-Reid, ed., Vol. 2, pp. 131-212, Academic Press, New York, 1970.

44. D. Kleinman, "Optimal Stationary Control of Linear Systems with Control-Dependent Noise," IEEE Trans. Autom. Contr., Vol. AC-14, pp. 673-677, 1969.

45. P. J. McLane, "Optimal Linear Filtering for Linear Systems with State-Dependent Noise," Int. J. Contr., Vol. 10, pp. 41-51, 1969.

46. P. McLane, "Optimal Stochastic Control of Linear Systems with State- and Control-Dependent Disturbances," IEEE Trans. Autom. Contr., Vol. AC-16, pp. 793-798, 1971.

47. D. Kleinman, "Numerical Solution of the State Dependent Noise Problem," IEEE Trans. Autom. Contr., Vol. AC-21, pp. 419-420, 1976.

48. U. Haussmann, "Optimal Stationary Control with State and Control Dependent Noise," SIAM J. Contr., Vol. 9, pp. 184-198, 1971.

49. J. Bismut, "Linear-Quadratic Optimal Stochastic Control with Random Coefficients," SIAM J. Contr., Vol. 14, pp. 419-444, 1976.

50. A. Ichikawa, "Optimal Control of a Linear Stochastic Evolution Equation with State and Control Dependent Noise," Proc. IMA Conference on Recent Theoretical Development in Control, Leicester, England, Academic Press, New York, 1976.

51. A. Ichikawa, "Dynamic Programming Approach to Stochastic Evolution Equations," SIAM J. Contr. Optim., Vol 17, pp. 152-174, 1979.

52. N. U. Ahmed, "Stochastic Control on Hilbert Space for Linear Evolution Equations with Random Operator-Valued Coefficients," SIAM J. Contr. Optim., Vol. 19, pp. 401-430.

53. C. W. Merriam III, Automated Design of Control Systems, Gordon and Breach, New York, 1974.

54. M. Aoki, "Control of Linear Discrete-Time Stochastic Dynamic Systems with Multiplicative Disturbances," IEEE Trans. Autom. Contr., Vol. AC-20, pp. 388-392, 1975.

55. D. E. Gustafson and J. L. Speyer, "Design of Linear Regulators for Nonlinear Systems," J. Spacecraft and Rockets, Vol. 12, pp. 351-358, 1975.

56. D. E. Gustafson and J. L. Speyer, "Linear Minimum Variance Filters Applied to Carrier Tracking," IEEE Trans. Autom. Contr., Vol. AC-21, pp. 65-73, 1976.

57. G. N. Milshtein, "Design of Stabilizing Controller With Incomplete State Data for Linear Stochastic System with Multiplicative Noise," Autom. and Remote Contr., Vol. 43, pp. 653-659, 1982.

58. M. Athans, R. T. Ku and S. B. Gershwin, "The Uncertainty Threshold Principle: Some Fundamental Limitations of Optimal Decision Making Under Dynamic Uncertainty," IEEE Trans. Autom. Contr., Vol. AC-22, pp. 491-495, 1977.

59. R. J. Ku and M. Athans, "Further Results on the Uncertainty Threshold Principle," IEEE Trans. Autom. Contr., Vol. AC-22, pp. 866-868, 1977.

60 T. L. Johnson and M. Athans, "On the Design of Optimal Constrained Dynamic Compensators for Linear Constant Systems," IEEE Trans. Autom. Contr., Vol. AC-15, pp. 658-660, 1970.

61. W. S. Levine, T. L. Johnson and M. Athans, "Optimal Limited State Variable Feedback Controllers for Linear Systems," IEEE Trans. Autom. Contr., Vol. AC-16, pp. 785-793, 1971.

62. K. Kwakernaak and R. Sivan, Linear Optimal Control Systems, Wiley-Interscience, New York, 1972.

63. D. B. Rom and P. E. Sarachik, "The Design of Optimal Compensators for Linear Constant Systems with Inaccessible States," IEEE Trans. Autom. Contr., Vol. AC-18, pp. 509-512, 1973.

64. M. Sidar and B.-Z. Kurtaran, "Optimal Low-Order Controllers for Linear Stochastic Systems, "Int. J. Contr., Vol. 22, pp. 377-387, 1975.

65. J. M. Mendel and J. Feather, "On the Design of Optimal Time-Invariant Compensators for Linear Stochastic Time-Invariant Systems, "IEEE Trans. Autom. Contr., Vol. AC-20, pp. 653-657, 1975.

66. S. Basuthakur and C. H. Knapp, "Optimal Constant Controllers for Stochastic Linear Systems, "IEEE Trans. Autom. Contr., AC-20, pp. 664-666, 1975.

67. R. B. Asher and J. C. Durrett, "Linear Discrete Stochastic Control with a Reduced-Order Dynamic Compensator, "IEEE Trans. Autom. Contr., Vol. AC-21, pp. 626-627, 1976.

68. W. J. Naeije and O. H. Bosgra, "The Design of Dynamic Compensators for Linear Multivariable Systems," 1977 IFAC, Fredricton, NB, Canada, pp. 205-212.

69. H. R. Sirisena and S. S. Choi, "Design of Optimal Constrained Dynamic Compensators for Non-Stationary Linear Stochastic Systems, "Int. J. Contr., Vol. 25, pp. 513-524, 1977.

70. P. J. Blanvillain and T. L. Johnson, "Invariants of Optimal Minimal-Order Observer Based Compensators, "IEEE Trans. Autom. Contr., Vol. AC-23, pp. 473-474, 1978.

71. C. J. Wenk and C. H. Knapp, "Parameter Optimization in Linear Systems with Arbitrarily Constrained Controller Structure, "IEEE Trans. Autom. Contr., Vol. AC-25, pp. 496-500, 1980.

72. J. O'Reilly, "Optimal Low-Order Feedback Controllers for Linear Discrete-Time Systems," in Control and Dynamic Systems, Vol. 16, edited C. T. Leondes, ed., Academic Press, 1980.

73. D. P. Looze and N. R. Sandell, Jr., "Gradient Calculations for Linear Quadratic Fixed Control Structure Problems," IEEE Trans. Autom. Contr., Vol. AC-25, pp. 285-8, 1980.

74. M. Aoki, "Control of Large-Scale Dynamic Systems by Aggregation," IEEE Trans. Auto. Contr., Vol. AC-13, pp. 246-253, 1968.

75. R. E. Skelton, "Cost Deconposition of Linear Systems with Application to Model Reduction," Int. J. Contr., Vol. 32, pp. 1031-1055, 1980.

76. B. C. Moore, "Principal Component Analysis in Linear Systems: Controllability, Observability, and Model Reduction," IEEE Trans. Autom. Contr., Vol. AC-26, pp. 17-32, 1981.

77. L. Pernebo and L. M. Silverman, "Model Reduction via Balanced State Space Representations," IEEE Trans. Autom. Contr., Vol. AC-27, pp. 382-387, 1982.

78. K. V. Fernando and H. Nicholson, "On the Structure of Balanced and Other Principal Representations of SISO Systems," IEEE Trans. Autom. Contr., Vol. AC-28, pp. 228-231, 1983.

79. S. Shokoohi, L. M. Silverman, and P. M. Van Dooren, "Linear Time-Variable Systems: Balancing and Model Reduction," IEEE Trans. Autom. Contr., Vol. AC-28, pp. 810-822, 1983.

80. E. I. Verriest and T. Kailath, "On Generalized Balanced Realization," IEEE Trans. Autom. Contr., Vol. AC-28, pp. 833-844, 1983.

81. E. A. Jonckheere and L. M. Silverman, "A New Set of Invariants for Linear Systems - Application to Reduced-Order Compensator Design," IEEE Trans. Autom. Contr., Vol. AC-28, pp. 953-964, 1983.

82. R. E. Skelton and A. Yousuff, "Component Cost Analysis of Large Scale Systems," Int. J. Contr., Vol. 37, pp. 285-304, 1983.

83. A. Yousuff and R. E. Skelton, "Controller Reduction by Component Cost Analysis," IEEE Trans. Autom. Contr., Vol. AC-29, pp. 520-530, 1984.

84. J. S. Gibson, "An Analysis of Optimal Modal Regulation: Convergence and Stability," SIAM J. Contr. Optim., 19(1981), pp. 686-707.

85. J. S. Gibson, "Linear-Quadratic Optimal Control of Hereditary Differential Systems: Infinite Dimensional Riccati Equations and Numerical Approximations, SIAM J. Contr. Optim., 21(1983), pp. 95-139.

86. H. T. Banks and K. Kunisch, "The Linear Regulator Problem for Parabolic Systems," SIAM J. Contr. Optim., 22(1984), pp. 684-698.

87. H. T. Banks, K. Ito and I. G. Rosen, "A Spline Based Technique for Computing Riccati Operators and Feedback Controls in Regulator Problems for Delay Equations," ICASE Report 82-31, Institute for Computer Applications in Science and Engineering, Hampton, VA, 1982; SIAM J. Sci. Stat. Comput., 5(1984).

88. T. L. Johnson, "Optimization of Low Order Compensators for Infinite Dimensional Systems," Proc. of 9th IFIP Symp. on Optimization Techniques, Warsaw, Poland, September 1979.

89. R. K. Pearson, "Optimal Fixed-Form Compensators for Large Space Structures," in ACOSS SIX (Active Control of Space Structures), RADC-TR-81-289, Final Technical Report, Rome Air Development Center, Griffiss AFB, New York, 1981.

90. R. K. Pearson, "Optimal Velocity Feedback Control of Flexible Structures, Ph.D. Dis., MIT. Dept. Elec. Eng. Comp. Sci., 1982.

91. R. E. Skelton and P. C. Hughes, "Modal Cost Analysis for Linear Matrix Second-Order Systems," J. Dyn. Syst. Meas. and Contr., Vol. 102, pp. 151-180, September 1980.

92. F. M. Ham, J. Shipley and D. C. Hyland, "Design of a Large Space Structure Vibration Control Experiment," 2nd IMAC, Orlando, FL, February 1984.

93. F. M. Ham and D. C. Hyland, "Vibration Control Experiment Design for the 15-M Hoop/Column Antenna," JPL Workshop on Identification and Control of Flexible Space Structures, San Diego, CA, June 1984.

94. L. W. Taylor and A. V. Balakrishnan, "A Mathematical Problem and a Spacecraft Control Laboratory Experiment (SCOLE) Used to Evaluate Control Laws for Flexible Spacecraft ... NASA/IEEE Design Challenge," NASA/IEEE Report, June, 1984.

95. D. C. Hyland and L. Davis, "Application of the Maximum Entropy Design Approach to the Spacecraft Control Laboratory Experiment (SCOLE)," presented at SCOLE Workshop, December 6-7, 1984, NASA Langley Research Center.

N87
22742
UNCLAS

N87-22742

c-5

VIBRATION ISOLATION FOR LINE OF SIGHT PERFORMANCE IMPROVEMENT

J.J. Rodden, H.J. Dougherty, W.B. Haile

LOCKHEED MISSILES & SPACE CO., INC.
SPACE SYSTEMS DIVISION
SUNNYVALE, CA 94086

Presented at the
Workshop on Structural Dynamics and Control Interaction of Flexible Structures

GEORGE C. MARSHALL SPACE FLIGHT CENTER

22 - 24 APRIL 1986

HST

1

Lockheed Missiles & Space Company, Inc.
SPACE SYSTEMS DIVISION • SUNNYVALE, CALIFORNIA

ORIGINAL PAGE IS
OF POOR QUALITY

Pointing Control System Block Diagram

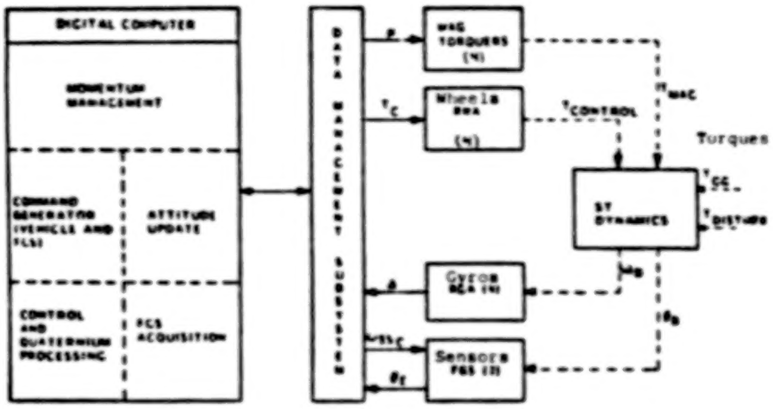

DIGITAL COMPUTER
MOMENTUM MANAGEMENT
COMMAND GENERATING (VEHICLE AND FGS)
ATTITUDE UPDATE
CONTROL AND QUATERNION PROCESSING
FGS ACQUISITION
DATA MANAGEMENT SUBSYSTEM
MAG TORQUERS (4)
Wheels RWA (4)
Gyros RGA (4)
Sensors FGS (3)
ST DYNAMICS
Turques
τ_C
$\tau_{CONTROL}$
τ_{MAG}
$\tau_{DISTURB}$
ω_B
θ_B
θ_E

Jitter Error Model

- TOTAL JITTER BUDGET IS 0.007 ", RMS

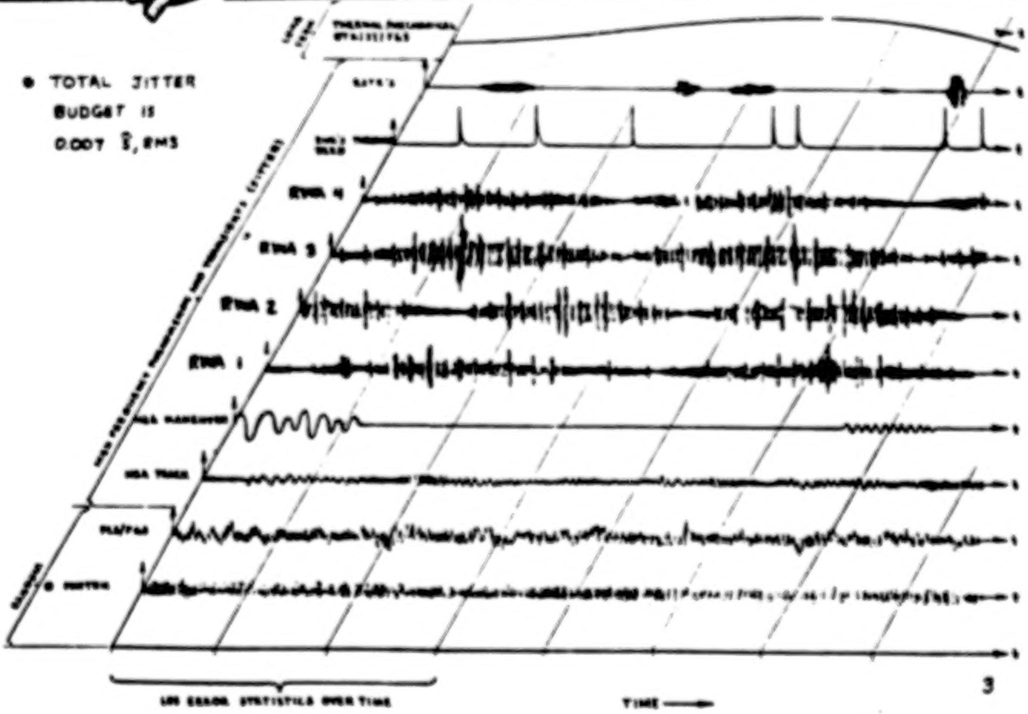

ORIGINAL PAGE IS
OF POOR QUALITY

RWA UNIT / EQUIPMENT SECTION BAY DETAILS

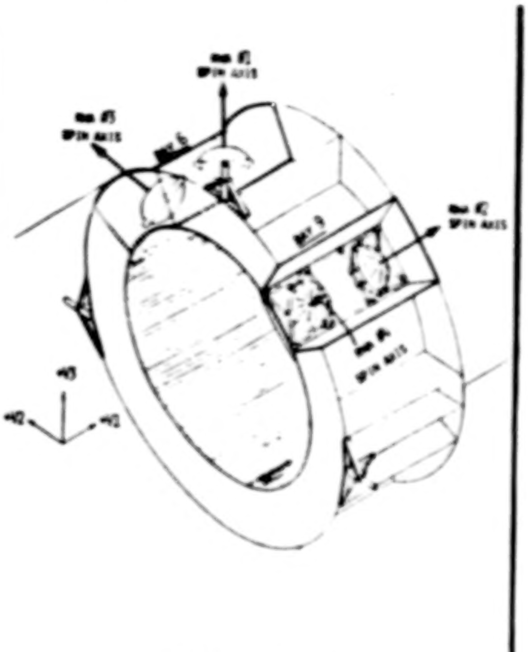
SPIN AXIS
SPIN AXIS
SPIN AXIS
SPIN AXIS

OVERVIEW : SSM EQ. SECT.

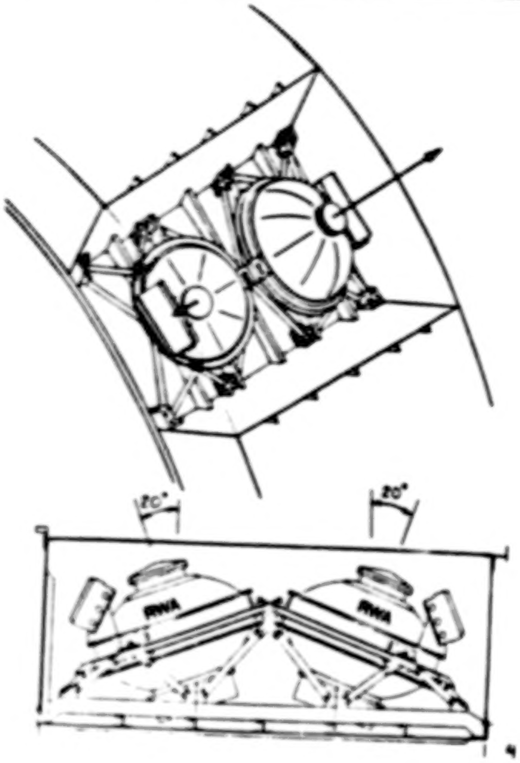
20°
20°
RWA
RWA

4

ST RWA INDUCED VIBRATION TEST

810 RPM WHEEL SPEED

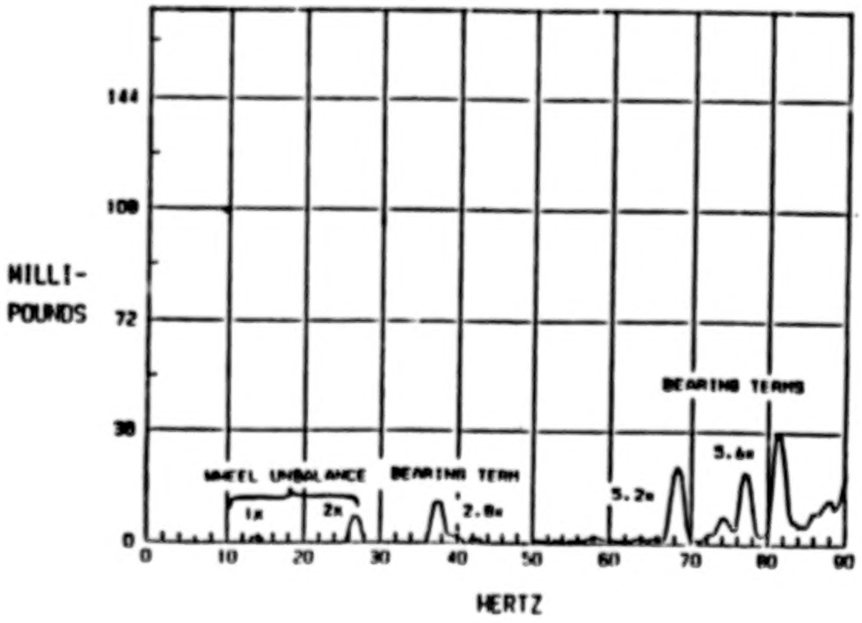

MODE, AXIAL

5

RWA JITTER PREDICTION FOR #1005 (4/85)

HARDMOUNTED RWA INDUCED JITTER: 1005

NOV 84 ST DYNAMIC MODEL - JITTER AT WF/PC (F/30)

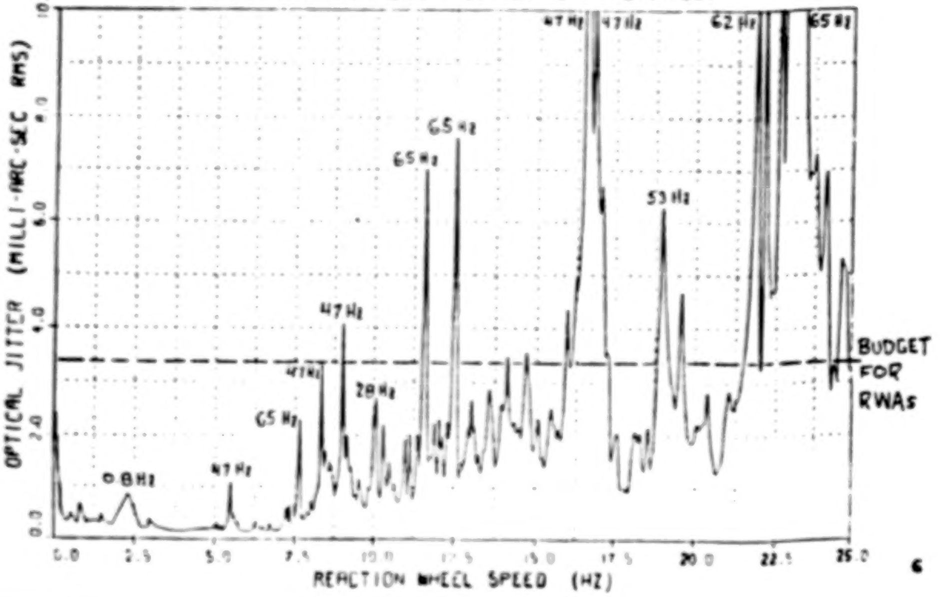

RWA WHEEL SPEED / AERO TORQUE SENSITIVITY RESULTS—V2 POP

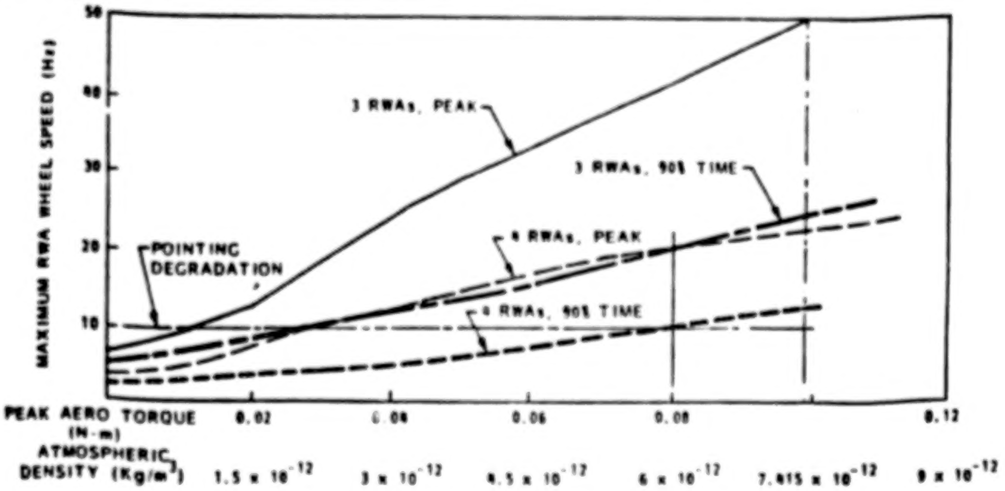

SOLAR ACTIVITY	ALTITUDE (Km)					
LOW	535	480	455	430	410	405
HIGH	750	655	605	570	535	525

NOMINAL HST ALTITUDE IS 580 KM

ORIGINAL PAGE IS
OF POOR QUALITY

NOISY WHEEL

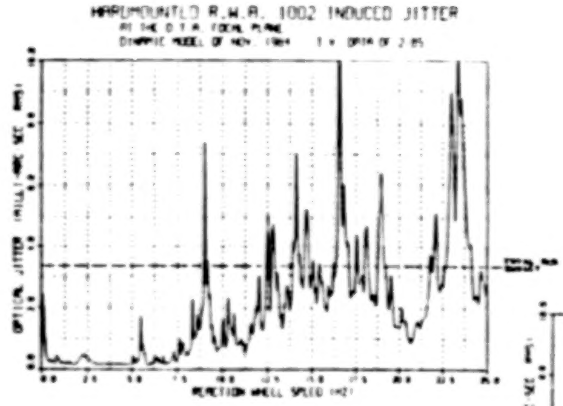

QUIET WHEEL

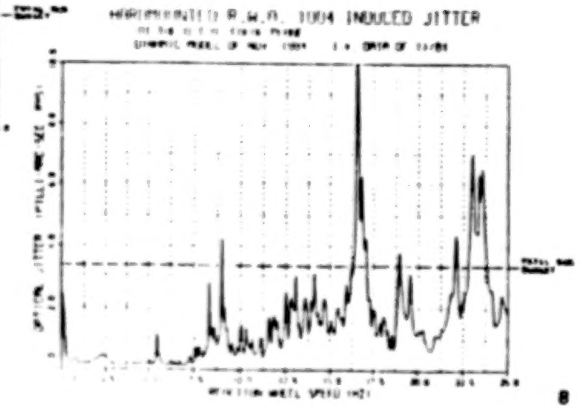

- ANALYSIS SHOWS RWAs WILL EXCEED THEIR JITTER BUDGETS

RWA ISOLATOR SPEC REQUIREMENTS

PARAMETER	REQUIREMENT
• AXIAL STIFFNESS	900-1100 LB/IN
• LATERAL STIFFNESS	1380-1870 LB/IN
• AXIAL DAMPING	.300-.060 (Q = 3 TO 20)
• LATERAL DAMPING	.170 - .025 (Q = 3 TO 20)
• MEET DYNAMIC PROPERTIES WITH STATIC 1G LOAD ON 3 UNITS	37.0 LB AXIAL 102.0 LB RADIAL
• ENVIRONMENT	TEMP: -20 F TO +120 F PRESSURE: 810 TO 10^{-13} TORR ACCEL.: 9.2 g's FOR 1.5 MIN. RANDOM VIB: 6.18 g (rms) OVERALL
• LIFE	UNIT: 2 YEARS GROUND 5 YEARS ORBITAL DAMPING ELEMENT: 7 YEARS
• WEIGHT	4.0 LBS MAX PER ISOLATOR

VIBRATION ISOLATION SYSTEM ON AN RWA

REACTION WHEEL
ASSEMBLY WITH 3
ISOLATOR UNITS

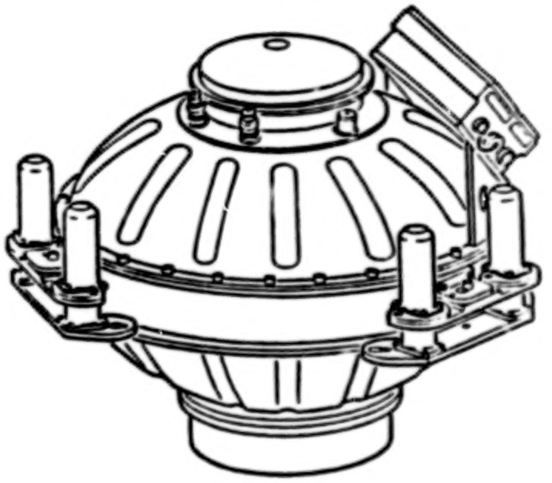

DAMPER SUBASSEMBLY
CUT-AWAY

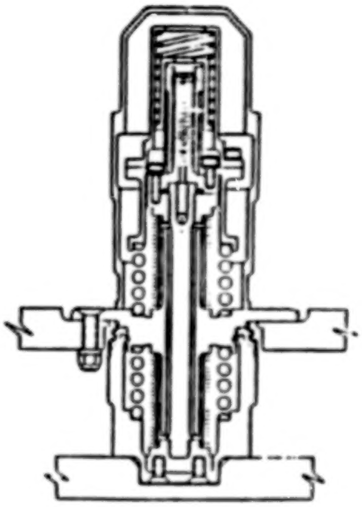

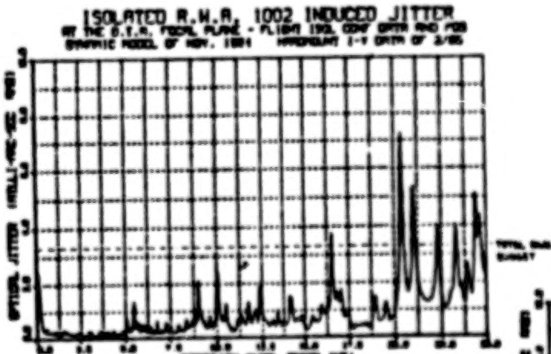

- ANALYSIS SHOWS THAT ISOLATED RWAs WILL MOSTLY REMAIN WITHIN THEIR JITTER BUDGETS

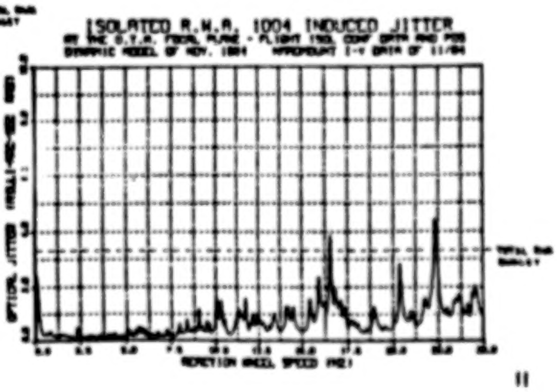

ORIGINAL PAGE IS
OF POOR QUALITY

ORIGINAL PAGE IS
OF POOR QUALITY

Unit Isolator

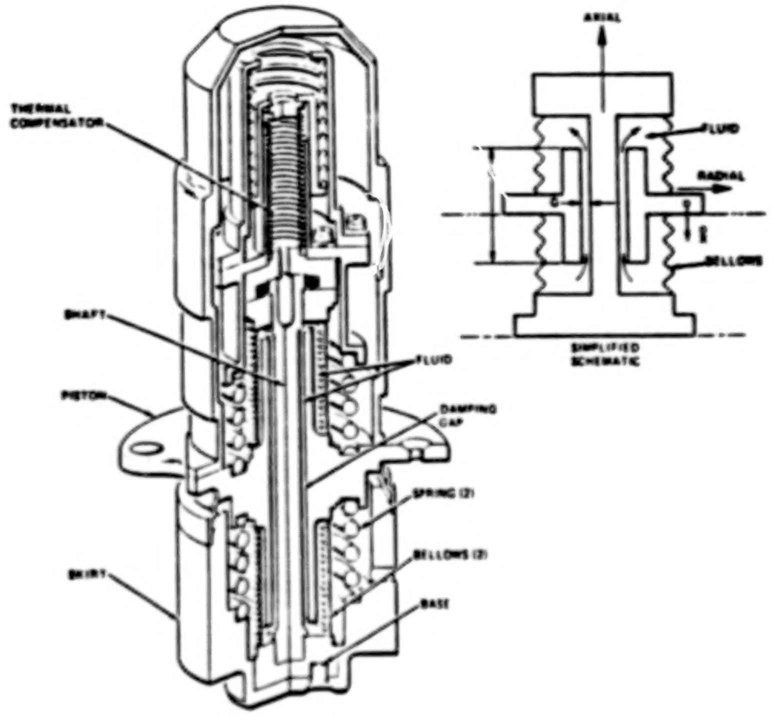
THERMAL COMPENSATOR
SHAFT
PISTON
SKIRT
FLUID
DAMPING GAP
SPRING (2)
BELLOWS (2)
BASE
AXIAL
FLUID
RADIAL
BELLOWS
SIMPLIFIED SCHEMATIC

Radial Displacement Transfer Function

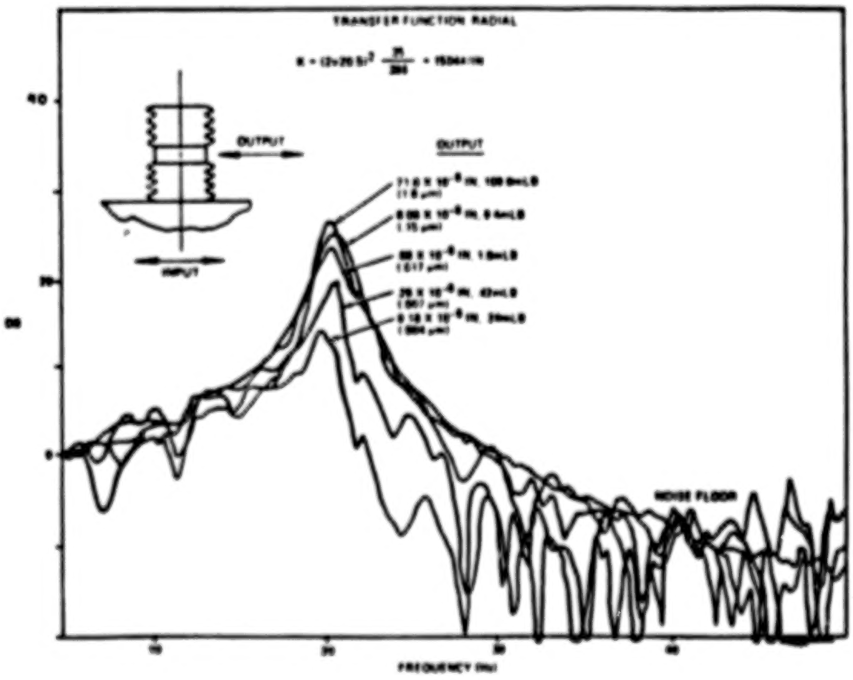

Axial Displacement Power Spectral Density

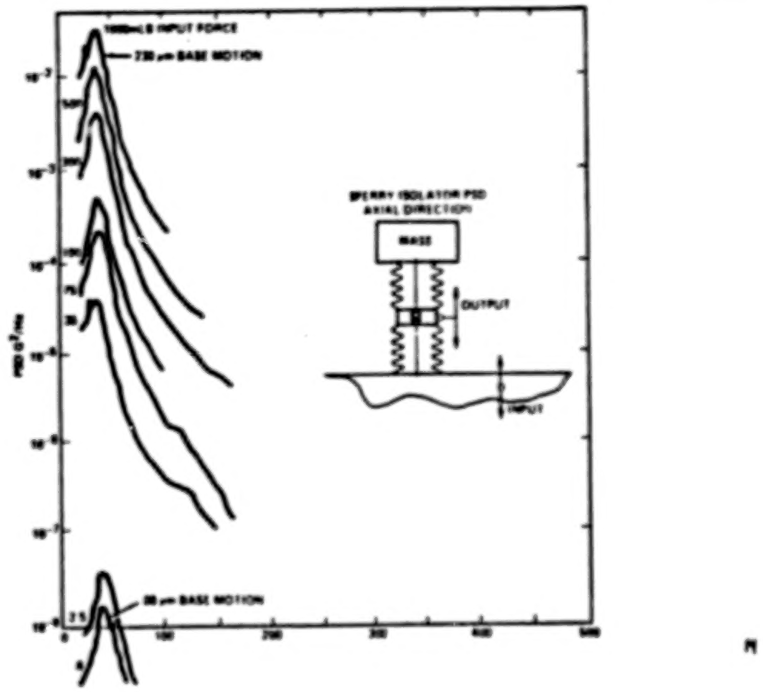

N87
22743
UNCLAS

N87-22743

A NEW APPROACH FOR VIBRATION CONTROL IN LARGE SPACE STRUCTURES

K. Kumar* and J. E. Cochran, Jr.†

Auburn University, Alabama

Abstract

A new approach for augmenting vibration damping characteristics in space structures with large panels is presented. It is based on generation of bending moments rather than forces. The moments are generated using bimetallic strips, suitably mounted at selected stations on both sides of the large panels, under the influence of differential solar heating, giving rise to thermal gradients and stresses. The collocated angular velocity sensors are utilized in conjunction with mini-servos to regulate the control moments by flipping the bimetallic strips. A simple computation of the rate of dissipation of vibrational energy is undertaken to assess the effectiveness of the proposed approach.

---

*Visiting Professor, Department of Aerospace Engineering, on leave from I.I.T., Kanpur, India.

†Professor, Department of Aerospace Engineering.

Introduction

Recent trends in space technology have been toward significantly larger and lighter weight structures.[1-3] The successful experimental mission of Communications Technology Satellite (Hermes) which employed a pair of solar panels measuring 11 x 7.3 m each is already behind us. One of the Large Space Structures (LSS) currently under development is the wrap-rib mesh deployable antenna[4,5] with a diameter of 100 m and surface thickness of 0.0254 mm. Another example is the spinning sail[6] which consists of a spacecraft propelled by photon light pressure impinging upon 12 blade-like surfaces, each measuring 8 m x 4000 m x 0.00254 mm and made of extra-light material. With Space Transportation System already in operation, several other space missions demanding varying sizes of LSS are under consideration for technological applications such as power generation and transmission, earth-resources observations and large scale communications related to mass education and electronic mail systems.[7]

Space structures with large dimensions and minimal weight characterized by distributed mass and elasticity properties are extremely flexible and, thus, are highly susceptible to on-board disturbances causing surface deformations and vibrations. Since, achieving adequate performance of LSS generally relies on precise pointing and/or precise structural configuration, it is necessary to minimize their structural response to disturbances through judicious design and by incorporating suitable control devices.

The dynamic analysis, design and control of an LSS poses a formidable technological challenge, calling for a major all-out effort.

The structural flexibility may interact with attitude control systems of spacecraft in a variety of ways. A NASA special report[8] has presented an excellent review of the earlier efforts in this area. It is interesting to note that what began as isolated efforts to understand the anomalous behavior of some specific orbiting spacecrafts by accounting for flexibility has emerged into a new field of astroelasticity.[9] In the early era, there had been considerable emphasis on developing adequate models[10] of the LSS which could account for the flexibility of the appendages. Even concise formulations of the spacecraft structures treating them as "hybrid" assembly of rigid and flexible components seem to represent a significant achievement.[11,12] Simulations of the dynamics of spinning and non-spinning systems with flexible arrays were attempted in several specific cases. The results of some of these analyses have also been verified by ground testing. During the last ten years, the emphasis seems to have shifted to investigations related to the problems involved in controlling the LSS, the stability of controls and the interaction of dynamics and control functions.

The methods most often proposed for controls are active ones although some passive approaches not requiring direct use of energy have also been suggested. For example, stiffening of an LSS can be utilized to improve its dynamic characteristics in a number of situations but only at the expense of severe weight penalties imposed. Besides, additional stiffness does not automatically add to structural damping. A feasible damping technique considered in the past is to incorporate mechanical dampers such as linear viscous dashpots into the structure.

Even this approach appears to be inadequate and has not gained much acceptance with spacecraft designers. This is perhaps due to only marginal improvements in damping characteristics associated with the rather large weight penalties involved.

Suggested here is a new approach for achieving positive damping action based on the use of moments rather than forces. In order to provide for the development of the controlling bending moments, it is proposed to have a number of moment generating units suitably spread on both sides of the large spacecraft appendages (Fig. 1). A suitable combination of strips of two different metals forms these units with constraints at the ends to obstruct any possible relative elongation or contraction of the strips under differential solar heating. This in turn generates the tensile and compressive stresses in the two members giving rise to a bending moment M_Y at the pin through which the whole unit is mounted on the panel.

For control implementation, the use of an "on-off" controller is proposed here. The sensors, essentially collocated with the bimetallic strips are required to measure the local angular velocities of the appendages. The mini-servo units are utilized to rotate/flip the strips in "on-off" positions depending upon the direction of the local angular velocity as indicated by the sensor. While in "on" position, the strips generate the bending moment through their differential thermal heating under the influence of the solar radiations. When the positive Z face of the strips is exposed to the sun and the local angular velocity of the panel about Y-axis is positive, the corresponding moment about this axis remains negative causing dissipation of vibrational energy. On the other hand, during the vibration phase of negative local angular velocity, the strips are turned into "off" position by flipping them through 90° about x-axis when the controlling moment virtually disappears. In this sun-orientation, the strips on the other side of the panel remaining unexposed to the sun do not generate any moment and may be kept in "off" position. However, when the sun moves to the other side of the panel, heating the negative Z face of the strips, the moment generated about the Y-axis becomes positive in the "on" position, thus requiring the control law to be reversed. Now, the strips are kept in the "on" position, generating positive moment while the local angular velocity of the panels remains negative. At other times, the strips are flipped into the "off" position.

Rates of Energy Dissipation

The success of the proposed control mechanism depends upon the level of rates of vibrational energy dissipation that can be achieved. The computation of these is the objective of the analysis undertaken here. It may be emphasized that since the objective is to establish the feasibility of the proposed concept, only an approximate analysis is attempted.

The feasibility study is based on a simple cantilever beam model of an LSS. Several moment units/packets are assumed distributed along the length of the beam. Both the metallic pieces in the packets are assumed to have rather small cross-sectional dimensions as compared to the length. Therefore, 1-d analysis permitting temperature variation only along the thickness would be sufficient. In steady thermodynamic state, the differential equation governing the temperature distribution across the thickness of any of the two pieces can be written as (Fig. 2)

$$\frac{d^2T}{d\xi^2} = 0 \tag{1}$$

where T is the temperature at position ξ. In order to maximize the temperature differences, an insulating material is introduced into the gap between the two pieces. Then, the boundary conditions for the "hot" piece can be stated as follows:

$$- K_1 \frac{\partial T}{\partial \xi} = \alpha_a S - \alpha_e \sigma T^4 = 0 \text{ at } \xi = - a_t \tag{2}$$

where

K_1 = Thermal conductivity of material for the "hot" piece.

$\alpha_a, \alpha_\varepsilon$ = Absorptivity and emisivity of the metallic surface, respectively.

S = Rate of solar energy received per unit area of the exposed surface; is same as the solar constant at normal incidence.

σ = Stefan-Boltzmann constant.

From Eq. (2), the temperature of the "hot" piece is given by

$$T = \left(\frac{\alpha_a S}{\alpha_\varepsilon \sigma}\right)^{1/4} \tag{3}$$

Since the other piece virtually does not receive any heat radiations, it can be assumed to be at 0° absolute. Under the temperature differences thus set up and neglecting the effect of insulating material on the thermal stresses, the resulting tensile and compressive forces in the two members can be obtained using geometric compatibility condition

$$F = \frac{\alpha_1 \ \Delta T}{(A_1E_1)^{-1} + (A_2E_2)^{-1}} \tag{4}$$

where

$$\Delta T = (\alpha_a S/\alpha_\varepsilon \sigma)^{1/4}$$

α_i = coefficient of thermal expansion; $i = 1,2$

A_i = area of cross section; $i = 1,2$

E_i = modulus of rigidity; $i = 1,2$

The subscripts 1 and 2 refer to the "hot" and "cold" members of the assembly. At 0° absolute, the two members in the assembly are assumed to have been kept in "free-force" condition.

The resulting moment in the steady state is given by

$$M_Y = \frac{\alpha_1 \delta(\alpha_a S/\alpha_\varepsilon \sigma)^{1/4}}{(A_1 E_1)^{-1} + (A_2 E_2)^{-1}} \qquad (5)$$

where δ = mean distance between the two pieces.

The local angular rate of the large panel ($\dot{\theta}$)can be expressed as follows:

$$\dot{\theta} = - \frac{\partial^2 W}{\partial X \partial t}$$

where W = deflection along Z-axis at the station X.

The instantaneous rate of energy dissipation ($-\dot{E}$) is then given by

$$(-\dot{E}) = - M_Y \dot{\theta} \qquad (6)$$

The standard modal analysis of the appendage vibrations leads to the following expression for $\dot{\theta}$.

$$\dot{\theta} = - \sum_{j=1}^{\infty} \left(\frac{d\phi_j}{dX} \dot{\xi}_j\right)$$

where

$\phi_j = c_1\ (\sinh u - \sin u) + c_2\ (\cosh u - \cos u)$

$u = (i\pi/L)X$

L = length of the appendage

$\xi_j = \xi_{j\max} \sin\ (\omega_j t + B)$

$\xi_{j\max}$ = amplitude of the jth mode of panel vibrations

$\omega_j = (i^2\pi^2/L^2)\ a$

$a = \sqrt{EI/m}$

i = 0.597 for j=1; 1.49 for j=2; (n-1/2) for j=3,4,...

(EI),m = section modulus and mass/length of the appendage, respectively.

On isolating the rate of energy dissipation corresponding to the jth mode and integrating it, one finds that the average loss of kinetic energy for this mode per vibration cycle is given by

$$\Delta E_j = \frac{2\alpha_1 \delta(\alpha_a S/\alpha_\varepsilon \sigma)^{1/4}}{(A_1E_1)^{-1} + (A_2E_2)^{-1}} \left(\frac{d\phi_j}{du}\right)\Big|_{X=L_i} \xi_{j\max} \sqrt{\omega_j/a} \tag{7}$$

where L_i specifies the position of the ith station where the moment-unit is located. This now must be compared to the maximum kinetic energy of vibrations corresponding to the jth mode (E_j). It is easy to show that

$$E_j = (1/2)\ m\xi^2_{j\max}\ \omega^2_j \int_{X=0}^{X=L} \phi^2_j\ du \sqrt{a/\omega_j} \tag{8}$$

On dividing (7) by (8), the loss factor η_j is obtained as

$$\eta_j = \frac{4\alpha_1 \delta(\alpha_a S/\alpha_\varepsilon \sigma)^{1/4}}{(A_1E_1)^{-1} + (A_2E_2)^{-1}}\ \frac{1}{\xi_{j\max}}\ \frac{1}{\omega_j\sqrt{EI\ m}}\ \frac{(d\phi_j/du)\big|_{X=L_i}}{\int_{X=0}^{X=L} \phi^2_j\ du}$$

In case the moment generating units distributed along the length of the appendage are at distances L_1, L_2,... from the clamped end of the appendage, the above results modify to:

$$\eta_j = \eta_{oj}\, f_j \tag{9}$$

where

$$\eta_{oj} = p_m/[\omega_j\, \xi_{j\max}\sqrt{EIm}] \tag{10}$$

$$p_m = \frac{4\alpha_1\,\delta(\alpha_a S/\alpha_\varepsilon \sigma)^{1/4}}{(A_1E_1)^{-1} + (A_2E_2)^{-1}}\text{ , the moment parameter} \tag{11}$$

$$f_j = [(d\phi_j/du)_{X=L_1} + (d\phi_j/du)_{X=L_2} + ---]/\int_{X=0}^{X=L} \phi_j^2\, du \tag{12}$$

Results and Discussion

The approximate analytical results developed here are of considerable significance. Mere observation suggests the effects of various system and design parameters on the loss factor, denoting the fraction of kinetic energy dissipated per cycle in various vibrational modes. The loss coefficient rapidly increases with increase in length of the appendage and hence decreasing frequency. In fact, this factor increases in proportion to L^2. It also suggests that the damping effectiveness progressively declines for higher modes of vibrations, as is usually the case with other damping techniques as well.

It is evident that the vibrational energy dissipation can be maximized by maximizing the design parameters p_m and f_j. The maximization of p_m demands the use of materials which provide the highest values of thermal coefficients, α_1, and modulii of rigidity, E_1 and E_2.

Further increase in p_m can be achieved by moving the two pieces apart to maximize the moment arm and of course by taking the higher areas of cross-section.

The parameters f_j merit special attention. By changing the longitudinal distribution of the moment-strips, it is possible to augment the damping effects in certain chosen/critical modes. However, it will result in compromising with dissipation rates associated with other modes. Rather simple algebraic calculations can be performed to determine the "best" locations. It is interesting to note that this approach enables attaining fairly significant values of loss factor even for higher modes. Since the control effectiveness increases with decreasing frequency, it appears particularly attractive for LSS.

Conceptually, the approach suggested here is a simple one. However, it involves several challenging problems at the design stage. The problems of mounting of the moment-strip units at various stations on a flexible light-weight structure, providing for the measuring sensors and the mini-servos which can control the orientation of the moment-strip unit according to the control policy proposed have to be tackled. The loss factors undergo periodic variation becoming zero during the periods of grazing solar incidence on the strips. Thus, in this phase, the damping mechanism appears to be ineffective. However, this problem can be overcome to a large extent simply by flipping the moment-strips through small angles (~30-45°) so as to ensure a significant differential solar heating even in this situation.

No doubt, the proposed control mechanism involves significant weight penalty associated with the use of the moment-strips and other accessories; however, it is hoped that a judicious design can keep it to within acceptable limits. Besides, the addition of this mass may also serve the secondary purpose of stiffening the system. Furthermore, the power required to drive the servos is expected to remain at low level. In a nutshell, this investigation brings out several interesting and useful features of the proposed scheme to augment the system damping.

References

1. Modi, V. J., "Altitude Dynamics of Satellites with Flexible Appendages - A Brief Review," Journal of Spacecraft and Rockets, Vol. 11, No. 11, November 1976, pp. 743-751.

2. Meirovitch, L. (Ed.), "Dynamics and Control of Large Flexible Spacecraft," Proceedings of a VPI & SU/AIAA Symposium, Blacksburg, Virginia, June 1977.

3. Meirovitch, L. (Ed.), "Dynamics and Control of Large Flexible Spacecraft," Proceedings of the Second VPI & SU/AIAA Symposium, Blacksburg, Virginia, June 1979.

4. Chen, Jay-Chung, "Response of Large Space Structures with Stiffness Control," Journal of Spacecraft and Rockets, Vol. 21, No. 5, Sept.-Oct. 1984, pp. 463-467.

5. El-Raheb, M., and Wagner, P., "Static and Dynamic Characteristics of Large Deployable Space Reflectors," AIAA/ASME/ASCE/AHS 22nd Structures, Structural Dynamics, and Materials Conference, Atlanta, Georgia, April 1981.

6. MacNeal, R. H., "Structural Dynamics of the Heliogyro," NASA Contract Report CR-1745, 1971.

7. Reddy, A. S. S. R., Bainum, P. M., Krishna, R., and Hamner, H. A., "Control of Large Flexible Platform in Orbit," Journal of Guidance and Control, Vol. 4, No. 6, Nov.-Dec. 1981, pp. 642-649.

8. Noll, R. B., Zvara, J., and Deyst, J. J., "Effects of Structural Flexibility on Spacecraft control Systems," NASA SP-8016, April 1969.

9. Yu, Y. Y., "Some Problems in Astroelasticity--Dynamics and Control of Flexible Vehicles and Spacecraft," Proc. VIIIth International Symposium on Space Technology and Science, Tokyo, 1969, pp. 349-358.

10. Likins, P. W., and Bouvier, M. K., "Attitude Control of Non-Rigid Spacecraft," Astronautics and Aeronautics, Vol. 9, No. 5, May 1971, pp. 64-71.

11. Keat, J. F., "Dynamical Equations of Nonrigid Satellites," AIAA Journal, Vol. 8, No. 7, July 1970, pp. 1344-1345.

12. Kane, T. R., and Wang, C. F., "On the Derivation of Equations of Motion," Journal of the Society for Industrial and Applied Mathematics, Vol. 13, No. 2, June 1965, pp. 487-492.

13. Hughes, P. C., "Attitude Dynamics of a Three Axis Stabilized Satellite with a Large Flexible Solar Array," The Journal of the Astronautical Sciences, Vol. XX, No. 3, Nov.-Dec. 1972, pp. 166-189.

14. Cherchas, D. B., and HUghes, P. C., "Attitude Stability of a dual-Spin Satellite with a Large Flexible Solar Array," Journal of Spacecraft and Rockets, Vol. 10, No. 2, Feb. 1973, pp. 126-132.

15. Hughes, P. C., "Dynamics of Flexible Space Vehicles with Active Attitude Control," Celestial Mechanics, Vol. 9, No. 1, 1976, pp. 21-39.

16. Lin, J. G., Hegg, D. R., Lin, Y. H., and Keat, J. E., "Output Feedback Control of Large Space Structures: An Investigation of Four Design Methods," Dynamics and Control of Large Flexible Spacecraft, Proc. Second VPI & SU/AIAA Symposium, Blacksburg, Virginia, June 1979, pp. 1-18.

17. Ashley, Holt, "On Passive Damping Mechanisms in Large Space Structures," Journal of Spacecraft and Rockets, Vol. 21, No. 5, Sept.-Oct. 1984.

18. Modi, V. J., and Kumar, K., "Planar Librational Dynamics of Satellite with Thermally Flexed Appendages," The Journal of the Astronautical Sciences, Vol. XXV, No. 1, Jan.-March 1977, pp. 3-20.

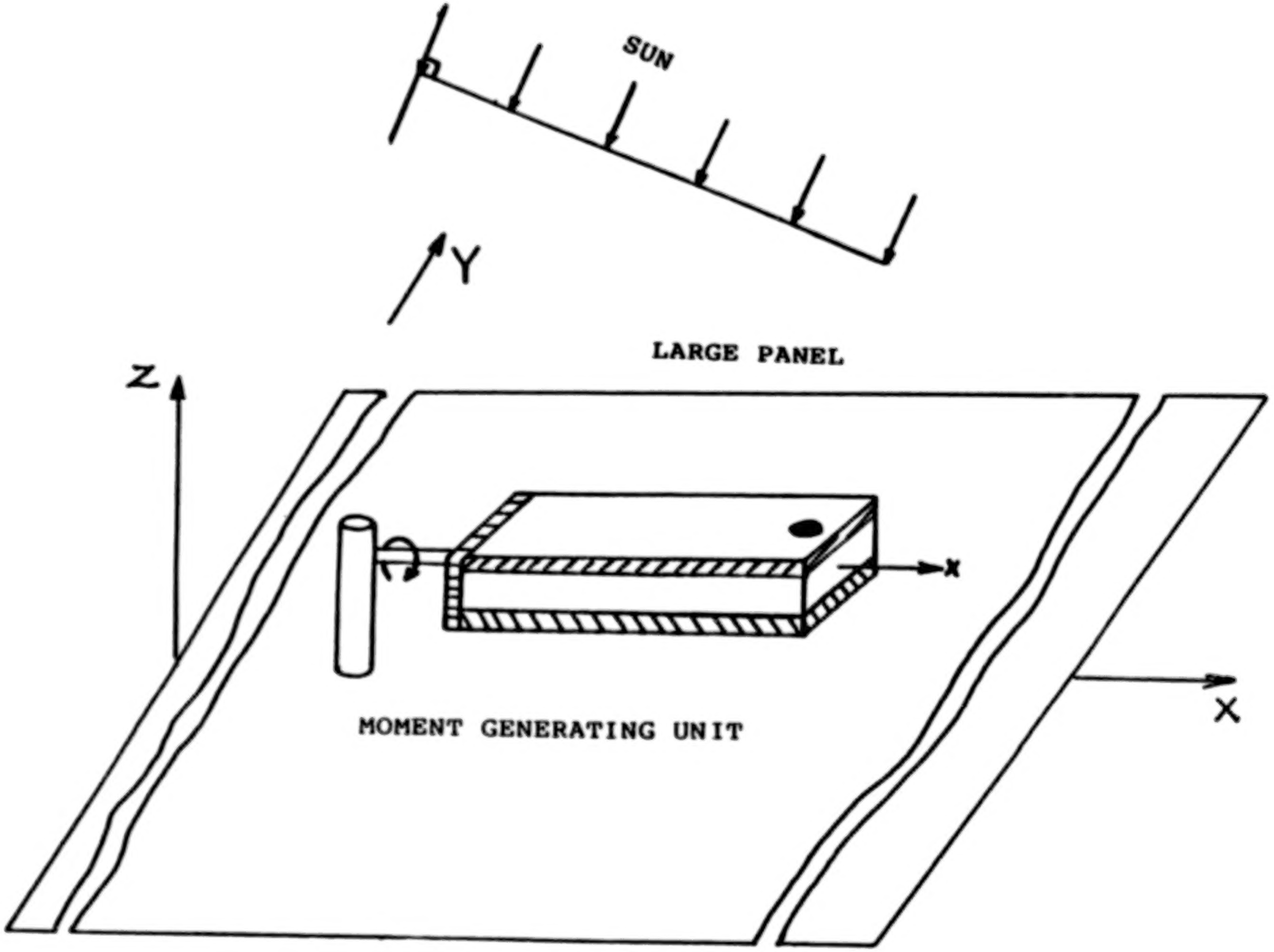
SUN
Y
LARGE PANEL
Z
x
X
MOMENT GENERATING UNIT

Fig 1.   A moment generating unit mounted on the large panel.

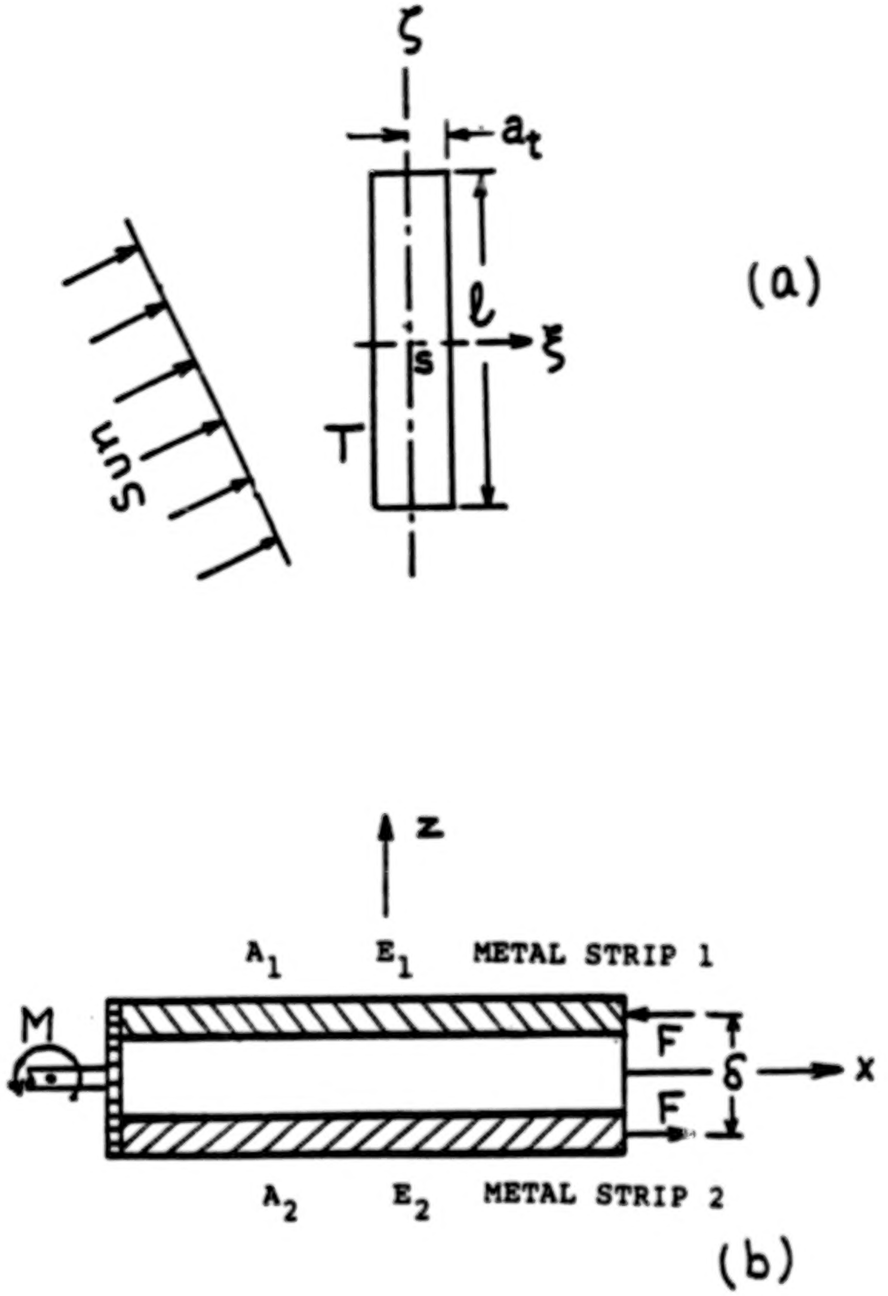
ζ
a_t
ℓ
ξ
s
T
sun
(a)
z
A_1
E_1
METAL STRIP 1
M
F
δ
x
F
A_2
E_2
METAL STRIP 2
(b)

Fig. 2. (a) Coordinate System for Thermal Analysis

(b) Geometry of forces and moments in the moment-packet

N87
22744
UNCLAS

N87-22744

TECHNICAL PAPER

CREW ACTIVITY AND MOTION EFFECTS
ON THE SPACE STATION

By

Brian V. Rochon

Steven A. Scheer

Lockheed Engineering and Management Services Company, Inc.
Houston, Texas
NAS 9-15800

Presented to the

Workshop on
Structural Dynamics and Control Interaction
of Flexible Structures

George C. Marshall Space Flight Center
Huntsville, Alabama

April 22-24, 1986

PRECEDING PAGE BLANK NOT FILMED

ABSTRACT

CREW ACTIVITY & MOTION EFFECTS ON THE SPACE STATION

Among the significant sources of internal disturbances that must be considered in the design of Space Station vibration control systems are the loads induced on the structure from various crew activities. Flight experiment T013, flown on the second manned mission of Skylab, measured force and moment time histories for a range of preplanned crew motions and activities. This experiment has proved itself invaluable as a source of on-orbit crew induced loads that has allowed a Space Station forcing function data base to be built.

This will enable forced response such as accelerations and deflections, attributable to crew activity, to be calculated.
The flight experiment, resultant database and structural model pre-processor, analysis examples and areas of continued research shall be described.

I. Introduction

Since the early sixties, crew activity/motion (CA/M) has been a concern and important parameter in the areas of space vehicle stability, attitude and control during its on-orbit operation. Initially, the impact of CA/M on the pointing accuracies and control of spacecraft carried the most concern. More recently, however, the on-orbit 'micro-g' environments of the Space Shuttle and the forthcoming Space Station have provided the motivation for further crew disturbance studies.

Various ground simulations and one flight experiment have been conducted through the years, yielding sufficient amounts of data to promote an understanding of the potential impact man has on his spacecraft's on-orbit quiescent environment. For analysis purposes, modeling can yield only part of the CA/M disturbance spectrum; stochastic modeling techniques can be used for low-level restrained activities. Flight data can be used to build a forcing function database and a structural model pre-processor can be generated to yield the remainder of the CA/M disturbance spectrum; the deterministic or discrete high-level restrained and translational activities.

The following is dedicated to describing the evolution of a CA/M forcing function database and preprocessor, 'CREW', developed by Lockheed-EMSCO for the Loads & Dynamics Branch of the Structures & Mechanics Division at NASA/JSC. The description of this evolution will include: background discussion of early studies and ground simulations; a description of the only flight experiment conducted to date; modeling techniques; features of 'CREW' and the T-013 CA/M forcing function database; analysis examples and plans for continued work in this area.

II. Background & Evolution of Skylab Experiment T-013

To demonstrate the potential impact man has on his spacecraft, the following 'real world' examples of CA/M disturbances can be cited. On the manned Skylab missions, the astronauts found that they had a 'jogging' track at their disposal. At the top of the Orbital Workshop (OWS), a bank of lockers around the perimeter of that compartment were used by the astronauts to 'run' on. In doing so, they were able to achieve centripedal acceleration equivalent to the moon's gravity, and more importantly, the induced loads started to precess the entire spacecraft. Needless to say, ground controllers had the crew discontinue this activity because the Skylab Attitude and Pointing Control System (APCS) was not able to maintain control of the spacecraft, and the Apollo Telescope Mount Experiment Pointing Control System (ATM EPCS) pointing accuracy, required by the solar experiments, was threatened (refs. 1 and 2).

More recently, aboard the shuttle, various forms of CA/M disturbances have been examined. During STS-9, after the Spacelab 1 module had been powered up and run through a systems checkout, the crew was asked to participate in the Spacelab Environment Verification Flight Test (ref. 3). The activities investigated were coughing and soaring. Peak response in the module was measured as 0.007 g. In the Shuttle's crew cabin middeck, a treadmill is provided for the crew to satisfy their exercise requirement while on-orbit. On recent missions, NASA/LaRC's ACIP/HIRAP accelerometer package has measured peak accelerations that exceed 0.0001 g's (nominal treadmill operation aboard a 220,000 lb Orbiter).

Thus the effect of CA/M on a spacecraft's on-orbit environment can be a dramatic one. Consideration of this potential impact is especially important for a spacecraft such as the Space Station, which is dedicated to providing a pure micro-g environment for its payloads and experiments.

During the development of early long duration spacecraft, other investigators (refs. 4, 5) demonstrated that CA/M disturbances would exceed other sources such as gravity-gradient and aero drag effects using point-mass representations of man in the spacecraft equations of motion. In 1966, Fuhrmeister and Fowler (ref. 6) reported that the crew would have to be isolated to ensure fine pointing accuracies for their MDAC Manned Orbital Research Laboratory (MORL). In 1969 Goodman and Middleton of MDAC conducted a 60 day crew locomotion study in their Space Cabin Simulator (ref. 7). Using applied force data (measured in the 1966 MORL ground simulation) to drive a computer simulation of their spacecraft dynamics, they confirmed the Fuhrmeister and Fowler conclusion and added that basic attitude control would also be compromised by frequent crew motion over a long time interval.

The lack of flight data and the need to verify simulation results culminated in the proposal of a dedicated experiment to be conducted on what was to be called Skylab. In addition, the experiment would test the design of a control/isolation system which would be used to ensure pointing accuracies of the Skylab's Apollo Telescope Mount (ATM). In 1967, Martin Marietta, under contract to MSFC, began the development of experiment T-013; in parallel they began conducting detailed ground simulations using their 6 DOF servo-driven simulator and a predecessor of the T-013 force measurement system (refs. 8, 9).

Reinforcement to the need for experiment T-013 can be found in understanding the limitations of ground simulation and, consequently, the questionable applicability of the resultant data. Several techniques of simulating the zero-g environment of a manned spacecraft and their advantages/disadvantages with respect to a crew-motion experiment are listed in Table 1.

Table 1: CREW ACTIVITY SIMULATION METHODS

METHOD	ADVANTAGES	DISADVANTAGES
FMU	engineering design and computer program to reduce instrumentation already developed; can measure effectof similar limb motions in both the horizontal and vertical plane and thus obtain comparisons with and without gravity	presence of gravity can affect manner in which motions are performed
Three DOF air bearing simulator at JSC	provides good approximation to zero-gravity limb motion effects in two translational and one rotational DOF (horizontal plane); low cost because air bearing floor and other hardware already exist at JSC	additional instrumentation of current simulator configurations may be required; computer program must be written to reduce data from instrumentation system; torque & force from air & instrumentation wires are negligible except for all but smallest limb motions; cannot measure effect of limb motions in vertical plane
air bearing simulation	provides good low-g or zero-g effect in two dimensions (horizontal plane)	implementation of force measuring techniques difficult; requires extremely fine balance and CG shift compensation; must counteract gravity in many motions; mounting harnesses, etc., too restrictive; susceptible to ambient air movement
underwater neutral buoyancy	approx. actual zero-g for unsuited subject	drag excessive for all but slowest motions, breathing equipment restrictive
servo-drive simulation	can be tied together with computer simulation of spacecraft dynamics	must counteract gravity in many motions; mounting harnesses too restrictive
cable suspension	relatively low cost	degrees of freedom limited; pendulum effects present; support apparatus restrictive
zero-g aircraft	actual zero-g environment	short run times; unnatural positive g forces interspersed between zero-g runs

III. Skylab Experiment T-013

Skylab experiment T-013 was proposed to determine the characteristics of CA/M disturbances and to evaluate the performance of a dedicated isolation system that would ensure the pointing accuracies of the ATM's solar experiment package.

The principal investigator, Mr. Bruce Conway, outlines the development and design of experiment T-013 in reference 10. Two categories of CA/M would be explored; restrained activities including respiration exercises, limb motion, gross torso motion and simulated console operations; and translation activities including various levels of soaring.

The restrained activities would be conducted with the test subject attached to a force measurement unit (FMU) with foot restraints and the translation activities would have the test subject pushing off from one FMU, soaring across the Skylab Orbital Workshop and landing on another FMU; see Figures 1 and 2.

The forces and frequency content of the disturbances produced by the T-013 subject were generally, and notably higher than those measured in ground simulations. For the respiration exercises (breathing, coughing, sneezing), only coughing had the same force levels in flight as obtained in simulation. Sneezing produced up to twice the force and deep breathing resulted in over 25 times as much force. A lack of 1-g restraint on the subject's viscereal mass, allowing more acceleration and motion of this mass, appears to provide reasonable explanation for the larger on-orbit forces. The experiment was performed approximately three weeks into the Skylab 3 mission (second manned mision) and it is assumed that the crew had become well adapted to their zero-g environment.

The crew's zero-g adaptation may also explain why the preflight zero-g aircraft soaring data was not as high as the T-013 flight levels. Figure 3 is a plot of the zero-g aircraft data and Figure 4 is a plot of representative T-013 data. In addition to the force time histories, these plots include a trace of the cumulative absolute force impulse. In comparison, the T-013 data indicates forces two times greater and an impulse value five times greater than the zero-g aircraft data. It should be noted that Figure 3 represents only the force normal to the 'wall' and with the addition of the other components of the total force, as measured in experiment T-013, there is a significant increase in the energy imparted to the spacecraft.

POOR QUALITY

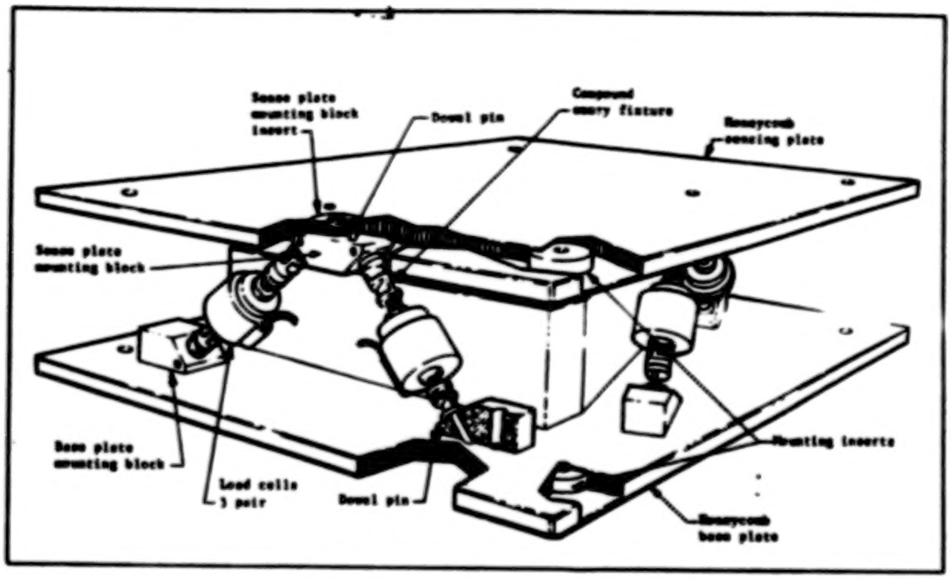
Sense plate mounting block insert
Dowel pin
Compound epoxy fixture
Honeycomb sensing plate
Sense plate mounting block
Base plate mounting block
Load cells 3 pair
Dowel pin
Mounting inserts
Honeycomb base plate

Figure 1 - Force Measurement Unit (FMU)

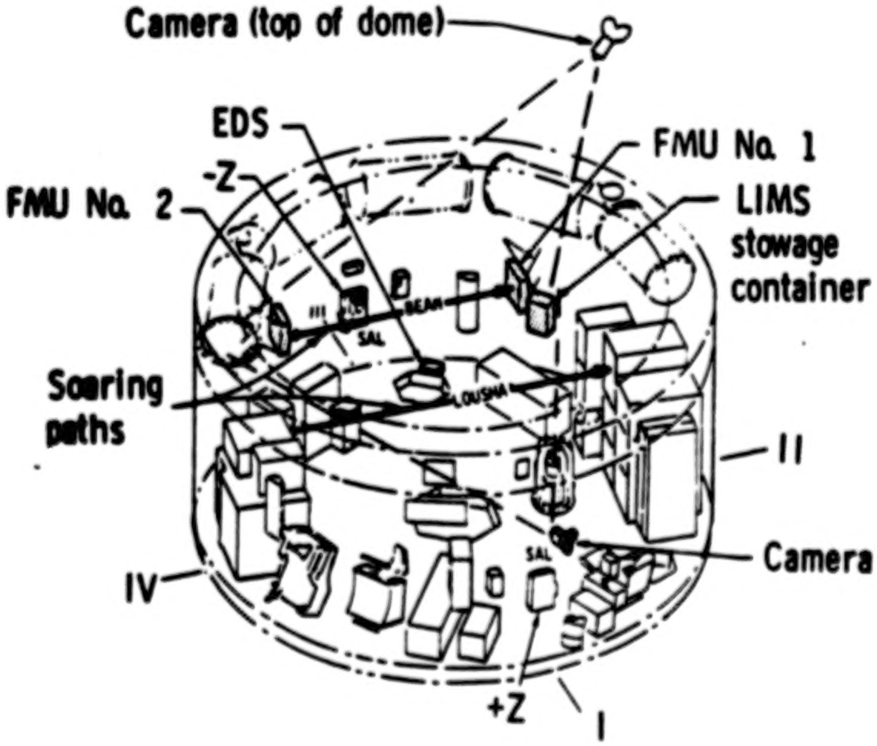
Camera (top of dome)
EDS
-Z
FMU No. 1
FMU No. 2
LIMS stowage container
BEAM
SAL
Soaring paths
II
Camera
IV
SAL
+Z
I

Figure 2 - T013 operations area of OWS indicating soaring paths

FIGURE 3 - ZERO G AIRCRAFT WALL PUSHOFF & LANDING

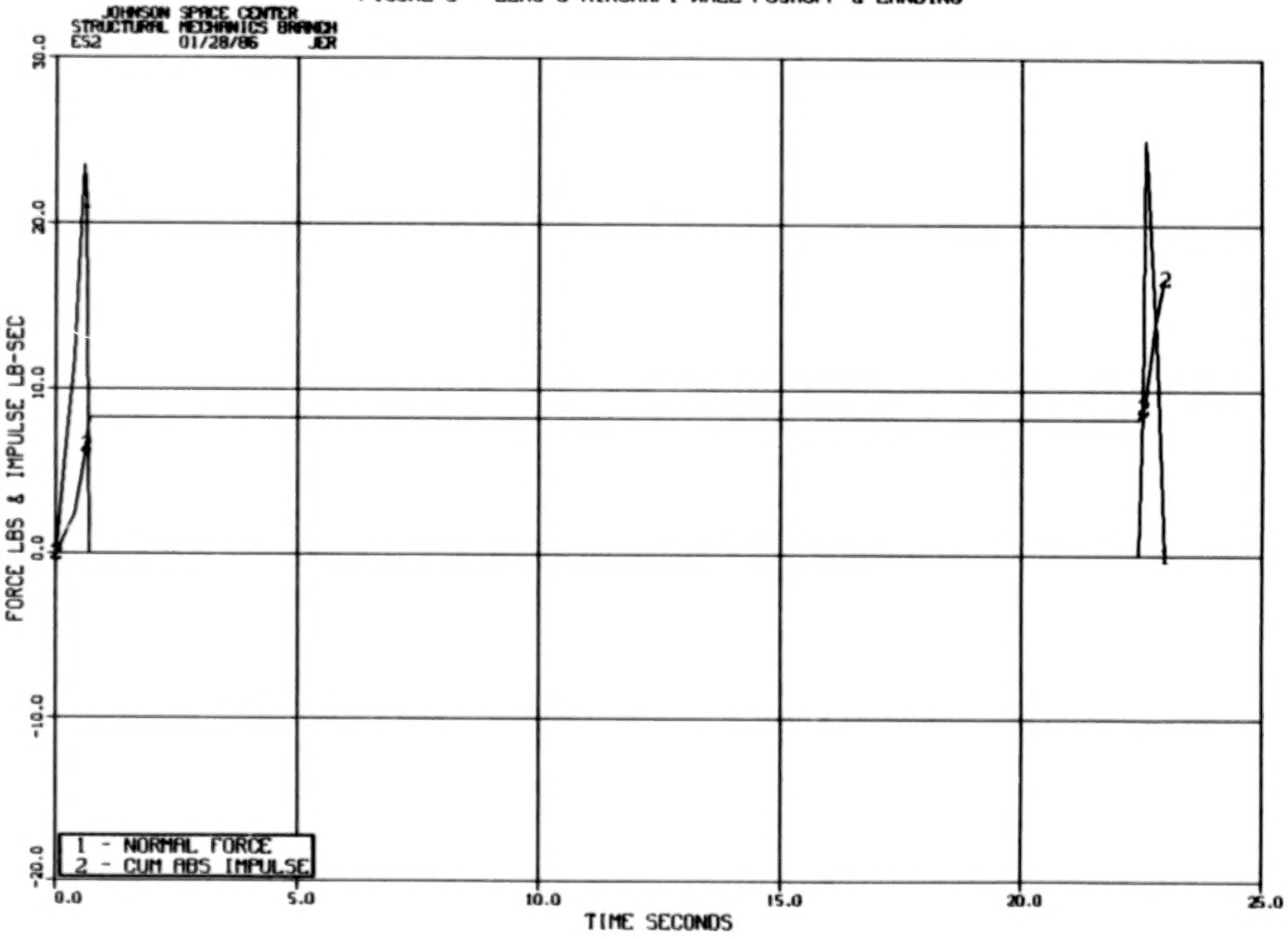

FIGURE 4 - TYPICAL EXPERIMENT T-013 WALL PUSHOFF & LANDING

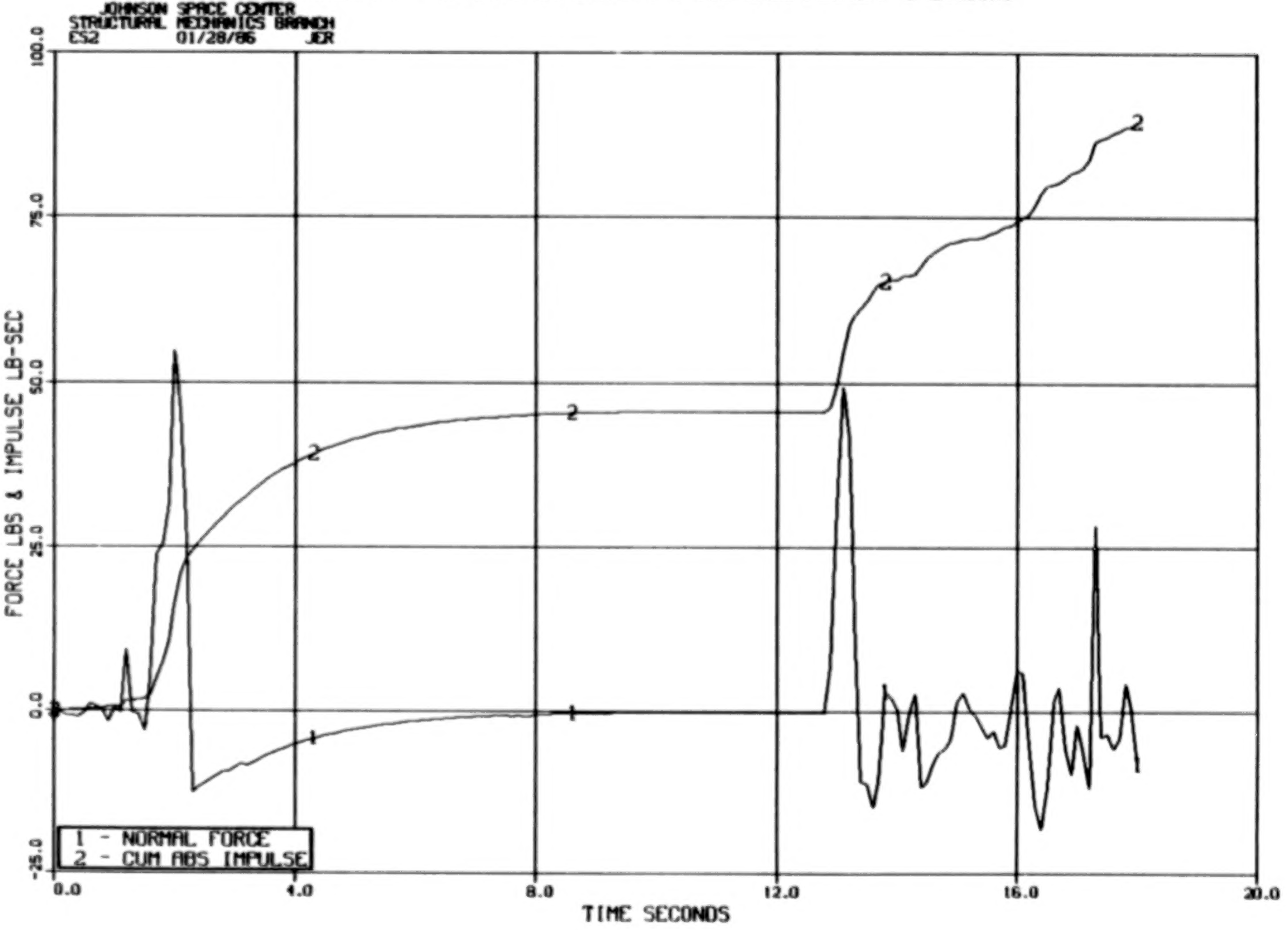

Thus it appears that short periods of zero-g interspersed with periods of greater than 1g would seem to preclude a complete adaptation and development of the large translation capabilities evidenced in Skylab. Those activities associated with gross body motion (subject restrained) and translation, simulated by Murrish and Smith, indicated poor correlation with T-013 results. The on-orbit force levels exceeded the simulated force levels by at least a factor of two. Analysis by Conway (ref. 11) showed that the discrepancy arises from the increased limb and torso velocities attained by the subjects during on-orbit activities (Conway noted that T-013 translation velocities were as much as two times the velocities measured during the ground simulations, and that limb motions showed a 35 percent increase compared to ground simulation predictions).

Console operations, as expected, produced the lowest forces and agreement with ground simulation data was very good. Hendricks and Johnson (ref. 12), Murrish and Smith conducted stochastic (deep breathing, console operations, coughing and sneezing) activity simulations using an FMU similar to that used in T-013. In brief, most of the low-level restrained motions were performed on mockups for console activities or hygiene functions, and after careful comparison of their results with the results collected from T-013, excellent correlation was evidenced. Thus motions necessary to personal hygiene, meal preparation, and console operations are considered stochastic and Kullas (ref. 13) feels that they are aptly represented using stochastic models. However, Conway noted that use of the T-013 flight data would be a more accurate 'model'.

Table 2 lists the peak forces for various activities collected from the MDAC MORL ground simulation, the pre T-013 ground simulations and the T-013 flight experiment. Table 3 lists summary data for all of the T-013 activities investigated. General conclusions derived from experiment T-013 by the principal investigator follow:

1) The Skylab APCS experienced significant disturbance inputs as a result of the T-013 activities.

2) In general, the forces generated were higher than those predicted from pre-flight ground simulations.

Table 2: CREW ACTIVITY & MOTION PEAK FORCES (LBS)

	MDAC/MORL	GROUND SIM (PRE T-013)	T-013
CONSOLE OPERATIONS	13.0	4.0	9.4
RESPIRATION EXERCISES	N/A	20.0	48.6
ARM MOTION	4.0	1.5	35.3
LEG MOTION	7.6	10.0	28.2
ARM FLAPPING	N/A	8.0	82.4
FORCEFUL THRUST	110.0	N/A	99.7
SOARING	350.0	10.0	77.3

TABLE #3
EXPERIMENT T-013 SUMMARY DATA
MAXIMUM VALUES

ACTIVITY	FORCE (lbs)			MOMENT (ft-lb)			PSD (lb^2 /htz)			PSD (lb^2 ft^2 /htz)		
	Fx	Fy	Fz	Mx	My	Mz	Fx	Fy	Fz	Mx	My	Mz
Respiration Exercises	12.73	47.81	8.95	9.35	7.92	13.74	0.11	2.54	0.16	2.74	0.07	0.51
Console Operations	7.54	7.26	3.03	11.32	5.21	10.02	0.79	0.32	0.54	8.89	0.51	4.10
Normal Body Exer:												
Arm Motion	5.80	33.56	12.02	8.20	7.74	6.20	0.19	5.21	0.83	0.99	0.65	0.38
Leg Motion	23.05	24.63	13.25	6.93	6.02	11.12	6.35	5.56	2.54	1.81	0.51	1.61
Bowing	17.73	52.12	8.68	19.04	9.36	6.51	1.21	155.58	3.94	34.19	0.55	1.71
Swaying	12.12	27.50	27.54	32.57	32.57	25.14	0.67	16.51	21.59	68.38	5.13	31.45
Gross Body Exer:												
Arm Flapping	14.71	88.96	28.18	21.64	8.97	11.55	0.41	165.11	10.16	5.81	0.24	1.16
Forceful Thrust	29.33	99.70	14.55	22.82	18.84	8.48	5.14	190.51	7.46	30.77	2.05	2.74
Oneman Soaring:												
Normal	18.53	69.51	27.42	23.18	11.86	19.37	2.86	34.93	2.06	11.62	1.30	5.47
Forceful	16.04	65.25	15.30	19.38	10.92	16.94	2.54	39.69	2.00	11.62	0.75	5.13
Twoman Soaring:												
Normal	13.54	64.03	14.17	19.73	11.26	16.21	1.17	50.80	2.16	19.49	0.62	4.79
Forceful	30.57	77.12	35.13	25.40	16.09	30.78	6.99	47.63	4.13	14.36	1.71	21.88

TABLE #3 (con't)
EXPERIMENT T-013 SUMMARY DATA
MAXIMUM VALUES

ACTIVITY	FREQUENCY (htz) @MAX PSD			FREQUENCY (htz) @ MAX PSD		
	Fx	Fy	Fz	Mx	My	Mz
Respiration Exercises	0.32	1.91	1.91	0.16	0.40	0.27
Console Operations	0.19	0.32	0.16	0.16	0.32	0.19
Normal Body Exer:						
Arm Motion	0.40	1.59	1.59	0.16	0.70	0.32
Leg Motion	0.92	1.40	0.92	0.40	0.51	1.40
Bowing	1.11	0.72	1.11	0.38	0.32	1.11
Swaying	0.16	0.32	0.32	0.13	0.13	0.16
Gross Body Exer:						
Arm Flapping	0.80	1.64	1.64	1.27	0.80	0.67
Forceful Thrust	0.80	0.99	0.37	0.37	0.95	0.32
Oneman Soaring:						
Normal	0.40	0.32	0.40	0.32	0.40	0.32
Forceful	0.51	0.80	0.70	0.19	0.32	0.40
Twoman Soaring:						
Normal	0.40	0.48	0.48	0.19	0.32	0.32
Forceful	0.32	0.38	0.32	0.19	0.32	0.32

3) The lack of 1-g restraint is the primary reason for the higher forces and velocities experienced.

4) Pre-flight locomotion capability study predictions were conservative.

5) The ATM EPCS provided adequate isolation from T-013 activities.

6) Use of the T-013 data is feasible for future multi-man crew spacecraft disturbance analyses.

7) Use of the T-013 data to develop a family of flight-verified CA/M models could prove useful for future spacecraft ACS design and analysis.

IV. CA/M Modeling Techniques

Prior to Experiment T-013, it had been realized that many of the low-level CA/M disturbances are stochastic in nature. The types of CA/M considered to be stochastic, or stationary random processes, are console operations, respiration, personal hygiene, etc. Realization of the above CA/M's stochastic nature came as a result of a search by investigators for a more convenient technique of incorporating CA/M forcing function data into a spacecraft dynmamic simulation. The lack of convenience was found to be in the necessity of recording the data from a physical simulation on analog or digital tape and then continuously feeding the data from the tapes into the spacecraft dynamic simulation programs, along with the inherent tape handling problems associated with computers of that era.

After Murrish and Smith had demonstrated the stationarity of their ground simulated console operations data, Hendricks and Johnson generated PSD curves of the data and set about synthesizing the digital filters to approximate the calculated PSD curves. Once the filter parameters were synthesized, they used a random number generator to drive the filter and generated PSD curves that were close approximations to the actual curves generated from the simulation data. They noted that because their approximation was made in the frequency domain, that one should not expect to see a similar forcing function generated for the time domain, once the inverse Fourier transform is completed.

For deterministic, or discrete, CA/M forcing function data, the sound approach is to use actual flight data, if it exists, as suggested by Conway and Kullas. If the analysis has a 'first-cut' flavor, then the investigator can employ a 'first order' model, which is an approximation of the actual time domain data, taking care to use peak force values.

After reviewing the above discussion, it seems logical and practical to employ the flight experiment forcing function data directly as input for time domain analysis routines where possible. Stochastic modeling techniques were desirable and convenient because of the logistics involved in handling large amounts of data, via magnetic tape on relatively 'weak' computers. However, with database management techniques used on computers capable of handling large amounts of I/O it seems prudent to use the actual flight data for both the stochastic and discrete CA/M disturbances.

V. Development of 'CREW'

The forcing function database was formed from all of the activities investigated during the flight experiment T-013, once the data tapes were acquired from NASA/GSFC. The experiment was conducted in a continuous manner, and after ground processing, all results were stored in one stream, requiring a breakdown of each event. The data from the tapes was broken down into the selected activities by following a chronological list of events for DOY 228 of the Skylab 3 mission. The data was seperated for each activity at its given start and stop time, as instructed by Conway.

For use with the pre-processor, the activities in the database are divided by physical description into three categories. The three categories are: 1 - respiration exercises (subject restrained), 2 - body movements (subject restrained), and 3 - soaring events.

The soaring portion of the experiment covered a larger time span, requiring breakdown into individual soaring events. Each of the four types of soaring were broken down into separate pairs involving a kickoff and the following landing (It should be noted that during experiment T-013, FMU #2 experienced a failure during a 'vigorous landing' by the test subject, thus the soaring data pairs were formed from FMU #1 data only). A section of the database contains the entire time span of each soaring category as one element for future use. One kickoff and landing pair was selected from each type of soaring as a representative example for analysis purposes.

The forcing function data is stored at a frequency of 10 Hz (unchanged from the original NASA/MSFC post-flight T-013 reduction effort) with six measurements pertaining to the three forces and three moments. An explanation of the data breakdown and force and moment plots for all T-013 CA/M activities are available in the 'CREW' User's Guide (ref. 14).

The major purpose of the menu-driven pre-processor is to build forcing function input files in the necessary format for dynamic analysis of a particular structural model. The program can output forcing function input formats for the following analysis routines: 1 - TRAP (Transient Response Analysis Program developed and used by JSC ES4), 2 - FRISBE (also developed and used by JSC/ES4), and 3 - NASTRAN. All three formats require similar user inputs which are: length of time for forcing function output file, requested activities (the number of selections is currently limited to five but can be increased), starting time, model node point (location), scaling values, and forcing function directions for each activity. The entire time span of an activity must be used, reduced time ranges are not available and the amount of data for the forcing function output file is limited to 250 seconds at this time. The output is available in both Fortran V and Fortran 77 while the program itself is written in Fortran 77. Output capabilities are discussed in further detail in the 'CREW' User's Guide along with examples.

There are three other options available from the 'CREW' pre-processor which complement the forcing function output routines. A helpful option is FORPLT, a plotting routine allowing the user to see the TRAP or FRISBE output graphically. The entire time span can be seen at once or in smaller time slices to improve clarity. The maximum and minimum force values are provided with the plot as an aid, and the model node point numbers for each forcing function activity are listed in a legend.

The two remaining options pertain to the individual activities of the database. The program allows the user to plot an individual activity, in its entirety, or selected time slices without building an output file. It also allows the user to dump the raw data from the database into a file for observation. Both options are discussed in detail in the User's Guide.

VI. CA/M Disturbance Analysis Example

The following analysis example has a dual purpose: (1) to demonstrate the use of 'CREW', and (2) to demonstrate the potential impact of CA/M on the Space Station microgravity environment. The results presented are preliminary and by no means represent the worst case for CA/M effects on the Station.

One of the expected disturbance sources of CA/M on the Space Station is that of a crew person undertaking a module to module transfer. A logical method for this crew translation would be to 'soar' from one node to another. Because of the fact that the laboratory modules will contain 'micro-g' sensitive payloads and/or experiments, it will be required to determine the vibration environment in those modules induced by CA/M such as a module to module transfer. Other areas of concern, in terms of Station vibration response to this type of CA/M will be the upper and lower booms, radiators, and the solar panels.

For comparison purposes, Station transient response induced by a crew person 'soaring' was generated from the following four different forcing function representations of an astronaut 'soaring':

1) Zero-g aircraft wall pushoff (ref. 11)
2) A first order soaring model used for preliminary CA/M analysis by the Space Station Program "Skunk Works" (ref. 15)
3) Soaring data from 'CREW'; normal force only
4) Soaring data from 'CREW'; all six components

For this analysis, a NASTRAN "stick" model of an early Dual Keel Space Station Configuration was used. The nine-foot deployable truss box-beam structure was represented by single NASTRAN CBAR elements with equivalent section properties (employing the so-called 'continuum' modeling philosophy often used for repeating truss structures). Radiators and solar panels were modeled as massless beams with concentrated masses located at each grid point. The modules and nodes were modeled by distributing one half of the mass in CBAR elements and concentrating the remaining mass at the geometric center of the module or node such that the given inertia properties were replicated.

For economy's sake, all of the NASTRAN runs utilized General Dynamic Reduction (Modified Givens) and modal methods ; extraction of normal modes for a frequency range of 0 to 2 Hz was selected based on an assumption that the error terms associated for the modal superposition method would not be dramatic (frequency content of the induced loads was 0.5 to 1.0 Hz). The analysis proceeded as follows:

1) Normal modes run (NASTRAN SOL 3)

2) Modal transient response (NASTRAN SOL 31), with 1% modal damping, from each type of soaring forcing function

3) Modal frequency response (NASTRAN SOL 30), again assuming 1% modal damping, using normalized force versus frequency from the T-013 normal force PSD (ref. 13) as excitation

From the normal modes run, 72 modes were extracted between 0.0 and 2.0 Hz. (with 51 between 0.0 and 1.0 Hz.). The lowest mode had a frequency of 0.14 Hz. and can be characterized, as expected, as a solar panel mast 'dominated' mode, as shown in Figure 5.

For each of the modal transient response runs, the soaring kickoff and landing were assumed to occur at grids 801002 and 800002, respectively; representing a module to module 'tunnel' transfer between habitation modules 1 and 2; see Figure 6. The kickoff and landing forcing functions are displayed in figures 7 through 9 for each type of soaring investigated. It should be noted that Figure 9 was generated by the program 'CREW', to serve as an example of its preprocessing capabilities.

Table 4 contains maximum acceleration values, in micro-g's, for each of the soaring types at various locations of the Dual Keel stick model; refer to Figures 6 and 10 for the grid point locations. Reviewing the tabulated values leads to the observation that both the zero-g aircraft and the first order model soaring representations yield response levels at least two times smaller in the Y axis direction than the T-013 representation, due to the fact that the peak and peak to peak values for the forcing functions exhibit the

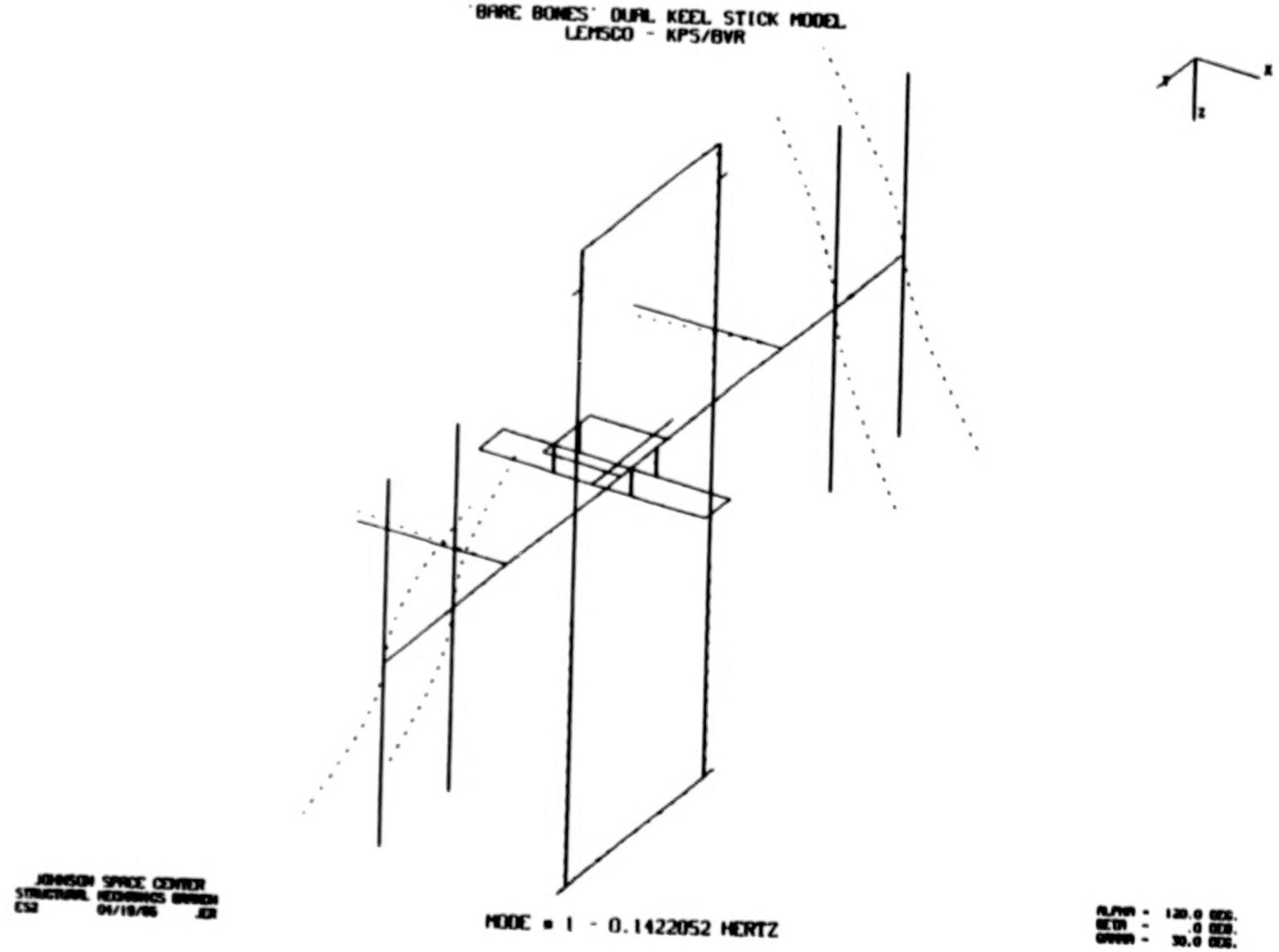
'BARE BONES' DUAL KEEL STICK MODEL
LEMSCO - KPS/BVR
X
Y
Z
JOHNSON SPACE CENTER
STRUCTURAL MECHANICS BRANCH
ES2 04/18/86 JER
MODE = 1 - 0.1422052 HERTZ
ALPHA - 120.0 DEG.
BETA - .0 DEG.
GAMMA - 30.0 DEG.

Figure 5

DUAL KEEL STICK MODEL
SOARING TRANSIENT RESPONSE
MODULE GRID LOCATIONS

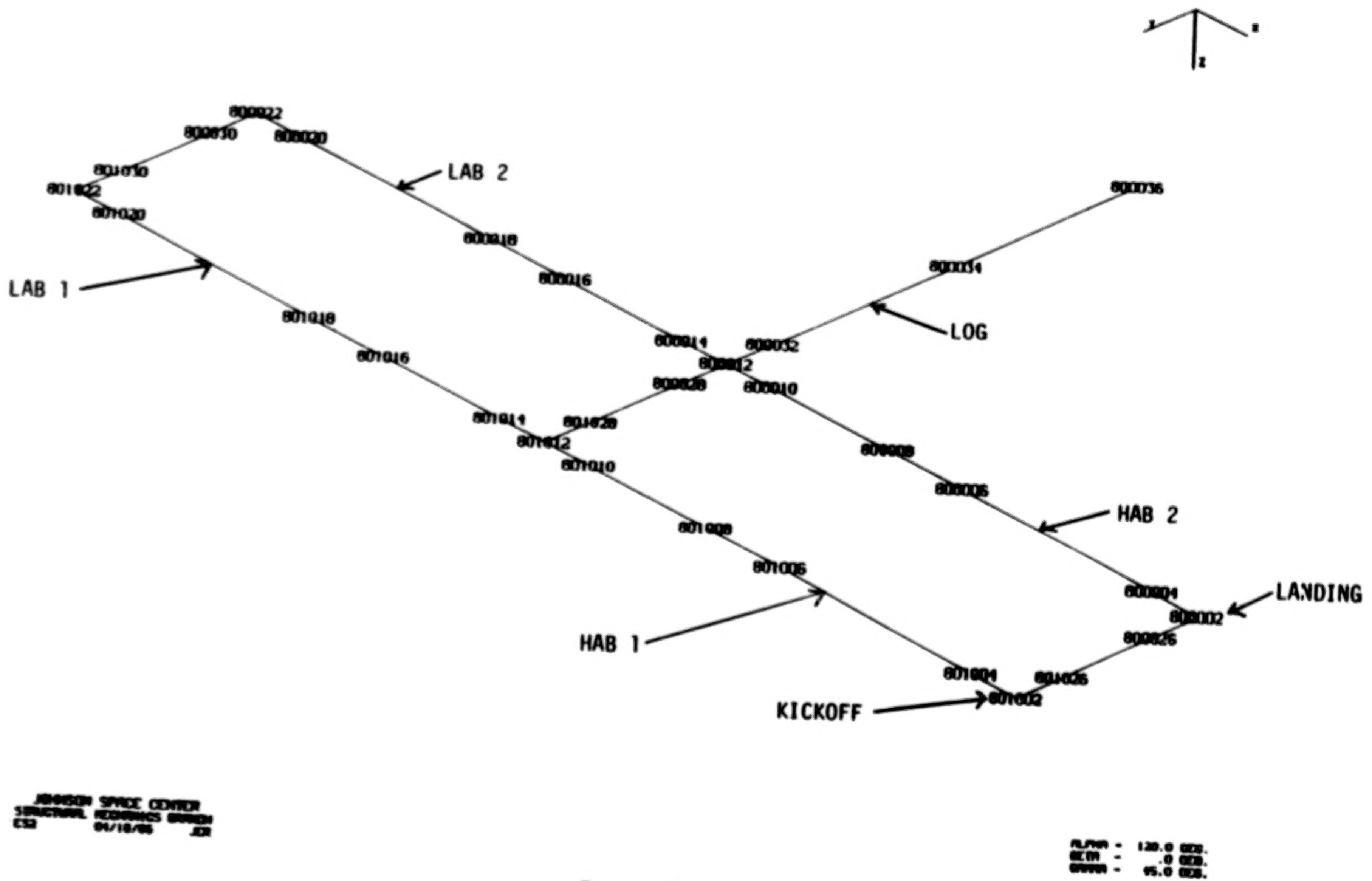
Y
X
Z
800022
800030
800020
801030
801022
801020
LAB 2
LAB 1
800018
800016
801018
801016
800014
800032
800012
800028
800010
LOG
800034
800036
801014
801028
801012
801010
800008
800006
HAB 2
801008
801006
HAB 1
800004
800002
LANDING
800026
801004
801026
801002
KICKOFF
JOHNSON SPACE CENTER
STRUCTURAL MECHANICS BRANCH
ES2 04/18/86 JER
ALPHA - 120.0 DEG.
BETA - .0 DEG.
GAMMA - 45.0 DEG.

Figure 6

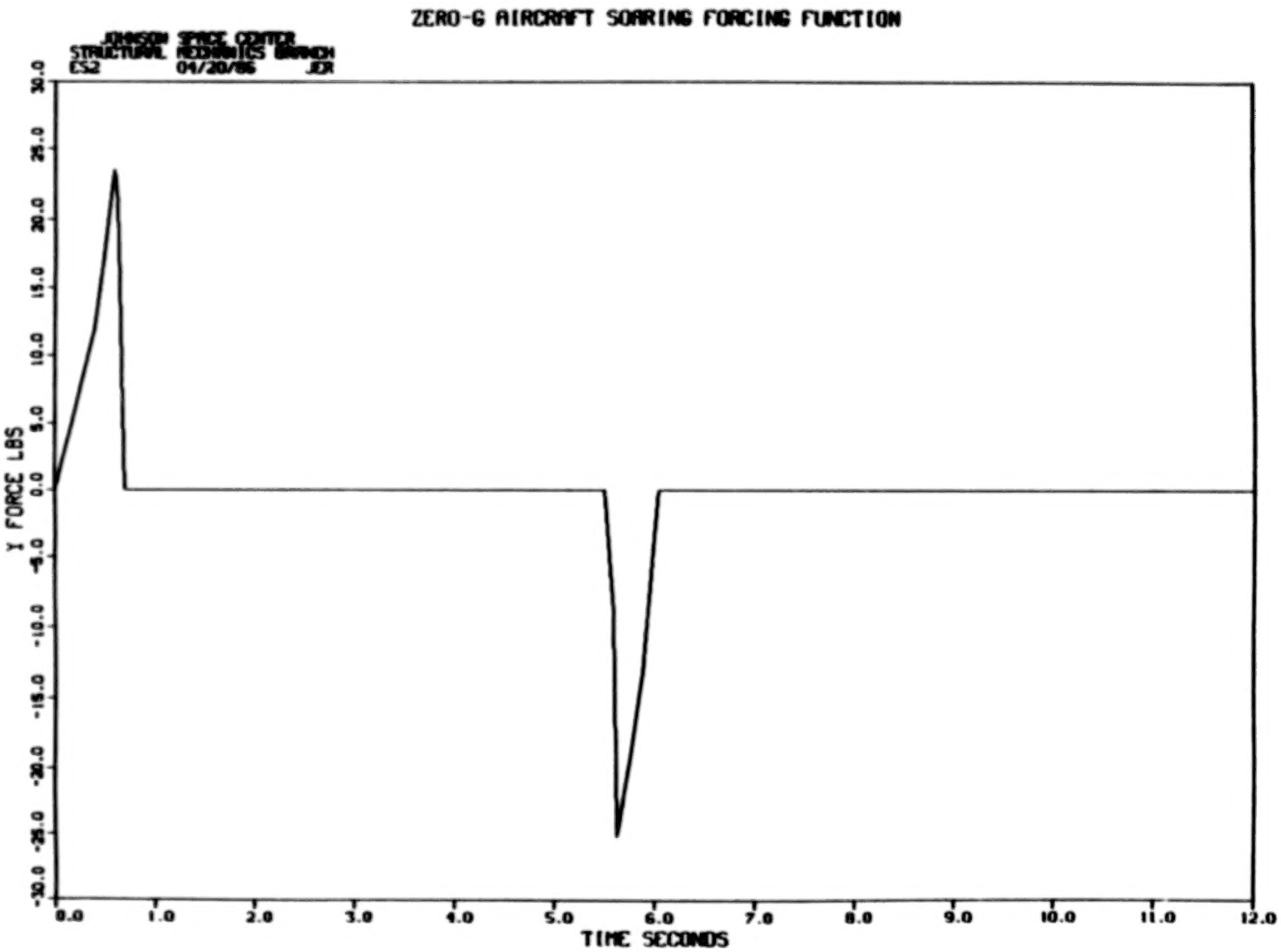
ZERO-G AIRCRAFT SOARING FORCING FUNCTION
JOHNSON SPACE CENTER
STRUCTURAL MECHANICS BRANCH
ES2 04/20/86 JER
Y FORCE LBS
30.0
25.0
20.0
15.0
10.0
5.0
0.0
-5.0
-10.0
-15.0
-20.0
-25.0
-30.0
0.0
1.0
2.0
3.0
4.0
5.0
6.0
7.0
8.0
9.0
10.0
11.0
12.0
TIME SECONDS

Figure 7

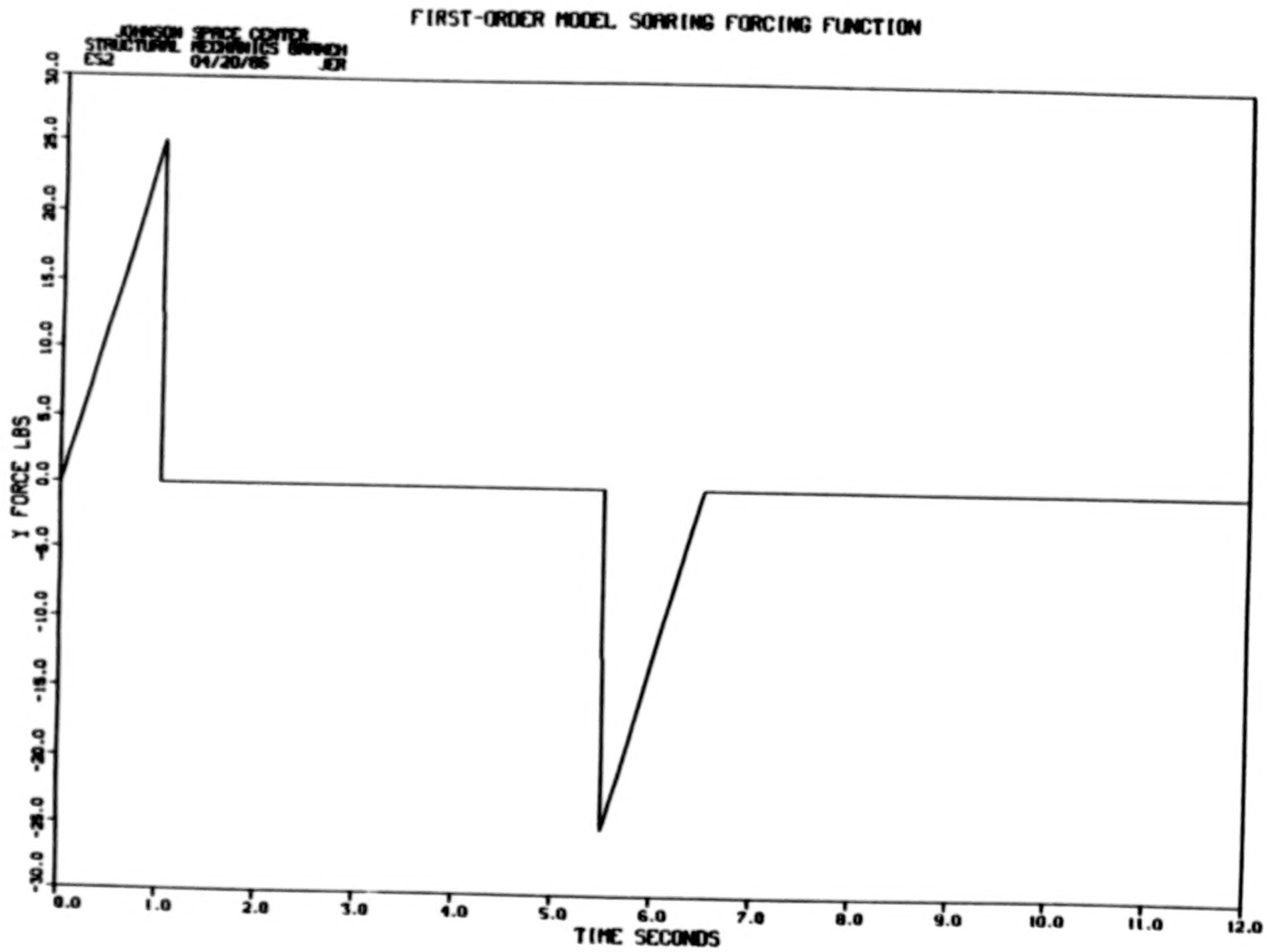
FIRST-ORDER MODEL SOARING FORCING FUNCTION
JOHNSON SPACE CENTER
STRUCTURAL MECHANICS BRANCH
ES2
04/20/86
JER
Y FORCE LBS
30.0
25.0
20.0
15.0
10.0
5.0
0.0
-5.0
-10.0
-15.0
-20.0
-25.0
-30.0
TIME SECONDS
0.0
1.0
2.0
3.0
4.0
5.0
6.0
7.0
8.0
9.0
10.0
11.0
12.0

Figure 8

CREW DISTURBANCE FORCING FUNCTION
DUAL KEEL STICK MODEL
T-013 KICKOFF & LANDING
ONEMAN FORCEFUL SOARING
MAX VALUE - 15.30 AT 6.50 SECONDS
MIN VALUE - -12.65 AT 2.20 SECONDS

LOCKHEED-EMSCO
BVR
04/20/86

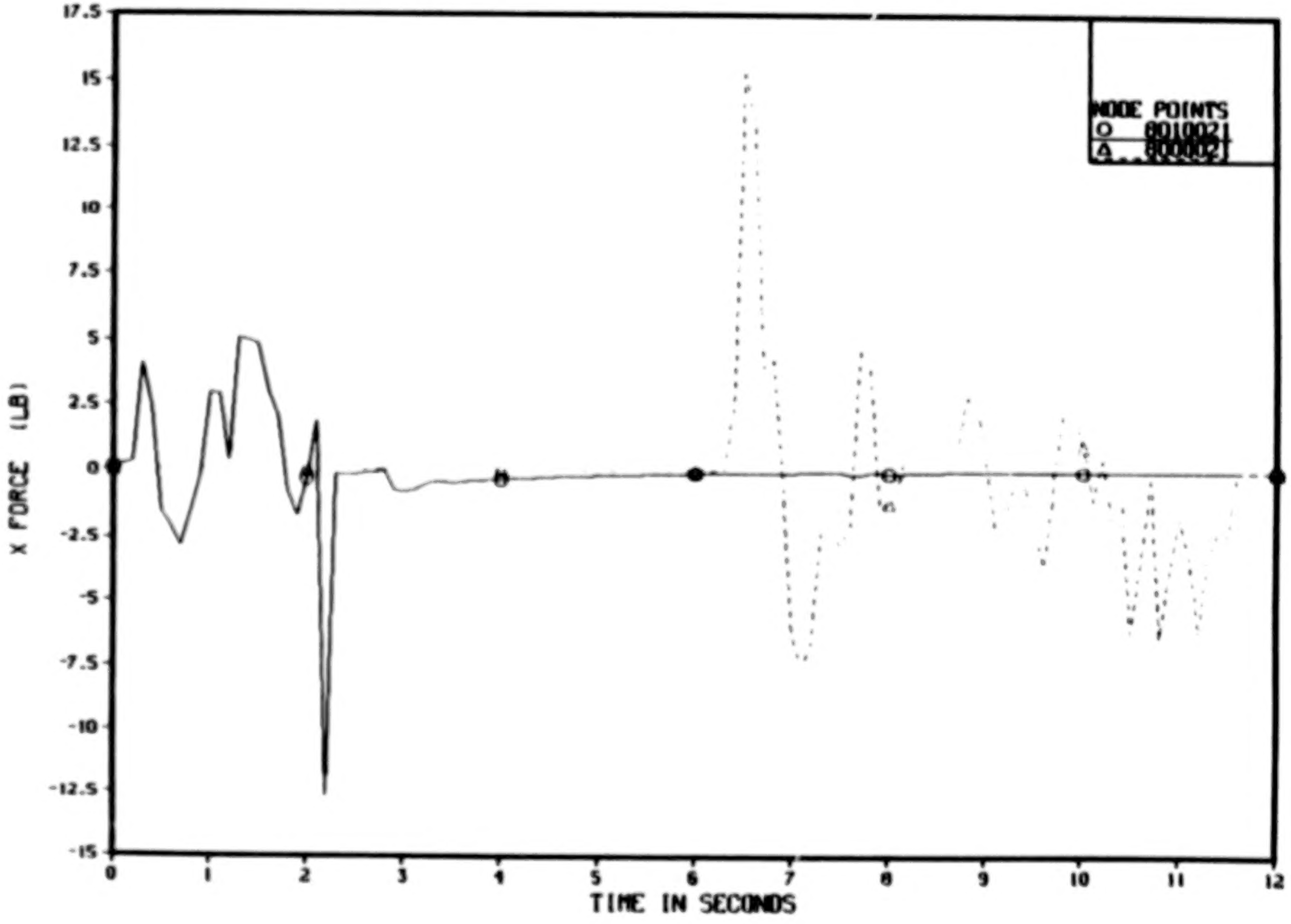

Figure 9

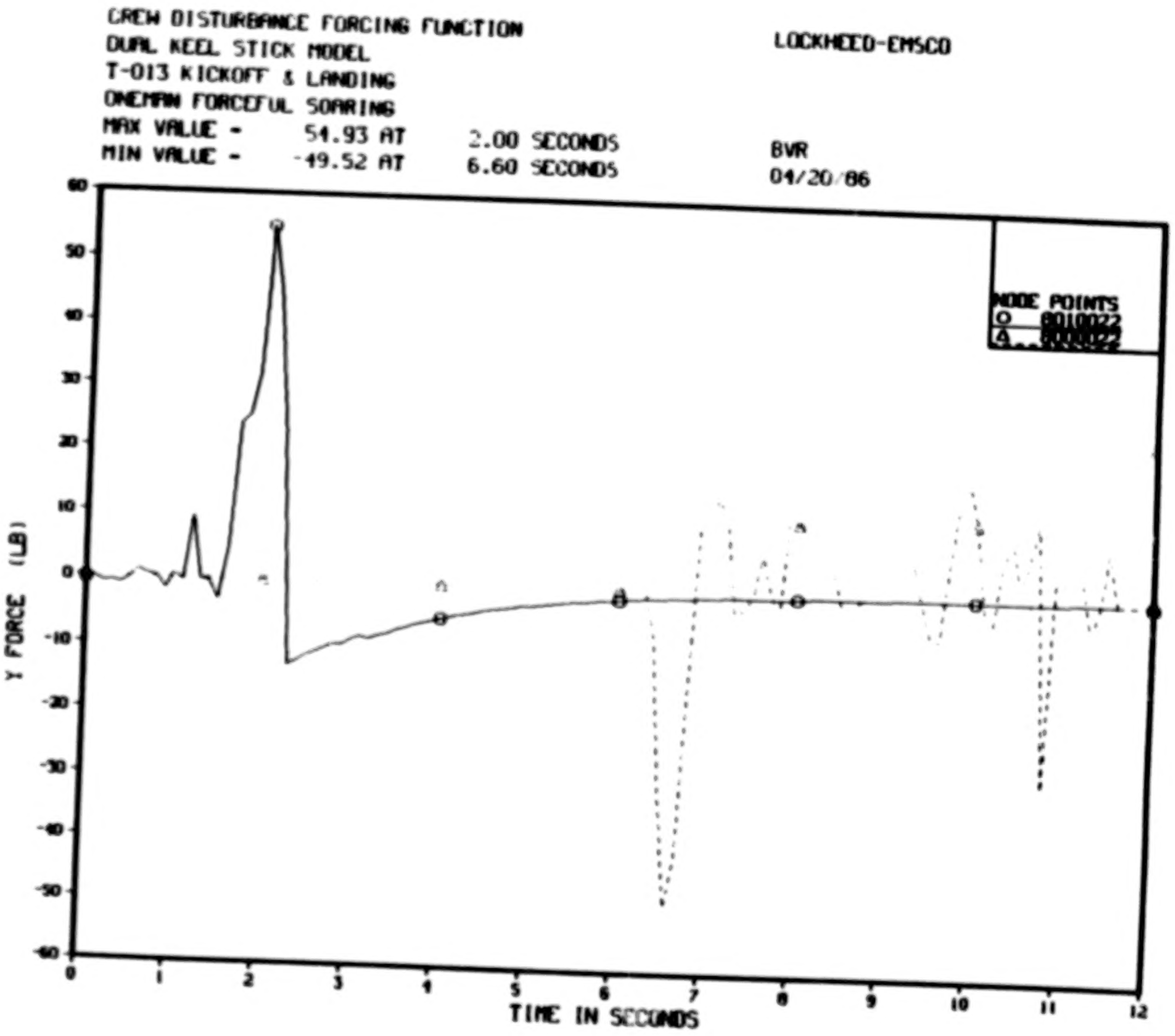

Figure 9 cont.

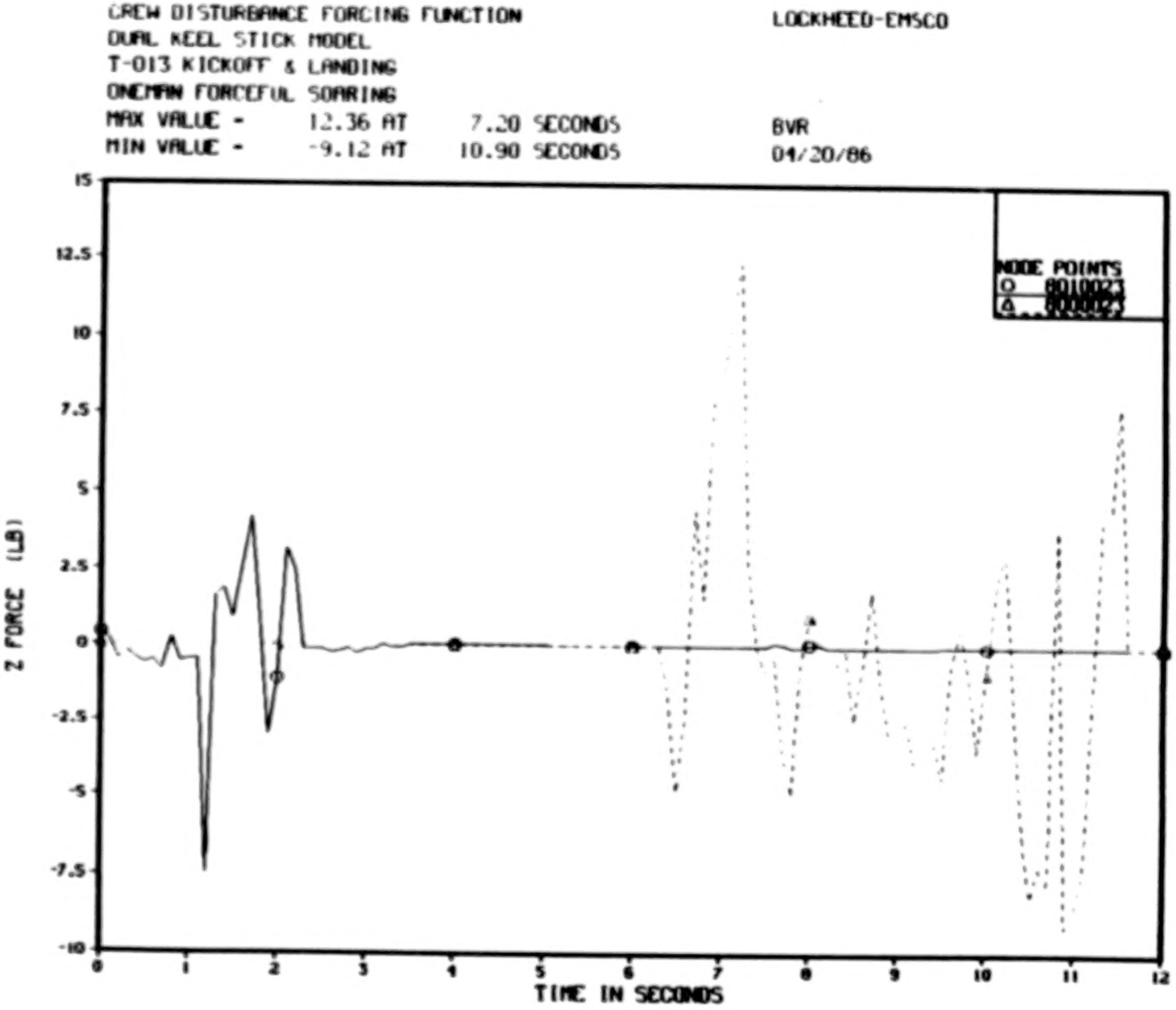

Figure 9 cont.

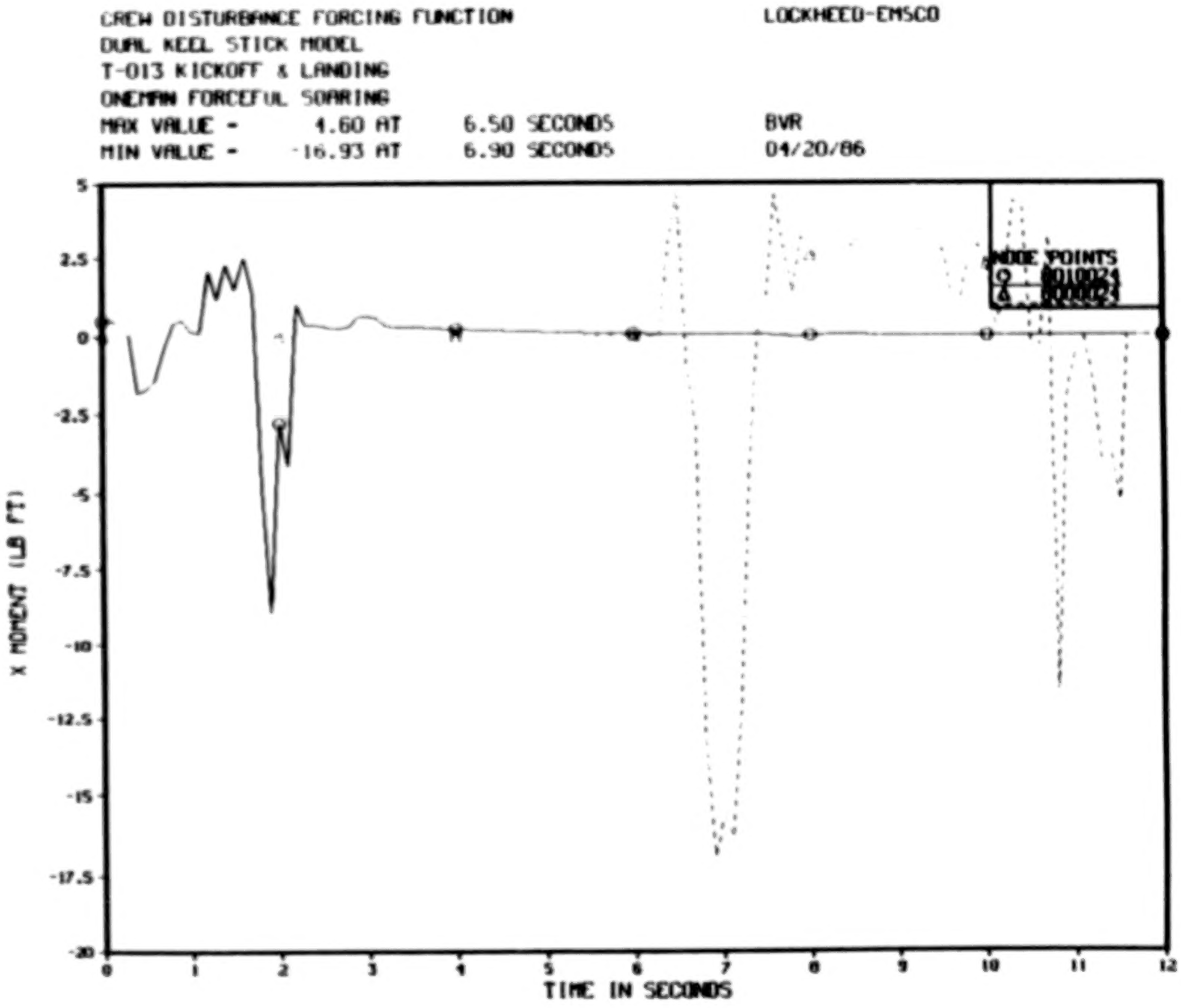

Figure 9 cont.

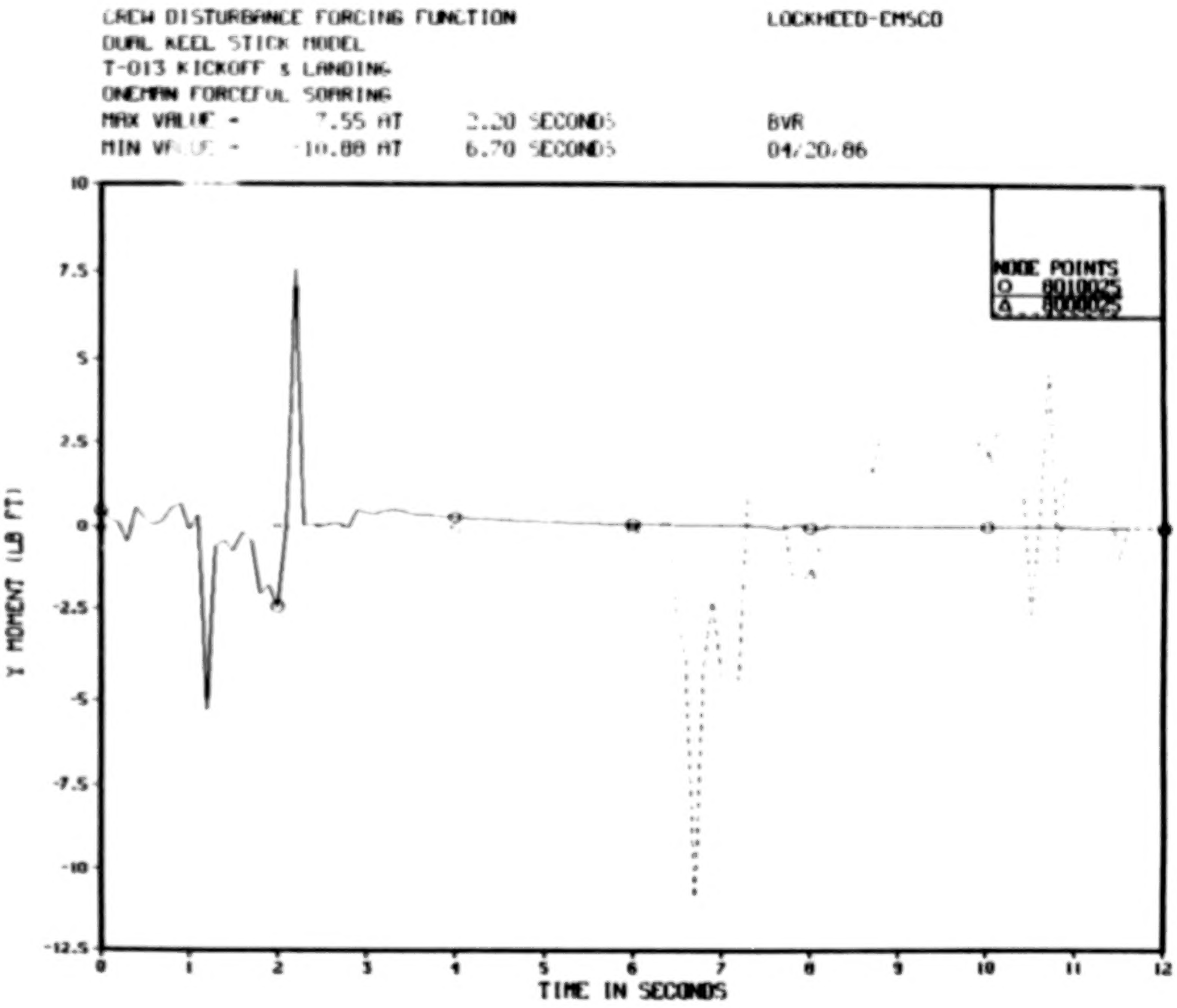

Figure 9 cont.

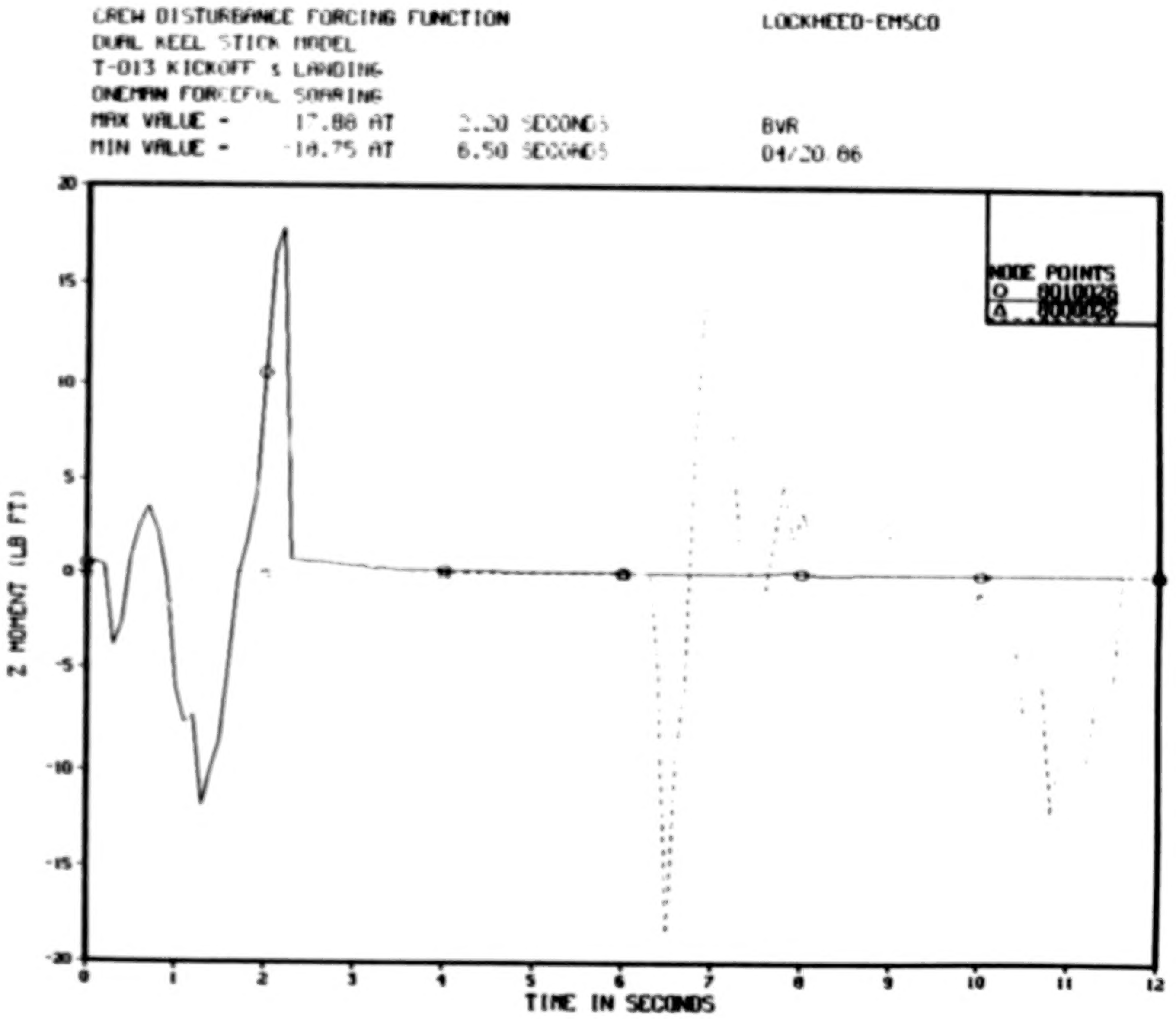

Figure 9 concluded

ORIGINAL PAGE IS
OF POOR QUALITY

DUAL KEEL STICK MODEL
SOARING TRANSIENT RESPONSE
GRID LOCATIONS

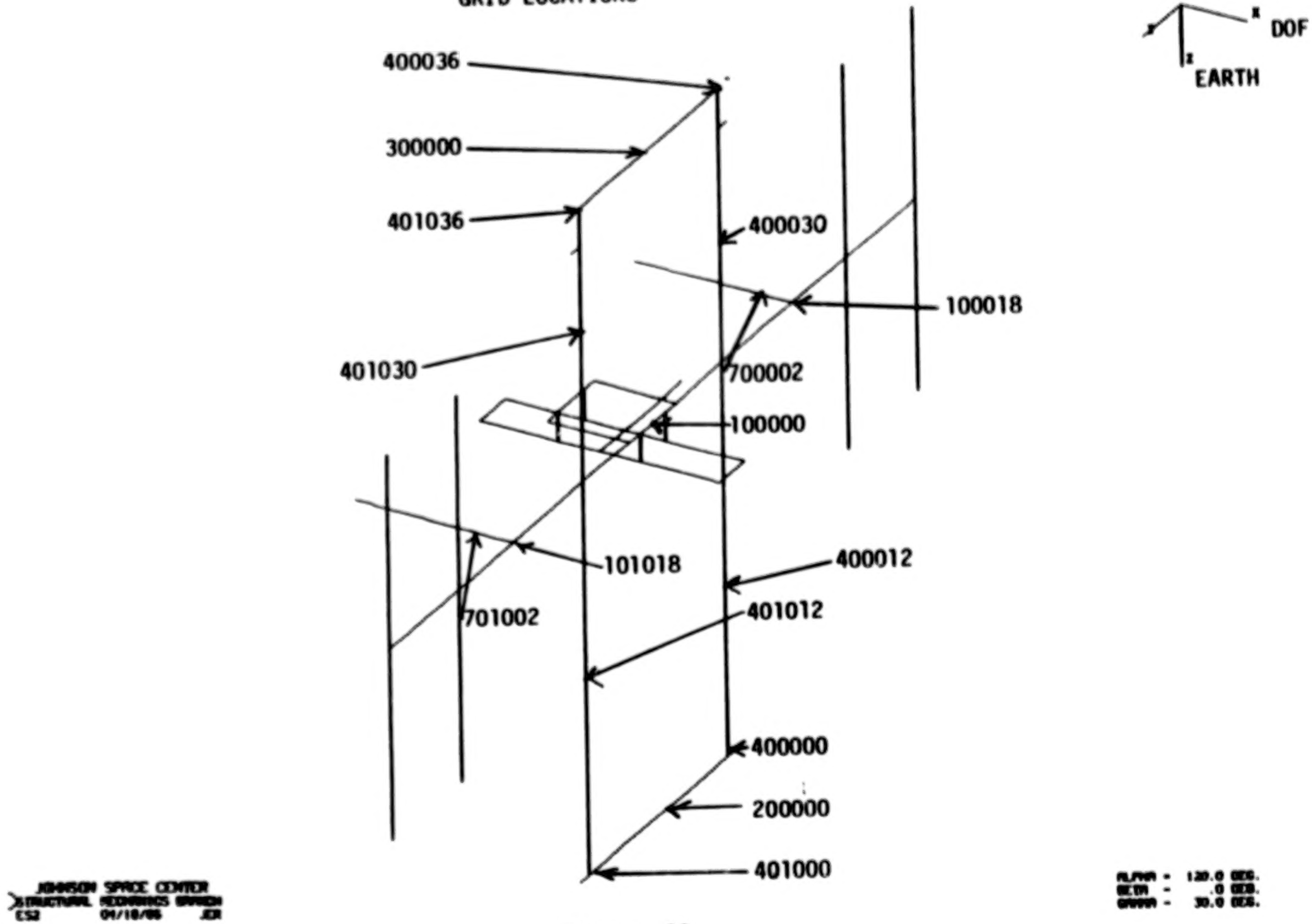
DOF
EARTH
x
y
z
400036
300000
401036
400030
100018
401030
700002
100000
101018
400012
701002
401012
400000
200000
401000
JOHNSON SPACE CENTER
STRUCTURAL MECHANICS BRANCH
ES2 04/10/86 JER
ALPHA - 120.0 DEG.
BETA - .0 DEG.
GAMMA - 30.0 DEG.

Figure 10

TABLE#4
DUAL KEEL 'CREW KO/LAND' RESPONSE
(PRELIMINARY RESULTS)
MAX ACCELERATION (MICRO - G'S)

LOCATION/ GRID	T-013 (ALL)			T-013 (NORMAL ONLY)		
	X	Y	Z	X	Y	Z
TRANSVERSE BOOM						
100000	68.18	344.27	105.24	44.43	347.49	17.72
100018	625.89	343.16	163.96	666.29	346.56	137.72
101018	714.54	343.08	137.73	684.02	346.49	96.37
LOWER BOOM						
200000	538.63	973.83	94.14	52.81	948.27	19.76
400000	1047.21	973.56	125.48	756.63	947.95	58.38
401000	1239.69	973.59	106.44	830.98	947.98	84.99
UPPER BOOM						
300000	295.04	757.31	93.91	133.45	753.19	19.65
400036	1251.72	756.97	128.57	1131.05	752.84	63.62
401036	1134.10	756.87	112.47	1123.09	752.79	88.56
KEELS						
400012	526.93	561.87	127.05	406.40	555.47	60.37
401012	557.49	578.66	109.11	448.97	557.69	86.87
400030	1025.59	677.14	128.58	924.23	671.36	63.13
401030	919.05	672.80	112.32	942.48	669.29	88.60
RADIATOR MASTS						
700002	625.89	329.10	158.17	666.30	332.67	148.40
701002	714.54	336.00	125.67	684.03	335.92	100.86
LAB MODULES						
800014 (2)	66.26	173.83	47.47	60.95	173.28	21.07
801014 (1)	155.34	173.96	55.62	146.80	173.39	45.29
800022 (2)	66.28	495.34	101.49	60.97	488.77	32.00
801022 (1)	155.37	495.35	148.93	146.84	488.77	39.42
HAB MODULES						
800002 (2)	66.27	639.94	215.09	60.97	632.25	7.86
801002 (1)	155.37	639.94	207.95	146.83	632.25	55.06
800006 (2)	66.26	422.41	136.44	60.97	415.16	10.65
801006 (1)	155.36	422.13	134.54	146.82	414.96	48.38
LOGISTICS MODULE						
800032	111.10	213.62	72.30	114.73	212.00	36.99
800036	550.74	213.62	220.34	548.81	212.00	189.50

TABLE 4 (con't)
DUAL KEEL 'CREW KO/LAND' RESPONSE
(PRELIMINARY RESULTS)
MAX ACCELERATION (MICRO - G'S)

LOCATION/ GRID	ZERO-G AIRCRAFT			FIRST ORDER MODEL		
	X	Y	Z	X	Y	Z
TRANSVERSE BOOM						
100000	13.94	166.09	6.97	12.28	122.96	7.41
100018	165.15	164.64	57.56	252.88	122.97	56.29
101018	179.84	164.55	46.22	265.13	122.97	42.83
LOWER BOOM						
200000	17.04	259.01	8.78	22.12	387.00	9.50
400000	341.02	258.91	33.63	207.48	387.87	34.70
401000	368.03	258.92	36.43	220.87	387.88	45.25
UPPER BOOM						
300000	38.32	299.81	8.70	43.02	255.96	9.42
400036	363.19	299.68	35.79	362.68	255.82	37.80
401036	404.44	299.65	38.59	358.84	255.80	48.33
KEELS						
400012	163.55	148.37	34.23	99.29	198.97	35.91
401012	173.51	151.87	37.04	111.16	200.95	46.45
400030	292.24	266.30	35.58	301.06	217.22	37.65
401030	321.96	265.22	38.39	296.61	216.30	48.19
RADIATOR MASTS						
700002	165.15	136.21	63.44	252.88	99.80	50.04
701002	179.84	136.22	47.32	265.13	99.60	46.74
LAB MODULES						
800014 (2)	23.03	80.27	8.39	17.30	86.83	8.95
801014 (1)	51.56	80.39	17.96	41.68	86.91	19.09
800022 (2)	23.04	102.94	12.10	17.31	146.01	12.83
801022 (1)	51.57	102.94	16.82	41.69	146.01	18.09
HAB MODULES						
800002 (2)	23.04	300.00	3.28	17.31	215.59	4.05
801002 (1)	51.57	300.00	21.99	41.68	215.59	23.66
800006 (2)	23.03	199.92	3.56	17.31	156.58	5.53
801006 (1)	51.56	199.73	19.08	41.68	156.40	20.74
LOGISTICS MODULE						
800032	42.35	99.47	14.97	32.64	97.00	16.01
800036	197.63	99.48	79.93	157.26	97.00	86.03

same relationship. For the X znd Z axis directions, the T-013 soaring, with all six components, yields response at least three times greater than the zero-g aircraft and first order model representations. The response in the laboratory modules is assumed to have the highest priority, so Figures 11 through 14 display the transient acceleration response (in micro-g's) at laboratory module one (grid 801022) to each of the soaring types.

For the modal frequency response analysis, a normalized force versus frequency excitation was derived from a PSD of the T-013 one man forceful soaring normal (Y axis) forcing function data; see Figures 15 and 16. The modal acceleration response (normalized) to this excitation at laboratory module one is shown in Figure 17. The X and Y axis response is dominated by modes 16 and 26, while the Z axis response is dominated by modes 26, 27, 34, 35, 49, 54, and 63. These mode shapes are shown in figures 18 through 26, and for the most part are primary structure modes coupled with solar array motion.

In terms of 'accuracy of representation', for the CA/M disturbances, it is believed that the T-013 data is the best because of its 'exact' magnitude and frequency characteristics. Furthermore, the T-013 data should be employed simply because it represents a nominal CA/M disturbance case, whereas the other 'models' probably better represent the middle of the CA/M spectrum in terms of magnitude.

Finally, the preliminary results presented above (T-013 soaring response) are somewhat dramatic; implying that 'a conflict of interest' may exist for a manned Station requiring a pure micro-g environment (based on a 'bare bones' Space Station with the nine-foot truss and having a mass of approx. 300,000 lbs).

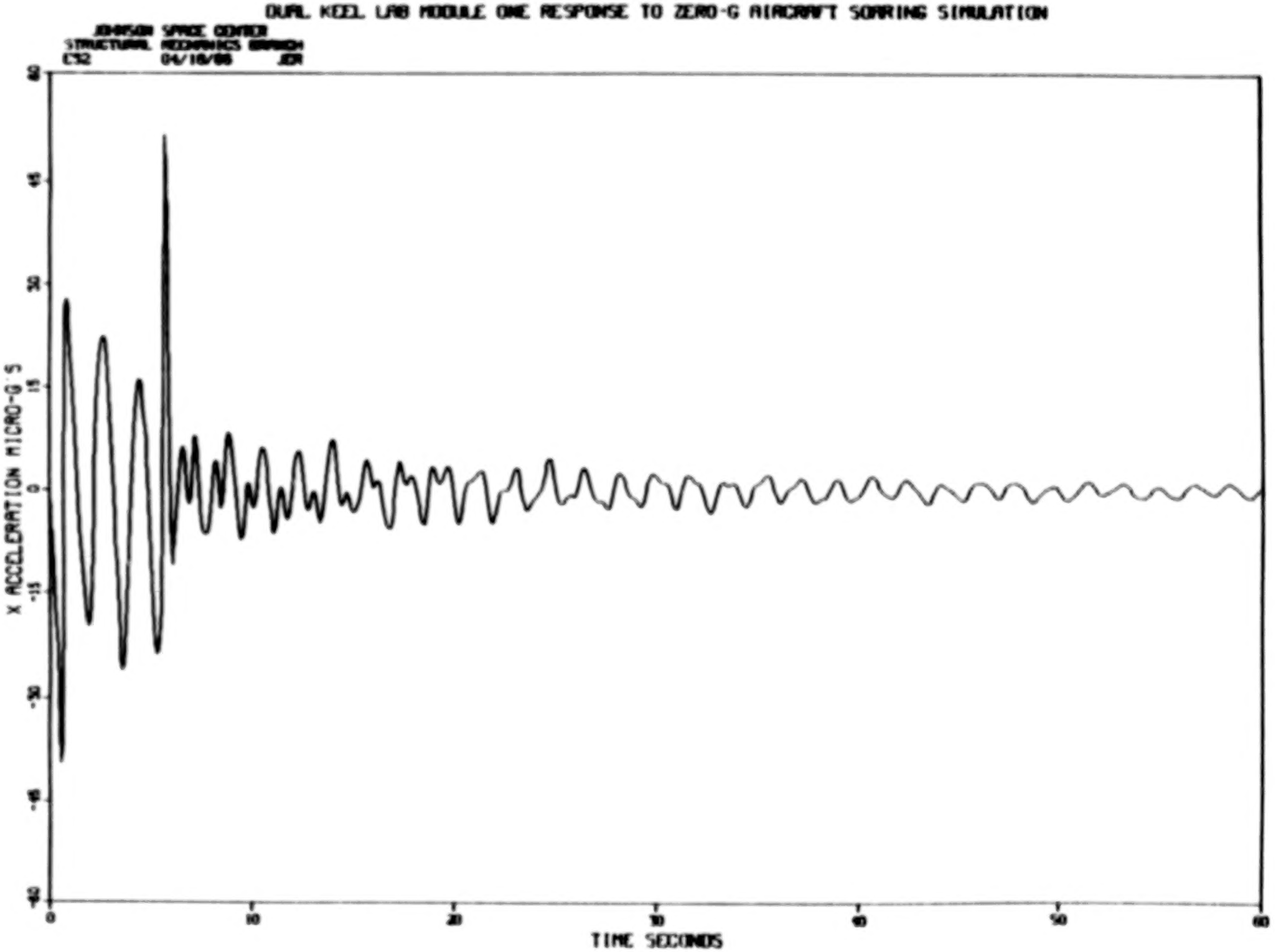
DUAL KEEL LAB MODULE ONE RESPONSE TO ZERO-G AIRCRAFT SOARING SIMULATION
JOHNSON SPACE CENTER
STRUCTURAL MECHANICS BRANCH
ES2 04/18/88 JER
X ACCELERATION MICRO-G'S
60
45
30
15
0
-15
-30
-45
-60
TIME SECONDS
0
10
20
30
40
50
60

Figure 11

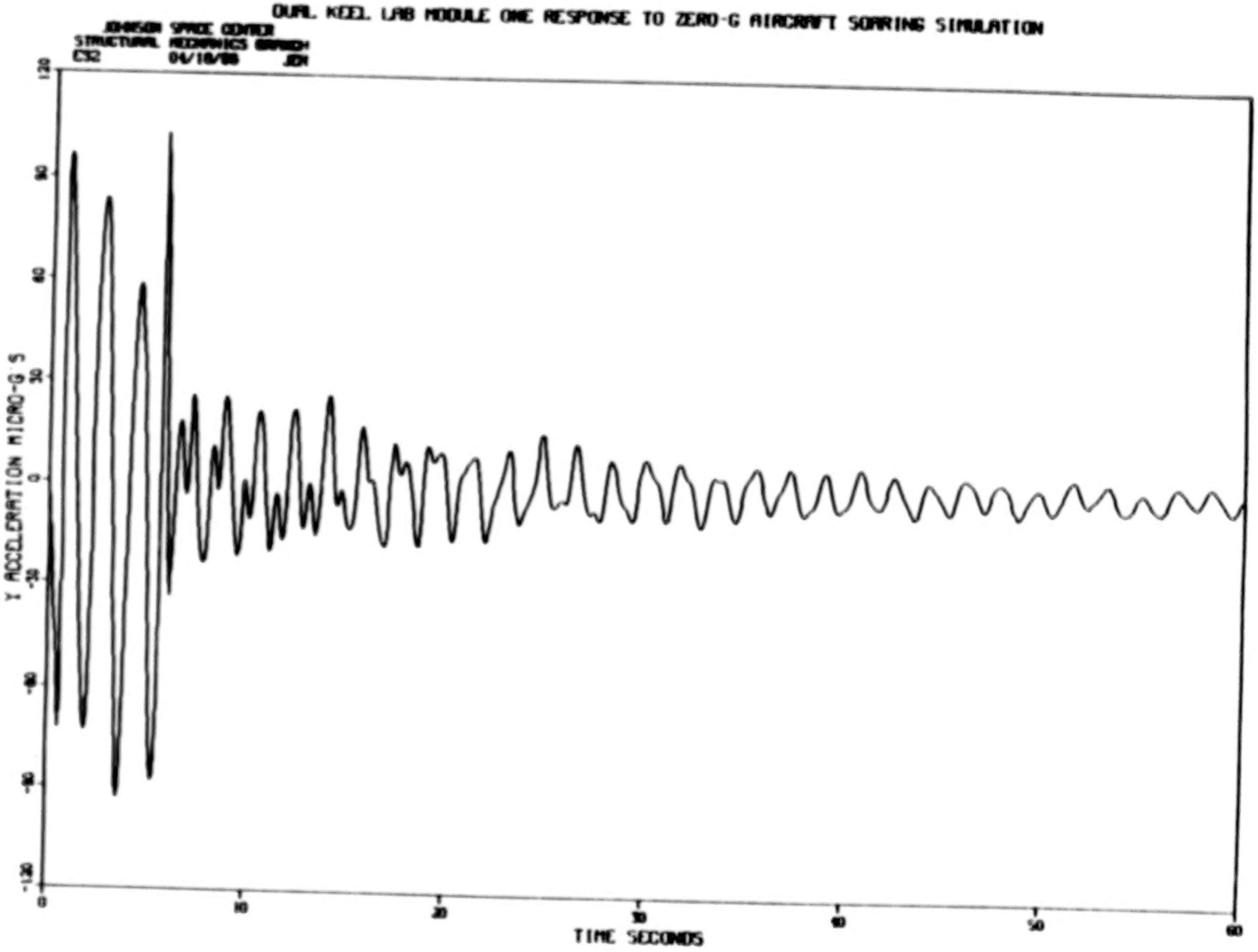

Figure 11 cont.

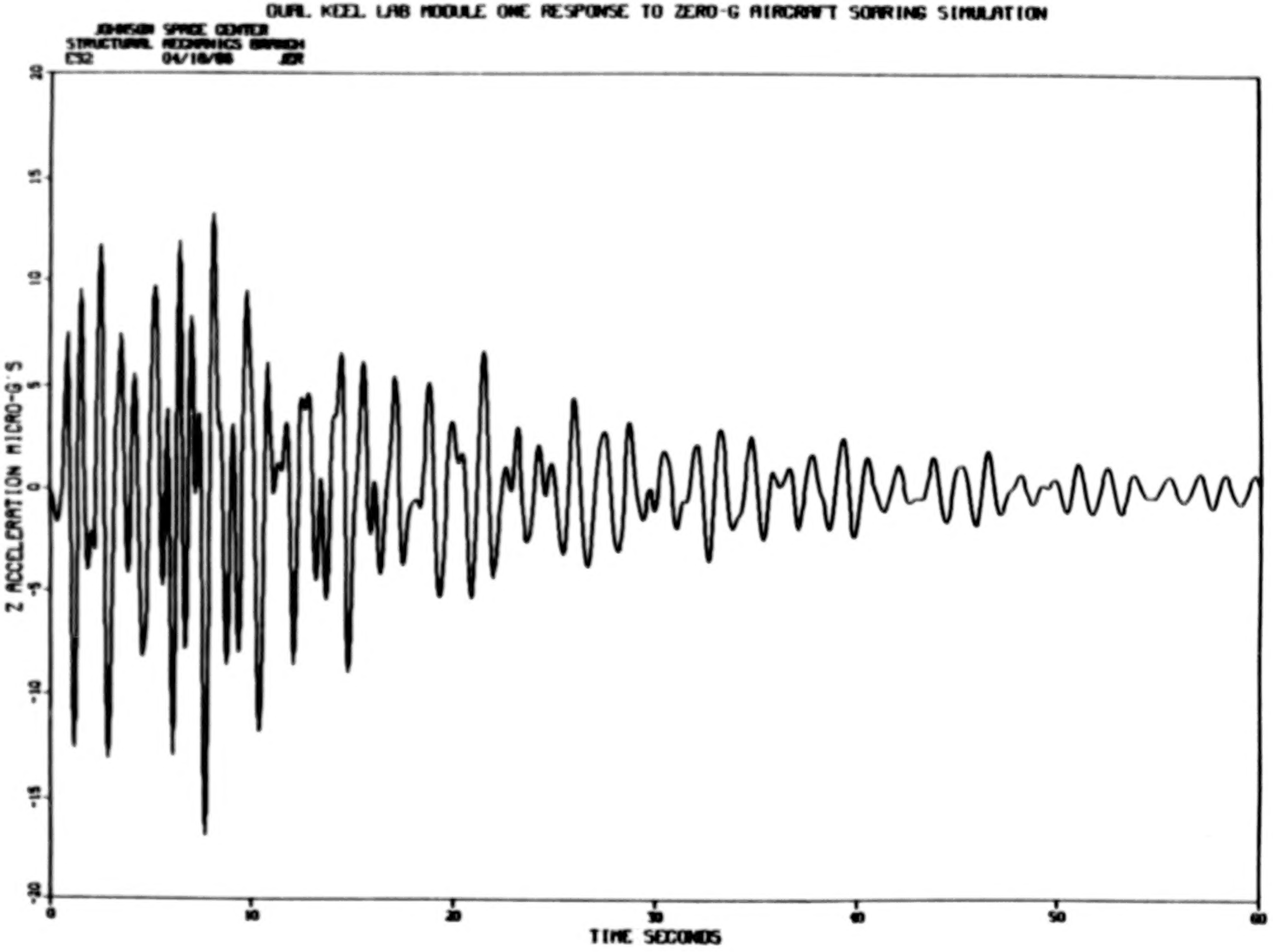

Figure 11 concluded

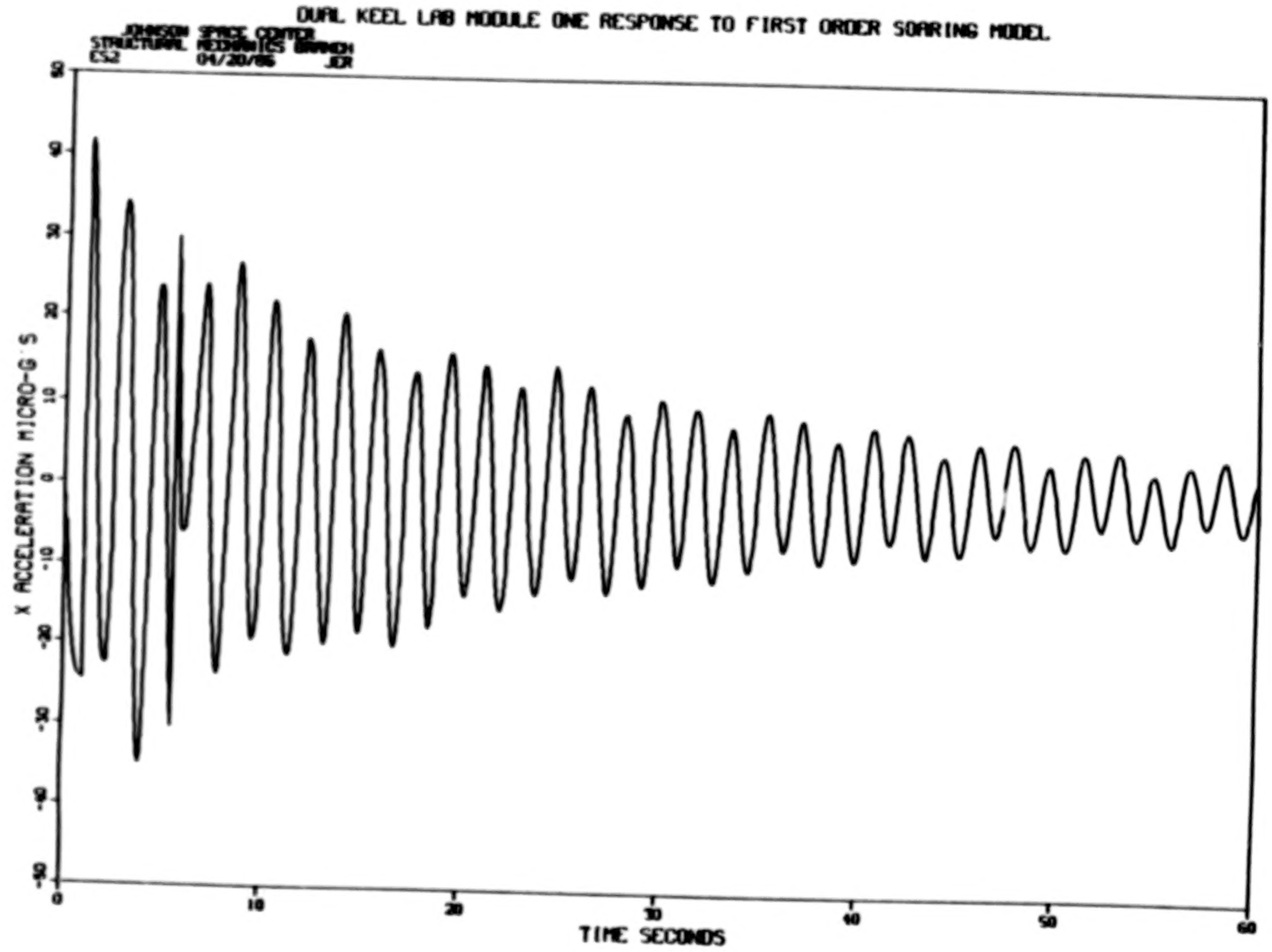
DUAL KEEL LAB MODULE ONE RESPONSE TO FIRST ORDER SOARING MODEL
JOHNSON SPACE CENTER
STRUCTURAL MECHANICS BRANCH
ES2 04/20/86 JER
X ACCELERATION MICRO-G'S
50
40
30
20
10
0
-10
-20
-30
-40
-50
0
10
20
30
40
50
60
TIME SECONDS

Figure 12

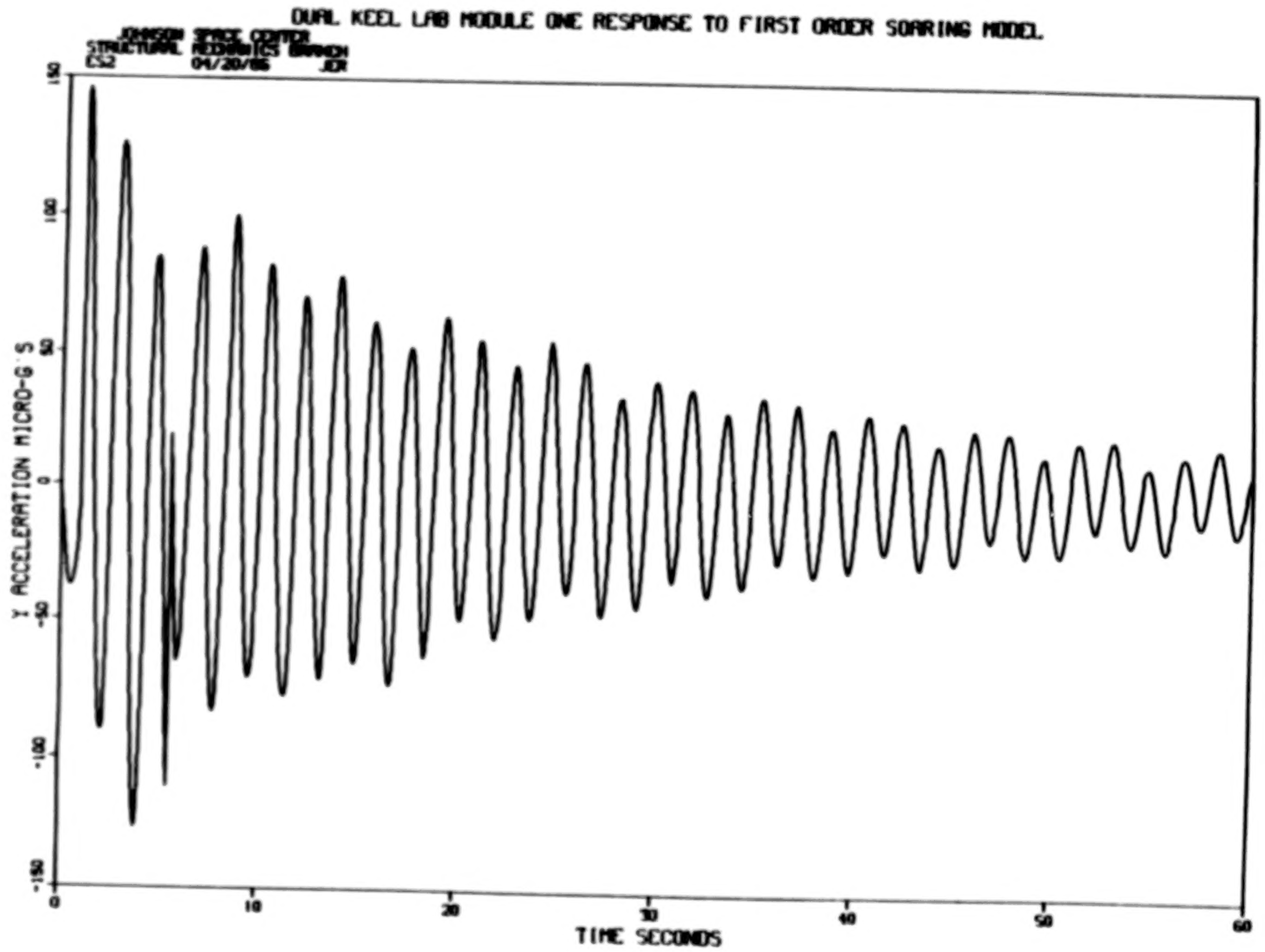

Figure 12 cont.

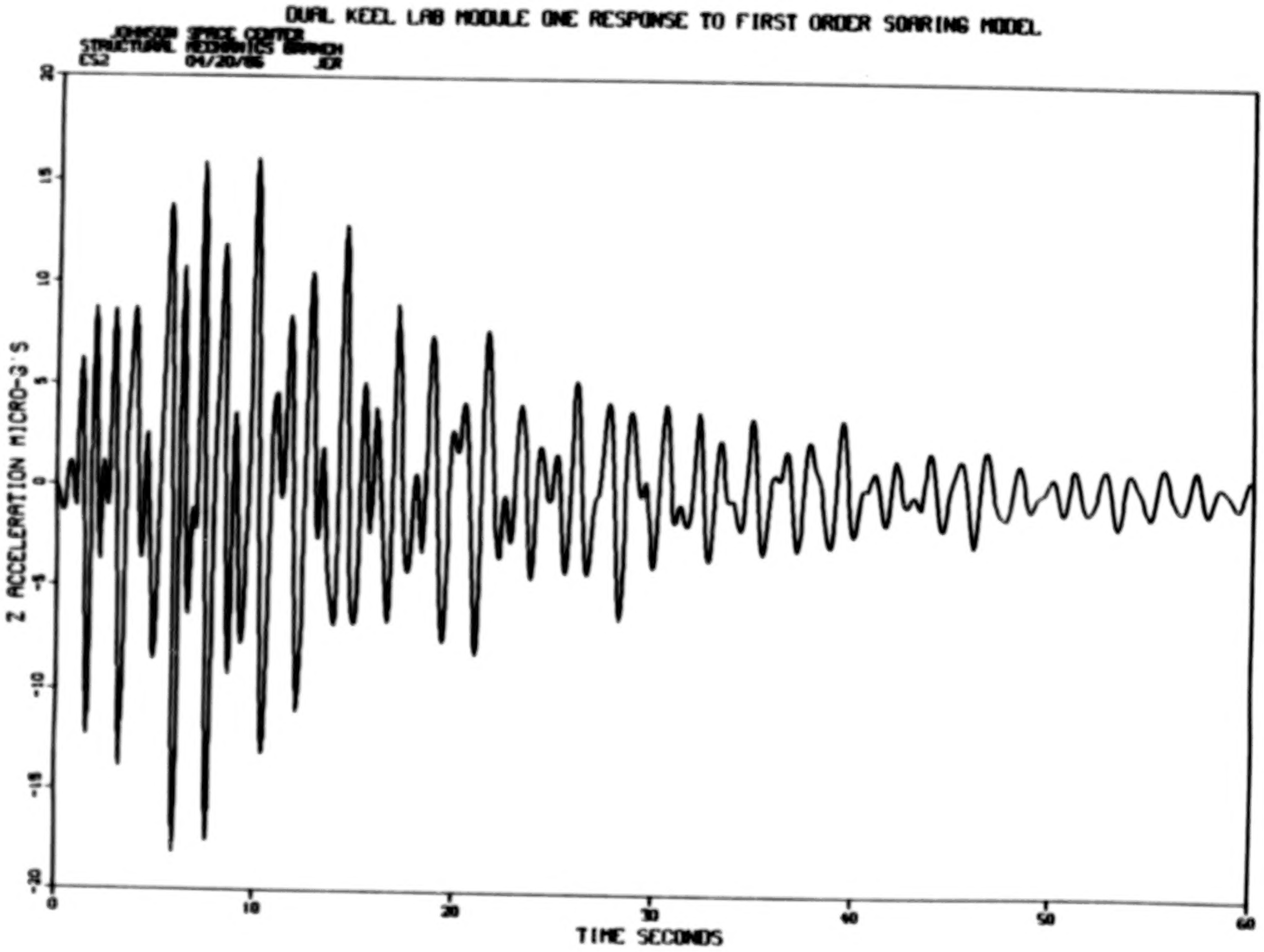

Figure 12 concluded

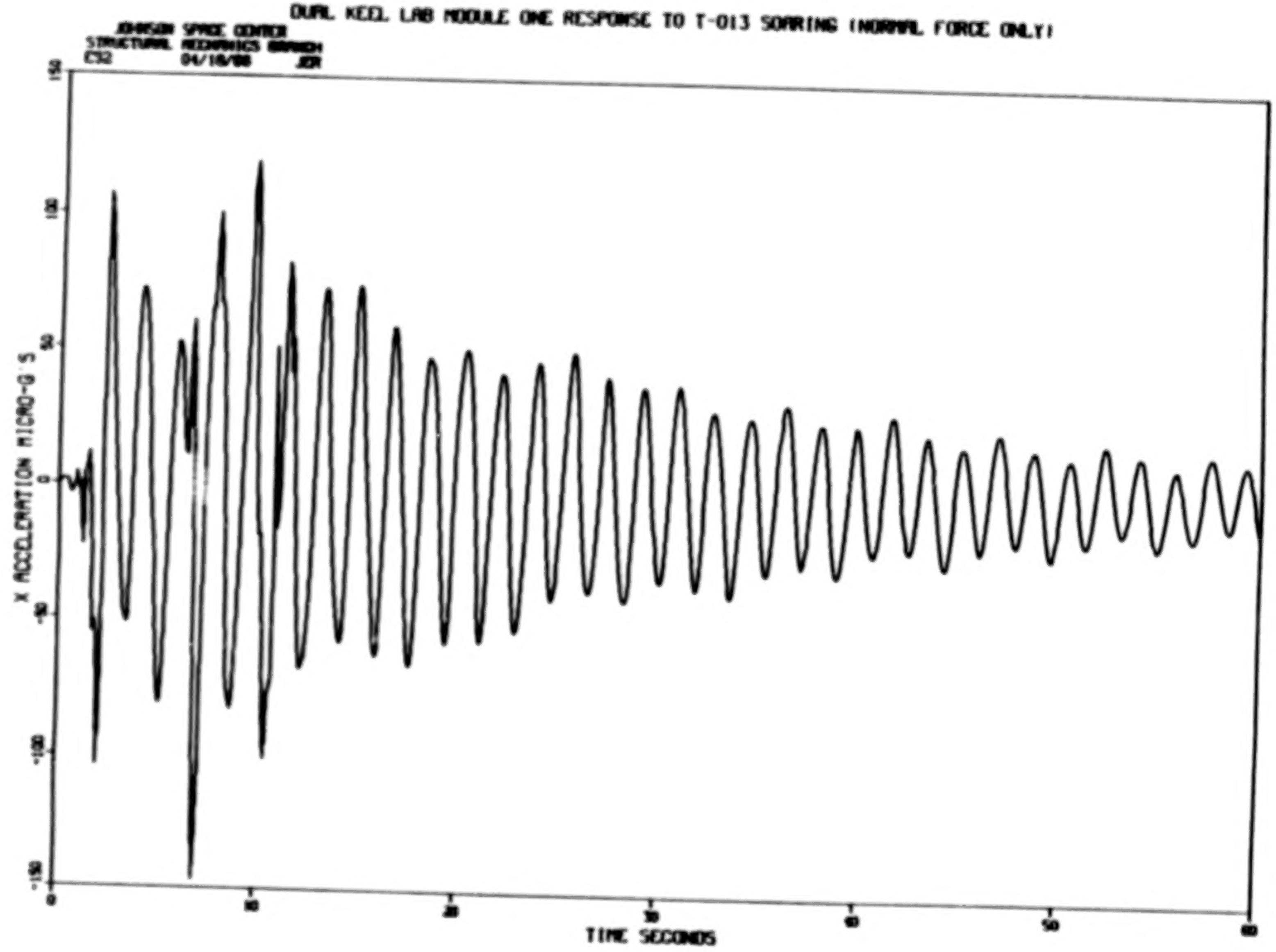
DUAL KEEL LAB MODULE ONE RESPONSE TO T-013 SOARING (NORMAL FORCE ONLY)

Figure 13

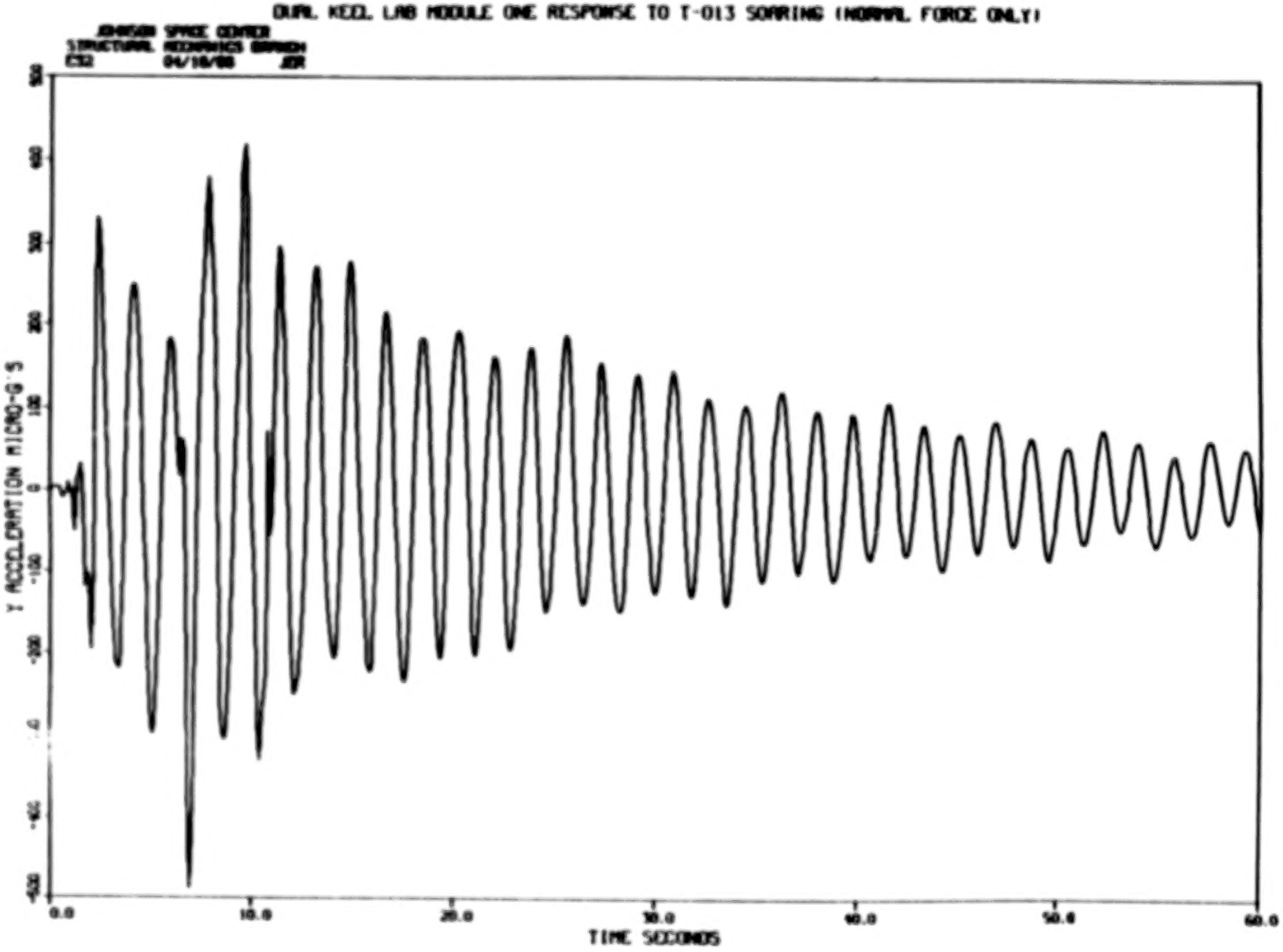

Figure 13 cont.

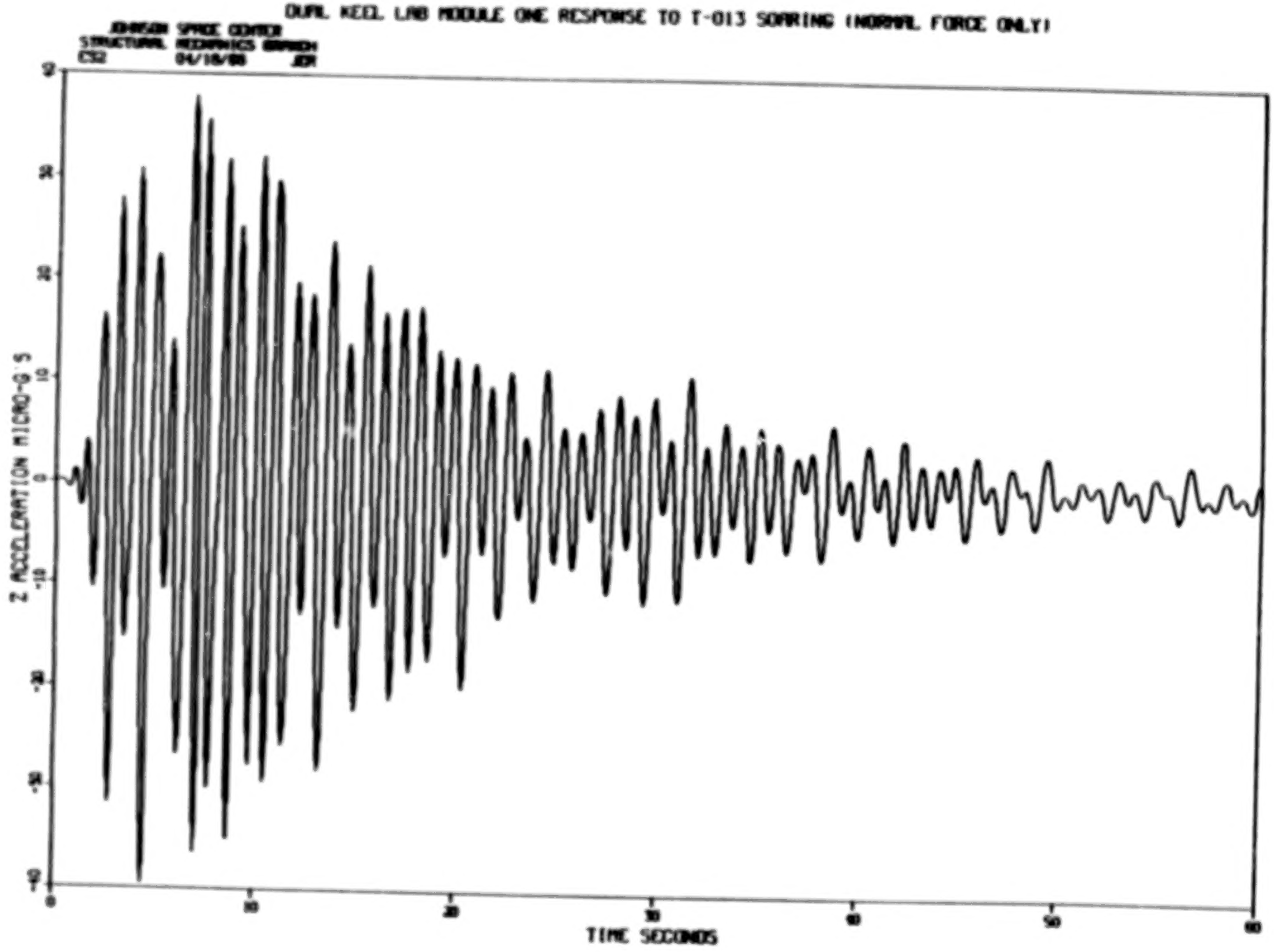

Figure 13 concluded

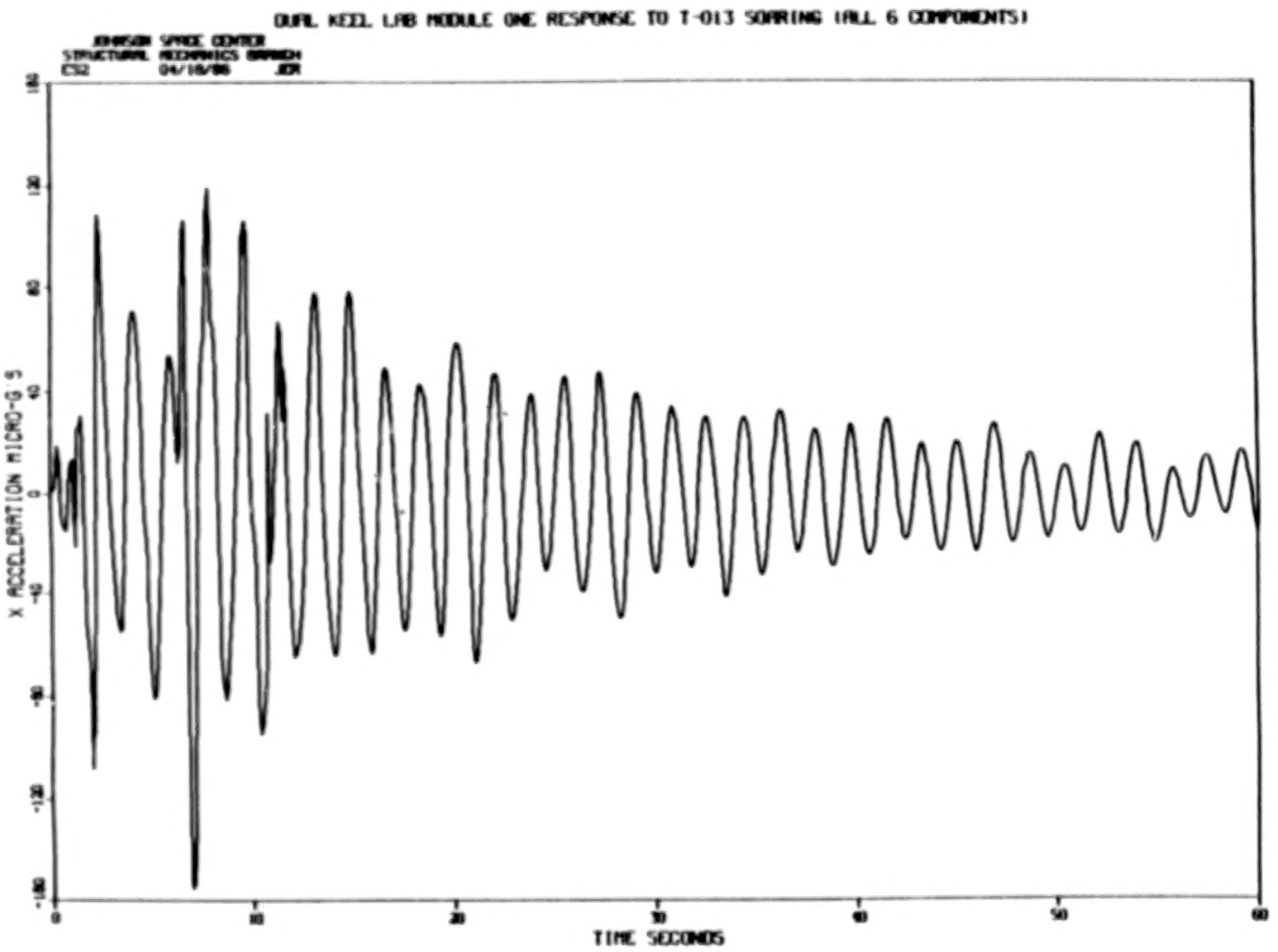DUAL KEEL LAB MODULE ONE RESPONSE TO T-013 SOARING (ALL 6 COMPONENTS)
JOHNSON SPACE CENTER
STRUCTURAL MECHANICS BRANCH
ES2 04/18/86 JER
X ACCELERATION MICRO-G'S
160
120
80
40
0
-40
-80
-120
-160
0
10
20
30
40
50
60
TIME SECONDS

Figure 14

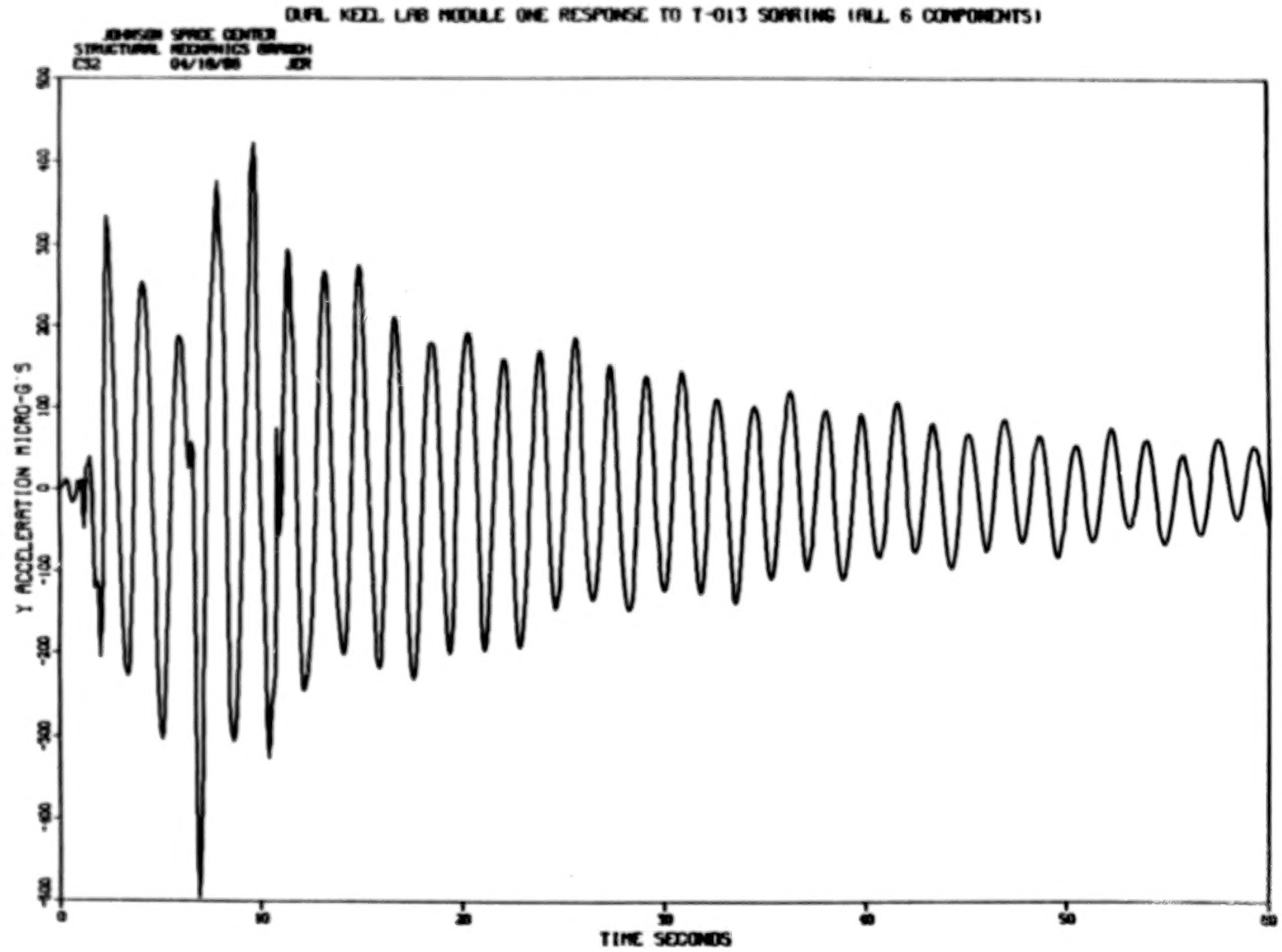

Figure 14 cont.

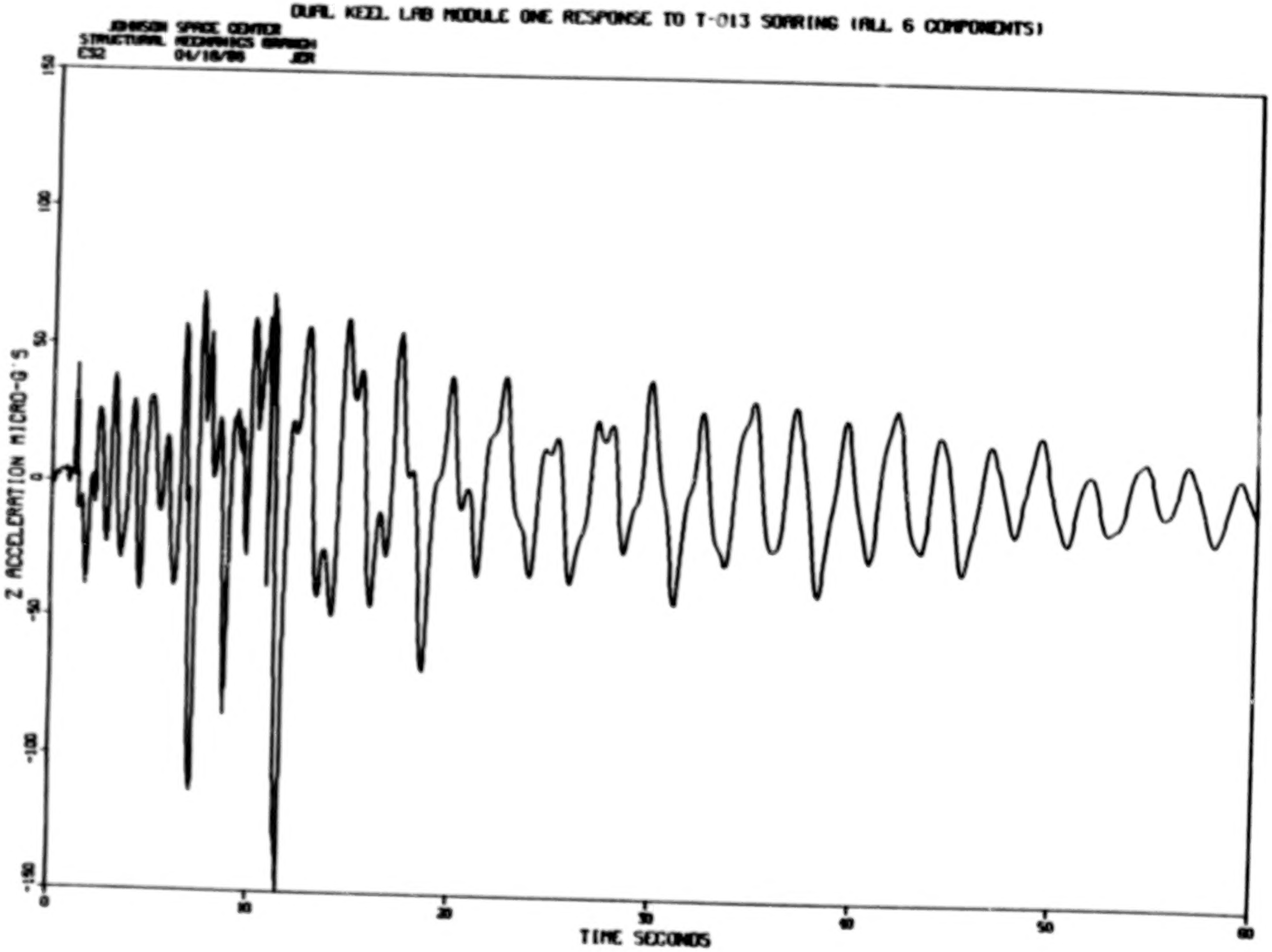

Figure 14 concluded

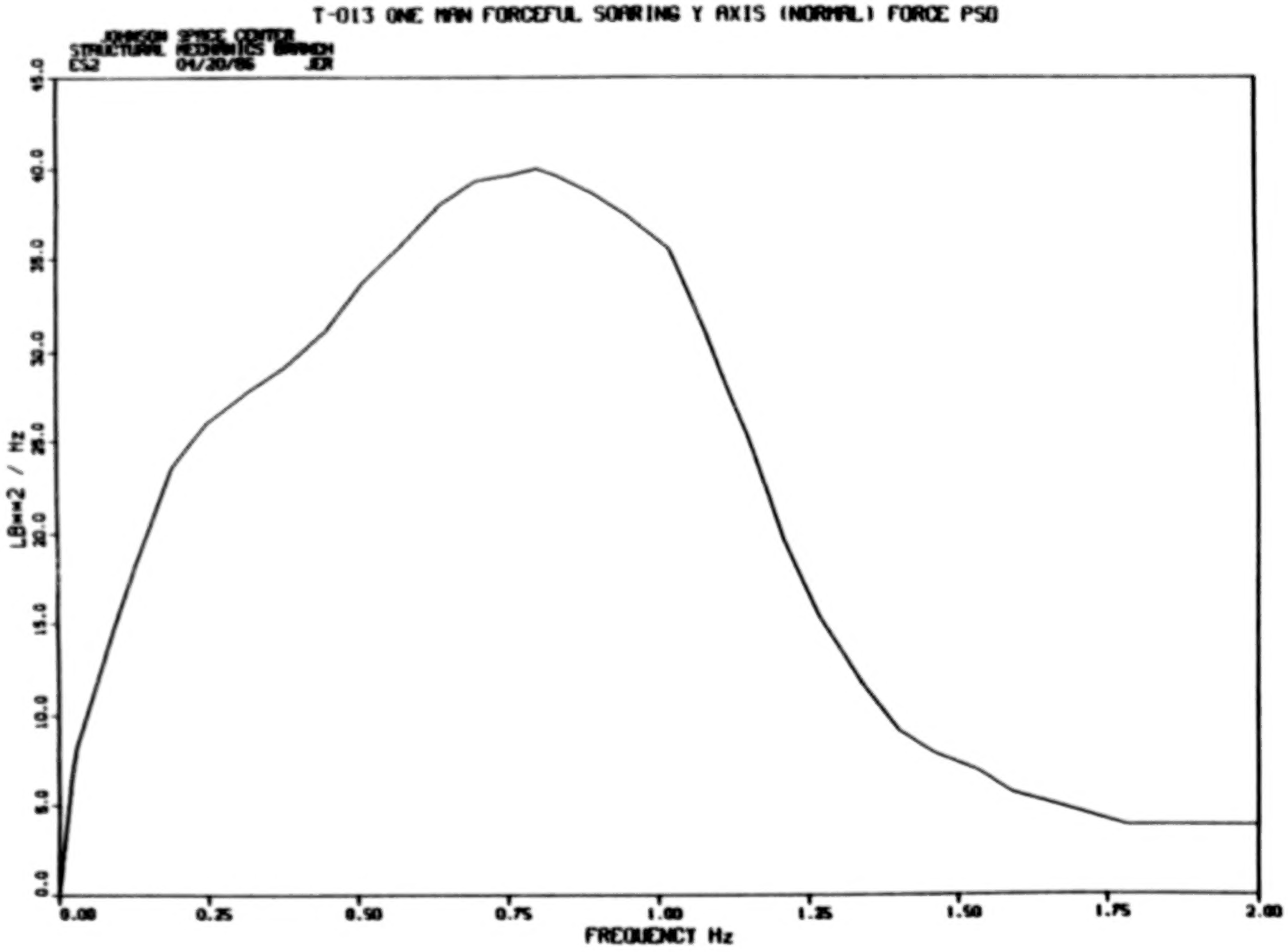
T-013 ONE MAN FORCEFUL SOARING Y AXIS (NORMAL) FORCE PSD
JOHNSON SPACE CENTER
STRUCTURAL MECHANICS BRANCH
ES2 04/20/86 JER
LB**2 / Hz
0.0
5.0
10.0
15.0
20.0
25.0
30.0
35.0
40.0
45.0
0.00
0.25
0.50
0.75
1.00
1.25
1.50
1.75
2.00
FREQUENCY Hz

Figure 15

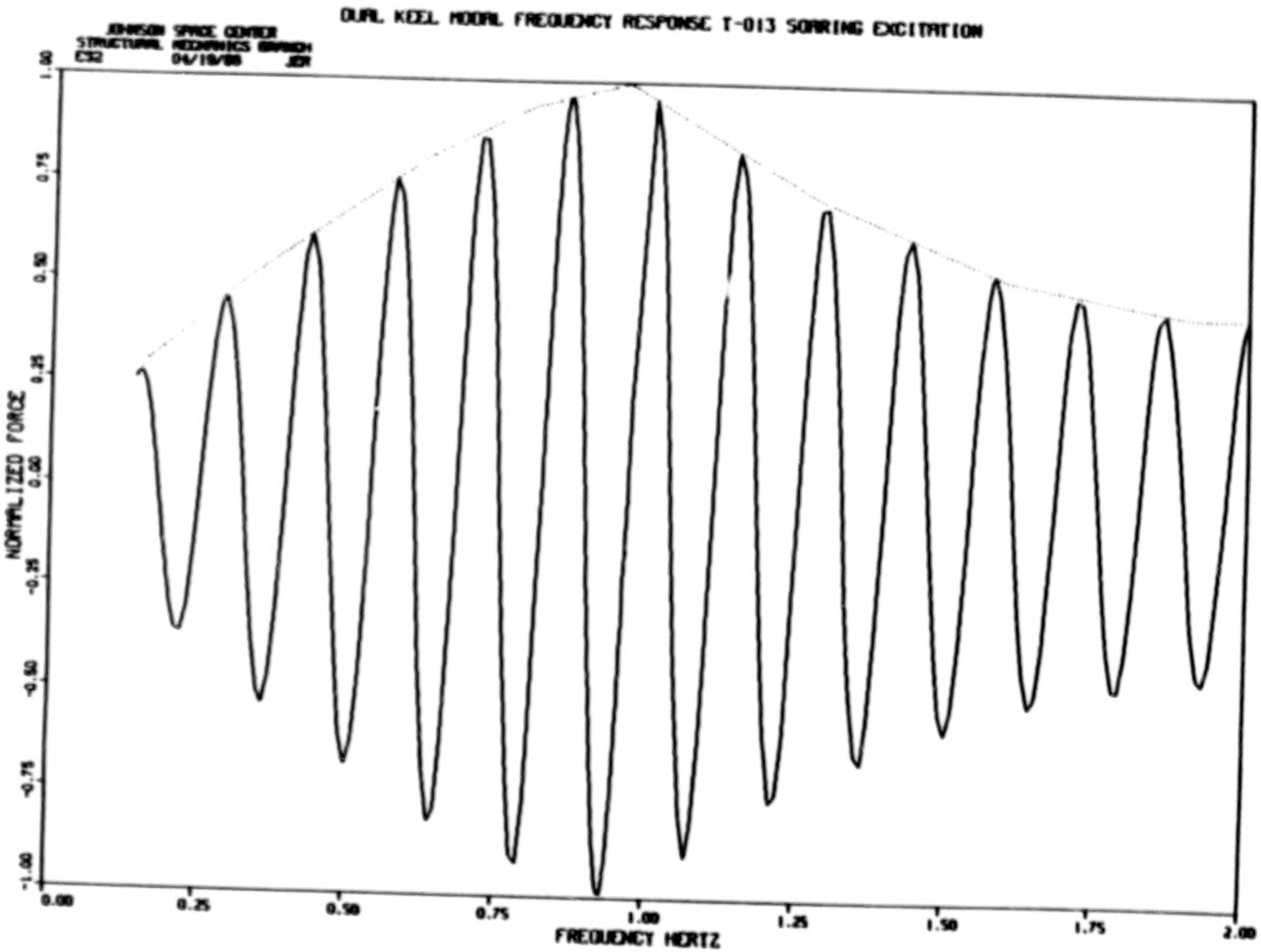

DUAL KEEL MODAL FREQUENCY RESPONSE T-013 SOARING EXCITATION
JOHNSON SPACE CENTER
STRUCTURAL MECHANICS BRANCH
ES2 04/19/88 JEM
NORMALIZED FORCE
1.00
0.75
0.50
0.25
0.00
-0.25
-0.50
-0.75
-1.00
0.00
0.25
0.50
0.75
1.00
1.25
1.50
1.75
2.00
FREQUENCY HERTZ

Figure 16

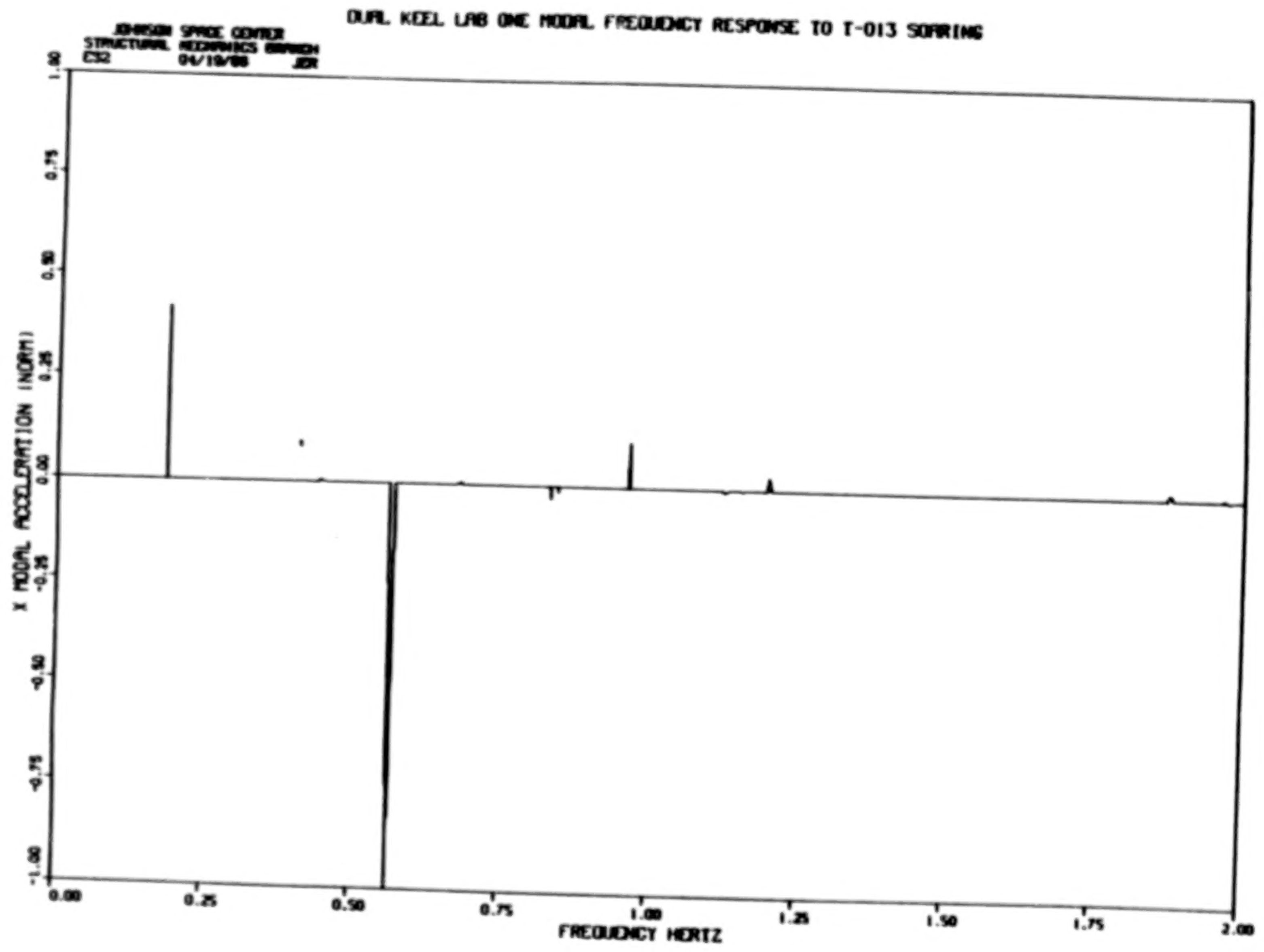
DUAL KEEL LAB ONE MODAL FREQUENCY RESPONSE TO T-013 SOARING
JOHNSON SPACE CENTER
STRUCTURAL MECHANICS BRANCH
ES2
04/19/88
JER
X MODAL ACCELERATION (NORM)
1.00
0.75
0.50
0.25
0.00
-0.25
-0.50
-0.75
-1.00
FREQUENCY HERTZ
0.00
0.25
0.50
0.75
1.00
1.25
1.50
1.75
2.00

Figure 17

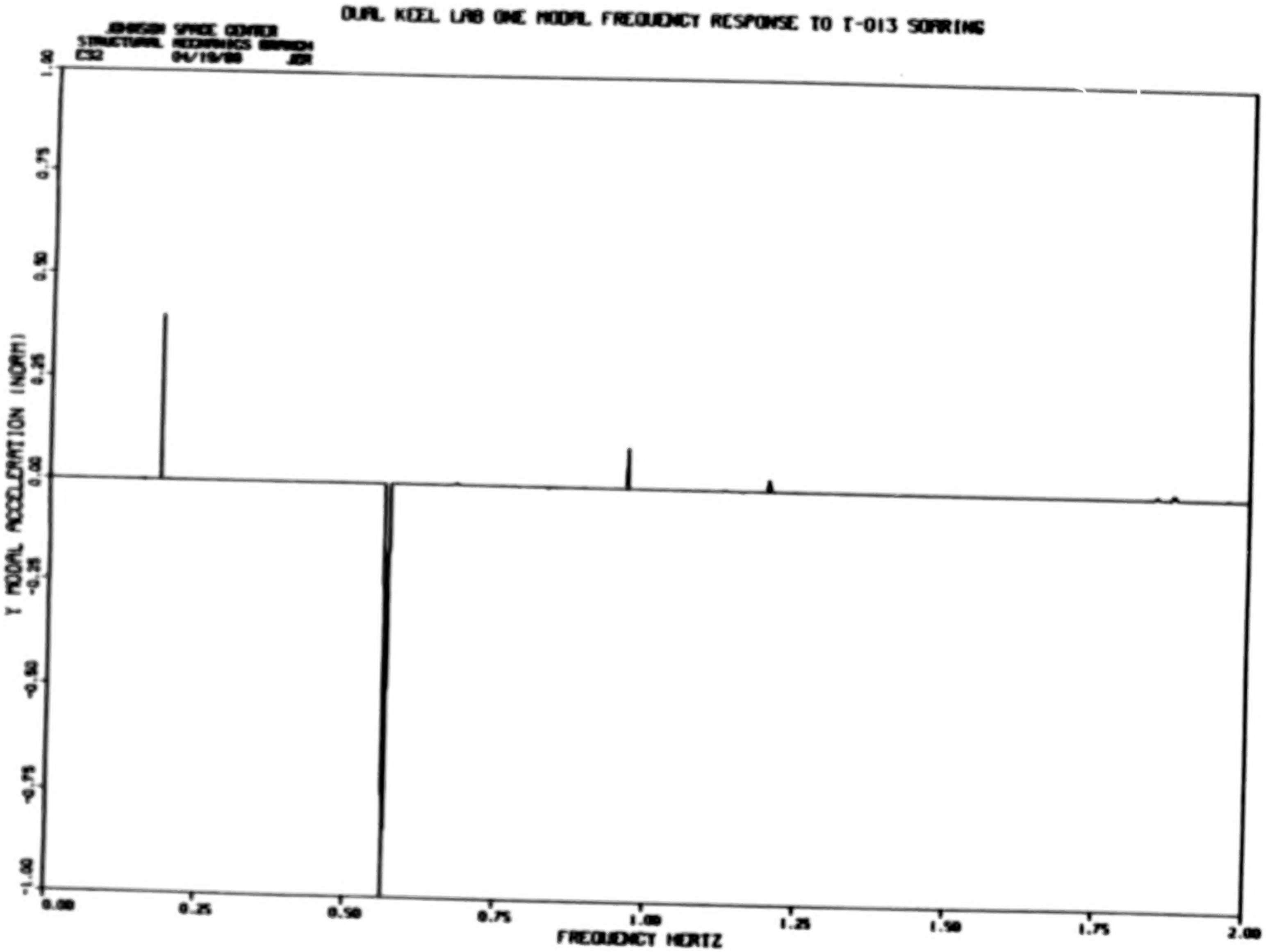

Figure 17 cont.

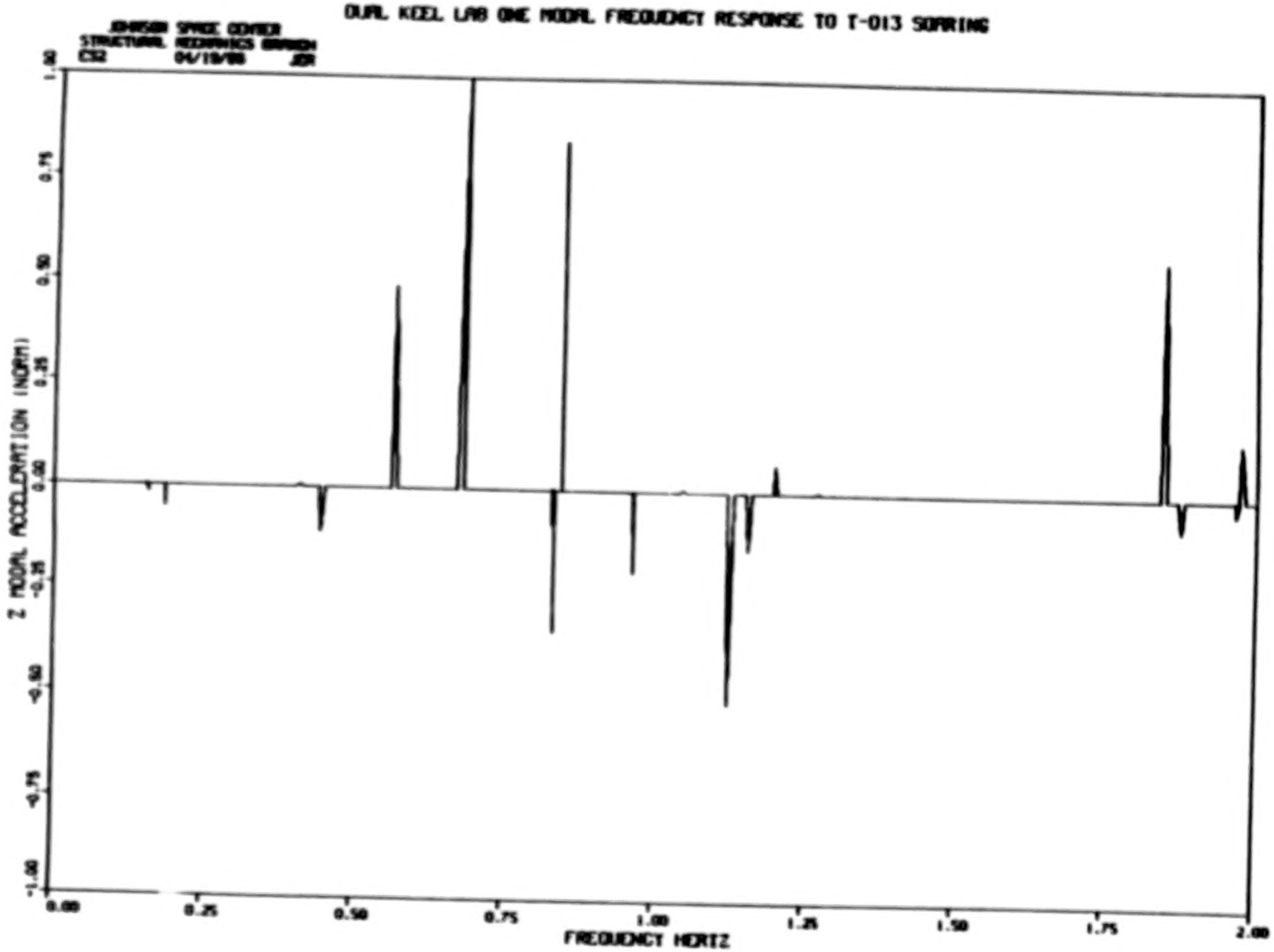

Figure 17 concluded

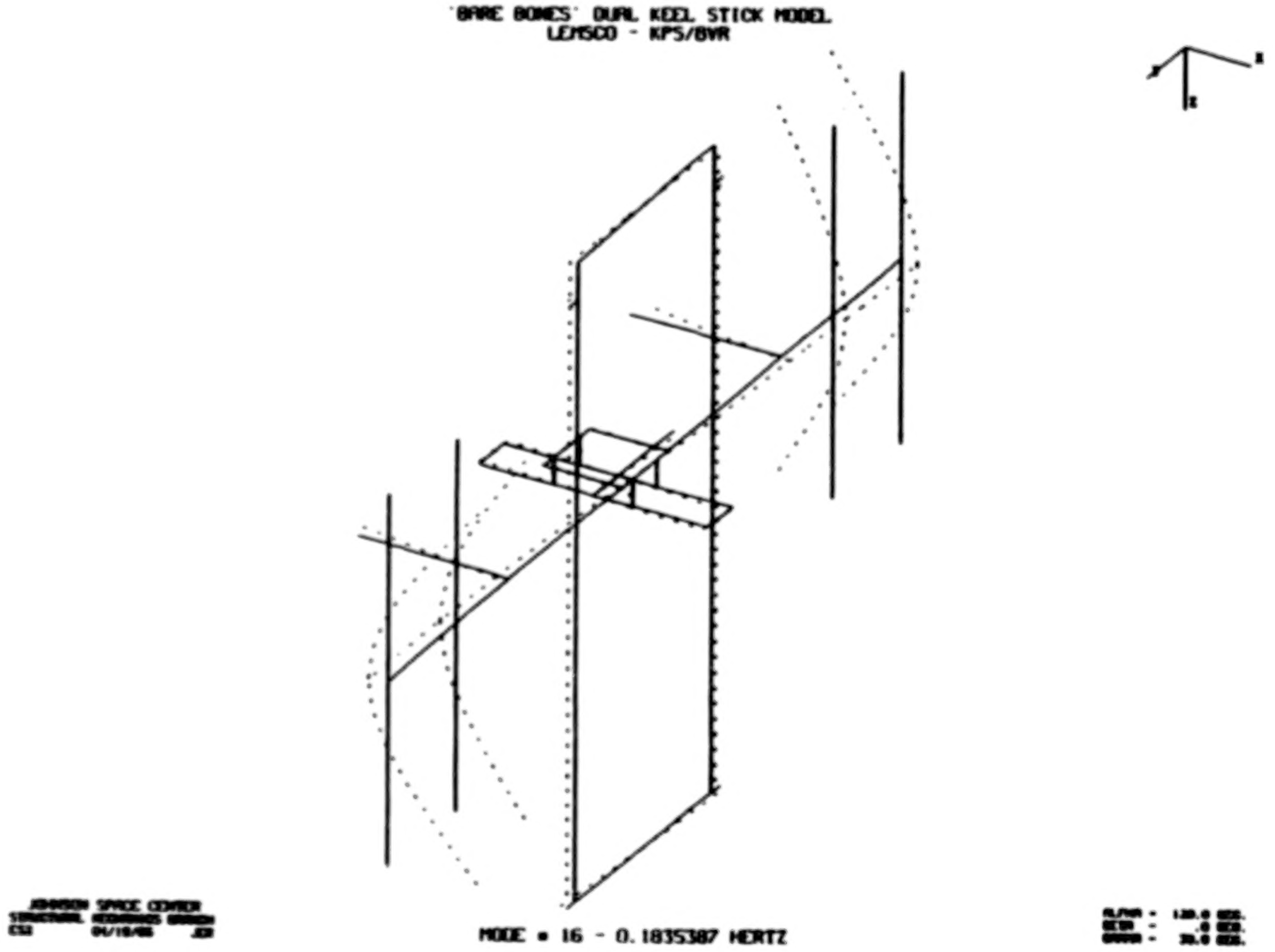
'BARE BONES' DUAL KEEL STICK MODEL
LEMSCO - KPS/BVR
X
Y
Z
JOHNSON SPACE CENTER
STRUCTURAL [illegible] BRANCH
CSI 04/18/85 JCD
MODE = 16 - 0.1835387 HERTZ
ALPHA : 120.0 DEG.
BETA : .0 DEG.
GAMMA : 30.0 DEG.

Figure 18

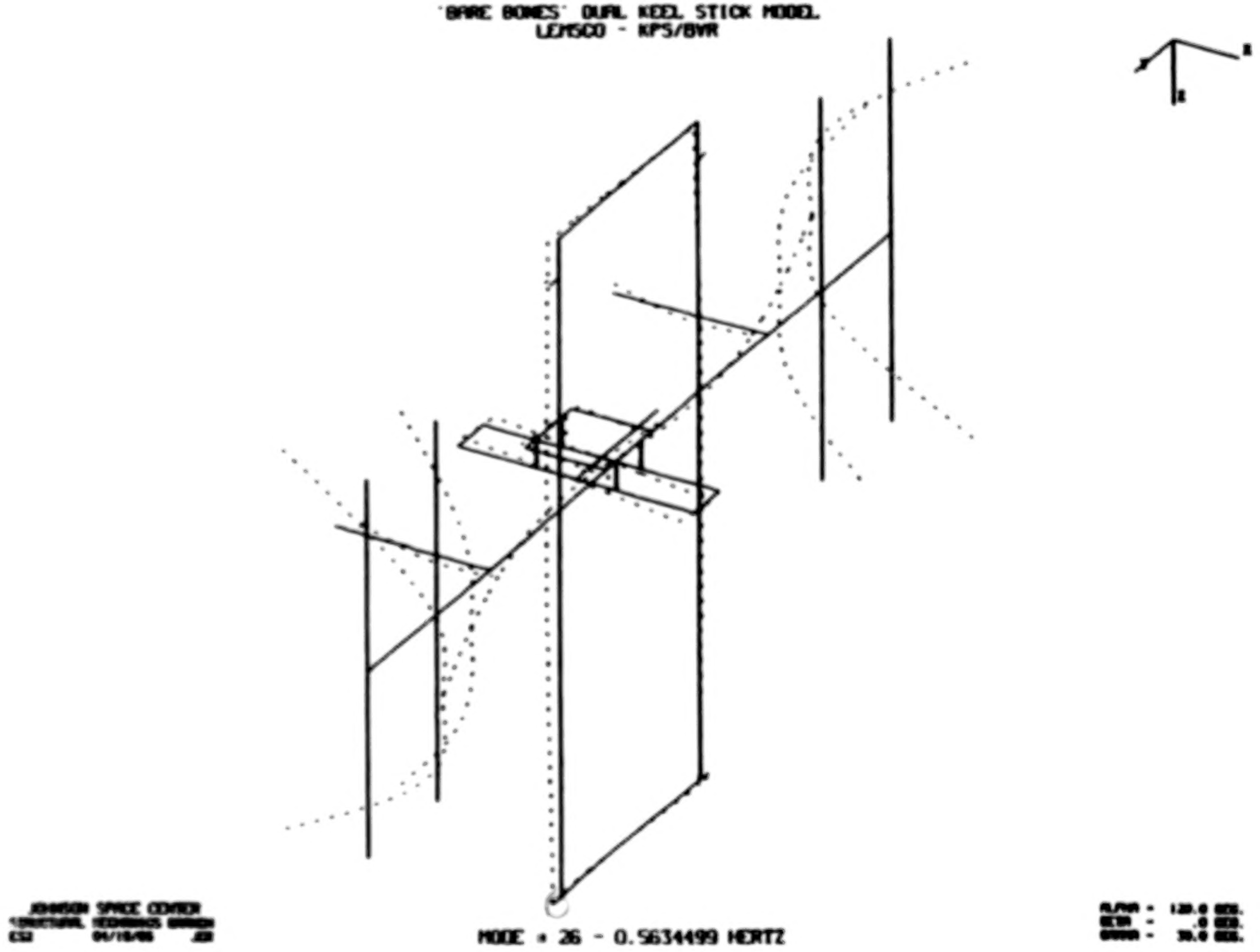
'BARE BONES' DUAL KEEL STICK MODEL
LEMSCO - KPS/BVR
JOHNSON SPACE CENTER
STRUCTURAL MECHANICS BRANCH
CSI 04/18/86 JER
MODE = 26 - 0.5634499 HERTZ
ALPHA = 120.0 DEG.
BETA = .0 DEG.
GAMMA = 30.0 DEG.

Figure 19

'BARE BONES' DUAL KEEL STICK MODEL
LEMSCO - XPS/BVR

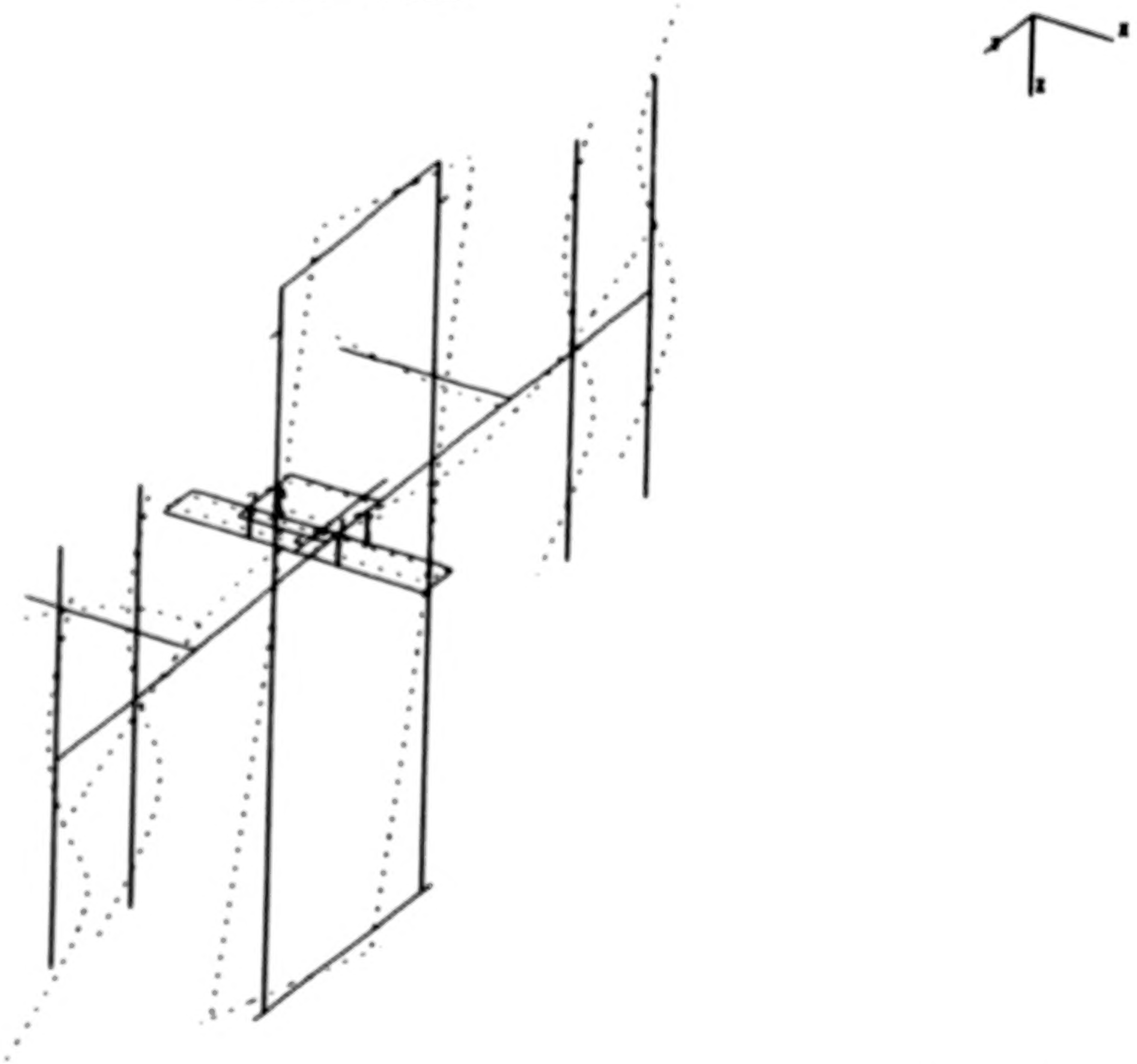

JOHNSON SPACE CENTER
STRUCTURAL MECHANICS BRANCH
ES2 04/18/86 JER

MODE = 27 - 0.6793752 HERTZ

ALPHA = 120.0 DEG.
BETA = .0 DEG.
GAMMA = 30.0 DEG.

Figure 20

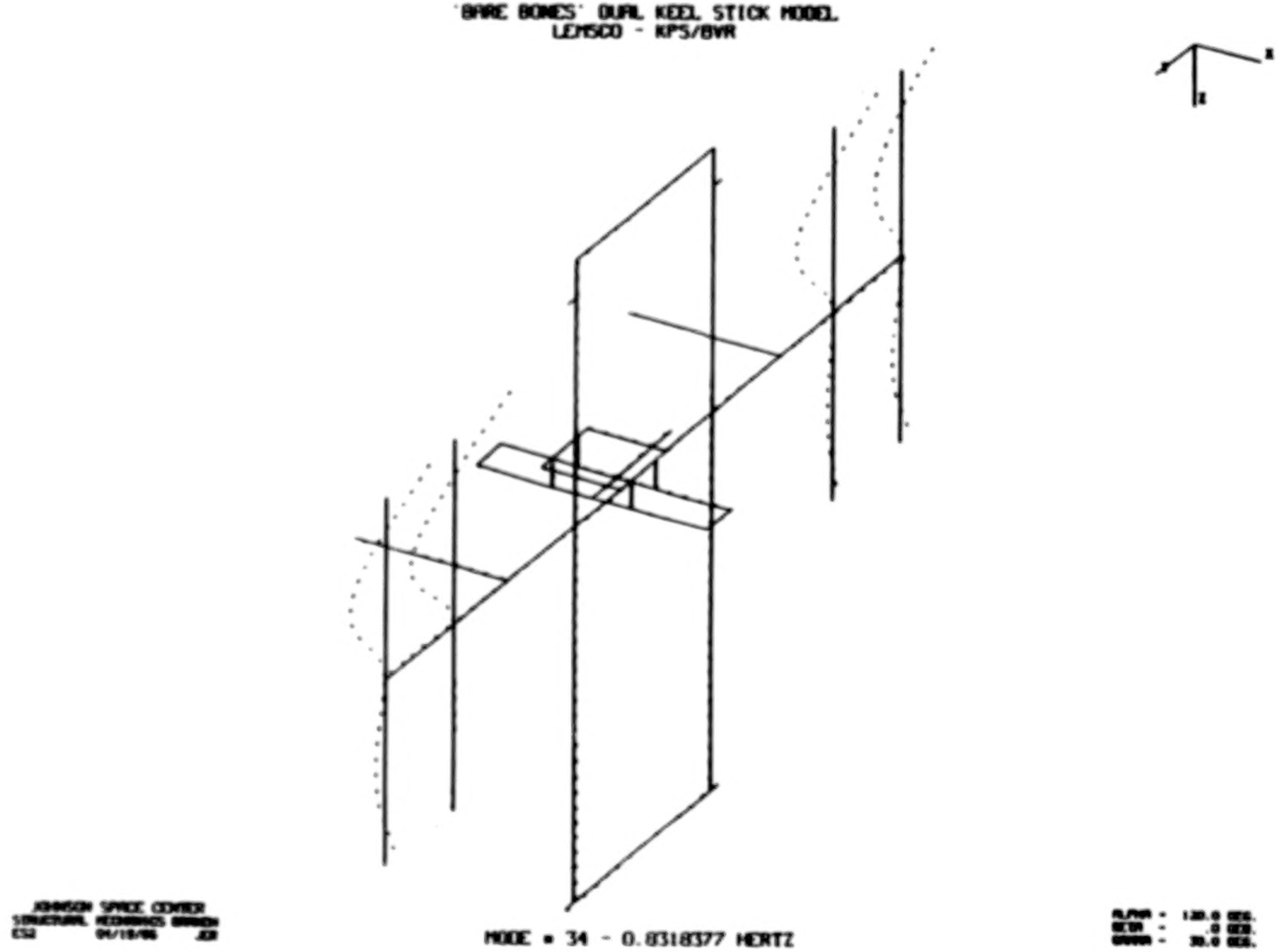
'BARE BONES' DUAL KEEL STICK MODEL
LEMSCO - KPS/BVR
X
Y
Z
JOHNSON SPACE CENTER
STRUCTURAL MECHANICS BRANCH
ES2 04/18/86 JCB
MODE = 34 - 0.8318377 HERTZ
ALPHA = 120.0 DEG.
BETA = .0 DEG.
GAMMA = 30.0 DEG.

Figure 21

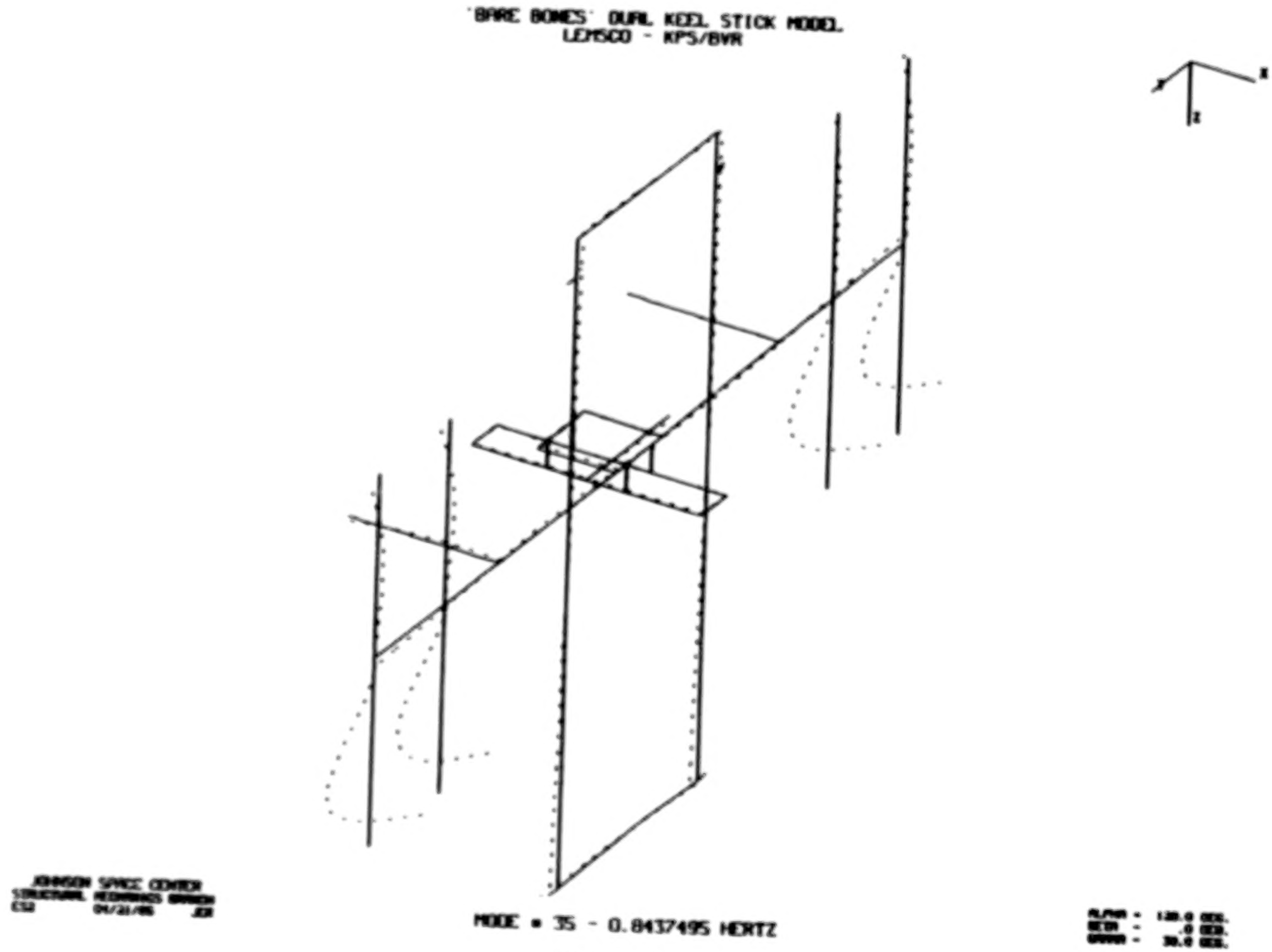
'BARE BONES' DUAL KEEL STICK MODEL
LEMSCO - KPS/BVR
X
Y
Z
JOHNSON SPACE CENTER
STRUCTURAL MECHANICS BRANCH
ES2 04/21/86 JCB
MODE = 35 - 0.8437495 HERTZ
ALPHA = 120.0 DEG.
BETA = .0 DEG.
GAMMA = 30.0 DEG.

Figure 22

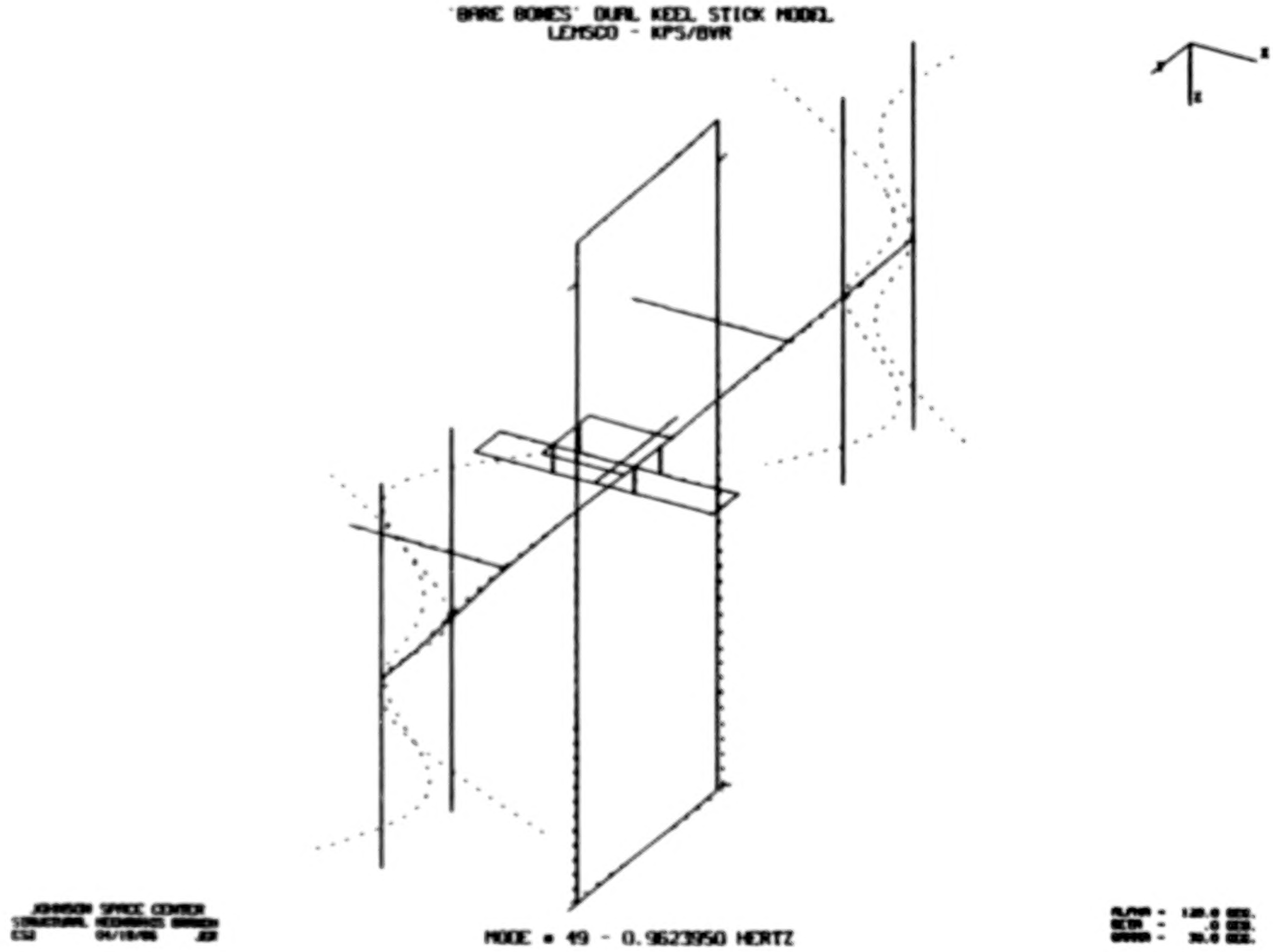
'BARE BONES' DUAL KEEL STICK MODEL
LEMSCO - KPS/BVR
X
Z
JOHNSON SPACE CENTER
STRUCTURAL MECHANICS BRANCH
ES2 04/18/86
MODE # 49 - 0.9623950 HERTZ
ALPHA - 120.0 DEG.
BETA - .0 DEG.
GAMMA - 30.0 DEG.

Figure 23

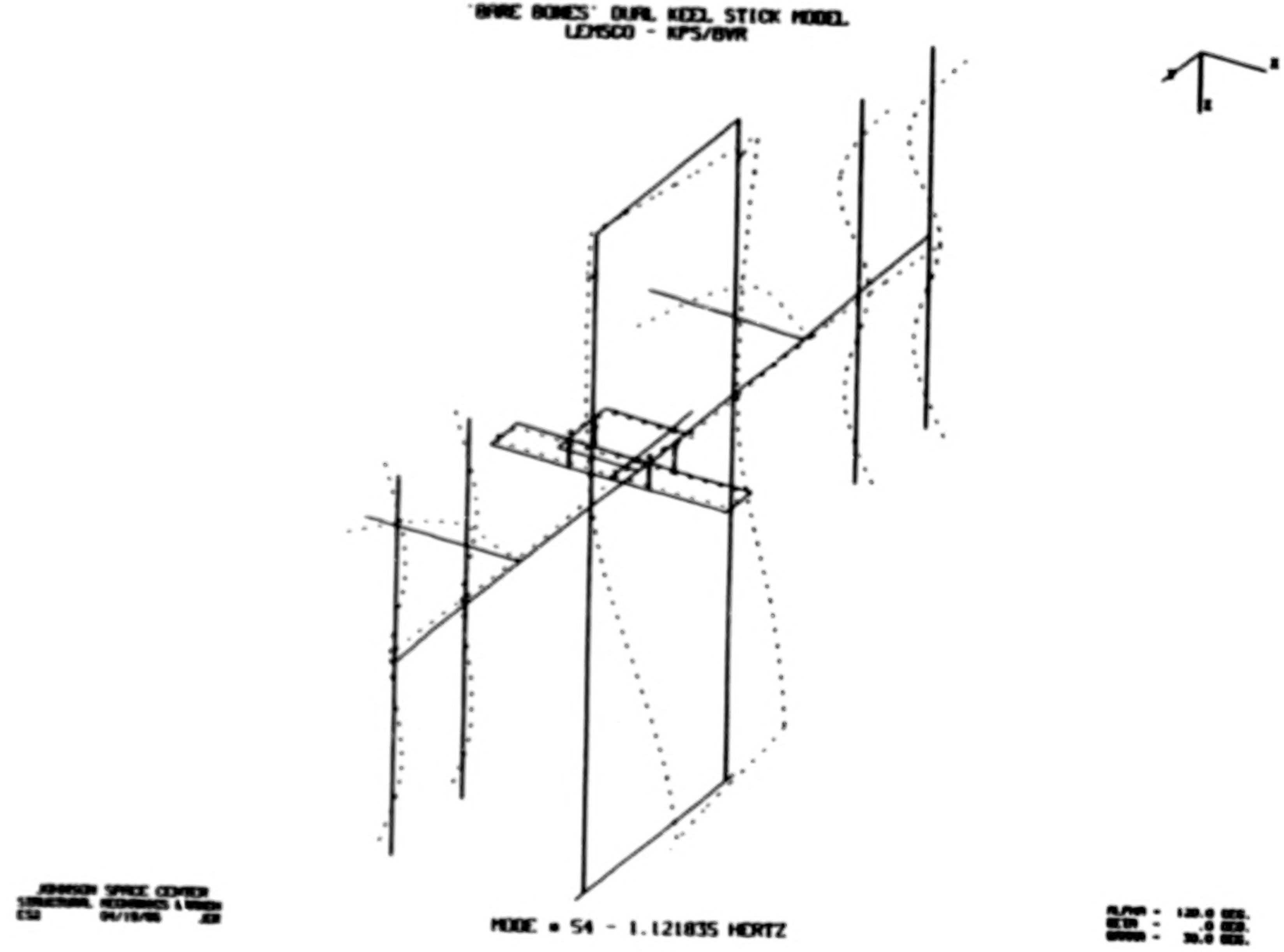
"BARE BONES" DUAL KEEL STICK MODEL
LEMSCO - KPS/BVR
X
Y
Z
JOHNSON SPACE CENTER
STRUCTURAL MECHANICS & BRANCH
ES2 04/18/86 JER
MODE = 54 - 1.121835 HERTZ
ALPHA - 120.0 DEG.
BETA - .0 DEG.
GAMMA - 30.0 DEG.

Figure 24

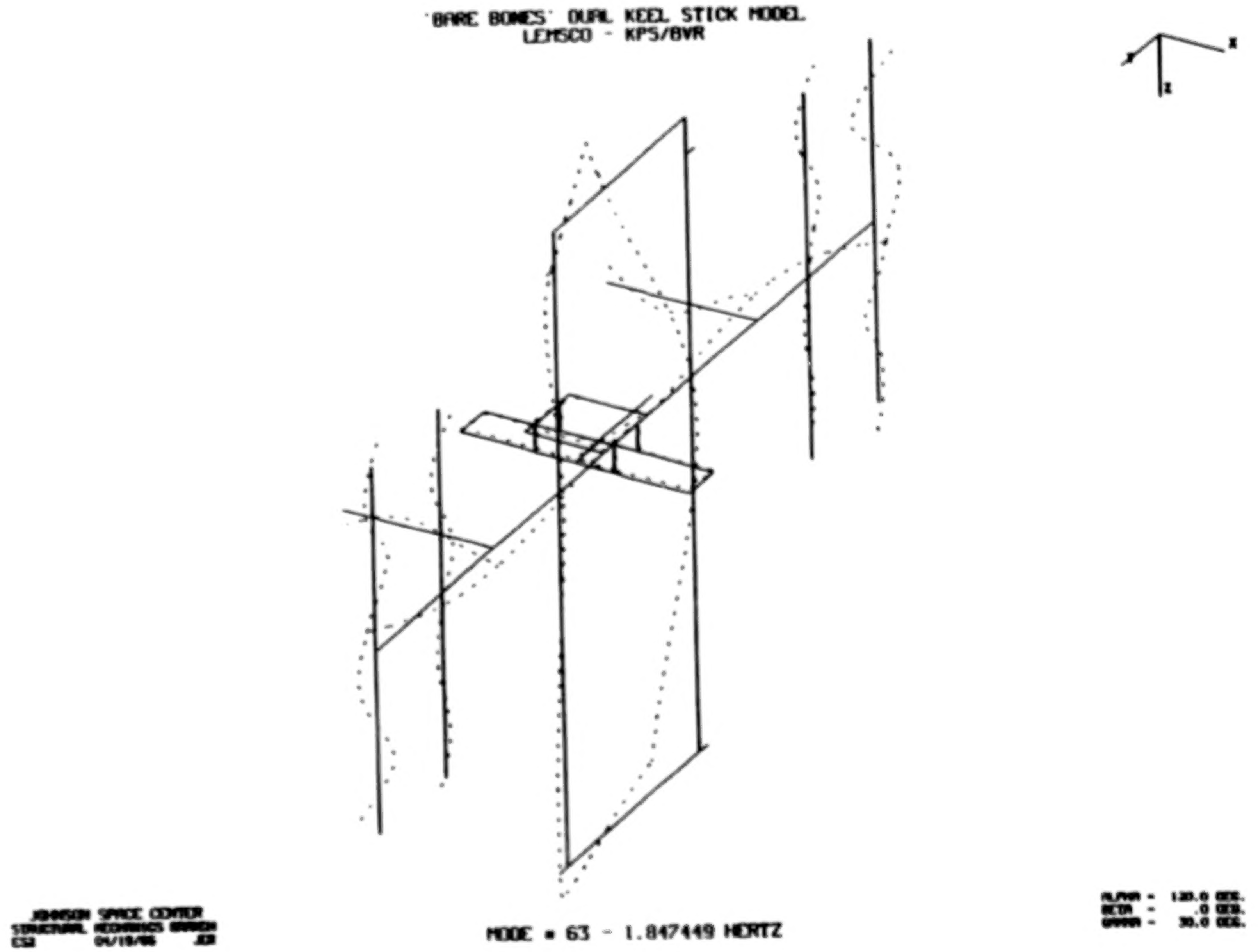
'BARE BONES' DUAL KEEL STICK MODEL
LEMSCO - KPS/BVR
X
Y
Z
JOHNSON SPACE CENTER
STRUCTURAL MECHANICS BRANCH
ES2 04/18/86
MODE = 63 - 1.847449 HERTZ
ALPHA = 120.0 DEG.
BETA = .0 DEG.
GAMMA = 30.0 DEG.

Figure 25

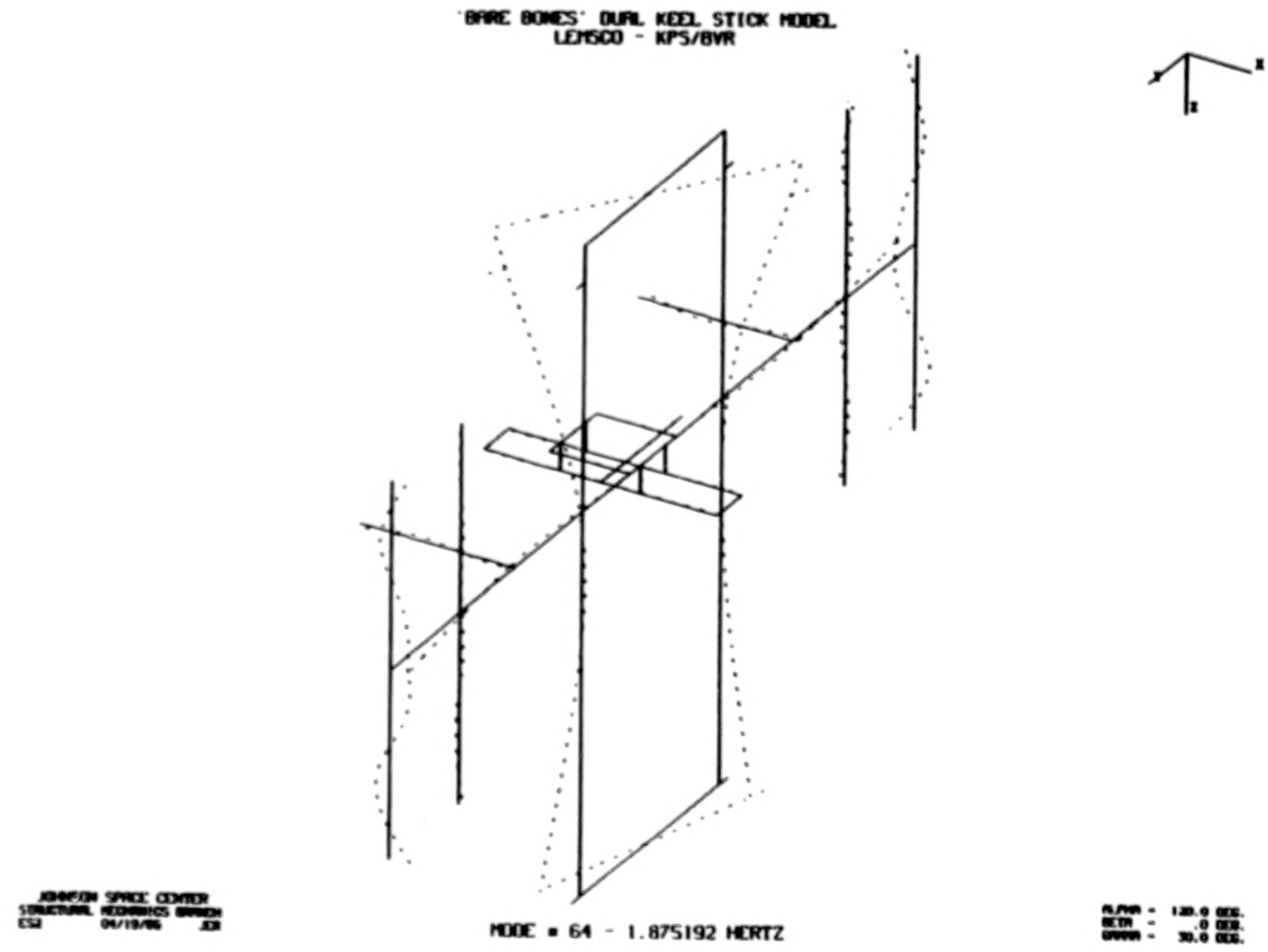'BARE BONES' DUAL KEEL STICK MODEL
LEMSCO - KPS/BVR
Y
X
Z
JOHNSON SPACE CENTER
STRUCTURAL MECHANICS BRANCH
ES2 04/19/86 JCR
MODE = 64 - 1.875192 HERTZ
ALPHA = 120.0 DEG.
BETA = .0 DEG.
GAMMA = 30.0 DEG.

Figure 26

VII. AREAS OF CONTINUED RESEARCH

The major portion of future work in the CA/M disturbance area will be towards expanding the present forcing function database. The current database is limited solely to CA/M results collected from Skylab experiment T-013, so it may be necessary to conduct additional flight experiments. There are deterministic (discrete) CA/M disturbances that cannot be simulated accurately or may have been modeled but need verification experimentally in a zero-g environment.

As part of the proposed work involving continued flight experimentation, a conceptual design is being developed for a force measurement system using a force platform similar to platforms currently used in biomechanics research. It will be a self-contained system integrating all sensors, data acquisition electronics, and power in one package to simplify procedures for flight certification and to eliminate the need for storage space aboard the Space Shuttle (middeck area).

The platform should be able to accomodate different equipment and loads but is presently being configured to handle the treadmill currently used by the crew for exercise aboard the Orbiter. The crew exercise treadmill is expected to be one of the major disturbance sources from CA/M on the Space Station, because it will probably be a part of the Health Maintenance Facility (HMF) so as to satisfy the crew's exercise requirement, which may call for daily use by each crew member. Thus without isolation of the apparatus, a seemingly constant disturbance will be present during its daily use (for a crew of 8). An experiment will be proposed to measure the disturbance caused by a member of the shuttle crew running on the treadmill apparatus. It is planned to gather Orbiter accelerometer data during the experiment; the measured accelerometer and forcing function data could then be used to predict Station and Orbiter response as well as for Orbiter structural math model verification.

It has been suggested to utilize ground simulations rather than actual flight experiments (due to the higher cost and time involved in preparing the experiment) for continued CA/M studies. During development of experiment T-013 questions were raised as to its necessity in light of the availability of a number of ground simulation techniques. However, with the benefit of hindsight and the wealth of T-013 data, there are still questions about the validity of ground simulation results. Several methods of simulation are available but have varying disadvantages and limitations (see Table 1). The results from ground simulations have been satisfactory for stochastic motions such as console operations, meal preparation, and personal hygiene. However, the results from simulating discrete, higher level restrained and translational CA/M did not correlate well with experiment T-013 results. No matter what the results, the simulated activities should be verified by on-orbit experimentation.

The ultimate goal of the work being conducted at NASA/JSC is to put together a handbook of induced loads and the resultant environments expected to affect Space Station operations. A significant portion of this data book will document the effects of CA/M disturbances.

VIII. Conclusions & Recommendations

Construction of the T-013 forcing function database and development of a structural analysis pre-processor has made it possible to evaluate the structural effects and response of CA/M disturbances on the space station. 'CREW' should prove itself invaluable as a tool for analysis in the near term. Efforts on modeling and synthesis of expected CA/M forcing function data are continuing and the results will be easily incorporated into the existing 'CREW' database.

Preliminary analysis has demonstrated that 'CREW', using the T-013 data, can accurately represent CA/M disturbances and that CA/M disturbances appear to be drivers that will compromise the Space Station's micro-g environment.

With crew capabilities and responsibilities expanding on a spacecraft with its purpose dedicated to using the micro-g environment, the spectrum of crew induced disturbances has widened. Thus the existing database needs to be expanded, and a choice has to be made between ground simulation (digital or physical) and flight experimentation. Various references have been reviewed and pertinant comments extracted leading to the recommendations that follow:

1) If the techniques exist for simulation of a disturbance,the results need to be experimentally verified.

2) If the techniques do not exist for simulation of a disturbance, then the disturbance must be measured by experimentation.

Both of the above recommendations lead to the same conclusion that for CA/M disturbance database expansion, a dedicated flight experiment should be conducted.

This conclusion is applicable to the majority of crew disturbances that need to be evaluated. The crew activity/motion requiring investigation falls into the category of gross body/torso motion and translation (exercise, IVA/EVA maintenance, hatch opening/closing, etc.), and based on experience gained from Skylab Experiment T-013, ground simulation of these activities resulted in very poor correlation with actual flight data. The remaining category (low level restrained activity such as console operations, personal hygiene, etc.) can be synthesized from existing flight data and can be modeled using stochastic techniques.

It is recommended that an experiment should be developed to investigate the crew motion/activity that cannot be modeled using the existing T-013 flight data. Such an experiment could use the Shuttle crew cabin or possibly a Spacelab module with a force measurement system similar to the one used in experiment T-013. Supporting this recommendation is the belief that some of the activities investigated will have force levels and frequency content greater than the T-013 activities (especially crew exercising on devices like the treadmill currently slated for use in the Station's HMF).

Acknowledgements

The authors wish to express their thanks to Ken Schultz, Paula Haddican and Patsy Barret, fellow LEMSCO employees, who shared a significant part in the effort to generate this paper. Also, the support and guidance provided by our JSC technical monitor, A. Rodney Rocha, was welcomed and appreciated.

References

1. Chubb, W. B., Kennel, H. F., Repp, C. C., and Seltzer, S. M., *Flight Performance of Skylab Attitude and Pointing Control System*, NASA TN D-8003, June, 1975.

2. *Skylab: Classroom In Space*, NASA SP 401, 1977.

3. *Initial Spacelab VFT Report, Volume VI Environment*, McDonnell Douglas Technical Services Co., MDAC H0843, September, 1984.

4. Poli, C. R., "Effects of Man's Motion on the Attitude of a Satelite", Journal of Spacecraft & Rockets, Vol. 4, No. 1, January, 1967.

5. Roberson, R. W., "Comments on the Incorporation of Man Into the Attitude Dynamics of Spacecraft", Journal of Astronautic Science, Vol. 10, 1963.

6. Fuhrmeister, W. F. and Fowler, J. L., *Experimental Study of Dynamic Effects of Crew Motion in a Manned Orbital Research Laboratory (MORL)*, NASA CR-66186, October 1966, McDonnell Douglas Aircraft Co., Western Div., Huntington Beach, Ca.

7. Goodman, M. and Middleton, W. C., "Crew Locomotion Disturbances in a Space Cabin Simulator", Journal of Spacecraft & Rockets, Vol. 6, October 1969.

8. Tewell, J. R. and Murrish, C. H., *Engineering Study and Experiment Definition for an Apollo Applications Program Experiment on Vehicle Disturbances Due To Crew Activity*, NASA CR-66277, March 1967, Martin Marietta Corp., Denver, Co.

9. Murrish, C. H. and Smith, G. W., *Apollo Applications Program Crew Motion Experiment - Program Defintion and Design Development*, NASA CR-66599, March 1968, Martin Marietta Corp., Denver, Co.

10. Conway, B. A. (Appendix A by Charles T. Wooley, Appendix B by Peter R. Kurzhals and Robert B. Reynolds), *Development of Skylab Experiment T-013 Crew/Vehicle Disturbances*, NASA TM D-6584, 1972.

11. Conway, B. A. and Hendricks, T. C., *A Summary of the Skylab Crew/Vehicle Disturbances Experiment T-013*, NASA TM D-8128, 1976.

12. Hendricks, T. C. and Johnson, C. H., "Stochastic Crew Motion Modeling", Journal of Spacecraft & Rockets, Vol. 8, No. 2, February, 1971.

13. Kullas, C. M., *Handbook on Astronaut Crew Motion Disturbances for Control System Desig*, NASA RP-1025, May 1979.

14. Scheer, S. A., *User's Guide For Version I of 'CREW' (Crew/Vehicle Disturbance Analysis)*, Lockheed Engineering & Management Services Co., LEMSCO-22064, September, 1985.

15. *Space Station Reference Configuration Descriiption*, JSC-19989, September, 1984.

N87
22745
UNCLAS

N87-22745

ORIGINAL PAGE IS
OF POOR QUALITY

MODELING OF CONTROLLED FLEXIBLE STRUCTURES WITH IMPULSIVE LOADS

M. Zak

Applied Technologies Section, Jet Propulsion Laboratory
California Institute of Technology, Pasadena, CA, USA

Abstract. The characteristic wave approach is developed as an alternative to modal methods which may lead to significant errors in the presence of impulsive or concentrated loads. The method is applied to periodic structures. Some special phenomena like cumulation effects and transitions to ergodicity are analyzed.

INTRODUCTION

Controlled large space structures, which will likely be composed of networks of long slender members, are subjected to disturbances (coming from the actuators) with a relatively small contact zone and short time interval. From the mathematical viewpoint such disturbances are characterized by discontinuities which can be considered as a very high frequency. In truncation techniques which are used in modal analysis the contribution of high frequencies is lost, and therefore, the impulsive concentrated loads are supposed to be treated by some other methods.

Since any discontinuity propagates with the characteristic speed, it is reasonable to turn to the characteristic wave approach in treating the impulsive loads. The advantage of this approach is in the fact that characteristic speeds depend only on the coefficients at the highest (second order) derivatives in the governing equation of structural members which significantly simplifies the analysis of characteristic waves.

Thus, it appears that the application of the characteristic wave approach is the most beneficial in the domains where spectral methods fail. That is why it can be used as a supplement to modal methods for linear analysis of controlled structures when loads can be decomposed in to "smooth" and impulsive components.

In this article, some aspects of characteristic wave propagation, reflection and transmission in structures with one-dimensional structural members as well as possible engineering tools for their analysis are discussed.

PROPAGATION OF IMPULSIVE LOADS IN ONE-DIMENSIONAL STRUCTURAL MEMBERS

We will start with a one-dimensional structural member subjected to a concentrated or impulsive load assuming that

$$\Delta\ell \ll L, \text{ and } \Delta t \ll \frac{L}{C} \tag{1}$$

in which L is the length of the structural member, $\Delta\ell$ is the width of the contact zone of the impulse, Δt is the duration of the concentrated load, and C is the characteristic speed of wave propagation, while

$$C_B^2 = \frac{E}{\rho},\ C_T^2 = \frac{G}{\rho},\ C_V^2 = \frac{GA_s}{\rho A},\ C_M^2 = \frac{EI}{\rho I},\ C_S^2 = \frac{T}{\rho} \tag{2}$$

Here C_B, C_T, C_V, C_M, and C_S are the characteristic speeds for longitudinal, torsional, shear, bending and transverse string waves, respectively. E is the Young modulus, G is the shear modulus, A is the cross-sectional area, A_s is an effective shear area of a Timoshenko beam, EI is the cross-sectional area moment of inertia, ρI is the rotatory inertia per unit length, ρ is the mass per unit length, T is the string tension, W. Flugge, 1962.

For homogenious structural members all the characteristic speeds (2) are constant, and consequently, the width $\Delta\ell$ as well as the duration Δt of the impulse will be constant too. However, the initial configuration of the impulse will be preserved only for the simple wave equation without damping.

In all other cases due to the dispersion phenomenon this configuration, strictly speaking, will not be preserved. Nevertheless, the dispersion can be ignored if the conditions (1) are satisfied. For further convenience we will introduce an equivalent rectangular impulse of the same length and energy. For such a rectangular impulse, all the waves listed in (2) are decoupled even if they propagate simultaneously in a structural member, and this is the most important advantage of the characteristic wave approach to propagation of impulsive loads.

As follows from the energy conservation law the height of the rectangular impulse expressed in terms of velocity, strain or stress will be constant if there is no material damping. If material damping is proportional to the velocity being characterized by the damping coefficient ξ then the height h of the rectangular impulse will exponentially decrease:

$$h^2 = h_o^2\, e^{-\xi t} \tag{3}$$

NON-HOMOGENEITY EFFECTS

The situation becomes more complicated even for a rectangular impulse if the speed of propagation is not constant. This effect can be caused by non-linear material properties (if the impulse is large enough to generate finite strains) or by non-homogenious properties of the structural member.

In the first case the speed becomes non-characteristic since it depends on the magnitude of the transmitted parameters, i.e., for a rectangular impulse

$$c = c(h) \tag{4}$$

This dependence may lead to a qualitatively new effects such as shock wave formation.

In the second case the speed remains characteristic, but it depends on the space coordinate:

$$c = c(x) \tag{5}$$

Although the governing equations for wave propagations remain linear (but with variable coefficients) the dependence (5) may lead to some surprising effects. In order to describe them, we will start with the energy balance. The energy E of a propagating impulse consist of potential and kinetic components:

$$E = \frac{1}{2}\int_{x_1}^{x_2} \rho(C^2[\varepsilon]^2 + [v]^2)\, dx \tag{6}$$

in which x_1 and x_2 are the space coordinates of the trailing and leading fronts of the propagating wave, $[v]$ and $[\varepsilon]$ are the impulsive velocity and strain, respectively, while

$$[\varepsilon] = -c[v] \tag{7}$$

as follows from the kinematical condition at the front of a discontinuity, Miklowitz, (1984). Hence, for a rectangular impulse:

$$E = \rho[v]^2\,(x_2 - x_1) \tag{8}$$

and instead of Eq. (3) now one obtains:

$$h^2(x_2 - x_1) = h_0^2\,\Delta\ell e^{-\zeta t} \tag{9}$$

The first effect which can be found from Eq. (9) is associated with the specific energy cumulation, i.e., with the unbounded growth of h due to shrinking width $(x_2 - x_1)$ of the propagating impulse. This effect was first described and explained by M. Zak, 1983.

The second effect is associated with a trapping of a propagating impulse within a localized area of a structural member. Similar effect of normal mode localization was predicted by C.H. Hodges, 1982, in connection with a system of coupled linear oscillators with damping. Thus, the trapping effect of a propagating impulse can be considered as a "continuum version" of the normal mode localization. A mathematical treatment of this effect is presented below.

Consider a function (5) in the following form:

$$C = \begin{cases} C_0 \text{ at } x < x_* \text{ and } x > x_{**} \\ \gamma C_0 \text{ at } x_* > x > x_{**},\ 0 < \gamma < 1 \end{cases} \tag{10}$$

Such a discontinuity of the characteristic speed C within a small segment $(x_{**} - x_*) < \Delta\ell$ can be caused by some structural irregularities (such as material inclusions, joints, etc.)

As follows from Eq. (10)

$$x_2 - x_1 = \begin{cases} \Delta\ell \text{ at } x_1 = x_* - \Delta\ell,\ x_2 = x_* \\ \Delta\ell - C_0(1-\gamma)t \text{ at } x_1 < x_* < x_2 < x_{**} \\ \Delta\ell - (x_{**} - x_*) \text{ at } x_1 < x_*,\ x_2 > x_{**} \\ \Delta\ell - (x_{**} - x_*) + C_0(1-\gamma)t \text{ at } x_* < x_1 < x_{**}, x_2 > x_{**} \\ \Delta\ell \text{ at } x_1,\ x_2 > x_{**} \end{cases} \tag{11}$$

Substituting (11) into (9) one finds:

$$h^2 = \begin{cases} h_0^2 e^{-\zeta t} \text{ at } x_1 = x_* - \Delta\ell,\ x_2 = x_* \\ h_0^2 e^{-\zeta t}/(1-\zeta t) \text{ at } x_1 < x_* < x_2 < x_{**} \\ h_1^2 e^{-\zeta t}/(1-\lambda) \text{ at } x_1 < x_*,\ x_2 > x_{**} \\ h_0^2 e^{-\zeta t}/(1-\lambda+\zeta t) \text{ at } x_* < x_1 < x_{**},\ x_2 > x_{**} \\ h_3^2 e^{-\zeta t} \text{ at } x_1,\ x_2 > x_{**} \end{cases} \tag{12}$$

in which

$$\zeta = \frac{C_0(1-\gamma)}{\Delta\ell},\ \lambda = \frac{x_{**} - x_*}{\Delta\ell}$$

$$h_1^2 = h_0^2 e^{-\zeta t_1},\ h_2^2 = h_0^2 e^{\zeta(t_1 + t_2)}$$

$$h_3^2 = h_0^2 e^{-\zeta(t_1 + t_2 + t_3)} \tag{13}$$

$$t_1 = \frac{\lambda}{\zeta},\ t_2 = \frac{1-\gamma-\lambda}{\zeta},\ t_3 = \frac{\lambda}{\zeta}$$

Simple analysis of Eq (12) shows that the function h(x) has maximum at $x_1 < x_* < x_2 < x_{**}$ if

$$\zeta < \xi < \frac{\zeta}{1-\lambda} \tag{14}$$

This maximum is:

$$h_{max}^2 = h_0^2 \frac{\xi}{\zeta} e^{(1 - \frac{\xi}{\zeta})} \tag{15}$$

The maximum of h_{max} as a function of ξ/ζ will be at

$$\frac{\xi}{\zeta} = \frac{1}{2}(1 + \sqrt{5}) \tag{16}$$

and therefore:

$$h^2_{max,max} = 8.15\, h^2_0 \tag{17}$$

Substituting (16) into (14) one obtains:

$$\lambda < 0.382 \tag{18}$$

But, as follows from (13):

$$h_3^2 = h_0^2 e^{-\frac{\xi}{\zeta}(1+\gamma+\lambda)t} \tag{19}$$

Hence, the trapping effect will be the strongest if

$$\lambda = 0.382 \tag{20}$$

ORIGINAL PAGE IS
OF POOR QUALITY

Indeed, in this case the function (12) has the sharpest shape since Eq. (16) provides the largest maximum (17), while Eq. (20) leads to the highest degree of dissipation after this maximum. Thus, the conditions (16) and (20) can be used as the key for structural implementation of the trapping effect.

Governing Equations

As shown by Zak, M. 1985, the governing equations for a propagation, reflection and transmission of an initial impulse in a two-member structure with isolated ends at $x = 1$, and $x = 3$, and a joint at $x = 2$ form a system of difference equations:

$$h_{k+1} = Ah_k \qquad (21)$$

where

$$A = \begin{pmatrix} 0 & \zeta_{12}\zeta_1 & 0 & 0 \\ -\zeta_{12}\zeta_2\varepsilon_2 & 0 & 0 & -\zeta_{12}\zeta_2(1-\varepsilon_2) \\ -\zeta_{23}\zeta_2(1-\varepsilon_2) & 0 & 0 & -\zeta_{23}\zeta_2\varepsilon_2 \\ 0 & 0 & -\zeta_{23}\zeta_3 & 0 \end{pmatrix}, \quad h_k = \begin{pmatrix} h_{12} \\ h_{21} \\ h_{23} \\ h_{32} \end{pmatrix} \qquad (22)$$

in which h_{12} is the wave at $x = 2$ coming from $x = 1$, etc. ζ_{12} and ζ_{13} are the damping coefficients in the corresponding structural members, ζ_1, ζ_2, ζ_3 are the damping coefficients at $x = 1, 2, 3$, respectively, ε_2 is the reflection coefficient at $X = 2$, while $\varepsilon_1 = \varepsilon_3 = 1$.

The same procedure can be applied to multi-member structural systems, while the matrix A will attain new submatrices corresponding to additional structural members (like a stiffness matrix in finite element methods).

Thus, any structure with n identical structural members subjected to impulsive loads is governed by the matrix difference equation (21) while the order of this system is $2n$.

Analysis of Solutions

In the case of n-member structure the solution to the governing equation (21) where the matrix A is of the order $2n$ can be written in the following form:

$$h_k = A^k h_0, \quad k = 0, 1, 2, \ldots \qquad (23)$$

All the qualitative properties of this solution are defined by the eigenvalues of the matrix A, i.e., by the roots of the characteristic polynomial:

$$|A - \lambda I| = 0 \qquad (24)$$

For instance, the solution is stable if

$$|\lambda i| < 1, \; i = 1, 2, \ldots 2n \qquad (25)$$

By applying a linear fractional transformation

$$\lambda = \frac{\tilde{\lambda}+1}{\tilde{\lambda}-1} \qquad (26)$$

to Eq. (25) one reduces the stability analysis to conventional methods.

Transition to Ergodicity

So far the only structures with identical members (characterized by the dimentionless time delay τ) were considered. It was demonstrated that there exists a formal analogy between the matrix techniques for treating these structures under impulsive loads and for conventional modal analysis (although the matrices have different physical nature). However, in reality the identicalness of structural members even in periodic structures is an exception rather than a rule. Indeed, different time delays for different structural members can be caused not only by different lengths, but also by different characteristic speeds. In turn, different characteristic speeds may occur if joints convert one type of deformation into another (see Eq. (2)). Another source of different time delays is associated with external forces if they applied not to joints. In this case, the points of their application must be considered as additional joints, but without reflection or damping, and this will lead to additional structural members with different time delays. As will be shown below, different time delays lead to new qualitative effects which do not occur in modal methods.

For simplicity, we will start with the two-member structure and assume the following (dimensionless) lengths:

$$AB = 4, \quad BC = 6 \qquad (27)$$

Then, the characteristic equation for this two-member system obviously has the order 24 (which is the least common multiple of 2x4 and 2x6)

But in the case

$$AB = 1, \; BC = \sqrt{2} \qquad (28)$$

the ratio of the time delays is irrational, and therefore, for successive rational approximations of $\sqrt{2}$ the order of the governing difference equation tends to infinity as:

$$4, 14, 282, 1414, \ldots \text{etc.} \qquad (29)$$

Now it is easy to deduce, that if in an n-member structure the time delays $\tau_1, \tau_2, \ldots \tau_n$ are commensurate, then the order of the governing difference equation will be finite and equal to the least common multiple of $2\tau_1, 2\tau_2, \ldots 2\tau_n$.

If at least two time delays are not commensurate, this order will tend to infinity. Obviously, this effect does not have an analogy in modal approach where the order of the governing differential equation depends only on the number of modes (or finite elements) considered.

In order to clarify the physical meaning of such a phenomenon let us start with the following question: during what time interval T an initial impulse will return to its original location in "one piece"? Simple geometrical consideration show that

$$\begin{aligned} T &= 2 \text{ if } AB = 1, \; BC = 1 \\ T &= 24 \text{ if } AB = 1, \; BC = 6 \qquad (30) \\ T &= \infty \text{ if } AB = 1, \; BC = \sqrt{2} \end{aligned}$$

In other words, this (dimensionless) interval is equal to the order of the governing difference equation.

Thus, if at least two time delays in an n-member structure are not commensurate, the system will never return to its initial position, i.e., the motion will lose its periodicity. In classical mechanics such systems are known as ergodic systems. For infinite number of times they pass through every state of motion (which is consistent with constraints) spending equal time intervals near ech state.

As however, the rational numbers are a set of measure zero, practically every motion of this type sooner or later become ergodic.

Nevertheless, in engineering applications there always can be found such a characteristic time interval within which the motion is approximately periodic, while the transition to ergodicity can be ignored due to damping.

It is worth emphasizing that the transition to ergodicity is not "inevitable" if one takes into account non-linear properties of real structures. Non-linearities may provide some mechanisms (such as dynamical synchronization effects) which depress the disorder and lead to periodical motion. In this connection, it is relevant to mention the experiment with coupled chain of harmonic oscillators performed by Fermi, Pasta and Ulam. Instead of ergodicity which was expected they found periodic oscillations. However, if dynamical synchronization effects do not depress ergodicity and if the characteristic time during which the motion can be approximated as periodic is too short one has to apply methods of statistical mechanics.

ACKNOWLEDGEMENTS

The research described in this paper was carried out by the Jet Propulsion Laboratory, California Institute of Technology, under NASA Contract No NAS7-918. The effort was supported by Dr. A. Amos, Air Force Office of Scientific Research.

REFERENCES

W. Flugge, (1962). Handbook of Engineering Mechanics, McGraw Hill Co., New York, pp 64-11.

J. Miklowitz, (1986). The theory of elastic waves and waveguides, North Hollywood, New York, pp 71.

M. Zak, (1983). Wrinking phenomenon in structures, Part II, Solid mechanics archives, 8, pp. 279-311.

C. H. Hodges, (1982). Confinement of vibrations by structural irregularities, J. Sound and vibrations, 82(3), 411-424.

M. Zak, (1986). Characteristic wave approach in controlled large space structures, AIAA/ASME/ASCE/AHS 27th Structures, Structural Dynamics and Material Conference, San Antonio, TX.

Modeling of Controlled Structures
with Impulsive Loads

by Michail Zak

Jet Propulsion Laboratory
Caltech

Spectral Methods

1. Modal Approach

$$U(x,t)=\sum_{m=1}^{\infty} X_m(x)\,T_m(t)$$

$$\left.\begin{aligned} X_m &= A_m' \cos \lambda_m x + A_m'' \sin \lambda_m x \\ T_m &= B_m' \cos \omega_m t + B_m'' \sin \omega_m t \end{aligned}\right| \begin{aligned} &\text{e.f.} \\ &\text{time f.} \end{aligned}$$

λ_m - shape parameter, ω - frequency

2. Travelling Wave Approach

$$U(x,t) = \sum_{m=1}^{\infty} A_m \cos(kx-\omega t) + B_m \sin(kx-\omega t)$$

$C = \dfrac{\omega}{k}$ - speed of wave propagation

Characteristic Wave Approach

$A_m, B_m \sim \left(\frac{1}{m}\right)^{n+1}$.

$f^{(n)}$ - continuous

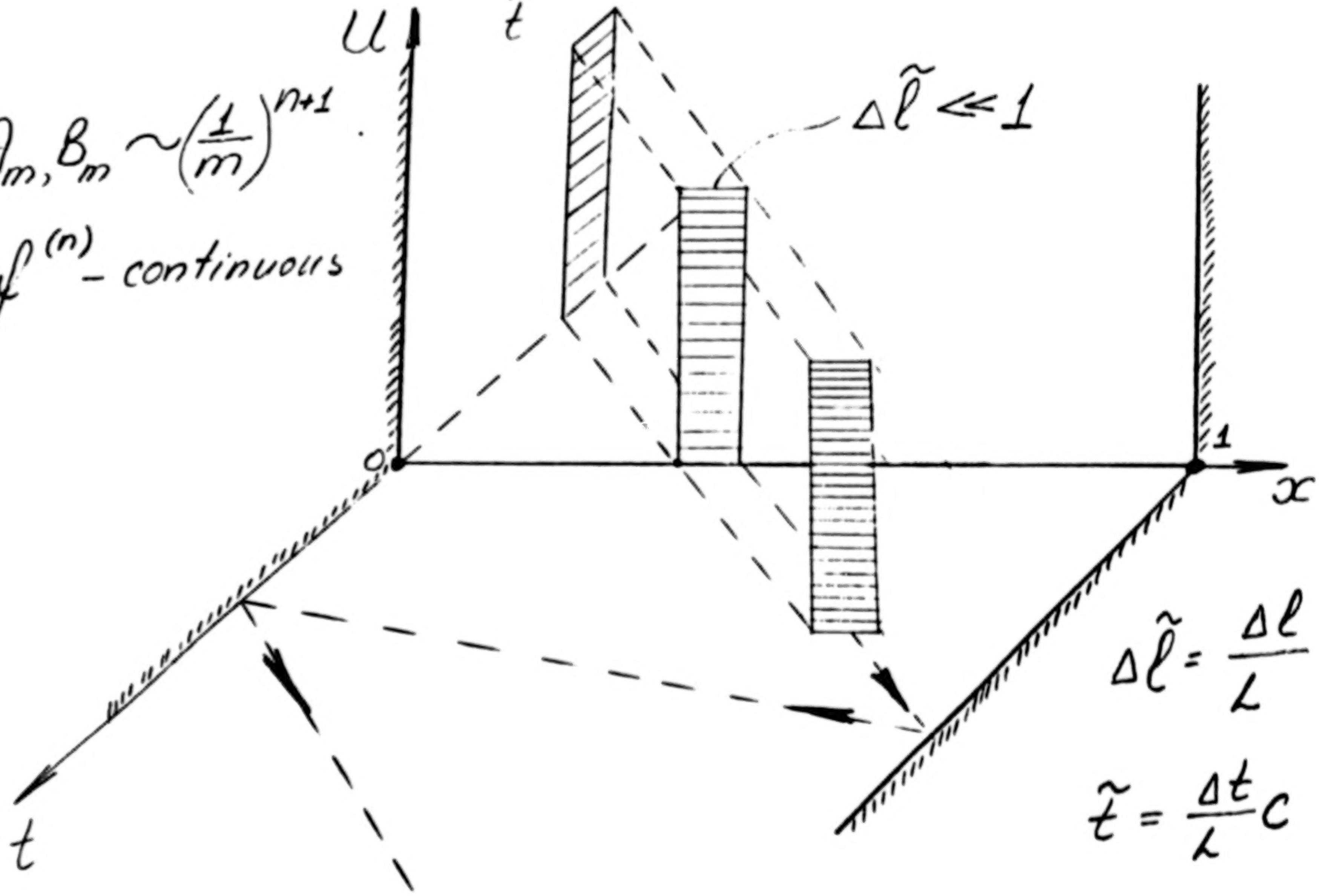
U
$\hat{t}$
$\Delta\tilde{l} \ll 1$
0
1
x
t

$\Delta\tilde{l} = \frac{\Delta l}{L}$

$\tilde{t} = \frac{\Delta t}{L} c$

Characteristic Speeds

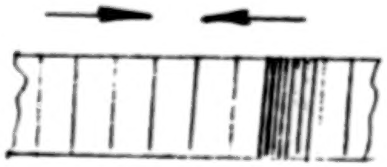

$C_B^2 = \frac{E}{\rho}$ - longitudinal wave

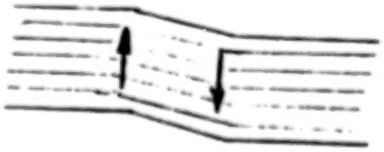

$C_V^2 = \frac{GA_s}{\rho A}$ - shear wave

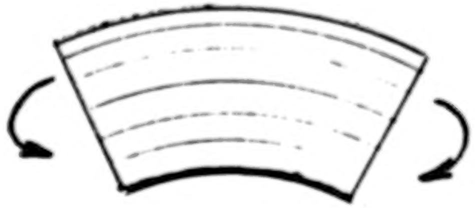

$C_M^2 = \frac{EI}{\rho I}$ - bending wave

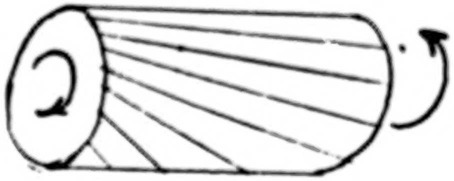

$C_T^2 = \frac{G}{\rho}$ - torsion wave

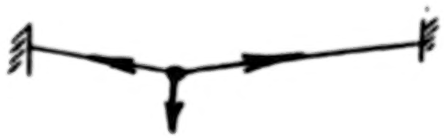

$C_S^2 = \frac{T}{\rho}$ - shear string wave

Linear Effects

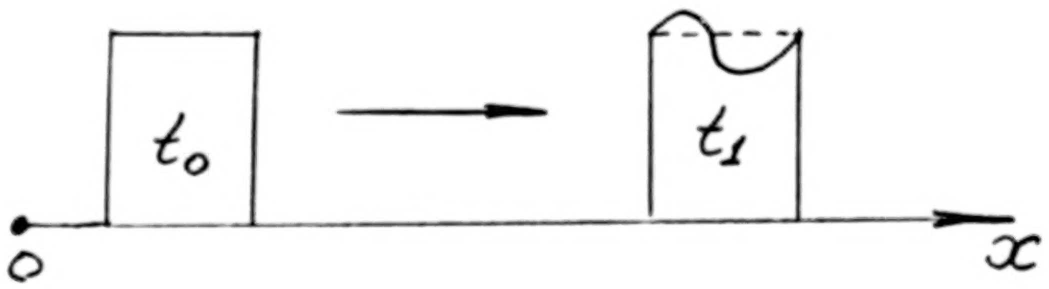

- Dispersion

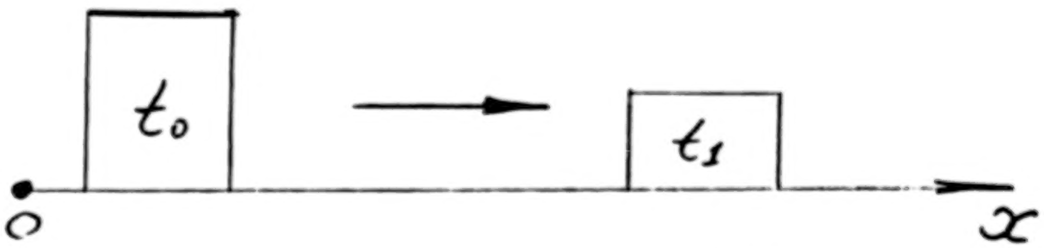

- Damping

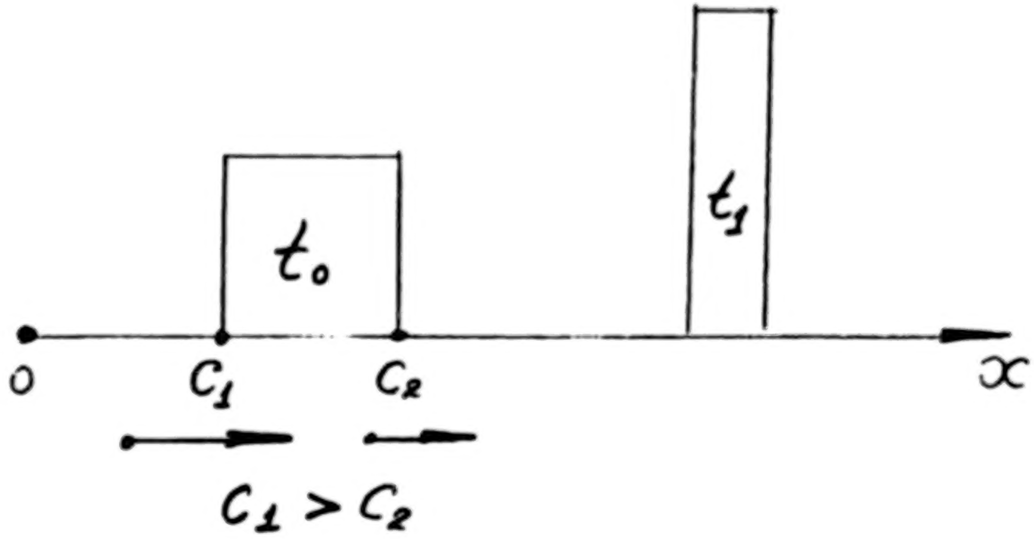
t_o
t_1
0
c_1
c_2
x
$c_1 > c_2$

- Cumulative effect

Periodic Structures: reflections

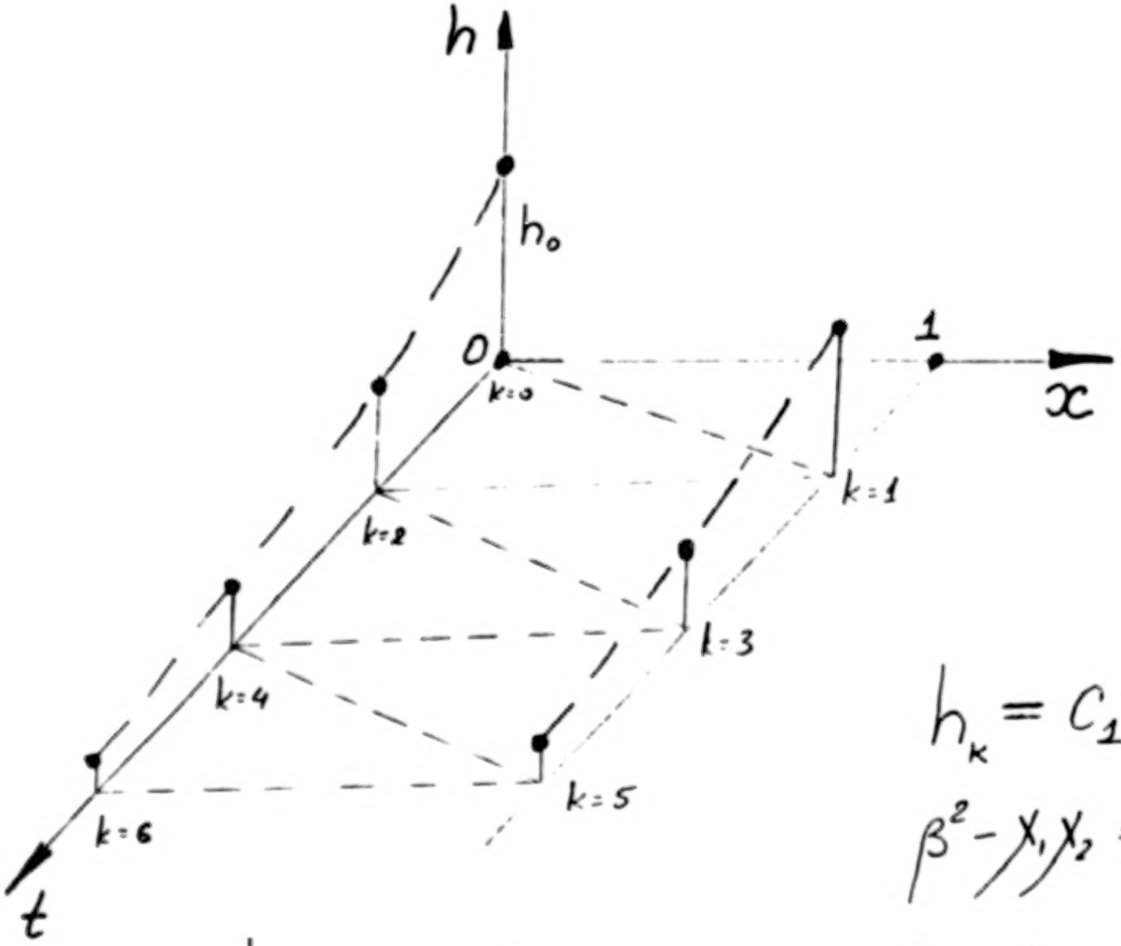

$$h(1, t+1) = \chi_1 h(0, t)$$

$$\underbrace{h(0, t+2) = \chi_2 h(0, t+1)}$$

$$\downarrow$$

$$h_{k+2} - \chi_1 \chi_2 h_k = 0$$

$$h_k = C_1 e^{r_1 k} + C_2 e^{r_2 k}, \quad r_m = \log \beta_m$$

$$\beta^2 - \chi_1 \chi_2 = 0, \quad \beta_1 = \sqrt{\chi_1 \chi_2}, \quad \beta_2 = -\sqrt{\chi_1 \chi_2}$$

$$\left.\begin{aligned} h_0 &= C_1 + C_2 \\ h_1 &= (C_1 - C_2)\sqrt{\chi_1 \chi_2} = 0 \end{aligned}\right\} \quad \begin{aligned} C_1 &= C_2 = \tfrac{1}{2} h_0 \\ h_{2n} &= h_0 (\chi_1 \chi_2)^n \,. \end{aligned}$$

Periodic Structures: transmission and reflection

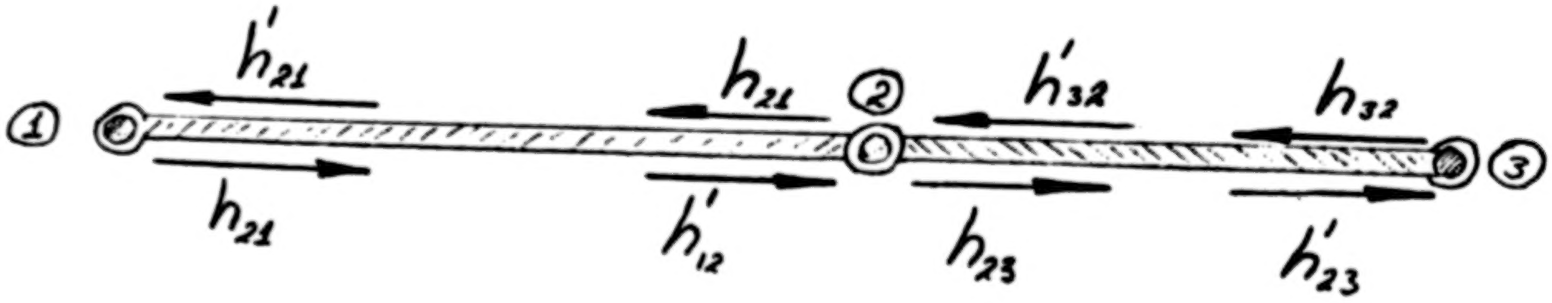

Propagation	Reflection- transmission
$h'_{12}(t+1) = \xi_{12}\, h_{12}(t)$	$h_{12} = \xi_1\, h_{21}$
$h'_{23}(t+1) = \xi_{23}\, h_{23}(t)$	$h_{21} = \xi_2\left[\eta_2\, h'_{12} + (1-\eta_2)\, h'_{32}\right]$
$h'_{32}(t+1) = \xi_{23}\, h_{32}(t)$	$h_{32} = \xi_3\, h'_{23}$
$h'_{21}(t+1) = \xi_{12}\, h_{21}(t)$	$h_{23} = \xi_2\left[\eta_2\, h'_{32} + (1-\eta_2)\, h'_{12}\right]$

$$0 \leq \xi_{ij} \leq 1, \qquad 0 \leq \xi_k \leq 1, \qquad -1 \leq \eta \leq 1$$

Governing Equations

$$h_{k+1} = A\mathbf{h}_k ,$$

$$A = \begin{pmatrix} 0 & -\xi_{12}\xi_1 & 0 & 0 \\ -\xi_{12}\xi_2\zeta_{12} & 0 & 0 & -\xi_{12}\xi_2(1-\zeta_{12}) \\ -\xi_{23}\xi_2(1-\zeta_{12}) & 0 & 0 & -\xi_{23}\xi_2\zeta_{12} \\ 0 & 0 & -\xi_{23}\xi_3 & 0 \end{pmatrix}$$

$$h_k = \begin{pmatrix} h'_{12} \\ h'_{21} \\ h'_{23} \\ h'_{32} \end{pmatrix}$$

Multi-member Structures

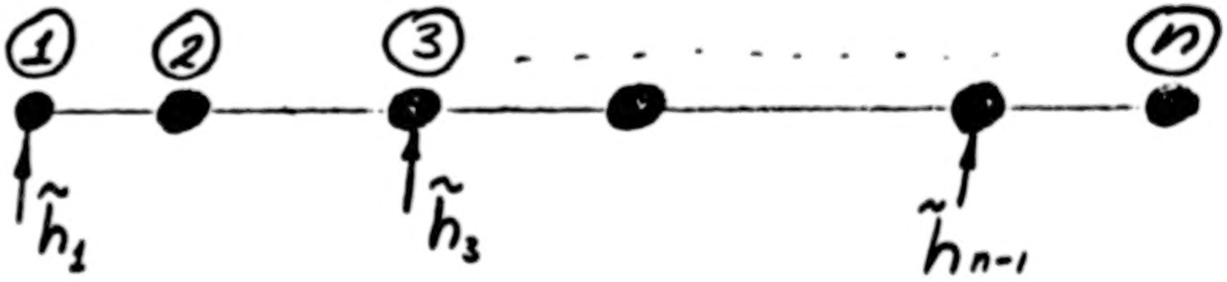
①
②
③
n
$\tilde{h}_1$
$\tilde{h}_3$
$\tilde{h}_{n-1}$

$$\mathbf{h}_{k+1} = A\,\mathbf{h}_k + \tilde{\mathbf{h}}_k$$

$$\tilde{\mathbf{h}}_k = \begin{Bmatrix} \tilde{h}_1 \\ \tilde{h}_2 \\ \vdots \\ \tilde{h}_n \end{Bmatrix}, \qquad A = \begin{pmatrix} A_{11} & A_{12} & \cdots & A_{1n} \\ A_{21} & \cdots & - & \cdots \\ \vdots & & & \\ A_{n1} & \cdots & & A_{nn} \end{pmatrix}$$

Analysis of Solutions

$$\boldsymbol{h}_k = A^k \boldsymbol{h}_0 + \sum_{j=0}^{k-1} A^j \tilde{\boldsymbol{h}}_{k-j-1}, \quad (k = 0, 1, 2, \dots)$$

$$|A - \lambda \bar{I}| = 0, \quad A^m = \sum_{j}^{2n} \lambda_j^m Z_j(A)$$

$$Z_r(A) = \left[\lambda_1^m \bar{I} + m \lambda_1^{m-1} (A - \lambda_1 \bar{I})\right) \frac{\prod_{p=3}^{2n} (A - \lambda_p \bar{I})}{\prod_{p=3}^{2n} (\lambda_1 - \lambda_p)}$$

Conditions of Stability

$$|\lambda_i| < 1, \quad i = 1, 2, \dots 2n,$$

$$\lambda = \frac{\tilde{\lambda} + 1}{\tilde{\lambda} - 1}$$

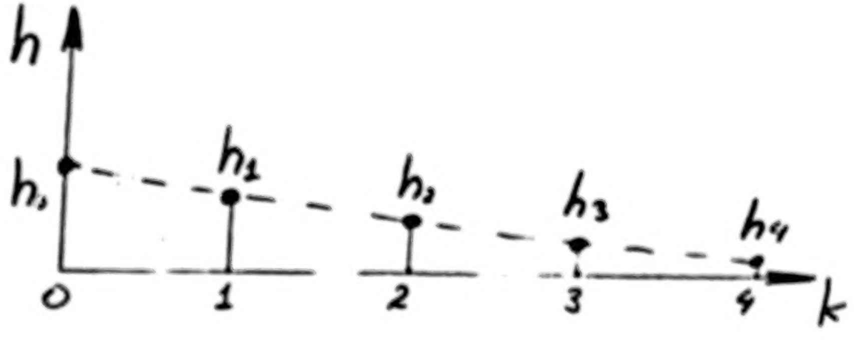

Transition to ergodicity

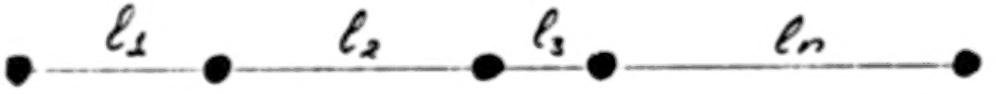

$$\lambda^n + \alpha_1 \lambda^{n-1} + \ldots = 0$$

n is the least common multiple of $2l_1, 2l_2, \ldots 2l_n$

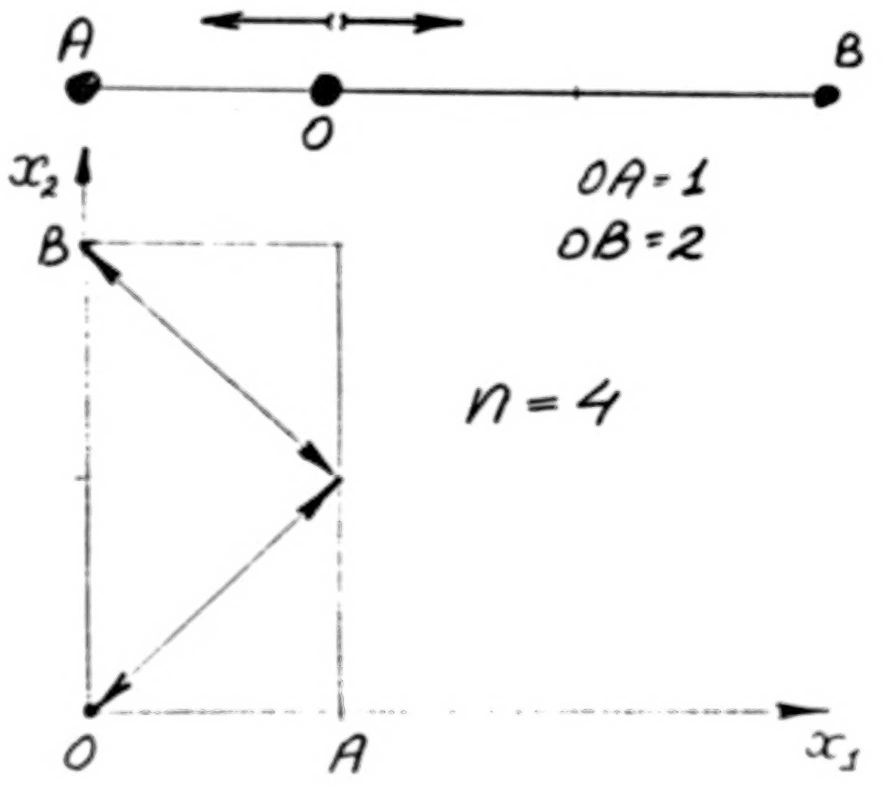
A
O
B
x_2
B
O
A
x_1

$OA = 1$
$OB = 2$

$n = 4$

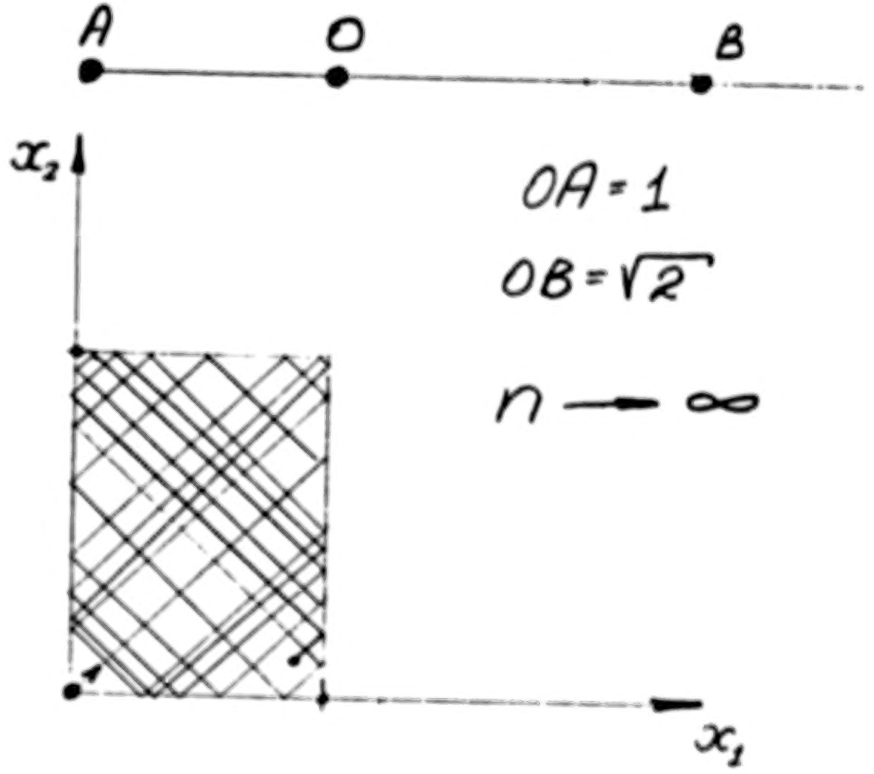

$OA = 1$
$OB = \sqrt{2}$

$n \rightarrow \infty$

Ergodicity in a Timoshenko beam

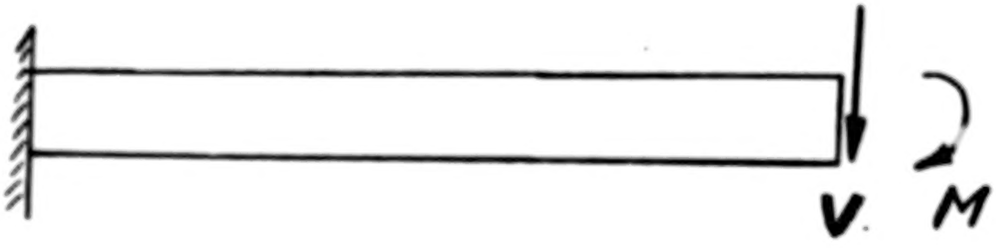

$$\frac{C_M}{C_V} = 2.8\sqrt{2}$$

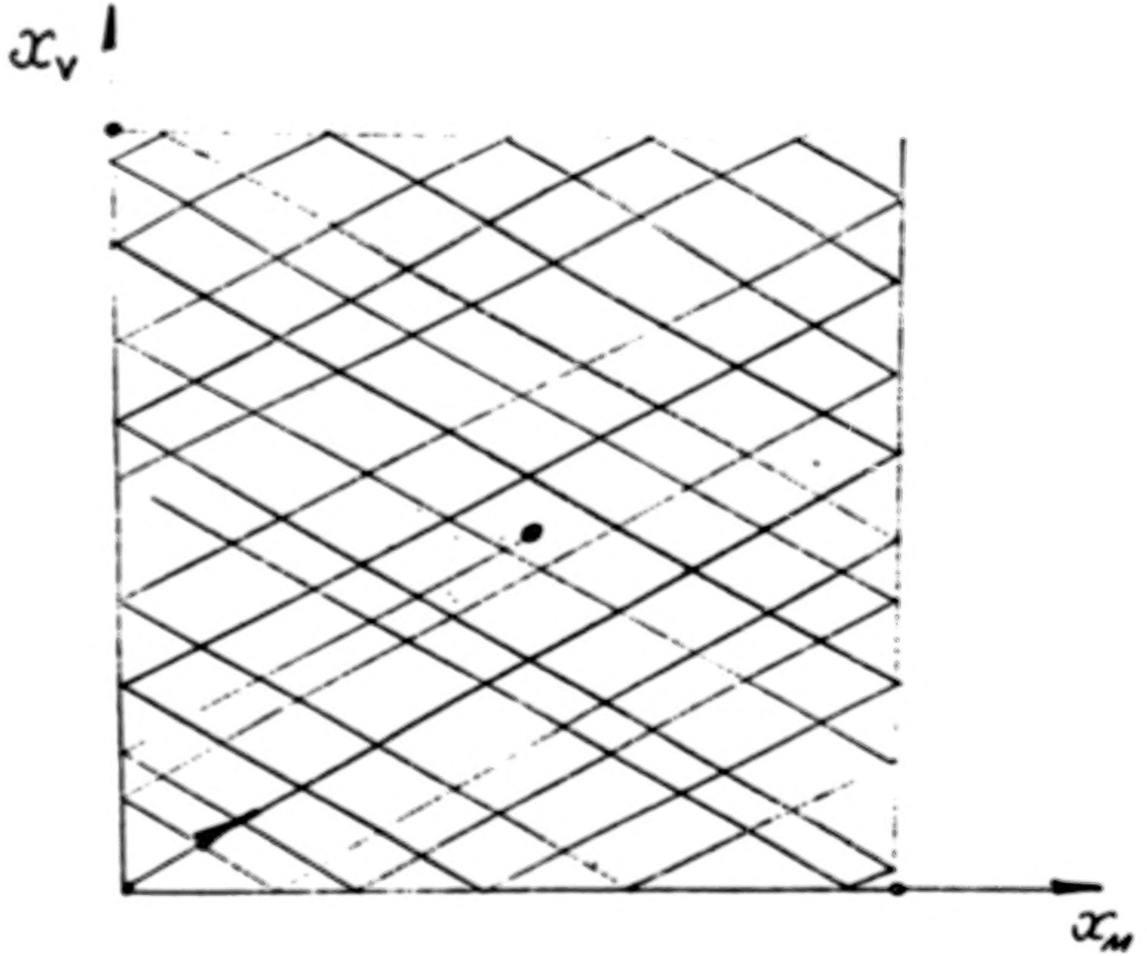

Thursday, April 24, 1986

SESSION 5

Critical Issues Forum

Control	Structures	Integrated
S. Seltzer	B. Wada	L. Pinson

(Concurrent Sessions on Integrated and Structures/Integrated)

Structures Integrated Session 5 - Carleton Moore, Chairman

Notes on Implementation of Coulomb Friction in Coupled Dynamical Simulations	R. J. VanderVoort, R. P. Singh, DYNACS
On the Control of Structures by Applied Thermal Gradients	D. R. Edberg and J. C. Chen, JPL
Finite Element Models of Wire Rope for Vibration Analysis	J. E. Cochran, Jr. N. G. Fitz-Coy, Auburn Univ.
Experimental Characterization of Deployable Trusses and Joints	R. Ikegami and S. Church, Boeing D. Kienholz and B. Fowler, CSA Eng.

Integrated Session 5 - Don McCutcheon, Chairman

System Identification for Large Space Structure Damage Assessment	J. C. Chen and J. A. Garba, JPL
Space Station Structures and Dynamics Test Program (Proposed)	E. W. Ivey, C. J. Moore, J. S. Townsend, MSFC
Analytical Determination of Space Station Response to Crew Motion and Design of Suspension System for Microgravity Experiments	F. C. Liu, UAH
Space Station Structural Dynamics/ Reaction Control System Interaction Study	M. Pinnamaneni, MMC

NASA MARSHALL SPACE FLIGHT CENTER

WORKSHOP

ON

DYNAMICS & CONTROL INTERACTION

OF

FLEXIBLE STRUCTURES

SESSION 5

CRITICAL ISSUES FORUM: CONTROL

CHAIRMAN: SHERM SELTZER

PRECEDING PAGE BLANK NOT FILMED

PRELIMINARIES

DEF. [WEBSTER'S NEW (1945) COLLEGIATE DICTIONARY]

FORUM (FO'RUM) [L.]

1. THE MARKET PLACE OR PUBLIC PLACE OF A CITY, CENTER OF JUDICIAL AND PUBLIC BUSINESS;
2. TRIBUNAL; COURT;
3. HENCE, A PUBLIC MEETING PLACE FOR OPEN DISCUSSION.

CONCURRENT ISSUES "FORA" [L.]:

- STRUCTURES
- INTEGRATED

DEF: FLEXIBLE STRUCTURE:

A LARGE SPACE STRUCTURE (LSS) WITH ...

... CERTAIN CHARACTERISTICS --> "PATHOLOGIES"

PROPOSED CONTROL CRITICAL ISSUES FORUM AGENDA

- PRIME THE PUMP

  1. EXPECTED LSS'S IN IMMEDIATE (?) FUTURE
  2. LSS PATHOLOGIES
  3. RESULTING CONTROL SYSTEM DESIGN REQUIREMENTS
  4. DEFINITIONS OF "CLASSES" OF LSS CONTROL
  5. DEFINE "THE PROBLEM"

- DISCUSSION OF THE "PROBLEM" --> CRITICAL ISSUES

EXPECTED LSS OF FUTURE

- NASA SPACE STATION
- VARIOUS STRATEGIC DEFENSE INITIATIVE (SDI) SPACECRAFT
- LARGE ANTENNAS OR REFLECTORS
- OTHER SHUTTLE-BORNE PAYLOADS

EXPECTED LSS CHARACTERISTICS → PATHOLOGIES

	NASA SPACE STATION	SDI S/C
SYSTEM		
• COMPLEX	X	X
• LARGE	X	X
• MIMO PLANT	X	X
• IGNORANCE OF CHARACTERISTICS	X	X
MISSION		
• STRINGENT POINTING, TRACKING REQUIREMENTS	0	X
• CHANGES IN FLIGHT CONFIGURATION (CONTINUOUS, DISCRETE)	X	?
• MANNED	X	0
• UNEXPECTED MISSION CHANGES	X	0
• MANEUVERS AND ATTITUDE VARIATIONS	X	X

EXPECTED LSS CHARACTERISTICS + PATHOLOGIES (CONTINUED)

	NASA SPACE STATION	SDI S/C
DYNAMICS		
• INTERACTION BETWEEN DYNAMICS AND CONTROL SYSTEM		
- FLEXIBLE STRUCTURE	X	?
- SIGNIFICANT MOVING PARTS	X	X
- ENVIRONMENT	X	X
- DISTURBANCES/NOISE	X	X
• LIMITED GROUND TEST/VALIDATION	X	0
• AMENABLE TO ON-ORBIT REFINEMENT	X	X
PERFORMANCE		
LONG DURATION FLIGHT	X	X
FAIL-SAFE	X	X
AMENABLE TO IN-FLIGHT UNIT REPLACEMENT(S)	X	X

RESULTING CONTROL SYSTEM DESIGN REQUIREMENTS

- MIMO
- DIGITAL
- ADAPTABLE
- ROBUST
- RELIABLE
- AMENABLE TO IN-FLIGHT UNIT REPLACEMENTS

? • RELATIVELY SIMPLE

DEFINITIONS OF LSS CONTROL

CAN DEFINE 4 CLASSES (TYPES) OF LSS CONTROL:

1. VERY SHORT TERM (HI BW)
    - FIGURE CONTROL
    - IMAGE MOTION COMPENSATION
    - OPTICAL TRAIN MOTION (BEAM CONTROL)
2. SHORT TERM (MED HI BW)
    - MANEUVERS
        - SLEWING (RETARGETING)
        - ACQUISITION
    - ATTITUDE CONTROL (POINTING)
    - VIBRATION SUPPRESSION
3. MEDIUM TERM
    - STATION KEEPING
4. LONG TERM (LO BW)
    - MOMENTUM MANAGEMENT

THE PROBLEM

- "ACCEPTABLE PERFORMANCE"
  - REASONABLE DYNAMIC RESPONSE TO STANDARD TEST INPUTS
  - REASONABLE REJECTION/ACCOMMODATION OF NOISE/DISTURBANCES
  - ROBUSTNESS TO INACCURACIES/CHANGES IN CURRENT SYSTEM CHARACTERISTICS
    - .. IGNORANCE
    - .. TIME-VARYING (CONTINUOUS AND/OR DISCRETE)

- COMPLICATIONS
  - MANAGEMENT → MYOPTIC SAVINGS IN RESOURCES/TIME
  - SYSTEMS ENGINEERS → NOT SCHOOLED IN CONTROLS AND DYNAMICS
  - LANGUAGE BARRIERS

- THE DEFINITION OF THE DESIGN GOALS
  - EMPHASIZE WHAT IS PRACTICAL → YOU (DESIGNER) MUST LIVE WITH IT
  - NEED FOR REAL COMMUNICATION AMONGST PARTICIPANTS
  - DETERMINE HOW TO VERIFY (AND WHY?)

CRITICAL ISSUES

1. DEMAND DEFINITION OF SYSTEM MISSION(S)
2. DEFINE & DETERMINE CONTROL SYSTEM REQUIREMENTS (SPECS)
3. PARTICIPATE IN DETERMINATION OF O/A SYSTEM CONFIGURATION
4. LEARN FROM HISTORY WHERE APPROPRIATE

   EXAMPLE: SKYLAB
5. ADEQUATE SENSING OF STRUCTURAL FLEXIBILITY
6. ADEQUATE VIBRATION SUPPRESSION DEVICES (ACTUATORS)
   - SUFFICIENT CONTROL AUTHORITY
   - LIGHTWEIGHT

CRITICAL ISSUES (Continued)

7. SUFFICIENTLY ACCURATE MODELS

- WHAT MUST BE MODELED?
  - THE "PLANT" (Incl. NL)
  - ACTUATORS (Incl. NL)
  - SENSORS (Incl. NL & Noise)
  - DISTURBANCES (Realism?)
  - COMPUTER CHARACTERISTICS
- ALTERNATES TO MODAL REPRESENTATIONS
- SYSTEM IDENTIFICATION
- VERIFICATION AND SUBSEQUENT MODIFICATION (DEMO. FLIGHT READINESS)
  - COMPUTER & HWIL SIMULATION
  - GROUND TEST
  - FLIGHT (ON-ORBIT) TEST

CRITICAL ISSUES (CONTINUED)

8. COMPUTATION ERRORS, FINITE WORDLENGTHS, SAMPLING

9. COPING WITH INACCURATE MODELS → NEED MIMO ROBUSTNESS
   - ADAPTIVE CONTROL
   - INSENSITIVE CONTROL
   - DISTURBANCE ACCOMMODATION
   - ON-ORBIT DESIGN

10. COPING WITH VIBRATIONS
    - ACTIVE "CONTROLS" TECHNOLOGY/TECHNIQUES: NEED ANY MORE?
    - DISTRIBUTED CONTROL (AND OBSERVABILITY)
    - DAMPING (PASSIVE, ACTIVE)
      - PHYSICAL AUGMENTATION
      - "LAC"

11. SIMULATION CAPABILITY
    - SPEED
    - CAPACITY

12. COST OF ENTIRE CONTROLS EFFORT

1. DEFINE SYSTEM MISSIONS

	(L)ST	SPACE STATION
WHO'S IN CHARGE?	?	?
OBJECTIVE(S): WHAT MUST SYSTEM DO?	ASTRONOMY	?
FIXED OR CHANGING CONFIGURATION	FIXED	CHANGING
DURATION	10 YEARS	?
TIME FRAME	1986-1996	?
DESIGN/VALIDATION SCHEDULE	-	-
MANNED?	NO	YES
MAINTENANCE	SHUTTLE VISITS	CONTINUOUS

2. DEFINE AND DETERMINE CONTROL SYSTEM REQUIREMENTS (SPEC'S)

- ACCURACY(<): $\widehat{A}$
- STABILITY(<): $\widehat{S}$
  (TIME DURATION)
- JITTER (</τ)
- ACQUISITION TIME
- RE-TARGETING
- EFFECTS OF
  - POORLY KNOWN SYSTEM CHARACTERISTICS
  - VARYING CHARACTERISTICS (CONTINUOUS AND/OR DISCRETE)
- STRUCTURAL MODE PLACEMENT
  - FILTERING
  - SHAPED MANEUVERS/COMMANDS
  - STIFFER STRUCTURE
  - DAMPING

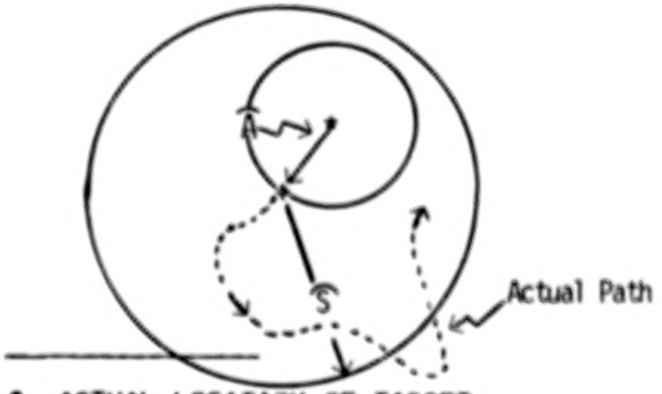

•: ACTUAL LOCATION OF TARGET

+: WHERE SENSOR(S) THINK TARGET IS LOCATED

3. DETERMINE O/A SYSTEM CONFIGURATION

- MOMENTUM MANAGEMENT
  - RCS
  - MAGNETIC DESATURATION
- MANEUVERS
- POINTING AND/OR TRACKING (ATTITUDE CONTROL)
- ENERGY SOURCE
  - SOLAR ARRAYS
  - OTHER

4. NASA SKYLAB

PROBLEMS ENCOUNTERED

- SYSTEM GREW SIGNIFICANTLY DURING DESIGN AND DEVELOPMENT
- UNPLANNED RADICALLY CHANGED GEOMETRY DURING LAUNCH
- RATE GYROS: REPLACED IN FLIGHT
- CMG'S: ONE FAILED, ONE THREATENED

NASA SKYLAB (CONTINUED)

LESSONS LEARNED

- ADAPTABILITY OF DIGITAL CONTROLLER
- AD HOC ON-ORBIT TEST
- NEED INSTRUMENT/ACTUATOR REPLACEMENT CAPABILITIES
- NEED FOR SIMPLE CONTROL LAW: COPE WITH UNEXPECTED
- FAILURE TOLERANT AND REPLACEMENT CAPABILITY RQD
- SYSTEM GROWTH (CMG REDUNDANCY)

N87
22746
UNCLAS

N87-22746

NOTES ON IMPLEMENTATION OF COULOMB FRICTION IN COUPLED DYNAMICAL SIMULATIONS

R. J. VanderVoort

R. P. Singh

DYNACS Engineering Company, Inc.
CLEARWATER, FLORIDA 33575

PRECEDING PAGE BLANK NOT FILMED

SYSTEM TOPOLOGY

A coupled dynamical system is defined as an assembly of rigid/flexible bodies that may be coupled by kinematical connections. Large relative displacement and rotation are permitted. The interfaces between bodies are modeled using hinges having 0 to 6 degrees of freedom. A hinge is defined as a pair of two material points, one on each of two adjoining bodies. A reference body is arbitrarily selected and it is assumed for convenience that the reference body is connected to an imaginary inertially fixed body. For consistency, a fictitious hinge is assigned to the reference body by assuming P_0 (See Figure), an inertial point. Thus the number of hinges equals the number of bodies in the system (as shown in Figure 2).

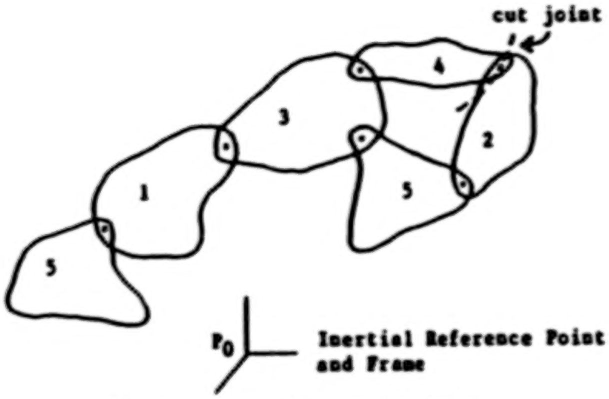
cut joint
4
3
2
1
5
5
P_0
Inertial Reference Point and Frame

Figure 1 An Arbitrary Topology

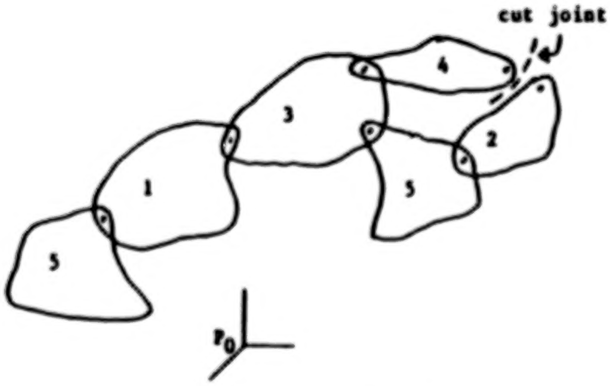
cut joint
4
3
2
1
5
5
P_0

Figure 2 Equivalent Tree Topology

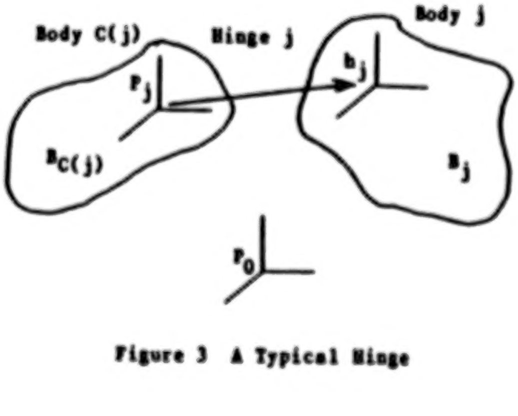
Body C(j)
Hinge j
Body j
P_j
h_j
$B_{C(j)}$
B_j
P_0

Figure 3 A Typical Hinge

CONSTRAINED DYNAMICAL SYSTEM

For a mechanical system of n flexible bodies in a topological tree configuration, the equations of motion are presented in Reference 1. Lagrange's form of D'Alembert's principle was employed to derive the equations. A detailed discussion of the approach is available in References 1 and 2. Equations (14), (15) in Reference 1 are the motion equations for the system of Figure 2. These equations are augmented by the kinematical constraint equations. This augmentation is accomplished via the method of singular value decomposition (see Reference 3).

CONSTRAINED DYNAMICAL SYSTEMS

- LET $q_1, \ldots, q_n$ DEFINE THE CONFIGURATION OF UNCONSTRAINED SYSTEM

- CONSTRAINT EQUATIONS

  $A \dot{q} = B$ $\qquad A_{m \times n}$

  $m < n$

- NUMBER OF INDEPENDENT COORDINATES

  = n-RANK A

- EQUATIONS OF MOTION

  $M \ddot{q} = f + f_c$

  f_c - FORCES/MOMENTS OF CONSTRAINT

- PROBLEMS OF PRACTICAL INTEREST

  - SIMPLE NON HOLONOMIC OR HOLONOMIC CONSTRAINTS

  - $n+m$ 2nd ORDER D.E.

    OR $2n+m$ 1st ORDER D.E.

SINGULAR VALUE DECOMPOSITION

- L $m \times n$ MATRIX

  THERE EXIST ORTHOGONAL MATRICES $U_{m \times m}$ AND $V_{n \times n}$

  SUCH THAT $U^T L V = \left[\begin{array}{c|c} X & 0 \\ \hline 0 & 0 \end{array} \right] = S$

  $X = \mathrm{DIAG}\ (\lambda_1 > \lambda_2 > \ldots . > \lambda_r)$ $\quad r = \mathrm{RANK}\ L$

- λ_i^2 - NONZERO EIGENVALUES OF $L^T L$

  $L = USV^T$

$$\Rightarrow [\ U_1 \mid U_2\ ] \left[\begin{array}{c|c} X & 0 \\ \hline 0 & 0 \end{array} \right] \left[\begin{array}{c} V_1^T \\ \hline V_2^T \end{array} \right]$$

V_2 SPANS NULL SPACE OF L

U_2 SPANS NULL SPACE OF L^T

$LV_2 = 0 \qquad L^+ = V \left[\begin{array}{c|c} X^{-1} & 0 \\ \hline 0 & 0 \end{array} \right] U^T$

L^+ = PSEUDO INVERSE OF L

APPLICATION OF SVD TO CONSTRAINED SYSTEMS

- $A\dot{q} = B$

  $\dot{q} = A^{+}B + V_2\dot{z}$ $\dot{z}$ COLUMN VECTOR (n-r)

  $V_2\dot{z}$ SOLUTION OF $A\dot{q} = 0$

  $A^{+}B$ PARTICULAR SOLUTION

- DIFFERENTIATE

  $A\ddot{q} = \dot{B} - \dot{A}\dot{q}$

  $A\ddot{q} = B'$

  $\ddot{q} = A^{+}B + V_2\ddot{z}$

- Z's ARE REDUCED SET OF n-r COORDINATES

  V_2 IS THE DESIRED TRANSFORMATION

- $M\ddot{q} = F + F^c$

  PROJECTION ON NULL SPACE OF A

  $V_2^T M\ddot{q} = V_2^T F + V_2^T F^c$

  SUBSTITUTE FOR $\ddot{q}$

  $V_2^T M V_2 \ddot{z} = V_2^T F + V_2^T F^c - V_2^T M A^+ B$

- $F^c = A^T \lambda$ λ - LAGRANGE MULTIPLIERS

  $V_2^T F^c = V_2^T A^T \lambda$

  $= [A V_2]^T \lambda = 0$

- $[V_2^T M V_2] \ddot{z} = V_2^T F - V_2^T M A^+ B$ GOVERNING DIFF. EQN.

  $\dot{q} = A^+ B + V_2 \dot{z}$

DAMPING LAW

- ACTUAL DAMPING LAW:

  $F_f(t_1)$ = f(LOAD OVER CONTACT AREA;

  $x(t),\ 0 < t < t_1,\ t_1,\ \ldots)$

  F_f = FRICTION FORCE

  $x(t),\ 0 < t < t_1$, REPRESENTS THE HISTORY OF MOTION PRIOR TO t_1

- IN GENERAL THE DAMPING LAW IS VERY COMPLICATED

- COULOMB DAMPING

  $F_f(t_1) = f(N,\ \mathrm{SIGN}(\dot{x}(t_1)),\ \mu_S,\ \mu_d$

  N - NORMAL LOAD

  μ_s - STATIC COEFFICIENT OF FRICTION

  μ_d - DYNAMIC COEFFICIENT OF FRICTION

$$\mathrm{SIGN}(x(t_1)) = \begin{cases} 1 & \dot{x}(t_1) > 0 \\ 0 & \dot{x}(t_1) = 0 \\ -1 & \dot{x}(t_1) < 0 \end{cases}$$

COULOMB DAMPING (CONT.)

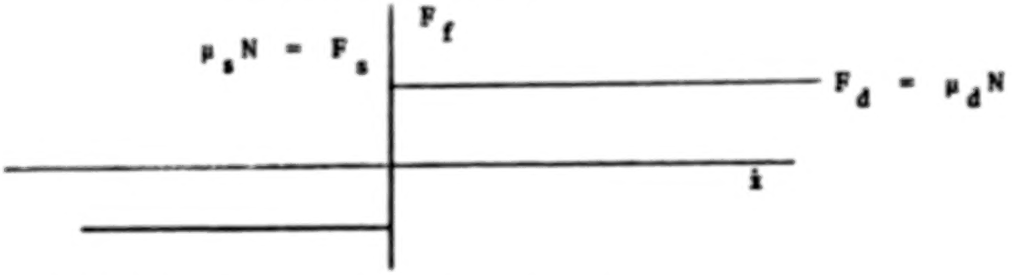

- THE MOST COMMON DRY FRICTION DAMPING LAW

  $\mu_s = \mu_d$ OR $F_s = F_d$

- MANY TIME DOMAIN AND FREQUENCEY DOMAIN STUDIES HAVE BEEN PERFORMED FOR HARMONICALLY EXCITED SYSTEMS WITH DRY FRICTION DAMPING. THERE ARE THREE BASIC METHODS OF ANALYSIS
  - EXACT
  - HARMONIC APPROXIMATIONS
  - TIME INTEGRATION

- OUR APPROACH IS TIME INTEGRATION

- STICK/SLIP MOTION

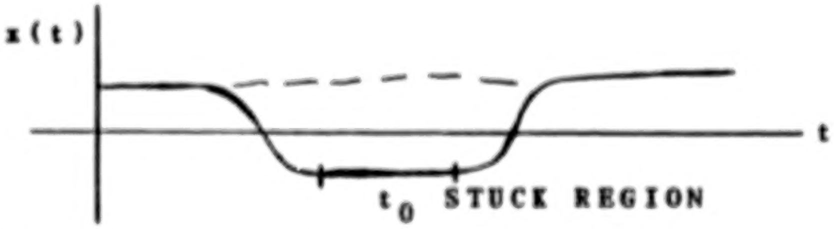

  t_0 BECOMES AN UNKNOWN.

- STUCK HINGE RESULTS IN ADDITIONAL CONSTRAINTS ON KINEMATICAL VARIABLES.

COULOMB DAMPER ALGORITHM

- A TYPICAL HINGE WITH COULOMB DAMPER

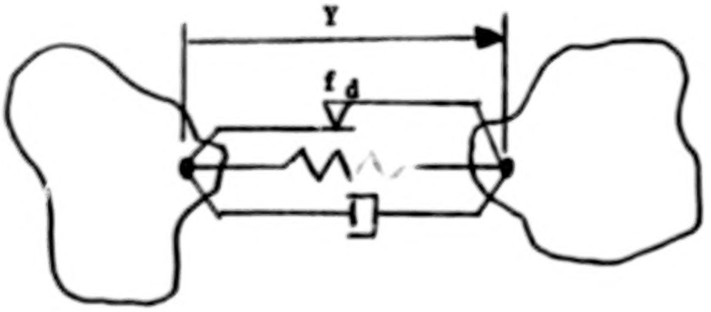

- TRACK $\dot{Y}$ (RELATIVE VELOCITY) FOR SIGN CHANGE

- $\dot{Y}$ CHANGES SIGN

  COMPARE $|\dot{Y}$ DIFFERENCE$|$ TO A PRESCRIBED $\epsilon \sim 0$

  IF GREATER THAN ϵ GO BACK TO PREVIOUS STEP AND REDUCE THE STEP SIZE AND REPEAT UNTIL $|Y$ DIFFERENCE$| < \epsilon$

  ACTIVATE THE CONSTRAINT $\dot{Y} = 0$ AND COMPUTE CONSTRAINT FORCE f_c FOR THIS CONSTRAINT

  IF f_c OVERCOMES f_d SLIP CONDITION, DEACTIVATE $\dot{Y} = 0$

  IF NOT, STICK CONDITION, RETAIN $\dot{Y} = 0$ AND KEEP COMPARING f_c WITH f_d UNTIL SLIP CONDITION

EXAMPLE

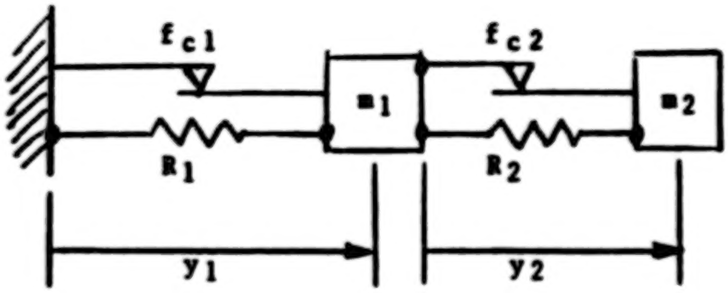

f_{c1}
f_{c2}
m_1
m_2
k_1
k_2
y_1
y_2

$m_1 = 1$ $m_2 = 1$

$k_1 = 2$ $k_2 = 2.5$

INITIAL CONDITION $y_1 = 1$ $y_2 = .2$

TEST CASES FOR VARIOUS COULOMB DAMPER LEVELS

	f_{c1}	f_{c2}
CASE 1	0	0
CASE 2	.1	0
CASE 3	.1	.1
CASE 4	.1	8000.

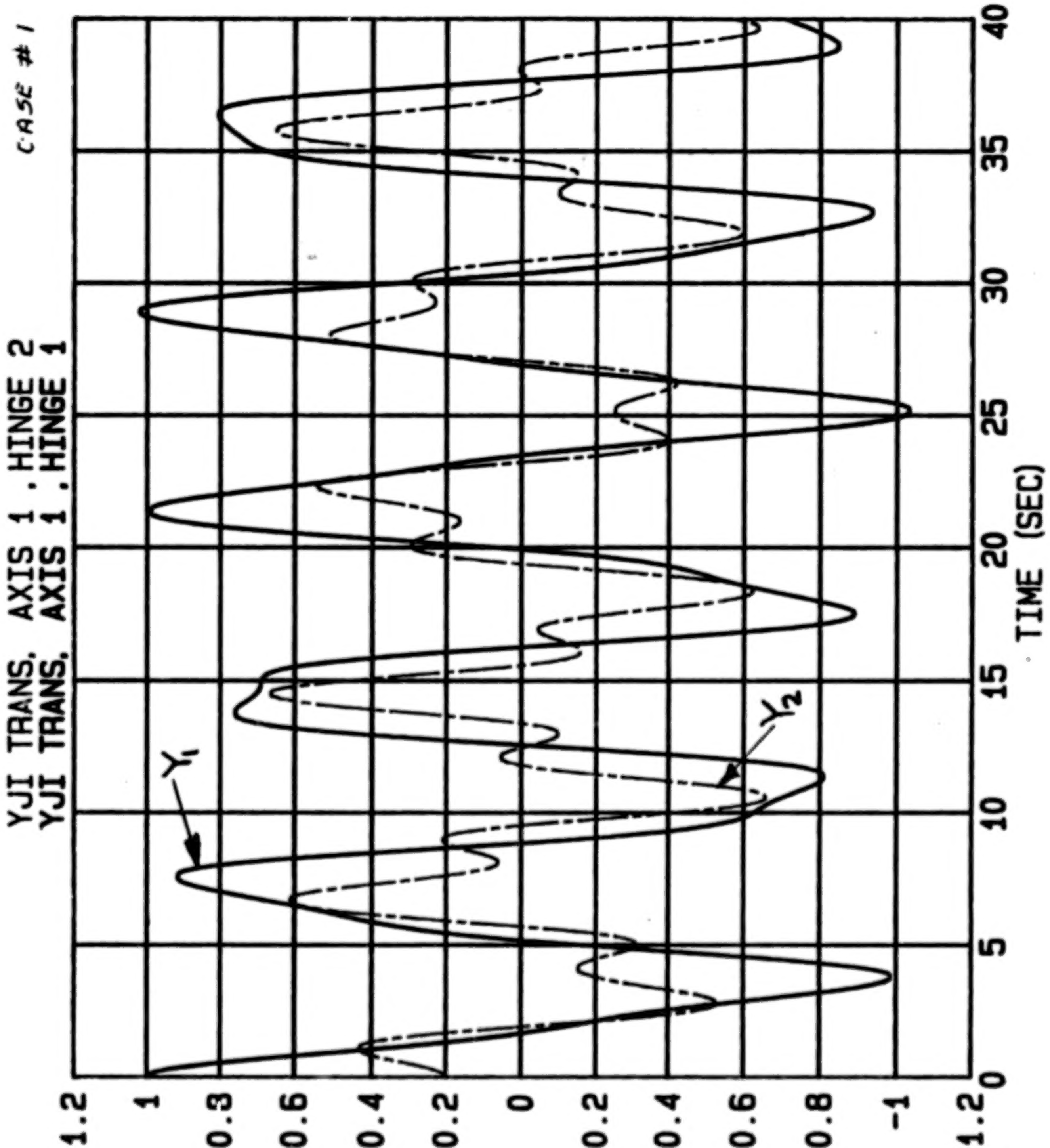
YJI TRANS. AXIS 1 ,HINGE 2
YJI TRANS. AXIS 1 ,HINGE 1
CASE # 1
Y1
Y2
1.2
1
0.3
0.6
0.4
0.2
0
-0.2
-0.4
-0.6
-0.8
-1
-1.2
0
5
10
15
20
25
30
35
40
TIME (SEC)

CASE # 2

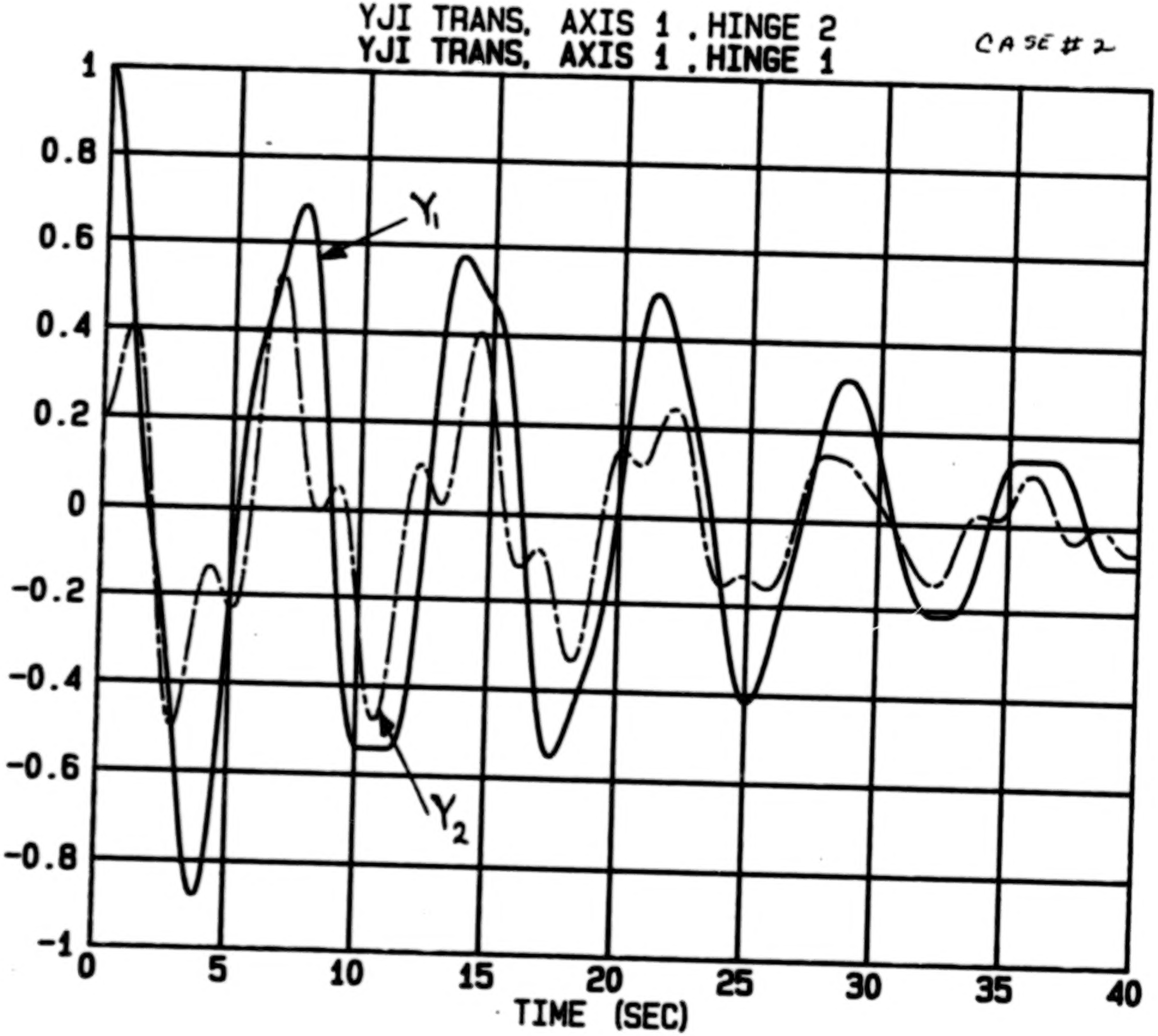
YJI TRANS, AXIS 1 , HINGE 2
YJI TRANS, AXIS 1 , HINGE 1
Y1
Y2
1
0.8
0.6
0.4
0.2
0
-0.2
-0.4
-0.6
-0.8
-1
0
5
10
15
20
25
30
35
40
TIME (SEC)

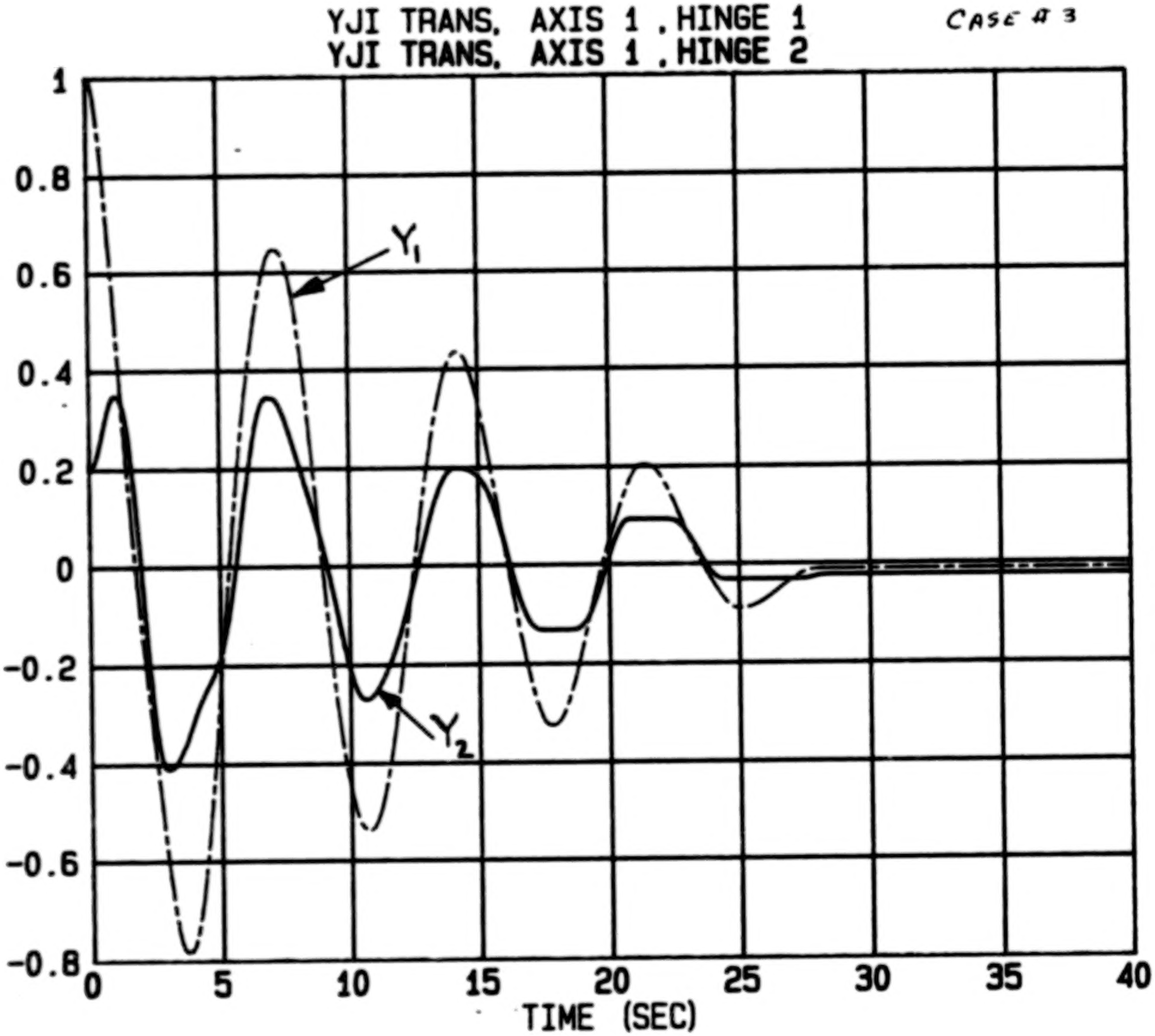
YJI TRANS. AXIS 1 .HINGE 1
YJI TRANS. AXIS 1 .HINGE 2
1
0.8
0.6
0.4
0.2
0
-0.2
-0.4
-0.6
-0.8
0
5
10
15
20
25
30
35
40
TIME (SEC)
Y_1
Y_2

CASE # 3

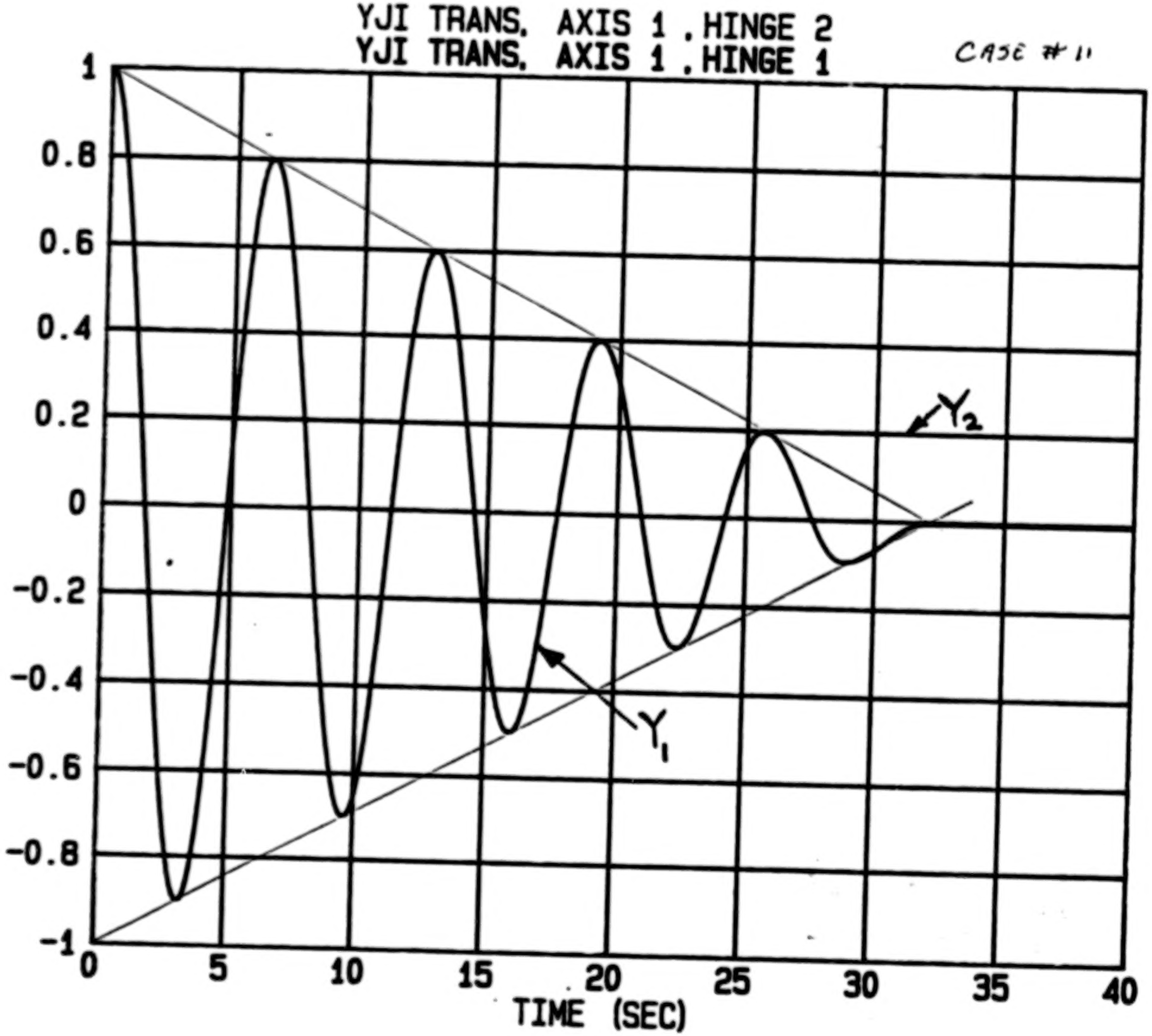
YJI TRANS. AXIS 1 . HINGE 2
YJI TRANS. AXIS 1 . HINGE 1
CASE # 11
1
0.8
0.6
0.4
0.2
0
-0.2
-0.4
-0.6
-0.8
-1
0
5
10
15
20
25
30
35
40
TIME (SEC)
Y_2
Y_1

REFERENCES

1. Singh, R. P., VanderVoort, R. J. and Likins, P. W. "Dynamics of Flexible Bodies in Tree Topology--A Computer Oriented Approach," AIAA Journal of Guidance Control and Dynamics, V8, No. 5, September 1985, pp. 584-590.

2. Singh, R. P. and Likins, P. W., "Manipulator Interactive Design with Interconnected Flexible Elements," Proceedings of 1983 Automatic Control Conference, San Francisco, CA, June 1983, pp. 505-512.

3. Singh, R. P. and Likins, P. W., "Singular Value Decomposition for Constrained Dynamical Systems," Transactions of ASME, Journal of Applied Mechanics, V52, No. 4, 1985, pp. 943-948.

CAPTIONS FOR DON EDBERG'S VIEWGRAPHS

This presentation gives some preliminary results of research on control of flexible structures carried out at Jet Propulsion Laboratory, Pasadena, California. This work has been underway since the summer of 1985. The research is supported by the NASA Office of Aeronautics and Space Technology. Don Edberg and Jay-Chung Chen are Members of the Technical Staff at the Jet Propulsion Laboratory.

N87
22747
UNCLAS

JPL

ON THE CONTROL OF STRUCTURES BY APPLIED THERMAL GRADIENTS

Don Edberg

Jay-C. Chen

Applied Technologies Section
Jet Propulsion Laboratory
California Institute of Technology

April 24, 1986

Workshop on Structural Dynamics
and Control Interaction of Flexible Structures

Marshall Space Flight Center, Alabama

N87-22747

The passive damping of large space structures is expected[1,2] to be small, on the order of about 1%. This figure is small enough that the performance of orbiting structures such as reflectors, antennae, and others with stringent pointing requirements will be hindered by the long settling time necessary for the subsidence of disturbances. We expect that some increase of damping will be required. This presentation discusses one prospective method.

[1] Edberg, D., "Measurement of Material Damping In a Simulated Space Environment," Stanford Dept. of Aero/Astro Report No. 546, Dec. 1984.

[2] Ashley, H., and Edberg, D., "On the Virtues and Prospects for Passive Damping in Large Space Structures," Paper DA, Proceedings of Vibration Damping Workshop II, Las Vegas, NV, Feb. 1986.

Passive Damping of Large Space Structures

- In general, passive damping is small ($\varsigma \approx 1\%$).
- More damping is required for "reasonable" performance.

A variety of techniques exist to control spacecraft. There are three different control problems which have to be considered: rigid-body pointing (attitude control), shape control, and vibration suppression. Conventional type actuators, such as thrusters and momentum wheels are satisfactory for attitude control. Thrusters use consumables, and reaction wheels can "saturate". Neither is suitable for shape control or vibration suppression.

For these categories, we need a so-called "internal" actuator, which does not produce inertial forces – only internal forces in the body. Two possible candidates are piezoelectric actuators[3,4], and thermoelectric actuators. We shall present some of our work on thermoelectric actuators.

---

[3] See, for example, "Use of Piezo-Ceramics as Distributed Actuators in Large Space Structures," by Crawley and de Luis, Paper 85-0626, AIAA 1985 SDM Conference, Orlando, FL.

[4] Refer to the presentation "Vibration Suppression by Stiffness Control," by Fanson and Chen in the proceedings of the present conference.

Methods of Increasing Damping

- "External" type actuators (inertial)
  - Thrusters
  - Control Moment Gyros and Pivoting Proof Masses
- Internal Actuators (produce no external forces)
  - Piezoelectric actuators
  - Thermoelectric actuators

There is good reason to try to control by using thermal-type actuators. Several works[5,6] have shown that material damping occurs because of a lag in conversion of vibrational to heat energy. In addition, civil engineers have known for years that thermal loading can produce very large forces.

[5] Ashley, H., "On Passive Damping Mechanisms in Large Space Structures," **Journal of Spacecraft and Rockets**, Sept./Oct. 1984.

[6] Lee, U., "Thermoelastic and Electromagnetic Damping Analysis," **AIAA Journal**, Nov. 1985.

Motivation for Thermal-Type Actuators

- Material damping occurs because of energy conversion between vibrational and heat
- Thermal loading can produce large forces

– Why not use applied thermal loading to control structural deformations?

There are several problems associated with use of applied temperatures. The thermal mass of a structure may cause a large time delay before there is a significant response. There may also be a large power consumption, because of the indirect way of converting thermal to strain energy. Finally, the actuator itself is a question.

Problems with Use of Applied Temperatures

- Time lags due to thermal inertia
- Possibly high power consumption
- What can be used as actuators?

Fortunately, there exist semiconductor devices that can act as a heat pump when voltage is applied. They are similar to the devices used in RTG's (radioisotope thermoelectric generators) used to power many spacecraft. These devices are reversible, and may be used as an actuator on a properly designed structure.

Because of finite physical properties, these thermoelectric devices have a finite response time. In addition, a structure must use a relatively large coefficient of thermal expansion to be controlled adequately.

Thermoelectric Actuators

- Used in RTG's as electricity generator
- Reversible – if current is applied, device becomes a heat pump
- May be used as a thermal actuator on a properly designed structure

Drawbacks to their use

- Finite response time due to thermal inertia
- Structural design must use relatively high α materials for maximum effectiveness

These figures show schematically what we employ in our experiment. The first shows that when the thermoelectric device is turned on, it pumps heat from one side of the beam to the other. This creates a bending moment, which will displace the beam.

The second illustration shows an exploded view of our experimental beam. It consists of two aluminum caps separating a number of thermoelectric devices. The two caps are bolted together with a number of screws and bolts. The beam is approximately 80 cm long.

EXPERIMENTAL DESIGN

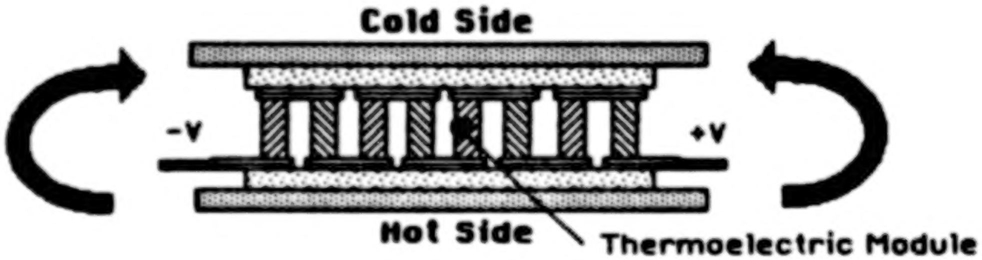
Cold Side
-V
+V
Hot Side
Thermoelectric Module

Thermally Induced Bending Moment

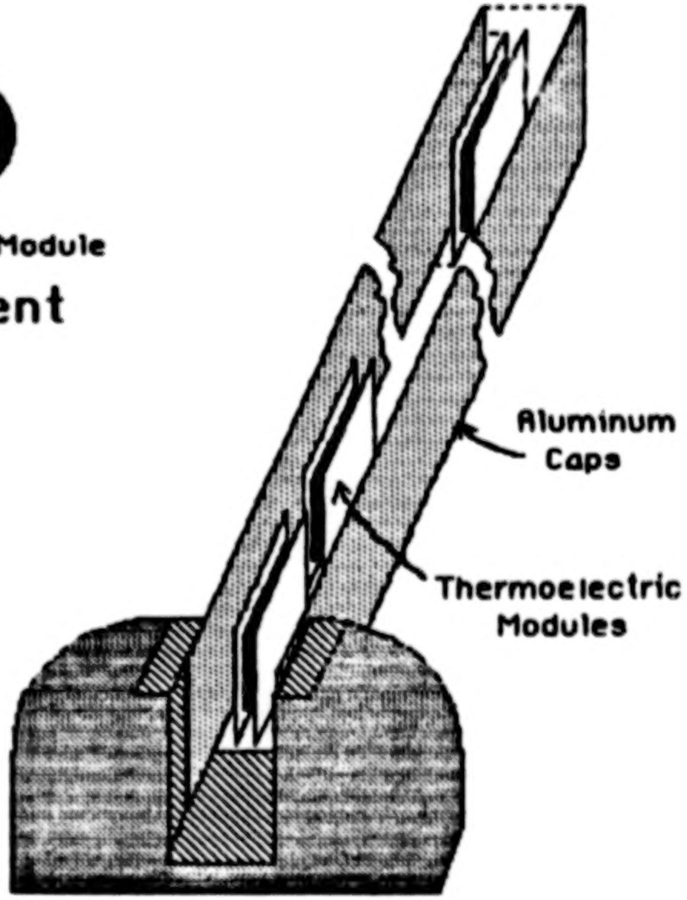
Aluminum Caps
Thermoelectric Modules

Test Setup

This photograph shows a side view of the beam. It is securely clamped in a heavy vise. The rule underneath is six inches long.

Photograph of Thermoelectric Beam

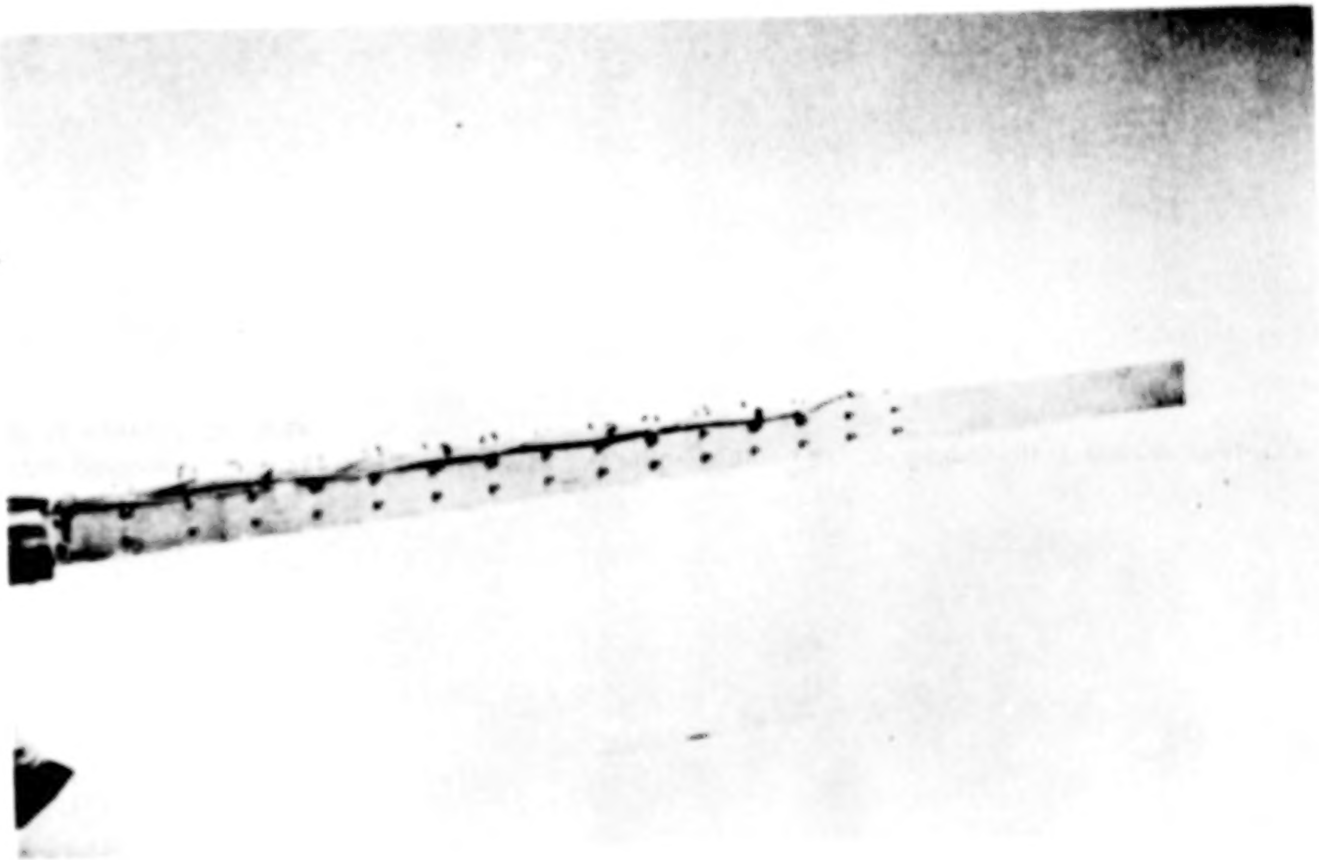

ORIGINAL PAGE IS
OF POOR QUALITY

This photograph shows the beam statically deflecting. The tip deflection is approximately 5 cm, on an applied 24 volts.

Static Deflection
from
Thermal Gradient

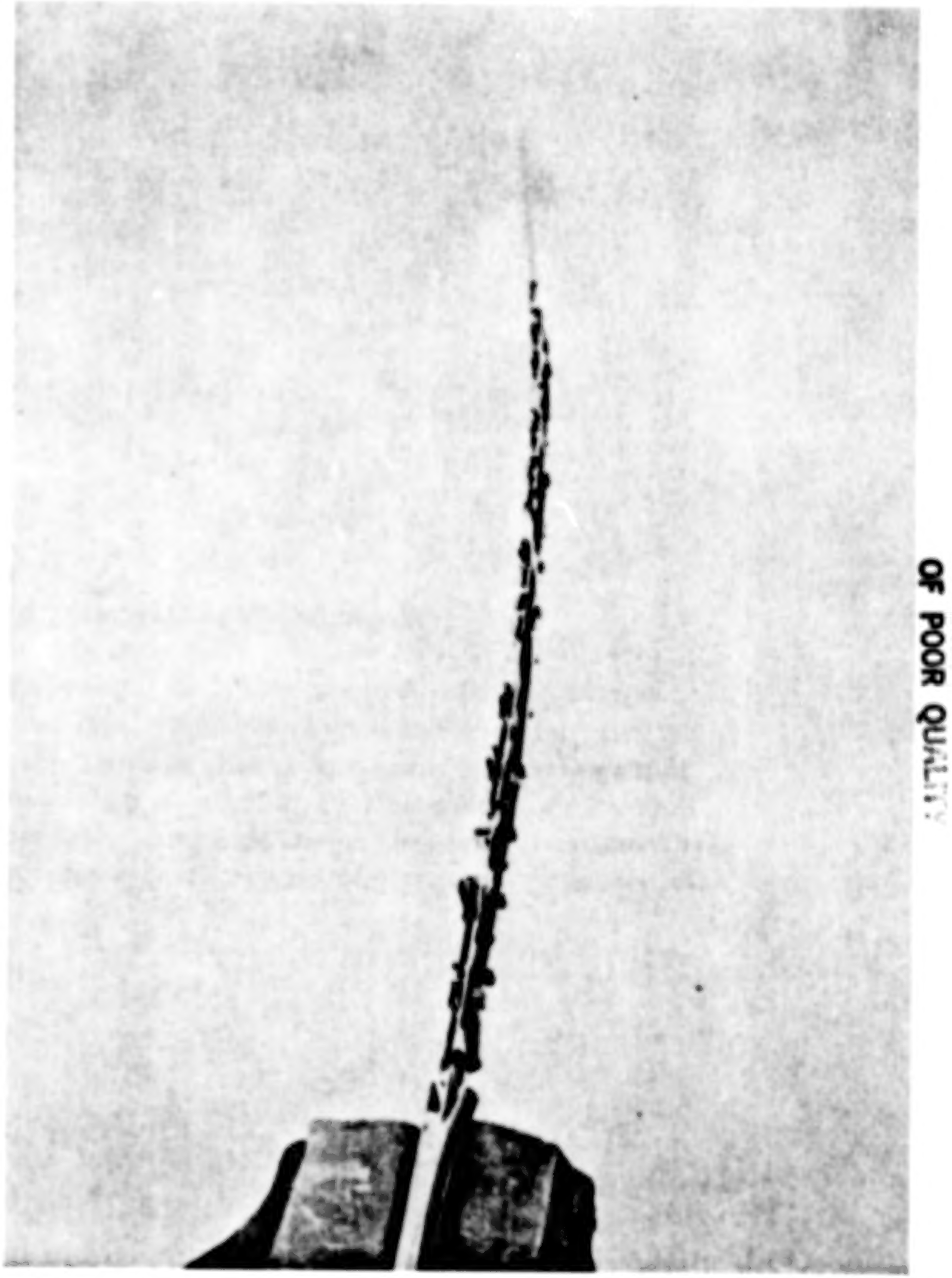

ORIGINAL PAGE IS
OF POOR QUALITY

The equation of motion of the beam is the standard fourth-order Bernoulli-Euler representation, with the exception of the term on the right hand side, which is found from energy considerations. The bending moment M_T is represented as a time function multiplying a step function which turns on at the beginning of the actuators and off at their end. If the deflection of the beam is separated into time and space functions, this results in a modal time function equation whose right hand side is a forcing term dependent on the slope of the (mass-normalized) modeshape at the two ends of the actuators, and the time history of the applied moment. For later analysis, it is convenient to take the Laplace Transform of the equation.

Equation of motion for beam

$$m(x)\frac{\partial^2 w(x,t)}{\partial t^2} + \frac{\partial^2}{\partial x^2}\left[EI(x)\frac{\partial^2 w(x,t)}{\partial x^2}\right] = \frac{\partial^2 M_T(x,t)}{\partial x^2}$$

$$M_T(x,t) = M_T(t)\cdot\left[H(x_1) - H(x_2)\right]$$

$$w(x,t) = \sum_{n=1}^{\infty}\varphi_n(x)\cdot\xi_n(t)$$

$$\xi^{''}(t) + 2\varsigma\,\omega\,\xi^{'}(t) + \omega^2\xi(t) = M_T(t)\left[\varphi^{'}(x_2) - \varphi^{'}(x_1)\right]$$

$$\left[s^2 + 2\varsigma\,\omega\,s + \omega^2\right]\xi(s) = M_T(s)\left[\varphi^{'}(x_2) - \varphi^{'}(x_1)\right]$$

To determine the time dependence of the applied moment, we must analyze the thermal time history of the beam. Its temperature history is determined by its heat capacity $\mathcal{M}c$. We further assume that the heating $Q(s)$ is proportional to the applied voltage $V(s)$. The $1/s$ dependence signifies that the thermal mass acts as an integrator.

The bending moment is calculated in the normal fashion, i.e., by integrating the strain across the section of the beam. The magnitude of the bending moment is found by substituting the thermal time history found earlier.

Thermal Equations

$$\frac{T(s)}{\frac{1}{2}Q(s)} = \left(\frac{1}{\mathcal{M}c}\right)\frac{1}{s}$$

$$Q(s) = C_{QV} \cdot V(s)$$

$$T(s) = \left(\frac{C_{QV}}{2\,n_s\,\rho\,A\,\ell_a\,c}\right)\frac{V_c(s)}{s}$$

Calculation of bending moment:

$$M_T(t) = \iint\limits_A E\,\alpha\,T(z,t)z\,dA$$

$$M_T(s) = \frac{E\alpha\,d\,C_{QV}}{\rho\,n_s\,\ell_a\,c}\;\frac{V_c(s)}{s}$$

When the bending moment relation is substituted into the beam equation, the open loop system equation results. It has two oscillatory roots in addition to a root at the origin. If proportional feedback is employed to attempt to control the system, the system goes unstable. This is verified by the root locus diagram, which shows that the system must be unstable with proportional feedback.

Open Loop System Equation

$$\frac{\xi(s)}{V_c(s)} = \frac{C}{s(s^2 + 2\zeta\omega s + \omega^2)}$$

Simple feedback leads to unstable system

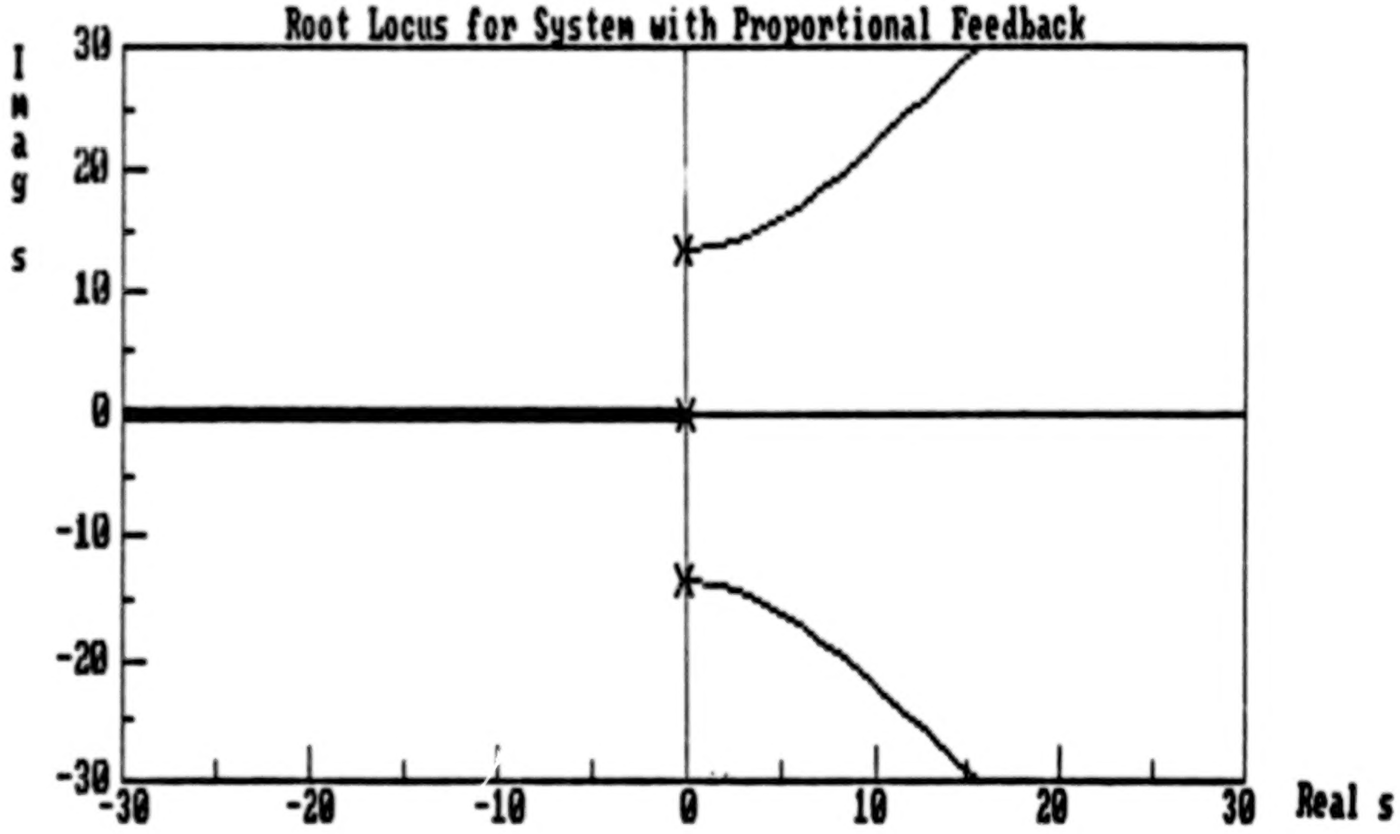

Because of the system behavior, more elaborate compensation is necessary to provide satisfactory behavior. If double lead compensation is added to the system, we can improve the performance. This results in the closed-loop block diagram shown.

Compensation Required

- Double lead compensation can stabilize, i.e. use

$$C(s) = K\frac{(s+a)^2}{(s+b)^2}$$

Closed-Loop Block Diagram

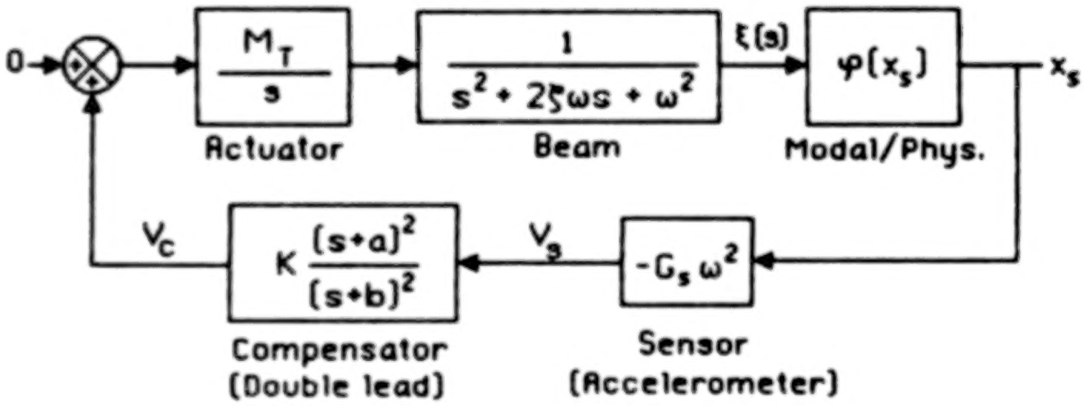
0
$\frac{M_T}{s}$
Actuator
$\frac{1}{s^2 + 2\zeta\omega s + \omega^2}$
Beam
$\xi(s)$
$\varphi(x_s)$
Modal/Phys.
x_s
$-G_s\,\omega^2$
Sensor
(Accelerometer)
V_s
$K\frac{(s+a)^2}{(s+b)^2}$
Compensator
(Double lead)
V_c

A plot of the closed loop poles is shown. Here we can see that all of the poles move into the left half plane with an increase of gain. We thus expect higher damping than exists in the open-loop system.

JPL

Closed Loop Root Locus

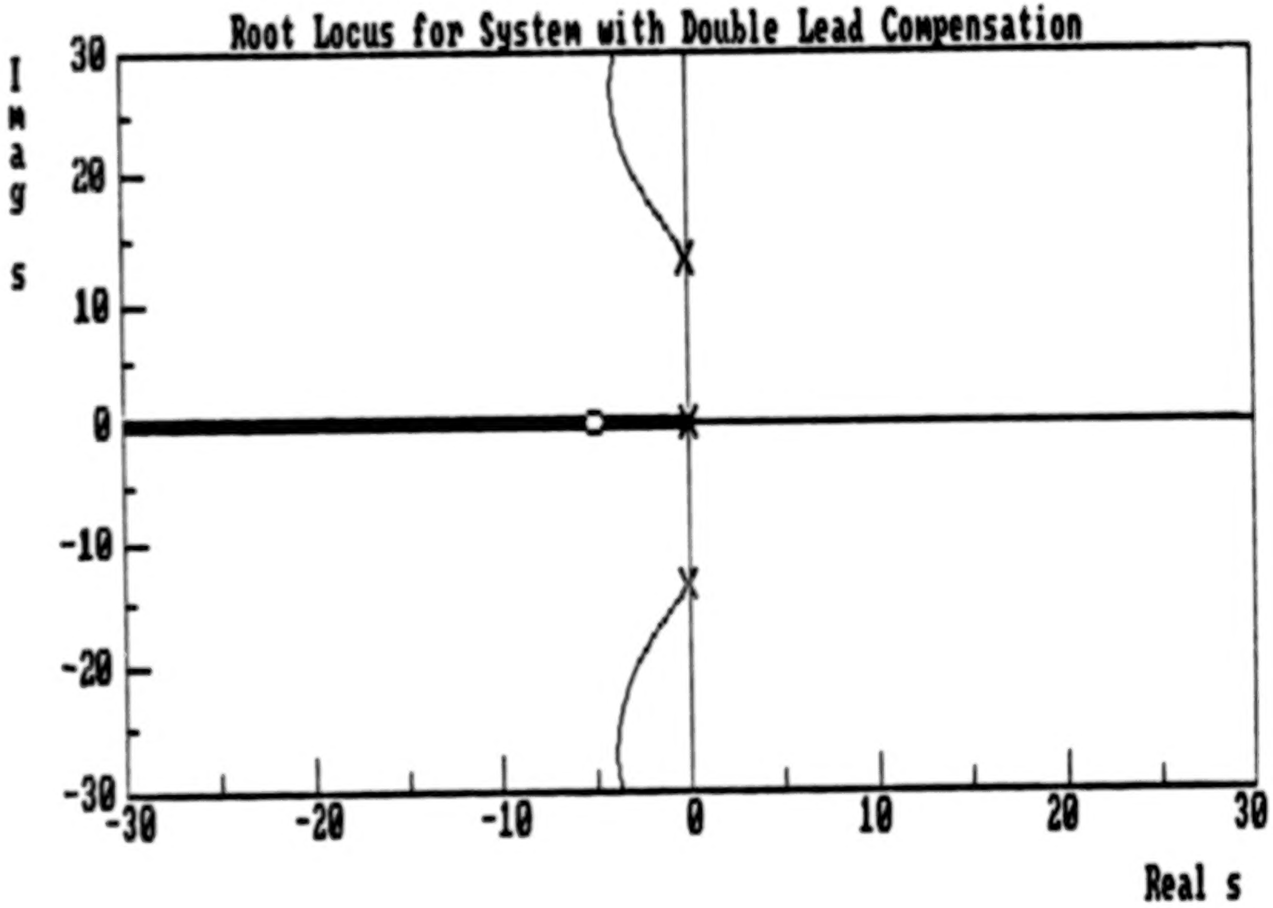

This plot shows the *measured* time history of the thermoelectric beam system. The dotted lines show the open loop free decay of the system, while the solid lines show the closed loop decay. One can observe a large increase in the system damping ratio, as expected.

Performance of Open-Loop and Closed-Loop Systems

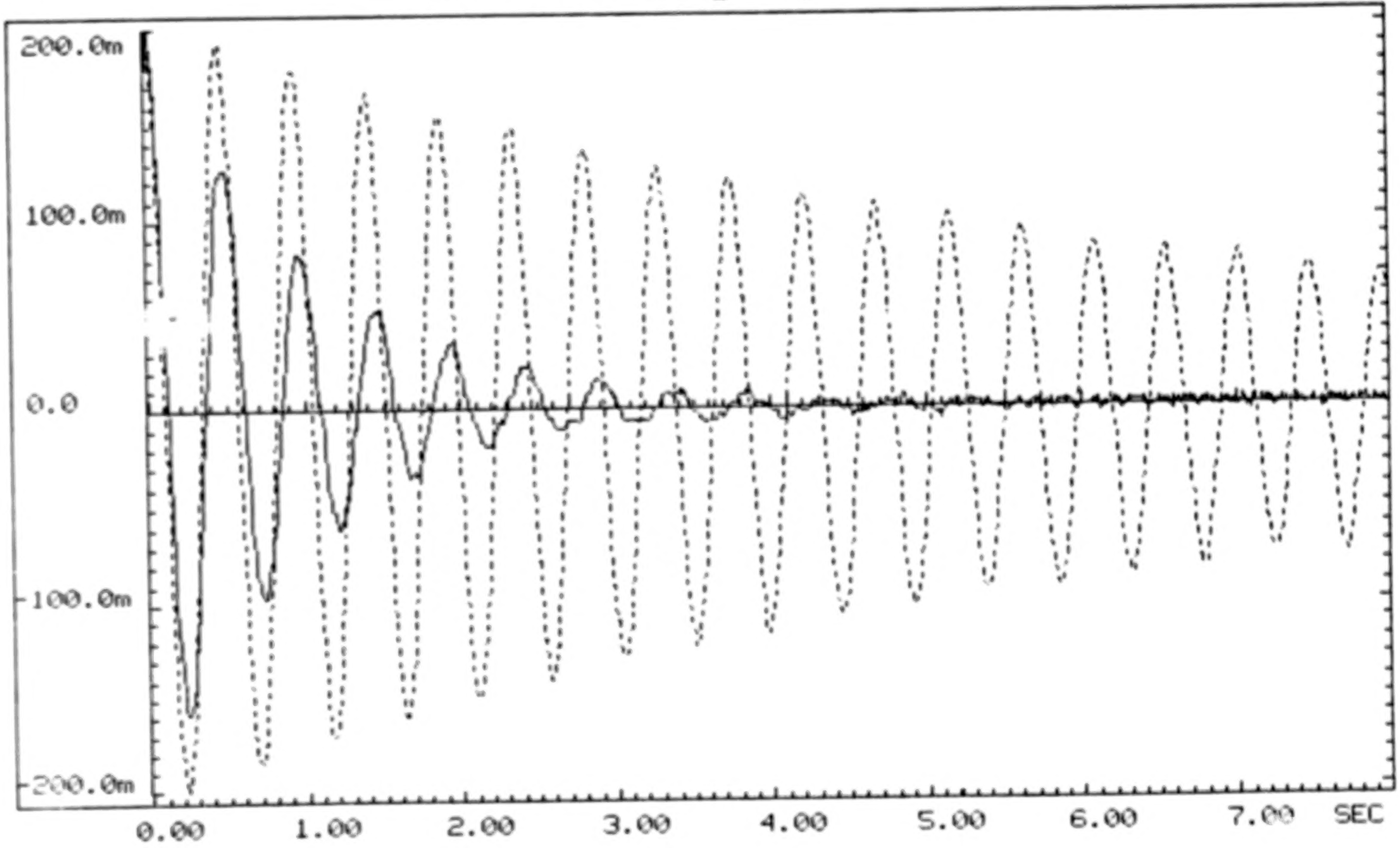

This table presents the results of the experiment. The system damping ratio has increased from 0.82% to 7.4%, nearly an order of magnitude. The frequency of oscillation has decreased slightly. Most importantly, the settling time factor has increases dramatically. This means that vibrations will be suppressed much faster in the closed-loop system.

Summary of Open-Loop vs. Closed-Loop Performance

System Type	Damping Ratio ς	Frequency $f\ (Hz)$	Settling Time $\varsigma\omega$
Open Loop	0.82%	2.154	1.502
Closed Loop	7.4%	2.078	12.61

We have shown that the thermoelectric device is a feasible actuator, and may effectively be used to control structures, provided the structure has a relatively low thermal inertia. The control law only depends on the open-loop system natural frequency.

CONCLUSIONS

- Feasibility of thermoelectric actuators shown
- Damping ratio of system increased by an order of magnitude
- Control law only loosely depends on system frequency

Future work in the field of thermoelectric actuators should address the following topics: power consumption, multimode control, and optimizing structural parameters (particularly thermal parameters). Our work will continue in these areas.

Recommendations for Future Work

- Thermoelectric power consumption
- Multi-mode control
- Optimal system definition (e.g. materials and geometry)

N87
22748
UNCLAS

N87-22748

FINITE ELEMENT MODELS OF WIRE ROPE FOR VIBRATION ANALYSIS

J. E. Cochran, Jr., N. G. Fitz-Coy and M. A. Cutchins
Auburn University, Alabama

Workshop on Structural Dynamics and Control

Interaction of Flexible Structures

Marshall Space Flight Center
Huntsville, Alabama

April 22-24, 1986

PRECEDING PAGE BLANK NOT FILMED

FINITE ELEMENT MODELS OF WIRE ROPE
FOR VIBRATION ANALYSIS

J. E. Cochran, Jr.,* N. G. Fitz-Coy† and M. A. Cutchins*

Auburn University, Alabama

Abstract

The usefulness of wire rope in shock and vibration isolation is briefly reviewed and its modeling for the purpose of vibration analysis is addressed. A model of a nominally straight segment of wire rope is described in which the rope structure is represented by a maiden, or central, strand of wire with one (or more) strand(s) wrapped around it in a helix (helices). The individual strands are modeled using finite elements and MSC NASTRAN. Small linear segments of each wire are modeled mathematically by dividing them lengthwise into triangular prisms (thick "pieces of pie") representing each prism by a solid NASTRAN element. To model pretensioning and allow for extraction of internal force information from the NASTRAN model, the "wound" strands are connected to the maiden strand and each other using "spring" (scalar elastic) elements. Mode shapes for a length of wire rope with one end fixed to a moving base and the other attached to a "point" mass, are presented. The use of the NASTRAN derived mode shapes to approximate internal normal forces in equations of motion for vibration analyses is considered.

---

*Professor, Aerospace Engineering
†Graduate Research Assistant

Introduction

Wire rope[1] is, from the basic point of view, simply several strands of wire twisted, or wound, together (see Fig. 1). Some types are commonly called "cable" and are used to carry electricity, support bridges and "cable cars," raise and lower heavy loads and in many other practical ways. A less obvious, but equally important, use of wire rope is in shock and vibration isolation devices.[2,3] The structure of wire rope provides many interfaces at which a portion of the relative motion of strands of wire is converted by friction into heat, thereby dissipating vibrational energy.[4] Furthermore, the stiffness of wire rope structures can be tailored to provide support and restoring forces. Stiffness and damping are adjusted by varying wire diameter, the number of strands, pretensioning and the arrangement of lengths of the wire rope. Commonly, helical coils of ropes[2,3] are fixed in clamps (see Fig. 2) to form individual shock and/or vibration isolators. The isolators are used to support and isolate communications equipment in vehicles which are subjected to large magnitude, short-term accelerations; i.e., "shocks." In addition to absorbing shock, the internal, or system, damping,[4,5] of the wire rope devices provides vibrational isolation over wide ranges of frequencies and amplitudes.

The damping characteristics of wire rope and vibration isolators made from it are not well understood from the theoretical standpoint. Apparently, the design of individual isolators is accomplished by experimentation by engineers with considerable experience in applications of these devices.[2] Realistic mathematical models of wire rope isolators would be useful in the design process and perhaps would allow the achievement of the confidence levels in isolator characteristics needed for more applications in which

ORIGINAL PAGE IS
OF POOR QUALITY

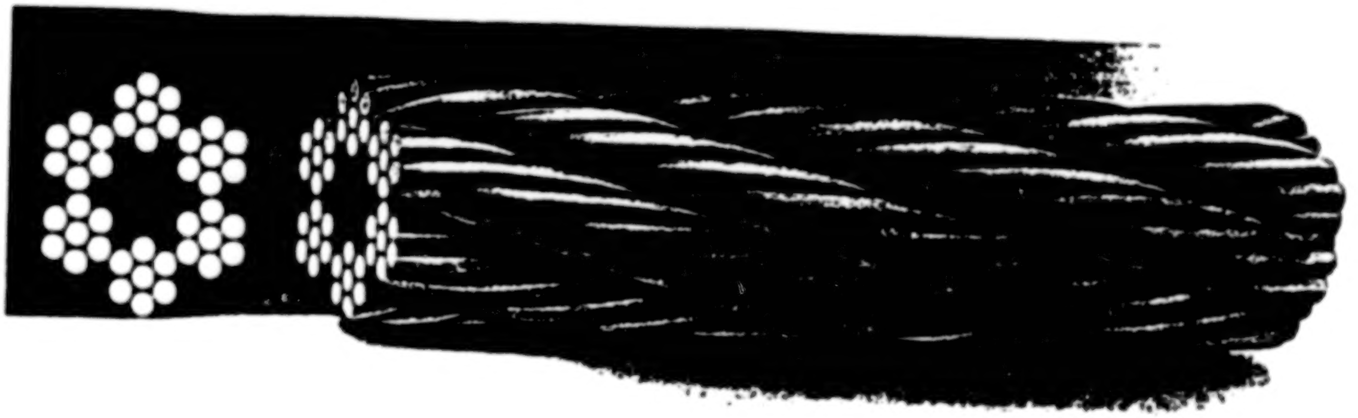

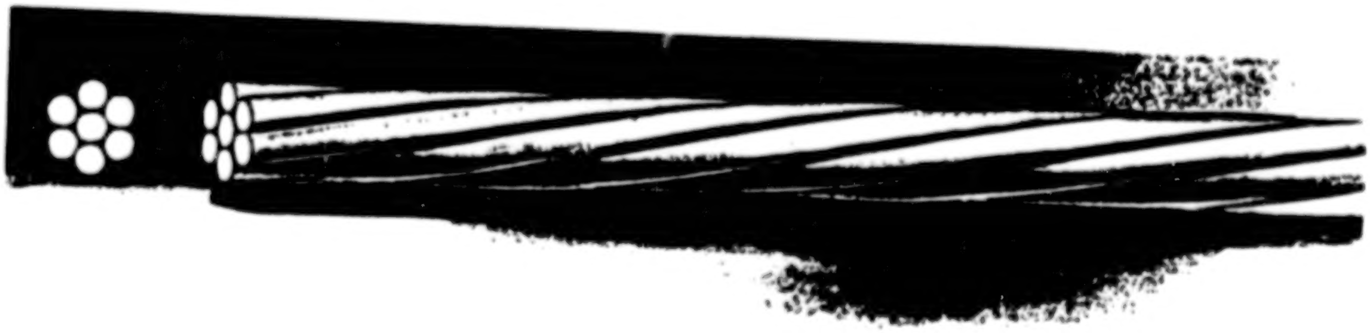

Fig. 1. Wire rope.

ORIGINAL
OF POOR QU

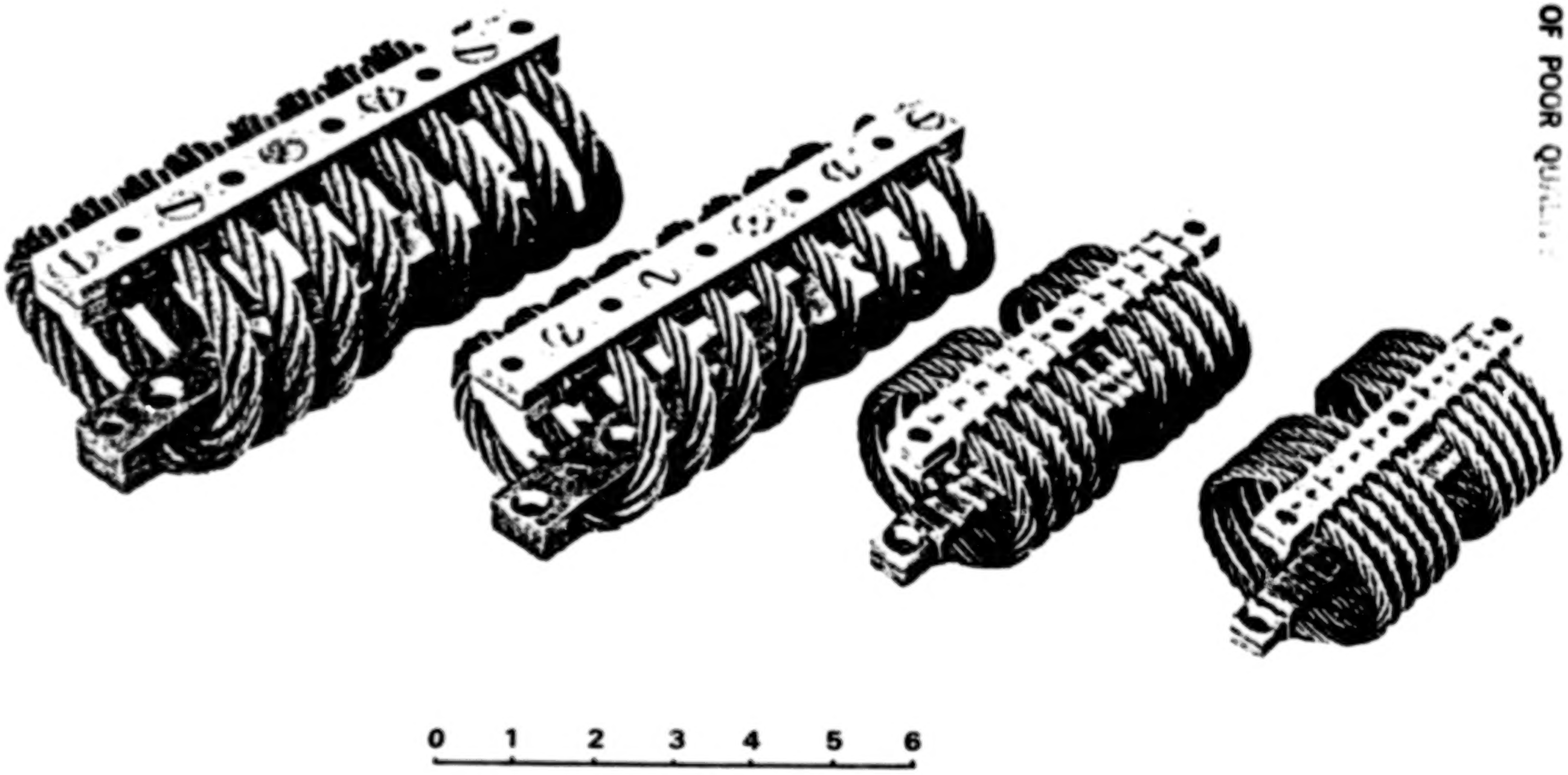

Fig. 2. Helical isolators.

damping rates and dynamic response must be very accurately known to prevent resonance and control interaction problems.

The purposes of this paper are (1) to present the results of work on the problem of obtaining accurate mathematical models of wire rope isolators using MSC NASTRAN and (2) to present some preliminary results of work toward obtaining equations of motion of a wire rope "pendulum" for use in correlating experimental and theoretical results.

Wire Rope Model

Basic Model

A sketch of a "wire rope" segment of length L, composed of a maiden wire strand and a single "wound" strand, is shown in Fig. 3. It is assumed that when the rope is in its undeformed state the angle of the helix formed by the centerline of the wound strand, α, is constant over the length L. For the finite element analysis, the maiden strand is divided into 372 elements such that each cross section of the strand looks like a hexagon cut into triangular pieces which have thicknesses equal to the radius of the strand. The other strands are modeled in a similar manner. In addition, scalar elastic elements ("springs") are used to connect the wound and maiden strands. These springs are incorporated so that the distribution of the normal force between the two strands can be determined for each mode shape computed (see Fig. 5). NASTRAN produced figures showing two-strand and seven-strand wire rope are given as Figures 6 and 7, respectively.

Boundary Conditions

The boundary conditions are chosen so that the "top" of the segment is fixed. Two choices for the boundary conditions on the other end are considered here. The first is to use a "free" end condition, (Case 1). The

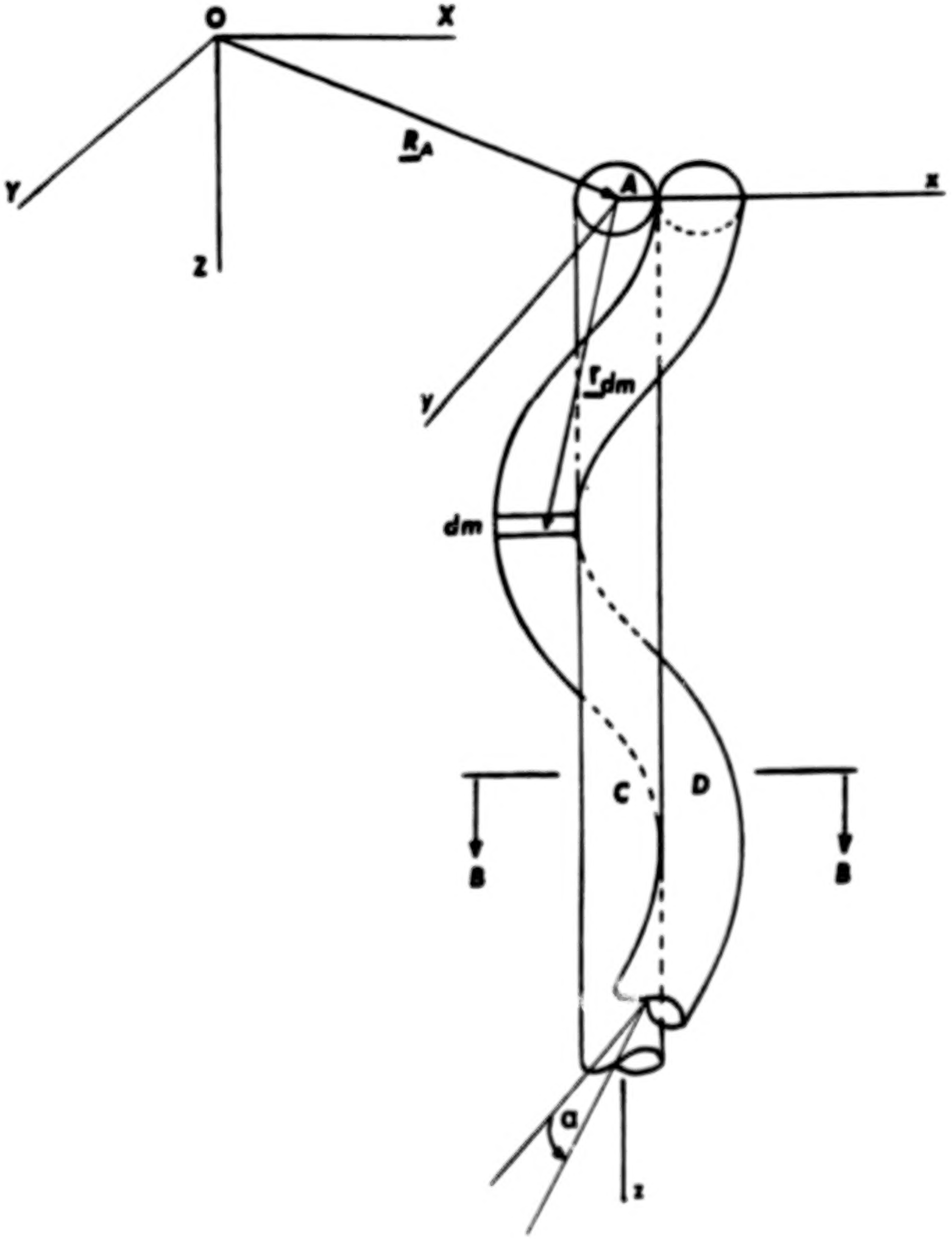
O
X
Y
Z
$\underline{R}_A$
A
x
y
$\underline{r}_{dm}$
dm
C
D
B
B
α
z

Fig. 3. Two-strand wire rope.

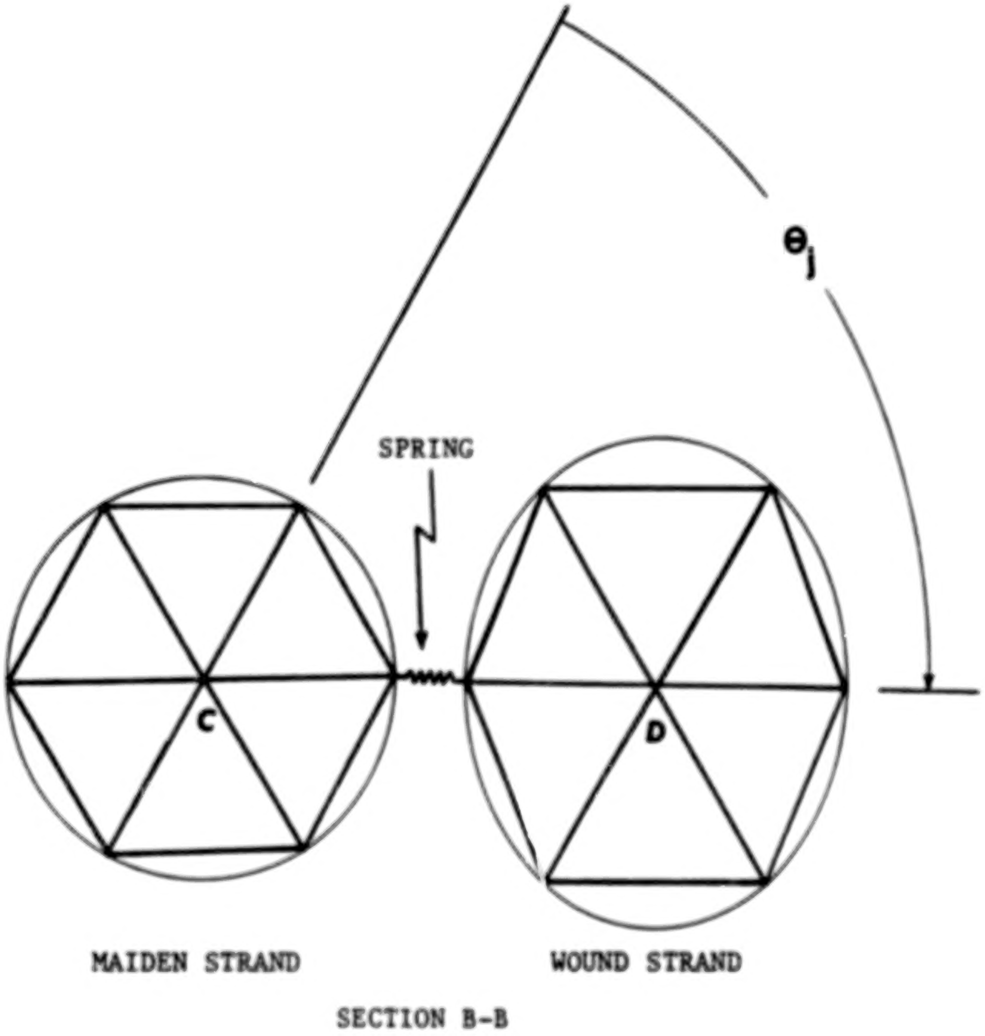
Θj
SPRING
C
D
MAIDEN STRAND
WOUND STRAND
SECTION B-B

Fig. 4. Cross section of two-strand wire rope showing finite elements.

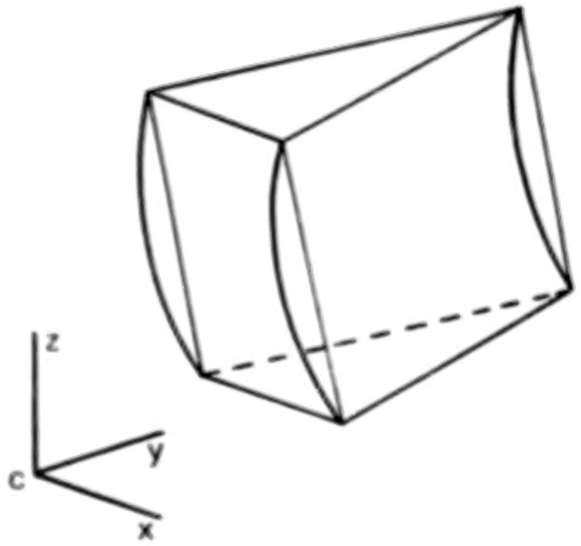

Fig. 5. PENTA MSC/NASTRAN solid element.

ORIGINAL PAGE IS
OF POOR QUALITY

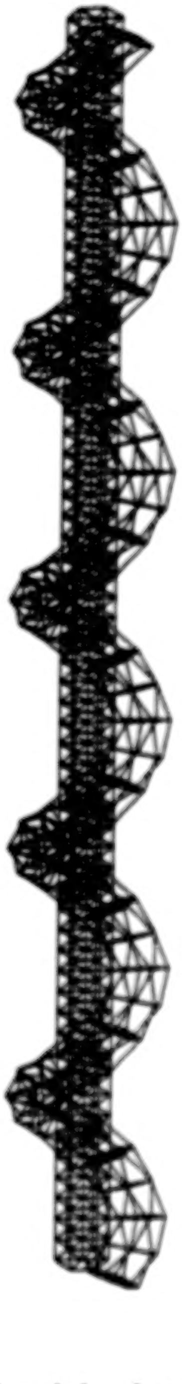

Fig. 6. NASTRAN model of two-strand wire rope.

ORIGINAL PAGE IS
OF POOR QUALITY

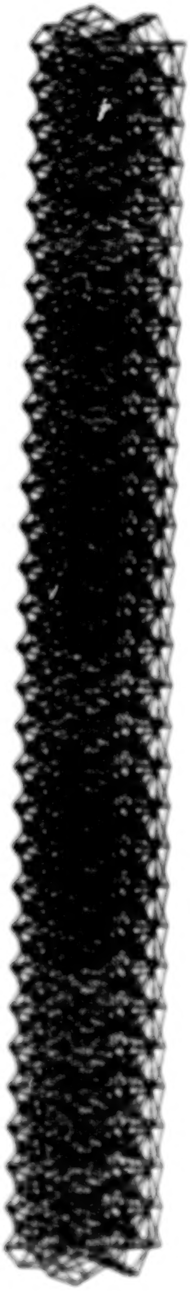

Fig. 7. NASTRAN model of seven-strand wire rope.

second choice (Case 2) is to attach to the "bottom" end a mass which is relatively large compared to the mass of the rope segment.

The fourth mode shape for the seven-strand rope alone (Case 1) is shown in Fig. 8. The corresponding mode shape for the Case 2 "pendulum" model is given in Fig. 9.

Equations of Motion

Our stated objective is to obtain "analytical" models of wire rope vibration isolation. Here, "analytical" implies that mode shapes from NASTRAN models without damping will be used rather than analytical mode shapes such as the classical ones for beams. The mode shapes are to be used to approximate the displacements of the wire rope and attach "rigid" bodies when linear damping is present and when nonlinear nonconservative and conservative forces act on the system. The wire rope "pendulum" is a simple system which we hope to use to test this method for modeling these effects.

Except for the determination of nonconservative internal forces, the most attractive way of deriving equations of motion for the pendulum is to use the Lagrangian formulation.

The Lagrangian

To obtain the Lagrangian $\mathcal{L}$, we must write the kinetic and potential energies of the pendulum. The support point, A, is assumed to move in a prescribed manner so that the vector $\underline{R}_A$ from the fixed point 0 is known. The kinetic energy, T, of the pendulum, assuming the mass M is a "point mass," is

$$T = \frac{1}{2} \sum_{i=1}^{N} \int_{m_i} (\underline{V}_A + \dot{\underline{r}}_{dm}) \cdot (\underline{V}_A + \dot{\underline{r}}_{dm}) dm$$

$$+ 1/2\ M\ (\underline{V}_A + \dot{\underline{r}}_M) \cdot (\underline{V}_A + \dot{\underline{r}}_M) \qquad (1)$$

ORIGINAL PAGE IS
OF POOR QUALITY

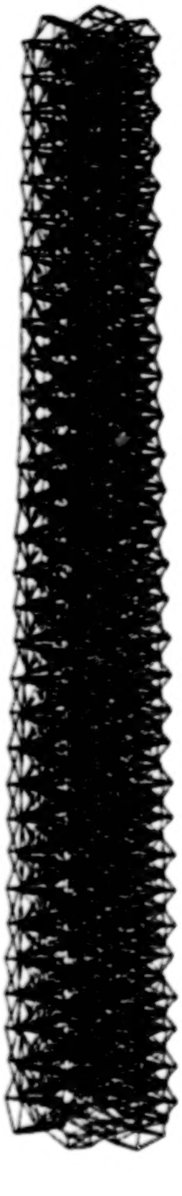

Fig. 8 Mode shape for wire rope model, Case 1.

C-7

ORIGINAL PAGE IS
OF POOR QUALITY

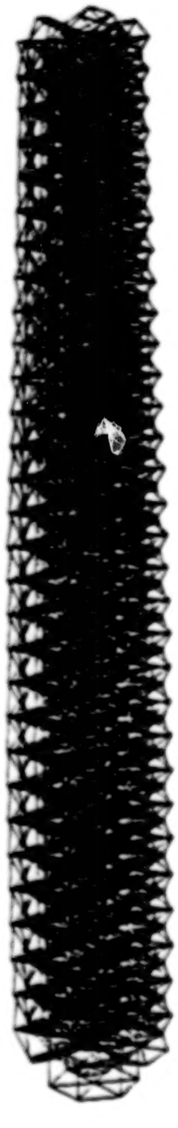

Fig. 9 Mode shape for wire rope model, Case 2.

where $\underline{V}_A = \dot{\underline{R}}_A$, the velocity of A, $\dot{\underline{r}}_{dm}$ is the velocity of a generic mass element dm, N is the number of strands (see Fig. 3), and m_i is the mass of the i^{th} strand. We approximate $\underline{r}_{dm}$ by $\sum_{j=1}^{m} \underline{\Phi}_j q_j$, where the $\underline{\Phi}_j$ are mode shapes, the q_j are generalized coordinates, m is the number of modes used and $\underline{r}_M = \sum_{j=1}^{m} \underline{\Phi}_j (0\ 0\ L) q_j$. The $\underline{\Phi}_j$ are functions of the coordinates x_o, y_o and z_o of dm in the undeformed "structure" and the q_j are, of course, functions of time to be determined.

In matrix form, Eq. (1) is

$$T = \frac{1}{2} M_T \underline{V}_A{}^2 + M \underline{V}_A^T \underline{\underline{\Phi}}_L \dot{\underline{q}} + \frac{1}{2} \dot{\underline{q}}^T \underline{\underline{\Phi}}_L^T \underline{\underline{\Phi}}_L \dot{\underline{q}} M$$

$$+ \underline{V}_A^T \sum_{i=1}^{N} \int_{m_i} \underline{\underline{\Phi}}\, \dot{\underline{q}}\, dm + \sum_{i=1}^{N} \frac{1}{2} \int_{m_i} \dot{\underline{q}}^T \underline{\underline{\Phi}}^T \underline{\underline{\Phi}}\, \dot{\underline{q}}\, dm \tag{2}$$

where M_T is the total mass of the system, $\underline{q} = (q_1 q_2 \cdots q_m)^T$ and $\underline{\underline{\Phi}} = (\underline{\Phi}_1\ \underline{\Phi}_2 \cdots \underline{\Phi}_m)$ and $\underline{\underline{\Phi}}_L$ is $\underline{\underline{\Phi}}$ evaluated at $x_o = y_o = 0$, $z_o = L$.

As expected, we may write

$$T = \frac{1}{2} \dot{\underline{q}}^T \underline{\underline{M}}\, \dot{\underline{q}} + \underline{a}^T \dot{\underline{q}} + \underline{b} \quad , \tag{3}$$

where

$$\underline{\underline{M}} = \sum_{i=1}^{N} \int_{m_i} \underline{\underline{\Phi}}^T \underline{\underline{\Phi}}\, dm + M\, \underline{\underline{\Phi}}_L^T \underline{\underline{\Phi}}_L \tag{4a}$$

$$\underline{a}^T = M \underline{V}_A^T \underline{\underline{\Phi}}_L + \underline{V}_A^T \sum_{i=1}^{N} \int_{m_i} \underline{\underline{\Phi}}\, dm \tag{4b}$$

and

$$\underline{b} = \frac{1}{2} M_T \underline{V}_A{}^2 \tag{4c}$$

the potential energy, V, is due to the elastic stiffness of the system and to gravity. For the former, write

$$V_s = 1/2\ \underline{q}^T\ \underline{\underline{K}}_s \underline{q} \tag{5}$$

where $\underline{\underline{K}}_s$ is the stiffness matrix.

The potential energy due to the location elements of mass in the rope and the mass M in a uniform gravity field is obtained by assuming that M is a point mass at the end of the length of rope and that the rope has mass per unit length $\sigma(z_o)$. Furthermore, the motion is restricted to the xz-plane and $dx/dz_o = (100)\ (d\underline{\phi}/dz_o\ \underline{q})$ is assumed small enough for terms of order q_j^3 and higher to be neglected. Then, the potential energy contribution due to gravity can first be written as

$$\begin{aligned} V_g = & \int_o^L Mg(1 - \cos\theta)dz_o \\ & + \int_o^L \sigma[1 - \int_0^{z_o} \cos[\theta(\zeta)]d\zeta]dz_o \end{aligned} \tag{6}$$

By noting that $\cos\theta \approx 1 - \frac{1}{2}(dx/dz_o)^2$, we may write

$$\begin{aligned} V_g = & \frac{1}{2} M \int_o^L \left(\frac{dx}{dz_o}\right)^2 dz_o \\ & + \frac{1}{2} \int_o^L \sigma \int_o^{z_o} \left[\frac{dx}{dz_o}\bigg|_{z_o=\zeta}\right]^2 d\zeta\ dz_o \end{aligned} \tag{7}$$

Obviously, V_g is of the form,

$$V_g = \frac{1}{2}\ \underline{q}^T\ \underline{\underline{K}}_g\ \underline{q} \tag{10}$$

The nonconservative forces acting on dm are assumed to be due to viscosity and coulomb friction between the strands. Viscous forces can be included in the equations by using some form of modal damping. For the coulomb friction, we need to consider the rope's structure.

Let the strands be renumbered so that the maiden strand is i=0, and at any value of z_o, the other strands are numbered 1 through N-1 in a counterclockwise manner about the z_o axis. Also, let $\underline{f}_{dm_i}$ denote the force on denote the force on the element dm_i of the i^{th} strand and let μ denote the coefficient of friction. Furthermore, let f_{ij} denote the magnitude of the normal force between the i^{th} and the j^{th} strands. Then, for dm_o, we have the coulomb friction force,

$$\underline{f}_{dm_o} = \sum_{i=1}^{N-1} \mu\, f_{oi}\ \mathrm{sgn}[(\dot{\underline{r}}_{dm_o} - \dot{\underline{r}}_{dm_i})\cdot(\hat{\underline{t}}_i\hat{\underline{t}}_i + \hat{\underline{b}}_i\hat{\underline{b}}_i)] \tag{11}$$

where $\hat{t}_i$ and $\hat{b}_i$ are the tangent and bi-normal unit vectors, respectively, of dm_i. For dm_j, $j > 0$, we may write.

$$\begin{aligned}\underline{f}_{dm_j} = &+ \mu f_{oj}\ \mathrm{sgn}[(\dot{\underline{r}}_{dm_o} - \dot{r}_{dm_j})\cdot(\hat{\underline{t}}_j\hat{\underline{t}}_j + \hat{\underline{b}}_j\hat{\underline{b}}_j)\\ &- \mu f_{jk}\ \mathrm{sgn}[(\dot{\underline{r}}_{dm_j} - \dot{\underline{r}}_{dm_k})\cdot(\hat{\underline{t}}_j\hat{\underline{t}}_j + \hat{\underline{b}}_j\hat{\underline{b}}_j)\\ &- \mu\, f_{j\ell}\ \mathrm{sgn}[(\dot{\underline{r}}_{dm_j} - \dot{\underline{r}}_{dm_\ell})\cdot(\hat{\underline{t}}_j\hat{\underline{t}}_j + \hat{\underline{b}}_j\hat{\underline{b}}_j)\end{aligned} \tag{12}$$

with j, k and ℓ in the following triplets:

$$\begin{bmatrix} j \\ k \\ \ell \end{bmatrix} = \begin{bmatrix} 1 \\ 2 \\ 6 \end{bmatrix}, \begin{bmatrix} 2 \\ 3 \\ 1 \end{bmatrix}, \begin{bmatrix} 3 \\ 4 \\ 2 \end{bmatrix}, \begin{bmatrix} 4 \\ 5 \\ 3 \end{bmatrix}, \ldots, \begin{bmatrix} N-1 \\ 1 \\ N-2 \end{bmatrix} \tag{13}$$

In Eqs. (12) we have also used[6]

$$\underline{\hat{t}}_j = \cos\alpha\,[-\sin\theta_j\,\hat{i} + \cos\theta_j\underline{\hat{j}}] + \sin\alpha\,\underline{\hat{k}} \tag{14a}$$

and

$$\underline{\hat{b}}_j = \sin\alpha[\sin\theta_j\,\underline{\hat{i}} - \cos\theta_j\underline{\hat{j}}] + \cos\alpha\,\underline{\hat{k}} \tag{14b}$$

where $\theta_j(z_o)$ is the angle of the centerline of the j^{th} strand at z_o.

Because $\underline{r}_{dm_i} = \underline{R}_A + \underline{\underline{\phi}}(x_o,y_o,z_o)\,\underline{q}$, where (x_o,y_o,z_o) is a point in the undeformed i^{th} strand, $\delta\underline{r}_{dm_i} = \underline{\underline{\phi}}\,(x_o,y_o,z_o)\delta\underline{q}$. The generalized force matrix is therefore[7]

$$\underline{Q} = \sum_{i=0}^{N-1} \int_{m_i} \underline{\underline{\phi}}^T\,\underline{f}_{dm_i}, \tag{15}$$

where the integral indicates a summation of the quantities within it.

The equations of motion then follow from $= T-V_s-V_g$, viz.,

$$\frac{d}{dt}\,\frac{\partial\mathcal{L}}{\partial\dot{\underline{q}}} - \frac{\partial\mathcal{L}}{\partial\underline{q}} = \underline{Q}^T - (\underline{\underline{D}}\,\dot{\underline{q}})^T\,, \tag{16}$$

where $-\underline{\underline{D}}\,\dot{\underline{q}}$ is the generalized viscous damping force. For normal modes of the undamped structure, we have (with $\underline{\underline{D}}$ a diagonal matrix),

$$M_j\,\ddot{q}_j + k_jq_j + \underline{K}^T_{gj}\underline{q} = Q_j - d_j\dot{q}_j - \dot{a}_j \tag{17}$$

where M_j is the generalized mass and k_j the generalized stiffness, respectively, for the j^{th} mode $\underline{K}^T_{gj}$ is the j^{th} row of $\underline{\underline{K}}_g$, Q_j is the j^{th} element of $\underline{Q}$, d_j the diagonal element of $\underline{\underline{D}}$ in the j^{th} row and a_j is the j^{th} element of $\underline{a}$.

The motion in q_j is coupled in two ways. First, through the gravity terms and, second, through the Q_j since up to m of the $\dot{q}_k$ appear in Q_j to determine its sign.

The next steps to be taken are (1) to obtain experimental data for the position of M and (2) to match it with

$$\underline{R}_M = \underline{R}_A + \underline{r}_M \qquad (18)$$

which can be determined when $\underline{R}_A$ is specified and the q_i are known.

Summary

The use of wire rope in shock and vibration isolation devices has been reviewed briefly. Finite element models of a nominally straight length of wire rope have been described. These models were developed as part of an effort to construct mathematical models of wire rope for use in the analysis of vibration isolation devices which are constructed from wire rope.

Equations of motion for one of the finite element models, a seven-strand rope suspended from one end and with a mass attached to the other end to form a "pendulum," were derived. The use of these equations to simulate the motion of the pendulum was discussed.

Further work needs to be done with the current models and new models of helical isolators should be developed.

Acknowledgment

The support of NASA, Marshall Space Flight Center, Huntsville, Alabama, under Grant NAG8-532 is gratefully acknowledged. The COTR for this effort is Mr. Stan Guest.

References

1. ______, American Wire Rope, American Steel and Wire Company, New York, 1913.

2. ______, "Helical Isolators Protect Communications Gear," National Defense, April 1986, pp. 72-73.

3. ______, "Shock-Free Flight Into the Future," Isolation News, Vol. 14, No. 1, Fall 1984, Newsletter published by Aeroflex International, Inc., Plainview, Long Island, NY.

4. Gobdman, L. E., "Material Damping and Slip Damping," in Shock and Vibration Handbook (C. M. Harris and C. E. Crede, editors), McGraw-Hill, New York, 1976, 36, pp. 1-28.

5. Badrakin, F., "Separation of and Determination of Combined Dampings from Free Vibrations," Journal of Sound and Vibration, Vol. 100, No. 2, 1985, pp. 243-255.

6. Miele, A., Flight Mechanics, Vol. I, Addison-Wesley Publishing Company, Inc., Reading, Mass., 1962, pp. 15-16.

7. Whittaker, E. G., A Treatise on the Analytical Dynamics of Particles and Rigid Bodies, Cambridge University Press, London 1936, reprinted 1970, pp. 34-38.

N87
22749
UNCLAS

N87-22749

Experimental Characterization of Deployable Trusses and Joints

By

Dr. R. Ikegami Mr. S. M. Church
Boeing Aerospace Company
Seattle, WA.
Dr. D. A. Keinholz Mr. B. L. Fowler
CSA Engineering, Inc.
Palo Alto, CA.

Presented at
Workshop On Structural Dynamics and Control Interaction of Flexible Structures
Marshall Space Flight Center
Huntsville, Alabama
April 22-24, 1986

ABSTRACT

The structural dynamic properties of trusses are strongly affected by the characteristics of joints connecting the individual beam elements. Joints are particularly significant in that they are often the source of nonlinearities and energy dissipation. While the joints themselves may be physically simple, direct measurement is often necessary to obtain a mathematical description suitable for inclusion in a system model. Force state mapping is a flexible, practical test method for obtaining such a description, particularly when significant nonlinear effects are present. It involves measurement of the relationship, nonlinear or linear, between force transmitted through a joint and the relative displacement and velocity across it. An apparatus and procedure for force state mapping are described. Results are presented from tests of joints used in a lightweight, composite, deployable truss built by the Boeing Aerospace Company. The results from the joint tests are used to develop a model of a full 4-bay truss segment. The truss segment was statically and dynamically tested. The results of the truss tests are presented and compared with the analytical predictions from the model.

EXPERIMENTAL CHARACTERIZATION OF DEPLOYABLE TRUSSES AND JOINTS

INTRODUCTION

This presentation describes preliminary results of some work that is currently being performed jointly by the Boeing Aerospace Company (BAC) and CSA Engineering Inc. The work performed was partially funded by Marshall Space Flight Center (MSFC) Contract NAS8-36420 "Development of Structural Dynamic Analysis Tools" under the direction of Ron Jewell, Tulon Bullock, and Carlton Moore. The deployable truss structure was designed and fabricated as part of a BAC IR&D program.

As shown in Figure 1, the objective of the work performed was to identify and develop experimental methods to obtain the data required to analytically model the nonlinear behavior of joint dominated truss structures. Briefly, the approach we employed was to utilize a compact deployable truss structure that was fabricated under a separate IR&D program. We identified several techniques to model individual joint behavior for incorporation into an overall truss model. The method selected as being most appropriate for our pruposes was based on the Force State Mapping technique developed by Prof. E.T. Crawley of M.I.T. The required testing of the individual joints was performed to characterize the joint behavior. An analytical model of a complete 4-bay truss was developed, and static and modal survey testing of the structure performed. The subsequent analysis/test correlation yielded several interesting conclusions regarding the analysis and testing technique, and the truss design which will be summarized.

BAC COMPACT DEPLOYABLE SPACE TRUSS

A picture of the fully deployed space truss is shown in figure 2. This truss was chosen not only because of its availability, but also because it was anticipated that the static and dynamic behavior would be dominated by the joints. In order to obtain a compact packaging ratio, hinged joints were incorporated at the midpoints of all horizontal members to allow them to fold. Deployment springs and a clothes pin type latching mechanism are designed into the hinged joints. Clevis joints are used at all five apex positions of the basic pentahedral truss bay. The 1 meter square bases of the pentahedrons are stabilized with crossed tension rods that pivot at their midpoints and ends. The rods are molded solid 0.125 inch diameter unidirectional graphite/epoxy. All of the truss fittings are discontinuous graphite fiber injection-molded thermo plastic resin. The 1 inch diameter truss tubes are graphite/epoxy and are designed for high stiffness, low weight, and near zero coefficient of thermal expansion.

TRUSS DEPLOYMENT SEQUENCE

Figure 3 depicts the deployment sequence of the 4-bay truss. As was mentioned previously, the truss was designed to provide a very compact packaging ratio. The truss which is nominally 4 meters x 1 meter x 0.71 meters when fully deployed, will fold up to a compact package which is 0.55 meters x 0.2 meters x 1.1 meters. The figure shows the truss fully folded, 50% deployed and fully deployed.

FIGURE 1

Introduction

ORIGINAL PAGE IS
OF POOR QUALITY

- Objective - Develop experimental methods to obtain data required to analytically model nonlinear joint dominated truss structures
- Approach
  - Fabricate compact deployable truss structure
  - Identify technique to represent individual joint behavior
  - Perform joint testing to develop data required to characterize joint behavior
  - Develop analysis model of complete truss structure
  - Perform static and modal survey testing of truss
  - Correlate test/analysis results
- Conclusions
- Work performed partially under MSFC contract NAS 8-36420 "Development of Structural Dynamic Analysis Tools"

FIGURE 2

BAC Compact Deployable Space Truss

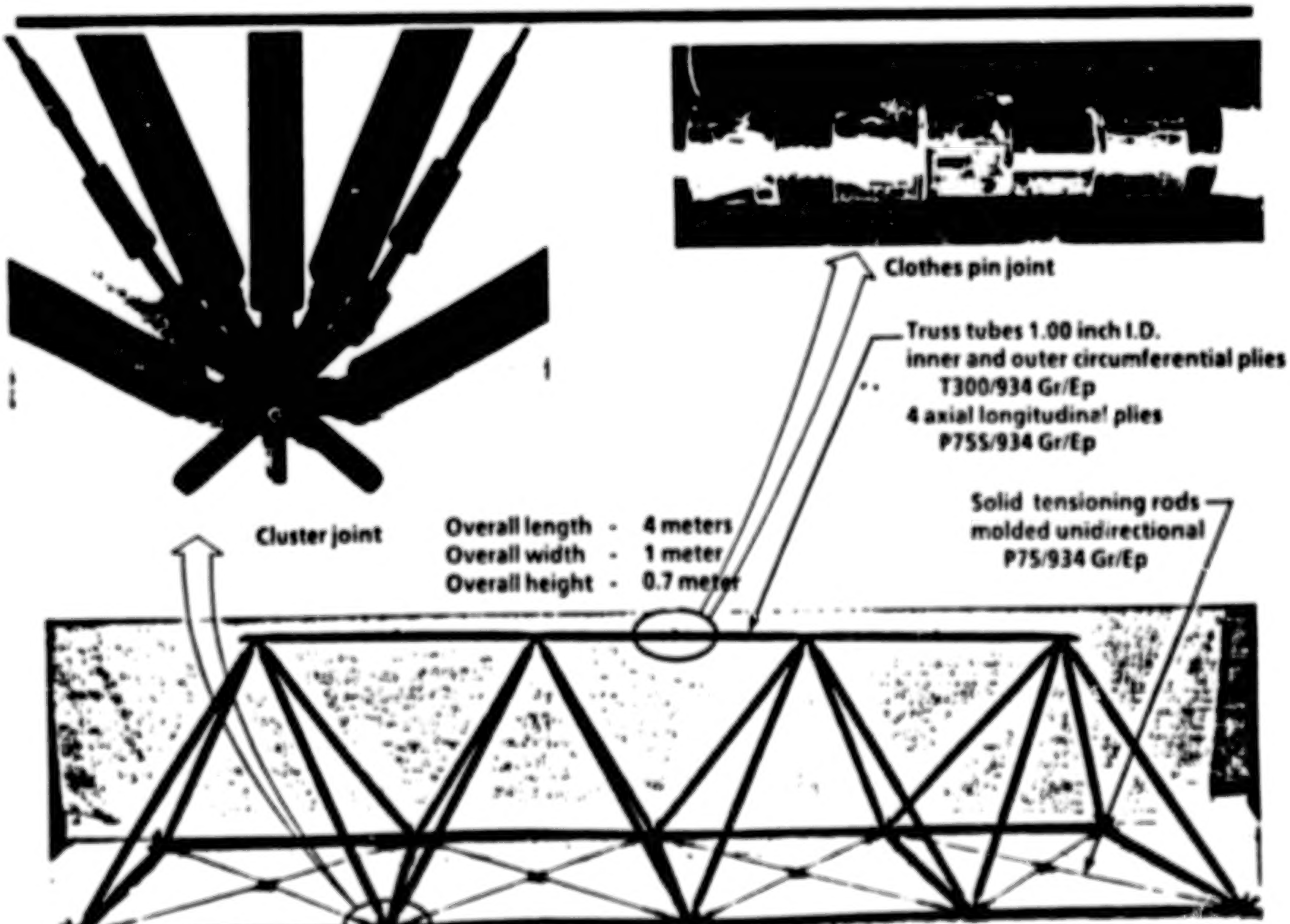
Clothes pin joint
Truss tubes 1.00 inch I.D.
inner and outer circumferential plies
T300/934 Gr/Ep
4 axial longitudinal plies
P75S/934 Gr/Ep
Cluster joint
Overall length - 4 meters
Overall width - 1 meter
Overall height - 0.7 meter
Solid tensioning rods
molded unidirectional
P75/934 Gr/Ep

ORIGINAL PAGE IS
OF POOR QUALITY

FIGURE 3

BAC Deployable Space Truss–Deployment Sequence

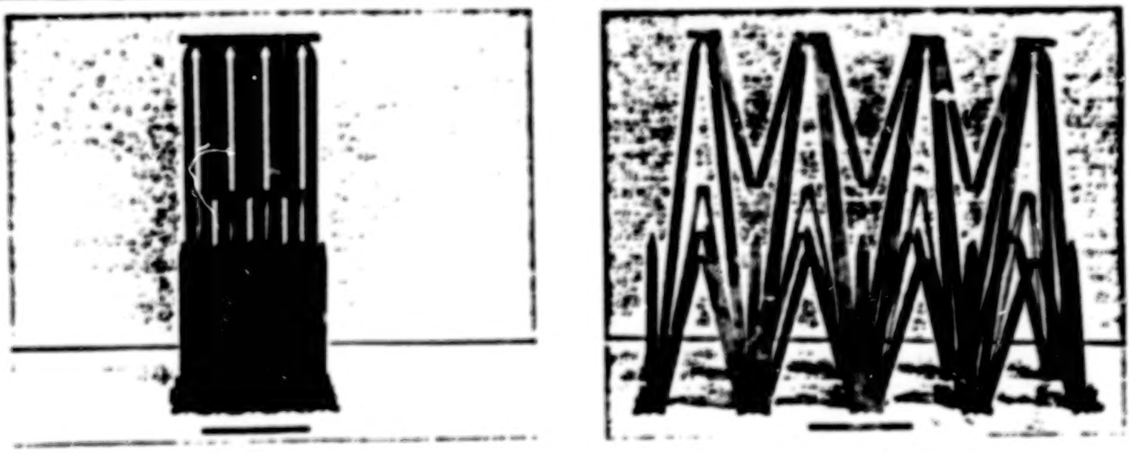

Folded

50 percent deployed

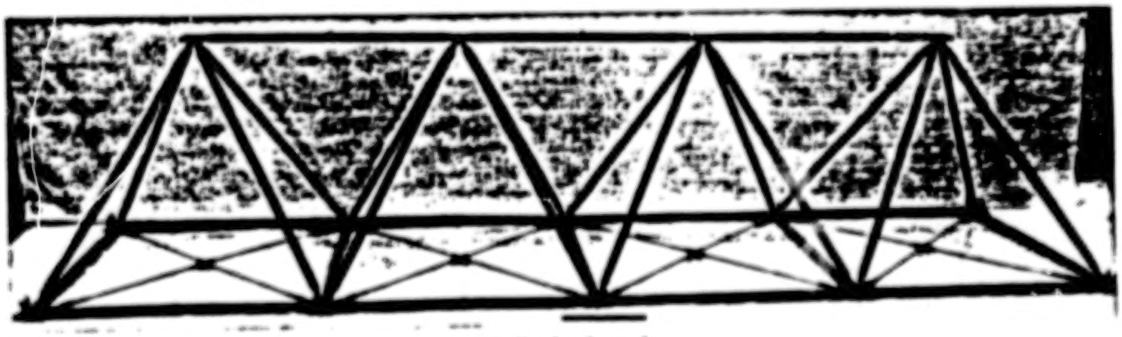

Fully deployed

FIGURE 4

Truss Testing/Modeling Approach

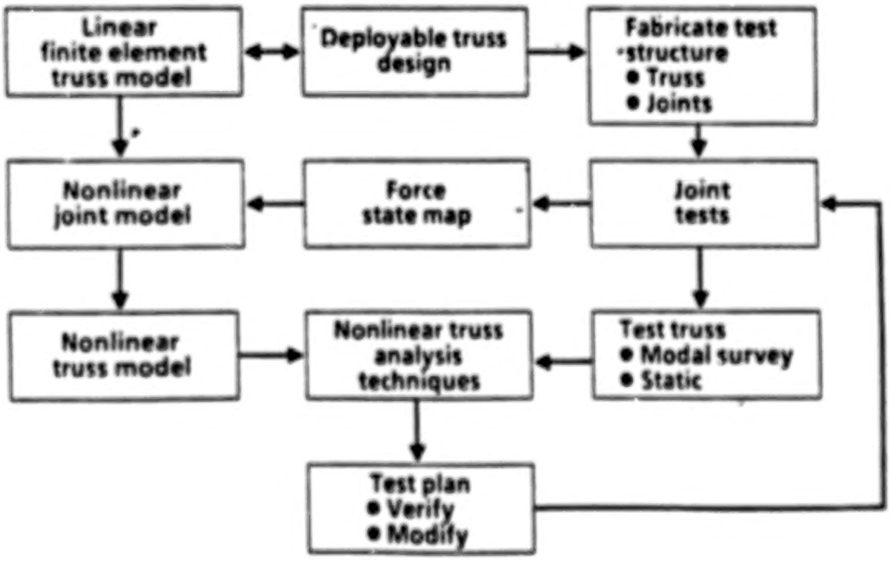
Linear finite element truss model
Deployable truss design
Fabricate test structure
• Truss
• Joints
Nonlinear joint model
Force state map
Joint tests
Nonlinear truss model
Nonlinear truss analysis techniques
Test truss
• Modal survey
• Static
Test plan
• Verify
• Modify

TRUSS TESTING/MODELING APPROACH

The approach that was taken in the development of a truss testing/modeling technique is shown in flow diagram form in figure 4. A linear finite element model of the truss was formulated to aid the truss design effort. The 4-bay truss structure was then fabricated along with several extra joints to be used in the joint characterization tests. Force state maps, described in figure 5, were developed from the joint test data. The maps were then used to in the formulation of nonlinear models of both types of truss joints. These models were then incorporated into a model of the 4-bay truss. An analysis was then performed to correlate with the results of static and modal survey tests of the truss. The test/analysis correlation indicated that the original test plan will require several modifications.

JOINTS CHARACTERIZATION - FORCE STATE MAPPING

Figure 5 gives a description of the Force State Mapping technique developed by Prof. E.F. Crawley and K.J. O'Donnell at the MIT Space Systems Laboratory. This technique represents the force transmitted through a joint as a function of the relative displacement and velocity across the joint. The resulting three dimensional plot provides a very compact, graphical description of the joint behavior. Common nonlinearities associated with joints produce surfaces that are easily recognizable which can give the analyst a qualitative idea for an applicable joint model. As an example, the Force State Map for a linear spring-damper in series with a gap is shown. A well defined testing procedure has been outlined to implement the technique. The results are also in a form in which tangent or secant moduli can be readily calculated to be used in equivalent linearization analyses.

CLEVIS JOINT TEST SETUP

A picture of the joint testing apparatus setup for the testing of the deployable truss clevis joint is shown in figure 6. The joint was held between a heavy steel "bookend" load reaction fixture and the armature of an electro-mechanical shaker. The shaker and fixture were bolted to a concrete slab floor. The force was applied to the joint along the axis of the truss tube leading into the joint. Displacement and velocity were sensed in the direction parallel to the applied load. The input force was sensed by a Kistler Model 922F3 piezoelectric force cell. The relative displacement across the joint was sensed with a Trans- Tek Model 240-0000 integrated linear variable differential transducer (LVDT), and the relative velocity across the joint with Trans-Tek Model 0101-0000 linear velocity transducer (LVT).

SCHEMATIC OF INSTRUMENTATION FOR FORCE-STATE MAPPING TESTS

Figure 7 shows a block schematic of the data acquisition system. The main components are a Zonic Model 6080 multichannel FFT analyzer and an LSI 11/73 minicomputer system. The 6080 provided the antialiasing filters, A/D conversion, and real-time DMA throughput of data to hard disk. Following acquistion, the raw time history data was moved to a VAX 11/750 for force map processing. The three quantitites of interest, force, displacement and velocity, were measured using three separate transducers. The controlled force input was an amplitude-modulated sine wave with a "carrier" frequency of 2 Hz. The modulating signal was a ramp function having a period of 120 seconds.

FIGURE 5

Joints Characterization–Force State Mapping

- **Reference:** "Identification of Nonlinear System Parameters in Space Structure Joints Using The Force State Mapping Technique", E. F. Crawley and K. J. O'Donnell SSL #16-85, July 1985
- Represents force transmitted by joint as function of displacement and velocity across joint
- 3 dimensional plot provides compact graphical description of nonlinear joint behavior
  - Established testing procedure
  - Common nonlinearities easily recognizable
  - Results directly usable for equivalent linearization analysis

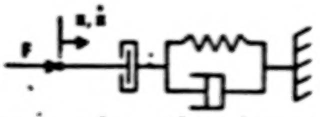

Force state map for spring-damper with gap

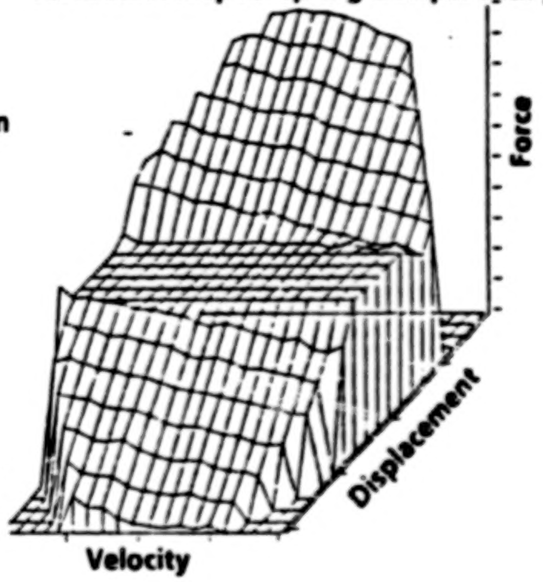

FIGURE 6

Clevis Joint Test Setup

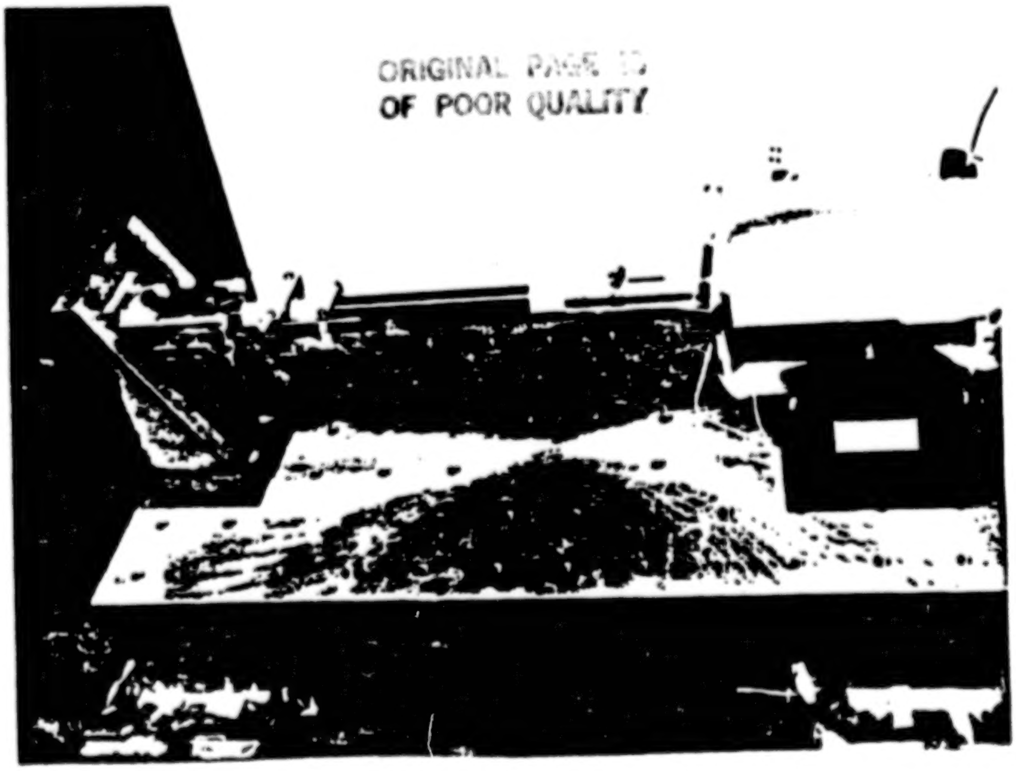

ORIGINAL PAGE IS
OF POOR QUALITY

FIGURE 7

Schematic of Instrumentation for Force State Mapping Tests

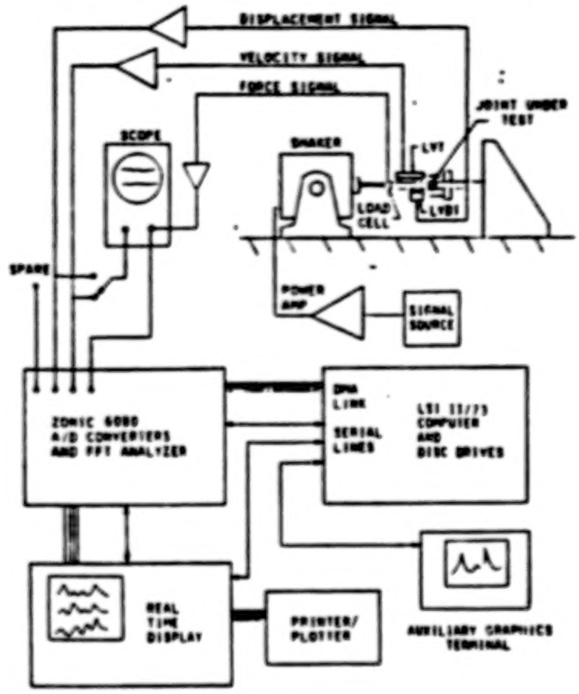
DISPLACEMENT SIGNAL
VELOCITY SIGNAL
FORCE SIGNAL
JOINT UNDER TEST
SCOPE
SHAKER
LVT
LOAD CELL
LVDT
SPARE
POWER AMP
SIGNAL SOURCE
ZONIC 6080 A/D CONVERTERS AND FFT ANALYZER
DMA LINK
SERIAL LINES
LSI 11/73 COMPUTER AND DISC DRIVES
REAL TIME DISPLAY
PRINTER/ PLOTTER
AUXILIARY GRAPHICS TERMINAL

FIGURE 8

Raw Data From Joint Testing at 2 Hz

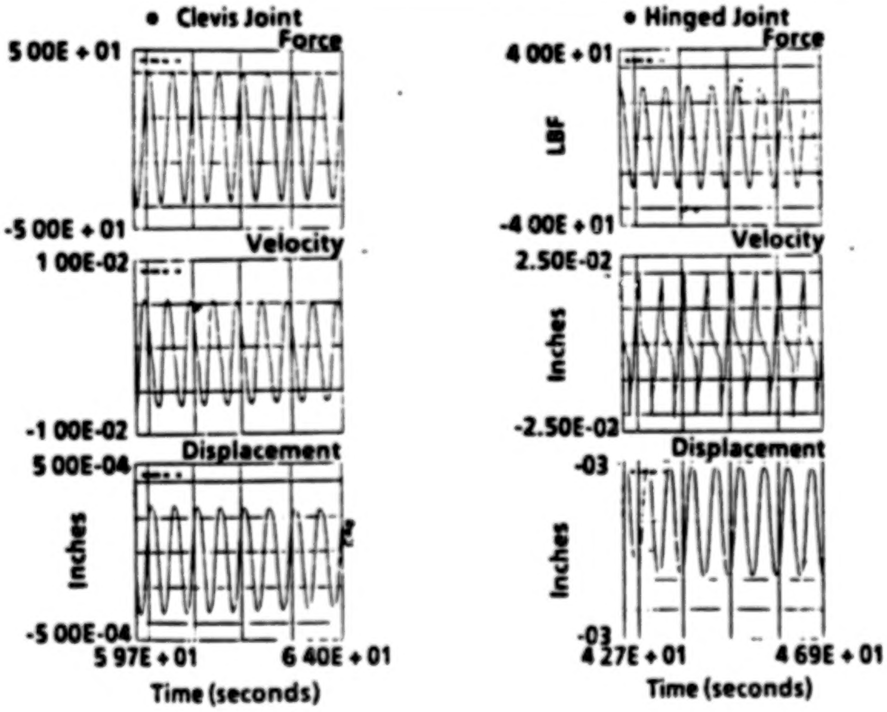

RAW DATA FROM JOINT TESTING AT 2 Hz.

The plots in figure 8 show segments of the raw time histories of force, velocity and displacement from tests of the clevis joint and hinged joint. Both the tongue and clevis fitting were fabricated of the injection- molded fiber-resin. Note that the force, velocity and displacement data for the clevis joint all appear to be sinusoidal, indicating that the clevis joint is essentially linear. The hinged joint however exhibited a more nonlinear behavior. Because the hinge axis does not intersect the axis of the tube, a bending moment around the hinge axis results when axial forces are applied to the tube. Although lateral motions of the joint were constrained by the test fixture, it is to be expected that some bending of the joints occurred. While the effect could not be eliminated, it was quantified by running the test with the transducers located at several different positions around the tube axis. It can be noted that the quantity which varies the most from a sinusoid is the velocity signal.

REDUCED FORCE STATE DATA FOR CLEVIS JOINT AT 2 Hz

A force-state map and a hysteresis curve of the clevis joint is shown in figure 9. The results were derived from the complete, amplitude-modulated time histories, a short segment of which was shown in the previous figure. Note that the surface is not perfectly flat, indicating that some amount of nonlinearity and energy dissipation are present. The hysteresis curve of the clevis joint shows force versus displacement for one load cycle at each of three peak load levels. It clearly shows that the joint is capable of dissipating a significant fraction of its peak energy in each cycle and that this dissipated fraction (proportional to damping) is a strong function of load level.

REDUCED FORCE STATE DATA FOR HINGED JOINT AT 2 Hz

The force-state map for the hinged joint is shown in figure 10. The characteristics of the joint were such that certain areas in the position-velocity plane could not be measured. The shape of the surface indicates a more pronounced nonlinear behavior than was noticed for the clevis joint. The corresponding hysteresis plot is also shown. The displacement offset is due to error in the DC-coupled transducing. As with the clevis joints, it can be seen that the hinged joint also exhibited a significant amount of damping.

DEPLOYABLE TRUSS STATIC AND MODAL SURVEY TEST SET-UP

Figure 11 shows the 4-bay deployable truss set-up for the static and modal survey testing. The truss was tested in a cantilevered configuration, mounted vertically with the fixed end at the floor of the test cell. A 208 lb tri angular tip mass was attached to the free end of the truss to decrease the structure modal frequencies. A pendulum suspension was used to off-load the 208 lb weight to eliminate any preload effects. During testing, the amount of off-load could be varied to assess the effects of a compressive joint preload. Electro-magnetic shakers were used to drive the tip mass for the modal survey tests, and a pulley/weight system was used to apply the forces for the static test. Modal shape data was obtained from 72 accelerometers mounted to the truss and tip mass. Deflection indicators were used to measure the displcement of the centroid of the tip mass during the static tests.

ORIGINAL PAGE IS
OF POOR QUALITY

FIGURE 9

Reduced Force State Data for Clevis Joint at 2 Hz

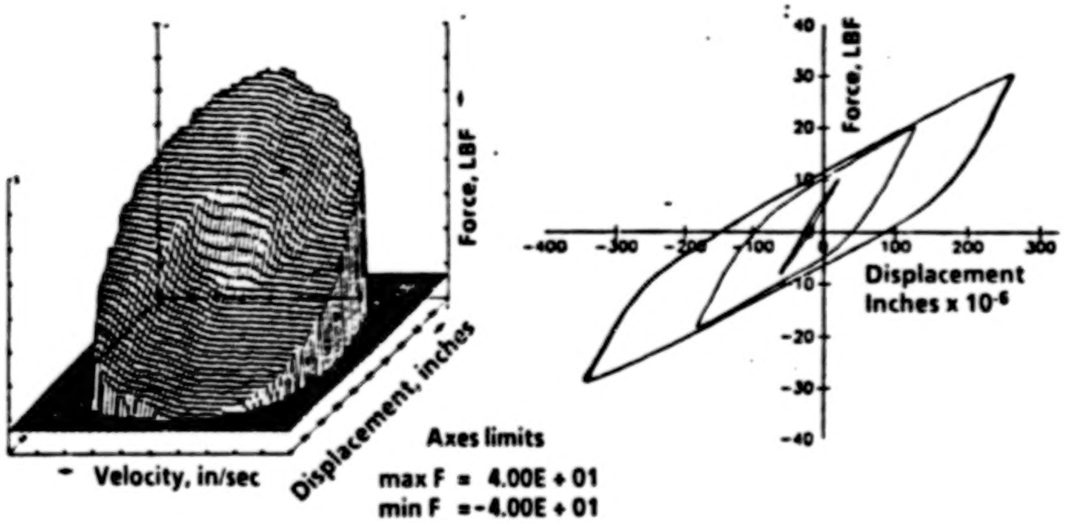

- Force State Map
- Hysteresis Plot

Axes limits

max F = 4.00E + 01
min F = -4.00E + 01
max d = 5.00E-04
min d = -5.00E-04
max v = 1.00E-02
min v = -1.00E-02

FIGURE 10

Reduced Force State Data for Hinged Joint at 2 Hz

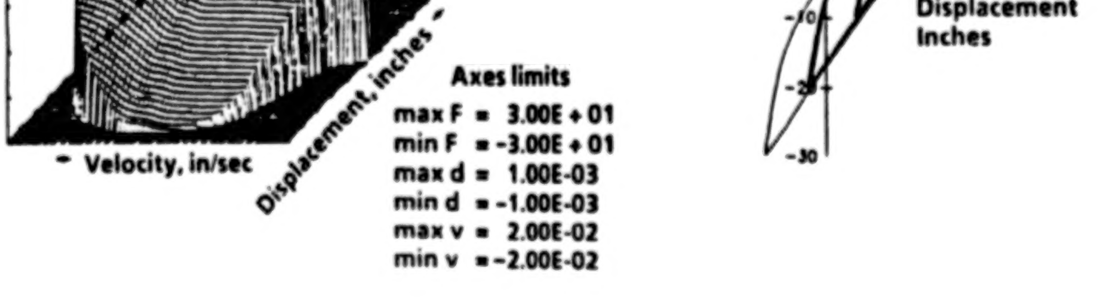

- Force State Map
- Hysteresis Plot

Axes limits

max F = 3.00E + 01
min F = -3.00E + 01
max d = 1.00E-03
min d = -1.00E-03
max v = 2.00E-02
min v = -2.00E-02

FIGURE 11

Deployable Truss Modal Survey and Static Test Set-Up

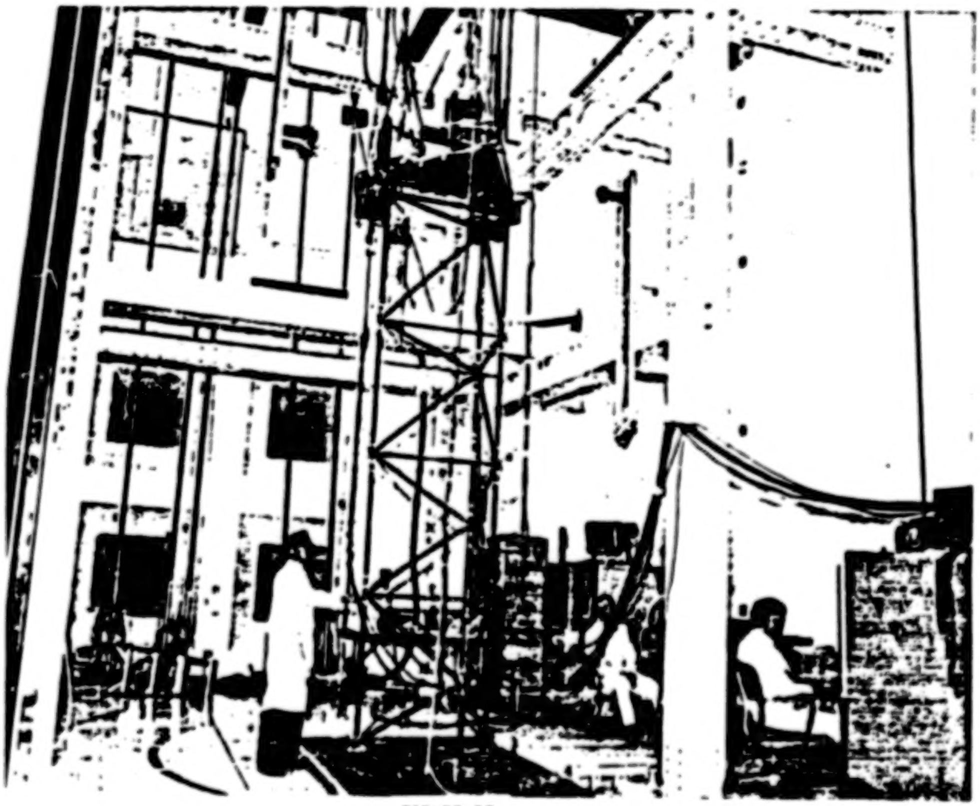

FIGURE 12

Truss Modal Survey Accelerometer Installation

- 72 Accelerometer measurements
- All clevis joints
- Hinged joints on one longeron

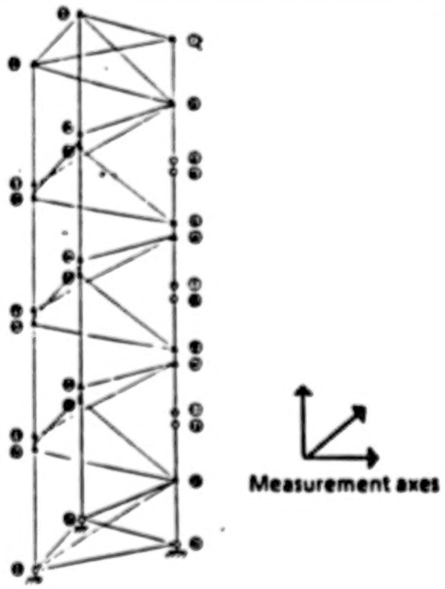

○ Single axis

△ Triaxis

ORIGINAL PAGE IS
OF POOR QUALITY

TRUSS MODAL SURVEY ACCELEROMETER INSTALLATION

The accelerometer installation for the truss modal survey tests is shown in figure 12. A total of 72 accelerometer measurements were made. The accelerometers were generally mounted in triaxial configuration adjacent to joints on small plexiglass mounting blocks. For several of the clevis joints, a triaxial set was mounted on both sides of the joint to measure joint rotation effects. Single axis lateral acceleration measurements were also made on both sides of the hinged joints along one longeron. All truss mounted accelerometers were lightweight, Endevco Models 2222 or 2250. Other locations utilized PCB Model 308 type. All accelerometers were mounted parallel to the rectangular X,Y,Z measurement axes system.

TRUSS MODAL SURVEY BENDING MODE SHAPES

Mode shape data for the first two lowest truss modes obtained from the modal survey testing are plotted in figure 13. These two modes were the cantilever bending modes in the Y and Z directions, respectively. In both of these mode shape plots, a significant amount of rotation of the clevis joints and lateral buckling at the hinged joints can be noticed. This behavior is most pronounced in the single longeron on the left side of the truss only because it contained the most instrumentation. The joints in the other longerons were observed to exhibit a similar behavior. This differed significantly from the strictly axial deformations that are generally expected in truss longerons.

TRUSS MODAL SURVEY TEST/ANALYSIS MODAL FREQUENCIES

A comparison of the modal frequencies obtained from the modal survey test and those predicted by a linear finite element modal analysis performed in NASTRAN is given in figure 14. The NASTRAN finite element model is also shown. Beam elements with pinned connections were used to model the truss members. The clevis joints were also modeled in detail with beam elements. The hinged joints, however, were assumed to be rigid. It can be seen that the analysis significantly overpredicted the frequencies of all of the overall truss modes. This is due primarily to the flexibility introduced by the lateral buckling of the longeron hinged joints. The effects of clevis joint rotation were modeled fairly well as can be seen by the comparisons with the joint rotation modes obtained in the modal survey test. A possible secondary effect on the overall flexibility of the test structure that was not modeled is the joint rotation that may be caused by an initial angular misalignment of the clevis joints. The lateral buckling and joint rotation effects cannot be readily incorporated into an analytical model and should be eliminated in the truss design process if an accurate model of the truss is needed.

TRUSS MODAL SURVEY VARIATION OF MODE FREQUENCY WITH FORCE AMPLITUDE

Figure 15 shows the variation of test frequencies for the first Y-bending mode for different shaker force levels. A narrow band sine sweep technique was used to map the test modes. The total shaker force was varied from 1.0 to 3.0 lbs rms. Tests were run with the truss structure completely off-loaded, and also with a total axial compressive preload of 50 lbs. In both cases, the mode frequencies decreased with increased shaker force. This is consistent with the behavior noticed in the joint tests, figures 9 and 10, in which it could be seen from the hysteresis plots that the joints appear to be stiffer at the lower load levels.

FIGURE 13

Truss Modal Survey Bending Mode Shapes

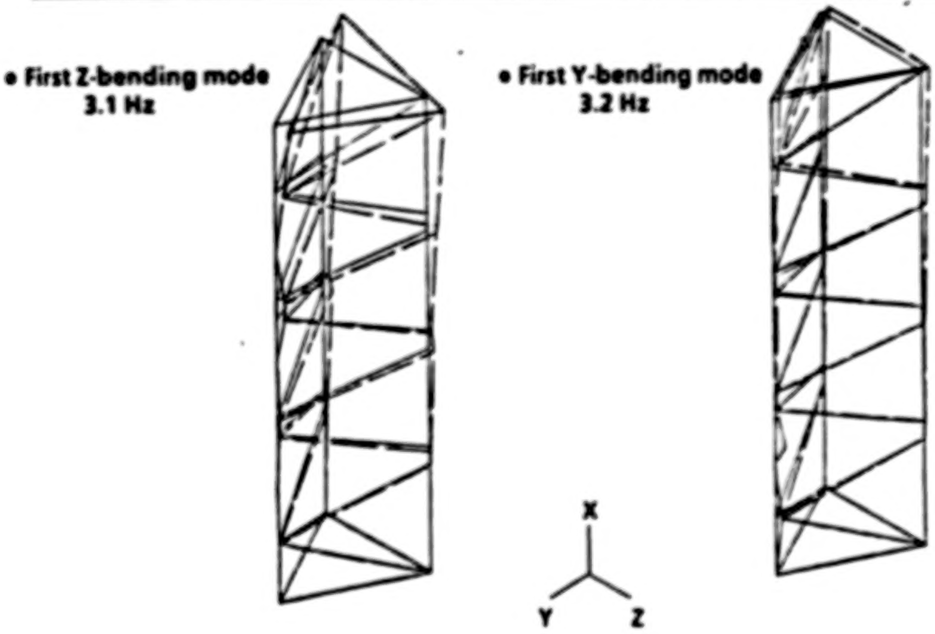
• First Z-bending mode
3.1 Hz
• First Y-bending mode
3.2 Hz
X
Y
Z

FIGURE 14

Truss Modal Survey Test/Analysis Modal Frequencies

Mode	Frequency-Hz	
	Test	Analysis
First Z-bending	3.1	4.4
First Y-bending	3.2	4.6
First axial	21.0	28.7
Torsion	9.5	14.6
Clevis joint rotation	15.4	15.3
Clevis joint rotation	19.6	17.1

- Nastran linear finite element modal analysis
  - Beam elements with pinned connections
  - Clevis joints modeled

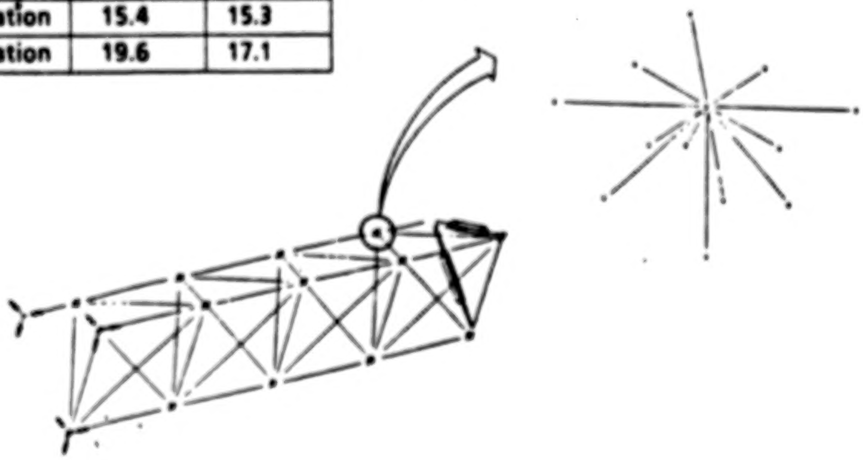

FIGURE 15

Truss Modal Survey Variation of Mode Frequency With Force Amplitude

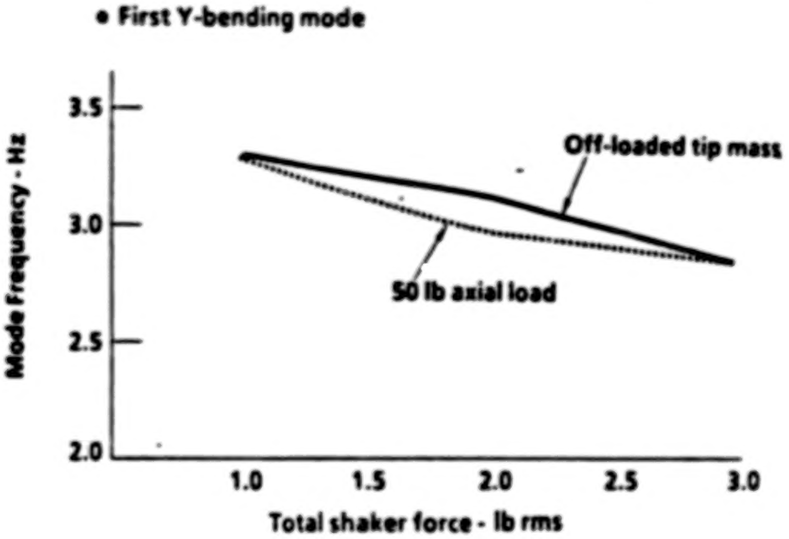

FIGURE 16

Truss Static Test/Analysis Comparison

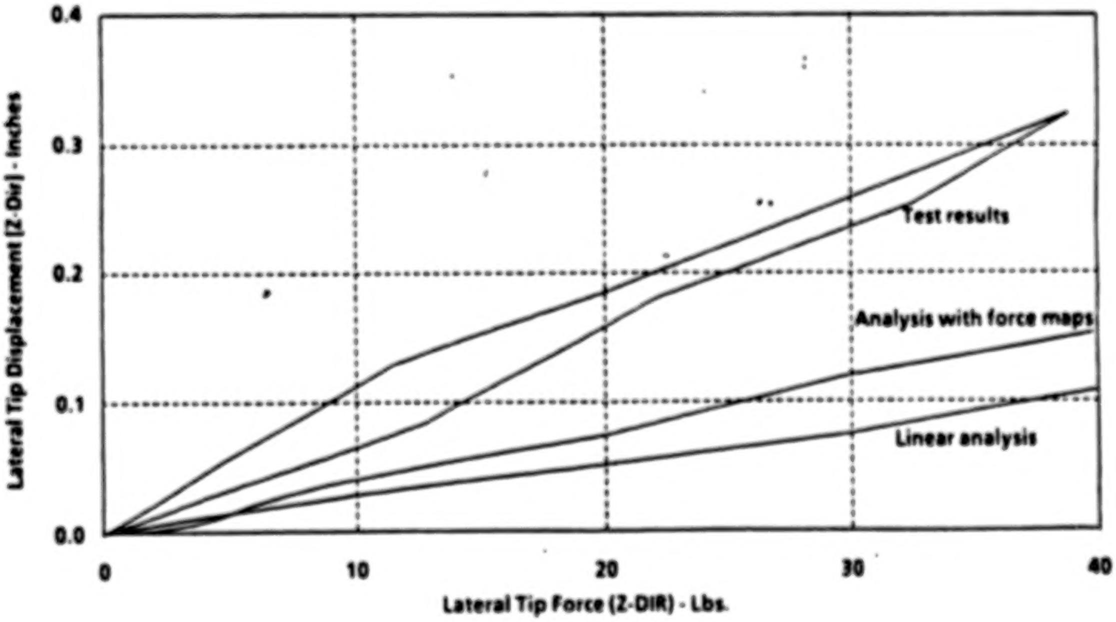

TRUSS STATIC TEST/ANALYSIS COMPARISON

The deflection at the tip of the truss in the Z-direction as a static loading of up to 38.7 lbs was first applied then removed is shown in figure 16. Some nonlinearity and hysteresis was noticed in the test data. For comparison purposes, first a linear static analysis was performed in NASTRAN using the finite element model shown in figure 14. As was observed in the modal survey results, the linear analysis model significantly overpredicted the stiffness of the truss structure. A second analysis was then performed incorporating the force state map data shown in figures 9 and 10 for the models of the clevis and hinged joints. The force maps were included in a residual force modal nonlinear analysis (reference: "Dynamics of Trusses Having Nonlinear Joints", by J. M. Chapman, F. H. Shaw, and W. C. Russell, presented previously at this workshop), in which only the stiffness components of the force maps at zero velocity were included. In the analysis, the load was ramped slowly from 0 to 40 lbs. The results are shown plotted in the figure. Although the correlation with the test data is closer than the strictly linear analysis, the analysis with the joint force maps still significantly overpredicts the truss stiffness.

TRUSS STATIC TEST COMPARISON - EFFECTS OF HINGE JOINT LATERAL BUCKLING

An analysis was performed incorporating the combined effects of axial deformation, hinged joint rotational gap and flexibility, and cable tension and end shortening due to bending using the residual force nonlinear analysis technique. The results are shown plotted in figure 17. The most sensitive parameters were found to be the hinge joint rotational stiffness and the gap. The 5000 in-lb/Rad rotational stiffness used in the analysis was felt to be conservative for the hinge joint. This analysis produced a much closer correlation with the test data than the linear finite element analysis, although it still over predicts the truss stiffness.

TRUSS STATIC TEST COMPARISON - EFFECT OF CLEVIS JOINT ROTATION

A NASTRAN geometric nonlinear analysis, including large deformation effects, was performed to assess the effects of having an initial angular misalignment of the clevis joints. Assumed 2 degree clevis joint rotations were written into the unstressed geometry, and runs were made with static loadings of 10, 20, 30, and 40 lbs. The resulting truss tip displacements are shown in figure 18. Again, the results are much closer to the test data than the linear analysis; however, the overall truss stiffness is still overpredicted. As was noticed in the discussion of the modal survey results, the flexibility of the test structure is probably due to the combined effects of hinge joint lateral buckling and clevis joint rotation.

CONCLUSIONS

In summary, several conclusions were drawn as a result of this work regarding the design of the deployable truss, and the testing and analysis of nonlinear joint dominated trusses. As shown in figure 19, the first conclusion was that a study of the load path through the truss joints in tension and compression should be performed early in the design process to determine the susceptibility of the joint to rotation or lateral buckling. This behavior decreases the overall stiffness and generally makes it impossible to develop an accurate analytical model of the truss structure. Since the hinged type folding joints are particularly

FIGURE 17

Truss Static Test Comparison-Effect of Hinge Joint Lateral Buckling

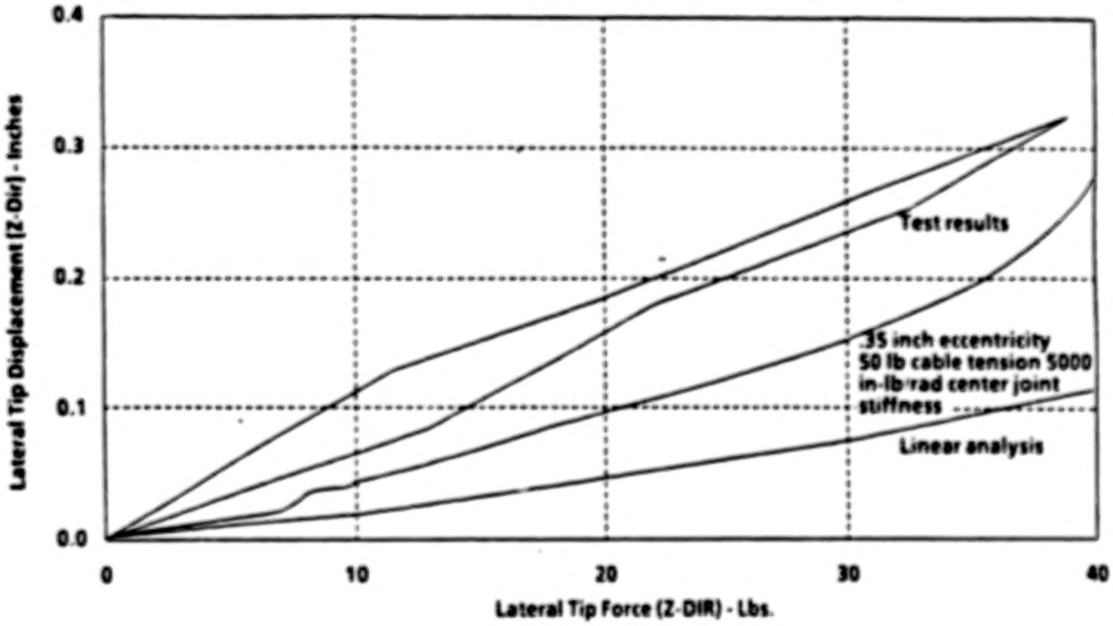

FIGURE 18

Truss Static Test Comparison– Effect of Clevis Joint Rotation

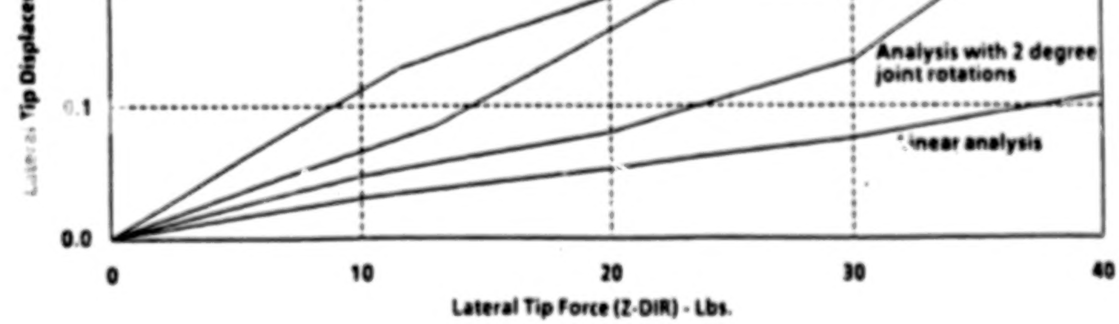

FIGURE 19

Conclusions

- Deployable truss design
  - Joints designed without consideration of load path can exhibit rotation or lateral buckling
    - Introduces structural flexibility
    - Impossible to characterize in analytical model
  - Avoid hinged type folding joints in longeron members
- Truss testing/analysis
  - Force state mapping excellent technique for characterizing joints
    - Straight forward test method
    - Compact representation of joint behavior
  - Link testing may be required to describe truss behavior and verify analytical models
  - Fabrication and testing of subscale models or links should be required during design development

susceptible to lateral buckling due to the eccentric load path of the truss should be avoided if possible.

The force state mapping has proven to be an excellent technique for characterizing the nonlinear behavior of joints. The required instrumentation and test methods are relatively straightforward and do not present any unique problems. The 3-dimensional force state map provides a compact qualitative and quantitative method of representing the test data required to define the joint behavior. However, due to the possibility that some of the joint degrees of freedom may be unintentionally constrained during the joint test, a link test involving several joints and truss members in series may be required to completely describe the truss behavior and verify analytical models. It is therefore recommended that the fabrication and testing of scaled truss models or links be performed during the design development to identify joint problems, especially if an accurate analytical model of the truss structure will be required.

The need for monitoring the dynamic characteristics of large structural systems for purposes of assessing the potential degradation of structural properties has been established. This paper develops a theory for assessing the occurance, location, and extend of potential damage utilizing on-orbit response measurements. Feasibility of the method is demonstrated using a simple structural system as an example.

N87
22750
UNCLAS

N87-22750

JPL

SYSTEM IDENTIFICATION FOR LARGE SPACE STRUCTURE DAMAGE ASSESSMENT

J. C. CHEN
J. A. GARBA

Applied Technologies Section
Jet Propulsion Laboratory
California Institute of Technology
Pasadena, California

Workshop on Structural Dynamics and Control
Interaction of Flexible Structures

April 23-24, 1986
Marshall Space Flight Center
Alabama

It becomes clear that continuous monitoring of structural integrity and the detection/assessment of damage and its subsequent compensation, repair, and control are important considerations for large flexible space structures. The ultimate future requirement will be a remote data acquisition system with rapid on board analysis for almost real time assessment. The present study will focus on the feasibility of such a methodology which will provide a damage assessment capability for large space structures.

BACKGROUND

- Early warnings for structural damage are necessary for prevention of catastrophic failure.
- For safety, the damage should be continuously monitored as to its occurrence, its location and as to the extend of the damage.
- Certain damage such as the material degradation cannot be detected by visual inspection.
- Damage detection permits real time corrective action to minimize further damages and to maintain operational requirement.

Techniques of using experimentally measured data for determining the parameters in the equations of motion of a system is commonly called system identification. A typical procedure involves the modal test of the structural system during which the responses due to external excitations are measure. From the response data, the dynamic characteristics of the system such as the natural frequencies and mode shapes can be determined directly or through data processing techniques depending on the test method employed. Because the natural frequencies and mode shapes of a structural system are functions of the system parameters such as the mass and stiffness, these system parameters may be "identified" by comparing those determined by test to those dynamic characteristics predicted from the mathematical model.

JPL

TECHNICAL APPROACH

Objective:

Detect Occurrence
Identify Location
Quantity Damage

Methodology:

Comparison of dynamic characteristics between the healthy state and damaged state.

Identification procedure for model changes.

Relating model changes to damages.

The fundamental questions for damage assessment are whether it is feasible to identify the occurrence, location and extend of the damage from given measured structural dynamic characteristics. Therefore, the relationship between the physical parameters such as the mass and stiffness and the dynamic characteristics such as the eigenvalues and eigenvectors or natural frequency and mode shape must be established.

It is clear that values of ω_i and $(\phi)_i$ are functions of the mass [M] and stiffness [K] of the system. In other words, any changes in [M] and [K] due to the loss of mass or loss of stiffness of certain parts of the structural system will be reflected in its natural frequency and mode shape measurements. A discovery of a deviation of the measured natural frequency and mode shape with respect to those previously measured when the system was in an undamaged condition is an indication of the occurrence of damage. Certain changes in the physical parameters will effect certain modes but not others.

GOVERNING EQUATION FOR STRUCTURES

$$[M]\{\ddot{x}\} + [C]\{\dot{x}\} + [K]\{x\} = \{F(t)\}$$

Eigensolution:

$$[K]\{\phi\}_i - \omega_i^2 [M]\{\phi\}_i = 0$$

$\{\phi\}_i$, ω_i are function of $[M]$, $[K]$

Any changes of $\{\phi\}_i$ and ω_i are indications of occurrence.

First, it will be postulated that the mass distribution of the system [M] remains unchanged or is changed by only a known quantity. This is a reasonable assumption in that most structural damage for the large space structures will result in stiffness losses instead of complete separation or breakage with a loss of mass. Also for certain large space structures, such as the space station, the major distribution to the mass matrix came from non-load carrying components such as instrument packages, fluid containers and power generation units. These weights can be accurately estimated.

The kinetic energy distribution at each degree-of-freedom for the ith mode is equal to the potential energy distribution. The potential energy distribution is a function only of the stiffness matrix and the modal displacements.' For a localized damage, the mode shape should be similar to or only slightly deviated from that of the undamaged system. Hence the potential energy distribution will be similar except for those degrees-of-freedom associated with the damaged component. The location of the damage can be found by identifying those degrees-of-freedom whose kinetic energies are different from those of the undamaged system. Since the correct stiffness matrix for the damaged system is unknown, the kinetic energy distribution can be used for this purpose instead.

JPL

KINETIC AND POTENTIAL ENERGY

$$\lceil \phi_i \rfloor [K] \{\phi\}_i = \omega_i^2 \lceil \phi_i \rfloor [M] \{\phi\}_i$$

$$\{\phi_{ij} (K_{jk} \phi_{ik})\} = \omega_i^2 \{\phi_{ij} (M_{jk} \phi_{ik})\}$$

i = mode number,
j = DOF number, sum over k = 1, 2, 3

For diagonal mass matrix j = k

$$\{\phi_{ij} (K_{jk} \phi_{ik})\} = \omega_i^2 \{M_{jj} \phi_{ij}^2\}$$

- Assume [M] remain unchanged.
- Damage causes small changes in mode shapes but substantial changes in local potential energy.

It should be noted that the dimensions of the vectors $(y)_i$ and (Δk_{ij}) are different. The dimension of $(y)_i$ is equal to the number of degrees-of-freedom of the system and the dimension of (Δk_{ij}) will be equal to the number of independent elements in the stiffness matrix. Although the stiffness matrix is highly banded, the number of independent elements is usually larger than the number of the degrees-of-freedom of the system.

QUANTIFICATION OF DAMAGE

Decomposition of Stiffness Matrix

$[K] = [Ko] + [\Delta K]$

$[Ko]$ = Stiffness for undamaged system

$[\Delta K]$ = Perturbation stiffness due to damage.

GOVERNING EQUATION

$$[\Delta K]\{\Phi\}_i = \left(\omega_i^2 [M] - [K_o]\right)\{\Phi\}_i = \{\gamma\}_i$$

$$[C]_i \{\Delta k_{ij}\} = \{\gamma\}_i$$

$[C]_i$ = Connectivity matrix, function of

Δk_{ij} = Elements in $[\Delta K]$ matrix, representing damages as reduction of stiffness in the associated structural elements.

For using multiple modes, the equation can be obtained by stacking the single mode equations. The number of unknowns remains the same, however, the number of equqtions will be increased. It is possible that the number of equations may become larger than that of the unknowns. In principle, a solution will not exist for such case, but an approximation can be obtained.

QUANTIFICATION OF DAMAGE (CONTINUE)

For multiple modes

$$\begin{bmatrix} [C]_1 \\ [C]_2 \\ \vdots \\ [C]_n \end{bmatrix} \{\Delta k_{ij}\} = \begin{Bmatrix} \{y\}_1 \\ \{y\}_2 \\ \vdots \\ \{y\}_n \end{Bmatrix}$$

or

$$\underset{n \times m}{[C]} \; \underset{m \times 1}{\{\Delta k_{ij}\}} = \underset{n \times 1}{\{Y\}}$$

n = number of equations = number of modes x DOF

m = number of Δk_{ij}'s, the unknown

in general $n \not\gtrless m$

Due to the nature of the problem, namely to seek the changes in the stiffness structural elements as represented by the quantities Δk_{ij}, it is reasonable to postulate that the "optimal" solution is the one with the smallest Euclidian norm. Thus, the solution procedure becomes a constrained minimization

JPL

QUANTIFICATION OF DAMAGE (CONTINUE)

Case I m > n (more unknowns than equations)

- Infinite number of solution.
- Seeking one with minimum Euclidean norm.

$$E = \frac{1}{2}\|\Delta k_{ij}\| + \{\lambda\}^T \left(\{\Upsilon\} - [C]\{\Delta k_{ij}\} \right)$$

where $\|\Delta k_{ij}\| = \{\Delta k_{ij}\}^T \{\Delta k_{ij}\}$ Euclidean Norm

$\{\lambda\}$ = vector of Lagrange multipliers

$$\left\{\frac{\partial E}{\partial(\Delta k_{ij})}\right\} = 0 \qquad \text{AND} \qquad \left\{\frac{\partial E}{\partial \lambda}\right\} = 0$$

$$\{\Delta k_{ij}\} = [C]^T \left([C][C]^T \right)^{-1} \{\Upsilon\}$$

If number of equations is greater than the number of unknowns, no exact solution exists. Therefore, one may look for an approximate solution in which the Euclidian norm of the error is minimized.

JPL

QUANTIFICATION OF DAMAGE (CONTINUE)

Case II $n > m$ **(more equations than unknowns)**

- **No solution**
- **Seeking approximation with minimum error**

$$\{\epsilon\} = \{\Upsilon\} - [C]\{\Delta k_{ij}\}$$

$$\|\epsilon^2\| = \{\epsilon\}^T\{\epsilon\}$$

$$\left\{\frac{\partial\|\epsilon^2\|}{\partial(\Delta k_{ij})}\right\} = 0$$

$$\{\Delta k_{ij}\} = \left([C]^T[C]\right)^{-1}[C]^T\{\Upsilon\}$$

ILLUSTRATIVE EXAMPLE

A simple example will be used for the purpose of illustrating the proposed approach for the assessment of structural damage. Figure 1 shows a 3 degree-of-freedom system to be used as an example for both the undamaged and damaged configurations. The "damage" is assumed to be the complete breakage of the spring K_4. The mass and stiffness matrices for the undamaged configuration are as follows:

$$[M] = \begin{bmatrix} 6 & 0 & 0 \\ 0 & 4 & 0 \\ 0 & 0 & 4 \end{bmatrix} , \qquad [K] = \begin{bmatrix} 6 & -3 & 0 \\ -3 & 6 & -3 \\ 0 & -3 & 4 \end{bmatrix}$$

The mass matrix for the damaged system is the same as that of the undamaged system but the stiffness matrix will be assumed unknown.

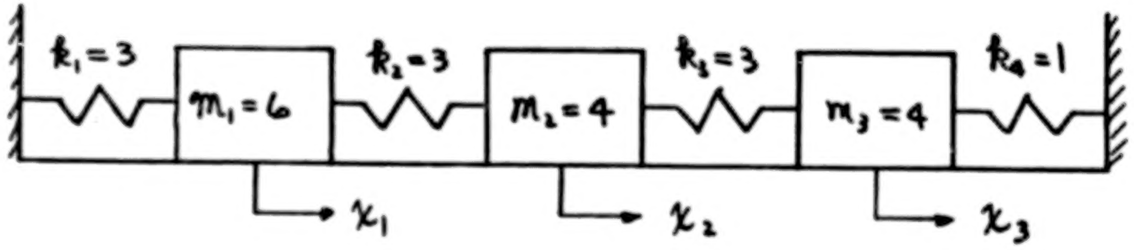
$k_1=3$
$m_1=6$
$k_2=3$
$m_2=4$
$k_3=3$
$m_3=4$
$k_4=1$
x_1
x_2
x_3

Undamaged System

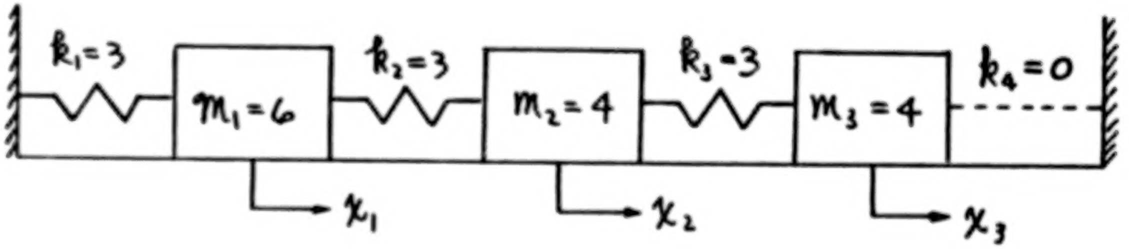
$k_1=3$
$m_1=6$
$k_2=3$
$m_2=4$
$k_3=3$
$m_3=4$
$k_4=0$
x_1
x_2
x_3

Damaged System

ILLUSTRATIVE EXAMPLE

The eigenvalues and eigenvectors of both systems are shown in Table 1. The following conditions will be assumed; (1) the mathematical model of the undamaged system, i.e., the mass and stiffness distribution, are known and have been verified by test data, (2) the mass distribution and geometric configuration of the damaged system remain unchanged, and (3) the natural frequencies and mode shapes of the damaged system are measured, they may be incomplete in the sense that not all the modes are measured. It is obvious that substantial changes exist for the first mode. This is an indication that the structural system has changed and since the mass distribution for this type of damage remains the same, it must be the stiffness that has changed.

TABLE 1

Eigenvalues and Eigenvectors

		Undamaged			Damaged		
Mode		1	2	3	1	2	3
Frequency		0.500	1.000	1.500	0.375	0.953	1.483
Mode Shape	X_1	2.000	1.000	2.000	2.184	1.101	2.312
	X_2	3.000	0	-5.000	3.756	0.200	-5.549
	X_3	3.000	-1.000	3.000	4.624	-0.944	2.870

TABLE 2

Comparisons of Frequency and Mode Shape

Mode No.	1	2	3
Frequency (%)	25.00	4.70	1.13
Mode Shape	0.271	0.232	0.083

kinetic energy distribution for the undamaged and damaged system have been calculated and are shown in Table 3. The kinetic energy distribution for each mode is listed in percentages for both the undamaged and damaged system. The comparison indicates that biggest difference between the two system is always occur at the degree-of-freedom X_3. It is reasonable to postulate that the damaged element is associated or physically attached to X_3. There are two structural elements associated with the X_3 degree-of-freedom, namely, the K_3 and K_4 springs. The K_3 spring is also associated with the X_2 degree-of-freedom whose kinetic energy remains relatively unchanged between the undamaged and damaged system for all three modes. This implies that the corresponding strain energy distribution in the elements associated with X_2 degree-of-freedom, i.e., the springs, K_2 and K_3, is relatively unchanged. Therefore, the only element whose strain energy must be changed to accommodate the kinetic energy distribution change is the K_4 spring. This concludes that the damage location is at the spring K_4.

TABLE 3

Kinetic Energy Distribution
(%)

Mode	1		2		3	
DOF	Undamaged	Damaged	Undamaged	Damaged	Undamaged	Damaged
X_1	25.00	16.77	60.00	66.15	15.00	17.07
X_2	37.50	32.98	0	1.47	62.50	65.45
X_3	37.50	50.16	40.00	32.39	22.50	17.49

From the mode one results, the stiffness reductions for spring K_1 to K_3 are from 1.56% to 4.22%. However, for spring K_4, the stiffness reduction is 97.69%. It is obvious that the spring k_4 has suffered major damage and in view of the large stiffness reduction, one may conclude that the spring has been broken. Mode one test data correctly assesses the damage. As expected mode 2 and 3 test data provide somewhat ambiguous results because of the small differences between the data from the damaged and the undamaged systems. Although the spring K_4 is identified to be damaged by a 71.46% or 64.06% stiffness reduction, these numbers are not convincing enough to indicate a breakage. However, these numbers should be sufficient to indicate that a damage has occurred at the spring K_4.

TABLE 4

Damage Assessment for Each Mode

Mode / Element	1		2		3	
	ΔK_j	Stiffness Reduction (%)	ΔK_j	Stiffness Reduction (%)	ΔK_j	Stiffness Reduction (%)
K_1	-.0468	1.56	.2391	-7.97 (increased)	-.4440	14.8
K_2	-.0694	2.31	-.2992	9.97	.1293	-4.31
K_3	-.1265	4.22	-.2378	7.93	-.1236	4.12
K_4	-.9769	97.69	-.7146	71.46	-.6406	64.06

It is clearly demonstrated that the proposed approach works perfectly in this case. The K_4 spring is identified as have 100% stiffness reduction which is total breakage and the springs K_1, K_2, and K_4 are identified as having less than 1% of stiffness changes. It is interesting to note when mode 2 and 3 data used separately, it provided less accurate assessment but when combined, a very accurate assessment is obtained.

TABLE 5

Damage Assessment for Multiple Modes

Mode / Element	1 and 2		2 and 3		3 and 1		1, 2 and 3	
	ΔK_j	Stiffnes Reduction(%)	ΔK_j	Stiffness Reduction(%)	ΔK_j	Stiffness Reduction(%)	ΔK_j	Stiffness Reduction(%)
K_1	-.0003	.01	-.0036	.13	.0018	-.06 (increased)	.0010	.03 (increased)
K_2	-.0039	.13	-.0003	.01	-.0019	.06	-.0017	.06
K_3	-.0049	.16	-.0025	.08	-.0011	.04	-.0012	.04
K_4	-.9996	99.96	-.9961	99.61	-1.0000	100	-1.0000	100

Acknowledgement

The research was carried out by the Jet Propulsion Laboratory, California Institute of Technology, under NASA Contracrt No. NAS7-918. This task was sponsored by Samuel L. Venneri, NASA Office of Aeronautics and Space Technology, Code RM.

JPL

CONCLUDING REMARKS

- Theory for the detection of damage occurrence, location and extend of stiffness reduction is developed.
- Theory is tested on a simple structure and a truss type mast structure.
- Further development is required, especially the application of actual field measurement.

N87
22751

UNCLAS

N87-22751

SPACE STATION STRUCTURES AND DYNAMICS TEST PROGRAM

Bugg, Ivey, Moore, and Townsend

Marshall Space Flight Center

April 1986

PRECEDING PAGE BLANK NOT FILMED

INTRODUCTION

The design, construction, and operation of a low-earth orbit Space station poses unique challenges for developement and implementation of new technology. The technology arises from the special requirement that the Station be built and constructed to function in a weightless environment, where static loads are minimal and secondary to system dynamics and control problems. One specific challenge confronting NASA is the devopment of a dynamics test program for (1) defining Space Station design requirements, and (2) identifying and charaterizing phenomena affecting the Station's design and developement. A general definition of the Space Station dynamic test program, as proposed by MSFC, forms the subject of this report.

The test proposal, as outlined herein, is a comprehensive structural dynamics program to be launched in support of the Space Station. The test program will help to define the key issues and/or problems inherent to large space structure analysis, design, and testing. Development of a parametric data base and verification of the math models and analytical analysis tools necessary for engineering support of the Station's design, construction, and operation provide the impetus for the dynamics test program. Four test phases are planned:

1) Phase I - Testing of Space Station Applicable Structural Concepts
2) Phase II - Testing of Space Station Prototypes
3) Phase III - Testing of Actual Space Station Structural Hardware
4) Phase IV - On-Orbit Testing of Space Station Construction

The philosopy being to integrate dynamics into the design phase through extensive ground testing and analytical ground simulations of generic systems, prototype elements, and subassemblies. On-orbit testing of the Station will also be used to define its capability.

PHASE I - TESTING OF SPACE STATION APPLICABLE STRUCTURAL CONCEPTS

MSFC recognized the need for static and dynamic testing of Large Space Structures applicable to Space Station design at an early stage. The purpose of these tests was to gain insight into the pecularities and requirements of not only the support fixtures, modal excitation, and data acquisition system, but also for the investigation into the static and dynamic behavior of truss structures exhibiting linear and nonlinear characteristics. Tasks have already begun to perform additional testing, modeling, and analyzing of these type structures. Some of the Large Space Structures that have been tested or are in the process of being tested are:

1. 46′ Rockwell deployable truss
2. 50′-30" diameter super astromast
3. 20′-30" diameter super astromast
4. SASP truss
5. 16½ meter Grumman beam

46 FOOT ROCKWELL DEPLOYABLE TRUSS TEST - The Rockwell truss is a box structure with telescoping diagonal joints with a housing frame assembly at one end as shown in Fig. 1. The truss has joints at each corner of the 10 bays where the diagonal battens and longerons meet. These joints contain a certain amount of free-play and hence the structures will exhibit nonlinearity with varying stiffness and damping. To reduce the amount of free-play, cables parallel to each of the longerons through each joint can be pretensioned up to 400 pounds each.

A static and dynamic test of this truss has been planned and is currently in progress. The truss will be tested in the horizontal with housing assembly at the free end. The bays will be supported in the vertical such that the loading at the joints will be reduced as much as possible. Static tests will be run laterally, axially, and torsionally. Deflection curves, with incremental loading of the four cables from 0-400 pounds, will be generated to characterize the linearity/nonlinearity of the truss.

After completion of the static tests, a modal survey test will be run to characterize the modes of the truss. Frequencies and damping will be determined for various preloads in the cables and with varying amplitudes to assess the nonlinearity effects. These dynamic tests of the truss will be for both cantilevered and free-free boundary conditions.

20-FOOT 30-INCH DIAMETER SUPER ASTROMAST TEST - The Astro-Research Corporation astromast consists of three continuous glass longerons with glass/epoxy batterns and diagonals. A finite element model of the truss structure and a test setup schematic are shown in Figures 2 and 3. Each end of the truss is attached to a 36-inch thick aluminum plate. The astromast is supported in the vertical by an overhanging beam/plate which is bolted to the top plate of the astromast.

The joint test performed was dynamic, with the truss supported vertically. A single point random testing technique was used to calculate the bending, torsional, and axial modes of vibration. Good agreement between the analysis and test was

INSTRUMENTATION LOCATIONS ON 46–FOOT TRUSS

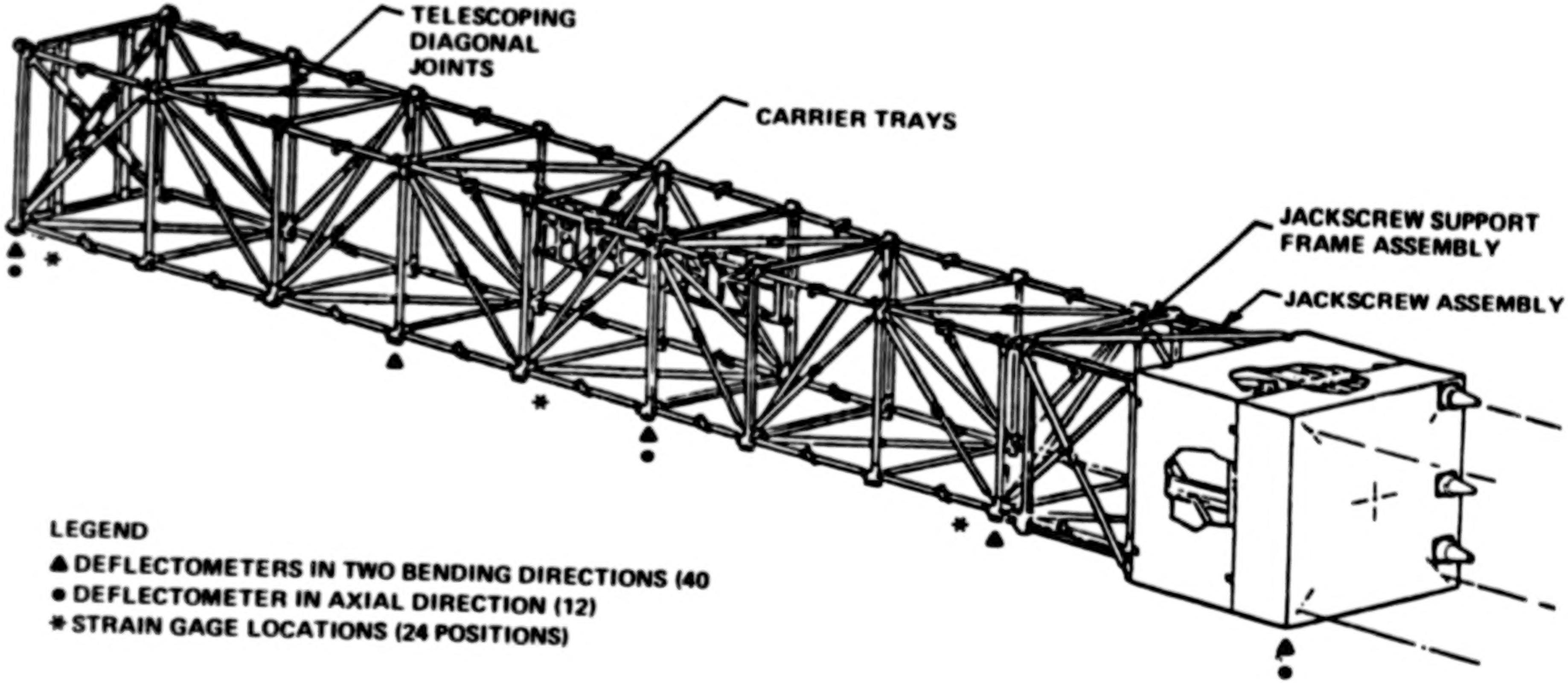
TELESCOPING
DIAGONAL
JOINTS
CARRIER TRAYS
JACKSCREW SUPPORT
FRAME ASSEMBLY
JACKSCREW ASSEMBLY
LEGEND
▲ DEFLECTOMETERS IN TWO BENDING DIRECTIONS (40
● DEFLECTOMETER IN AXIAL DIRECTION (12)
* STRAIN GAGE LOCATIONS (24 POSITIONS)

FIGURE 1.

ORIGINAL PAGE IS
OF POOR QUALITY

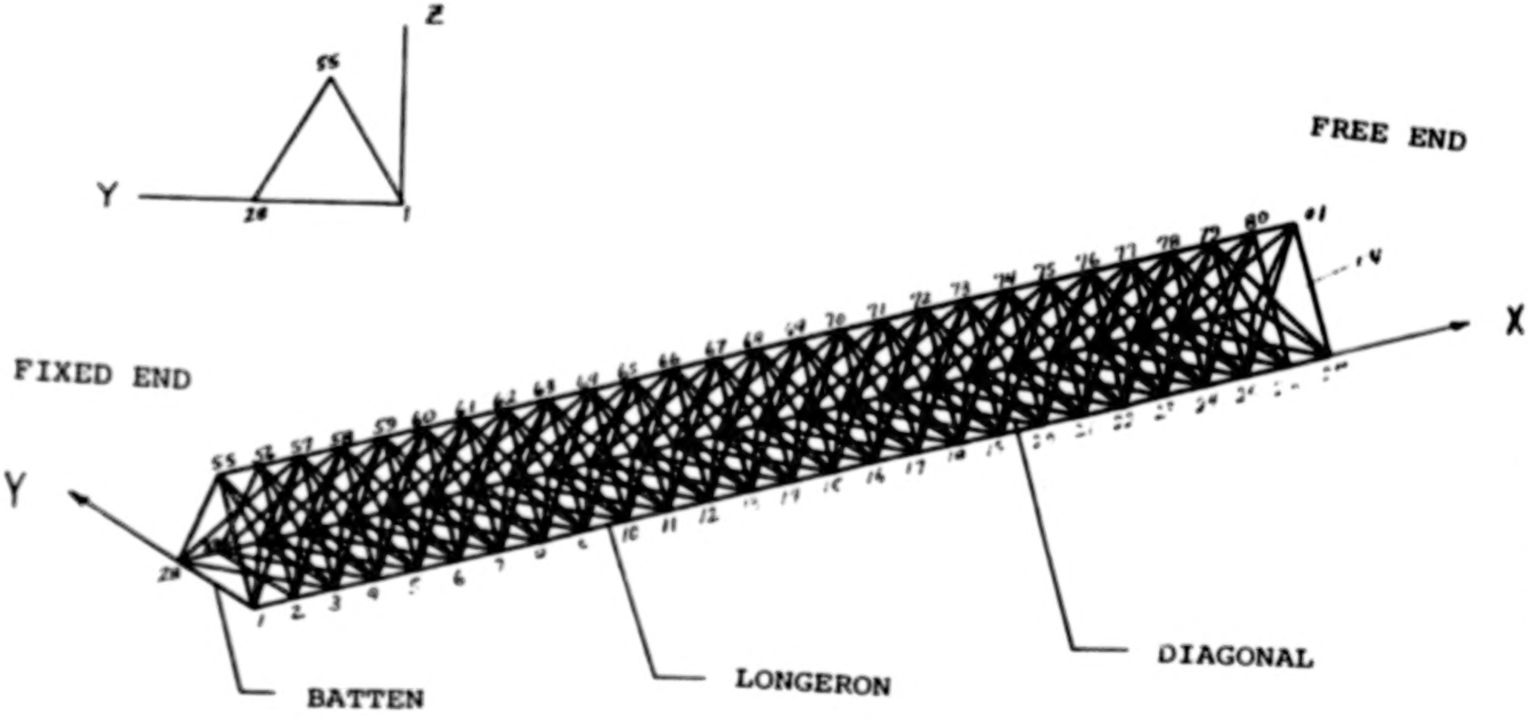
Z
55
Y
28
1
FREE END
81
X
FIXED END
Y
28
55
1
BATTEN
LONGERON
DIAGONAL

OF POOR

FIG. 2. 20-FOOT SUPER ASTROMAST NASTRAN PLOT

20' SUPER ASTROMAST STATIC TEST SETUP*

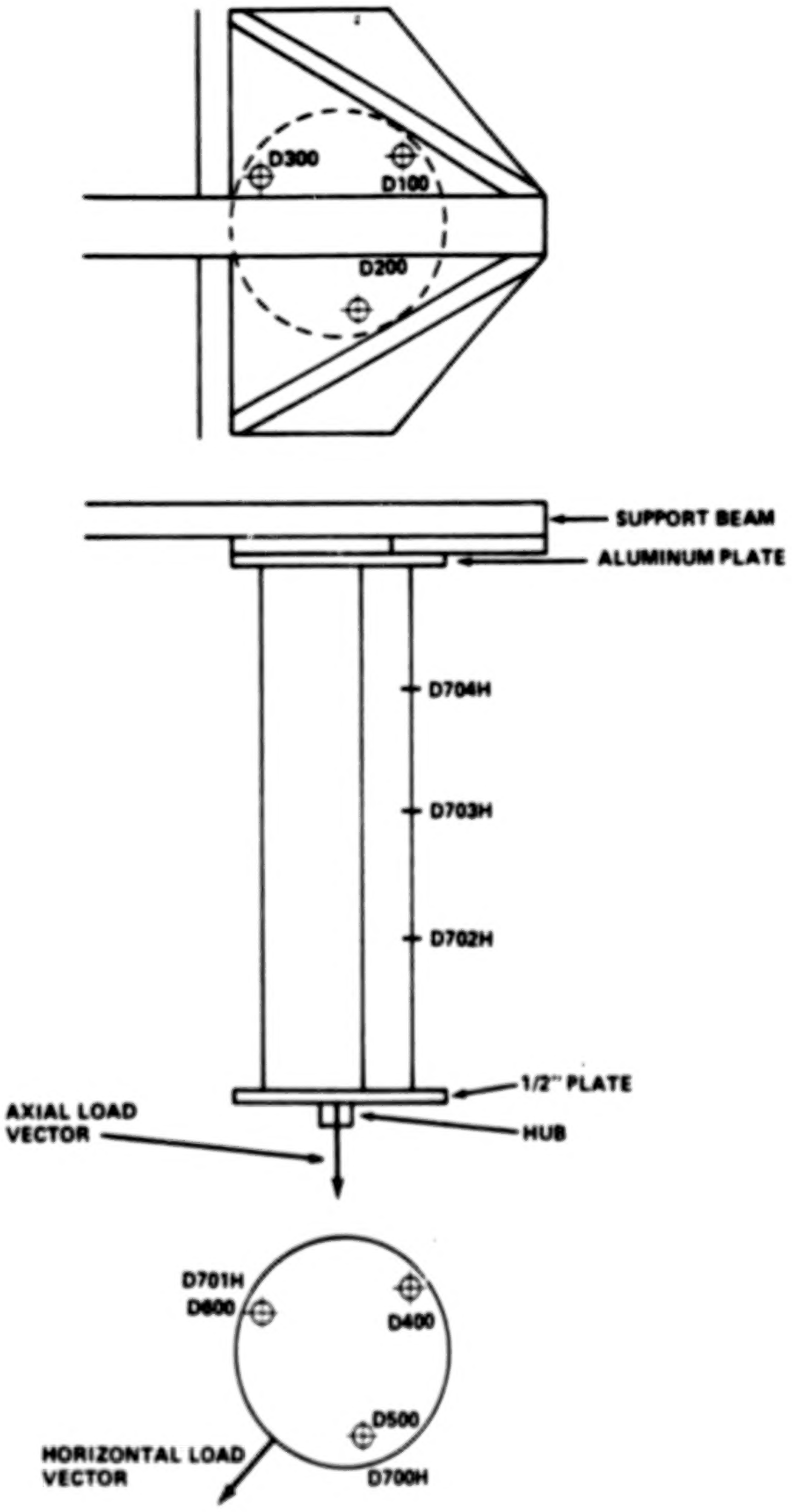
D300
D100
D200
SUPPORT BEAM
ALUMINUM PLATE
D704H
D703H
D702H
1/2" PLATE
AXIAL LOAD VECTOR
HUB
D701H
D600
D400
D500
HORIZONTAL LOAD VECTOR
D700H

*NOT TO SCALE

FIGURE 3 TEST SETUP

obtained except for the axial mode (see Table 1). The predicted frequency of 59.8 Hz did not agree with the test frequency of 37.7 Hz. After considerable analysis and some additional testing, it was found that the 1/2-inch aluminum plate at the free end, where the shaker was attached, had an inplane frequency of 37.7 Hz. As a result, the test personal were unable to shake out the higher first axial mode. A 2-inch plate was subsequently bolted to the 1/2-inch plate and the test was repeated. For this configuration, the first axial mode was easily obtained and compared well with analysis.

The static test followed the dynamic testing. Using the same configurations and boundary conditions, as in the dynamic test, axial and lateral static tests were conducted. For the axial test, loads up to 1200 pounds in increments of 200 pounds were applied in the center of the 1/2-inch plate attached to the free end. Several interesting results arose from this test:

a) The three longerons which ideally carried the total axial load in fact did not. The load in the longerons was also unsymmetric which caused seemingly random deflection patterns as shown in Fig. 4. This was caused by the following factors: 1) bowing of the bottom base plate introduced loads in the diagonals, 2) small off-set c.g. loading of the plate, 3) bending of the truss support beam, and 4) deflections observed between the 1/2-inch aluminum plate and the support beam/plate (A random bolt pattern was used for the attachment of the top plate to the support plate on the beam).

b) Due to the above problems, the stiffness of the longerons were recalculated by determining the load and deflections in each longeron separately. The results are plotted in Fig. 5. Although this technique required additional instrumentation, the findings are conclusive.

For the horizontal test, loads up to 100 pounds were applied in 20- pound increments. The bending of the upper beam support was again a factor and resulted in a 25 percent larger deflection than predicted.

For future testing of truss support structures, having proper boundary conditions and understanding these boundaries is a must. Static tests should always precede dynamics test. It is also recomended that the diagonals and longerons be instrumented with strain gages to better understand the load path.

TABLE 1

20′ SUPER ASTROMAST
DYNAMIC TEST RESULTS VS. ANALYSIS

MODE NO.	TEST FREQUENCY (Hz)	ANALYTICAL FREQUENCY (Hz)	MODE DESCRIPTION
1	3.7	4.2	1ST BENDING
2	3.7	4.2	1ST BENDING
3	12.4	11.5	1ST TORSION
4	25.8	31.6	2ND BENDING
5	25.8	31.6	2ND BENDING
6	38.9	38.3	2ND TORSION
7	37.7*	57.3	1ST AXIAL

*NOTE: FREQUENCY OF PLATE

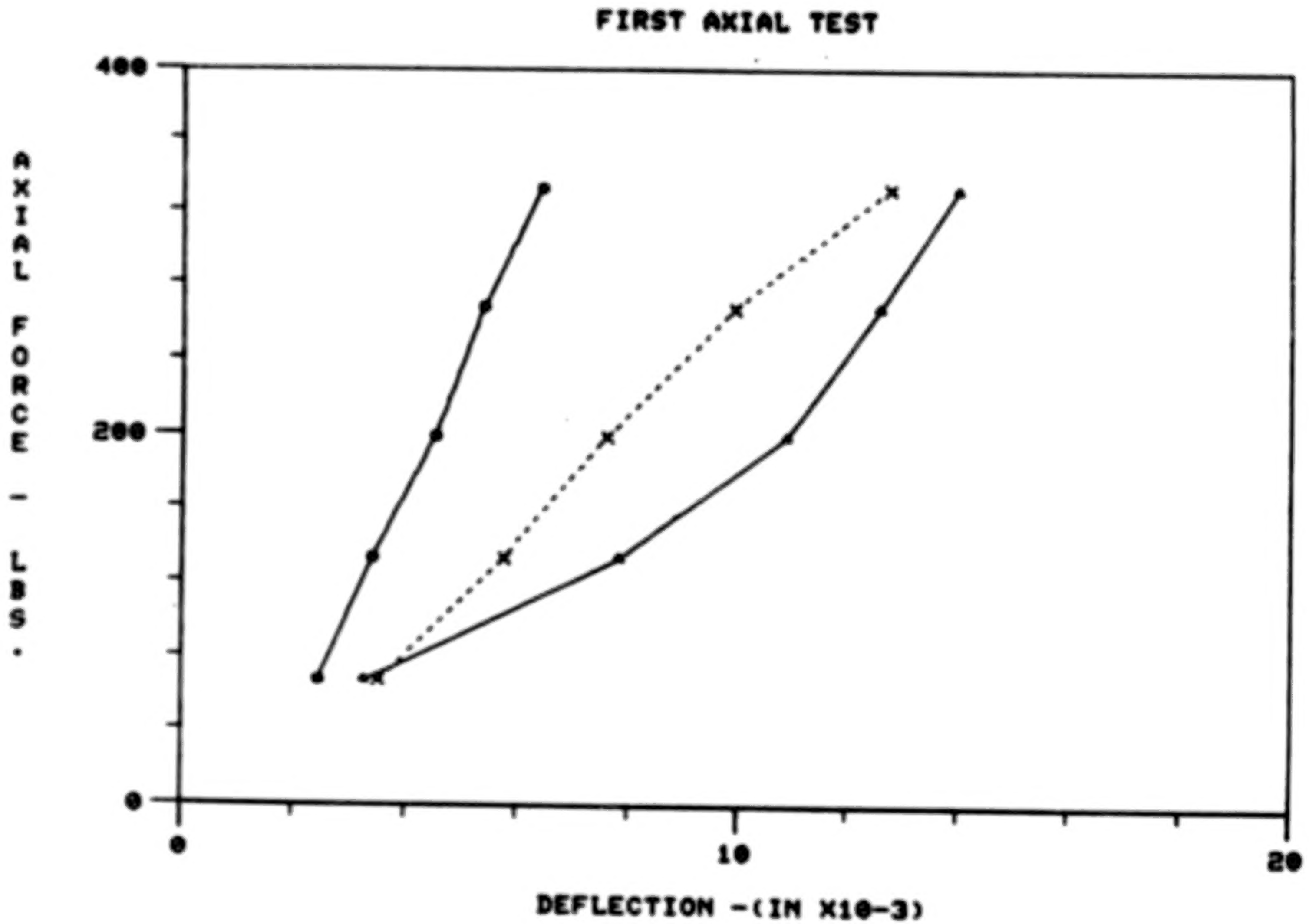

FIG. 4. STATIC FORCE DEFLECTION DATA ASSUMING SYMMETRIC LOADING

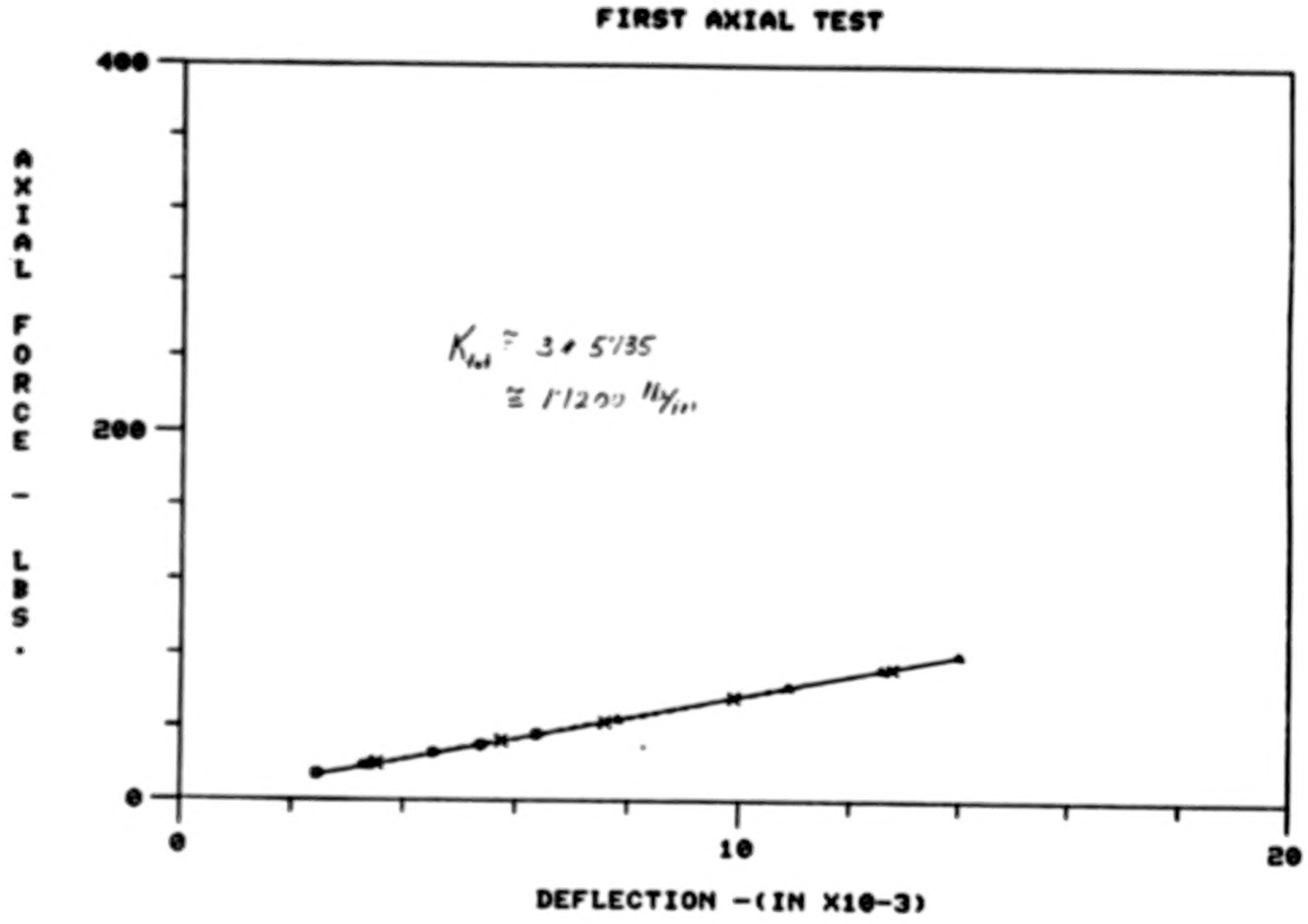

FIG. 5. STATIC FORCE DEFLECTION DATA WITH FORCE CALCULATED FROM STRAIN

PHASE II - TESTING OF SPACE STATION PROTOTYPES

The second phase of the test program will address the structural development and testing of candidate Space Station prototypes and concepts. While Phase I characterized and verified pre-Space Station structures and math modeling techniques, Phase II will characterize specific Space Station structural concepts. For example, the following structural investigation is anticipated.

1) Static and dynamic analysis and testing of Space Station erectable and deployable prototype hardware.

2) Static and dynamic analysis and testing of truss members and joint concepts.

3) Experimental and analytical characterization of the truss member buckling phenomenon.

4) Investigation into the applied usage of composite materials for Space Station joint and truss design.

5) Experimental and analytical simulation of Space Station dynamic events such as construction, payload handling, berthing, docking, etc.

The objectives of the phase two test program are as follows:

1) Continued investigation and characterization of nonlinear phenomena on prototype concepts and hardware. For example, define nonlinear load deflection curves and evaluate the influence of structural preloads on these curves.

2) Characterize the amount and types of damping inherent to these structures and investigate methods of increasing damping.

3) Access the effects of nonlinear stiffness and damping on the systems dynamic response in the zero-g environment.

4) Develop and verify with testing nonlinear dynamic structural math models which are suitable for control system studies and evaluation.

5) Develop and verify isolation systems and mechanisms for the low frequency zero-g environment.

6) Develop and pursue dynamic simulation of construction and other dynamic events, which will be encountered in the Space Station working environment. This ground based analysis and experimental simulation capability will verify procedures and loads and develop potential ground capability for mission support.

7) Develop analysis methods and construction methods for the use of composite materials in truss structure joints and members. (It should be noted that the current state of the art for composite structural analysis is based on the Plane Stress assumption, which is not valid for truss joint design. Also, the nature of truss structures is that they produce large concentrated loads. Current composite material construction methods deal well with distributed loads, but a concentrated loads is at this point in time the Achilles' heel of composites.)

PHASE III - TESTING OF ACTUAL SPACE STATION STRUCTURAL HARDWARE

Hardware verification is Phase III of the Space Station test program. The objective being the characterization of flight hardware, verification of math models, and anomaly identification. Three test classifications are envisioned:

Structural Elements - testing of truss elements, for example, short rods, diagonal rods, and joint clusters.

Truss Subassemblies - testing of one bay of the truss structure, five bays, and power boom/keel intersection.

Large Assemblies - testing of keels/end booms/partial power boom and nested common modules with interface structure.

The verification phase of the test program must proceed in stages, as outlined. Since the truss structure is to be made up of multiple elements of the same design, material stiffness variations are expected. Variations in joint combinations for freeplay will also influence modal stiffness. Detail testing, static and dynamic, of individual structural elements and truss assemblies will provide the database necessary for insuring modal/model predictability of the Space Station configuration.

PHASE IV - ON-ORBIT TESTING OF SPACE STATION CONSTRUCTION

Phase IV of the test program addresses on-orbit verification and control of structural design, space construction, ground based math modeling, growth evolution, and structural damage and deterioation. The Space Station is unique in that it will only be totally assembled on-orbit with no possible ground experimental verification for its zero-g environment.

NASA's experience with on-orbit structural dynamic testing began with SAFE (Solar Array Flight Experiment). This experiment showed a larger than anticipated damping and also demonstrated unexpected thermal effects. NASA's experience with the erection of space structures began with EASE/ACCESS (Experimental Assembly of Structures in Extravehicular Activity/Assembly Concept for Construction of Erectable Space Structures). Although the EASE/ ACCESS mission demonstrated space construction, it did not attempt to do any structural testing. NASA's past experience with on-orbit test and construction points the way for future effort.

The first step in on-orbit testing of Space Station applicable structures is at this time envisioned to be a demonstration of onorbit eractable construction of a 5-meter-square cross section truss beam. The 5-meter construction experiment would be tested on-orbit for its dynamic response in the zero-g environment. This testing would allow determination of the Space Station structural damping and the effects of joints in the zero-g environment.

Successful completion of the large construction and testing experiment would allow the initial construction of the Space Station. On-orbit testing would follow a natural progression at the end of each construction phase of the Space Station. The purpose of these tests will be to verify space structural assembly and assembly techniques, and provied basis for verification and revsion of ground based math models. These verified and revised math models will provide a basis for updated control system software and gains.

An on-orbit structural verification and acceptance test will be performed on the Space Station upon completion of the main structural assembly. This testing will be performed prior to the addition of payloads. Also, as the Space Station grows there will be continued on-orbit structural dynamic testing to verify the system capability and to access structural damage over the life of the station. This continued testing will allow verification and update of ground based math models and revision of control systems.

N87
22752
UNCLAS

N87-22752

1985

NASA/ASEE SUMMER FACULTY RESEARCH FELLOWSHIP PROGRAM

MARSHALL SPACE FLIGHT CENTER

THE UNIVERSITY OF ALABAMA

ANALYTICAL DETERMINATION OF SPACE STATION RESPONSE TO CREW MOTION AND DESIGN OF SUSPENSION SYSTEM FOR MICROGRAVITY EXPERIMENTS

Prepared By:	Frank C. Liu, Ph.D., PE
Academic Rank:	Professor
University and Department:	The University of Alabama in Huntsville Department of Mechanical Engineering
NASA/MSFC	
Division:	Mechanical
Branch:	Mechanical System Development
MSFC Counterpart:	Harold Smyly
Date:	August 1, 1985
Contract No.:	NGT-01-008-021 The University of Alabama in Huntsville

PRECEDING PAGE BLANK NOT FILMED

ANALYTICAL DETERMINATION OF SPACE STATION RESPONSE TO CREW MOTION AND DESIGN OF SUSPENSION SYSTEM FOR MICROGRAVITY EXPERIMENTS

by

Frank C. Liu

Professor of Mechanical Engineering
The University of Alabama in Huntsville
Huntsville, Alabama

ABSTRACT

The objective of this investigation is to make analytical determination of the acceleration produced by crew motion in an orbiting space station and define design parameters for the suspension system of microgravity experiments. A simple structural model for simulation of the IOC space station is proposed. Mathematical formulation of this model provides the engineers a simple and direct tool for designing an effective suspension system.

ACKNOWLEDGMENT

It has been an exciting experience for me to work on this interesting project. I am grateful to Mr. Doug Lamb, Chief of Mechanical Division, Structures and Propulsion Laboratory, and his staff Mr. Charles Cornelius, Mr. Harold Smyly, and Mr. Charles Miller for giving me an enjoyable summer to carry out this investigation. I express appreciation to Mr. Mike Moore, my office mate, for making all the computer graphs. Special thanks are due to Ms. Margarete Landers for typing this report.

1. Introduction

Some microgravity experiments to be performed on the IOC space station require an environment in which the acceleration level must be below 10^{-5} g. Among the various sources of disturbances, crew motion is the severe one which can produce acceleration to a magnitude of 10^{-4} g. The objectives of this investigation are to define design characteristics for the suspension system and to find effective means for isolation of the experiment packages from disturbance. To achieve these goals, the following have been accomplished.

1. Analytical formulation of acceleration response of IOC to crew motion

Assumed modes method and modal transformation are used to obtain mathematical solution for the normal coordinates to an input function due to crew motion. Acceleration response of any point in the space station can be analytically formulated.

2. Structural modeling for IOC space station

The finite element model for IOC space station, shown in Figure 1, used by JFC [1] for vibration analysis generates a wide range and closely spaced spectrum of vibration frequencies (see Table 4.3.3.3-3, reference 1). It makes it extremely difficult for mechanical design engineers to identify a particular mode which has dominant effect on the experiment package. A simple structural model which is made of a rigid main body (extension of keel frame which supports all the massive modules), a cantilever beam (the keel frame), and a transverse cantilever beam (the solar boom) is proposed for simulation of the IOC. A complete analytical formulation for this model is made. This formulation provides the design engineers a simple and direct tool for determination of acceleration and disturbing frequencies acting on the experiment package. Computations can be carried out by using a pocket calculator. This model can be easily improved by increasing the degrees-of-freedom. A simple computer program will do this work.

3. Derivation of design characteristics for suspension system

Consider that a microgravity experiment package is supported by a spring and a mass-spring-damper vibration absorber is attached to it. The acceleration magnification factor and the ratio of acceleration response of package to acceleration input of the support is then derived. The plots of this factor versus frequency ratio (IOC to mass-spring) provide engineers design parameters of the suspension system.

4. Significant findings for effective isolation of disturbance

The microgravity laboratory is 23.3/83.2 feet from the center of mass of IOC with/without the orbiter attached. It is shown by numerical study that the acceleration disturbance is greatly reduced when the orbiter is not present (i.e., microgravity lab is actually 59.9 feet farther away from the C.M. of IOC). This shows that the most favorable location beside the C.M. of IOC is the node of the fundamental elastic vibration mode of the IOC.

2. Analytical Formulation

2.1 Modal analysis of a structure system

A brief presentation of modal analysis of a structure is given here. Let P be the coordinate of a generic mass point P in a structure and u(P,t) be its displacement which is expressed in the form [2]

$$u(P,t) = \sum_{i=1}^{N} \psi_i(P) q_i(t) \tag{2.1}$$

where $\psi_i(P)$ is an admissible function and $q_i(t)$ is the ith generalized coordinate of a set N. The equation of motion of the structure system in matrix form is

$$[m]\ \{\ddot{q}\} + [k]\ \{q\} = \{Q\} \tag{2.2}$$

where [m], [k], and {q} are the generalized mass, stiffness, and force matrices, respectively.

The kinetic and bending strain energies of the system are formulated from the following integrals:

$$T = \tfrac{1}{2}\int_B m_P[\dot{u}(P,t)]^2\ dP = \tfrac{1}{2}\sum\int_B m_P\psi_i{}^2(P)dP\dot{q}_i{}^2 \tag{2.3}$$

$$V = \tfrac{1}{2}\int_B EI[u''(P,t)]^2 dP = \tfrac{1}{2}\sum\int_B m_P[\psi_i''(P)]^2\ dPq_i{}^2 \tag{2.4}$$

where m_P is the mass density at P and EI is the bending stiffness of the structure at P, the prime denotes partial differentiation with respect to spatial coordinates and the symbol B with the integral sign means integration over the entire body B. From the above integrals, the elements of the [m] and [k] matrices are obtained respectively,

$$m_{ij} = \frac{\partial^2 T}{\partial\dot{q}_i\partial\dot{q}_j} = \int_B m_P\psi_i(P)\psi_j(P)dP \tag{2.5}$$

$$k_{ij} = \frac{\partial^2 V}{\partial q_i \partial q_j} = \int_B EI\psi_i''(P)\psi_j''(P)dP \tag{2.6}$$

Denoting the force acting at P in the direction of $u(P,t)$ by $f_P(t)$, then the virtual work is

$$\delta W = \int_B f_P(t)\delta u dP = \sum \int_B f_P \psi_i(P)\delta q_i dP \tag{2.7}$$

It follows that

$$Q_i = \frac{\partial W}{\partial q_i} = \int_B f_P \psi_i(P)dP \tag{2.8}$$

Next, the natural frequencies of the system are determined from the determinant

$$|[k] - \omega^2[m]| = 0 \tag{2.9}$$

and the eigenvectors (or modal columns) $\{\phi_i\}$ are the solution of the matrix equations,

$$([k] - \omega_i^2[m])\ \{\phi_i\} = \{0\} \qquad i = 1,2,\ldots,N \tag{2.10}$$

The normal coordinates $\{\eta\}$ and the generalized coordinates are related by the transformation

$$\{q\} = [\Phi]\ \{\eta\} \tag{2.11}$$

where the modal matrix

$$[\Phi] = [\{\phi_1\},\ \{\phi_2\},\ \ldots,\ \{\phi_N\}]\ .$$

Applying Eq. (2.11) to Eq. (2.2) and making use of the property of generalized orthogonality of the eigenvector with respect to [m] and [k], the equation of motion in normal coordinates is

$$\ddot{\eta}_j + \omega_j^2\ \eta_j = N_j(t)/M_{jj} \qquad j = 1,2,\ldots,N \tag{2.12}$$

where

$$M_{jj} = \{\phi_j\}^T[m]\{\phi_j\} \tag{2.12a}$$

$$\omega_j^2 = \{\phi_j\}^T[k]\{\phi_j\}/M_{jj} \qquad (2.12b)$$

$$N_j(t) = \{\phi_j\}^T\{Q\} \qquad (2.12c)$$

2.2 Structure response to disturbing force

Consider that a disturbing force $f_a(t)$ is applied to the structure at P_a, from Eqs. (2.8) and (2.12c) one obtains

$$N_j(t) = \sum_{k=1} \phi_{kj}\psi_k(P_a)f_a(t) \qquad (2.13)$$

where ϕ_{kj} is the kth element of the jth eigenvector. The response at point P_e in the structure, $u(P_e,t)$, can be obtained by using Eqs. (2.1), (2.11), and (2.13). It results in

$$\begin{aligned} u(P_e,t) &= \sum_i \psi_i(P_e)q_i(t) = \sum_i \sum_j \psi_i(P_e)\phi_{ij}\eta_j(t) \\ &= \sum_j \left[\left(\sum_i \phi_{ij}\psi_i(P_e)\right)\left(\sum_k \phi_{kj}\psi_k(P_a)\right)\right] \bar{\eta}_j(t)/M_{jj} \qquad (2.14) \end{aligned}$$

where $\bar{\eta}_j(t)$ denotes the solution of the differential equation,

$$\ddot{\eta}_j + \omega_j^2\eta_j = f_a(t) \qquad \text{with} \qquad \eta_j(0) = \dot{\eta}_j(0) = 0 \quad . \qquad (2.15)$$

2.3 Model of crew motion and response function

The motion of an astronaut inside a space module is started by pushing one wall and motion is stopped by pushing the opposite wall. A simple mathematical model is suggested [1] as shown in Figure 2.

$$f_a(t) = \begin{cases} (f_o/t_1)t & 0 < t \le t_1 \\ 0 & t_1 < t \le t_{13} \\ (f_o/t_1)(t - t_{14}) & t_{13} < t \le t_{14} \\ 0 & t_{14} < t \end{cases} \tag{2.16}$$

The magnitude of f_o is 25 lbs and t_1, t_{13}, and t_{14} are 1, 13, and 14 seconds, respectively. These notations for time will be kept through the formulation for the sake that one may wish to change their magnitudes and secondly, that the equation involved will have appropriate units (use $\sin\omega t_{13}$ rather than $\sin 13\omega$ where ω is in rad/s). The solution of equation (2.15) is readily obtained. Denoting that

$$\eta(t) = (f_o/\omega^3 t_1)U(t) \tag{2.17}$$

the dimensionless displacement function U(t) is given by

$$0 < t \le t_1 \qquad U(t) = \omega t - \sin\omega t \tag{2.17a}$$

$$t_1 < t \le t_{13} \qquad U(t) = -\sin\omega t + \sin\omega(t - t_1) + \omega t_1 \cos\omega(t - t_1) \tag{2.17b}$$

$$\begin{aligned} t_{13} < t \le t_{14} \qquad U(t) = {} & \omega(t - t_{14}) - \sin\omega t + \sin\omega(t - t_1) \\ & - \sin\omega(t - t_{13}) + \omega t_1[\cos\omega(t - t_1) \\ & + \cos\omega(t - t_{13})] \end{aligned} \tag{2.17c}$$

$$\begin{aligned} t_{14} < t \qquad U(t) = {} & -\sin\omega t + \sin\omega(t - t_1) - \sin\omega(t - t_{13}) \\ & + \sin\omega(t - t_{14}) + \omega t_1[\cos\omega(t - t_1) \\ & + \cos\omega(t - t_{13})] \end{aligned} \tag{2.17d}$$

The function U(t) is continuous and has continuous first derivative (velocity); its second derivative is only piecewise continuous. Denoting

$$\ddot{\eta}(t) = (f_o/\omega t_1)A(t) \tag{2.18}$$

and differentiating Eq. (2.17) twice, one obtains the dimensionless acceleration A(t),

$$0 < t \leq t_1 \qquad A(t) = \sin\omega t \tag{2.19a}$$

$$t_1 < t \leq t_{13} \qquad A(t) = \sin\omega t - \sin\omega(t - t_1) - \omega t_1 \cos\omega(t - t_1) \tag{2.19b}$$

$$\begin{aligned} t_{13} < t \leq t_{14} \qquad A(t) = {} & \sin\omega t - \sin\omega(t - t_1) + \sin\omega(t - t_{13}) \\ & - \omega t_1 \, [\cos\omega(t - t_1) + \cos\omega(t - t_{13})] \end{aligned} \tag{2.19c}$$

$$\begin{aligned} t_{14} < t \qquad A(t) = {} & \sin\omega t - \sin\omega(t - t_1) + \sin\omega(t - t_{13}) \\ & - \sin\omega(t - t_{14}) - \omega t_1 \, [\cos\omega(t - t_1) \\ & + \cos\omega(t - t_{13})] \end{aligned} \tag{2.19d}$$

The functions of U(t) and A(t) are plotted versus time for frequencies ranging from 0.1 to 0.4 as shown in Figures 3 and 4 respectively. Now, the displacement and acceleration response of point P_e in the space station can be expressed in the form

$$u(P_e,t) = \sum_j \left(\sum_i \phi_{ij}\psi_i(P_e) \right) \left(\sum_k \phi_{kj}\psi_k(P_a) \right) U_j(t)(f_o/\omega_j{}^3 t_1 M_{jj}) \tag{2.20a}$$

$$a(P_e,t) = \sum_j \left(\sum_i \phi_{ij}\psi_i(P_e) \right) \left(\sum_k \phi_{kj}\psi_k(P_a) \right) A_j(t)(f_o/\omega_j t_1 M_{jj}) \tag{2.20b}$$

The subscript "j" with U and A denotes that these functions are corresponding to $\omega = \omega_j$.

2.4 Modeling of IOC space station

The structure of the IOC space station may be treated as a structural system having three elements. The main body is a frame structure which supports all the massive members, the vertical and horizontal HAB modules, the vertical and horizontal LAB modules, logistic and common modules, and above all, the orbiter. Attached to the main body is a keel frame structure 296 feet in length which supports an antenna system at its other end and a transverse boom at a distance 165.5 feet from the main body. The third member of the system is a transverse boom which is a frame structure 264 feet long. Its main purpose is to carry eight solar arrays and power system radiators.

A simple structural model for the IOC proposed consists of a rigid main body which supports a cantilever beam (keel frame) and a transverse cantilever beam (solar boom) mounted on the keel. As shown in Table 1 in Appendix A, the modules, equipment, solar arrays, fuel tanks, orbiter, etc., are treated as concentrated masses. However, the rotational moments of inertia of the orbiter and solar arrays must be included in forming the mass matrix.

Motions of the IOC in X-Z and Y-Z planes will be treated separately. In each plane the proposed IOC has four degrees-of-freedom, namely, rigid-body translation, rigid-body rotation, and one bending mode for each cantilever beam. Thus, the corresponding admissible functions are

$$\psi_1(P) = 1 \tag{2.21a}$$

$$\psi_2(P) = \bar{z} \tag{2.21b}$$

$$\psi_3(P) = \bar{z}^2 - \bar{z}^3/3 \tag{2.21c}$$

$$\psi_4(P) = \bar{y}^2 - \bar{y}^3/3 \tag{2.21d}$$

where $\bar{z} = z/\ell_k$ and $\bar{y} = y/\ell_s$ in which ℓ_k and ℓ_s are the length of the keel (296 ft) and solar boom (132 ft), respectively.

2.5 Modal analysis of IOC model

Based on Eq. (2.21) the mass and stiffness matrices for the model are formulated in Appendices A and B. The matrix equation of free motion of the IOC is

$$\begin{bmatrix} m_{11} & m_{12} & m_{13} & m_{14} \\ m_{21} & m_{22} & m_{23} & m_{24} \\ m_{31} & m_{32} & m_{33} & m_{34} \\ m_{41} & m_{42} & m_{43} & m_{44} \end{bmatrix} \begin{bmatrix} \ddot{q}_1 \\ \ddot{q}_2 \\ \ddot{q}_3 \\ \ddot{q}_4 \end{bmatrix} + \begin{bmatrix} 0 & 0 & 0 & 0 \\ 0 & k_{22} & 0 & 0 \\ 0 & 0 & k_{33} & 0 \\ 0 & 0 & 0 & k_{44} \end{bmatrix} \begin{bmatrix} q_1 \\ q_2 \\ q_3 \\ q_4 \end{bmatrix} = \begin{bmatrix} 0 \\ 0 \\ 0 \\ 0 \end{bmatrix} \tag{2.22}$$

One may eliminate the rigid-body translation q_1 from the system by solving q_1 in terms of the rest of q's from the first equation of Eq. (2.22) and substituting it into the remaining equations. A further simplification can be made by disregarding the small coupling effect of the rigid-body rotation q_2 and the elastic modes q_3 and q_4 due to gravity gradient torque. Thus, one may eliminate both q_1 and q_2 from the system and obtain the following:

$$\begin{bmatrix} q_1 \\ q_2 \end{bmatrix} = [T] \begin{bmatrix} q_3 \\ q_4 \end{bmatrix} \tag{2.23}$$

$$\begin{bmatrix} m_{33} & m_{34} \\ m_{43} & m_{44} \end{bmatrix} \begin{bmatrix} \ddot{q}_3 \\ \ddot{q}_4 \end{bmatrix} + \begin{bmatrix} k_{33} & 0 \\ 0 & k_{44} \end{bmatrix} \begin{bmatrix} q_3 \\ q_4 \end{bmatrix} = \begin{bmatrix} 0 \\ 0 \end{bmatrix} \tag{2.24}$$

where

$$[T] = - \begin{bmatrix} m_{11} & m_{12} \\ m_{21} & m_{22} \end{bmatrix}^{-1} \begin{bmatrix} m_{13} & m_{14} \\ m_{23} & m_{24} \end{bmatrix}$$

$$\begin{bmatrix} \overline{m}_{33} & \overline{m}_{34} \\ \overline{m}_{43} & \overline{m}_{44} \end{bmatrix} = \begin{bmatrix} m_{33} & m_{34} \\ m_{43} & m_{44} \end{bmatrix} + \begin{bmatrix} m_{31} & m_{32} \\ m_{41} & m_{42} \end{bmatrix} [T]$$

The two elastic frequencies of the IOC can be written out directly in the form

$$\omega_{1,2}^2 = \frac{\overline{m}_{33}\, k_{44} + \overline{m}_{44}\, k_{33} \mp \sqrt{(\overline{m}_{33}\, k_{44} - \overline{m}_{44}\, k_{33})^2 + 4\overline{m}_{34}\, \overline{m}_{43}\, k_{33}\, k_{44}}}{2(\overline{m}_{33}\, \overline{m}_{44} - \overline{m}_{34}\, \overline{m}_{43})} \tag{2.25}$$

and the eigenvector is

$$\{\phi_i\} = \begin{bmatrix} T_{11}(\overline{m}_{34}\, \omega_i^{\,2}) + T_{12}(k_{33} - \overline{m}_{33}\, \omega_i^{\,2}) \\ T_{21}(\overline{m}_{34}\, \omega_i^{\,2}) + T_{22}(k_{33} - \overline{m}_{33}\, \omega_i^{\,2}) \\ \overline{m}_{33}\, \omega_i^{\,2} \\ k_{33} - \overline{m}_{33}\, \omega_i^{\,2} \end{bmatrix} \quad i = 1,2 \tag{2.26}$$

2.6 Rigid-body librational motion of IOC

The equations of librational motion of an orbiting body which has its principal axes parallel to the orbital axes subjected to disturbing torque M can be written directly in the form [3]

$$I_x\ddot{\theta}_x + 3\,\omega_o^2(I_y - I_z)\theta_x = M_x \tag{2.27}$$

$$I_y\ddot{\theta}_y + 3\,\omega_o^2(I_x - I_z)\theta_y = M_y \tag{2.28}$$

where the I's are the moments of inertia about their respective principal axes through the center of mass. The orbital frequency of a circular orbit is

$$\omega_o = \sqrt{\mu/R^3}\ \text{rad./s} \tag{2.29}$$

where R is the orbital radius and the gravitational constant

$$\mu = 1.407 \times 10^{16}\ \text{ft}^3/\text{s}^2$$

$$= 3.986 \times 10^{14}\ \text{m}^3/\text{s}^2$$

Thus, Eqs. (2.27) and (2.28) yield the librational frequencies

$$\omega_x = \omega_o\sqrt{3(I_y - I_z)/I_x} \tag{2.30a}$$

$$\omega_y = \omega_o\sqrt{3(I_x - I_z)/I_y} \tag{2.30b}$$

2.7 Response of IOC to crew motion due to rigid-body modes

As shown in Figure 6, due to the arrangement of the modules, crew motion will create a disturbing force either in x-direction (motion in horizontal modules) or z-direction (motion in vertical modules). Hence, the torque M_x is negligible in comparison with M_y which has the magnitudes,

$$M_y = \begin{cases} f_x Z_a & \text{(motion in horizontal modules)} \\ f_z X_a & \text{(motion in vertical modules)} \end{cases} \tag{2.31}$$

As indicated by Eq. (2.30), the librational frequency is approximately equal to $\sqrt{3}$ times the orbital frequency ($I_x \approx I_y$, $I_z << I_x$, see Table 1). The crew kicking motion is completed in a time interval of 1 second which is very short in comparison with the period of librational motion of 3,300 second. This means that the torque can be treated as an impulse torque. The action of an impulse torque is equivalent to give the space station an initial angular velocity, i.e.,

$$\hat{M}_y = \int_0^t M_y(t)dt = \dot{\theta}_y(0)\ I_y \tag{2.32}$$

The solution of Eq. (2.28b) is simply

$$\theta_y = (\hat{M}_y/\omega_y)\sin\omega_y t \tag{2.33}$$

Using the mathematical model for crew motion given by Eq. (2.16), one obtains the response at P_e

$$u(P_e,t) = Z_e\theta_y$$

$$= \begin{cases} \frac{1}{2}\ Z_e Z_a f_o t_1/\omega_y I_y)\sin\omega_y t & \text{(motion in horizontal module)} \\ \frac{1}{2}\ Z_e X_a f_o t_1/\omega_y I_y)\sin\omega_y t & \text{(motion in vertical module)} \end{cases} \tag{2.34}$$

The magnitude of acceleration produced by crew motion at P_e is

$$a(P_e) = \begin{cases} Z_e Z_a f_o \omega_y t_1/2I_y & \text{(motion in horizontal module)} \\ Z_e X_a f_o \omega_y t_1/2I_y & \text{(motion in vertical module)} \end{cases} \tag{2.35}$$

3. Numerical Results of Acceleration Due to Crew Motion

Using data given in Table 4.3.3.4-2 to 4.3.3.4-4 of Reference 1, Table 3 is formed for the formulation of the mass matrix for IOC space station. Note that the total weight given by Tables 4.3.3.4-2 and 4.3.3.4-4 [1] is 77,600 lbs heavier than that given by Table 2. In an effort to match the total weight given in Table 2, some of the weights are not included. There is a significant difference on the location of the center of mass between the present model to that given in Table 2, as shown in the following:

	Table 2	Present Model	Difference
With Orbiter	68.3 ft	113.8 ft	14.4 ft
Without Orbiter	128.2	59.5	8.8

Consider that the distance from the reference point to the microgravity experiment is equal that of the location of crew motion, i.e., $z_e = z_c = -55$ ft. The magnitude of acceleration on the microgravity experiment due to crew motion as given by Eq. (2.20b) is

$$a_e = [\phi_{1j} + \phi_{2j}(z_e/\ell_k)]^2 (f_o/M_{jj}\omega_j t_1) [A_j(t)]_{max} \qquad j = 1,2 \qquad (3.1)$$

The value of $[A_j(t)]_{max}$ can be estimated from curves given in Figure 4 for a given value of ω. The summation is omitted so that a_e is calculated for each mode. Based on the librational motion approach, one has from Eq. (2.35)

$$a_e = Z_e^2 f_o \omega_y t_1/2I_y \qquad (3.2)$$

The numerical resulted obtained are summarized in Table 4.

It is important to note the following:

(1) No direct comparison can be made on the frequencies obtained to that given in Table 4.3.3.3-3 [1] due to the difference of inertia properties of the models, and furthermore, the JSC model has no distinct fundamental mode that can be singled out.

(2) The acceleration level obtained here is about one order smaller than that given by Table 4.3.3.5-15 [1]. This is due to the fact that the inertia data given by Table 4.3.3.5-6 [1] is about 1/3 of that given by Table 4.3.3.5-6 [1] (without orbiter). In addition, the disturbance torque given by Table 4.3.3.5-7 [1] is more than 2 times the value used here. Thus, the magnitude of accelerations presented in Table 5 are reasonable.

(3) Motion of the space station in Y-Z plane will occur if the disturbing force is in the direction parallel to the solar boom.

(4) The acceleration given by the librational motion is 10^{-3} of that given by elastic motion. This, due to the frequency of librational motion, is only 10^{-3} of the frequency of elastic motion.

4. Design Characteristics of Suspension System

4.1 Acceleration response of a vibration absorber system

Consider that a microgravity experiment package is mounted on the laboratory module structure which has motion $u_o(t)$ as a result of crew motion or other disturbance. As shown in Figure 3, $u_o(t)$ is approximately a harmonic. It is required to design a suspension system which can effectively reduce this disturbance over some frequency range. Vibration can be effectively reduced by using a vibration absorber [4] which is a mass-spring-damper system attached to the main mass-spring system as shown in Figure 7.

Denoting u_o, u_1, u_2, the absolute displacement of the structure, main mass, and absorber mass, respectively, the equations of motion of the system are

$$m_1\ddot{u}_1 + c\dot{u}_1 + (k_1 + k_2)u_1 - c\dot{u}_2 - k_2u_2 = k_1u_o(t) \tag{4.1a}$$

$$m_2\ddot{u}_2 + c\dot{u}_2 + k_2u_2 - c\dot{u}_1 - k_2u_1 = 0 \tag{4.1b}$$

Letting the input $u_o(t)$ be a harmonic disturbance, one may put

$$u_o(t) = U_oe^{i\omega t} \quad , \quad u_1 = U_1e^{i\omega t} \quad , \quad \text{and} \quad u_2 = U_2e^{i\omega t} \quad i = \sqrt{-1} \tag{4.2}$$

where U_1 and U_2 are complex quantities that can be determined from the matric equation

$$\begin{bmatrix} (k_1 + k_2 - m_1\omega^2 + ic\omega) & -(k_2 + ic\omega) \\ -(k_2 + ic\omega) & (k_2 - m_2\omega^2 + ic\omega) \end{bmatrix} \begin{bmatrix} U_1 \\ U_2 \end{bmatrix} = \begin{bmatrix} k_1U_o \\ 0 \end{bmatrix} \tag{4.3}$$

If one wishes to determine acceleration response rather than displacement, set

$$\ddot{u}_1 = A_1e^{i\omega t} \quad \text{with} \quad A_1 = -\omega^2B_1 \tag{4.4}$$

Now, let M_a denote the magnification factor of acceleration, the ratio of A_1 to input acceleration,

$$M_a = |A_1|/U_o\omega^2 \tag{4.5}$$

First, introduce the following dimensionless parameters:

$$k = k_1/k_2 \quad \mu = m_2/m_1 \quad \zeta = c/2\sqrt{m_2k_2} \quad r = \omega/\omega_n \tag{4.6}$$

It can be shown that

$$M_a = \left\{[(1 - \mu kr^2)^2 + 4\mu k\zeta^2r^2]/D\right\}^{1/2} \tag{4.7}$$

where

$$D = \left\{1 - [1 + (1+k)\mu]r^2 + \mu kr^2\right\}^2 + 4\mu k\zeta^2r^2\,[1 + (1+\mu)r^2]^2$$

4.2 Design considerations

The magnitude of the magnification factor of acceleration depends on four parameters:

k, the spring ratio (main spring/absorber spring),

μ, the mass ratio (absorber mass/main mass),

ζ, damping factor (damping coefficient/critical damping),

r, frequency ratio (space station frequency/natural frequency of main mass-spring system).

To plot M_a versus frequency ratio squared as shown in Figure 8, six sets of curves are illustrated for $\zeta = 0.2$. The first three sets are for fixed values of $\mu = 0.01$, 0.025, and 0.05, respectively, with various values of k. The next three sets are for fixed values of $k = 10$, 15, and 20, respectively, with various values of μ. All these curves have one common characteristic, M_a which can be effectively reduced for $r^2 > 2$. Since the frequency of the IOC space station in elastic vibration is about 1 rad/s, it requires that $k_1 > 2W_1/g$. For a microgravity experiment package of 1,000 lbs, the spring constant of the suspension must be less than 5 lb/in. For the frequency range $0.5 < r^2 < 2$, M_a can be made less than 0.5 by a proper combination of μ and k.

5. Conclusions

A simple structural model for simulation of IOC space station has been presented and formulation of this simple model provides engineers a simple and direct method for computing the fundamental frequencies of the space station and determining the magnitude of acceleration at any point produced by crew motion. Acceleration response of a mass-spring-absorber system to a moving support is also formulated. Design engineers can use plots of acceleration magnification factor versus frequency ratio squared to determine design parameters for the suspension system of the microgravity experiment package.

The following are some significant findings:

(1) The acceleration due to librational rigid-body motion is 3 orders smaller than that due to elastic bending motion.

(2) The frequency of librational motion is 1.8×10^{-3} rad/s, which is approximately $\sqrt{3}$ times the orbital frequency.

(3) The frequencies of elastic motion of the simple model are in the range 0.6 to 1.5 rad/s.

(4) Only the fundamental bending mode has dominant contribution to the acceleration, therefore, a simple model is adequate.

(5) An effective suspension system can reduce the acceleration to 1/4 of its magnitude, at most.

(6) The ideal location of the microgravity lab does not have to be near the center of mass of the space station.

(7) The most effective means to eliminate acceleration is to have the experiment module near the nodal point of the fundamental bending mode, as illustrated in Figure 9. This means that the factor $(\phi_{11} + \phi_{21}\, z_e/\ell_k)$ in Eq. (4.1) becomes very small. Example: The IOC without orbiter has moved the lab module 59.9 ft further away from the center of mass, but the acceleration is reduced 3 orders smaller than the IOC with orbiter.

(8) It is favorable to perform the microgravity experiments when the orbiter is not present.

(9) It is possible that by rearranging some massive elements, a minimum value of $(\phi_{11} + \phi_{21}\, z_e/\ell_k)/M_{11}$ can be reached. However, this has to be done by trial and error method.

Appendix A. Formulation of Mass Matrix

Notations:

I_{ox}, I_{oy}	moment of inertia of orbiter about x- and y-axis through C.M. of orbiter, respectively
I_{sx}, I_{sy}	moment of inertia of solar arrays about x- and y-axis through solar boom at the attachment, respectively
I_{UB}	moment of inertia of upper boom about x-axis through end of keel
I_{LB}	moment of inertia of lower boom about x-axis through attachment
ℓ_k	length of keel frame
ℓ_s	length of solar boom
M_k	mass of keel frame alone
m_k	kth concentrated mass attached to keel at distance z_k
M_s	mass of solar boom frame alone
m_s	sth concentrated mass attached to solar boom at y_s
m_r	rth concentrated mass attached to rigid main body at z_r
m_o	mass of orbiter
u_x, u_y	displacement in x and y direction respectively
$\overline{y}_s$	$= y_s/\ell_s$, coordinate of concentrated mass attached to solar boom
$\overline{z}_k$	$= z_k/\ell_k$, coordinate of concentrated mass attached to keel
z_o	coordinate of orbiter
subscripts & summation index	k(keel), r(rigid main body), s(solar boom)

A-1. Motion of IOC in X-Z Plane

The kinetic energy of rigid main body is

$$T_R = 1/2 \sum_r m_r \dot{u}_x^{\,2}(z_r)$$

$$= 1/2 \sum_r m_r[\psi_1(z_r)\dot{q}_1 + \psi_2(z_r)\dot{q}_2]^2 + 1/2\ I_{oy}[\psi_2'(z_o)\ \dot{q}_2]^2 \qquad \text{(A-1)}$$

The kinetic energy of keel structure is

$$T_K = 1/2 \sum_k m_k[\psi_1(z_k)\dot{q}_1 + \psi_2(z_k)\dot{q}_2 + \psi_3(z_k)\dot{q}_3]^2$$

$$+ 1/2\ M_k \int [\psi_1\dot{q}_1 + \psi_2(z)\dot{q}_2 + \psi_3(z)\dot{q}_3]^2\ dz/\ell_k$$

$$+ 1/2 \sum_s I_{sy}[\psi_2(z_s)\dot{q}_2 + \psi_3'(z_s)\dot{q}_3]^2 \qquad \text{(A-2)}$$

The kinetic energy of solar boom is

$$T_S = 1/2\ M_s \int [\psi_1(z_s)\dot{q}_1 + \psi_2(z_s)\dot{q}_2 + \psi_4(y_s)\dot{q}_4]^2 dy_s/\ell_s$$

$$+ 1/2 \sum_s m_s[\psi_1(z_s)\dot{q}_1 + \psi_2(z_s)\dot{q}_2 + \psi_4(y_s)\dot{q}_4]^2$$

$$+ 1/2 \sum_s I_{sx}[\psi_4'(y_s)\dot{q}_4]^2 \qquad \text{(A-3)}$$

By using Eq. (2.5) the elements of the mass matrix are obtained as follows:

$$m_{11} = M_{total} = M_r + M_k + \sum_k m_k + M_s + \sum_s m_s$$

$$m_{12} = \sum_r m_r\bar{z}_r + 1/2\ M_k + \sum_k m_k\bar{z}_k + (M_s + \sum_s m_s)\bar{z}_s$$

$$m_{13} = 1/4\ M_k + \sum_k m_k(\bar{z}_k^{\,2} - 1/3\ \bar{z}_k^{\,3}) + (M_s + \sum_s m_s)(\bar{z}_s^{\,2} - 1/3\ \bar{z}_s^{\,3})$$

$$m_{14} = 1/4\ M_s + \sum_s m_s(y_s^{\ 2} - 1/3\ y_s^{\ 3})$$

$$m_{22} = \sum_r m_r\bar{z}_r^{\ 2} + 1/3\ M_k + \sum_k m_k\bar{z}_k^{\ 2} + (M_s + \sum_s m_s)\bar{z}_s^{\ 2} + \sum_s I_{sy}/\ell_k^{\ 2} + I_{oy}(\psi_2')^2$$

$$m_{23} = \frac{11}{60} M_k + \sum_k m_k\bar{z}_k^{\ 3}(1 - 1/3\ \bar{z}_k) + (M_s + \sum_s m_s)(1 - 1/3\ \bar{z}_s)\ \bar{z}_s^{\ 3}$$

$$+ (\sum_s I_{sy})\ \bar{z}_s(2 - \bar{z}_s)/\ell_k^{\ 2}$$

$$m_{24} = \bar{z}_s m_{14}$$

$$m_{34} = (\bar{z}_s^{\ 2} - 1/3\ \bar{z}_s^{\ 3})\ m_{14}$$

$$m_{33} = (11/105)M_k + \sum_k m_k(\bar{z}_k^{\ 2} - 1/3\ \bar{z}_k^{\ 3})^2 + (M_s + \sum_s m_s)(\bar{z}_s^{\ 2} - 1/3\ \bar{z}_s^{\ 3})^2$$

$$+ (\sum_s I_{sy})\ (2\bar{z}_s - \bar{z}_s^{\ 2})^2/\ell_k^{\ 2}$$

$$m_{44} = (11/105)M_s + \sum_s m_s(\bar{y}_s^{\ 2} - 1/3\ \bar{y}_s^{\ 3})^2 + 4I_{sx}\{[\bar{y}_{s1}(2 - y_{s1})^2$$

$$+ [\bar{y}_{s2}(2 - y_{s2})^2\}/\ell_s^{\ 2}$$

A-2. Motion in Y-Z Plane

The kinetic energy of rigid main body is

$$T_R = 1/2 \sum_r m_r[\psi_1(z_r)\dot{q}_1 + \psi_2(z_r)\dot{q}_2]^2 + 1/2\ I_{ox}[\psi_2'(z_o)\dot{q}_2]^2$$

$$+ 1/2\ I_{UB}[\psi_2'(z_{UB})\dot{q}_2]^2 \qquad \text{(A-4)}$$

The kinetic energy of the keel structure is

$$T_K = 1/2 \sum_k m_k[\psi_1\dot{q}_1 + \psi_2(z_k)\dot{q}_2 + \psi_3(z_k)\dot{q}_3]^2$$

$$+ 1/2\ M_k \int_k [\psi_1\dot{q}_1 + \psi_2(z_k)\dot{q}_2 + \psi_3(z_k)\dot{q}_3]^2 dz_k/\ell_k$$

$$+ 1/2\ I_{UB}[\psi_2'(z_s)\dot{q}_2 + \psi_3'(z_s)\dot{q}_2]^2 \qquad \text{(A-5)}$$

The kinetic energy of the solar boom structure is

$$T_S = 1/2\ M_s \int_s [\psi_1\dot{q}_1 + \psi_2(z_s)\dot{q}_2 + \psi_3(z_s)\dot{q}_3]^2 dy_s/\ell_s$$

$$+ 1/2\ M_s \int_s \{[\psi_2'\dot{q}_2 + \psi_3'(z_s)\dot{q}_3]y_s - \psi_4(y_s)\dot{q}_4\}^2 dy_s/\ell_s$$

$$+ 1/2 \sum_s \{m_s[\psi_1\dot{q}_1 + \psi_2(z_s)\dot{q}_2 + \psi_3(z_s)\dot{q}_3]^2$$

$$+ [\psi_2'\dot{q}_2 + \psi_3'(z_s)\dot{q}_3]y_s - \psi_4(y_s)\dot{q}_4]^2\}$$

$$+ 1/2 \sum_s I_{sx}[\psi_2'\dot{q}_2 + \psi_3'(z_s)\dot{q}_3 - \psi_4'(y_s)\dot{q}_4]^2 \qquad \text{(A-6)}$$

Applying Eq. (2.5) results in the mass matrix for motion in Y-Z plane:

$$m_{11} = M_T = (m_{11})_{xz}$$

$$m_{12} = (m_{12})_{xz}$$

$$m_{13} = (m_{13})_{xz}$$

$$m_{14} = 0$$

$$m_{22} = (m_{22})_{xz} + (\psi_2')^2 \, [\sum_s (I_{sx} - I_{sy}) + 1/3 \, M_s \ell_s^{\,2} + \sum_s m_s y_s^{\,2}$$

$$+ I_{ox} - I_{oy} + I_{UB} + I_{LB}]$$

$$m_{23} = (m_{23})_{xz} + \psi_2' \psi_3'(z_s) [\sum_s ({}_{sx} - I_{sy}) + \sum_s m_s y_s^{\,2} + 1/3 \, M_s \ell_s^{\,2}]$$

$$+ I_{UB} \psi_2' \psi_3'(\ell_k)$$

$$m_{24} = -\left[\frac{13}{30} M_s \ell_s + \sum_s m_s y_s \psi_4(y_s) + \sum_s I_{sx} \psi_4'(y_s)\right] \psi_2'$$

$$m_{33} = (m_{33})_{xz} + \left[\sum_s m_s y_s^{\,2} + \sum_s (I_{sx} - I_{sy})\right] [\psi_3'(z_s)]^2 + I_{UB} [\psi_3'(\ell_k)]^2$$

$$m_{34} = -\left[\frac{13}{30} M_s \ell_s + \sum_s m_s \psi_4(y_s) y_s + \sum_s I_{sx} \psi_4'(y_s)\right] \psi_3'(z_s)$$

$$m_{44} = (m_{44})xz$$

The subscript "xz" denotes element of mass matrix of motion in X-Z plane.

A-3. Mass and inertia properties for IOC model

Table 3 is formed based on data given by Table 4.3.3.4-2 to 4.3.3.4-4 [1] for the purpose of formulation of the mass matrix.

Appendix B. Determination of Stiffness Matrix

B-1. Bending strain energy

The bending strain energy of keel and solar boom structure is given by

$$V = 1/2 \int_{0}^{\ell_k} (EI)_k[\psi_3'' q_3]^2 dz_k + 1/2 \int_{0}^{\ell_s} (EI)_s[\psi_4''(y_s) q_4]^2 dy_s$$

Applying Eq. (2.6), one obtains the following non-zero elements of the stiffness matrix

$$k_{33} = 4(EI)_k/3\ell_k^3 \qquad k_{44} = 4(EI)_s/3\ell_s^3$$

B-2. Moment due to gravity gradient

Using the formula given by Reference 3, the following are obtained:

Motion in X-Z Plane

$$M_y = -3(\mu/R^3)(I_x - I_z)q_2 \quad , \qquad k_{22} = 3(\mu/R^3)(I_x - I_z)$$

Motion in Y-Z Plane

$$M_x = -3(\mu/R^3)(I_y - I_z)q_2 \quad , \qquad k_{22} = 3(\mu/R^3)(I_y - I_z)$$

where the moments of inertia are about the axes through the c.m. of the IOC space station.

Appendix C. Numerical Results

C-1. Motion in X-Z plane (IOC with orbiter attached)

$$[m] = \begin{bmatrix} 18900 & -2758 & 1096 & 171.6 \\ -2758 & 3168 & 831.9 & 96.0 \\ 1096 & 831.9 & 483.7 & 43.7 \\ 171.6 & 96.0 & 43.7 & 122.9 \end{bmatrix} \qquad \omega_1^2 = 1.0431 \qquad \omega_2^2 = 6.64$$

$$\{\phi_1\} = \begin{bmatrix} 1.1135 \\ .9546 \\ -10.118 \\ .1639 \end{bmatrix} \qquad \{\phi_2\} = \begin{bmatrix} .2770 \\ .1165 \\ -6.49 \\ -411.87 \end{bmatrix} \qquad M_{11} = 29157 \qquad M_{22} = 1488$$

C-2. Motion in X-Z plane (IOC without orbiter attached)

$$[m] = \begin{bmatrix} 11590 & 376.2 & 1096 & 171.6 \\ 376.2 & 1829.6 & 831.9 & 96.0 \\ 1096 & 831.9 & 483.7 & 43.7 \\ 171.6 & 96.0 & 43.7 & 115.2 \end{bmatrix} \qquad \omega_1^2 = 2.0243 \qquad \omega_2^2 = 7.436$$

$$\{\phi_1\} = \begin{bmatrix} .1936 \\ 1.054 \\ -2.429 \\ .1095 \end{bmatrix} \qquad \{\phi_2\} = \begin{bmatrix} .9485 \\ 4.769 \\ -8.923 \\ -17.603 \end{bmatrix} \qquad M_{11} = 191.5 \qquad M_{22} = 32169$$

C-3. Motion in Y-Z plane (IOC with orbiter attached)

$$[m] = \begin{bmatrix} 18900 & -2758 & 1096 & 0 \\ -2758 & 3298 & 872.3 & -92.5 \\ 1096 & 872.3 & 513.5 & -74.5 \\ 0 & -92.5 & -74.5 & 122.9 \end{bmatrix} \qquad \omega_1^2 = .8022 \qquad \omega_2^2 = 7.881$$

$$\{\phi_1\} = \begin{bmatrix} .3673 \\ 1.\text{[illegible]}94 \\ -2.\text{[illegible]}32 \\ .1674 \end{bmatrix} \qquad \{\phi_2\} = \begin{bmatrix} .3332 \\ .9829 \\ -3.274 \\ -5.779 \end{bmatrix} \qquad M_{11} = 959.8 \qquad M_{22} = 3312$$

C-4. Motion in Y-Z plane (IOC without orbiter attached)

$$[m] = \begin{bmatrix} 11590 & 369.8 & 1096 & 0 \\ 369.8 & 3298 & 872.3 & -92.5 \\ 1096 & 872.3 & 513.5 & -74.5 \\ 0 & -92.5 & -74.5 & 11 \end{bmatrix} \qquad \omega_1^2 = .4301 \qquad \omega_2^2 = 7.046$$

$$\{\phi_1\} = \begin{bmatrix} .1906 \\ .510 \\ -2.191 \\ -1.716 \end{bmatrix} \qquad \{\phi_2\} = \begin{bmatrix} .3221 \\ .5438 \\ -3.589 \\ -13.17 \end{bmatrix} \qquad M_{11} = 927.5 \qquad M_{22} = 18582$$

C-5 Computation of accelerations

Using the data given above, Eq. (3.1), and with the aid of Figure 4 for the value of $[A(t)]_{max}$, acceleration of the experiment package can be calculated. The results are shown in Table 4.

References

1. "Space Station Configuration Description," Systems Engineering Integration Space Station Program Office, L.B.J. Space Center, August, 1984.

2. Craig, R. R., Jr.: "Structural Dynamics," Wiley, 1981.

3. Kane, T. R.; Likins, P. W.; and Levinson, D. A.: "Spacecraft Dynamics," McGraw-Hill, 1983, p. 177.

4. Tong, K. N.: "Theory of Mechanical Vibrations," Wiley, 1960.

C-8

C-8

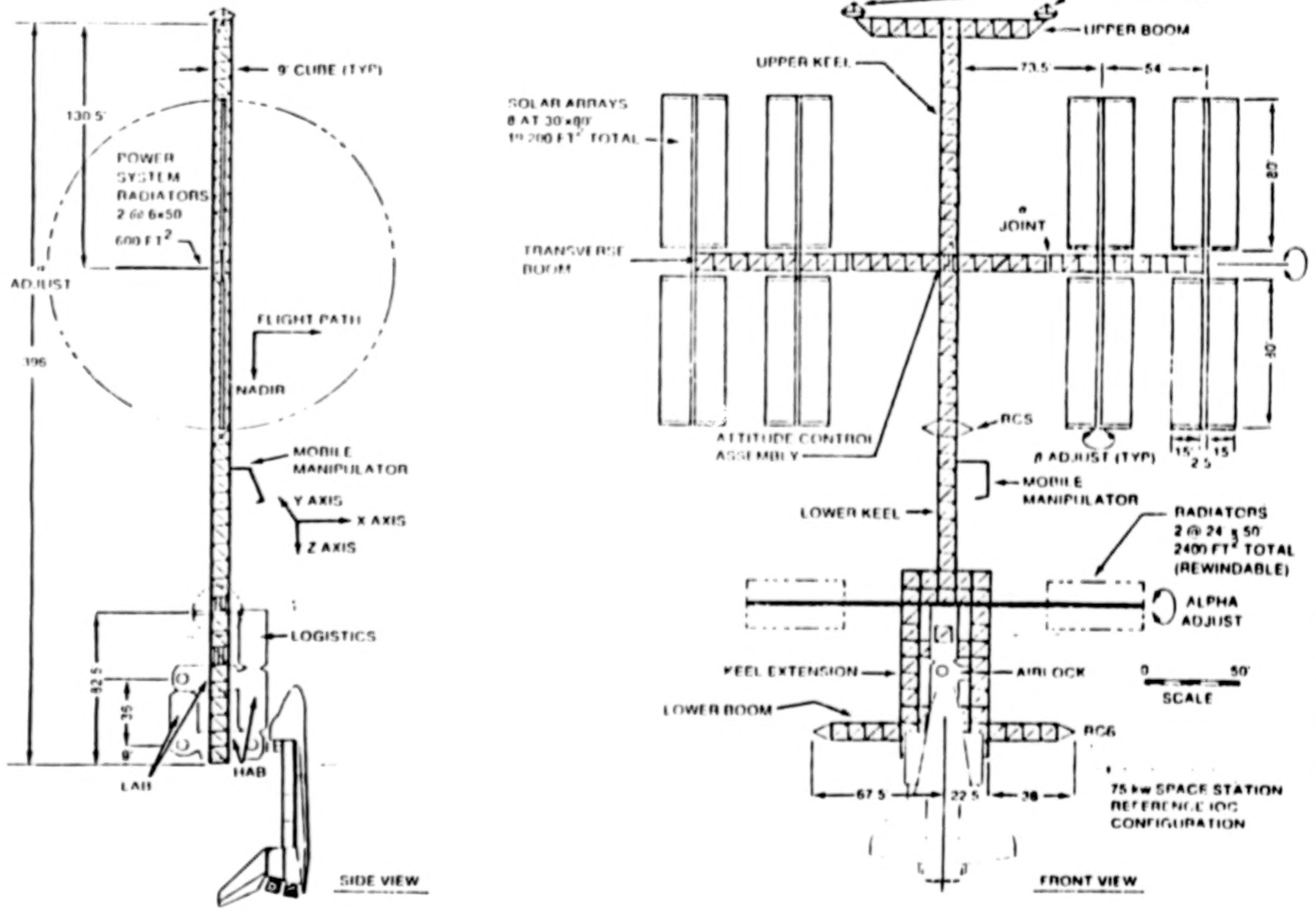
9' CUBE (TYP)
130.5'
POWER SYSTEM RADIATORS 2 @ 6×50 600 FT^2
ADJUST
396
FLIGHT PATH
NADIR
MOBILE MANIPULATOR
Y AXIS
X AXIS
Z AXIS
LOGISTICS
92.5
35
8
LAB
HAB
SIDE VIEW
ANTENNA SYSTE
UPPER BOOM
UPPER KEEL
73.5
54
SOLAR ARRAYS 8 AT 30'×80' 19 200 FT^2 TOTAL
80'
α JOINT
TRANSVERSE BOOM
40'
RCS
ATTITUDE CONTROL ASSEMBLY
β ADJUST (TYP)
15' 15'
2.5
MOBILE MANIPULATOR
LOWER KEEL
RADIATORS 2 @ 24 x 50' 2400 FT^2 TOTAL (REWINDABLE)
ALPHA ADJUST
KEEL EXTENSION
AIRLOCK
0 50'
SCALE
LOWER BOOM
RCS
67.5
22.5
38
75 kw SPACE STATION REFERENCE IOC CONFIGURATION
FRONT VIEW

ORIGINAL PAGE IS OF POOR QUALITY

Figure 1 (Figure 4.2.1-1[1])IOC REFERENCE CONFIGURATION

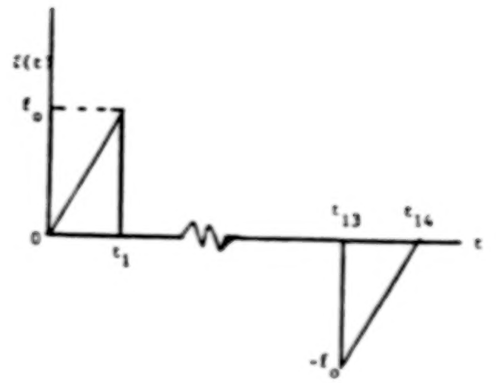

Figure 2 Mathematical Model of Crew Motion

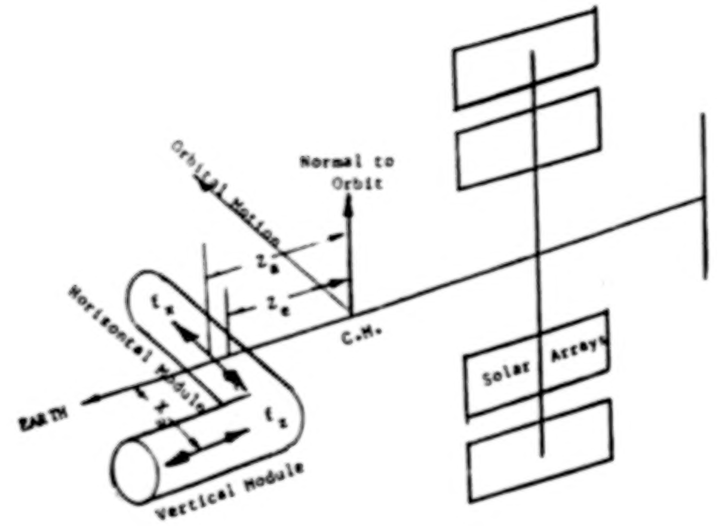
Orbital Motion
Normal to Orbit
z_a
z_e
C.M.
Horizontal Module
f_x
x_e
EARTH
f_z
Vertical Module
Solar Array

Figure 6 Reference of Crew Motion

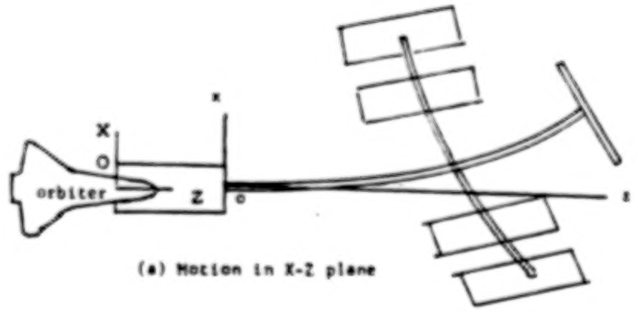
X
O
x
orbiter
Z
o
z

(a) Motion in X-Z plane

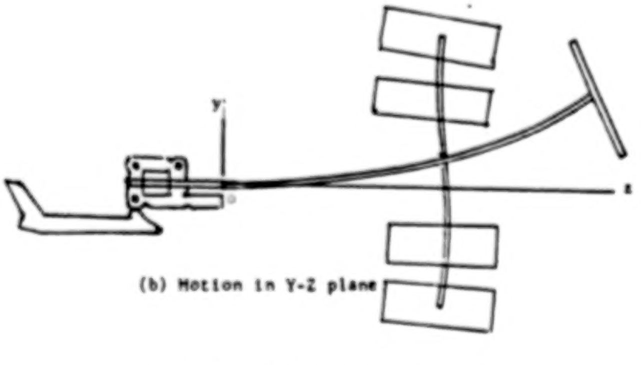

(b) Motion in Y-Z plane

Figure 5 Model of IOC Space Station

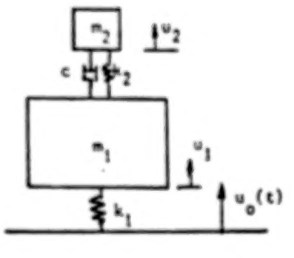
m_2
u_2
c
k_2
m_1
u_1
u_o(t)
k_1

Figure 7 Model of SuspensionSystem

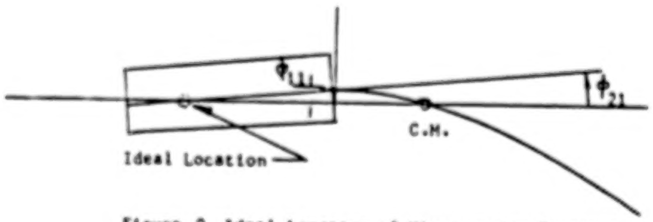
φ_11
φ_21
C.M.
Ideal Location

Figure 9 Ideal Location of Microgravity Experiment

ORIGINAL PAGE IS
OF POOR QUALITY

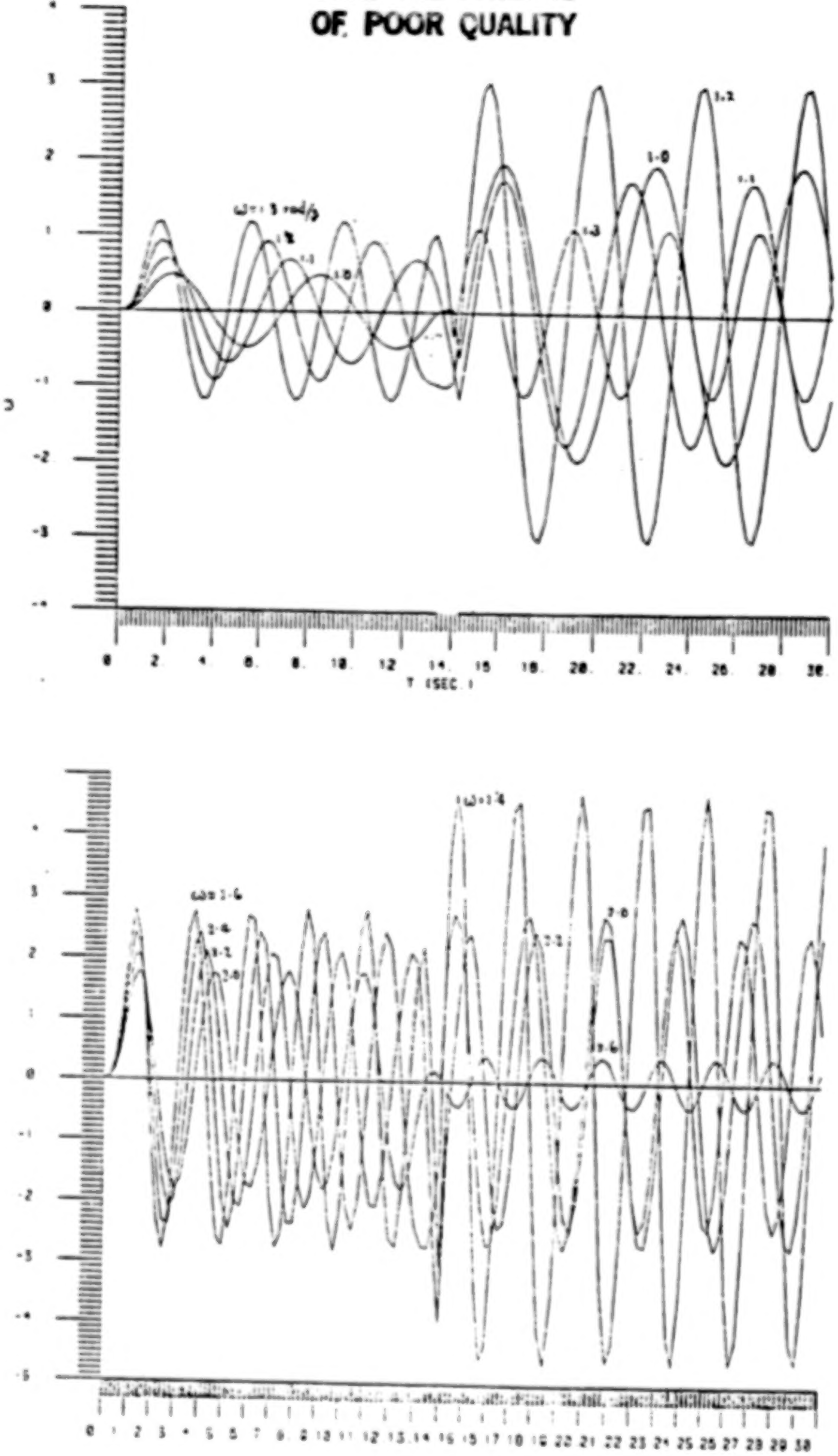

Figure 3 Displacement Functions

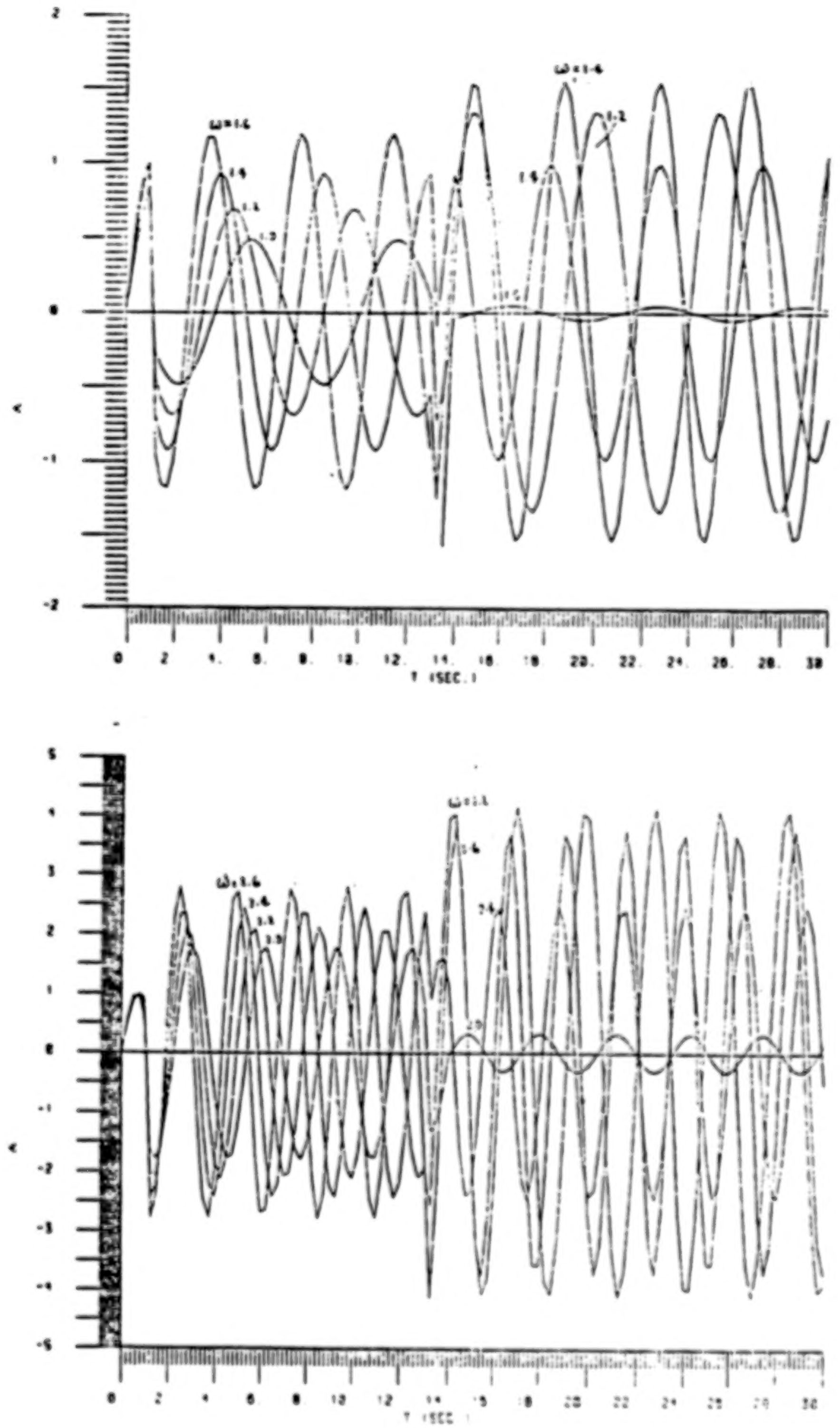

Figure 4 Acceleration Functions

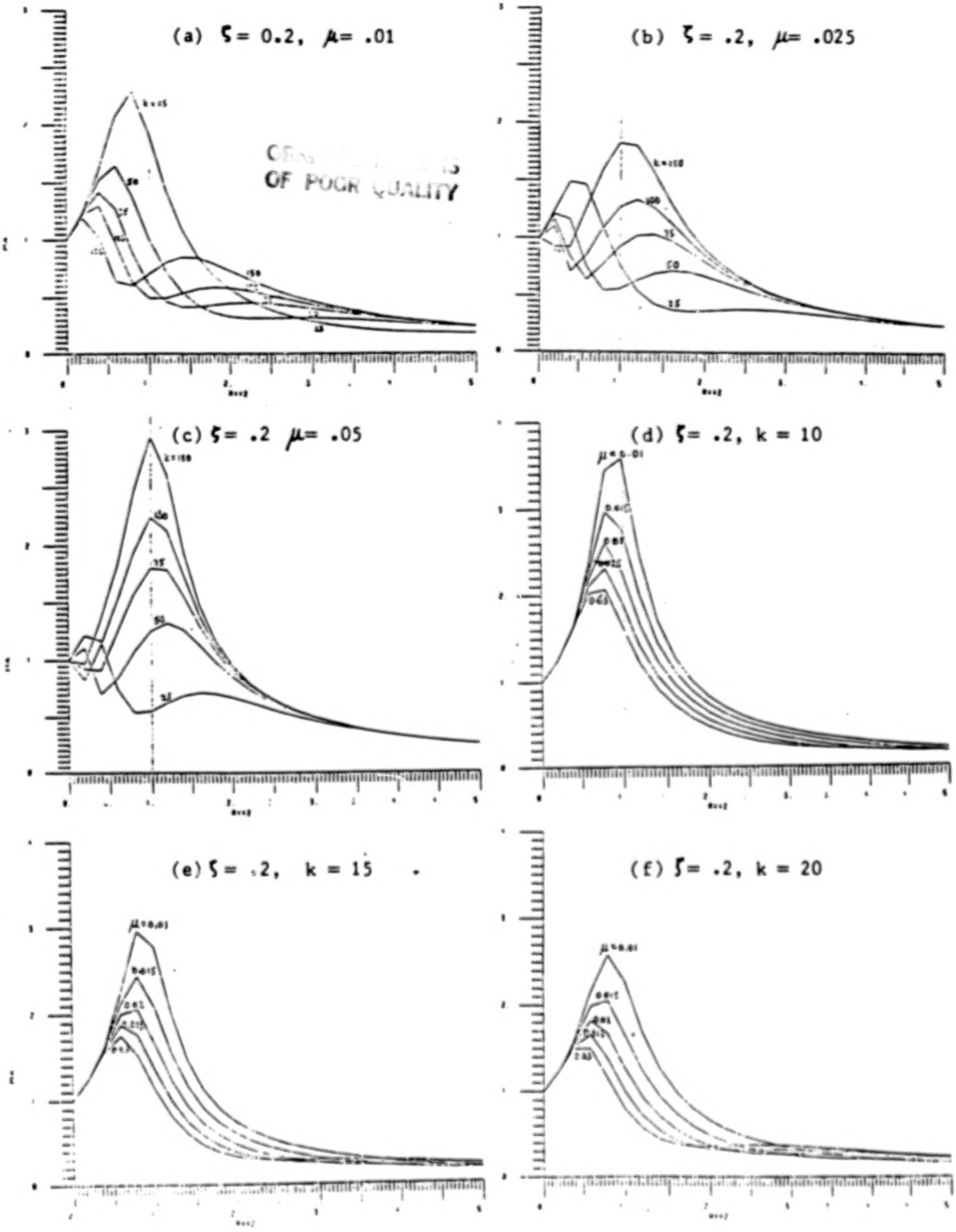
(a) ζ = 0.2, μ = .01

(b) ζ = .2, μ = .025

(c) ζ = .2 μ = .05

(d) ζ = .2, k = 10

(e) ζ = .2, k = 15

(f) ζ = .2, k = 20

Figure 8 Acceleration Magnification Factor

ORIGINAL PAGE IS
OF POOR QUALITY

Table 1. Properties of Analytical Reference Configuration Space Station Model (Table 4.3.3.3-1 [1])

Component	Bending Stiffness	Torsional Stiffness	Mass Length	Bending Strength	Torsional Strength
	(ft-lbs-ft)		(Slugs/ft)	(ft-lbs)	
Booms and Keels	1.31 E+9	3.18 E+8	0.25	35,000	15,000
30-Inch Astro Mast	3.13 E+6	2.08 E+5	2.3	3,480	208

Table 2. Inertial Properties of Analytical Model (Table 4.3.3.3-2 [1])

Case	Weight (lbs)	C. G. Coordinates (ft)	Moments of Inertia ($lb-ft-sec^2$)
Without Payloads and Orbiter	269,000	(1.1,0,84.2)	(8.63 E+7, 7.82 E+7, 1.20 E+7)
With Payloads Only	373,200	(-1.1,0,128.2)	(2.06 E+8, 1.98 E+8, 1.45 E+7)
With Orbiter Only	508,800	(5.7,0,34.4)	(1.45 E+8, 2.37 E+8, 1.35 E+7)
With Payloads and Orbiter	608,600	(3.59,0,68.3)	(3.21 E+8, 3.14 E+8, 1.62 E+7)

Table 3. Masses and Inertia Properties Used for IOC Model

r	Masses attached to main body	Z_r ft	z_r ft	W_r lbs
1	Fuel tank and gases	94.5	- 5.5	17,002
2	Module radiators	82.5	- 17.5	3,000
3	Five-bay platform	76.5	- 23.5	1,403
4	COM 1203	64.0	- 26.0	11,000
5	Logistics module	71.5	- 28.5	37,823
6	OMV and kits	67.5	- 32.5	23,750
7	Horizontal lab	45.0	- 55.0	54,295
8	Vertical lab	34.5	- 65.5	27,067
9	Keel extension	27.0	- 73.0	970
10	Vertical lab	19.5	- 80.5	47,709
11	Lower boom	13.5	- 86.5	728
12	Horizontal lab, SAA0207 and SAA0201	9.0	- 91.0	37,089
13	Orbiter	-26.66	-126.66	235,400

s	Masses attached to solar boom	Z_s ft	z_s ft	y_s ft	W_s lbs
	Solar boom structure	265.5	165.5	0-132	2,345
1	Power system radiators	265.5	165.5	54.0	750
2	TDM 2010	265.5	165.5	63.4	1,540
3	4 inboard solar arrays	265.5	165.5	78.0	4,787
4	4 outboard solar arrays	265.5	165.5	132	4,787

k	Mass attached to keel	Z_k ft	z_k ft	W_k lbs
	Upper and lower keel structure	100-396	0-296	2,504
1	Remote manipulator	162.0	62.0	2,000
2	Refuel attachment, tanks and tools	107.5	7.5	4,625
3	TDM 2570	210.5	110.5	2,000
4	Instruments and storage shelter	212.5	112.5	4,625
5	Storage boxes and tools	272.5	172.5	9.850
6	Service attachments	290.5	190.5	3,750
7	TDM 2560	295.5	195.5	7,055
8	Satellite	324.5	224.5	20,000
9	Upper boom and antenna system	396.0	296.0	17,734

Rotational Moment of Inertia	I_x ft-lb-s^2	I_y ft-lb-s^2
Orbiter (about c.m. of orbiter)	7×10^6	8×10^6
Solar array (about attachment) each		
Parallel to Nadir	101,000	107,300
Normal	2,790	107,300
Upper boom with antenna system	158,800	small
Module radiators (about attachment)	583,500	4,470
Power system radiators (about attachment)	750	25,120

Note: Z is measured from the bottom end of the keel extension and z is measured from the joint of keel and keel extension

Table 4. Numerical Results for IOC Model

		Motion in X-Z Plane		Motion in Y-Z Plane	
Motion	ω and a_e	With Orbiter	Without Orbiter	With Orbiter	Without Orbiter
Bending	ω rad/s	1.021	1.423	0.896	0.656
	a_e	$1.14\ g \times 10^{-5}$	$1.44\ g \times 10^{-8}$	$0.86\ g \times 10^{-5}$	$1.17\ g \times 10^{-5}$
	ω rad/s	2.577	2.730	2.810	2.654
	a_e	$2.26\ g \times 10^{-6}$	$1.38\ g \times 10^{-7}$	$0.66\ g \times 10^{-5}$	$2.9\ g \times 10^{-6}$
Libra. Motion	ω rad/s	1.89×10^{-3}	1.89×10^{-3}	1.85×10^{-3}	1.81×10^{-3}
	a_e	$0.254\ g \times 10^{-8}$	$5.13\ g \times 10^{-8}$	$0.24\ g \times 10^{-8}$	4.72×10^{-8}

N87
22753
UNCLAS

N87-22753

SPACE STATION STRUCTURAL DYNAMICS/ REACTION CONTROL SYSTEM INTERACTION STUDY

M. Pinnamaneni [1] and J. Murray [2]

Martin Marietta Denver Aerospace, Denver, Colorado

Abstract

The performance of the Reaction Control System is impacted by the extreme flexibility of the space station structure. This paper [3] presents the method used to analyse the periodic thrust profile of a simple form of phase plane logic. The results illustrate the effect on flexible body response of 1) the type of phase plane logic utilized and 2) the choice of control parameters: cycle period and attitude deadband.

---

1. Staff Engineer, Analytical Mechanics. Member AIAA.
2. Staff Engineer, Guidance Navigation and Control. Member AIAA.
3. Sponsored by Martin Marietta Corporation, Independent Research and Development, D37S.

Glossary

a'_n = Fourier coefficient, normalized by the control torque
A = complex harmonic response
  suffix R: real component
  suffix I: imaginary component
$\Delta P'$ = thrust pulse, normalized by P
Δt = cycle period fraction
  suffix 1: control phase
  suffix 2: coast phase
ε = attitude error angle
  suffix DB: deadband half-angle
ε = error angle rate
  suffix MAX: maximum
  suffix H: hard-cycle
f_C = duty cycle
f = frequency (Hz)
  suffix S: structural
  suffix H: harmonic
F = thrust profile harmonic coefficient
H = transfer function
I = inertia
L = propulsion efficiency losses
  suffix F: thrust losses
  suffix I: impulse losses
ϕ = attitude angle
n = Fourier harmonic
  suffix PEAK: corresponding to a peak
P = cycle period
  suffix S: soft-cycle
  suffix SC: coast
  suffix C: hard-cycle
$\Sigma\phi$ = attitude deadband
t = time
T = applied torque
T' = angular acceleration
  suffix C: control
  suffix D: disturbance

1. INTRODUCTION

Due to the extreme mechanical flexibility of the space station, the use of thrusters to control attitude presents new challenges to control system designers. The lightweight materials being used to construct the space station effect low rigidity and low natural damping. This, in turn, causes the presence of a large number of low frequency structural modes which place stringent limits on the control system bandwidth. The objective of this paper is to describe an approach to designing the control algorithm via analysis of the flexible body response to thrust profiles.

There is a very practical reason for this approach: as thrust profile requirements become more exacting and sophisticated, the propulsion system life cycle costs can become prohibitive. It is therefore expedient to analyse the interaction between thruster control and structural dynamics in order to affect thruster attitude control requirements that are cost effective.

The analysis covers two operational scenarios: space station reboost and back-up control during failure of the primary Attitude Control System (ACS). In each case the goal is to keep the attitude error within a 10 degree band, although minimizing the thrust cosine losses during reboost is also considered. (The essential difference between the two is the size of the disturbing torque seen by the space station, the reboost disturbance is significantly larger). The same phase plane logic has been used to generate thrust profiles for both scenarios. Based on attitude error and error rate, it has been used in other systems where structural modes are easily excited. As will be shown, thrust profile demands can be generated which restrict the harmonic content responsible for exciting the structure.

The approach to the dynamic analysis is to first analyse the space station rigid body response to the thrust profiles generated by the phase plane logic. These profiles are periodic and can be stipulated based on attitude control requirements and space station inertias, the shape of the thrust profile will vary according to the size of the disturbing torque and control torque.With the variation in shape determined, the Fourier coefficients are calculated showing the harmonic content of each profile. This enables a first cut at establishing the profile period.

A structural dynamic model is used during the second stage of the analysis, based upon the MMA Twin Keel configuration (dated 1/15/86.) The frequency response to thrust pulses is determined at various locations on the station to identify the significant elastic modes which might influence the phase plane logic design, and also establish a lower bound to the profile period. The final step is to define thrust profiles which restrict structural response and compute the actual response from model results.

This paper provides an insight into the development of Reaction Control System (RCS) requirements by analysing the sensitivety of thrust profiles to attitude control requirements and space station flexibility. It also illustrates how a relatively simple control algorithm can effect a 2 degree attitude band during the space station reboost and ACS backup.

2. PHASE PLANE LOGIC THRUST PROFILES

2.1 PHASE PLANE ROTATION

Introduction

The approach taken to develop the phase plane logic is to allow the space station to "float" within a deadband. Torques are applied only to reverse the direction of rotation when an attitude error limit has been reached. This is illustrated in Figure 2.1.

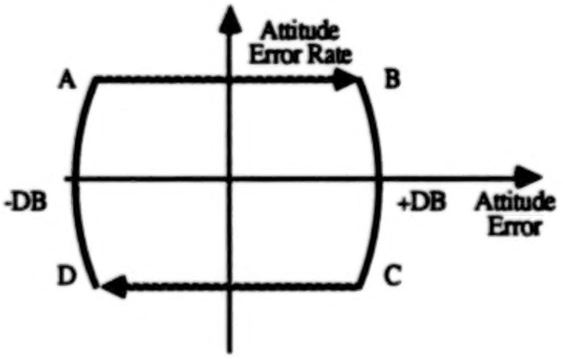

Fig. 2.1 Phase Plane Limit Cycle

As can be seen, the space station is allowed to float from one side of the dead band to the other (A to B and C to D). Control torques are applied when the space station attitude reaches the deadband (B to C and D to A).

This kind of limit cycle is referred to as hard due to there being two torque impulses for each cycle. In comparison, a soft limit cycle utilizes disturbance torques such that only one torque impulse is required to complete a cycle[1]. This is illustrated in Figure 2.2.

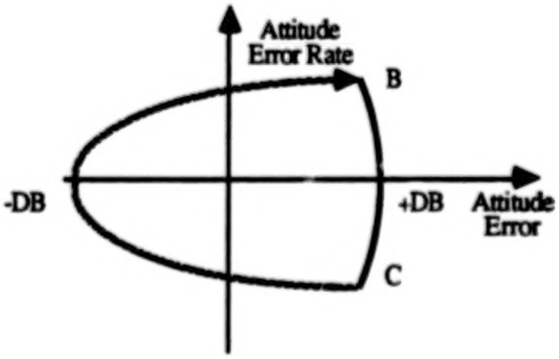

Fig. 2.2 Soft Limit Cycle

As shown, only one torque pulse is required for each cycle (B to C). The disturbance torque acts to rotate the space station back (C to B).

Rigid Body Rotational Equations of Motion

The set of rigid body equations for a single rotation axis can be described by the following equations:

$$\ddot{\phi} = T' \tag{2.1}$$

$$\dot{\phi}(t) = T'.[t-t_0] + \phi(t_0) \tag{2.2}$$

$$\phi(t) = T'.[t-t_0]^2/2 + \dot{\phi}(t_0).[t-t_0] + \phi(t_0) \tag{2.3}$$

where: $T' = T/I$

$T =$ applied torque, assumed constant

$I =$ space station inertia

$t_0 =$ initial time

$\phi(t_0) =$ initial attitude angle

Cycle Period of a Soft Limit Cycle

The soft-cycle period is the sum of the torque impulse period, Δt_1, and the soft-cycle coast period, Δt_2. Equation 2.2 yields the torque impulse period:

$$\Delta t_1 = 2.\dot{\varepsilon}_{MAX} / T'_C \tag{2.4}$$

where: $\dot{\varepsilon}_{MAX} =$ maximum soft-cycle error rate

$T'_C =$ control angular acceleration

The soft-cycle coast period, Δt_2, is calculated from equation 2.2 and 2.3 assuming a constant disturbance torque, T_D. Hence:

$$\Delta t_2 = 8.\varepsilon_{DB}/\dot{\varepsilon}_{MAX} \tag{2.5}$$

$$\dot{\varepsilon}_{MAX}^2 = 4.(T'_D.\varepsilon_{DB}) \tag{2.6}$$

where: $\varepsilon_{DB} =$ attitude deadband half-angle

$T'_D =$ disturbance angular acceleration

The soft-cycle can be summarized by:

$$P_S = P_{SC}.\{ 1 + T_D/T'_C \} \tag{2.7}$$

where: $$P_{SC} = 4.\{\varepsilon_{DB}/T_D \}^{1/2} \tag{2}$$

Comparison of Hard and Soft Limit Cycles

Because the hard limit cycle has no disturbance torque, the cycle period is simply computed from:

$$P_C = 2.\{2.\dot{\varepsilon}_H/T'_C + 2.\varepsilon_{DB}/\dot{\varepsilon}_H\} \qquad \_\_\_\_ \; 2.9$$

where: $\dot{\varepsilon}_H$ = equivelant hard-cycle error rate

From equations 2.8 and 2.9 an equivalent hard-cycle error rate can be related to the maximum soft-cycle error rate for identical periods and deadbands. This yields:

$$\dot{\varepsilon}_H = \dot{\varepsilon}_{MAX}/2 \qquad \_\_\_\_ \; 2.10$$

As can be seen, the resultant change in angular velocity over a complete cycle is the same. Consequently, the torque impulse is also identical, as illustrated in Figure 2.3.

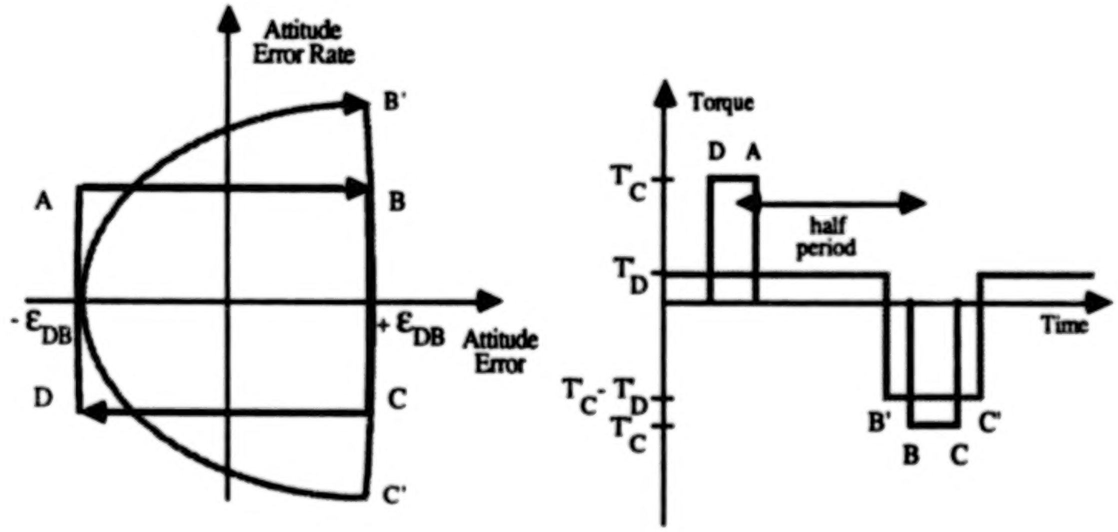

Figure 2.3 Phase Plane and Torque Profile Comparison

Space Station utilization of the Soft Limit Cycle

During reboost, the space station thrust axis is sufficiently displaced off the CG to cause a large disturbance torque and, as a result, the hard-cycle phase plane logic is not feasible. Given a fixed deadband and a knowledge of the disturbance torque, the torque profile can be shaped to effect the largest practicle cycle period. This minimizes the thruster harmonics as will be shown.

Should the RCS be used to backup an ACS failure, the disturbance torque (a function of the gravity gradient and aerodynamic torques) is small. The soft-cycle is still the optimum solution as long as the torque requirement (B' to C') does not effect a thrust impulse less than the minimum impulse bit. In comparison to the reboost case, the same deadband will effect a longer cycle period (ref. equation 2.8) further reduces the thruster harmonics.

2.2 THRUST IMPULSE LOSSES

Calculating the losses

During reboost the thrust vector is rotating about about the velocity vector as the space station attitude rotates about the deadband. This effects a reduction in effective impulse due to cosine losses. The fractional thrust loss can be calculated from:

$$L_F(t) \quad = \quad 1 - \cos \varepsilon(t) \qquad \_\_\_\_\ 2.11$$

and the fractional impulse loss over half of the coast period:

$$L_I \quad = \quad 1/\Delta t \int_0^{\Delta t} [\, 1 - \cos \varepsilon(t)\,] \,.\, dt \qquad \_\_\_\_\ 2.12$$

For the hard limit cycle we have:

$$\Delta t \quad = \quad 2.\varepsilon_{DB}/\dot{\varepsilon}_H$$

$$\text{and} \qquad \varepsilon(t) \quad = \quad \varepsilon_{DB} - \dot{\varepsilon}_H . t \qquad \_\_\_\_\ 2.13$$

substituting into 2.12 we have:

$$L_I \quad = \quad \{ \cos \phi_{DB}/2 \,.\, \sin \phi_{DB} - \sin \phi_{DB}/2 \,.\, (\cos \phi_{DB} - 1) \} / \phi_{DB} \qquad \_\_\_\_\ 2.14$$

$$\text{where:} \qquad \phi_{DB} \quad = \quad 2.\varepsilon_{DB}$$

For the soft-limit cycle the integral is evaluated after substituting equations 2.3 and 2.6:

$$L_I \quad = \quad 2/\Delta t \int_0^{\Delta t/2} \{ 1 - \cos [(a.t - b)^2 - \varepsilon_{DB}] \} \, dt \qquad \_\_\_\_\ 2.15$$

$$\text{where:} \qquad a \quad = \quad \{T_D / 2\}^{1/2}$$

$$b \quad = \quad \phi_{DB}$$

Integrating 2.15 we have:

$$L_I \quad = \quad 1 - \cos \phi_{DB}/2 \,.\, \Sigma\{ (-1)^n . \phi_{DB}{}^{2n} / [(4n+1).(2n)!] \} - \sin \phi_{DB}/2 \,.\, \Sigma\{ (-1)^n . \phi_{DB}{}^{2n+1} / [(4n+3).(2n+1)!] \} \qquad \_\_\_\_\ 2.16$$

Estimating the Losses

For small deadbands a simplifying approximation, ϕ_{DB}=sin ϕ_{DB}, can be made to equations 2.14 and 2.15:

$$L_{I(HC)} = 1 - (\cos \varepsilon_{DB} + \varepsilon_{DB}^2)$$

and

$$L_{I(SC)} = 1 - (\cos \varepsilon_{DB} + 2.\varepsilon_{DB}^2/3) \qquad \_\_\_\_ 2.17$$

As can be seen, the two limit-cycle types have nearly identical impulse loss characteristics. The actual losses described by equations 2.14 and 2.16 are illustrated in Figure 2.4. In both cases the impulse loss is relatively insensitive to the deadband size, with a 25 degree deadband the impulse loss is little more than 1%. It can be concluded that impulse loss is not a descriminator.

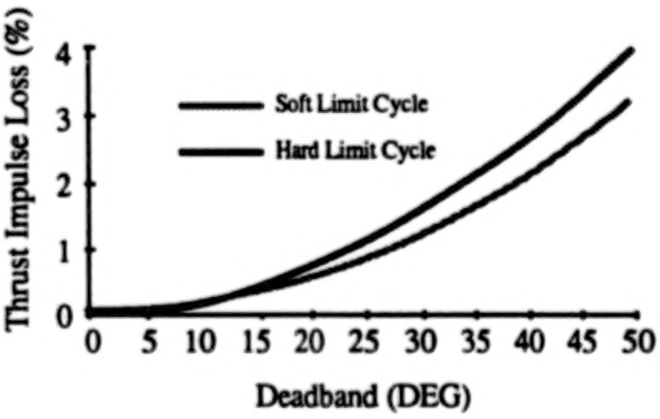

Figure 2.4 Estimate of Thrust Impulse Losses

2.3 SOFT LIMIT CYCLE PERIODS AND DUTY CYCLE

Duty Cycle

Figure 2.5 illustrates a worst case reboost thrust off-set in the space station pitch plane. This off-set is the effect of the bottom set of propulsion modules being further displaced from the space station CG than the top set.

The disturbance-control torque ratio can be calculated as follows:

$$T_C = F * 6.5 \text{ bays}$$

$$T_D = 2.F * 1 \text{ bay}$$

Hence

$$T'_D/T'_C = 0.31 \qquad \_\_\_\_ 2.18$$

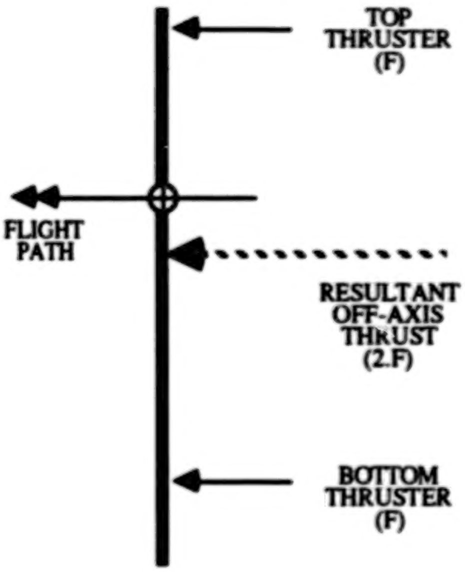
TOP
THRUSTER
(F)
FLIGHT
PATH
RESULTANT
OFF-AXIS
THRUST
(2.F)
BOTTOM
THRUSTER
(F)

Figure 2.5 Space Station Thrust Misalignment during Reboost

The duty cycle required to effect a pitch control is calculated using a rearrangement of equation 2.7:

$$f_C = [P_S - P_{SC}]/P_S$$

$$= [T'_D/T'_C]/[1 + T'_D/T'_C] \qquad 2.19$$

where f_C = duty cycle

This is illustrated in Figure 2.6 for a torque ratio range (0,0.3).

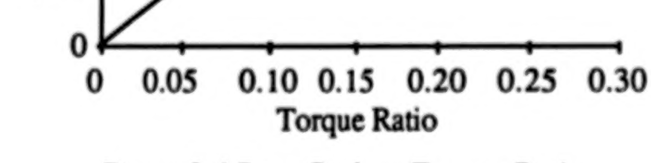

Figure 2.6 Duty Cycle vs Torque Ratio

In comparison to the reboost case, during ACS backup the disturbance due to gravity gradient and aerodynamic torques are small, in the region of 20 to 40 Nm. The range of available control torques depends on the final thruster size and the control mode: top thruster only, bottom thruster only or both sets of thrusters to provide a couplet. The impact of these possibilities on the torque ratio is illustrated in Table 2.1.

	Top Thruster Set	Bottom Thruster Set	Combined Thruster Set
Control Torque Range (Nm)	2,400-6,000	4,000-10,000	6,400-16,000
Torque Ratio Range (40N thruster)	0.008-0.016	0.005-0.010	0.003-0.006
Torque Ratio Range (100N thruster)	0.003-0.006	0.002-0.004	0.001-0.005

Table 2.1 Torque Ratio Variation with Thruster Size and Usage

As can be seen, the thruster duty cycle during the ACS backup mode are two orders less than those of the reboost mode. There are two critical parameters related to the duty cycle: the minimum impulse bit and thruster heat pumping. Assuming a 60 second limit cycle period, the required minimum impulse is in the 60 to 100 msec range which should not impact the design. The second parameter concerns thruster heat pumping; this is where the fuel flow is insufficient to cool the thruster due to its being discontinuous. Figure 2.7 illustrates this phenomenon for a typical hydrazine application showing the operating modes for both the reboost and ACS backup modes. The ACS backup mode presents the most severe operating condition. However, because this mode is abnormal it cannot be assumed that it will effect either design or life cycle difficulties.

Cycle Period

The cycle period determines the thruster harmonics exciting the structure. It is therefore desirable to maximize the cycle period to the extent possible in order to minimize the magnitude of the higher frequency harmonics. This is acheived by increasing the deadband.

The attitude control deadband has two components, illustrated in Figure 2.8: the error angle (ε_{DB}) seen during the coast phase of the cycle, and the control error angle (ϕ'_{DB}) seen during the control phase of the cycle. Equations 2.7 and 2.8 define the cycle period as a function of the error angle and the torque ratio, the deadband is determined a follows:

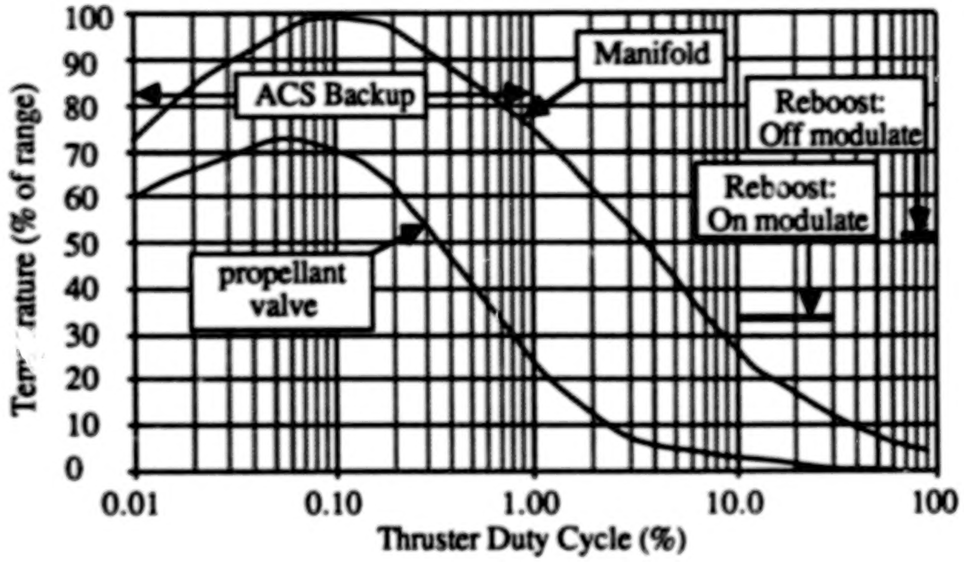

Figure 2.7 Heat Pumping vs Duty Cycle

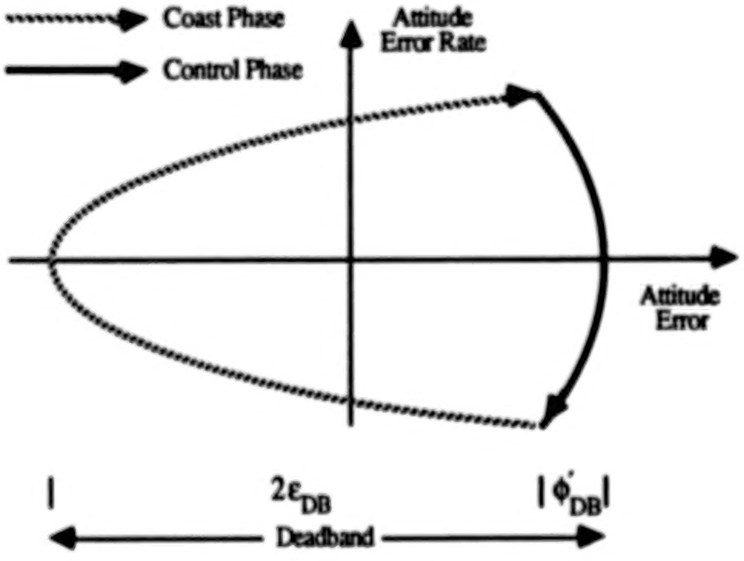
Coast Phase
Control Phase
Attitude
Error Rate
Attitude
Error
$2\varepsilon_{DB}$
$|\phi'_{DB}|$
Deadband

Figure 2.8 Soft Limit Cycle Deadband

From equation 2.3 we have:

$$\phi'_{DB} = [T_C/2].(\Delta t_1/2)^2 + \dot{\varepsilon}_{MAX}.(\Delta t_1/2) \qquad \_\_\_\_ \; 2.20$$

and, $\dot{\varepsilon}_{MAX} = T'_C.\Delta t_1/2$

therefore, $\phi'_{DB} = 3.\dot{\varepsilon}_{MAX}{}^2 / (2.T'_C)$ ____ 2.21

Substituting in equation 2.6 we have:

$$\phi'_{DB} \quad = \quad [T'_D/T'_C].6.\varepsilon_{DB} \qquad \text{\_\_\_\_ } 2.22$$

The error angle can now be defined as a function of the total deadband, $\Sigma\phi$:

$$\varepsilon_{DB} \quad = \quad \Sigma\phi\ /\{\ 2.(1 + 3.[T'_D/T'_C])\ \} \qquad \text{\_\_\_\_ } 2.23$$

From equations 2.7, 2.8 and 2.23 the soft-cycle period can be plotted against the total deadband as illustrated in Figure 2.9. A comparison of 30% and 0.1% torque ratio is given in Figure 2.10.

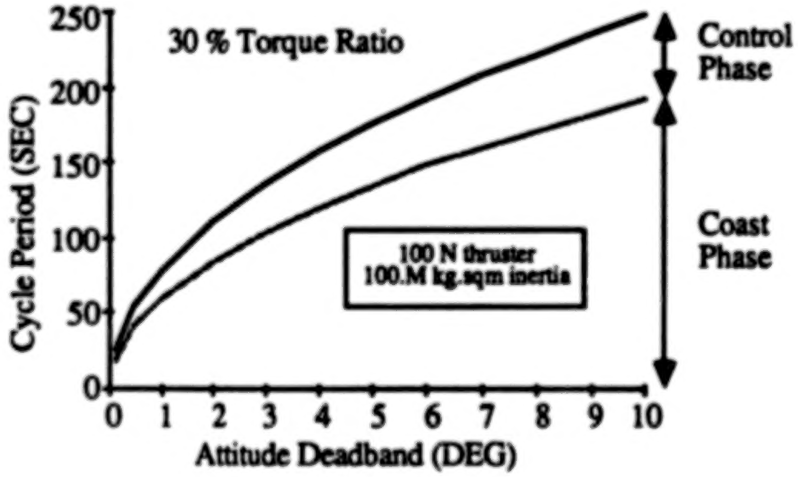

Figure 2.9 Variation of Cycle Period with Attitude Deadband

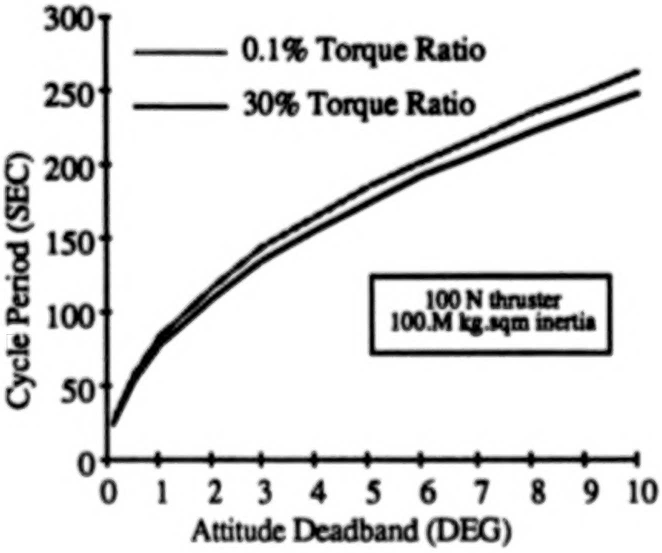

Figure 2.10 Variation of Cycle Period with Torque Ratio

From Figures 2.9 and 2.10 it can be seen that the cycle period is sensitive to the attitude deadband. The configuration used to generate these characteristics is a worse case as 100N thrusters were modelled; 40N thrusters would increase the period by 60%, and during the ACS backup mode the period would be increased ten-fold.

It can be concluded that a period range of 60 to 240 seconds for the space station is quite feasible with an attitude deadband during ACS backup within 2 degrees.

2.4 PRELIMINARY CONCLUSIONS

Reboost Mode

It has been shown that a soft limit cycle can be implemented to effect attitude control. This requires on-off modulation of the thrusters; either off-modulating thrusters with the largest moment arm at a 20% rate (80% duty cycle), or on-modulating the redundant thrusters having the smallest moment arm at a 20% rate (20% duty cycle). The remainder of this study will consider the latter as a worst case scenario.

The attitude deadband is largely insensitive to impulse losses and mostly dependent upon the required cycle period. Periods of 60 to 240 seconds in the pitch plane are quite feasible using deadbands of 1 to 10 degrees. An analysis of the structural response to thruster harmonics is required to determine the sensitivity to cycle period.

ACS Backup Mode

It has been shown that a soft limit cycle is equally effective during ACS backup. Although the duty cycle is significantly smaller than that of the reboost mode, the minimum impulse requirement is still significantly larger than the minimum impulse bit (2 seconds as compared to 40 msecs.) A more significant problem may be the heat pump phenomenon at the low duty cycle rate experienced. However, given that this mode is abnormal it is not considered to be a serious handicap.

3.LIMIT CYCLE HARMONICS

3.1 SOFT LIMIT CYCLE

Analysis of the thruster induced harmonics provides insight into the space station structural excitation. To determine the affect of the soft limit cycle, the torque profile illustrated in Figure 2.3 is used to calculate the Fourier coefficients as follows:

$$a_0 = [1/P].\int_{-P/2}^{P/2} [T'_D + T'_C(t)].dt$$

$$a_n = [2/P].\int_{-P/2}^{P/2} [T'_D + T'_C(t)].\cos n\omega t.dt$$

$$b_n = [2/P].\int_{-P/2}^{P/2} [T'_D + T'_C(t)].\sin n\omega t.dt \qquad \text{\_\_\_\_ } 3.1$$

Since the function has even symmetry, $b_n = 0$. Also, by definition the integral of torque over the cycle period is zero, therefore $a_0 = 0$. The Fourier coefficient (normalized by the control torque) is:

$$a'_n = [2/n\pi].\sin(n.\Delta P'.\pi) \qquad \text{\_\_\_\_ } 3.2$$

where: $\Delta P'$ = thrust pulse duration, normalized by the cycle period.

The frequency spectrum of T'_C is illustrated in Figure 3.1 for a 20% pulse duration (note that for a soft limit cycle the pulse duration is analogous to the duty cycle.)

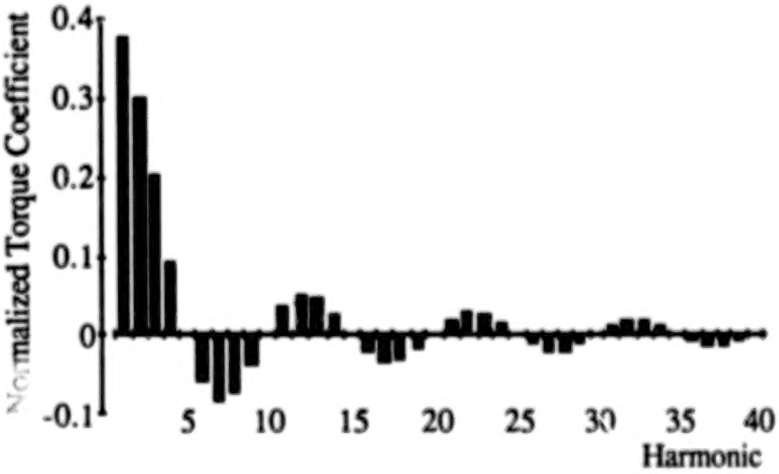

Figure 3.1 Soft Limit Cycle Frequency Spectrum

The significance of this spectrum lies in recognizing the fast decay in the size of the higher frequency harmonics. The correct choice for cycle period will effectively restrict the size of the harmonics that excite the space station structural modes. The cycle period can be set using:

$$P_S > n / f_M \qquad \text{\_\_\_\_ } 3.3$$

For example; if the structural mode of concern has a 0.1 Hz frequency and the 10th harmonic is considered the breakpoint, then the cycle period must exceed 100 seconds. The detailed analysis of this control-dynamics interaction is the subject of section 5 of this paper.

3.2 COMPARISON OF HARD AND SOFT CYCLE HARMONICS

The derivation of Fourier coefficients for the eqivelent hard limit cycle is identical to that of the soft. For the torque profile illustrated in Figure 2.3, the coefficients can be calculated using:

$$a'_n = [2/n\pi].\{\sin(n.\Delta P'.\pi/2) + (-1)^n.\sin(n.\Delta P'.\pi/2)\} \qquad \_\_\_\ 3.4$$

Figure 3.2 compares the two cycle types illustrating two principle differences:

a. The decay of the hard limit cycle harmonics is slower than that of the soft limit cycle.

b. The hard limit cycle has less harmonics. (Although in reality the space station would not have the identical opposing torque impulses used to derive the results given in Figure 3.2, consequently there would not be the exact cancellation shown here.)

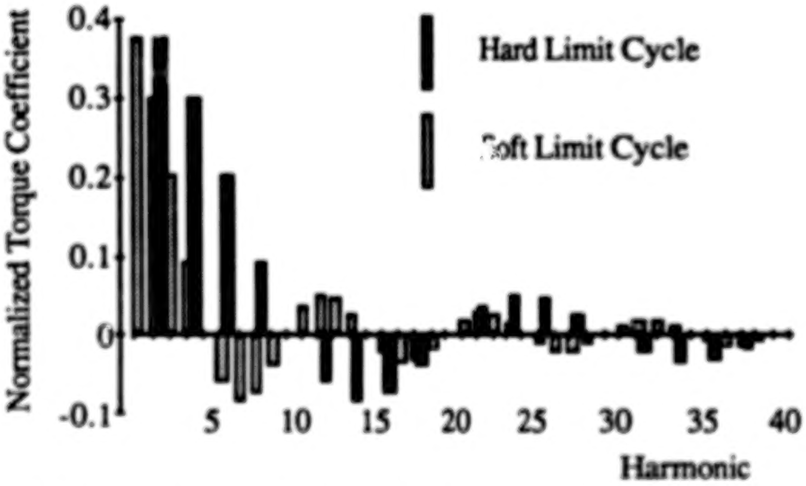

Figure 3.2 Comparison of Hard and Soft Limit Cycle Frequency Spectrums

To effect a separation of torque profile harmonics and structural modes identical to that of the soft limit cycle would require a period twice the size. This can be seen from the comparison in Figure 3.2; the 20th harmonic of the hard-cycle is equivelent to the 10th harmonic of the soft-cycle with respect to the magnitude of the torque coefficients. It should be noted, however, that a complete dynamic response analysis is necessary to validate this assertion.

3.3 EFFECT OF COEFFICIENT DECAY ON DYNAMIC RESPONSE

Peak Torque Decay in the Frequency Domain

The amplitude of the peak torque Fourier coefficients can be determined from equation 3.2:

$$A_P = 2.T_C / n.\pi \qquad \_\_\_\_ \; 3.5$$

Substituting the harmonic, n, with frequency and expressing in db, the variation of peak amplitude with frequency as described by:

$$20 \log A_P = 20 \log[\, 2.T_C/\pi.\Delta P/P \,] - 20 \log[\, \Delta P.f \,] \qquad \_\_\_\_ \; 3.6$$

This is described graphically in Figure 3.3.

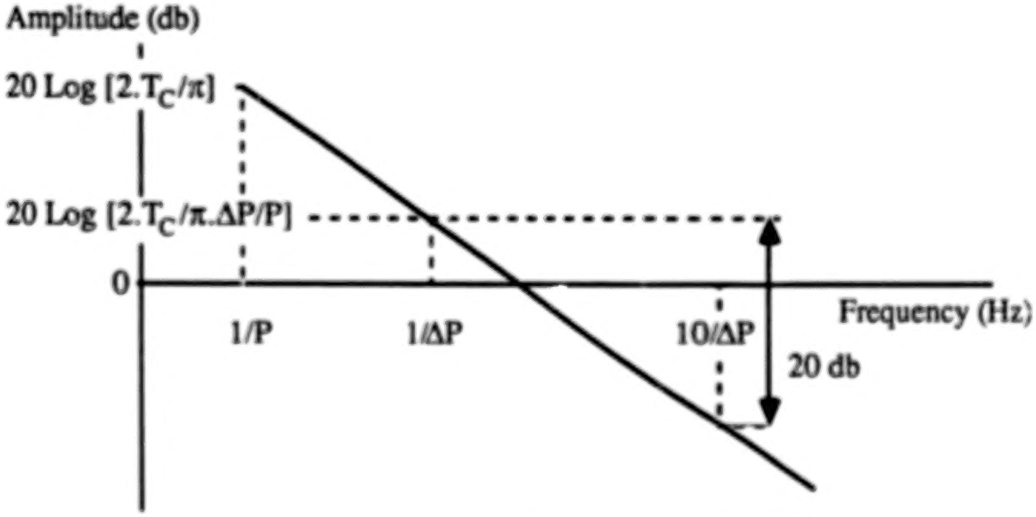

Figure 3.3 Decay of Peak Disturbance with Frequency

As can be seen the peak amplitudes decay at a 20db/decade rate. There are three significant parameters that will determine the eventual frequency response: the control torque, duty cycle and the thruster pulse width. From equation 2.19, the following simplification can be made to equation 3.6:

$$20 \log A_P = 20 \log[\, 2.T_D/\pi \,] - 20 \log[\, P.(T_D/T_C).f \,] \qquad \_\_\_\_ \; 3.7$$

From equation 3.7 it is more evident that the driving parameters are the disturbance torque, the cycle period and the torque ratio. Hence, recalling Figure 2.9, it can be seen that constraining the high frequency content of the thrust profile requires decreasing the size of the disturbance torque and increasing the deadband.

Effect of Peak Torque Decay on Flexible Body Response

The need to restrict the high frequency content of the thruster profile becomes evident when the flexible body response is assessed. This is illustrated qualitatively in Figure 3.4 as two predominant flexible body modes, the second larger than the first (note that in reality there will tend to be alot more than two!)

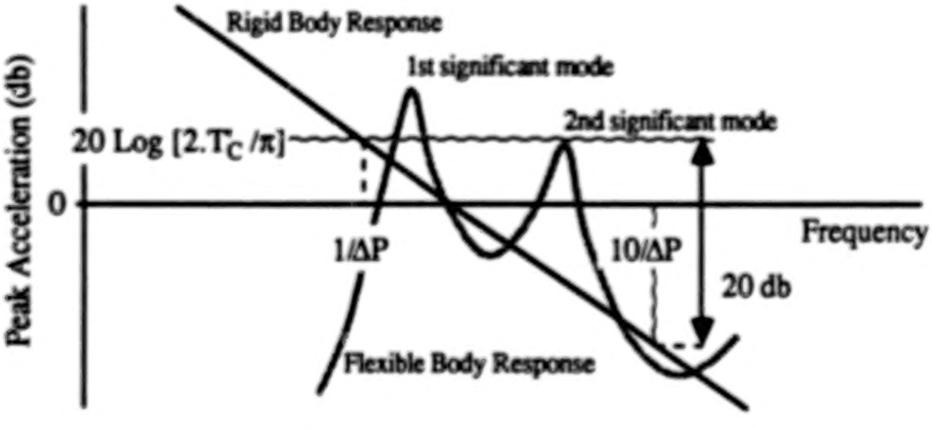

Figure 3.4 Flexible Body Response

Figure 3.4 illustrates the rigid body response, with the flexible body response superimposed. As the thruster pulse width is reduced, the response of both modes will increase. Also, because the exciting torque has a -20db/decade slope, the second mode has a smaller response even though it is more "excitable".

4. FLEXIBLE BODY DYNAMIC RESPONSE ANALYSIS

4.1 STRUCTURAL DYNAMIC MODEL.

In order to analyse the RCS-Structural dynamics interaction, a finite element model has been developed based on the Martin Marietta Space Station dual keel 5 meter configuration (dated 1/15/86). The truss members were modelled with ROD elements and the solar panels, radiators and modules were assumed rigid and modelled with mass elements at the corresponding interfaces neglecting the moment of inertias. These simplifications eliminate the very low frequency local modes and provide the primary modes necessary for the RCS/Structural Dynamics interaction study. The mass properties of the finite element model illustrated in Figure 4.1 are described in the Table 4.1. The size of the finite element model (1596 d.o.f) was reduced to a smaller dynamic model (42 d.o.f) using MSC/NASTRAN generalised dynamic reduction procedure. The reduced model has the fidelity of generating natural frequencies accurately up to 2.0 Hz.

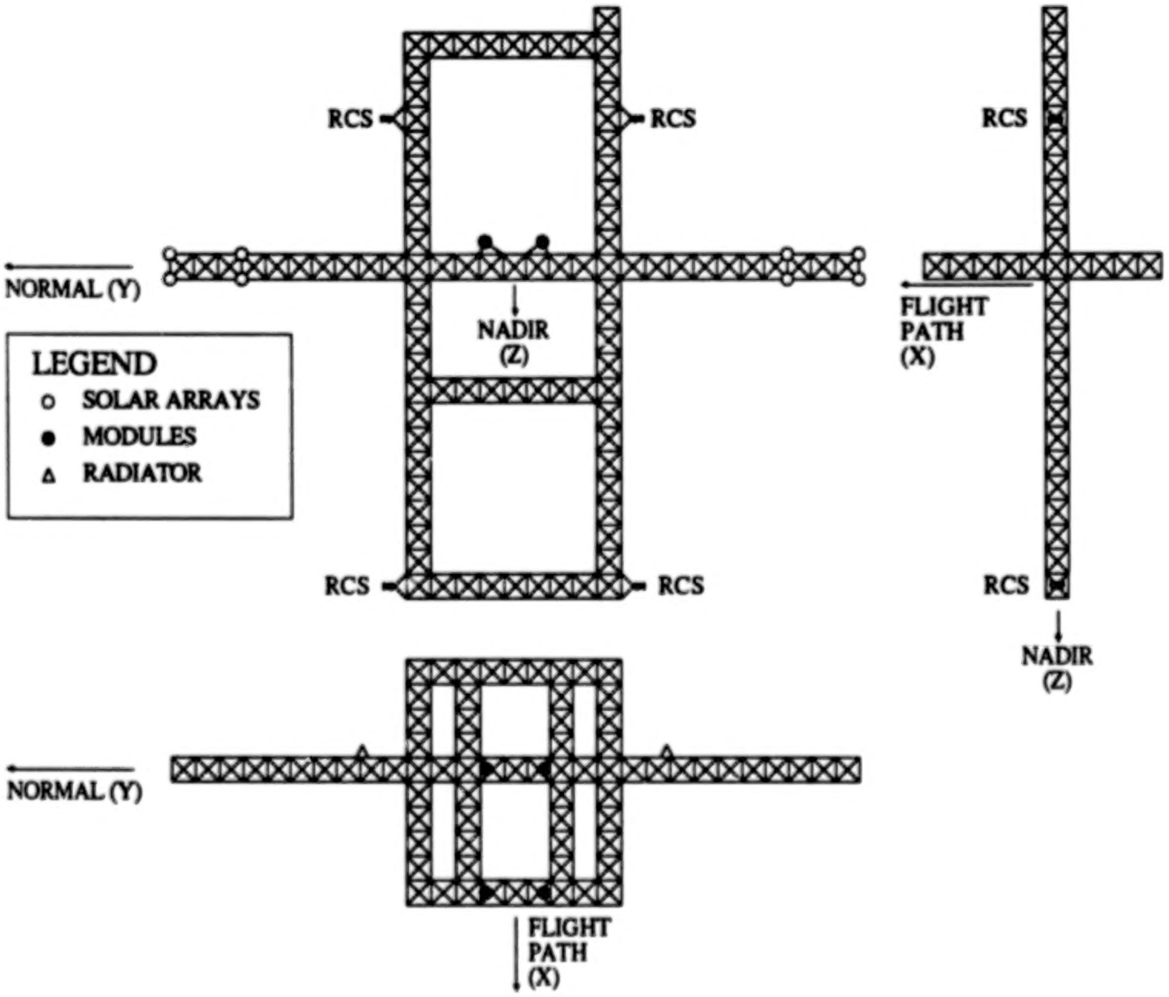

Figure 4.1 Martin Marietta Space Station Dual Keel 5m Configuration NASTRAN Model

Mass (kg)	217,404		
Centre of Gravity	X 5.316	Y -0.248	Z -3.513
Inertia (kg.m^2)	I_{XX} $1.08*10^8$	I_{YY} $8.71*10^7$	I_{ZZ} $7.75*10^7$
Inertia (kg.m^2)	I_{XY} $2.17*10^6$	I_{XZ} $2.36*10^6$	I_{YZ} $4.59*10^6$

Table 4.1 MMA Dual Keel 5m Space Station Configuration Mass Properties

4.2 NORMAL MODES.

MSC/NASTRAN SOL 3 was used to obtain the natural frequencies and mode-shapes up to 2.0 Hz. The frequencies of the elastic modes are listed in the Table 4.2 along with the modal strain and kinetic energy participations of the different structural components. These energy participations provide insight into identifying the most significant modes that make up the dynamic response. For example, the thruster located on the top keel in the flight direction (X-axis) significantly excites the 0.36 Hz and 0.54 Hz elastic modes. Similarly, the thruster located on the bottom keel excites the 0.42 Hz, 0.94 Hz and 1.17 Hz modes. Since the present study considers only the thruster on the top keel, the 0.36 and 0.54 elastic mode-shapes are presented in the Figures 4.2 and 4.3 .

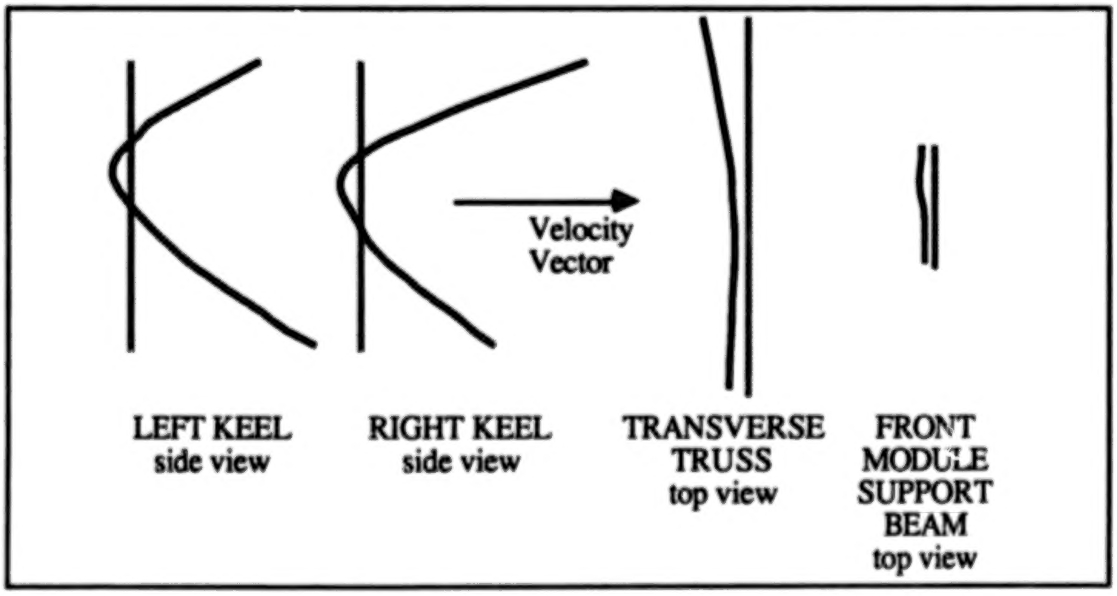
Velocity
Vector
LEFT KEEL
side view
RIGHT KEEL
side view
TRANSVERSE
TRUSS
top view
FRONT
MODULE
SUPPORT
BEAM
top view

Figure 4.2 Mode-Shape deflections at 0.36 Hz

Freq (Hz)	Model Percentage Strain-Kinetic Energy							Mode and Mode Description
	1	2	3	4	5	6	7	
0.36	2-1	2-1	62-60	8-14	21-6	3-17	2-1	1. UPPER KEEL FIRST X BENDING (SYM)
0.42	4-2	4-2	2-2	40-49	43-41	5-2	3-2	2. LOWER KEEL FIRST X BENDING (SYM)
0.53	27-47	26-42	5-2	4-1	34-6	2-1	2-1	3. TRANSVERSE BOOM FIRST Z BENDING
0.54	5-1	5-2	56-77	7-5	13-13	11-1	7-1	4. UPPER KEEL FIRST TORSION, BEND, PITCH
0.56	24-46	25-46	2-1	2-1	37-4	5-1	5-1	5. TRANSVERSE BOOM FIRST X BENDING
0.57	3-25	3-15	48-52	2-1	18-5	3-1	3-1	6. UPPER KEEL Y , TRANSVERSE X BENDING
0.62	26-28	25-44	3-1	4-10	28-15	7-1	7-1	7. TRANSVERSE BOOM X & Z BENDING
0.67	19-26	20-16	16-13	8-18	27-23	4-1	3-3	8. UPPER KEEL Y, TRANSVERSE X & Z BEND
0.91	8-2	8-2	11-7	54-62	10-22	5-2	4-2	9. LOWER KEEL FIRST TORSION
0.94	8-1	8-1	3-3	48-42	18-49	9-1	6-1	10. LOWER KEEL FIRST Y BENDING
0.97	11-2	11-3	11-6	3-3	14-76	34-2	16-10	11. KEEL TORSION AND BOOM BENDING
1.17	6-1	6-1	2-1	64-63	11-32	7-1	3-1	12. LOWER KEEL MODE - X DIR
1.29	21-2	18-2	9-14	5-10	28-68	14-2	6-2	13. TRANSVERSE BOOM MODE - Z DIR
1.40	11-2	13-2	1-2	4-3	14-82	49-2	8-7	14.TRANSVERSE BOOM MODE - X DIR
1.46	12-2	11-2	3-6	5-2	16-70	44-2	9-6	15. TRANSVERSE BOOM MODE - Z DIR
1.78	10-2	9-2	5-2	61-47	9-43	3-2	2-2	16. TRANSVERSE BOOM MODE -Y DIR
1.86	17-1	18-1	2-1	3-1	16-78	40-1	12-17	17. TRANSVERSE BOOM MODE - X DIR
1.91	17-1	17-1	20-22	3-23	13-47	5-1	5-5	18. TRANSVERSE BOOM/UPPER KEEL - Z DIR

☐ Significant Modes in the Flight Path Direction

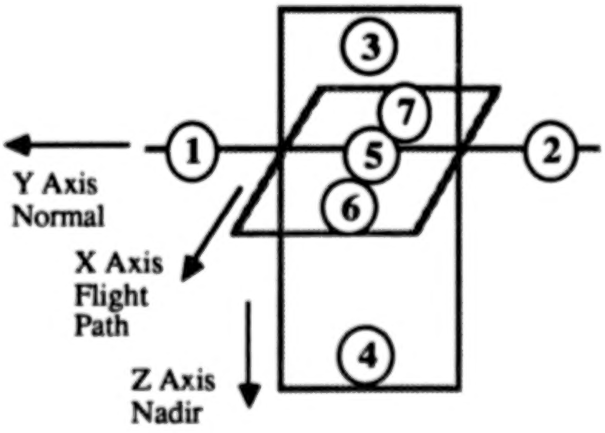

Table 4.2 Modal Strain and Kinetic Energy Participations

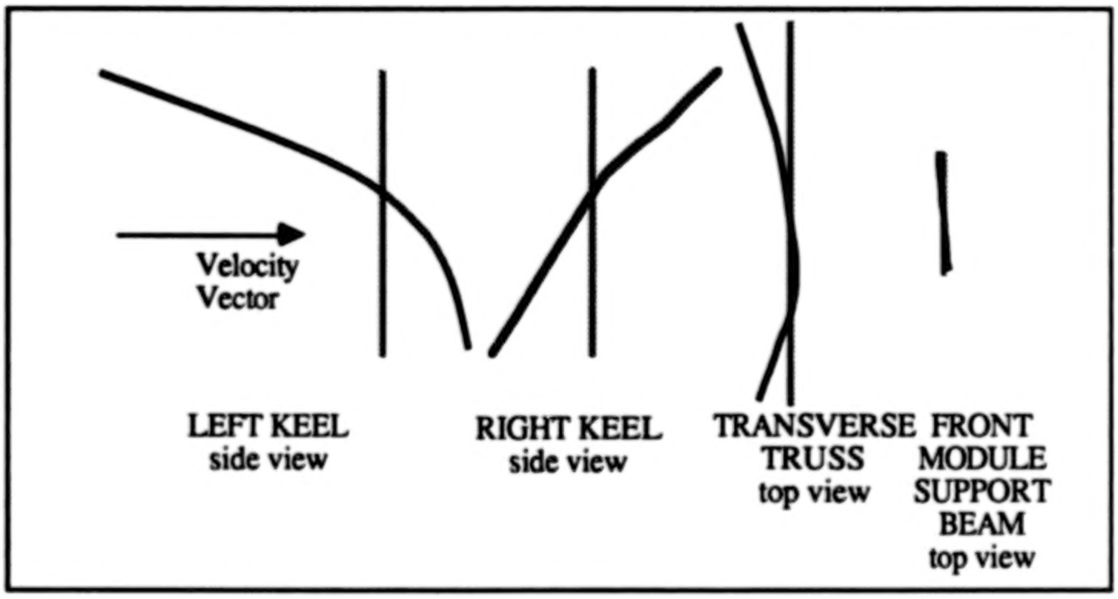

Figure 4.3 Mode-Shape deflections at 0.54 Hz

4.3 TRANSFER FUNCTIONS.

MSC/NASTRAN SOL 30 (modal frequency response solution) was used to compute the transfer functions at different points on the space station structure. By definition these are defined as the complex frequency response outputs due to unit input forces applied at the thruster locations. As stated earlier, the present study considers only the soft cycle harmonic inputs of the thrusters located at the top left and right keel locations (X=92.5m). A uniform modal damping coefficient of 0.5% was assumed in the present analysis and the transfer functions computed over the range of 0-2 Hz at different locations. The consequent acceleration amplitude/frequency plots at critical points are shown in Figures 4.4 through 4.9. The frequencies associated with the peak amplitudes identify the significant elastic modes. The points on the top keel are exicited by the 0.36 Hz and 0.54 Hz modes and the points on the bottom keel are excited by the 0.36 Hz, 0.54 Hz, 0.94 Hz and 1.17 Hz modes. Similarly the points at the module interfaces are exicited by 0.36 Hz, 1.4 Hz and 1.86 Hz modes.

4.4 DYNAMIC RESPONSE DUE TO THRUST PROFILE INPUTS

The number of harmonics and the harmonic frequencies for a specific thrust profile depend on the Cycle Period of the Thrust Profile. These can be computed using the Fourier series expressions discussed in the section 3.4. As mentioned above, the significant modes are exicited by the thrusters located on the top keel are 0.36 Hz and 0.54 Hz. The cycle periods chosen in the analysis are calculated by matching the thrust profile peak amplitude harmonic frequencies with the dominant structural frequencies. This selection procedure is based upon the following:

$$P_S = n_{PEAK} / f_S \qquad \text{\_\_\_\_4.1}$$

where:
P_S = Cycle Period
f_S = Structural Frequency in Hz.
n_{PEAK} = Harmonic corresponding to a peak Fourier Coefficient.

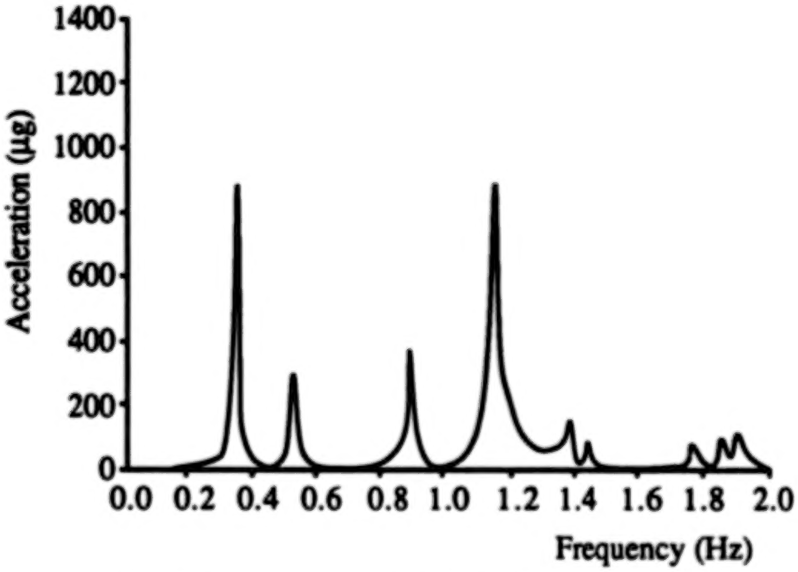

Figure 4.4 Bottom Keel (left) Transfer Function

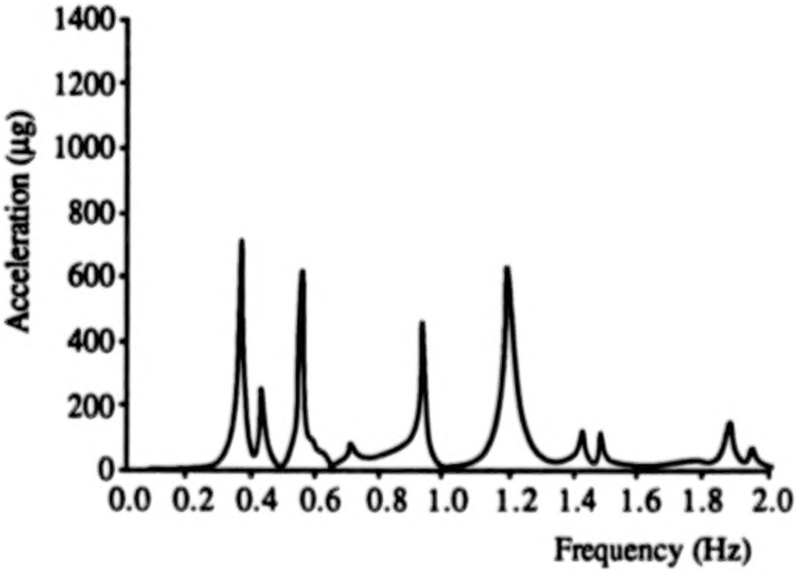

Figure 4.5 Botttom Keel (right) Transfer Function.

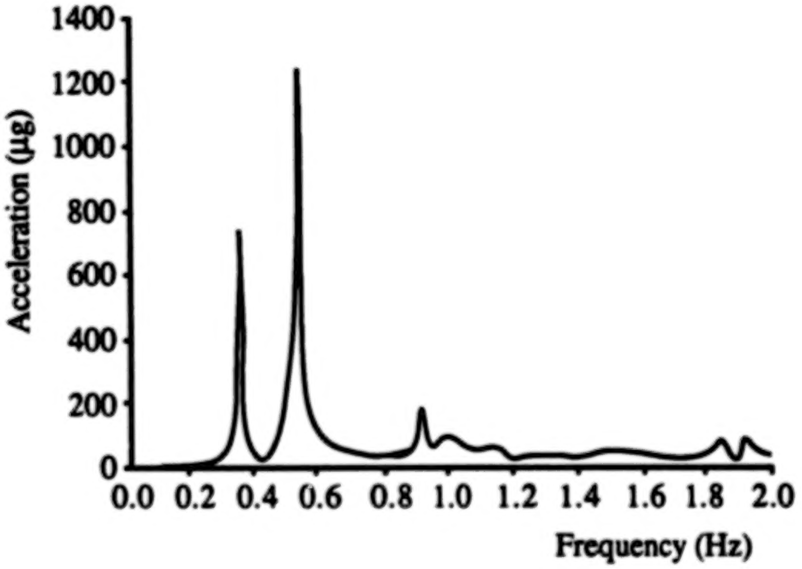

Figure 4.6 Top Keel (left) Transfer Function

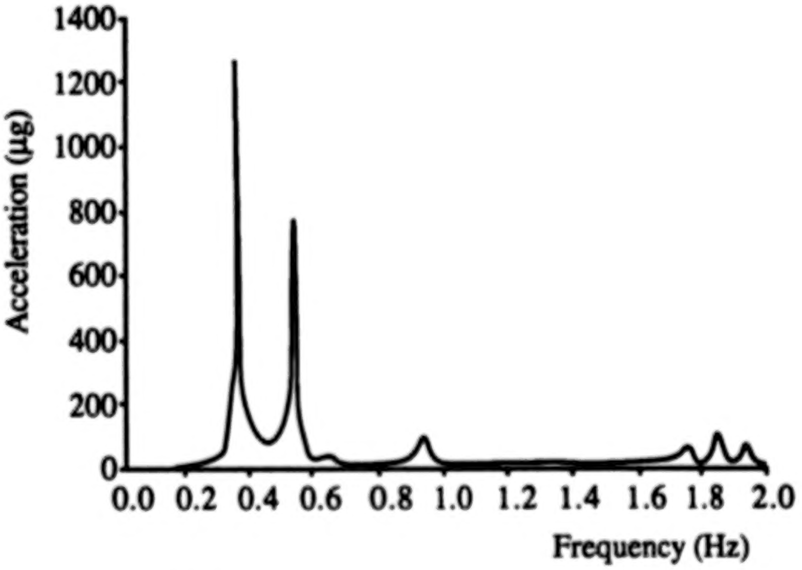

Figure 4.7 Top Keel (right) Transfer Function

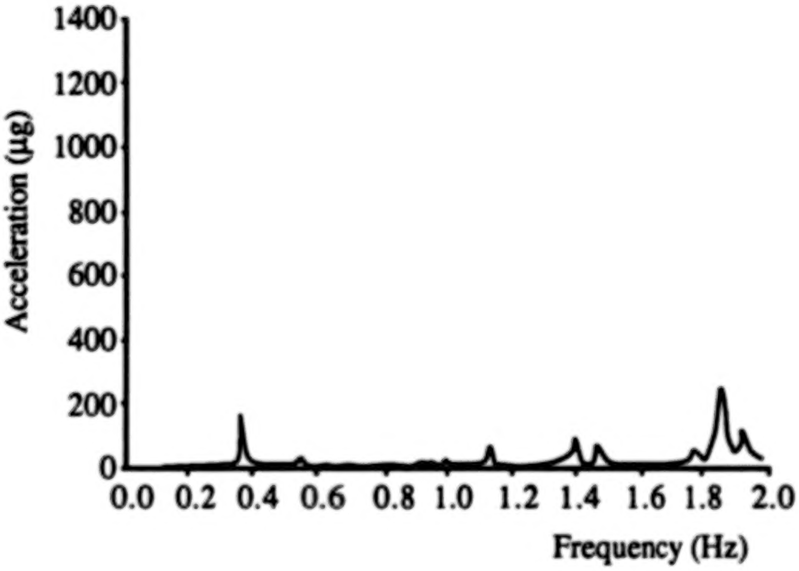

Figure 4.8 Module Interface with Central Transverse Boom Transfer Function

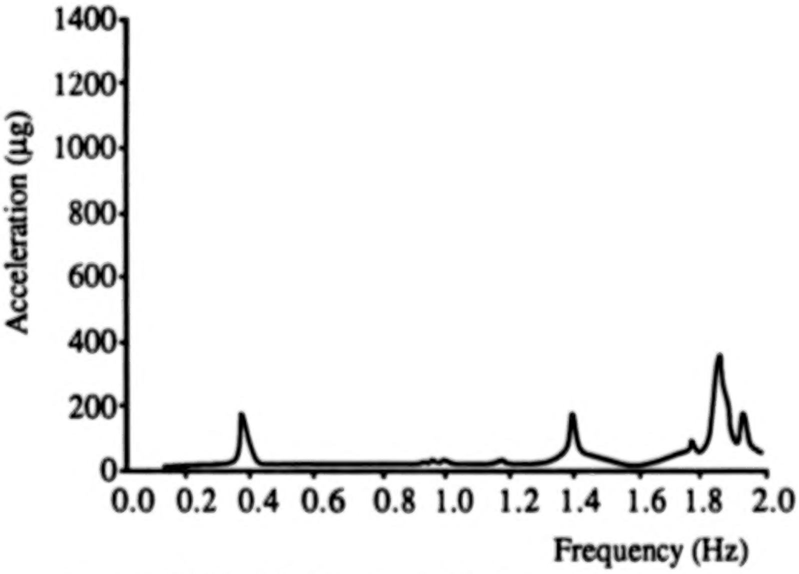

Figure 4.9 Module Interface with Front Support Beam Transfer Function

The harmonic response at the different points on the space station structure are computed using the following expression:

$$A(f_H) \quad = \quad H(f_H)^* \, F(f_H) \qquad \text{\_\_\_\_ 4.2}$$

where:
f_H = Harmonic Frequency
H = Transfer Function
F = Thrust Profile Harmonic Coefficient
A = Complex Harmonic Response

The maximum harmonic amplitude response versus period at a point on the keel and at the module interface point are shown in Figure 4.10.

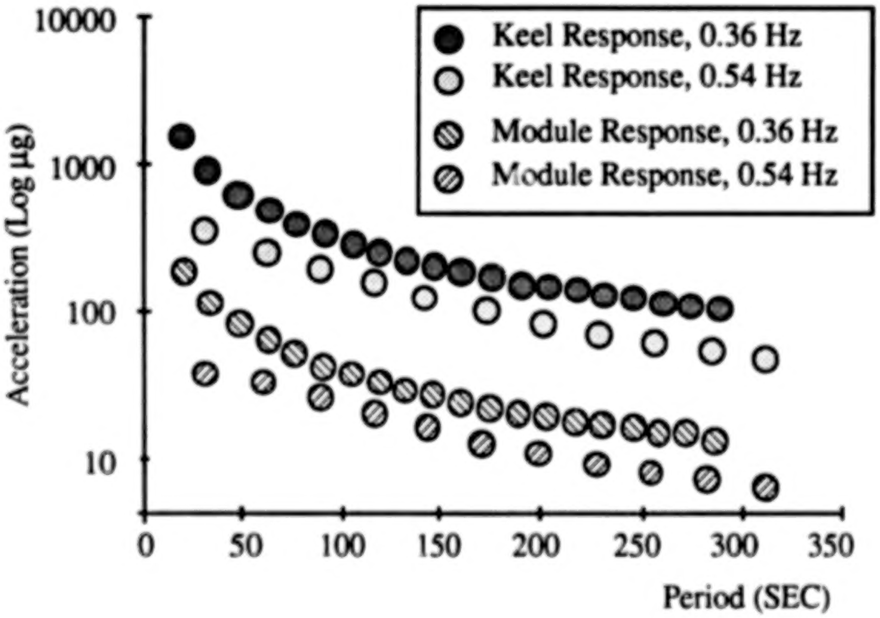

Figure 4.10 Frequency Response Amplitude vs Cycle period

The complex harmonic frequency response solutions are combined to yield the corresponding time response solutions using the expression

$$A(t) \quad = \quad \sum A_R(f_j).\cos(2\pi.f_j.t) + A_I(f_j).\sin(2\pi.f_j.t) \qquad \text{\_\_\_\_ 4.3}$$

where $A_R(f_H)$ and $A_I(f_H)$ are the real and imaginary components of the complex harmonic response.

The peak acceleration in the time domain are shown in Figure 4.11.

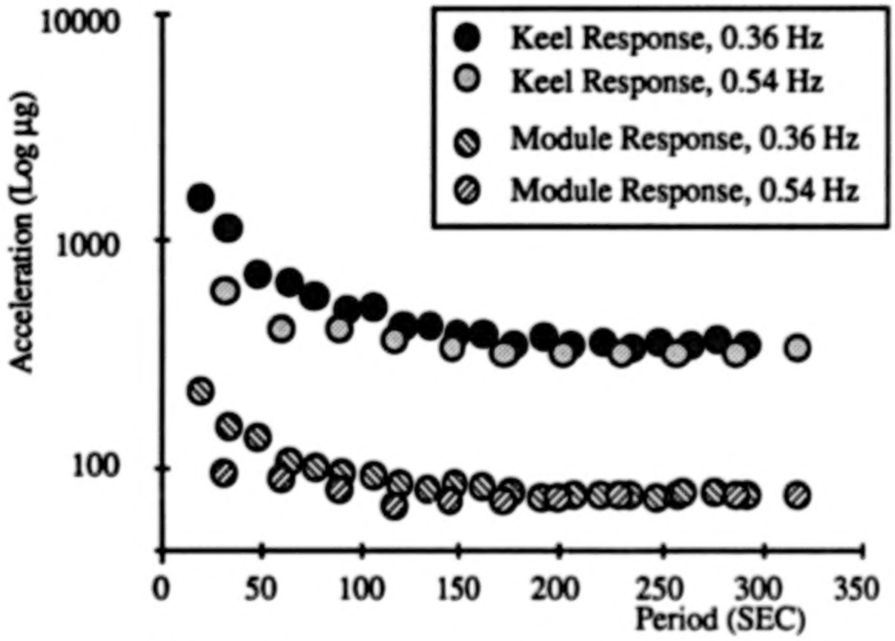

Figure 4.11 Time Response Maximum Amplitude vs Cycle period

4.5 INTERACTION ASSESSMENT.

From the results of the analysis presented in the previous section it can be seen that the lowest elastic mode frequency which contributed most to the response due to thrust profile harmonic inputs is 0.36 Hz. The other significant modal frequencies are 0.54, 0.94, 1.17, 1.4 and 1.86 Hz. The large number of harmonics associated with the large period thrust profiles excite a large number of structural modes. This can be seen from the relatively slow drop in the peak time response (Figure 4.11) compared to the peak amplitude response in the frequency domain (Figure 4.10). The flexible body response can be minimised by selecting thrust profile periods greater than about 30 times the period of the dominant elastic mode (0.36 Hz).

5.0 CONCLUSIONS

This paper has presented preliminary results from a study into the RCS/Structures interaction of the space station. The results indicate that a soft-limit cycle is an effective form of phase-plane logic; use of impulse is minimized and structural response can be restricted by choosing a suitably large attitude deadband.

Analysis of the frequency response and harmonic content of the thrust profiles suggest a continual reduction in flexible body response with increasing cycle perod. However, due to the increasing harmonic content with larger cycle periods, the reduction in response seen in the time domain actually plateaus. For periods greater than 30 times that of the fundamental mode the response was unchanged.

For the mode of control considered (uncoupled top keel thrusters) the resultant cycle period can be set at 100 seconds, effecting an attitude deadband of ±1 degree. The resultant flexible body peak accelerations are ±70μg at the modules and ±400μg at the top keel. This result was based upon the use of 50N thrusters; should larger thrusters be used then the accelerations would increase linearly.

Further analysis is required into the use of off-modulation of the bottom keel thrusters during reboost. Differing harmonic content ($\Delta P'=80\%$) and frequency response should reduce the peak accelerations.

Acknowledgements

The authors would like to express their gratitude to R. Odbert for creating the structural dynamic model and his support throughout this study.

References

1. Marshall H. Kaplan, "Modern Spacecraft Dynamics & Control" pp.262.

SESSION 6

Panel
Morris Auditorium

Dr. G. F. McDonough, MSFC, Chairman
Dr. John L. Junkins, Texas A&M
Dr. Roy R. Craig, Jr., U. of Texas
Dr. Robert Skelton, Purdue University
Dr. Sherman Seltzer, Control Dynamics
Dr. Larry Pinson, LaRC
Dr. Ken Richards, MMC

PRECEDING PAGE BLANK NOT FILMED

PANEL DISCUSSION

SUMMARY OF THE STRUCTURES ISSUES SESSION - BEN WADA

WADA: These are some of the more interesting conclusions that came out of the Structures areas; some of which are fairly critical issues (see Figure 1). First of all, the general feeling is that we are not able to provide precise dynamic data. I think frequencies and mode shapes can be predicted pretty well but the prediction of damping is going to be very, very difficult. A second issue is that, for many of the structures that we have flown, we had validated the dynamic model of entire structures with a total system level test. Often when we have run these tests, we have found errors in the math model, and these tests have been very valuable in picking out these errors. On future large space structures, we will not be able to validate the system dynamic model; therefore, we have to rely more on analysis and somehow we are going to have to work harder to convince management that we are able to do a good job. At least, I know, at JPL they believe math models are good but most program managers are not willing to commit a $5 million or $1 billion program without the tests to validate our math models. Another thing that we have brought out is that most of our experience in modeling and running tests has been on the prediction of dynamic characteristics for high excitation levels. We have been interested primarily in launch load analysis. We find that when you start getting down into low excitation levels our experience does not always hold. Recently, we ran a low level test on the Centaur booster and got some very poor results. We had to shake it harder in order to get the kind of dynamic characteristics we had anticipated.

There has been a lot of effort to build what we refer to as "clean" type structures with tight joints so that we can better understand what the structure is in order to better model it. When you look at a structure in space, what you find is that the utilities (i.e., cables, fluid system) will have 2 to 3 times the weight of the structure. Frequently, the utilities are not precisely mounted on the structure. So the problem is that the utilities tend to pollute the structure, and the question is whether it is worthwhile to build a clean structure when there are other things that completely pollute the structure itself? Generally, our group said yes, there is some value, because from a controls point of view, the first two or three modes may really be of value and this type of structure could help us predict the first two or three modes more accurately, although the utilities might give us imprecise higher modes.

Another thing brought up was the flight test program, is it of value? Generally, the feeling was that it does uncover unexpected problems. There are certain problems that we expect

PRECEDING PAGE BLANK NOT FILMED

FIGURE 1

B. WADA

STRUCTURES

- CAN'T PROVIDE PRECISE DYNAMICS DATA
- CAN'T VALIDATE SYSTEMS DYNAMIC MATH MODEL BY GROUND TESTS.
- EXPERIENCE ON PREDICTION OF DYNAMIC CHARACTERISTICS FOR HIGH EXCITATION LEVELS.
- VALUE TO BUILD CLEAN "TIGHT" STRUCTURE-UTILITIES MAY BE 2-3 TIMES STRUCTURAL WEIGHT.
- FLIGHT TEST PROGRAM — UNCOVER UNEXPECTED PROBLEMS.
- ON-ORBIT TESTING - DIFFICULT TO OBTAIN STRUCTURAL DYNAMIC CHARACTERISTICS
- BELIEVE WE CAN HELP DESIGN MORE "CONTROLLABLE" STRUCTURES.

but often there are unexpected problems that we have to understand and we find that the flight test program will help us to uncover some of these problems we do not understand. The next point is that people feel that when you don't understand the dynamic characteristics of a structure before flight, we can test it in orbit and gain the needed understanding. I feel that it is going to be very, very difficult to obtain structural dynamic characteristics of large space structures from on-orbit testing. First of all, we have a very difficult time determining the characteristics on the ground where we use 100 to 200 accelerometers and we are able to go back and look at the structure again if the data are questionable. On-orbit test is going to be much more difficult with fewer sensors and probably fewer locations to apply the shaker to excite the structure. We, the structures people, believe that we could help design a more easily controllable structure, if we knew that was wanted by the control system designers. However, we have no idea what is required or what we can do to help make the structure be more controllable.

Let me give you an illustration of the difficulty in even measuring dynamic properties of structures. On the Galileo spacecraft, we had approximately half a dozen companies take the same data from the same spacecraft and perform a modal analysis. The companies we picked were leaders in the industry. We had Langley do the ERA analysis. We had SDRC to do poly reference analysis, STI do the swift and other analysis. We at JPL did some other analyses, and we compared the results of the damping, frequencies, and mode shapes. Frequency and mode shape compared fairly well, but damping data had considerable scatter (see Figure 2). I think the way to look at it is that this is probably one mode at a given frquency, and these are the estimates of damping we obtained from a modal test. This is what I consider the state-of-the-art of modal testing with the best techniques being applied by the developers of the methods and gives an indication of how well we are going to be able to predict damping, which is not very well. So, if this is as well as we can do on the ground, my question is how well can you do it on-orbit?

McDONOUGH: Any questions or anything to add?

DICK SCHOCK: I would like to say that, having done on-orbit testing on one program, I favor doing it. I think we proved from that on-orbit test that it is a feasible thing to do. Admittedly, in both our on-orbit testing and the photogrammetric work by Langley, we flat out did not get one mode and could not get it. We did not have control of the excitation capability, but I think you get down to a choice on these large space structures eventually of which is the worst way to do it, you

FIGURE 2

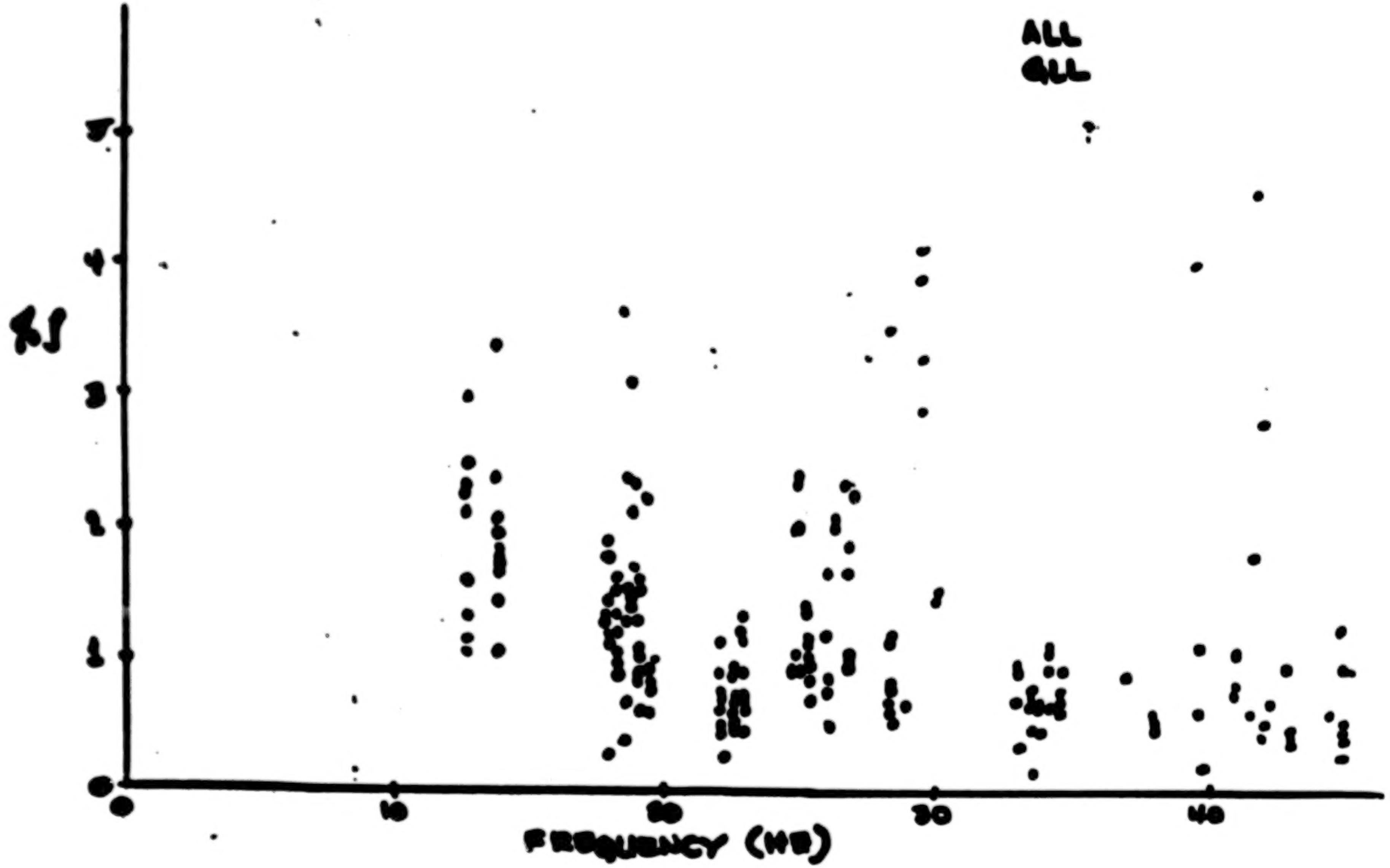

are simply picking the best of the worst. On-orbit testing may be easier and simpler and a lot more accurate than trying to test in 1-g. structures that are not designed for 1 g. and that are not basically amenable to that type of testing. We could not test the solar array in 1 g. There wasn't any choice but to conduct the system test on-orbit. For years, when we system tested something that could stand up to 1 g, the philosophy was to model what you test then to convert the model to fit flight conditions. I am afraid with these large structures coming up, that the choice is not there. You just simply do not have the capability of doing much testing at the assembly level, in my opinion, on some of these large space structures.

BOB JONES, BOEING: I would like to ask, did you really mean it when you said we are going to do pretty well on the mode shapes and frequencies, or would you be willing to qualify that and say that perhaps in a certain frequency range like the very lowest frequencies, we will be able to do fairly well and at the high frequency range, we probably cannot give the controls people any good information at all?

BEN WADA: It was all relative. What I was trying to point out is the comparison on prediction of damping would be very very difficult to do. Based on our experience, we find that even mode shapes and frequencies, predicted by various methods differ from one another so that it is difficult to determine what is the real frequency and mode shape. Often, many of these methods predict mode shapes and frequencies that do not exist because somehow during the data analysis, noise was processed or some other data that gives pseudo modes, this does give more problems. It is difficult to predict high frequency modes.

BOB JONES: I was anticipating someone asking how controls are going to simulate the structural response, and I remember my controls friends telling me that you can't lie to the filter. I am convinced we will lie to the filters. I just wanted to make sure that my bias is clear on that.

LARRY PINSON: I think the situation in the systems identification (let me call that modal extraction from ground tests to be very clear about that) is probably in pretty good shape in that most of the high frequency modes can be identified without too much difficulty. I realize Dick's exception to that. If you are running a ground test, and it is a valid ground test, then I think that our ability to analyze it and get most of the correct responses is not too bad. I am not willing to say that we could apply the same kind of algorithm to an on-orbit test, reduce the data on-orbit in some kind of automated fashion, and be very confident that was the correct answer. But in the case of ground tests, where you can work the data, massage it, iterate it, we can identify most of the response characteristics from a structures standpoint pretty well.

KEN RICHARDS: I would like to comment on the ability to identify damping. It is certainly true, and I am sure this is what Ben meant, that damping values are certainly harder to identify in a modal test where you are evaluating things at resonances and that peak response is very sensitive to that value of damping. Also, it is not necessarily clear that if I shift the same structure from place to place that inadvertent damping has not been changed in handling. Intentional damping with carefully designed damping treatments, we have shown on a limited basis can be predicted very accurately, and it is at least in our charter to show on a more complicated basis that we can predict that damping. But this is intentional designed-in damping as opposed to the inadvertent damping. These are two different things.

SUMMARY OF THE INTEGRATED ISSUES SESSION - LARRY PINSON

PINSON: A couple of points need to be made about the Integrated session. One is that it was heavily dominated by structures people. This is supposed to be the integrated session. It is my understanding that there were an estimated 40-60 people in the control session. We had 28. The Structures session had half a dozen or so, and here we had one person who came in 15 minutes prior to the end of the session who identified himself as a control person. We had two people who would condescend to call themselves structural dynamics and controls, and the rest of them were structures and dynamics and one systems guy whom I know has a dynamics background. That was the makeup of our so-called integrated session. I would invite comments on this.

The way I conducted the session was that I divided things into two parts. The first part had to do with technical, administrative, managerial, political, whatever you want to call it, more broad general issues and later we got into some of the nontechnical issues that then led to other issues that came out of the forum that were not listed originally. My intention in doing this was merely to stimulate discussion, and I think we had a good session. First of all, organization is one. We had a long discussion about co-location and new organization entities. In that regard, there was a fair amount of disagreement on this subject, as a matter of fact. I think probably companies, that is the private sector, have a little better ability to function in this co-location because they are organized in a matrix fashion and they seem to be able to work things like that a little better than, say, us "govies" and so that is not so much an issue. The point is thought that by having people in the different disciplines together so they can interact on a day to day basis, you encourage communication and you get a synergism out of that that you wouldn't get otherwise. A guy sitting in a structural dynamics area will not abandon his desk, go across the street, and talk about some hairbrain scheme he just thought up but he might if he were just sitting in a swivel chair and could turn around and ask his control compatriot, "What do you think about this?" So, the communication is encouraged by co-location. The point was made that projects force an integration of the controls and structures disciplines by their requirements and that's true, but the other side of the coin is that once the project is over, you have this team formed, they work well together, and they solve the problem, now each guy goes back to his original abode and becomes just as parochial as he ever was a short time later. The thought was, why don't we have an entity identified organizationlly as a control/structure group and, I think, that people feel the term "cyberelastician" is a little bit obscure, we need a catchier phrase. (Laughter) By the way, that was one thing the panel agreed on; we do need a phrase. Terminology is a major issue, and it doesn't get enough attention. A large number of people in controls tend to have an electrical engineering background, whereas the people in structural dynamics tend to have a structures oriented background. I think that is pretty generally true, and even though the equations of motion and all that have the same form, over the years being separated and not communicating very much, people learn to think differently and so the communications difficulties that occur because of terminology are hard to estimate. I didn't realize it was as big as it was until I got into this a little myself. We talked about education, and there is a feeling that there is a lot happening in the universities. You can argue about the pace of it, but there are a lot of people getting Ph.D.'s in the universities whose dissertations involve both structures and control disciplines, trying to work that interface. You see more and more of it. The point was made also, though, that how many companies go out and find Ph.D.'s that sit down and design actual control systems? what we need to do is get that worked into the curriculum earlier than it is presently being worked in. With regard to professional societies, we felt that professional societies are doing about as much as they can do or probably should do, in that there are a lot of control-structural interaction workshops being held. The SDM conference which has the dynamic specialist conference attached to it every third year. The last one had as its theme control of flexible structures; so there are a lot of things going on to encourage interaction in the professional societies. You could probably think of a lot more they could do, but it's debatable whether they should.

With regard to integrated program, this is getting into more technical issues now. In analysis, I said (and I didn't get a whole lot of disagreement here) that the area of simulation was a really difficult area, one that needs a lot of attention and to quote the justification for that, you talk about modeling just a few modes, a few elastic modes plus rigid body modes and you end up talking about days of computer run time on a VAX 780 or so. This is one bench mark. There are improvements. TREETOPS certainly is one of those that now has the closed topology capability, and there are others. We are doing lattice deployment with our structure program at Langley, etc. So there are some things happening there, but it is still a very difficult problem and needs a lot of work. Design is the next item we discussed. This question runs deeper than simply using the term simultaneous, and I put this in and it stimulated a fair amount of discussion. The thought was, consider the way we design things now and consider just the two disciplines of structures and controls, there are others, of course. The structures people compute modes and they give those to controls people who design a control system using that set of modes. Ken Richards made the comment that wouldn't it be nice if they would come back and as a part of their design process, let's say, structural dynamicists, can you design 5 percent damping on mode #7 for me? And, wouldn't that help? The point is, yes, it would and still using the existing setup of iterating back and forth between the structures and control people, wouldn't it be nice to have a framework within which you could do simultaneous design of structures and control where the trade between structural weight and control effort was made on an internal basis to a design code? Okay, what was the response to that? The response to it was, boy, you are way premature. There is not enough computer time in the world to work that problem. I guess my response to that was, okay, we don't even know at this point whether systems that are being proposed really need this kind of activity, but let's say that if we could design such a code to work only simple things, we would at least have something to attack, improve, work on, and have a much more integrated structural control kind of code. I guess something that I forgot to mention in the area of simulation analysis was the things that are going on that are improving this situation. The paper we heard yesterday by Bob Jones fills a big gap in that it is an approach to saying let's not get half percent accuracy necessarily; let's get something that's 10 percent or so, that embodies the essence of the problem or something that we can turn around quickly and do independent trades with. I think that is a very good thing. Another thing going on is the CAPPS (Custom Architectured Parallel Processing System) at TRW which is a different approach in that you try to tailor both the process of hardware and software to work in a class of structures. Okay, moving on now to the systems. This is an area where we got into a discussion that sort of boiled down to error budgets. The point of discussion was the effect of mission requirements on the integrated structures and control requirements that get levied on these people. It was pointed out that probably the structures people don't share in the responsibility in an equitable way. What happens typically is that the requirements come down like, let's say line of sight or something and that requirement gets imposed on the controls people. The controls people say, hey, structures guys, we need to have a certain RMS accuracy, etc. Why differentiate that error between structures and controls, why not leave that as one error, and let these guys iterate back and forth and share equally in the responsibility of matching a single performance requirement? Maybe this goes back to the new entity question that we talked about earlier.

We had other issues that came up during the discussion. Systems identification is an issue that seems to go across the board. We sort of boiled that down into two parts. Parameter identification which says basically you know what the fundamental structure equations are. Let's do a parameter identification and verify that we have the right numbers. System identification would be a litle broader than that. You say, well, that may be a part of it but you have a bunch of nonlinearities and let's try to identify what they are. In addition, the emphasis, I think, here in the system identification was on, let's identify the entire system including the controls, presumably what that would mean is the closed loop properties of the system. That might be expressed, for example, in terms of complex modes. Error bounds on the combined system received a fair amount of attention. Error bounds we could probably identify on a given math model by assuming we could run a proper test. You might identify error bounds on the properties of the control system. How about when you put them together and you have the interaction between the two? How do you go about assessing what the overall error bounds are? This leads to the third one, verification of combined systems. Typically, we run mode surveys on structures, and basically, we identify the open loop properties. What happens to close the loop? You turn the control system on. Is there any way in combining that to get a verification of a combined system? How do we do that on a very large complex system before you ever fly? Reduced model size, and by model here, I mean the math model not the scale model. An issue here was how can we get the smallest model that will adequately describe the entire system and include such effects as gyroscopic forces and that sort of thing. It might be a model embodying the Lanzcos vectors that Roy [Craig] talked about plus gyroscopic terms might work that. Something of that nature. That is an issue yet. Again, early identification of structural requirements kind of goes back to the period of involvement of people. Typically, in the structural dynamics world, the structure is designed, it's even working in a fashion, a problem develops, then the question is okay, dynamicists, go fix it. We tend to work in that mode a lot. Necessarily, the controls people are involved up front and are involved in the design process very early. The thought was that perhaps getting a single entity would force a melding or coalescence of the time when these people got involved. Any comments?

JOHN HEDGEPETH: I just want to defend cyberelasticity (laughter) and to make a couple of historical comments. Bernie Budianski pointed out several years ago that there is an analogy between what's happening with respect to controls and structures, etc., in space with what existed in the early 30's with respect to airplanes and structures and aerodynamics. The fact is that back then we were flying airplanes, it became obvious that if we were going to have increased performance airplanes, we were going to have to start dealing with this interaction between the airstream and the structural flexibility. There came about during the next decades a body of knowledge which became known as aeroelasticity. I can recall pretty far back when I was in college, I took an undergraduate course in aeroelasticity. I believe that there are going to be courses in the future in this combined thing we are talking about, and there may already be as far as I know. I am talking at the undergraduate level. The statistics are interesting because, historically, aeroelasticity made its advances primarily with the efforts of these structures and structural dynamics people. The aerodynamicists largely refused to "dirty" their hands at such kinds of things that they had to do in order to deal practically with the situation of interfacing the aerodynamics with the structures. It's only because of a few very capable aerodynamicists like Ed Garrett, Dorsen, Kusner, and Bogner did indeed agree to get involved in such things that we were able to make the advances that we did make in the area of aeroelasticity. I am not surprised that we have mostly structures and structural dynamics people looking at this integrated problem. I am glad to see a few good controls people involved in this issue. Finally, to get back to cyberelasticity. The term really comes from Norbert Weiner. Norbert Weiner coined the term cybernetics as a name for what you controls people do. Maybe you would rather have elastic-cybernetics as a name for what we are talking about and maybe that rolls neatly off the tongue. What do you want, elastic controls, controllo-elasticity? (Laughter) I think that Norbert Weiner was a pretty perspicacious fellow when he coined the term, because after all, Cyberus was a steersman for the boat which goes across the river Styx and takes us to our final resting place where we all have to go eventually. Thank you.

DR. SKELTON: If I might just respond to one point there. I agree with you that we need help from the university in marrying the disciplines, and I do find that there is interest both in the practical and new theoretical questions that fall within the gap between the two disciplines that are not answered by either one. On the other hand, I have a question for you. The structures and controls marriage is one that this conference is concerned about, but there are other marriages going on. There have been problems with propulsion interaction with controls, the pogo problems, of course, you could argue that part of that is structures too, but the point is, do you coin a name for every marriage of controls plus something?

PINSON: I would like to make one comment. Pogo is a dynamic instability that is a result of an interaction between the structure, in particular, structural dynamics and the dynamics of the propulsion system. It is not involved primarily with control, although on an asymmetric vehicle, there is a secondary effect there. But, primarily, it is a structural dynamics and propulsion system dynamics interaction. There is an instability there, and again, it was worked primarily by structural dynamics people.

SCOFIELD: There is one small correction that should be made, Larry, that all modern engines have electronics controls system.

PINSON: Of course, but in a solution of the pogo problem, that's modeled as a part of the transfer function for the engine.

SUMMARY OF THE CONTROL ISSUES SESSION - SHERM SELTZER

SELTZER: I had the pleasure of trying to lead the controls critical issues forum composed of some 40 or 50 shy, retiring members of the controls mafia and what I tried to do under direction was to put onto one viewgraph and about 10 minutes of talking a summary of what these people had to say. You will be subjected to that now. My partner Gene Worley accuses me of writing ancient Aramaic. The 8 topics for those who might have difficulty communicating with me, the first is communications with management. This is a critical issue. Some very harsh things were said about motherhood during our meeting and I'm trying to relate those to you now. I suppose those of you who were in the thing know though. What we are talking about is we designers have got to communicate with the management no matter how painful and difficult we think that is. We've got to participate in the development of the configuration of the system we are going to control, for instance. We have to be able to participate in the definition of the specifications on the control system that we are going to have to meet and live with throughout the design, so we had better get with those people in management and make sure they give us something we can really live with and understand. Some folks disagreed with this, I might point out, and felt that this was too political an issue for engineers to participate in. We had some disagreements on that, and it was proposed as a critical issue. The second one is more technical in nature. It has to do with designing, not waiting until you are done and building it in, but designing reliability and maintainability into your design right from the beginning. Also, to have the ability in the design to replace units if you think the system is going to last very long, and hopefully, it will. Something is going to fail ultimately. You had better have a plan of how you are going to replace what failed. The last point brought up was very important, that you must have in mind the cost, primarily, the dollars but also your resources, your own time, the cost involved in what you are designing. We talked quite a bit about modeling. This came up in the other two sessions, as you know. Normally, it is terribly important. The form of the model should be finite element coming out with modal representations or should be some kind of frequency domain modeling or perhaps a traveling wave phenomenon. I know that most of us agree we are not too happy with the form of models we have now, the form of plant that we must control. A few had ideas on how we might maku it better. We know that with the models that we use if we controls peple are asked how many modes did you include, we say ten. Someone thumbs their nose at us and say that's not enough. But, what is enough? How we truncate the model, that is something we can grapple with, and design about. It is very important. We have seen a number of truncation techniques that have been developed, some here and some elsewhere. These are difficult critical issues that must be resolved. How to come up with a model that is a reasonable size, that we can design, simulate, etc. Advocates of control hardware had to do with having sensors that can sense the parameters that you may have to control, where we talked about modes or whatever, and also the actuators, the things that we are going to use to control things that we sense. We have to have enough control authority to grapple with the deflections or whatever. They also have to be light enough in weight so that we don't go over our weight budget. Of course, we have to be able to get the information in a form that's sufficient for our needs. In other words, we may need to know very high frequency content of some things. Yet, we have a sensor whose output is sampled by a telemetry system to send the data down and we have lost our goal there. We talked about education. That was an interesting discussion. Are people being educated properly where they know how to communicate with other members like the controls people communicating with aerodynamicists, etc.? A very interesting side discussion occurred on whether young people can really influence us old timers on their new techniques. I may have been the oldest person in the room. I took immediate offense, but the point is that sure they can. They've got to be persistent and perhaps a little tactful with us, but yes, new techniques ought to be tried out and pushed and you shouldn't give up doing that. It can be done. Simplicity, now there was something we kicked around quite a bit, and strangely enough, we finally agreed on. Here, the idea was the control technique must end up simple. It must be simple enough, first of all, to get the sponsor to fund it. It must be simple enough that it can be implemented properly in a reasonable size computer, an onboard computer. It must be simple enough that you can assure beyond any reasonable doubt that your system will be flightworthy before it flies or the program manager will not fly it. That's what we need. The road to that simple system might be very tortuous and difficult and might be hard to understand, and that's okay as long the result is simple so that you can meet these goals. Let me give an example all of you will understand. The LaPlace transform is a terribly easy but nifty way of solving ordinary differential equations and that came from Heavyside, who used the symbol P for those of us who are old timers. Heavyside was unable to explain this very complicated development of the Heavyside operator, now the LaPlace operator. He just couldn't do it in front of the Royal Mathematical Society. But even though he couldn't describe it, it was that complicated, the results were terribly simple. We all use it, pardon me, a lot of us use it, That's a beautiful example of something that's simple although it's gotten to in a very tortuous way. So, the end result is simplicity. It doesn't have to be that your road to getting there is simple.

We talked about optimal. There's a nice word, we all like to use the optimal. But, how do we optimize something? We typically optimize subsystems, we come up with sub-optimal results. Is the final result when put all together going to be optimal? Likely not. Then, finally, we talked about the need to focus our efforts on something that's liable to be used in the future, so we don't just fritter away effort on just working on a problem that's elegant to work on but it's never going to be used. We observed that NASA and DARPA, in particular, are very good about providing models to the scientific and engineering community that we could all focus our efforts on and compare results. That's a summary of what, I think, we talked about in the controls critical issues forum. Thank you.

McDONOUGH: Anybody want to add to that or ask any questions? I would add one admonition as a fellow "old folk." We don't like quick motions and loud noises. (Laughter) So, if you have an idea that revolutionary, we would like to have it in small pieces, spread out over a few weeks. Also, I guess I could say the key to success is making us think we thought of it.

I see a lot of younger people out here. One of the problems we have, those of us who are managers and get in somewhat lofty positions, it is difficult to bring out the young people sometimes, and you would like them to come and bring ideas. People are often afraid of what they say would be considered dumb or useless or whatever. This is really not the case. I think the younger people tend to teach us a lot more than we teach them. If anybody's having problems with that, I would hope you would put that behind you.

SELTZER: I see one young person in the audience who is not afraid to approach management periodically. There a few.

McDONOUGH: Any other comments? John, do you have anything you would like to add?

JOHN JUNKINS: Well, I think one thing that connects loosely to what Sherm was saying, that I believe also affects the enthusiasm perhaps for structural designers and structural optimizers to get into the structural dynamics and controls business is, perhaps in some circles, lack of enthusiasm. I believe, it is a fair statement that structural optimization, and that's not to say controls structural optimization but the structural optimization discipline, has been around for probably 30 years, and there are virtually zero things to point to, or very few things to point to, where this discipline has impacted real hardware in terms that it was designed in a sense using structural optimization concepts. It's been largely an academic discipline. On the other hand, in optimal control and control of the dynamic systems, there are numerous systems flying where optimization principles have been successfully applied to the given plant or to a given system to make that system work. So, it is somewhat paradoxical that the structural dynamics or the structural community is enthusiastic for yet another quest, namely to get into the structural/control interaction business. But this is by way of a preface to saying that many of the techniques and ideas that really led to very little practical implementation had success or were precisely what we need in this structural/controller interaction game we need to start playing. More specifically, let me say that I think we need to start looking at the structural model as a member of a parametric family of structures. We need to look at the structural model and modeling process in a crude analysis sense as a subroutine with argument list and input and output being the mass matrix and perhaps the frequencies and mode shapes that depend upon a set of arguments. It might not be a global argument list, in a sense that I may not make everything fair game in the structural model, but we need to parameterize structures and especially identify those parameters that can be modified. It's a straightforward process to propagate the sensitivity of the structural model output, namely the mass and stiffness characteristics of the structure as a function of the parameters. Those sensitivity formulas are well known. These would then be the input to a controlled system sensitivity analysis. Whether or not we ultimately iterate indefinitely in a formal sense, structural/control optimization can remain a moot point, but at least we'll know how to ask some intelligent questions because we can propagate these sensitivities to the measure of closed loop performance that we hold dearest to our hearts and say, what if we turn this structural parameter knob a little to the right or the left, what happens to the closed loop performance? I believe it is time that we start moving in that direction, and I don't really think it's a tremendous big step. We just need to decide to do it. I think the methodology will evolve.

PAWEL DISCUSSION - GENERAL

McDONOUGH: We're going to shift gears a little bit now. We talked about the summaries of what was said in the sessions this morning and what we distilled from those sessions. We didn't really cover everything in the sessions but the things we thought were the salient points. We discussed among ourselves what some issues were that maybe weren't fully brought out this morning, which we wanted to say some more about or to embellish what might have been said this morning. So, we're going to go around the table and let the people who have these ideas bring them up and discuss them. Bob Skelton is first.

SKELTON: Another point is that the data is important. I want to make a suggestion to the controls people. The point is this, even if we can agree on what the control objectives are at various points of the structure, and even if we can agree on what the mathematical model for that structure is (those are two big hurdles), even if we got that far, we still have a problem. There are multiple points on the structure at which the RMS deflections, or rates, or rotations are important. Not just one point, there are certain critical points of the structure where the deflections must be equal to or less than a certain specified number and at some other point on the structure, equal to something else, the acceptable RMS values of the deflections and their rates are other values. So, you can define a field of acceptable deflections over the whole surface of the structure. At some point, where there is an antenna and a very tight shape control requirement, other points are less important, for example. The point is, there is not a single scalar objective to give to the controls designer. You have multiple places on the structure where deflections are so weird, and we have a natural statement of the problem that is a multiple objective statement for the control designer. This is even putting all the other modes aside in the model. So, I am suggesting to the controls people that, even though multiple objectives formulate a natural statement of the control problem, there is no theory to do that. We ought to be concerned about that, how to do that. I used to think in working with the students back in 1981, that you just take the LQG (linear quadratic Gaussian) problem and use a weighted approach. So, you take all these outputs and weight them in some scalar cross function and try to tune the weights to get these results. It turned out that there may not exist weights to do that, and even if there are, there is no proof of convergence of the algorithm to do that. This is an issue that I think is important, and model reduction and control design, sensor actuator placement all have to have to be looking at the same objective. Otherwise, you are not cooperating with these tests, even though your optimizing of the total design might be complete. In the model reduction, I think, too, it's important to preserve the RMS values of the outputs of interest over the structure and yet most of the model reduction literature does not do this. So, I'll leave it at that.

McDONOUGH: I was a little surprised when the issues came down from the groups this morning. We started with political problems, I think, and then we got into some technical problems. These are mostly communications problems, how one group talked to another group, how do we get through to each other, and how do we work together, how do we form a discipline between structures and control, etc. Those of us who are in NASA are faced with the Space Station problem right now. We try to optimize the station for control of large flexible structures and you ask yourself, as Bob's been saying, whether our main concern is an antenna, where we are worried about keeping the shape, is it a pointing system, are we worried about the accuracy, the jitter, the dynamics; is it, for example, someplace we're doing low gravity work trying to form crystals? Where do you put the various things to the environments you want, how do you define what the environments are? We seem to have a problem that transcends any simple optimal technical solution. We can get optimal solutions for single purpose payloads, such as Hubble Space Telescope (I don't know if that's much smaller, but at least it's single purpose) where the purpose is to point at the sky and focus on individual targets. When we get to multipurpose orbiting platforms, such as Spacelab, there may be no overall solution other than the kind of solution that says, well, you do your thing first and I'll do mine next. If we could figure out some way to determine the characteristics of this system, modal characteristics of different places, possibly we could find ways to control it, but that's a big bite, too.

SELTZER: I get concerned about the form of the model before we talk about reducing it. I'm concerned whether we have the right form in modal characteristics, and yet all the reduction techniques are armed toward reducing modal characteristics. Some get very complicated to apply, and I'm wondering if we really end up with a sufficiently accurate model that way. I think maybe starting out with some other approach other than modal, say, one that ends up with modal characteristics might be more appropriate.

SKELTON: Well, some years ago, we wrote a paper asking a different question just from an academic point of view. Just suppose you had a linear mathematical model of the system and you wanted to consider the possibility of truncating things in a number of different coordinates, so you could choose modal coordinates or you could choose any set of coordinates you like. The question was, does there exist a set of coordinates that are best in the sense that, if you transform the system to those coordinates and then throw away the last part, does this set of coordinates have the property that you make the smallest possible degradation in the performance RMS values at the location on the structure then? We found there is, indeed, a set of coordinates that have that property and they are not modal coordinates. And, they are described in the literature.

SELTZER: I guess I would like to encourage people to consider modeling things entirely different from that. Perhaps, as traveling waves, if we have very large structures where the disturbance moves along the structure and the wave. Perhaps, in the frequency domain approach, as a transfer function or voting block between selected sensors and actuators. These are just a couple I can think of, but surely there are many other ways that we ought to attack to model things that would end up with a simpler model that would be easier to truncate and that we could implement into a computer simulation for our design purposes.

PINSON: The idea of multiple objective functions does, I think, bring up the subject that came up in our forum that I didn't mention when I was up there. I think it was McCutchen or somebody brought it up. That you really design a system to accomplish multiple functions, like Space Station is going to have many experiments on it and many things going on at the same time, and how you go about designing something like that, like a Space Station, for a global optimum, in a sense, that you consider all of the functions that it has to perform or at least envelope the various configurations or functions that it has to perform and try to optimize for that. I don't know how it relates to what you have up there exactly, but it seems like that is something worth considering.

SKELTON: The part that I did show, Larry, was not as all encompassing as that. It was a much simpler statement. Even if you decided that RMS values at multiple points on the structure are points of interest, and only that, there are other things as you mentioned, where to put the equipment, etc. So, this is a problem for a controls person to say, even if you decide those things, there are certain decisions in existing control theory. That's the only point I was trying to make. I would like also to say that all controls engineers don't come from EE's.

PINSON: I would like to add one of the things that I stated in the critical issues forum, and I don't think very many people took issue with. Maybe it's something that might stimulate a discussion here. I said it was my impression that controls people tended to be more mathematically rigorous in the work they do than structures people. Structures people tend to be more intuitive in their approach to problems. As a result of dealing with some controls people in the structural dynamics area at Langley, I have seen a pretty sizable synergism coming in that looking at things from the opposite point of view was very productive and quite a learning experience. I just wondered if anybody here has a similar experience or would like to comment on the encompassing statement I just made about controls people tending to be more mathematically rigorous, while structures people tend to be more intuitive?

McDONOUGH: Sco might have a comment on that

(LAUGHTER)

SCOFIELD: I have a theory about that, Larry. After World War II, the operational methods and other analysis techniques that are taught in undergraduate school, first blossomed in the electrical engineering schools, not in mechanical. I think that the reason for that is we have a lot of neat linear components in electrical engineering and we have components that you can breadboard and try. You know when you build a bridge, you had better be right. When you make a filter, you can change it before you put it in the TV. So, my theory is that mechanical engineers and structural engineers are deprived, because they don't have the hardware to tinker with that the electrical engineers do. I don't know how that ties in with being more mathematical rigorous, but it did give birth to the proliferation of a whole bunch of linear analysis techniques. We are as stuck as anybody on the nonlinearity analysis techniques.

JUNKINS: I would like to add another point if I may, that applies to this perception, and this was primarily a perception by structural analysts. I think another way of stating it is many of the controls engineers are working in large space structures. First of all, they have to be a fairly hardy lot who are not intimidated by high dimensionality and partial differential equations, etc., because they are here. Also, concerning the structural analysts, often times an end product of their analysis is the equations of motion and the beginning point is the geometrical description and parameterization of the properties of that structure. So, the nature of the role they play is very physical. They start with the physical description of the system, and the output is the equations of motion and the mode shapes, frequencies, etc. Whereas, the input in the traditional operation of this scenario here to the controls engineer are the equations of motions. He doesn't start with geometrical descriptions of the system in question. I think that perception is fostered really by traditional separation of functions. I don't really believe one set of engineers are necessarily less physical than the other regardless of their opinions on Olivia Newton John. (LAUGHTER)

SKELTON: If I could say one thing. The last couple of days I've heard controls people talk about what the structures people don't know. And I've heard structures people talk about what the controls people don't know or do. I think it's not good to polarize us into categories. I think good mathematics and good intuition and experimental feeling for the application are important on both sides. Maybe it's even irrelevant whether one side of the aisle is more theory than the other. The important thing is how do we use the best of methods for getting a particular job done by cooperating. I remember too vividly when things go wrong in a control systems design, when the controls guy points to the structures and says it was your model that was bad. The structures guy says no, there is nothing wrong with our model; control theory is worthless. You know we've got to go beyond this polarization.

McDONOUGH: You know, we've been discussing what name this hybrid person has and what it is that he does. Do we really think there is another discipline in between structures and control that should take care of the interaction problem? Because if one person covers both areas, then there is no disagreement between groups. But, can one person be both?

KEN RICHARDS: It's possible to make a contribution to both fields, certainly not the cutting edge. I would remark that I've known Harold Scofield for 13 years or more. We initially worked together, he at Marshall and I at JSC, on ascent flight control stability. Harold introduced me as a controls engineer. Actually, Harold, I didn't have my first controls course until 2 years after my Ph.D. in mechanics, but I'm really happy to have been able to fool you this long. It is difficult, I can remember early in 1973 when I went to work at JSC, even trying to communicate with my NASA monitor, we spoke a different language. It was Bill Peters, he was known in ascent flight control and worked in there for a long time. The initial reaction when I talked about a real eigenvalue problem, he thought about plus or minus j omega. You know, I questioned him, and he wanted to know what Lockheed had sent him. So, the first year was getting the terminology straight, and after that, it was fairly effective but it was tough, it's getting easier now.

McDONOUGH: Well, I think it is, and of course, it's my hope when we get problems like Space Station, we are almost forced to look at the whole problem at the same time rather than structures guys starts it out, passes it over to controls, he takes it a certain distance. Now, it appears we all have to jump in at the beginning and lay things out, and one issue I think you brought up this morning, too, is how do we get the managers to allow some of this to happen before things get out of hand. How do we get in when the requirements are set so that we don't get things that are mutually exclusive? We can't do this and that, but we are forced to do both.

BILL HAILE, LOCKHEED: You know, I've been listening here for 2 1/2 days. It's been very informative, but I have a couple of things or observations I would like to put out just to see what you think. The purpose of this conference is interaction of structures and controls. As I go down the list, a lot papers were given and the critical items list that we had up on the board, and I notice that not many of the critical items have to do with interaction of structures and controls. In fact, I think there are only 3 of them. There are a lot of arguments with management, a lot about computer sizes, whatever, inexact problems, but a lot of those can be handled in a separate discipline. They can cross communicate. There are problems in communications but they can be solved, I think. The three that I've picked out, it looks like might be an issue here. One of them was lack of optimum design. You know, we design structures and controls systems separately. We don't get the optimum design because we don't have any single discipline that handles that, but my own view on that is that I'm not interested in the optimum design. If it works and meets the requirements, it's good enough for me. You could maybe fine tune that and make a better design but I'd rather spend my time designing something else. The optimum design issue may be an issue, but for me personally, I don't think that. We did mention system identification, how do you identify it once it's built, and I think that's a discipline that does require another person who can cross communicate between the control system and the rest of the system. I thought that system identification was a difficult problem for controls system alone to handle. It's a difficult problem for structural dynamics alone to handle. That was one I picked out. The third one that was mentioned, I lumped this into the lot in here, was, is there a best set of coordinates to define your structure? We talked a lot about truncating modes shapes, etc. You know I'm in structural dynamics, and I kind of resent the fact we're only talked about in terms of mode shapes. There's more in structural dynamics than mode shapes. You going to be faced with nonlinear structures, a number of problems in structures. Even with nonlinear structures, it looks to me like one of the problems was on the controls side, computers were too slow to handle the large size of problems we have. I don't mean slow computers, I mean maybe better techniques to solve those, but still is there a best set of coordinates, a better way to work the whole problem? I think that the third issue, a better way to work the whole problem is a real discipline between the two that is emerging. I would like us to consider here, whether we are talking about an evolution of present techniques just getting better, better communications solving some of the problems, or whether there is a need for a whole other discipline that is, what we've been throwing names around for. I thought that in the three issues I've listed, I didn't see the need for a new discipline. I think if you can't identify exactly what this discipline is going to do, you're going to have a tough time selling it. The optimum design issue may not be a critical issue, I'm not sure on that, but the system identification issue, a better way to solve the problems, and a different set of coordinates, are vital ones. Maybe somebody would comment on that.

GEORGE VON PRAGENAU: I would like comment on the identification and I would like to make a contrast between identification and robustness. We're mainly in a quandary with our robustness when you have a difficult way to achieve robustness, and then we lean heavily on the identification of the system and its accuracy. There's a tradeoff. It was discussed earlier in our controls session that if we have more robustness, we definitely have less problem in identification since we don't have such a heavy accuracy requirement. I think there are other possibilities to help ourselves to get the robustness. I would suggest you consider interstability, so that, if we have a system that's highly robust, it must be rather sensitive to interstability. When a flexible structure is impacting the control system which behaves like a mechnical system, it would be better to come up with how to design a system like this, then we have more robustness and identification is a lesser problem. This is my comment to that. There is always a tradeoff between identification and robustness.

JUNKINS: I think as structures people we have not contributed to the robustness of these systems as much as we could. I would like to put in a commercial here for passive damping. I would not be so bold as to say that that's the missing link between the two disciplines, or that's the new discipline that's needed. I don't believe it is that encompassing or elegant. But passive damping is frequently looked at as a bandaid technique. You slap the glue on it later. We have a term for that. After Walt Disney, we call that Tar Baby technology. It generally results in large weight penalties and very little good. There are some social myths about passive damping. One, it's a damping add-on if you do it, but it's not very efficient. Two, it adds weight. This is not necessarily true, in fact, if you can put in sufficient amount of passive damping, you can do away with actuators, etc., and reduce weight. It's not true it always adds weight. A third social myth is that you have to soften the structure. Actually, sometimes the structures increases in strength, but what I am proposing here is that these ideas be investigated by more than just a few of us specialists and factored into the system design process early enough to do some good and provide a little bit of the robustness, so that the entire burden doesn't have to fall on the controls engineer.

SKELTON: I want to make a comment about optimal design. When you're discussing optimal design, you're making an assumption that there exists a design that is adequate. The whole issue of optimization is existence, the question of whether there exists a design to do what you want in the first place. If the answer is no, then you don't know what to do unless you approach the question of optimum design.

CRAIG: Several people have spoken on the issue of system identification. I think the point that was just made about the relationship between that and robustness is certainly a very valid point. It is a very tough issue, and I think it was properly pointed out that it is one that will bring our disciplines together perhaps in a very significant way. There are a lot of real issues within the issue of verification or system identification, whether it's going to be the structure or whether it's going to be the system, open loop or closed loop. Whether it's going to be using the algorithms that are currently available that are very well refined for linear systems identification, or modal testing, whether we are going to have to get beyond that and look at some nonlinear testing. If so, how do we do it and what kind of nonlinearities are we looking for? How are we going to characterize those, and how are those people who are using the model going to use the nonlinearities that we come up with? Gyroscopic effect has been mentioned for the question about what sort of parameters do we want to get out of the testing. Do we want just mode shapes and frequencies, or do we want max physical parameters, just what do we want? One thing that I haven't heard too much about because I only heard two or three of the controls papers, and that is the issue of online identification as part of perhaps adaptive control versus the larger issue that we looked at usually in terms of modal testing which would probably have to be accomplished offline or on a less frequent basis than some kind of online testing. What kind of requirements are there for accuracy on those two different levels of models that are obtained by some kind of identification technique? Of course, the ground test versus on-orbit, again, we haven't heard too much about component level versus system level. At least my understanding is that the Space Station will be progressively built, different modules will come up; therefore, there will never be necessarily a time in which one would test the structure and that would be the last test that would be done. So, what do we need to know about different components, either before they are assembled or would another test have to be done once it comes up and docks? Related to this is that I didn't really learn the analytical side of structural dynamics until I participated in the test side of it. I have a laboratory, the last part down here relates to the fact that we're doing modal testing in the laboratory. I think that trying to get into also developing even simple control experiments, people may look down their nose at that. It's not really easy to go in and do a test when a beam that has modes at 1 Hz and below, to find the sensors, the actuators, to decide what the control objectives are going to be and to do that. I think that in the universities we certainly will be doing it with cruder equipment. We won't have flight qualified rate gyros, but hopefully, the reality therapy is doing some experiments in the lab will help these students be better integrated as they come out. At the University of Texas, we will be going with linear systems theory to provide both the structural dynamics and controls portions so that instead of being separate, sort of taking off in our own directions, we will have a little bit of glue to pull it together. So, I think those issues about verification have been discussed before, but I just wanted to bring up some of the details.

HAILE: A lot of the problems that we are having, I think, that if we had enough time and enough engineers and enough money, maybe lots more, but still they are all solvable that way. I look at the problems that we could solve with more of the same, but some of the problems we can't solve that way and those are the ones I think this conference should be looking at. They are beyond the state-of-the-art today. I think the systems identification issue might be beyond what we know right now. I think we ought to be looking at things that we cannot presently solve but might need a new discipline.

McDONOUGH: I think that we all agree with that. The question, of course, is usually how and where do we start? We should be talking more about that, and if anybody has a comment, we could add to it, but I think you've given us food for thought. That's about all I'd be willing to say right now. You are undoubtedly right.

JOHN JUNKINS: I thought I might give you a quote to take home and put in your circular file. I think the triple curse of the high dimensionality, the uncertainty, and the nonlinearity coupled with the fact that these issues cross the traditional boundaries, which is really why we're here. These models are in a strict sense, I think, unsolvable in that they have nice clean deterministic answers. What I would like to do is to focus the last of my discussion here, and rather than to dwell on the critical issues per se, I would like to point to things on this conference that have been significant contributions that seem to be promising steps in the right direction for dealing with these aspects of the triple curse. In the area of high dimensionality, where does the high dimensionality come from? Well, it comes into the structure-control problem usually out of the application of NASTRAN or some other structural modeling program, and there are all sorts of issues involved within this, but one of the things you find after playing with various substructure techniques and various finite element modeling techniques that on the average, misery is not conserved. (Laughter) There are good and bad ways of doing things, and in many cases, if you have a lot of insight about how to go about modeling your structure, with 50 degrees of freedom you may get accuracy that someone with less insight might get with 10 times that number of degrees of freedom as far as being convergent to an accurate set of modes and eigenvalues. I did see two things that caught my attention that I want to go home and think about more. One of them I had seen before, but the paper given by Remi Engels on his modification of the Craig-Bampton technique let me see something that is extremely important, at least it's important in my mind's eye right now, and I want to study it very carefully as a way to get at the dimensionality problem where it arises, mainly at the point of modeling the structure. Also, in that same paper, he had a very interesting technique of solving a sequence of small eigenvalue problems instead of one big one. You remember he was reporting some powers of 10 times gain in efficiency for solving for frequency and mode shapes with large structures. So, that seemed to me to be very significant and the same thing, I think, the Lanzcos vectors approach that was presented by Roy Craig looked very interesting. In the area of uncertainty and nonlinearity, now there are two aspects of uncertainty that I think are important, one of them is how to reduce it and the other is how to live with what's left. This basically lies at the heart of dual problems, one is those of system identification that has been discussed extensively here. The other one is the adaptive control and robust control methodology, and in this area and to some extent in the other areas, the work that Dave Hyland has been talking about for a number of years and has recently been doing in a sense applies to structural dynamics and looks to me to be very significant. The area of nonlinearity, I would like to suggest a philosophy. There is no doubt in my mind that regardless of how nonlinear a model is, a linear model of that nonlinear model or of that nonlinear system is going to remain at the heart of the engineering analysis of that system. We just don't have the methodoloy on the shelf for designing control systems for highly nonlinear systems. On the other hand, modeling the nonlinearities is going to be extremely important because we will then try the first approach which is to design a linearized control system for the linearized version of the model and then try to construct with our math model the nonlinearities you believe are present. Will the system work in the presence of nonlinearities?

McDONOUGH: Thank you, Johnny. We are about to reach the end of our time period. Would anybody like to comment on that or any other aspect of what we've talked about? Anybody at the panel like to summarize?

CRAIG: I would like to take the microphone for just a minute. I saw Bob Ryan step in. I think for those of us who participated, knowing the difficult problems that they've had over the past couple of months and to still go ahead with the conference and to have the kind of conference we've had, I would like to express my appreciation to Harold and Bob, and I think all of us should at this time. (APPLAUSE)

McDONOUGH: Thank you. I think we'll call the panel session closed now. Appreciate it.

U.S. GOVERNMENT PRINTING OFFICE:1987-726-123/45006

END

DATE

FILMED

AUG 12 1987